Journal of Biomedicine and Biotechnology

Animal Models of Human Pathology 2012

Guest Editors: Monica Fedele, Oreste Gualillo, and Andrea Vecchione

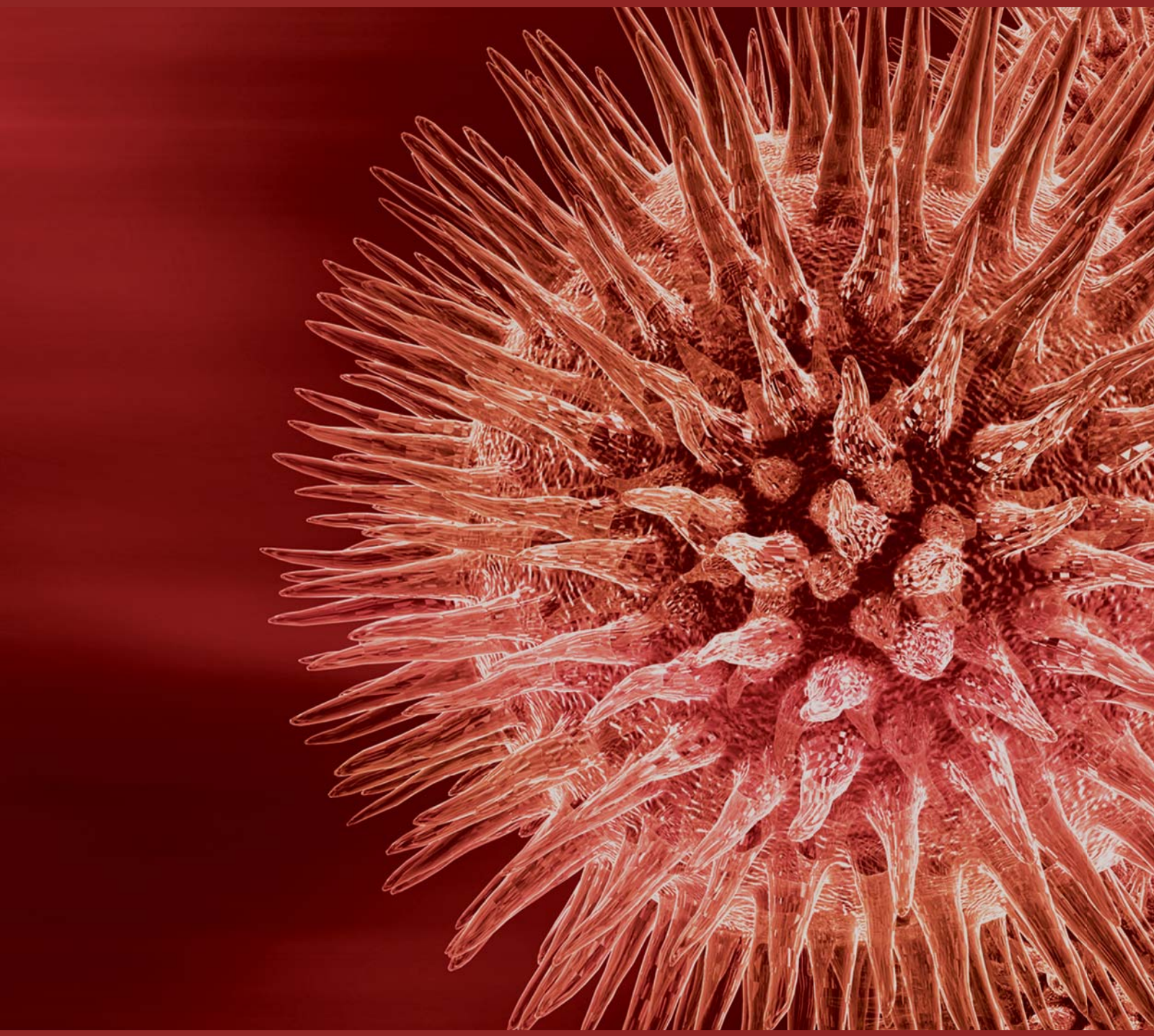

Animal Models of Human Pathology 2012

Journal of Biomedicine and Biotechnology

Animal Models of Human Pathology 2012

Guest Editors: Monica Fedele, Oreste Gualillo,
and Andrea Vecchione

Editorial Board

The editorial board of the journal is organized into sections that correspond to the subject areas covered by the journal.

Agricultural Biotechnology

Ahmad Zuhairi Abdullah, Malaysia
Guihua H. Bai, USA
Christopher P. Chanway, Canada
Ravindra N. Chibbar, Canada
Adriana S. Franca, Brazil
Ian Godwin, Australia
Hari B. Krishnan, USA
Carol A. Mallory-Smith, USA
Xiaoling Miao, China
Dennis P. Murr, Canada
Rodomiro Ortiz, Sweden
Encarnación Ruiz, Spain
B. C. Saha, USA
Abdurrahman Saydut, Turkey
Mariam B. Sticklen, USA
Kok Tat Tan, Malaysia
Chiu-Chung Young, Taiwan

Animal Biotechnology

E. S. Chang, USA
Bhanu P. Chowdhary, USA
Noelle E. Cockett, USA
Peter Dovc, Slovenia
Scott C. Fahrenkrug, USA
Dorian J. Garrick, USA
Thomas A. Hoagland, USA
Tosso Leeb, Switzerland
James D. Murray, USA
Anita M. Oberbauer, USA
Jorge A. Piedrahita, USA
Daniel Pomp, USA
Kent M. Reed, USA
Lawrence Reynolds, USA
Lawrence B. Schook, USA
Mari A. Smits, The Netherlands
Leon Spicer, USA
J. Verstegen, USA
Matthew B. Wheeler, USA
Kenneth L. White, USA

Biochemistry

David Ronald Brown, UK
Saulius Butenas, USA
Vittorio Calabrese, Italy
Miguel Castanho, Portugal
Francis J. Castellino, USA
Roberta Chiaraluce, Italy
D. M. Clarke, Canada
Francesca Cutruzzolà, Italy
Paul W. Doetsch, USA
Hicham Fenniri, Canada
Nick V. Grishin, USA
J. Guy Guillemette, Canada
Paul W. Huber, USA
Chen-Hsiung Hung, Taiwan
Maria Jerzykiewicz, Poland
Michael Kalafatis, USA
B. E. Kemp, Australia
Phillip E. Klebba, USA
Wen-Hwa Lee, USA
George Makhatadze, USA
Leonid Medved, USA
Susan A. Rotenberg, USA
Jason Shearer, USA
Andrei Surguchov, USA
John B. Vincent, USA
Y. George Zheng, USA

Bioinformatics

T. Akutsu, Japan
Miguel A. Andrade, Germany
Mark Y. Borodovsky, USA
Rita Casadio, Italy
David Corne, UK
Sorin Draghici, USA
Eugénio Ferreira, Portugal
Stavros J. Hamodrakas, Greece
Paul Harrison, USA
George Karypis, USA
Guohui Lin, Canada
Satoru Miyano, Japan
Zoran Obradovic, USA
Florencio Pazos, Spain
Zhirong Sun, China
Ying Xu, USA
Alexander Zelikovsky, USA
Albert Zomaya, Australia

Biophysics

Miguel Castanho, Portugal
P. Bryant Chase, USA
Kuo-Chen Chou, USA
Rizwan Khan, India
Ali A. Khraibi, Saudi Arabia
Rumiana Koynova, USA
Serdar Kuyucak, Australia
Jianjie Ma, USA
S. B. Petersen, Denmark
Peter Schuck, USA
Claudio M. Soares, Portugal

Cell Biology

Omar Benzakour, France
Sanford I. Bernstein, USA
Phillip I. Bird, Australia
Eric Bouhassira, USA
Mohamed Boutjdir, USA
Chung-Liang Chien, Taiwan
Richard Gomer, USA
Paul J. Higgins, USA
Pavel Hozak, Czech Republic
Xudong Huang, USA
Anton M. Jetten, USA
Seamus J. Martin, Ireland
Manuela Martins-Green, USA
Shoichiro Ono, USA
George Perry, USA
M. Piacentini, Italy
George E. Plopper, USA
Lawrence Rothblum, USA
Michael Sheetz, USA
James L. Sherley, USA
G. S. Stein, USA
Richard Tucker, USA
Thomas van Groen, USA
Andre Van Wijnen, USA
Steve Winder, UK
Chuanyue Wu, USA
Bin-Xian Zhang, USA

Genetics

Adewale Adeyinka, USA
Claude Bagnis, France
J. Birchler, USA
Susan Blanton, USA
Barry J. Byrne, USA
R. Chakraborty, USA
Domenico Coviello, Italy
Sarah H. Elsea, USA
Celina Janion, Poland
J. Spencer Johnston, USA
M. Ilyas Kamboh, USA
Feige Kaplan, Canada
Manfred Kayser, The Netherlands
Brynn Levy, USA
Xiao Jiang Li, USA
Thomas Liehr, Germany
James M. Mason, USA
Mohammed Rachidi, France
Raj S. Ramesar, South Africa
Elliot D. Rosen, USA
Dharambir K. Sanghera, USA
Michael Schmid, Germany
Markus Schuelke, Germany
Wolfgang Arthur Schulz, Germany
Jorge Sequeiros, Portugal
Mouldy Sioud, Norway
Rongjia Zhou, China

Genomics

Vladimir Bajic, Saudi Arabia
Margit Burmeister, USA
Settara Chandrasekharappa, USA
Yataro Daigo, Japan
J. Spencer Johnston, USA
Vladimir Larionov, USA
Thomas Lufkin, Singapore
John L. McGregor, France
John V. Moran, USA
Yasushi Okazaki, Japan
Gopi K. Podila, USA
Momiao Xiong, USA

Immunology

Hassan Alizadeh, USA
Peter Bretscher, Canada
Robert E. Cone, USA
Terry L. Delovitch, Canada
Anthony L. DeVico, USA
Nick Di Girolamo, Australia
Don Mark Estes, USA
Soldano Ferrone, USA
Jeffrey A. Frelinger, USA
John Robert Gordon, Canada
James D. Gorham, USA
Silvia Gregori, Italy
Thomas Griffith, USA
Young S. Hahn, USA
Dorothy E. Lewis, USA
Bradley W. McIntyre, USA
R. Lee Mosley, USA
Marija Mostarica-Stojković, Serbia
Hans Konrad Muller, Australia
Ali Ouaissi, France
Kanury V. S. Rao, India
Yair Reisner, Israel
Harry W. Schroeder, USA
Wilhelm Schwaeble, UK
Nilabh Shastri, USA
Yufang Shi, China
Piet Stinissen, Belgium
Hannes Stockinger, Austria
Graham R. Wallace, UK

Microbial Biotechnology

Suraini Abd-Aziz, Malaysia
Jozef Anné, Belgium
Nuri Azbar, Turkey
Yoav Bashan, Mexico
Marco Bazzicalupo, Italy
Hakan Bermek, Turkey
Nico Boon, Belgium
José Luis Campos, Spain
Yinguang Chen, China
Luca Simone Cocolin, Italy
Peter Coloe, Australia
Daniele Daffonchio, Italy
Han de Winde, The Netherlands
Raf Dewil, Belgium
Jos Domingos Fontana, Brazil
Petros Gikas, Greece
Tom Granstrom, Finland
Ismail Kiran, Turkey
Hongjuan Liu, China
Yanhe Ma, China
Paula Loureiro Paulo, Brazil
Bernd H A Rehm, New Zealand
Alberto Reis, Portugal
Muthuswamy Sathishkumar, Singapore
Ramkrishna Sen, India
Angela Sessitsch, Austria
Ya-Jie Tang, China
Orhan Yenigun, Turkey
Eileen Hao Yu, UK

Microbiology

D. Beighton, UK
Steven R. Blanke, USA
Stanley Brul, The Netherlands
Isaac K. O. Cann, USA
Stephen K. Farrand, USA
Alain Filloux, UK
Gad Frankel, UK
Roy Gross, Germany
Hans-Peter Klenk, Germany
Tanya Parish, UK
Gopi K. Podila, USA
Frederick D. Quinn, USA
Didier A. Raoult, France
Isabel Sá-Correia, Portugal
P. L. C. Small, USA
Michael Thomm, Germany
H. C. van der Mei, The Netherlands
Schwan William, USA

Molecular Biology

Rudi Beyaert, Belgium
Michael Bustin, USA
Douglas Cyr, USA
K. Iatrou, Greece
Lokesh Joshi, Ireland
David W. Litchfield, Canada
Wuyuan Lu, USA
Patrick Matthias, Switzerland
John L. McGregor, France
S. L. Mowbray, Sweden
Elena Orlova, UK
Yeon-Kyun Shin, USA
William S. Trimble, Canada
Lisa Wiesmuller, Germany
Masamitsu Yamaguchi, Japan

Oncology

Colin Cooper, UK
F. M. J. Debruyne, The Netherlands
Nathan Ames Ellis, USA
Dominic Fan, USA
Gary E. Gallick, USA
Daila S. Gridley, USA
Xin-yuan Guan, Hong Kong
Anne Hamburger, USA
Manoor Prakash Hande, Singapore
Beric Henderson, Australia
Daehee Kang, Republic of Korea
Abdul R. Khokhar, USA
Rakesh Kumar, USA
Macus Tien Kuo, USA
Eric W. Lam, UK
Sue-Hwa Lin, USA
Kapil Mehta, USA
Orhan Nalcioglu, USA
P. J. Oefner, Germany
Allal Ouhtit, Oman
Frank Pajonk, USA
Waldemar Priebe, USA
F. C. Schmitt, Portugal
Sonshin Takao, Japan
Ana Maria Tari, USA
Henk G. Van Der Poel, The Netherlands
Haodong Xu, USA
David J. Yang, USA

Pharmacology

Abdel A. Abdel-Rahman, USA
M. Badr, USA
Stelvio M. Bandiera, Canada
Ronald E. Baynes, USA
R. Keith Campbell, USA
Hak-Kim Chan, Australia
Michael D. Coleman, UK
J. Descotes, France
Dobromir Dobrev, Germany
Ayman El-Kadi, Canada
Jeffrey Hughes, USA
Kazim Husain, USA
Farhad Kamali, UK
Michael Kassiou, Australia
Joseph J. McArdle, USA
Mark J. McKeage, New Zealand
Daniel T. Monaghan, USA
T. Narahashi, USA
Kennerly S. Patrick, USA
Vickram Ramkumar, USA
Michael J. Spinella, USA
Quadiri Timour, France
Todd W. Vanderah, USA
Val J. Watts, USA
David J. Waxman, USA

Plant Biotechnology

Prem L. Bhalla, Australia
J. R. Botella, Australia
Elvira Gonzalez De Mejia, USA
Shi-You Ding, USA
Metin Guru, Turkey
H. M. Häggman, Finland
Liwen Jiang, Hong Kong
P. B. Kirti, India
Yong Pyo Lim, Republic of Korea
Gopi K. Podila, USA
Ralf Reski, Germany
Sudhir Sopory, India

Toxicology

Michael Aschner, USA
Juergen Buenger, Germany
Michael L. Cunningham, USA
Laurence D. Fechter, USA
Hartmut Jaeschke, USA
Y. James Kang, USA
M. Firoze Khan, USA
Pascal Kintz, France
Qaisar Mahmood, Pakistan
R. S. Tjeerdema, USA
Kenneth Turteltaub, USA
Brad Upham, USA

Virology

Contents

Hindawi Publishing Corporation
Journal of Biomedicine and Biotechnology
Volume 2012, Article ID 404130, 2 pages
doi:10.1155/2012/404130

Editorial
Animal Models of Human Pathology 2012

Monica Fedele,[1] Oreste Gualillo,[2] and Andrea Vecchione[3]

[1] *Istituto di Endocrinologia ed Oncologia Sperimentale (IEOS)–CNR, 80131 Naples, Italy*
[2] *SERGAS, Instituto de Investigación Sanitaria de Santiago, Santiago University Clinical Hospital, NEIRID Laboratory 9, 15706 Santiago de Compostela, Spain*
[3] *Human Cancer Genetics Program, Division of Pathology, Comprehensive Cancer Center, The Ohio State University, Columbus, OH 43216, USA*

Correspondence should be addressed to Monica Fedele, mfedele@unina.it

Received 29 July 2012; Accepted 29 July 2012

In this special issue we gather together 23 articles (15 reviews, 7 research articles, and 1 methodology report) with diverse information presently available on animal models of human disease.

The use of animal for studying human diseases, from the pathogenesis to the clinical aspects of diagnosis and therapy, has always been a very useful tool and indeed, has contributed enormously to our understanding of the mechanisms of diseases and to the development of numerous drugs.

The 15 comprehensive reviews critically inform the reader of the latest developments in the animal models of diseases such as Parkinson (Blesa et al.), glaucoma (Bouhenni et al.), dermatophytoses (Shimamura et al.), colitis (Perse and Cerar), HCV infections (Carcamo and Nguyen), Glomerulonephritis (Urushihara et al.), and posterior circulation stroke (Lekic and Ani). Moreover, Underbayev et al. provide a clear and concise review on the applications of induced pluripotent stem cells (iPS) for human disease mouse modeling, focusing on the use of microRNA manipulation in the generation and differentiation of iPS. Goldsmith and Jobin propose the use of zebrafish model to study human disease. Moro and colleagues review the significance of mouse models in the study of human cancer progression with particular emphasis on the possible application of patient-derived xenograft in the evaluation of chemoresistance, while Mendes-Braz et al. review the mechanisms of hepatic ischemia-reperfusion injury in animal models, and its translation to the clinical practice. Greco et al. describe the basic principles of high resolution imaging ultrasound equipment and the most important applications in preclinical studies, Li et al. examine different MRI sequences to explore a murine model of intracerebral hemorrhage, whereas Gargiulo et al. provide a review of the use of PET/CT for examining mouse models of myocardial ischemia and Sergi et al. propose an important role of hepatocellular to cholangiocytic metaplasia (as expressed by switch in keratin expression) in the causation of liver graft dysfunction (including cholestasis) in case of ischemia/reperfusion injury, based on personal observations and evidence from the literature. Di Domenico et al. present an exhaustive analysis of the role played by the vascular endothelial growth factor and some cytokines in periodontal ligament remodeling and bone resorption at the pressure side of orthodontic tooth movement.

The research articles deal with the molecular mechanisms involved in the pathogenesis of a particular disease. Vitale et al. report synaptic differences between wild-type and FDDki mice, essentially in the expression levels of selected proteins, in a model of familial dementia; Venancio et al. demonstrate that sleep deprivation alters rat ventral prostate morphology; Neri et al. analyze the effect of colic vein ligature in rats with loperamide-induced constipation, and Allan et al. evaluate the ability of an antimicrobial peripherally inserted central catheter (PICC) to reduce microbial migration and colonization compared to an uncoated PICC. Dunn and Pinkert provide evidence supporting allotopic expression as a tool for mtDNA disease research with implications in development of DNA-based therapeutics, while Mingchang et al. propose a pilot study to examine the use of T1, T2, and T2* weighted images for evaluating hematoma size and extent of edema in mouse brain at high field.

In further contributions animal models have been used to implement therapeutic approaches. It is the case of the studies (a research article and a methodology report) by Pereira et al. which develop an animal model to study deep second-degree thermal burning and characterize *in vivo* hydrogel formulation for burn healing.

In conclusion, as it is shown in the collection of contributions assembled in this special issue, we believe that animal models of human pathologies, because of the tremendous bulk of information that they can supply to scientific community, particularly genetic and alternative models, might lead us into a new era of disease research and drug discovery.

Acknowledgments

We thank all the authors, the reviewers, and the Hindawi Publishing staff for their strong effort in making possible the realization of this project.

Monica Fedele
Oreste Gualillo
Andrea Vecchione

Hindawi Publishing Corporation
Journal of Biomedicine and Biotechnology
Volume 2012, Article ID 921617, 12 pages
doi:10.1155/2012/921617

Research Article

An *In Vivo* Rabbit Model for the Evaluation of Antimicrobial Peripherally Inserted Central Catheter to Reduce Microbial Migration and Colonization as Compared to an Uncoated PICC

Nicholas D. Allan,[1] Kamna Giare-Patel,[2] and Merle E. Olson[1,3]

[1] *Innovotech Inc., Suite 101, 2011 94th Street, Edmonton, AB, Canada T6N 1H1*
[2] *Research and Development Department, Teleflex Medical Incorporated, 2400 Bernville Road, Reading, PA 19605, USA*
[3] *Department of Biomedical Engineering, University of Alberta, Edmonton, AB, Canada T6G 2V2*

Correspondence should be addressed to Merle E. Olson, merle.olson@innovotech.ca

Received 9 January 2012; Accepted 6 May 2012

Academic Editor: Oreste Gualillo

Infection is the leading complication associated with intravascular devices, and these infections develop when a catheter becomes colonized by microorganisms. To combat this issue, medical device manufacturers seek to provide healthcare facilities with antimicrobial medical devices to prevent or reduce the colonization. In order to adequately evaluate these devices, an *in vivo* model is required to accurately assess the performance of the antimicrobial devices in a clinical setting. The model presented herein was designed to provide a simulation of the subcutaneous tunnel environment to evaluate the ability of an antimicrobial peripherally inserted central catheter (PICC), coated with chlorhexidine based technology, to reduce microbial migration and colonization compared to an uncoated PICC. Three samples of control, uncoated PICCs and three samples of coated PICCs were surgically tunneled into the backs of female New Zealand White rabbits. The insertion sites were then challenged with *Staphylococcus aureus* at the time of implantation. Animals were evaluated out to thirty days and sacrificed. Complete *en bloc* dissection and evaluation of the catheter and surrounding tissue demonstrated that the chlorhexidine coated catheter was able to significantly reduce microbial colonization and prevent microbial migration as compared to the standard, un-treated catheter.

1. Introduction

Indwelling intravascular devices, which are becoming integral components of modern medical practice, are associated with the high incidence of nosocomial bloodstream infections especially in intensive care patients, those receiving chemotherapy and those dependent upon haemodialysis. Central venous catheters (CVCs) account for approximately 90% of all catheter-related bloodstream infections (CRBSIs) [1]. PICCs are associated with similar rates of CRBSI as CVCs, placed in internal jugular or subclavian veins (2 to 5 per 1,000 catheter days) [2]. It has been estimated that nearly 80,000 CRBSIs occur in intensive care units alone and result in costs approaching 2 billion dollars and 20,000 deaths annually [3–5]. Colonization of the catheter by microorganisms forming a biofilm is the first stage of the infection process [6]. Sources for microbial colonization may be environmental contamination, skin organisms, post-placement subcutaneous tract infection, intraluminal contamination, or hematogenous seeding [7]. Whether derived from the patient's skin, hematogenously, or from a health care worker, microorganisms present in the catheter display the characteristic reduced susceptibility to antimicrobials, which has become a hallmark of biofilms [8]. Biofilms are a cohesive matrix of microorganisms, mucopolysaccharides (slime), and extracellular constituents that exist in virtually every natural environment [9]. They form on a solid surface (such as a catheter or other implanted medical device) in the presence of shear force or flow (as would be encountered in the environment surrounding an implant medical device), as a mechanism to avert being removed from that environment [10]. Biofilm formation is a developmental process moving

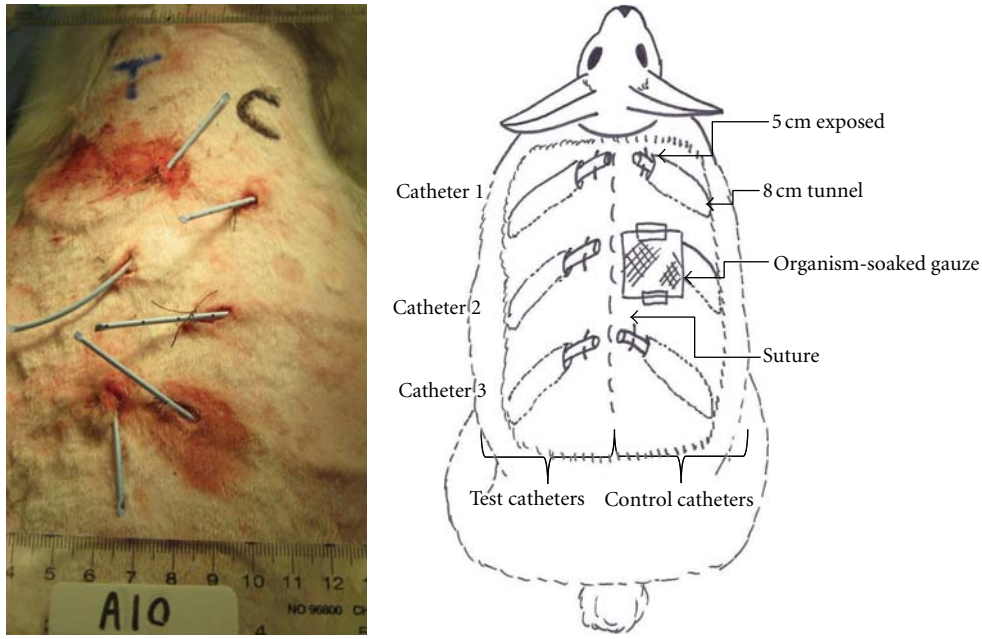

(a) (b)

Figure 1: Left side image shows actual catheter placement (rabbit 10 shown) prior to challenge and bandaging. Right side is a cartoon diagram representing catheter placement and challenge procedures. The diagram displays only those portions of the device which are evaluated. Note that the test and control sides are randomized between animals and groups.

Table 1: A diagram and table describing the preparation of the explanted catheter. Note that 13 cm sections are implanted, but 3 cm which is heat sealed and remains outside of the animal is removed prior to evaluation.

(a) The bolded (underlined numbers) represent tissue segments and catheter material that were exposed to the subcutaneous tunnel environment

1	2	**3**	**4**	**5**	**6**	**7**	**8**	**9**	**10**

(b) The table describes what the various segments were used for in the analysis of each segment

Segment no.	Microbiology	Histology	SEM
1	X		
2	X		
3	X		
4	X		
5		X	X
6	X		
7		X	X
8	X		
9		X	X
10	X		

from attachment to microcolony formation and then to mature biofilm development under the control of specific biofilm genes [11]. The production of a mucopolysaccharide (slime) on the surface, which further protects the biofilm, can often be seen with the naked eye [9]. Microbial biofilms demonstrate recalcitrance towards a wide range of antimicrobial treatments and have been reported to be 100–1,000 times less susceptible than their planktonic counterparts [12]. This resistance is due to the presence of extracellular polysaccharide matrix, the physicochemical heterogeneity developed within such consortia, acquiring of multiantimicrobial resistance genes, and the presence of cells of highly recalcitrant physiology (persisters) [13]. Thus, once an implanted medical device (such as a PICC) is colonized by biofilm bacteria, the bacteria are protected from both immune response and antimicrobial therapy, and thus, such infections are rarely resolved [14–16]. This fact often leads to the failure of conventional antibiotic therapy and necessitates the removal of infected devices. Removal of the infected device is often not practical (as in the case in pace makers or artificial joints) or not at good strategy as this can lead to the production of detached, slime-enclosed, antibiotic-resistant aggregates that can initiate endocarditis or pneumonia by dissemination in the blood stream [17]. With this in mind, medical device manufacturers and researchers in biofilm microbiology have developed strategies and technologies to prevent the initial colonization and prevent the subsequent biofilm colonization of various implant medical devices. A good approach to the reduction of CRBSI includes surface modification of devices to reduce microbial attachment and biofilm development as well as the use of CVCs precoated with antimicrobials such as chlorhexidine and/or silver sulfadiazine and antibiotics such as minocycline and rifampin [18–22].

The proper development and evaluation of antibiofilm efficacy of antimicrobial coated or eluting medical devices

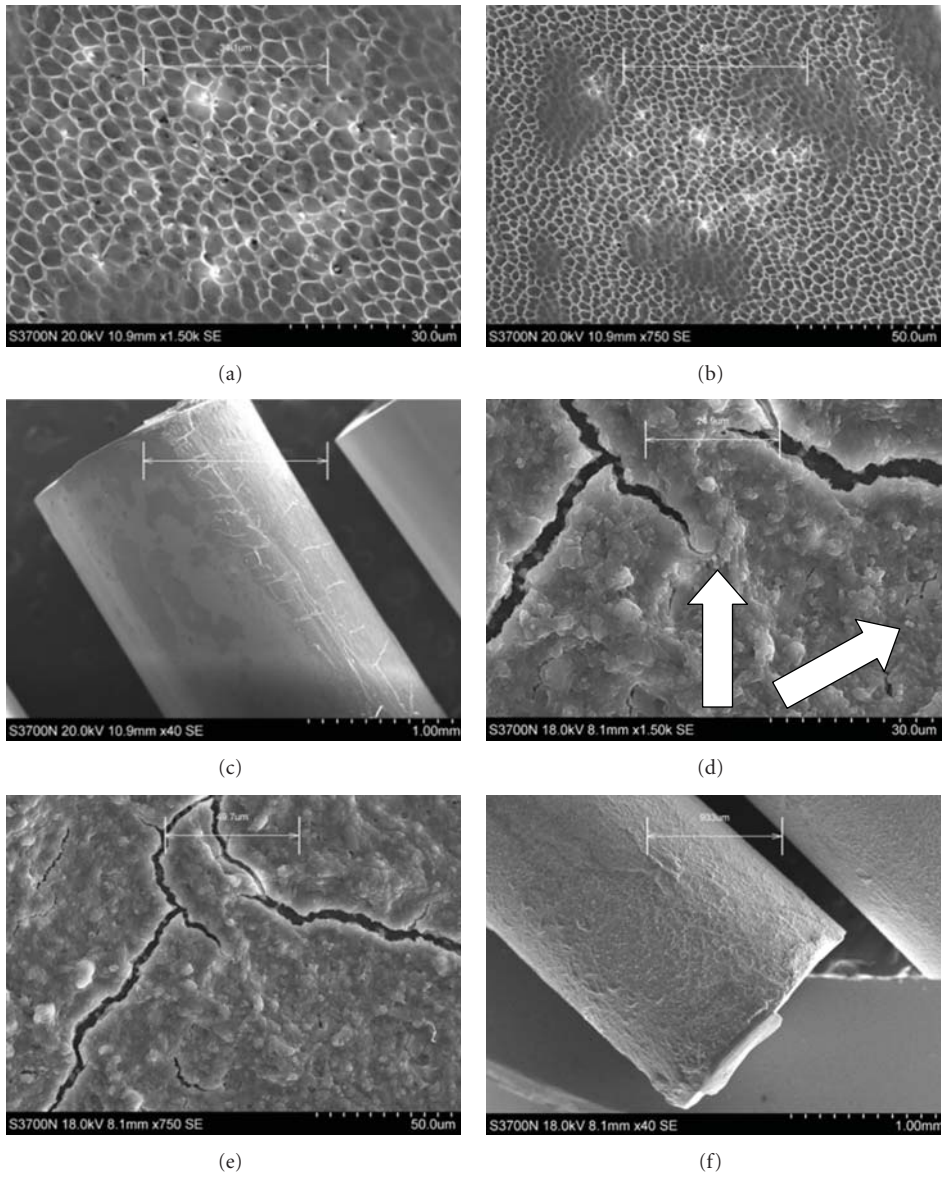

Figure 2: Representative SEM micrographs taken of test catheter 3 (segment 7) and control catheter 3 (segment 7) from animal 10 on day 21. (a) 1500x magnification of test catheter, (b) 750x magnification of test catheter, (c) 40x magnification of test catheter, (d) 1500x magnification of control catheter, (e) 750x magnification of control catheter, and (f) 40x magnification of control catheter. Note: the fissures seen in the biofilm in images D & E are artifacts from the SEM preparation process. Scale bars are presented on each image. Arrows point to isolated cocci.

has proven to be a daunting task due to the limitations of good *in vitro* evaluation tools. Rapid screening tools like the MBEC assay can be utilized to evaluate short-term exposures and isolated antimicrobials and potential antibiofilm agents [23–25] but do not evaluate the antimicrobial agent as it is presented on the actual medical device. Most commonly, the testing of potential implant materials or medical devices is often done by measuring planktonic growth in the presence of the respective material or by "zone of inhibition" determination [26, 27]. Placing selected bacterial suspensions and exposing them to short-term incubation (<24 hr) directly on implant/coated materials and analyzing viable counts is also a standardized method to examine antibacterial activity (Japanese Industrial Standards, as described in [28]). Capillary flow cells that study different biofilm stages under constant nutrient, salt, and pH conditions [29] or disc/drip flow reactors that expose implant/coated materials to biofilm under shear [30] account for the dynamic environment the devices may be exposed to and the biofilm state of the organisms colonizing the device but are limited in that only partial devices or components thereof can be assessed. The so-called "roll plate," method first described by Maki et al.

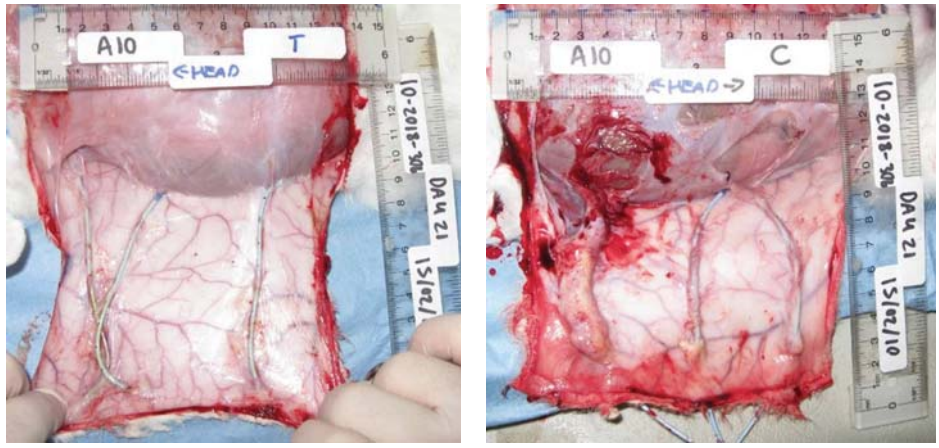

(a) (b)

Figure 3: Representative digital micrographs taken during catheter explant and necropsy on rabbit 10. (a) Test article side: note that the fibrous capsule is minimal, and there is no evidence of pus or irritation. (b) Control article side: the digital image demonstrates indicators of infection uniformly across the three control replicates. Extensive pus, hyperemia, and fibrosis can be seen associated with the tissue around the control catheters.

[31], can evaluate the entire surface of the catheter but is also limited in its practicality and potential operator errors associated with the manipulations of the catheters.

When evaluating and developing implant medical devices with surface modifications, the study of the antibacterial/antibiofilm effects must take into account the actual device itself and be tested while exposed to an appropriate *in vitro* test system that mimics the environment in which it is expected to perform. In addition, demands of regulatory agencies such as the American Food and Drug Administration (FDA) [32] require the utilization of effective *in vitro* (preferably supported by *in vivo*) data to support any label claims. This evaluation needs to simulate human clinical situation which includes (1) using the actual device (preferably sterile finished goods), (2) preconditioning or exposure of the device to body fluid, (3) using a dynamic (rather than static) environment, (4) evaluating the actual contact time with the body, (5) at body temperature, and (6) assuring that the organisms used are relevant to the label claim [32, 33].

To address the needs and testing gaps described above, we developed an *in vivo* test method to provide a high-throughput, repeatable, and cost-effective simulation of the subcutaneous tunnel environment with multiple end points to evaluate the ability of an antimicrobial PICC to reduce microbial migration and colonization as compared to an uncoated PICC.

2. Methods and Materials

2.1. Animals. A total of 10 healthy, ~15-week-old, ~3 Kg, New Zealand white female rabbits (Charles River Laboratories, Canada) were used in this study. Five rabbits were allocated to each sample time (21 and 30 days, resp.). All animals received a thorough physical examination before entry into the study. Any animal that did not meet the health and weight criteria was excluded from the study. Animals with any infection, inflammation, dermatitis, muscular disease, or apparent abnormalities of the urinary tract as well as any animal deemed unsuitable by the study director were also excluded from this study. The study was conducted in compliance with the guidelines of the Canadian Council on Animal Care after the appropriate review by the Institutional Animal Care and Use Committee.

2.2. Catheters. All catheter materials were custom manufactured to 13 cm lengths from the tip and heat sealed at ends. The catheters were individually packaged and sterilized by Arrow International, Inc. (Reading, PA). The test article consisted of 5.5 French (Fr) double lumen Arrow Antimicrobial PICC with Chlorag + ard Technology (Teleflex Medical Inc, Reading, PA). The control/predicate material consisted of uncoated 5.5 Fr double lumen PICC material (Teleflex Medical Inc, Reading, PA).

2.3. Experimental Design. Animals were allocated to test groups using a random block procedure and randomly assigned to groups 1 (21-day catheterization) and 2 (30-day catheterization). As each animal served as its own control and treatment, control/treatment sides were allocated to each treatment group using a random block procedure and randomly assigned to each rabbit. Test and control sides were randomized between animals and groups (see Figure 1).

2.4. Preparation of Inoculum. Staphylococcus aureus ATCC 29213 (American Type Culture Collection, Manassas, VA) was selected due to its role in CRBSI [33]. This strain was selected because it has been used successfully based on our experience to cause infection in NZW rabbits, and this strain was used in an *in vitro* challenge experiment using artificially aged PICC material and demonstrated as significant (>Log_{10} 4 reduction compared to controls). Using

Table 2: Tissue (CFU/g) Log reduction summary tables for day 21. Log reduction values higher than 4 are bold and underlined.

(a) For pairwise comparison, the mean Log_{10} CFU/g recovered from the three replicates of test articles/rabbit was subtracted from the mean Log_{10} CFU/g recovered from the three replicates of control articles/rabbit per segment

		Sample location				
	Sample no.	3	4	6	8	10
Day	Rabbit no.	Log*R* (pairwise comparison)				
21	1	0.81	**4.28**	**6.03**	289	2.44
	P	0.50	0.05	0.00	0.31	0.83
21	4	−2.46	−1.54	−0.44	1.93	1.18
	P	0.18	0.35	0.86	0.37	0.59
21	7	2.90	3.08	1.87	1.70	3.22
	P	0.13	0.14	0.37	0.50	0.12
21	9	1.23	1.10	1.48	0.00	1.59
	P	0.37	0.37	0.37	N/A	0.37
21	10	**5.30**	3.68	3.73	**5.02**	**4.48**
	P	0.00	0.13	0.14	0.01	0.01

(b) For test article log reduction, the mean Log_{10} CFU/g recovered from the three replicates of test articles/rabbit was subtracted from the mean Log_{10} CFU from the initial inoculum counts that were exposed to the catheters at implantation

		Sample location				
	Sample no.	3	4	6	8	10
Day	Rabbit no.	Test article Log*R* (based on initial inoculum)				
21	1	2.62	**5.67**	**6.86**	**5.55**	**5.72**
	P	0.50	0.05	0.00	0.31	0.83
21	4	1.49	2.53	**4.41**	**6.86**	**5.38**
	P	0.18	0.35	0.86	0.37	0.59
21	7	**6.86**	**6.86**	**6.86**	**5.29**	**6.86**
	P	0.13	0.14	0.37	0.50	0.12
21	9	**6.86**	**6.86**	**6.86**	**6.86**	**6.86**
	P	0.37	0.37	0.37	N/A	0.37
21	10	**6.86**	**6.86**	**6.86**	**6.86**	**6.86**
	P	0.00	0.13	0.14	0.01	0.01

(c) For control article log reduction, the mean Log_{10} CFU/g recovered from the three replicates of control articles/rabbit was subtracted from the mean Log_{10} CFU from the initial inoculum counts that were exposed to the catheters at implantation

		Sample location				
	Sample no.	3	4	6	8	10
Day	Rabbit no.	Control article Log*R* (based on initial inoculum)				
21	1	1.81	1.39	0.82	265	3.28
	P	0.50	0.05	0.00	0.31	0.83
21	4	3.95	**4.07**	**4.85**	**4.93**	**4.20**
	P	0.18	0.35	0.86	0.37	0.59
21	7	3.96	3.77	**4.99**	3.59	3.64
	P	0.13	0.14	*0.37*	0.50	0.12
21	9	**5.63**	**5.75**	**5.38**	**6.86**	**5.26**
	P	0.37	0.37	0.37	N/A	0.37
21	10	1.56	3.18	3.13	1.84	2.38
	P	0.00	0.13	0.14	0.01	0.01

Table 3: Catheter (CFU/catheter segment) Log reduction summary tables for day 21. Log reduction values higher than 4 are bold and underlined.

(a) For pairwise comparison, the mean Log_{10} CFU/g recovered from the three replicates of test articles/rabbit was subtracted from the mean Log_{10} CFU/g recovered from the three replicates of control articles/rabbit per segment

		Sample location						
	Sample no.	1	2	3	4	6	8	10
Day	Rabbit no.	Log*R* (pairwise comparison)						
21	1	−0.47	−0.07	1.58	2.44	0.49	0.00	0.87
	P	0.78	0.94	0.37	0.15	0.78	1.00	0.37
21	4*	−1.99	0.71	0.17	−0.87	1.45	1.95	0.00
	P	0.23	0.76	0.93	0.50	0.27	0.27	1.00
21	7	1.84	2.38	1.31	0.97	1.03	1.03	0.00
	P	0.12	0.12	0.37	0.37	0.37	0.37	1.00
21	9	−0.67	0.43	1.15	1.28	0.00	0.00	0.00
	P	0.65	0.06	0.37	0.37	1.00	1.00	1.00
21	10	2.08	0.33	1.48	3.18	2.92	2.60	1.50
	P	0.08	0.85	0.37	0.16	0.13	0.14	0.37

(b) For test article log reduction, the mean Log_{10} CFU/g recovered from the three replicates of test articles/rabbit was subtracted from the mean Log_{10} CFU from the initial inoculum counts that were exposed to the catheters at implantation

		Sample location						
	Sample no.	1	2	3	4	6	8	10
Day	Rabbit no.	Test article Log*R* (based on initial inoculum)						
21	1	1.33	2.49	**6.86**	**6.86**	**5.99**	**6.86**	**6.86**
	P	0.78	0.94	0.37	0.15	0.78	1.00	0.37
21	4*	**4.86**	**5.62**	**5.73**	**5.99**	**6.86**	**6.86**	**6.86**
	P	0.23	0.76	0.93	0.50	0.27	0.27	1.00
21	7	**6.86**	**6.86**	**6.86**	**6.86**	**6.86**	**6.86**	**6.86**
	P	0.12	0.12	0.37	0.37	0.37	0.37	1.00
21	9	**5.12**	3.34	**6.86**	**6.86**	**6.86**	**6.86**	**6.86**
	P	0.65	0.06	0.37	0.37	1.00	1.00	1.00
21	10	**5.12**	**5.89**	**6.86**	**6.86**	**6.86**	**6.86**	**6.86**
	P	0.08	0.85	0.37	0.16	0.13	0.14	0.37

(c) For control article log reduction, the mean Log_{10} CFU/g recovered from the three replicates of control articles/rabbit was subtracted from the mean Log_{10} CFU from the initial inoculum counts that were exposed to the catheters at implantation

		Sample location						
	Sample no.	1	2	3	4	6	8	10
Day	Rabbit no.	Control article Log*R* (based on initial inoculum)						
21	1	1.80	2.56	**5.27**	**4.42**	**5.50**	**6.86**	**5.99**
	P	0.78	0.94	0.37	0.15	0.78	1.00	0.37
21	4*	**6.86**	**4.90**	**5.55**	**6.86**	**5.40**	**4.90**	**6.86**
	P	0.23	0.76	0.93	0.50	0.27	0.27	1.00
21	7	**5.02**	**4.47**	**5.54**	**5.89**	**5.83**	**5.83**	**6.86**
	P	0.12	0.12	0.37	0.37	0.37	0.37	1.00
21	9	**5.79**	2.90	**5.71**	**5.58**	**6.86**	**6.86**	**6.86**
	P	0.65	0.06	0.37	0.37	1.00	1.00	1.00

(c) Continued.

		Sample location						
	Sample no.	1	2	3	4	6	8	10
Day	Rabbit no.	Control article Log*R* (based on initial inoculum)						
21	10	3.04	**5.56**	**5.37**	3.68	3.94	**4.25**	**5.35**
	P	0.08	0.85	0.37	0.16	0.13	0.14	0.37

* indicates that control catheter 3 on rabbit 4 was not available for analysis.

a cryogenic stock (at −70°C), a first subculture of the bacterial organisms listed above was streaked out on tryptic soy agar (TSA) (Becton Dickinson, Sparks, MD). The plate was incubated at 35 ± 2°C for 24 hours and stored wrapped in parafilm at 4 ± 2°C. From the first sub-culture, a second sub-culture was streaked out on TSA and incubated at 35 ± 2°C for 24 hours. The second sub-culture was used within 24 hours starting from the time it was first removed from incubation. From a fresh streak plate, each study organism was inoculated in 200 mL of sterile Trypticase Soy Broth (TSB) (Becton Dickinson, Sparks, MD). Organisms were grown in TSB at 37 ± 2°C on a rotary shaker (at approximately 150 rpm) for 12–18 hours. This achieved an inoculum density of approximately 10^9 colony-forming units (CFU)/mL. The inoculum was adjusted to an approximate cell density of 10^6 CFU/mL by diluting *Staphylococcus aureus* in sterile 0.9% saline (Baxter, Canada). The cell density was confirmed by serially diluting and spot plating triplicate samples of the inoculum.

2.5. Surgical Procedures and Catheterization. Rabbits were fasted approximately 12 hours prior to surgery. Anesthesia (Isoflurane) (Benson Medical, Markham, ON, Canada) was administered by the qualified veterinary staff per test facility standard operating procedure. Selection of the dose and agents followed the standard operating procedures of the test facility. The hair over the dorsal thorax and abdomen was clipped with a number 40 Osler clipper blade and scrubbed with a soap that did not contain any disinfectant or antibiotic. Three incisions were made on either side of the dorsal midline for catheter insertion. The catheters (13 cm long) were inserted subcutaneously in each rabbit so ~ 8 cm tunneled under the skin and 6 cm was on the skin surface (see Figure 1). The catheters were anchored to the skin with adhesive tape and sutures. Animals were observed for any adverse reactions. The catheters were challenged by inoculating the insertion site with ~1 mL of inoculum. To supplement this significant challenge, a gauze sponge with 5 mL of the prepared bacterial suspension was also placed over each insertion site. Opsite (Smith and Nephew, Hull, England) was placed over all catheters and inoculum-soaked sponges. Tensoplast (BSN Medical, Pinetown, South Africa), an occlusive bandage, was then placed over all catheters to prevent self-mutilation and removal of the catheters. All animals were observed for morbidity and mortality, overt signs of toxicity (including abstinence of water), and any signs of distress throughout the study per test facility procedures.

Table 4: Tissue (CFU/g) Log reduction summary tables for day 30. Log reduction values higher than 4 are bold and underlined.

(a) For pairwise comparison, the mean Log_{10} CFU/g recovered from the three replicates of test articles/rabbit was subtracted from the mean Log_{10} CFU/g recovered from the three replicates of control articles/rabbit per segment

		Sample location				
	Sample no.	3	4	6	8	10
Day	Rabbit no.	Log*R* (pairwise comparison)				
30	2	0.98	0.00	0.00	0.00	−0.74
	P	0.37	0.00	0.00	0.00	0.76
30	3	−1.05	2.43	1.16	2.48	**4.52**
	P	0.37	0.13	0.37	0.12	0.00
30	5	−2.57	2.18	2.41	1.06	1.04
	P	0.12	0.12	0.12	0.37	0.37
30	6**	3.91	0.00	0.00	0.00	0.00
	P	N/A	N/A	N/A	N/A	N/A
30	8	**4.90**	2.24	3.70	3.68	**5.18**
	P	0.01	0.37	0.14	0.13	0.00

(b) For test article log reduction, the mean Log_{10} CFU/g recovered from the three replicates of test articles/rabbit was subtracted from the mean Log_{10} CFU from the initial inoculum counts that were exposed to the catheters at implantation

		Sample location				
	Sample no.	3	4	6	8	10
Day	Rabbit no.	Test article Log*R* (based on initial inoculum)				
30	2	**6.86**	**6.86**	**6.86**	**6.86**	**5.02**
	P	0.37	0.00	0.00	0.00	0.76
30	3	**5.81**	**6.86**	**6.86**	**6.86**	**6.86**
	P	0.37	0.13	0.37	0.12	0.00
30	5	**4.28**	**6.86**	**6.86**	**6.86**	**6.86**
	P	0.12	0.12	0.12	0.37	0.37
30	6**	**6.86**	**6.86**	**6.86**	**6.86**	**6.86**
	P	N/A	N/A	N/A	N/A	N/A
30	8	**6.86**	**6.86**	**6.86**	**6.86**	**6.86**
	P	0.01	0.37	0.14	0.13	0.00

(c) For control article log reduction, the mean Log_{10} CFU/g recovered from the three replicates of control articles/rabbit was subtracted from the mean Log_{10} CFU from the initial inoculum counts that were exposed to the catheters at implantation

		Sample location				
	Sample no.	3	4	6	8	10
Day	Rabbit no.	Control article Log*R* (based on initial inoculum)				
30	2	**5.87**	**6.86**	**6.86**	**6.86**	**5.76**
	P	0.37	0.00	0.00	0.00	0.76
30	3	**6.86**	**4.42**	**5.70**	**4.37**	2.34
	P	0.37	0.13	0.37	0.12	0.00
30	5	**6.86**	**4.67**	**4.44**	**5.80**	**5.81**
	P	0.12	0.12	0.12	0.37	0.37
30	6**	2.95	**6.86**	**6.86**	**6.86**	**6.86**
	P	N/A	N/A	N/A	N/A	N/A
30	8	1.95	4.62	3.15	3.18	1.67
	P	0.01	0.37	0.14	0.13	0.00

** indicates that control tunnels 1 and 3 on rabbit 6 were not available for analysis.

Table 5: Catheter (CFU/catheter segment) Log reduction summary tables for day 30. Log reduction values higher than 4 are bold and underlined.

(a) For pairwise comparison, the mean Log_{10} CFU/g recovered from the three replicates of test articles/rabbit was subtracted from the mean Log_{10} CFU/g recovered from the three replicates of control articles/rabbit per segment

		Sample location						
	Sample no.	1	2	3	4	6	8	10
Day	Rabbit no.	Log*R* (pairwise comparison)						
30	2*	0.30	1.80	0.00	0.00	1.75	1.60	0.00
	P	0.88	0.27	0.00	0.00	0.27	0.27	0.00
30	3	−1.72	2.98	3.43	3.49	0.87	2.71	1.19
	P	0.34	0.10	0.00	0.00	0.37	0.12	0.37
30	5*	0.00	0.00	0.00	0.00	0.00	0.00	0.00
	P	0.00	0.00	0.00	0.00	0.00	0.00	0.00
30	6**	0.00	0.00	2.60	0.00	0.00	0.00	0.00
	P	N/A	N/A	N/A	N/A	N/A	N/A	N/A
30	8	2.49	2.56	1.97	2.40	2.38	2.40	1.13
	P	0.12	0.12	0.12	0.12	0.12	0.12	0.37

(b) For test article log reduction, the mean Log_{10} CFU/g recovered from the three replicates of test articles/rabbit was subtracted from the mean Log_{10} CFU from the initial inoculum counts that were exposed to the catheters at implantation

		Sample location						
	Sample no.	1	2	3	4	6	8	10
Day	Rabbit no.	Test article Log*R* (based on initial inoculum)						
30	2*	**5.71**	**6.86**	**6.86**	**6.86**	**6.86**	**6.86**	**6.86**
	P	0.88	0.27	0.00	0.00	0.27	0.27	0.00
30	3	**4.27**	**5.50**	**6.86**	**6.86**	**6.86**	**6.86**	**6.86**
	P	0.34	0.10	0.00	0.00	0.37	0.12	0.37
30	5*	**6.86**	**6.86**	**6.86**	**6.86**	**6.86**	**6.86**	**6.86**
	P	0.00	0.00	0.00	0.00	0.00	0.00	0.00
30	6**	**6.86**	**6.86**	**6.86**	**6.86**	**6.86**	**6.86**	**6.86**
	P	N/A	N/A	N/A	N/A	N/A	N/A	N/A
30	8	**6.86**	**6.86**	**6.86**	**6.86**	**6.86**	**6.86**	**6.86**
	P	0.12	0.12	0.12	0.12	0.12	0.12	0.37

(c) For control article log reduction, the mean Log_{10} CFU/g recovered from the three replicates of control articles/rabbit was subtracted from the mean Log_{10} CFU from the initial inoculum counts that were exposed to the catheters at implantation

		Sample location						
	Sample no.	1	2	3	4	6	8	10
Day	Rabbit no.	Control article Log*R* (based on initial inoculum)						
30	2*	**5.40**	**5.06**	**6.86**	**6.86**	**5.10**	**5.25**	**6.86**
	P	0.88	0.27	0.00	0.00	0.27	0.27	0.00
30	3	**5.99**	2.52	3.42	3.36	**5.99**	**4.15**	**5.67**
	P	0.34	0.10	0.00	0.00	0.37	0.12	0.37
30	5*	**6.86**	**6.86**	**6.86**	**6.86**	**6.86**	**6.86**	**6.86**
	P	0.00	0.00	0.00	0.00	0.00	0.00	0.00
30	6**	**6.86**	**6.86**	**4.25**	**6.86**	**6.86**	**6.86**	**6.86**
	P	N/A	N/A	N/A	N/A	N/A	N/A	N/A

(c) Continued.

		Sample location						
	Sample no.	1	2	3	4	6	8	10
Day	Rabbit no.	Control article Log*R* (based on initial inoculum)						
30	8	**4.36**	**4.30**	**4.89**	**4.46**	**4.48**	**4.46**	**5.73**
	P	0.12	0.12	0.12	0.12	0.12	0.12	0.37

* indicates that control catheter 1 on rabbits 2 and 5 was not available for analysis.
** indicates that control catheters 1 and 3 on rabbit 6 were not available for analysis.

Table 6: Infection prevention in the tissue samples: the total number of samples where significant (≥3.0 Log) bacterial load was recovered (from sample locations 4, 6, 8, and 10) is divided by the total number of catheters/tracts in each group. This is separated by sample type (tissue and catheter).

Sample day	Test catheter tunnel	Control catheter tunnel	*P**
21	40% (6 of 15 tracts)	80% (12 of 15 tracts)	0.030216 (S)
30	6% (1 of 15 tracts)	76% (10 of 13 tracts)	0.000203 (S)

* Fisher exact test for statistical significance (for statistical significance (S), $P \leq 0.05$).

Table 7: Infection prevention on the catheter segments: the total number of samples where significant (≥3.0 Log) bacterial load was recovered (from sample locations 4, 6, 8, and 10) is divided by the total number of catheters/tracts in each group. This is separated by sample type (tissue and catheter).

Sample day	Test catheter	Control catheter	*P**
21	0% (0 of 15 catheter segments)	43% (6 of 14 catheter segments)	0.006322 (S)
30	0% (0 of 15 catheter segments)	54% (6 of 11 catheter segments)	0.002007 (S)

* Fisher exact test for statistical significance (for statistical significance (S), $P \leq 0.05$).

2.6. Euthanasia and Harvesting of Samples. Animals were euthanized with an overdose of intracardiac-injected sodium pentobarbital at 21 (group 1) and 30 (group 2) days after catheterization, based on Alberta Veterinary Medical Association (AVMA) procedures and guidelines. Animals were immediately prepared for aseptic collection of tissue samples. A complete *en bloc* dissection was made excising the skin and catheter at the insertion site and the tissue underlying and surrounding the catheter. The distal and proximal ends of the tissue were surgically stapled to the PICC line to secure the location. A photo was taken to record complete length of the catheter positioned in the tissue bloc (*in situ*). The catheter (and surrounding tunnel) was segmented into 10 × 1 cm segments for analysis as described in Table 1. The procedure was repeated for each catheter.

2.7. Microbiology Procedures

Catheter Segments. 1 cm segments were aseptically separated from the surrounding tissue. Each catheter segment was

inserted into a sterile 6-well plate (Becton Dickinson, Franklin lakes, NJ) containing 4 mL of D/E neutralizing broth (Becton Dickinson, Sparks, MD) in each well. The entire 6-well plate assembled above was sonicated in a bath sonicator (VWR 550T, VWR, Canada) for 30 minutes. Following sonication, 100 μL from each well of the six-well plates was placed into the first 12 empty wells of the first row of a 96-well microtiter plate (Nunc, Roskilde, Denmark). 180 μL of 0.9% sterile saline was placed in the remaining rows. A serial dilution (10^0–10^{-7}) was prepared by moving 20 μL down each of the 8 rows. 10 μL was removed from each well and spot plated on a prepared TSA plate. Plates were incubated at 37 ± 2°C and counted after approximately 24 hours of incubation. Data was evaluated as CFU/catheter segment.

Tissue Segments. Each 1 cm tissue segment was aseptically homogenized (Brinkman Polytron PT (VWR, Canada) in 2.5 sterile phosphate buffered saline (PBS: 2 g KCl, 2.4 g KH2PO4, 80 g NaCl, and 14.4 g Na2HPO4, to 1000 mL; pH 7.4)) in sterile preweighed 50 mL conical centrifuge tubes (Fisher Scientific, Mexico). Following homogenization, 100 μL from each tissue homogenate specimen was placed into the first 12 empty wells of the first row of 96-well microtiter plates. The remaining wells all contained 180 μL of 0.9% sterile saline. A serial dilution (10^0–10^{-7}) was prepared by moving 20 μL down each of the 12 rows. From each well, 10 μL was removed and spot plated on TSA plates. Culture plates were incubated at 37 ± 2°C for 24 hours, after which the numbers of CFU were counted as CFU per gram of tissue.

2.8. Calculation of Log Reduction. Catheter efficacy is presented by Log_{10} reduction [23–25, 32]. Sample calculations to describe the data presented in Tables 2, 3, 4, and 5, are presented below.

Tissue Log Reduction. Total CFU recovered per gram of tissue = (raw plate count/0.01 mL {the volume plated}) ∗ 2.5 mL {the total volume homogenized}/tissue sample weight. Log transformed value = Log_{10}(CFU/sample + 1) [23].

Log reduction (Log$R$) = (mean Log_{10} control) − (mean Log_{10} test).

Catheter Log Reduction. Total CFU recovered per gram of tissue = (raw plate count/0.01 mL {the volume plated}) ∗ 4.0 mL {the total sonication volume}. Log transformed value = Log_{10}(CFU/sample + 1) [23].

Log reduction (Log$R$) = (mean Log_{10} control) − (mean Log_{10} test).

For statistical analysis, a nonpairwise, two-tailed Student's t-test was used. $P \leq 0.05$.

2.9. Scanning Electron Microscopy (SEM) Samples. One cm catheter segments were aseptically separated from the surrounding tissue. The samples were placed into empty receiver vials. In a fume hood, primary fixative (5% glutaraldehyde in 0.1 M Na cacodylate buffer pH = 7.5) was added to each vial to completely cover all samples. The vials were capped and incubated at 4 ± 2°C for 16 to 24 hours. After-fixation, the samples caps were loosely removed. The loosely capped sample vials were placed into a fume hood, and the samples were allowed to air dry for 72 to 96 hours. Appropriate standard operating procedures (SOPs) for use of a Hitachi S3700N Scanning Electron Microscope were followed. SEM data was recorded as images and through notes describing each sample.

2.10. Histopathology. Tissue specimens were excised and fixed in 10% neutral buffered formalin. The samples were embedded in paraffin and sectioned, mounted, and stained with hematoxylin and eosin (H&E) per facility SOPs. Samples were reviewed by a blinded third-party board-certified pathologist for a scored report detailing findings.

3. Results

Animals 2, 5, and 6 removed some of the control catheters prior to the scheduled removal at day 30. This behavior is associated with infection and inflammation of the tissue around the catheters as animals cannot ethically be restrained to totally prevent them from accessing the catheters. At the time of sacrifice, the tissue tract associated with the catheter could be clearly identified allowing removal and analysis on animals 2 and 5. The loss of these samples is denoted by an asterisk (*) in the supporting data tables.

Animal models of infection of medical devices generally tend to produce variability. Infections may be associated with the test catheters due to the significant level of challenge. Also, infection may not be observed in all control devices due to the ability of the healthy (nonimmunocompromised) animal to resist or eliminate the infection. In this model, a significant and continual challenge was provided to both the control and the test catheters. In spite of the heavy challenge (10^6 CFU/mL), the test catheters consistently demonstrated prevention of catheter and associated tissue bacterial colonization and reduction in catheter and tissue colonization by the challenge bacteria (see Tables 2–5). *In vivo* efficacy was demonstrated by meeting the acceptance criteria (4 Log reduction of adhered biomass) [32] over a 30-day time period. This is further demonstrated by the observation that the test catheters significantly reduced tissue colonization (40% test article tissue colonization versus 80% control tissue colonization) on day 21 and (6% test article tissue colonization versus 76% control tissue colonization) on day 30 (see Table 6). More significantly, the test catheters significantly reduced catheter colonization (0% test article colonization versus 43% control article colonization) on day 21 and (0% test article colonization versus 54% control article colonization) on day 30 (see Table 7). The plate count data was further supported by the scanning electron microscopic (SEM) evaluation of the selected catheter segments analyzed. Generally, irrespective of sample location or time point, no major differences were seen between the various samples of the coated catheter material. Occasional patchy deposition of host proteins and occasional areas of

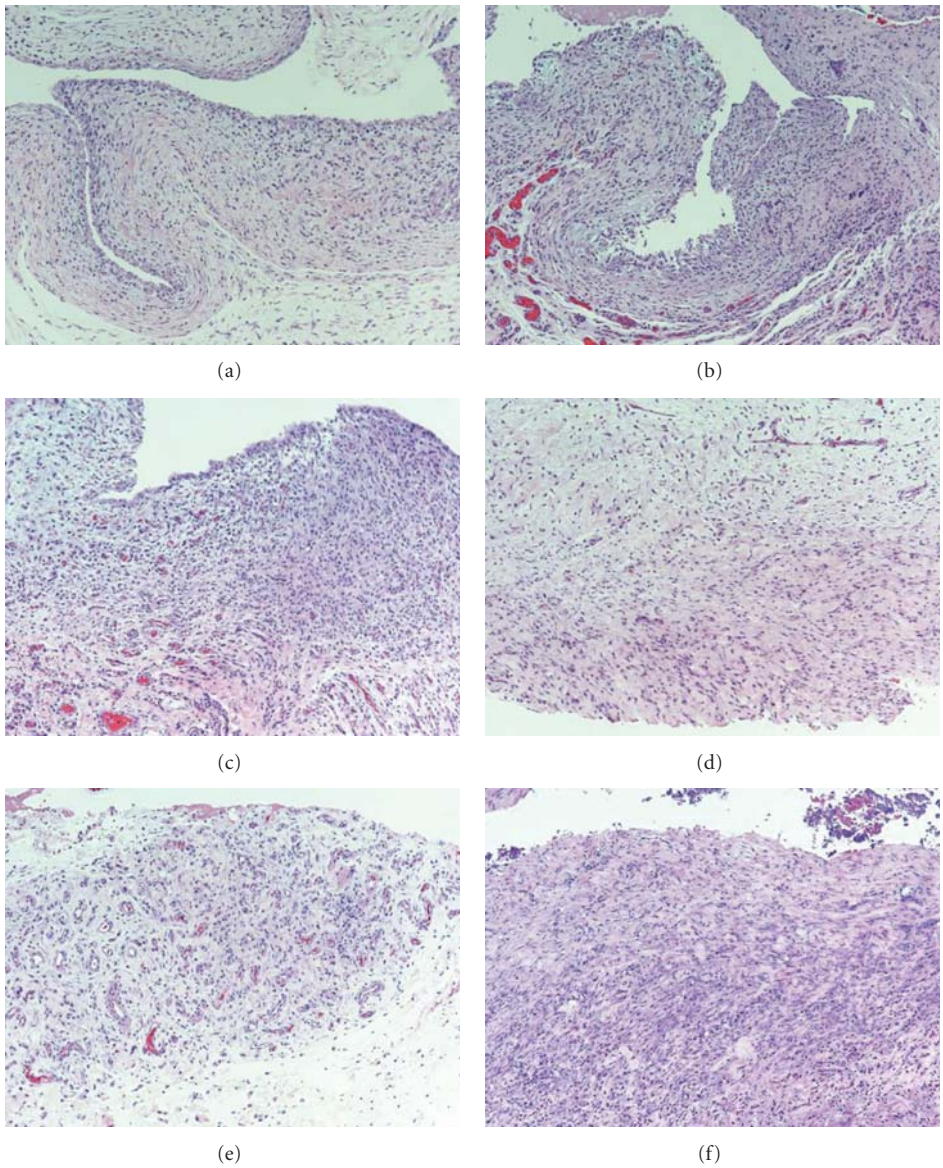

Figure 4: Representative digital micrographs (100x magnification) taken during the histological review of tissue segments from animal 10. (a) Test catheter 3, segment 5: neutrophils and/or macrophages are present, with inflammation in the lumen, (b) test catheter 3, segment 7: neutrophils and/or macrophages are present, with inflammation in the lumen. There is an inner layer which would have been adjacent to the catheter which is composed of well-vascularised immature connective tissue with a mild inflammatory reaction. There is also an outer layer of mature, well-organized, and uninflamed fibrous connective tissue. (c) Test catheter 3, segment 5: neutrophils and/or macrophages are present; inflammation extends to include the subcutis outside the connective tissue tunnel. (d) Control catheter 3, segment 5: neutrophils and/or macrophages are present, with inflammation in the lumen. (e) Control catheter 3, segment 7: neutrophils and/or macrophages are present; inflammation extends to include the subcutis outside the connective tissue tunnel. (f) Control catheter 3, segment 9: neutrophils, macrophages and lymphocytes are present; inflammation extends to include the subcutis outside the connective tissue tunnel. There is a thick necrotic mass of debris in lumen, with more general inflammation of wall.

aggregated host red blood cells (RBCs) were seen on the catheter surfaces. The catheter surface was largely visible on most samples. No significant amounts of bacteria were observed indicating that the log reduction data obtained during this study was due to the device preventing the adherence of the challenge microorganism, rather than killing or inactivating adhered cells (Figure 2). The control (or reference catheters) on the other hand, typically presented with heavy deposition of host proteins, RBCs, and bacterial proteins and exopolysaccharide, was consistently observed across all samples. Heavy fibrin deposition was observed on several samples (data not shown). Most bacteria were embedded in the host/bacterial extracellular protein/polysaccharide matrix. Occasional healthy bacterial cocci were visible at the surface (Figure 2(d)). These observations are consistent with the viable cell count data obtained (Tables 2–5).

Clinical Efficacy. In addition to the plate count data, gross pathological findings clearly demonstrate the efficacy of the antimicrobial PICC as demonstrated by the digital images presented in Figure 3. The antimicrobial PICC presented with minimal pathological signs of infection (device associated swelling, capsule, pus), while the untreated control devices uniformly demonstrated clinical signs of infection (pus, swelling, extensive capsule surrounding the device, and necrotic tissue). A sample comparison set (animal 10) is presented to highlight this discussion point in Figure 3. The impact on the surrounding tunnel tissue was further examined by histological evaluation (Figure 4).

4. Discussion

This model was effective in comparing the patterns of microbial migration along the catheter segments proximal and distal to the entry site, comparing microbial colonization for antimicrobial PICC to that for untreated PICC and comparing the efficacy of the antimicrobial PICC for microbial colonization and inflammation mitigation up to 21 and 30 days after catheter insertion as compared to untreated catheters. In addition, the results showed that chlorhexidine-based technology was effective in reducing bacterial colonization on catheters and their surrounding tissue for up to 30 days. This model represents the subcutaneous space and not the vasculature; however, it is the subcutaneous space that is frequently infected, and tracking of the infection leads to vasculitis and cellulitis. In addition, the model does not simulate the use of the device in the clinical setting that includes repeated manipulations of the device under repeated challenge conditions and up to the projected life of the device. Rather, this model simulates the *in vivo* environment that the catheter is expected to be in contact with up to the projected life of the device. This feature of the model is important in that the risks of CRBSI increase as the duration of implantation increases [34, 35], and the replacement of PICCs is not a recommended strategy [17, 34] underlying the need for devices with long-acting antimicrobial coatings and models that can accurately evaluate these technologies.

The authors recognize that this model has several limitations: the first is that not all organisms will reproducibly colonize rabbit tissue, as such *S. aureus* was chosen for this model due to reproducibility in this model and in the literature and due to the fact that this species represents the causative agent of the majority of clinical CRBSIs [33]. Therefore, for product label claims that seek to cover the full spectrum of causative agents of CRBSI or catheter colonization, it is recommended that this model be used in conjunction with other recognized *in vitro* assays that can specifically test against this diverse group of organisms [33]. Secondly, these are healthy animals, and their immune systems can clear the infection over the duration of the study (see Tables 2–5). It can be hypothesized that the catheters may provide protection for only a few days, and then the animal's immune system clears the infection. For that reason, it is critical that control (nonantimicrobial) catheters be run concurrently within the same animal to demonstrate that the antimicrobial effect is in fact due to the antimicrobial agent and not just the animal's immune response. This limitation was not valid and pertinent in this study because antimicrobial catheters did clearly demonstrate reduction in colonization on catheter surface, surrounding tissue, and clinical/localized infection symptoms. Lastly, to accurately predict and demonstrate duration of the efficacy, it is important to run a parallel *in vitro* study utilizing unchallenged 21- and 30-day explant materials or artificially aged materials followed by an *in vitro* challenge of the organism to test whether the materials can still resist biofilm colonization. Also, chronic irritation of a chronic wound will cause a rabbit to remove its bandage and its catheter. It is ethically not possible to provide such restraint to prevent removal of a severely irritated catheter. However, despite these limitations, this model does represent an effective *in vivo* assessment of antimicrobial implant medical device performance over an extended time period. We present this work to further expand the research tool box available to medical device manufacturers and regulatory agencies to develop, review, and assess new antimicrobial implant medical devices.

While many factors affect microbial colonization of the catheter, duration of implantation is a major complication leading to infection [33, 34]. Clearly preventing infections on the surface of indwelling medical devices over extended time frames is an important issue with the increased use of medical devices. To provide healthcare facilities with another tool to attain and sustain their goal of zero catheter-related infections, Teleflex has developed both a 4.5 Fr single lumen and a 5.5 Fr double lumen Arrow Antimicrobial PICC with Chlorag + ard Technology to reduce the potential risk for catheter colonization. Both the indwelling external surface and entire fluid pathway of the catheters are treated with chlorhexidine-based technology to address this issue. This model successfully demonstrated that this technology was effective in catheter colonization reduction up to 30 days and showed promise in reducing CRBSI.

Acknowledgments

This project was funded by Teleflex Medical Inc and was executed by Innovotech Inc.

References

[1] M. Mer, A. G. Duse, J. S. Galpin, and G. A. Richards, "Central venous catheterization: a prospective, randomized, double-blind study," *Clinical and Applied Thrombosis/Hemostasis*, vol. 15, no. 1, pp. 19–26, 2009.

[2] N. Safdar and D. G. Maki, "Risk of catheter-related bloodstream infection with peripherally inserted central venous catheters used in hospitalized patients," *Chest*, vol. 128, no. 2, pp. 489–495, 2005.

[3] L. A. Mermel, L. Mermel, and B. Hudson, "Prevention of intravascular catheter-related infections," *Annals of Internal Medicine*, vol. 132, no. 5, pp. 391–402, 2000, (Erratum, 133:5.).

[4] D. Pittet, D. Tarara, and R. P. Wenzel, "Nosocomial bloodstream infection in critically ill patients: excess length of stay,

extra costs, and attributable mortality," *Journal of the American Medical Association*, vol. 271, no. 20, pp. 1598–1601, 1994.

[5] L. Soufir, J. F. Timsit, C. Mahe, J. Carlet, B. Regnier, and S. Chevret, "Attributable morbidity and mortality of catheter-related septicemia in critically ill patients: a matched, risk-adjusted, cohort study," *Infection Control and Hospital Epidemiology*, vol. 20, no. 6, pp. 396–401, 1999.

[6] I. Raad, W. Costerton, U. Sabharwal, M. Sacilowski, E. Anaissie, and G. P. Bodey, "Ultrastructural analysis of indwelling vascular catheters: a quantitative relationship between luminal colonization and duration of placement," *Journal of Infectious Diseases*, vol. 168, no. 2, pp. 400–407, 1993.

[7] R. J. Sherertz, "Pathogenesis of vascular catheter-related infections," in *Catheter-Related Infections*, H. Seifert, B. Jansen, and B. M. Farr, Eds., pp. 1–29, Marcel Dekker, New York, NY, USA, 1997.

[8] H. Ceri, M. E. Olson, C. Stremick, R. R. Read, D. Morck, and A. Buret, "The Calgary Biofilm Device: new technology for rapid determination of antibiotic susceptibilities of bacterial biofilms," *Journal of Clinical Microbiology*, vol. 37, no. 6, pp. 1771–1776, 1999.

[9] J. W. Costerton, Z. Lewandowski, D. E. Caldwell, D. R. Korber, and H. M. Lappin-Scott, "Microbial biofilms," *Annual Review of Microbiology*, vol. 49, pp. 711–745, 1995.

[10] Y. Liu and J. H. Tay, "Metabolic response of biofilm to shear stress in fixed-film culture," *Journal of Applied Microbiology*, vol. 90, no. 3, pp. 337–342, 2001.

[11] J. W. T. Wimpenny, A. Peters, and M. Scourfield, "Modelling spatial gradients," in *Structure and Function of Biofilms*, W. G. Characklis and P. A. Wilderer, Eds., pp. 111–127, John Wiley & Sons, Chichester, UK, 1989.

[12] P. Gilbert and A. J. McBain, "Biofilms: their impact on health and their recalcitrance toward biocides," *American Journal of Infection Control*, vol. 29, no. 4, pp. 252–255, 2001.

[13] P. Gilbert, T. Maira-Litran, A. J. McBain, A. H. Rickard, and F. W. Whyte, "The physiology and collective recalcitrance of microbial biofilm communities," *Advances in Microbial Physiology*, vol. 46, pp. 203–256, 2002.

[14] I. Atela, P. Coll, J. Rello et al., "Serial surveillance cultures of skin and catheter hub specimens from critically ill patients with central venous catheters: molecular epidemiology of infection and implications for clinical management and research," *Journal of Clinical Microbiology*, vol. 35, no. 7, pp. 1784–1790, 1997.

[15] R. M. Donlan and J. W. Costerton, "Biofilms: survival mechanisms of clinically relevant microorganisms," *Clinical Microbiology Reviews*, vol. 15, no. 2, pp. 167–193, 2002.

[16] I. Raad and H. Hanna, "Intravascular catheters impregnated with antimicrobial agents: a milestone in the prevention of bloodstream infections," *Supportive Care in Cancer*, vol. 7, no. 6, pp. 386–390, 1999.

[17] M. E. Olson, K. Lam, G. P. Bodey, E. G. King, and J. W. Costerton, "Evaluation ofstrategies for central venous catheter replacement," *Critical Care Medicine*, vol. 20, no. 6, pp. 797–804, 1992.

[18] M. Hannan, R. N. Juste, S. Umasanker et al., "Antiseptic-bonded central venous catheters and bacterial colonisation," *Anaesthesia*, vol. 54, no. 9, pp. 868–872, 1999.

[19] R. A. Harvey, D. V. Alcid, and R. S. Greco, "Antibiotic bonding to polytetrafluoroethylene with tridodecylmethylammonium chloride," *Surgery*, vol. 92, no. 3, pp. 504–512, 1982.

[20] D. G. Maki, "Infections caused by intravascular devices used for infusion therapy: pathogenesis, prevention and management," in *Infections Associated with Indwelling Medical Devices*, A. I. Bisno and F. A. Waldvogel, Eds., pp. 155–212, ASM Press, Washington, DC, USA, 2nd edition, 2004.

[21] K. D. Marciante, D. L. Veenstra, B. A. Lipsky, and S. Saint, "Which antimicrobial impregnated central venous catheter should we use? Modeling the costs and outcomes of antimicrobial catheter use," *American Journal of Infection Control*, vol. 31, no. 1, pp. 1–8, 2003.

[22] S. A. McConnell, P. O. Gubbins, and E. J. Anaissie, "Do antimicrobial-impregnated central venous catheters prevent catheter-related bloodstream infection?" *Clinical Infectious Diseases*, vol. 37, no. 1, pp. 65–72, 2003.

[23] J. J. Harrison, C. A. Stremick, R. J. Turner, N. D. Allan, M. E. Olson, and H. Ceri, "Microtiter susceptibility testing of microbes growing on peg lids: a miniaturized biofilm model for high-throughput screening," *Nature Protocols*, vol. 5, no. 7, pp. 1236–1254, 2010.

[24] H. Ceri, M. E. Olson, C. Stremick, R. R. Read, D. Morck, and A. Buret, "The Calgary Biofilm Device: new technology for rapid determination of antibiotic susceptibilities of bacterial biofilms," *Journal of Clinical Microbiology*, vol. 37, no. 6, pp. 1771–1776, 1999.

[25] L. Ali, F. Khambaty, and G. Diachenko, "Investigating the suitability of the Calgary Biofilm Device for assessing the antimicrobial efficacy of new agents," *Bioresource Technology*, vol. 97, no. 15, pp. 1887–1893, 2006.

[26] B. Jose, V. Antoci, A. R. Zeiger, E. Wickstrom, and N. J. Hickok, "Vancomycin covalently bonded to titanium beads kills *Staphylococcus aureus*," *Chemistry and Biology*, vol. 12, no. 9, pp. 1041–1048, 2005.

[27] B. Li, X. Liu, C. Cao, Y. Dong, and C. Ding, "Biological and antibacterial properties of plasma sprayed wollastonite/silver coatings," *Journal of Biomedical Materials Research B*, vol. 91, no. 2, pp. 596–603, 2009.

[28] T. Shirai, H. Tsuchiya, T. Shimizu, K. Ohtani, Y. Zen, and K. Tomita, "Prevention of pin tract infection with titanium-copper alloys," *Journal of Biomedical Materials Research B*, vol. 91, no. 1, pp. 373–380, 2009.

[29] J. Pratten and D. Ready, "Use of biofilm model systems to study antimicrobial susceptibility," *Methods in Molecular Biology*, vol. 642, pp. 203–215, 2010.

[30] D. M. Goeres, M. A. Hamilton, N. A. Beck et al., "A method for growing a biofilm under low shear at the air-liquid interface using the drip flow biofilm reactor," *Nature Protocols*, vol. 4, no. 5, pp. 783–788, 2009.

[31] D. G. Maki, C. E. Weise, and H. W. Sarafin, "A semiquantitative culture method for identifying intravenous catheter related infection," *New England Journal of Medicine*, vol. 296, no. 23, pp. 1305–1309, 1977.

[32] "Draft guidance for industry and FDA Staff-Premarket notification [510(k)] submissions for medical devices that include antimicrobial agents," July 2007, http://www.fda.gov/MedicalDevices/DeviceRegulationandGuidance/GuidanceDocuments/ucm071380.htm.

[33] A. I. Hidron, J. R. Edwards, J. Patel et al., "Antimicrobial-resistant pathogens associated with healthcare-associated infections: annual summary of data reported to the National Healthcare Safety Network at the Centers for Disease Control and Prevention, 2006-2007," *Infection Control and Hospital Epidemiology*, vol. 29, no. 11, pp. 996–1011, 2008.

[34] A. Sengupta, C. Lehmann, M. Diener-West, T. M. Perl, and A. M. Milstone, "Catheter duration and risk of CLA-BSI in neonates with PICCs," *Pediatrics*, vol. 125, no. 4, pp. 648–653, 2010.

[35] P. Viale and S. Stefani, "Vascular catheter-associated infections: a microbiological and therapeutic update," *Journal of Chemotherapy*, vol. 18, no. 3, pp. 235–249, 2006.

Hindawi Publishing Corporation
Journal of Biomedicine and Biotechnology
Volume 2012, Article ID 285938, 6 pages
doi:10.1155/2012/285938

Research Article

Sleep Deprivation Alters Rat Ventral Prostate Morphology, Leading to Glandular Atrophy: A Microscopic Study Contrasted with the Hormonal Assays

Daniel P. Venâncio,[1] Monica L. Andersen,[2] Patricia S. L. Vilamaior,[3] Fernanda C. Santos,[4] Adriano Zager,[2] Sérgio Tufik,[2] Sebastião R. Taboga,[3] and Marco T. De Mello[2]

[1] *Departamento de Nutrição, Universidade Federal de São Paulo (UNIFESP-EPM), Rua Marselhesa, 630, Vila Clementino, 04020-620 São Paulo, SP, Brazil*
[2] *Departamento de Psicobiologia, Universidade Federal de São Paulo (UNIFESP-EPM), Rua Napoleão de Barros, 295, Vila Clementino, 04024-002 São Paulo, SP, Brazil*
[3] *Departmento de Biología, Instituto de Biociências, Letras e Ciências Exatas (IBILCE), Universidade Estadual Paulista (UNESP), Rua Cristóvão Colombo 2265, Jardim Nazareth, 15054-000 São José do Rio Preto, SP, Brazil*
[4] *Departamento de Morfologia, Universidade Federal de Goiás, Campus II Samambaia, Caixa Posta 131, 74001-970 Goiânia, GO, Brazil*

Correspondence should be addressed to Sebastião R. Taboga, taboga@ibilce.unesp.br

Received 30 December 2011; Accepted 16 June 2012

Academic Editor: Oreste Gualillo

We investigated the effect of 96 h paradoxical sleep deprivation (PSD) and 21-day sleep restriction (SR) on prostate morphology using stereological assays in male rats. After euthanasia, the rat ventral prostate was removed, weighed, and prepared for conventional light microscopy. Microscopic analysis of the prostate reveals that morphology of this gland was altered after 96 h of PSD and 21 days of SR, with the most important alterations occurring in the epithelium and stroma in the course of both procedures compared with the control group. Both 96 h PSD and 21-day SR rats showed lower serum testosterone and higher corticosterone levels than control rats. The significance of our result referring to the sleep deprivation was responsible for deep morphological alterations in ventral prostate tissue, like to castration microscopic modifications. This result is due to the marked alterations in hormonal status caused by PSD and SR.

1. Introduction

Sleep deprivation (SD) is a frequent condition in modern life due to the demands of our lifestyles [1], and sleep loss may trigger several alterations in organisms, including immunological effects [2–5], memory deficits [6–8], and hormonal abnormalities [9–14]. Shift work, obstructive sleep apnea, and other sleep disturbances may cause metabolic syndrome, which is strongly associated with male sex hormone alterations [15]. For instance, men affected by SD showed accentuated reduction of testosterone levels or hypogonadism [16]. Additionally, obstructive sleep apnea syndrome is frequently associated with decreased testosterone concentrations [17], fatigue, and erectile dysfunction [18, 19].

Our laboratory group has consistently demonstrated the effects of paradoxical sleep deprivation (PSD) on overall hormonal profiles in male rats; specifically we have found lower testosterone and estrone levels, but higher levels of progesterone, prolactin, corticosterone, and adrenocorticotropic hormone (ACTH) [11, 12]. Interestingly, in contrast to humans, these rats showed increased genital reflexes, reflected in penile erections and ejaculatory frequency [9–12, 20, 21]. In the male rat's reproductive system, 4-day PSD decreased the weight of the seminal vesicle and ventral prostate, indicating reduced steroidogenesis or diminished expression of androgens in target glands [22]. Indeed, PSD is inherently a stress condition, and other stress modalities

that have been examined, such as immobilization, also lead to lower testosterone concentrations [9, 10]. This can impair gonadal function by altering testicular maturation and the production of maturing sperm [23]. Moreover, it has been demonstrated that after castration, blood androgen levels as well as blood flow in the prostate (which is controlled by androgen levels) decrease abruptly. This reduction induces apoptosis in both endothelial and secretory epithelial cells [24]. However, the specific effects of PSD on prostate morphology have not been determined. Therefore, our objective was to examine the effect of PSD (96 h) and chronic sleep restriction (21 days) on hormonal profiles and prostate histological patterns.

2. Material and Methods

2.1. Animals. Wistar male rats, aged 3 months and weighing 300–350 g at the beginning of the experiment, were obtained from the Instituto Nacional de Farmacologia (INFAR) colony at UNIFESP. The rats were housed inside standard polypropylene cages in a temperature-controlled (23 ± 1°C) room with a 12:12 h light-dark cycle (lights on at 06:00 hours). All procedures used in the present study complied with the guide for care and use of laboratory animals, and the experimental protocol was approved by the UNIFESP Ethical Committee (0876/09).

2.2. Paradoxical Sleep Deprivation/Sleep Restriction Procedure. Naïve rats were randomly distributed into three groups: paradoxical sleep deprivation (PSD), sleep restriction (SR), and home-cage controls (CTRL). The chronic partial SR group was subjected to SR for 18 h (beginning at 16:00 h) per day for 21 consecutive days (SR21 $n = 10$). After each 18 h sleep deprivation period, the rats were allowed to sleep for 6 h (sleep window beginning at 10:00). Throughout the SR procedure, rats slept an average of 30–40% of the time, corresponding to 8-9 h per day. This sleep interval (10:00–16:00 h) was chosen because this is when paradoxical sleep attains its highest expression, and slow wave-sleep homeostatic pressure is generated [25–27].

The SD procedure consisted of placing rats in a container with a narrow cylindrical platform 6.5 cm in diameter surrounded by water about 1 cm below the platform surface. Each rat was placed individually in the container, and food and water were available *ad libitum* throughout the entire experimental period. At the onset of a paradoxical sleep episode, rats experienced loss of muscle tonus and fell into the water, thus being awakened.

2.3. Hormonal Assay. After the PSD/SR period, the rats were brought to an adjacent room and decapitated with minimum discomfort between 09:00 h and noon. The control group rats were euthanized at the same time as the experimental group and the other 50% were euthanized on the first day of the experimental procedure. Blood was collected in glass tubes and centrifuged to obtain samples of serum or plasma. The samples were maintained at −20°C until assay. Each hormone assay of the samples from the five groups was analyzed on the same day. The intraassay coefficient variations are given in parentheses. Testosterone concentration (6.7%) was measured by chemiluminescent immunometric assay (Immulite Automated Analyses; Diagnostic Products Corporation, Los Angeles, CA, USA), with a detection threshold of 10 ng dL^{-1}. Corticosterone (10.3%) concentrations were assayed by a double-antibody RIA method specifically for rats and mice, using a commercial kit (ICN Biomedicals, Costa Mesa, CA, USA). The sensitivity of the assay is 0.25 ng dL^{-1}.

2.4. Tissue Collection. For light microscopy, the ventral prostates were removed and immediately fixed by a 24 h immersion in Karnovsky fixative (0.1 M phosphate buffer, pH 7.2, containing 4% paraformaldehyde and 2.5% glutaraldehyde). Fixed tissues were dehydrated in a graded ethanol series and embedded in paraffin or glycol methacrylate resin (Historesin embedding kit, Leica, Heidelberg, Germany). Sections were cut at 3 μm and stained with hematoxylin and eosin (H&E) for general histological studies. Analyses were carried out using either a Zeiss Jenaval light microscope (Carl Zeiss, Jena, Germany) or an Olympus BX60 (Hamburg, Germany).

2.5. Morphometric and Stereological Analyses. Random prostatic fields from H&E sections were analyzed using the software Image-Pro-Plus version 4.5 for Windows (Media Cybernetic). Stereological analyses were carried out using Weibel's multipurpose graticulate with 130 points and 60 test lines [28], to compare the relative proportion (relative volume) of each prostatic tissue component (epithelium, lumen, and stroma), as described by Huttunen and collaborators (1981) and modified by Vilamaior and collaborators (2006) for prostatic tissue [29, 30]. Thirty microscopic fields were chosen at random. In summary, the relative values were determined by counting the coincident points of the test grid and dividing them by the total number of points. The absolute volume of each of these compartments was determined by multiplying the relative volume value by the mean prostatic weight, based on the determination that 1 mg of fresh rat ventral tissue had a volume of approximately 1 mm^3 [30]. For the morphometrical analyses, 200 random measurements of epithelium height were also obtained.

2.6. Statistical Analysis. The quantitative results are expressed as means ± standard errors. One-way ANOVA was followed by Tukey's test. The level of statistical significance was set at $P \leq 0.05$.

3. Results

3.1. Hormonal Levels. Plasma testosterone fell drastically in both groups. After 96 h PSD, testosterone was 87% lower than in the control group (436.0 ± 68.0 versus 58.0 ± 8.2 ng dL^{-1}; $P < 0.01$). The 21-day SR group's testosterone levels fell 65% in regarding control group (436.0 ± 68.0 versus 152.7 ± 22.2 ng dL^{-1}; $P < 0.01$), as shown in Figure 1.

Corticosterone values are shown in Figure 2. The ANOVA test showed the effect of the PSD and SR groups on corticosterone levels [$F(3.49) = 13.92$; $P < 0.001$]. Subsequent post hoc analysis revealed that corticosterone

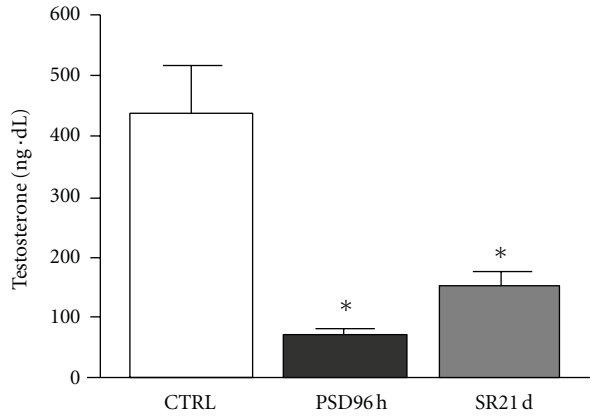

Figure 1: Mean ± SD concentration of serum testosterone (in ng dL^{-1}) control group (CTRL), paradoxal sleep deprivation (PSP) and sleep restriction (SR) at different time points. *Different from control group ($P < 0.01$).

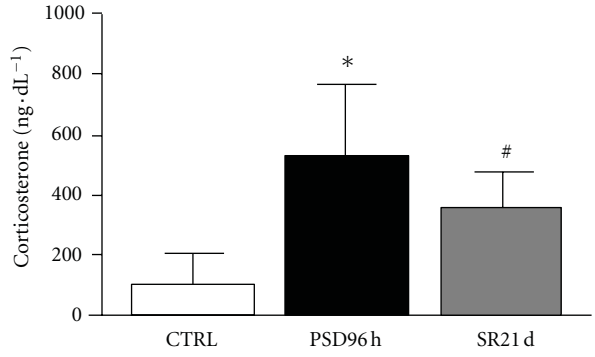

Figure 2: Mean ± SD concentration of plasma corticosterone (in ng dL^{-1}) of control group (CTRL), sleep deprivation (PSP), and sleep restriction (SR) at different time points. *Different from all groups ($P < 0.01$); #different from control group ($P < 0.01$).

concentrations after 96 h of PSD ($P < 0.001$) were higher than in the control 8 group and 21 days of SR. Furthermore, corticosterone levels after 21 days of SR were statistically different from the control group ($P < 0.01$).

3.2. Prostate Histology. Structural analysis of the ventral prostate using ordinary light microscopy demonstrated that the ventral prostate tissue was affected in the PSD 96-h and SR 21-day protocols. Figure 3 shows major alterations in prostatic tissue morphology, evidenced by epithelium alterations. Epithelial infoldings of apoptotic figures appeared and interestingly, there was an accumulation of fat cells in prostatic gland stroma, particularly in rats subjected to the SR procedure.

Morphometric and stereological evaluation of prostatic compartments (Table 1) showed regression of epithelium height in PSD96 and SR groups ($P < 0.001$) relative to the control group. The relative epithelial volume did not show any differences relative to the control groups. On the other hand, relative volumes of the stroma and lumen in the SR group were significantly different from the control and PSD96 volumes ($P < 0.001$). However, the absolute volume of the lumen in the SR group declined relative to both the control and PSD96 rats ($P < 0.001$).

Table 1

	Control	PSD96 h	SR21
Morphometry			
Epithelium height (μm)	43.42 ± 7.3	38.7 ± 5.4*	38.5 ± 5.2*
Estereology			
Epithelium			
RV (%)	33.84 ± 2.33	31.6 ± 7.2	29.1 ± 7
AV (mg)	35.43 ± 2.44	25.88 ± 1.71*	22.52 ± 1.08*
Stroma			
RV (%)	10.7 ± 0.67	12.2 ± 6*	20.2 ± 8.7*#
AV(mg)	11.17 ± 0.67	10.02 ± 0.97	15.65 ± 1.35*#
Lumen			
RV (%)	55.5 ± 13.3	56.2 ± 10	50.8 ± 9*#
AV (mg)	58.07 ± 2.79	45.99 ± 1.63*	39.36 ± 1.40*

Values represent means ± SEMs of the data obtained for stereological and morphometrical analyses of three experimental groups: control, PSD96 h and SR21. Statistical analyses based on ANOVA and Tukey tests. Significance $P < 0.05$. *Different from control group and different from PSD96 h. RV: relative volume. AV: absolute volume.

4. Discussion

The purpose of this study was to evaluate the effects of 96-hour SD and 21-day SR on prostate morphology in rats. The main findings were that prostate tissue responded to 96 h PSD with the presence of apoptotic bodies and diminished epithelium height, which indicates regression of the prostatic secretion function (glandular atrophy). The SR group showed diminished epithelium and lumen height. In addition, fat cells were observed in the stroma in the SR group. Both sleep-deprivation procedures caused higher corticosterone and lower testosterone levels.

Our data confirm previous findings about how sleep deprivation affects testosterone and corticosterone concentrations [9, 10, 31, 32]. The abrupt fall in testosterone levels may be influenced by an elevation of hormones involved in the hypothalamic-pituitary-adrenal (HPA) axis, such as corticosterone. Therefore, it seems that glucocorticoids have the ability to suppress endocrine signaling in the reproductive axis [9, 10, 31, 33]. *In vitro* studies show that Leydig cells are negatively regulated by the administration of corticosteroids [34]. Indeed, glucocorticoids directly inhibit transcription of genes responsible for the enzymatic mechanism that activates testosterone synthesis. Hales and Payne [34] reported that after treating Leydig cells with glucocorticoid *in vitro*, the gene transcription and subsequent synthesis of the protein responsible for cholesterol cleavage (which produces testosterone) was also inhibited.

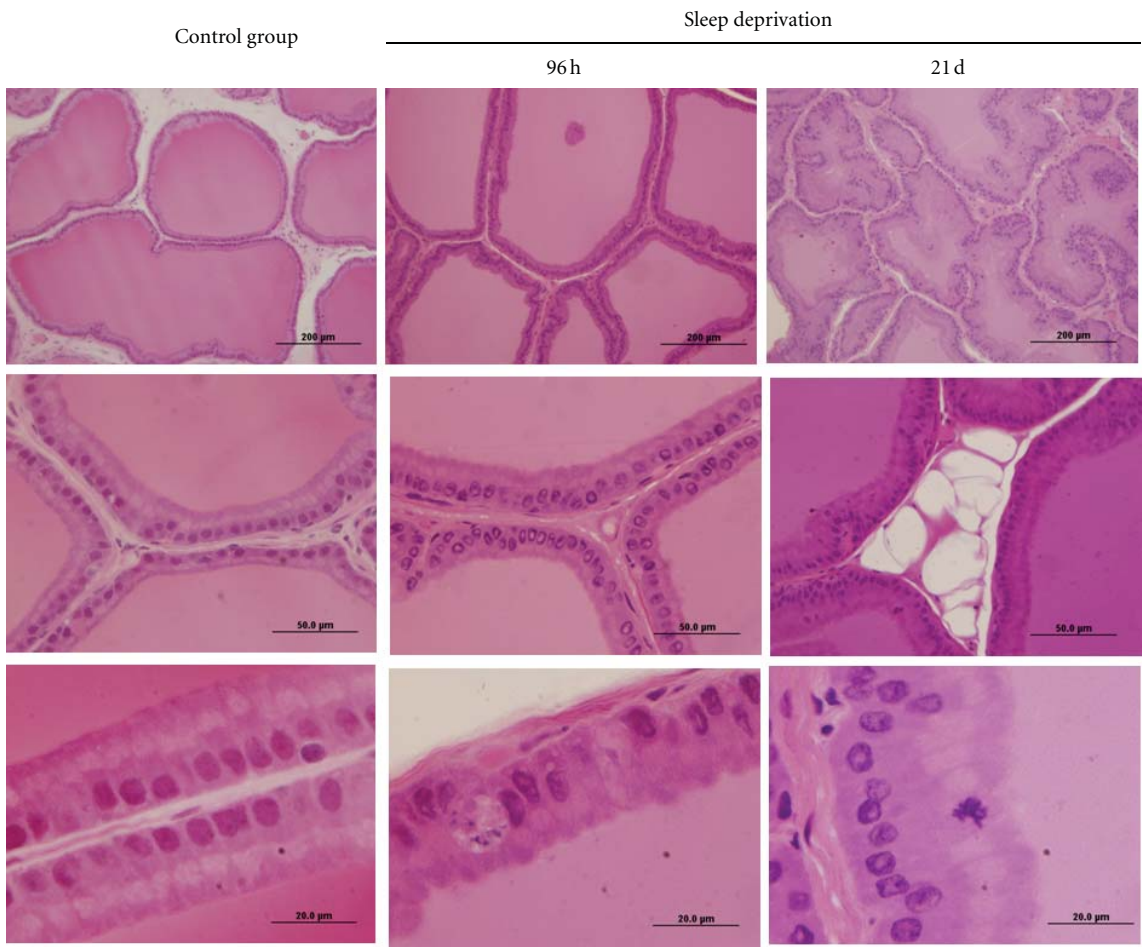

Figure 3: Haematoxylin and eosin stained histological sections of rat ventral prostatic tissue under different conditions of sleep deprivation. The prostate of control group shows the acini (Ac) with great amount of secretion in the luminal region (Lu), and the epithelium (Ep) is visualized with conspicuous Golgi's region (star), indicative of high secretion activity. During the sleep deprivation conditions, the acini compartment is decreased, and the presence of unilocular adipose tissue is evident (*). The thin arrow indicates an apoptotic body in the epithelium. Stroma (S).

High glucocorticoid concentrations downmodulate the reproductive axis at the hypothalamus and pituitary levels, showing that they have deleterious effects on the expression of gonadotrophin-releasing hormone (*GnRH*) mRNA and reduce LH plasma concentrations [35]. As shown by Andersen and coworkers, plasma testosterone reduction during sleep deprivation is directly related to higher corticosterone levels [11, 12].

Testosterone is a critical hormone for prostate development, growth, and maintenance [30]. Prostatic morphogenesis is determined not genetically, but by exposure to androgens produced by the testes in the fetus [36, 37]. Therefore, insensitivity to androgens hinders prostate development. It has been shown that androgen stimulation at the correct time during embryogenesis can modulate prostate tissue growth in both males and females [38]. Several studies have shown that the prostate undergoes more marked alterations in epithelial and stromal compartments after hormonal and surgical ablation. These procedures lead to a decrease in glandular function, with consequent declines in epithelium thickness and stromal volume [39, 40]. In the current study, we found diminished epithelium height in rats subjected to PSD 96 h and SR. Androgen levels are clearly lowered during sleep deprivation [9–12, 41]. Maintenance of prostate physiology depends on circulating androgens and more specifically on dihydrotestosterone levels [42, 43]. Therefore, this hormone seems to be more potent than testosterone in stimulating epithelium growth and maintenance, although they have the same ability to prevent cell death after castration [44]. Androgens play a central role in regulating growth and maintenance of the active functional state of the prostate gland in mammals and can stimulate and inhibit the death of epithelial glandular cells [24, 45]. There is strong evidence that the low levels of circulating androgens seen in the PSD96 group may have started the apoptotic process in the rat ventral prostate, which led to diminished volume and thus glandular atrophy and decreased function.

Ribeiro and collaborators (2008) showed that dexamethasone treatment in male rats induced atrophy and reduced the proliferative capacity of epithelial cells. The same

treatment also led to altered epithelium-stroma interactions. Smooth muscle cells showed an atrophic contractile pattern and high electron density of the mitochondrial matrix [46]. The high concentration of circulating corticosterone may have led to the reduced epithelium height in the experimental groups studied here. In addition, accumulation of fat cells in the stroma was observed in the group of rats subjected to SR21. We do not know what impact reduced circulating levels of androgens has in this phenomenon, since we found that animals castrated after 21 days did not present this phenomenon; it is not even known whether this may be related to high levels of corticosterone or some other hormone [47].

Taken as a whole, our results suggest that both paradoxical sleep deprivation and sleep restriction strongly influence the ventral prostate alterations observed in this study. These observed morphological alterations could be induced by two mechanisms mediated by SD and/or SR: the drastic reduction in testosterone levels (important for organ morphology maintenance) or the increase in corticosterone levels, which can act directly on the cytoplasmic receptors of the prostate cells.

Conflict of Interests

The authors declare that they have no conflict of interests associated with this paper.

Acknowledgments

This paper is part of the thesis presented by D. P. Venâncio to the Department of Nutrition of the Universidade Federal de São Paulo (UNIFESP-EPM), in partial fulfillment of the requirement for a doctoral degree in science. The authors wish to thank to Mr. Luiz Roberto Falleiros Júnior for technical assistance. This work was supported by National Council of Scientific and Technological Development (CNPq): Research Fellowships to M. L. Andersen, S. R. Taboga, S. Tufik, M. T. De Mello.

References

[1] S. M. Rajaratnam and J. Arendt, "Health in a 24-h society," *The Lancet*, vol. 358, no. 9286, pp. 999–1005, 2001.

[2] C. A. Everson, "Sustained sleep deprivation impairs host defense," *American Journal of Physiology*, vol. 265, no. 5, pp. R1148–R1154, 1993.

[3] B. D. Palma, A. Gabriel Jr., F. A. B. Colugnati, and S. Tufik, "Effects of sleep deprivation on the development of autoimmune disease in an experimental model of systemic lupus erythematosus," *American Journal of Physiology*, vol. 291, no. 5, pp. R1527–R1532, 2006.

[4] F. S. Ruiz, M. L. Andersen, A. Zager, R. C. S. Martins, and S. Tufik, "Sleep deprivation reduces the lymphocyte count in a non-obese mouse model of type 1 diabetes mellitus," *Brazilian Journal of Medical and Biological Research*, vol. 40, no. 5, pp. 633–637, 2007.

[5] A. Zager, M. L. Andersen, F. S. Ruiz, I. B. Antunes, and S. Tufik, "Effects of acute and chronic sleep loss on immune modulation of rats," *American Journal of Physiology*, vol. 293, no. 1, pp. R504–R509, 2007.

[6] T. A. Alvarenga, C. L. Patti, M. L. Andersen et al., "Paradoxical sleep deprivation impairs acquisition, consolidation, and retrieval of a discriminative avoidance task in rats," *Neurobiology of Learning and Memory*, vol. 90, no. 4, pp. 624–632, 2008.

[7] R. H. Silva, V. C. Abílio, A. L. Takatsu et al., "Role of hippocampal oxidative stress in memory deficits induced by sleep deprivation in mice," *Neuropharmacology*, vol. 46, no. 6, pp. 895–903, 2004.

[8] J. L. Tartar, C. P. Ward, J. T. McKenna et al., "Hippocampal synaptic plasticity and spatial learning are impaired in a rat model of sleep fragmentation," *European Journal of Neuroscience*, vol. 23, no. 10, pp. 2739–2748, 2006.

[9] M. L. Andersen, M. Bignotto, R. B. Machado, and S. Tufik, "Different stress modalities result in distinct steroid hormone responses by male rats," *Brazilian Journal of Medical and Biological Research*, vol. 37, no. 6, pp. 791–797, 2004.

[10] M. L. Andersen, L. A. Papale, and S. Tufik, "Diurnal variation in the genital reflexes and hormone levels induced by paradoxical sleep deprivation and cocaine in male rats," *Brain Research Bulletin*, vol. 64, no. 3, pp. 215–220, 2004.

[11] M. L. Andersen, V. D'Almeida, P. J. F. Martins, H. K. M. Antunes, and S. Tufik, "Effects of paradoxical sleep deprivation and cocaine on genital reflexes in hyperlipidic-fed rats," *Pharmacology Biochemistry and Behavior*, vol. 81, no. 4, pp. 758–763, 2005.

[12] M. L. Andersen, P. J. F. Martins, V. D'Almeida, M. Bignotto, and S. Tufik, "Endocrinological and catecholaminergic alterations during sleep deprivation and recovery in male rats," *Journal of Sleep Research*, vol. 14, no. 1, pp. 83–90, 2005.

[13] E. Y. Kim, G. S. Mahmoud, and L. M. Grover, "REM sleep deprivation inhibits LTP in vivo in area CA1 of rat hippocampus," *Neuroscience Letters*, vol. 388, no. 3, pp. 163–167, 2005.

[14] C. Mirescu, J. D. Peters, L. Noiman, and E. Gould, "Sleep deprivation inhibits adult neurogenesis in the hippocampus by elevating glucocorticoids," *Proceedings of the National Academy of Sciences of the United States of America*, vol. 103, no. 50, pp. 19170–19175, 2006.

[15] R. Wolk and V. K. Somers, "Sleep and the metabolic syndrome," *Experimental Physiology*, vol. 92, no. 1, pp. 67–78, 2007.

[16] F. Singer and B. Zumoff, "Subnormal serum testosterone levels in male internal medicine residents," *Steroids*, vol. 57, no. 2, pp. 86–89, 1992.

[17] R. Luboshitzky, L. Lavie, Z. Shen-Orr, and P. Herer, "Altered luteinizing hormone and testosterone secretion in middle-aged obese men with obstructive sleep apnea," *Obesity Research*, vol. 13, no. 4, pp. 780–786, 2005.

[18] M. A. Gonçalves, C. Guilleminault, E. Ramos, A. Palha, and T. Paiva, "Erectile dysfunction, obstructive sleep apnea syndrome and nasal CPAP treatment," *Sleep Medicine*, vol. 6, no. 4, pp. 333–339, 2005.

[19] D. Margel, M. Cohen, P. M. Livne, and G. Pillar, "Severe, but not mild, obstructive sleep apnea syndrome is associated with erectile dysfunction," *Urology*, vol. 63, no. 3, pp. 545–549, 2004.

[20] M. L. Andersen, J. C. Perry, M. C. Battisti et al., "Association of paradoxical sleep deprivation and ecstasy (MDMA) enhances genital reflexes in male rats," *Behavioural Brain Research*, vol. 170, no. 2, pp. 287–292, 2006.

[21] M. L. Andersen, J. C. Perry, I. B. Antunes, and S. Tufik, "Involvement of nitric oxide in cocaine-induced erections and ejaculations after paradoxical sleep deprivation," *Progress in*

Neuro-Psychopharmacology and Biological Psychiatry, vol. 31, no. 3, pp. 652–657, 2007.

[22] S. Mathur and P. P. Chattopadhyay, "Effect of sleep deprivation on the physiological status of rat testis," *Andrologia*, vol. 23, no. 1, pp. 49–51, 1991.

[23] R. Demura, T. Suzuki, S. Nakamura, H. Komatsu, E. Odagiri, and H. Demura, "Effect of immobilization stress on testosterone and inhibin in male rats," *Journal of Andrology*, vol. 10, no. 3, pp. 210–213, 1989.

[24] N. Kyprianou and J. T. Isaacs, "Activation of programmed cell death in the rat ventral prostate after castration," *Endocrinology*, vol. 122, no. 2, pp. 552–562, 1988.

[25] P. Franken, I. Tobler, and A. A. Borbely, "Sleep homeostasis in the rat: simulation of the time course of EEG slow-wave activity," *Neuroscience Letters*, vol. 130, no. 2, pp. 141–144, 1991.

[26] R. B. Machado, D. C. Hipólide, A. A. Benedito-Silva, and S. Tufik, "Sleep deprivation induced by the modified multiple platform technique: quantification of sleep loss and recovery," *Brain Research*, vol. 1004, no. 1-2, pp. 45–51, 2004.

[27] C. Timo-Iaria, N. Negrào, W. R. Schmidek, K. Hoshino, C. E. L. de Menezes, and T. L. da Rocha, "Phases and states of sleep in the rat," *Physiology and Behavior*, vol. 5, no. 9, pp. 1057–1062, 1970.

[28] E. R. WEIBEL, "Principles and methods for the morphometric study of the lung and other organs," *Laboratory Investigation*, vol. 12, pp. 131–155, 1963.

[29] E. Huttunen, T. Romppanen, and H. J. Helminen, "A histoquantitative study on the effects of castration on the rat ventral prostate lobe," *Journal of Anatomy*, vol. 132, no. 3, pp. 357–370, 1981.

[30] P. S. L. Vilamaior, S. R. Taboga, and H. F. Carvalho, "Postnatal growth of the ventral prostate in Wistar rats: a stereological and morphometrical study," *Anatomical Record A*, vol. 288, no. 8, pp. 885–892, 2006.

[31] D. C. Hipólide, D. Suchecki, A. P. de Carvalho Pinto, E. Chiconelli Faria, S. Tufik, and J. Luz, "Paradoxical sleep deprivation and sleep recovery: effects on the hypothalamic-pituitary-adrenal axis activity, energy balance and body composition of rats," *Journal of Neuroendocrinology*, vol. 18, no. 4, pp. 231–238, 2006.

[32] A. Sgoifo, B. Buwalda, M. Roos, T. Costoli, G. Merati, and P. Meerlo, "Effects of sleep deprivation on cardiac autonomic and pituitary- adrenocortical stress reactivity in rats," *Psychoneuroendocrinology*, vol. 31, no. 2, pp. 197–208, 2006.

[33] T. E. Orr and D. R. Mann, "Role of glucocorticoids in the stress-induced suppression of testicular steroidogenesis in adult male rats," *Hormones and Behavior*, vol. 26, no. 3, pp. 350–363, 1992.

[34] D. B. Hales and A. H. Payne, "Glucocorticoid-mediated repression of P450(SCC) mRNA and de novo synthesis in cultured Leydig cells," *Endocrinology*, vol. 124, no. 5, pp. 2099–2104, 1989.

[35] A. C. Gore, B. Attardi, and D. B. DeFranco, "Glucocorticoid repression of the reproductive axis: effects on GnRH and gonadotropin subunit mRNA levels," *Molecular and Cellular Endocrinology*, vol. 256, no. 1-2, pp. 40–48, 2006.

[36] G. R. Cunha, A. A. Donjacour, P. S. Cooke et al., "The endocrinology and developmental biology of the prostate," *Endocrine Reviews*, vol. 8, no. 3, pp. 338–362, 1987.

[37] G. Pointis, M. T. Latreille, and L. Cedard, "Gonado-pituitary relationships in the fetal mouse at various times during sexual differentiation," *Journal of Endocrinology*, vol. 86, no. 3, pp. 483–488, 1980.

[38] H. Takeda, I. Lasnitzki, and T. Mizuno, "Analysis of prostatic bud induction by brief androgen treatment in the fetal rat urogenital sinus," *Journal of Endocrinology*, vol. 110, no. 3, pp. 467–470, 1986.

[39] R. S. Cordeiro, W. R. Scarano, R. M. Góes, and S. R. Taboga, "Tissue alterations in the Guinea pig lateral prostate following antiandrogen flutamide therapy," *Biocell*, vol. 28, no. 1, pp. 21–30, 2004.

[40] L. S. Corradi, R. M. Gòes, H. F. Carvalho, and S. R. Taboga, "Inhibition of 5-α-reductase activity induces stromal remodeling and smooth muscle de-differentiation in adult gerbil ventral prostate," *Differentiation*, vol. 72, no. 5, pp. 198–208, 2004.

[41] M. R. Gonzalez-Santos, O. V. Gaja-Rodriguez, R. Alonso-Uriarte, I. Sojo-Aranda, and V. Cortes-Gallegos, "Sleep deprivation and adaptive hormonal responses of healthy men," *Archives of Andrology*, vol. 22, no. 3, pp. 203–207, 1989.

[42] J. Imperato-McGinley, R. S. Sanchez, J. R. Spencer, B. Yee, and E. D. Vaughan, "Comparison of the effects of the 5α-reductase inhibitor finasteride and the antiandrogen flutamide on prostate and genital differentiation: dose- response studies," *Endocrinology*, vol. 131, no. 3, pp. 1149–1156, 1992.

[43] J. D. Wilson, J. E. Griffin, and D. W. Russell, "Steroid 5α-reductase 2 deficiency," *Endocrine Reviews*, vol. 14, no. 5, pp. 577–593, 1993.

[44] A. S. Wright, L. N. Thomas, R. C. Douglas, C. B. Lazier, and R. S. Rittmaster, "Relative potency of testosterone and dihydrotestosterone in preventing atrophy and apoptosis in the prostate of the castrated rat," *Journal of Clinical Investigation*, vol. 98, no. 11, pp. 2558–2563, 1996.

[45] J. T. Isaacs, "Antagonistic effect of androgen on prostatic cell death," *Prostate*, vol. 5, no. 5, pp. 545–557, 1984.

[46] D. L. Ribeiro, A. Rafacho, J. R. Bosqueiro, S. R. Taboga, and R. M. Góes, "Cellular changes in the prostatic stroma of glucocorticoid-treated rats," *Cell and Tissue Research*, vol. 332, no. 3, pp. 499–508, 2008.

[47] P. S. L. Vilamaior, S. R. Taboga, and H. F. Carvalho, "Modulation of smooth muscle cell function: morphological evidence for a contractile to synthetic transition in the rat ventral prostate after castration," *Cell Biology International*, vol. 29, no. 9, pp. 809–816, 2005.

Hindawi Publishing Corporation
Journal of Biomedicine and Biotechnology
Volume 2012, Article ID 601786, 6 pages
doi:10.1155/2012/601786

Review Article

Involvement of the Intrarenal Renin-Angiotensin System in Experimental Models of Glomerulonephritis

Maki Urushihara, Yukiko Kinoshita, Shuji Kondo, and Shoji Kagami

Department of Pediatrics, Institute of Health Biosciences, The University of Tokushima Graduate School, Kuramoto-cho 3-18-15, Tokushima, Tokushima 770-8503, Japan

Correspondence should be addressed to Maki Urushihara, urushihara@clin.med.tokushima-u.ac.jp

Received 9 January 2012; Accepted 9 June 2012

Academic Editor: Oreste Gualillo

The intrarenal renin-angiotensin system (RAS) has several pathophysiologic functions not only in blood pressure regulation but also in the development of glomerulonephritis (GN). Angiotensin II (Ang II) is the biologically active product of the RAS. Locally produced Ang II induces inflammation, renal cell growth, mitogenesis, apoptosis, migration, and differentiation, regulates the gene expression of bioactive substances, and activates multiple intracellular signaling pathways, leading to tissue damage. Activation of the Ang II type 1 (AT1) receptor pathway results in the production of proinflammatory mediators, cell proliferation, and extracellular matrix synthesis, which facilitates glomerular injury. Previous studies have shown that angiotensin-converting enzyme inhibitors and/or AT1 receptor blockers have beneficial effects in experimental GN models and humans with various types of GN, and that these effects are more significant than their suppressive effects on blood pressure. In this paper, we focus on intrarenal RAS activation in the pathophysiology of experimental models of GN.

1. Introduction

The role of the renin-angiotensin system (RAS) in blood pressure regulation and sodium and fluid homeostasis is well recognized [1, 2]. The biologically active peptides that are formed from angiotensinogen (AGT) include angiotensin II (Ang II) and Ang 1-7. The balance between the vasoconstricting actions of Ang II, which are mediated by the Ang II type 1 (AT1) receptor, are countered by the vasodilating actions of Ang II, which are mediated by the AT2 receptor [3] and the actions of Ang 1-7 on the G protein-coupled receptor Mas [4]. Formation of Ang II is dependent upon the substrate availability of AGT and Ang I and the activities of renin, angiotensin-converting enzyme (ACE), ACE2, and ACE-dependent enzymatic pathways, including serine proteases, tonin, cathepsin G, trypsin, and kallikrein. The actions of Ang II are determined by signaling via AT1 and AT2 receptors and the putative Ang 1-7 receptor Mas [5].

Local/tissue RAS in specific tissues has become the focus of much recent interest [6]. Emerging evidence has demonstrated the importance of tissue-specific RAS in the brain [7], heart [8], adrenal glands [9], vasculature [10, 11], and the kidneys [12]. Renal RAS in particular is unique, because all of the components necessary to generate intrarenal Ang II are present along the nephron in both interstitial and intratubular compartments [2, 5]. AGT is the only known substrate for renin that is a rate-limiting enzyme of the RAS. Because the level of AGT is close to the Michaelis-Menten constant for renin, not only renin levels but also AGT levels can control RAS activity, and AGT upregulation may lead to elevated angiotensin protein levels and increased blood pressure [13]. Recent studies have shown that AGT plays an important role in the development and progression of hypertension and kidney disease [2, 12]. Renin mRNA and renin-like activity have been observed in cultured proximal tubular cells [14]. The brush border membrane of proximal human kidney tubules also expresses abundant levels of ACE, mRNA [15], and protein [16]. ACE has been measured in proximal and distal tubular fluid, with greater concentrations observed in proximal tubule fluid [17]. Therefore, all the major components required to generate Ang II are expressed within the kidneys [2, 12].

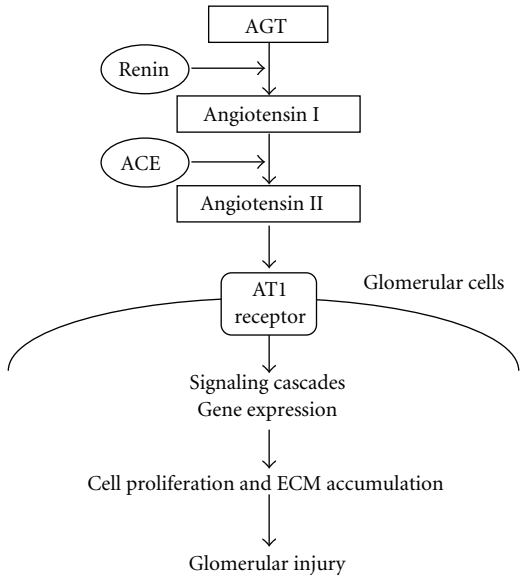

Figure 1: Working schematic of the renin-angiotensin system in glomerulonephritis. AGT: angiotensinogen, ACE: angiotensin-converting enzyme, AT1 receptor: angiotensin II type 1 receptor, and ECM: extracellular matrix.

Chronic glomerulonephritis (GN) resulting in substantial renal damage is frequently characterized by relentless progression to end-stage renal disease. Renal Ang II, the production of which is enhanced in chronic GN, can elevate intraglomerular pressure, increase glomerular cell hypertrophy, and augment extracellular matrix (ECM) accumulation [18, 19] (Figure 1). ACE inhibitors and/or AT1 receptor blockers (ARBs) are often administered to patients with proteinuric nephropathies [20, 21]. The efficacy of these agents in this indication suggests that factors other than Ang II play an important role in the progression of renal disease. This paper explores recent findings concerning the involvement of intrarenal RAS activation in experimental models of GN.

2. RAS Activation in a Model of Progressive Mesangioproliferative GN

Anti-Thy-1 antibody-induced GN is the most common model of experimental nephritis [22, 23], because selective damage to mesangial cells (MCs) allows for the study of mesangial function and pathophysiology. This antibody-antigen reaction initiates complement activation to form a membrane attack complex. Repeated anti-Thy-1 antibody injections may produce progressive glomerular lesions ending in sclerosis, resembling human progressive GN [24]. Glomerulosclerosis is characterized by a continuative accumulation of the ECM, due to increased synthesis and decreased degeneration of the ECM, and overproduction of transforming growth factor (TGF)-β1 in the glomerulus. Furthermore, uninephrectomized rats treated with a single injection of the anti-Thy-1 antibody develop hypertension, massive proteinuria, and severe glomerular injury, finally resulting in chronic mesangioproliferative glomerulosclerosis [25].

To elucidate the involvement of intrarenal RAS activation in the development of glomerulosclerosis during the course of anti-Thy-1 GN with uninephrectomy, we performed an interventional study using the ARB candesartan in a rat model of progressive mesangioproliferative GN [26]. Reactive oxygen species (ROS) produced by NADPH oxidase have been implicated in the development and progression of GN [27, 28]. Ang II induces the activation of NADPH oxidase and the development of oxidative stress in GN [29]. We therefore also examined whether the interaction between the RAS and ROS is important for the development of progressive GN. Nephritis was induced in rats by a single intravenous injection of 2 mg of the nephritogenic anti-Thy-1 antibody 1 week after uninephrectomy. Rats were divided into 4 groups and administered daily oral doses of (1) vehicle, (2) 1% probucol, a free radical scavenger, (3) 70 mg/L candesartan in drinking water, or (4) probucol plus candesartan. Rats in each group were killed at 56 days after the injection of anti-Thy1-1 antibody. As controls, rats were injected with phosphate-buffered saline 1 week after unilateral nephrectomy and were killed on day 56. The ARB candesartan was found to considerably reduce proteinuria, the level of TGF-β1, and ECM accumulation, finally inhibiting the progression of glomerulosclerosis. The combination of probucol and candesartan not only completely eliminated NADPH oxidase components and superoxide production, but also normalized urinary protein excretion and TGF-β1 expression and prevented ECM accumulation, resulting in full prevention of the progression of GN. It seems likely that the beneficial effect of such combined treatment is due to the synergistic action of Ang II inhibition with a receptor antagonist and the elimination of ROS with a radical scavenger. These findings suggest that RAS activation and NADPH oxidase-associated ROS production may play a pivotal role in the progression of GN.

Hydrogen peroxide-inducible clone-5 (Hic-5) was originally discovered as a gene that is induced by TGF-β1 and hydrogen peroxide (H_2O_2), in a study on the growth-inhibitory functions of TGF-β1 in cellular senescence [30]. Recently, Hic-5 has been shown to function as an adaptor protein in focal adhesions and to be involved in integrin-mediated signal transduction, remodeling of the actin cytoskeleton, and regulation of the cellular phenotype [31–33]. To investigate the significance of Hic-5 expression in GN, we analyzed the changes in Hic-5 expression in a rat model of progressive mesangial proliferative GN and examined the combined effects of an ARB and probucol on Hic-5 expression in GN [34]. Glomerular Hic-5 expression increased in parallel with α-smooth muscle actin (SMA) expression in progressive mesangial proliferative GN. Combined therapy with an ARB and probucol in this model improved the histology and expression of Hic-5 and α-SMA. These results suggest that Hic-5 is involved in changes in the MC phenotype, which produce abnormal ECM remolding in GN.

The mitogen-activated protein kinase (MAPK) signaling pathway is a highly conserved module involved in various

cellular functions, including cell proliferation, cell survival, differentiation, and migration [35]. Extracellular stimuli, such as growth factors and environmental stress, induce sequential activation of the MAPK cascade. At least 4 members of the MAPK family have been identified, namely, extracellular signal-regulated kinase 1/2 (ERK1/2), c-Jun-amino-terminal kinase, p38, and ERK5 [35]. It was recently reported that ERK1/2 activation occurs in the rat Thy-1 model of mesangioproliferative nephritis, and that blocking of the ERK1/2 pathway results in a significant reduction in MC proliferation in this model [36]. In addition, ERK1/2 activation in human glomerulopathies is associated with cell proliferation, histologic lesions, and renal dysfunction [37]. ERK5-mediated MC growth has been reported to be involved in the pathogenesis of diabetic nephropathy [38]. To further elucidate whether ERK signaling is involved in the pathogenesis of GN, we examined the expression and phosphorylation levels of glomerular ERK signals in progressive models of rat mesangioproliferative GN characterized by MC proliferation and ECM accumulation. In addition, the potential role of ERK signaling in MC-mediated pathologic mesangial remodeling was investigated in cultured MCs [39]. Glomerular alterations in progressive models of rat mesangial proliferative GN were examined on days 3, 7, 14, 28, and 56 after anti-Thy1 antibody injection. Light microscopy revealed that almost all glomeruli exhibited faint MC proliferation on day 3, followed by mesangial matrix expansion on day 7. Thereafter, massive accumulation of mesangial ECM and MC proliferation were the prominent features of nephritic glomeruli on days 28 and 56. Immunostaining of kidneys obtained at different time points revealed that phospho-ERK1/2 expression increased on day 7 during the phase of enhanced MC proliferation and decreased thereafter. On the other hand, phospho-ERK5 was weakly expressed in control glomeruli but dramatically increased in a typical mesangial pattern after 28 and 56 days of GN. Semiquantitative assessment indicated that glomerular phospho-ERK5 expression closely paralleled the accumulation of ECM and collagen type 1, as well as glomerular expression of ROS and Ang II. The in vitro study revealed that H_2O_2 and Ang II each induced ERK5 phosphorylation by cultured MCs. Costimulation with both H_2O_2 and Ang II synergistically increased ERK5 phosphorylation in MCs. Cultured MCs transfected with ERK5-specific small interference RNA showed a significant decrease in H_2O_2 or Ang II-induced cell viability and soluble collagen secretion compared with control cells. Finally, treatment of GN rats with an ARB resulted in a significant decrease in phospho-ERK5 expression and collagen accumulation, accompanied by remarkable histologic improvement. Taken together, these results suggest that MC ERK5 phosphorylation by Ang II or H_2O_2 enhances cell viability and ECM accumulation in chronic GN.

Several studies demonstrated that the MAPK signaling controls cell behaviors via under RAS activation in other experimental GN models [40–42]. In diabetic conditions, high glucose generates ROS as a result of glucose autooxidation, metabolism, and formation of advanced glycation end production [43]. All these signaling molecules are involved into MAPK signaling pathways in glomerular cells [44]. High-glucose-induced diabetic complications have been implicated, in part, to the activation of MAPK [44]. Interestingly, the stimulation of Ang II by hyperglycemia or oxidative stress activates the MAPK cascade [45]. These results suggest that high-glucose-induced ROS/MAPK pathway and intrarenal RAS activation play key roles in diabetic nephropathy.

3. RAS Activation in a Model of Crescentic GN

Crescentic GN, also known as antiglomerular basement membrane (anti-GBM) disease or Goodpasture's syndrome, is characterized by the formation and deposition of antibodies on the basement membranes of glomeruli and alveoli [46]. The disease progresses rapidly, and patients present with renal failure, dyspnea, hemoptysis, a sudden decrease in hemoglobin level, pallor, and circulatory disturbances. Understanding the underlying proinflammatory responses may help to facilitate the identification of therapeutic targets for arresting the progression of anti-GBM disease. In Wistar-Kyoto (WKY) rats, the administration of a minute dose of anti-GBM antibodies induces severe proliferative and necrotizing GN with crescent formation [47, 48]. In rat models of anti-GBM disease, glomerular infiltration by T lymphocytes, monocytes/macrophages, and some neutrophils is the earliest and most prominent pathologic change [48]. To investigate whether local RAS activation occurs in nephritic glomeruli with crescent formation and whether the final effector molecule Ang II contributes to the induction of ROS and inflammation, as well as glomerular pathologic alterations, we studied the effects of an ARB on rat anti-GBM antibody-induced GN by evaluating indexes of glomerular RAS activation, oxidative stress, inflammation, and TGF-β1 expression in GN rats [49]. Progressive anti-GBM GN was induced in 7-week-old male WKY rats by a single injection of anti-GBM antiserum. Vehicle-treated nephritic rats showed severe proteinuria and developed crescentic GN accompanied by marked macrophage infiltration and enhanced expression of glomerular α-SMA, AGT, Ang II, AT1 receptor, and NADPH oxidase on day 28. Treatment with an ARB improved proteinuria and pathologic alterations such as crescent formation and glomerulosclerosis, and had a significant inhibitory effect on these parameters on day 28 of GN. Enhanced superoxide production in nephritic glomeruli was also decreased by the ARB. Moreover, Ang II and TGF-β1 in the supernatant of cultured glomeruli was increased significantly in vehicle-treated nephritic rats, whereas the production of these compounds was significantly inhibited in ARB-treated rats on day 28. These findings indicate that increased glomerular RAS activity and the resulting increase in Ang II production plays an important role in progressive glomerular injury by inducing oxidative stress and TGF-β1 expression.

Recent studies have revealed that monocyte chemoattractant protein-1 (MCP-1) is involved in the pathogenesis of crescentic GN [50]. MCP-1 is presumed to be a key mediator of chemotaxis and the activation of macrophages [51]. Chronic Ang II infusion in rats activates MCP-1 and

TGF-β1, which in turn induces macrophage infiltration in renal tissues [52]. CC chemokine receptor 2 (CCR2), a cognate receptor of MCP-1 expressed mainly on monocytes, has been reported to be involved in human crescentic GN [53]. Based on these principles, we hypothesized that therapeutic management of anti-GBM disease may be achieved by blocking the MCP-1/CCR2 signaling pathway and RAS [54]. Whereas treatment with a CCR2 antagonist (CA) or ARB alone only moderately ameliorated kidney injury in a rat model of crescentic GN, combination treatment with a CA and an ARB dramatically prevented proteinuria and markedly reduced glomerular crescent formation. Further, combination treatment suppressed macrophage infiltration, reduced MCP-1, AGT, Ang II, and TGF-β1 expression, and reversed the fibrotic change in glomeruli. Primary cultured glomerular MCs stimulated by Ang II showed significant increases in MCP-1 and TGF-β1 expression. Furthermore, a coculture model consisting of MCs, parietal epithelial cells, and macrophages showed an increase in Ang II-induced cell proliferation and collagen secretion. ARB treatment attenuated these effects. These data suggest that Ang II enhances glomerular crescent formation, and inhibition of the MCP-1/CCR2 pathway with a CA/ARB combination effectively reduces renal injury in anti-GBM nephritis.

Recent reports indicated roles of RAS activation and MCP-1/CCR2 pathway in other nephritis models [55–58]. Most studies concluded that activation of RAS is an important determinant of local MCP-1 expression, either directly or indirectly through glomerular hemodynamic effects. However, whether the manipulation of MCP-1/CCR2 pathway and RAS is beneficial with respect to the progression of human and experimental GN remains to be investigated.

4. Conclusion

The present studies reveal that intrarenal RAS activation has important pathophysiologic functions in the development of progressive mesangioproliferative and crescentic GN. Additional studies are needed to determine the relationship between RAS activation and glomerular injury, such as cell proliferation, sclerosis, and crescent formation, and to clarify the mechanisms underlying Ang II-induced pathologic glomerular changes. Furthermore, it is necessary to determine whether RAS inhibition may provide a clinically significant pharmacologic strategy for the therapeutic treatment of progressive GN.

Acknowledgments

The authors acknowledge the critical discussion and/or excellent technical assistance from Maki Shimizu, Masanori Takamatsu, Kenichi Suga, Sato Matuura, Naomi Okamoto (The University of Tokushima Graduate School), and L. Gabriel Navar, Hiroyuki Kobori (Tulane University). These studies were supported by grants-in-aid from the Ministry of Education, Culture, Sports, Science, and Technology of Japan and the National Institute of Diabetes and Digestive and Kidney Diseases and the National Center for Research Resources.

References

[1] L. G. Navar, L. M. Harrison-Bernard, J. D. Imig, C. T. Wang, L. Cervenka, and K. D. Mitchell, "Intrarenal angiotensin II generation and renal effects of AT1 receptor blockade," *Journal of the American Society of Nephrology*, vol. 10, supplement 12, pp. S266–S272, 1999.

[2] H. Kobori, M. Nangaku, L. G. Navar, and A. Nishiyama, "The intrarenal renin-angiotensin system: from physiology to the pathobiology of hypertension and kidney disease," *Pharmacological Reviews*, vol. 59, no. 3, pp. 251–287, 2007.

[3] R. M. Carey and H. M. Siragy, "The intrarenal renin-angiotensin system and diabetic nephropathy," *Trends in Endocrinology and Metabolism*, vol. 14, no. 6, pp. 274–281, 2003.

[4] R. A. S. Santos, A. C. Simoes e Silva, C. Maric et al., "Angiotensin-(1-7) is an endogenous ligand for the G protein-coupled receptor Mas," *Proceedings of the National Academy of Sciences of the United States of America*, vol. 100, no. 14, pp. 8258–8263, 2003.

[5] L. G. Navar, M. C. Prieto-Carrasquero, and H. Kobori, *Chapter 1: Molecular Aspects of the Renal Renin-Angiotensin System*, Taylor & Francis Medical, Oxfordshine, UK, 1st edition, 2006.

[6] V. J. Dzau and R. Re, "Tissue angiotensin system in cardiovascular medicine: a paradigm shift?" *Circulation*, vol. 89, no. 1, pp. 493–498, 1994.

[7] O. Baltatu, J. A. Silva Jr., D. Ganten, and M. Bader, "The brain renin-angiotensin system modulates angiotensin II-induced hypertension and cardiac hypertrophy," *Hypertension*, vol. 35, no. 1, part 2, pp. 409–412, 2000.

[8] L. J. Dell'Italia, Q. C. Meng, E. Balcells et al., "Compartmentalization of angiotensin II generation in the dog heart: evidence for independent mechanisms in intravascular and interstitial spaces," *Journal of Clinical Investigation*, vol. 100, no. 2, pp. 253–258, 1997.

[9] G. Mazzocchi, L. K. Malendowicz, A. Markowska, G. Albertin, and G. G. Nussdorfer, "Role of adrenal renin-angiotensin system in the control of aldosterone secretion in sodium-restricted rats," *American Journal of Physiology*, vol. 278, no. 6, pp. E1027–E1030, 2000.

[10] K. K. Griendling, C. A. Minieri, J. D. Ollerenshaw, and R. W. Alexander, "Angiotensin II stimulates NADH and NADPH oxidase activity in cultured vascular smooth muscle cells," *Circulation Research*, vol. 74, no. 6, pp. 1141–1148, 1994.

[11] A. H. J. Danser, P. J. J. Admiraal, F. H. M. Derkx, and M. A. D. H. Schalekamp, "Angiotensin I-to-II conversion in the human renal vascular bed," *Journal of Hypertension*, vol. 16, no. 12, part 2, pp. 2051–2056, 1998.

[12] L. G. Navar, L. M. Harrison-Bernard, A. Nishiyama, and H. Kobori, "Regulation of intrarenal angiotensin II in hypertension," *Hypertension*, vol. 39, no. 2, part 2, pp. 316–322, 2002.

[13] A. R. Brasier and J. Li, "Mechanisms for inducible control of angiotensinogen gene transcription," *Hypertension*, vol. 27, no. 3, part 2, pp. 465–475, 1996.

[14] W. L. Henrich, E. A. McAllister, A. Eskue, T. Miller, and O. W. Moe, "Renin regulation in cultured proximal tubular cells," *Hypertension*, vol. 27, no. 6, pp. 1337–1340, 1996.

[15] M. Sibony, J. M. Gasc, F. Soubrier, F. Alhenc-Gelas, and P. Corvol, "Gene expression and tissue localization of the two isoforms of angiotensin I converting enzyme," *Hypertension*, vol. 21, no. 6, part 1, pp. 827–835, 1993.

[16] C. P. Vío and V. A. Jeanneret, "Local induction of angiotensin-converting enzyme in the kidney as a mechanism of progressive renal diseases," *Kidney International, Supplement*, vol. 64, no. 86, pp. S57–S63, 2003.

[17] D. E. Casarini, M. A. Boim, R. C. R. Stella, M. H. Krieger-Azzolini, J. E. Krieger, and N. Schor, "Angiotensin I-converting enzyme activity in tubular fluid along the rat nephron," *American Journal of Physiology*, vol. 272, no. 3, part 2, pp. F405–F409, 1997.

[18] D. E. Kohan, "Angiotensin II and endothelin in chronic glomerulonephritis," *Kidney International*, vol. 54, no. 2, pp. 646–647, 1998.

[19] M. Urushihara and H. Kobori, "Angiotensinogen expression is enhanced in the progression of glomerular disease," *International Journal of Clinical Medicine*, vol. 2, no. 4, pp. 378–387, 2011.

[20] Y. Horita, M. Tadokoro, K. Taura et al., "Low-dose combination therapy with temocapril and losartan reduces proteinuria in normotensive patients with immunoglobulin A nephropathy," *Hypertension Research*, vol. 27, no. 12, pp. 963–970, 2004.

[21] P. Ruggenenti, A. Perna, G. Gherardi, F. Gaspari, R. Benini, and G. Remuzzi, "Renal function and requirement for dialysis in chronic nephropathy patients on long-term ramipril: REIN follow-up trial," *The Lancet*, vol. 352, no. 9136, pp. 1252–1256, 1998.

[22] M. Ishizaki, Y. Masuda, and Y. Fukuda, "Experimental mesangioproliferative glomerulonephritis in rats induced by intravenous administration of anti-thymocyte serum," *Acta Pathologica Japonica*, vol. 36, no. 8, pp. 1191–1203, 1986.

[23] N. Sakai, K. Iseki, S. Suzuki et al., "Uninephrectomy induces progressive glomerulosclerosis and apoptosis in anti-Thy1 glomerulonephritis," *Pathology International*, vol. 55, no. 1, pp. 19–26, 2005.

[24] H. Kawachi, T. Iwanaga, S. Toyabe, T. Oite, and F. Shimizu, "Mesangial sclerotic change with persistent proteinuria in rats after two consecutive injections of monoclonal antibody 1-22-3," *Clinical and Experimental Immunology*, vol. 90, no. 1, pp. 129–134, 1992.

[25] T. Nakamura, J. E. Obata, H. Kimura et al., "Blocking angiotensin II ameliorates proteinuria and glomerular lesions in progressive mesangioproliferative glomerulonephritis," *Kidney International*, vol. 55, no. 3, pp. 877–889, 1999.

[26] S. Kondo, M. Shimizu, M. Urushihara et al., "Addition of the antioxidant probucol to angiotensin II type I receptor antagonist arrests progressive mesangioproliferative glomerulonephritis in the rat," *Journal of the American Society of Nephrology*, vol. 17, no. 3, pp. 783–794, 2006.

[27] S. A. Gaertner, U. Janssen, T. Ostendorf, K. M. Koch, J. Floege, and W. Gwinner, "Glomerular oxidative and antioxidative systems in experimental mesangioproliferative glomerulonephritis," *Journal of the American Society of Nephrology*, vol. 13, no. 12, pp. 2930–2937, 2002.

[28] M. N. Budisavljevic, L. Hodge, K. Barber et al., "Oxidative stress in the pathogenesis of experimental mesangial proliferative glomerulonephritis," *American Journal of Physiology*, vol. 285, no. 6, pp. F1138–F1148, 2003.

[29] Y. Gorin, J. M. Ricono, B. Wagner et al., "Angiotensin II-induced ERK1/ERK2 activation and protein synthesis are redox-dependent in glomerular mesangial cells," *Biochemical Journal*, vol. 381, part 1, pp. 231–239, 2004.

[30] M. Shibanuma, J. I. Mashimo, T. Kuroki, and K. Nose, "Characterization of the TGFβ1-inducible hic-5 gene that encodes a putative novel zinc finger protein and its possible involvement in cellular senescence," *Journal of Biological Chemistry*, vol. 269, no. 43, pp. 26767–26774, 1994.

[31] M. Matsuya, H. Sasaki, H. Aoto et al., "Cell adhesion kinase β forms a complex with a new member, Hic-5, of proteins localized at focal adhesions," *Journal of Biological Chemistry*, vol. 273, no. 2, pp. 1003–1014, 1998.

[32] D. A. Tumbarello and C. E. Turner, "Hic-5 contributes to epithelial-mesenchymal transformation through a RhoA/ROCK-dependent pathway," *Journal of Cellular Physiology*, vol. 211, no. 3, pp. 736–747, 2007.

[33] G. Dabiri, D. A. Tumbarello, C. E. Turner, and L. Van de Water, "Hic-5 promotes the hypertrophic scar myofibroblast phenotype by regulating the TGF-β1 autocrine loop," *Journal of Investigative Dermatology*, vol. 128, no. 10, pp. 2518–2525, 2008.

[34] K. Suga, S. Kondo, S. Matsuura et al., "Glomerular expression of hydrogen peroxide inducible clone-5 in human and rat progressive mesagnial proliferative glomerulonephritis," *Nephron Experimental Nephrology*, vol. 120, no. 2, pp. e59–e68, 2012.

[35] S. Nishimoto and E. Nishida, "MAPK signalling: ERK5 versus ERK1/2," *EMBO Reports*, vol. 7, no. 8, pp. 782–786, 2006.

[36] D. Bokemeyer, D. Panek, H. J. Kramer et al., "In vivo identification of the mitogen-activated protein kinase cascade as a central pathogenic pathway in experimental mesangioproliferative glomerulonephritis," *Journal of the American Society of Nephrology*, vol. 13, no. 6, pp. 1473–1480, 2002.

[37] T. Masaki, C. Stambe, P. A. Hill, J. Dowling, R. C. Atkins, and D. J. Nikolic-Paterson, "Activation of the extracellular-signal regulated protein kinase pathway in human glomerulopathies," *Journal of the American Society of Nephrology*, vol. 15, no. 7, pp. 1835–1843, 2004.

[38] Y. Suzaki, M. Yoshizumi, S. Kagami et al., "BMK1 is activated in glomeruli of diabetic rats and in mesangial cells by high glucose conditions," *Kidney International*, vol. 65, no. 5, pp. 1749–1760, 2004.

[39] M. Urushihara, M. Takamatsu, M. Shimizu et al., "ERK5 activation enhances mesangial cell viability and collagen matrix accumulation in rat progressive glomerulonephritis," *American Journal of Physiology Renal Physiology*, vol. 298, no. 1, pp. F167–F176, 2009.

[40] H. Okada, T. Inoue, T. Kikuta et al., "A possible anti-inflammatory role of angiotensin II type 2 receptor in immune-mediated glomerulonephritis during type 1 receptor blockade," *American Journal of Pathology*, vol. 169, no. 5, pp. 1577–1589, 2006.

[41] N. Ohashi, M. Urushihara, R. Satou, and H. Kobori, "Glomerular angiotensinogen is induced in mesangial cells in diabetic rats via reactive oxygen speciesERK/JNK pathways," *Hypertension Research*, vol. 33, no. 11, pp. 1174–1181, 2010.

[42] A. P. Lakshmanan, R. A. Thandavarayan, K. Watanabe et al., "Modulation of AT-1R/MAPK cascade by an olmesartan treatment attenuates diabetic nephropathy in streptozotocin-induced diabetic mice," *Molecular and cellular endocrinology*, vol. 348, no. 1, pp. 104–111, 2012.

[43] H. Ha and Hi Bahl Lee, "Reactive oxygen species as glucose signaling molecules in mesangial cells cultured under high glucose," *Kidney International, Supplement*, vol. 58, no. 77, pp. S19–S25, 2000.

[44] D. R. Tomlinson, "Mitogen-activated protein kinases as glucose transducers for diabetic complications," *Diabetologia*, vol. 42, no. 11, pp. 1271–1281, 1999.

[45] E. Tsiani, P. Lekas, I. G. Fantus et al., "High glucose-enhanced activation of mesangial cell p38 MAPK by ET-1, ANG II, and platelet-derived growth factor," *American Journal of Physiology*, vol. 282, no. 1, pp. E161–E169, 2002.

[46] B. G. Hudson, K. Tryggvason, M. Sundaramoorthy, and E. G. Neilson, "Alport's syndrome, Goodpasture's syndrome, and

type IV collagen," *The New England Journal of Medicine*, vol. 348, no. 25, pp. 2543–2556, 2003.

[47] M. Shimizu, S. Kondo, M. Urushihara et al., "Role of integrin-linked kinase in epithelial-mesenchymal transition in crescent formation of experimental glomerulonephritis," *Nephrology Dialysis Transplantation*, vol. 21, no. 9, pp. 2380–2390, 2006.

[48] T. Wada, H. Yokoyama, K. Furuichi et al., "Intervention of crescentic glomerulonephritis by antibodies to monocyte chemotactic and activating factor (MCAF/MCP-1)," *The FASEB Journal*, vol. 10, no. 12, pp. 1418–1425, 1996.

[49] Y. Kinoshita, S. Kondo, M. Urushihara et al., "Angiotensin II type I receptor blockade suppresses glomerular renin-angiotensin system activation, oxidative stress, and progressive glomerular injury in rat anti-glomerular basement membrane glomerulonephritis," *Translational Research*, vol. 158, no. 4, pp. 235–248, 2011.

[50] T. Wada, K. Furuichi, N. Sakai et al., "A new anti-inflammatory compound, FR167653, ameliorates crescentic glomerulonephritis in Wistar-Kyoto rats," *Journal of the American Society of Nephrology*, vol. 11, no. 8, pp. 1534–1541, 2000.

[51] K. Matsushima, C. G. Larsen, G. C. DuBois, and J. J. Oppenheim, "Purification and characterization of a novel monocyte chemotactic and activating factor produced by a human myelomonocytic cell line," *Journal of Experimental Medicine*, vol. 169, no. 4, pp. 1485–1490, 1989.

[52] Y. Ozawa, H. Kobori, Y. Suzaki, and L. G. Navar, "Sustained renal interstitial macrophage infiltration following chronic angiotensin II infusions," *The American Journal of Physiology*, vol. 292, no. 1, pp. F330–F339, 2007.

[53] S. Segerer, Y. Cui, K. L. Hudkins et al., "Expression of the chemokine monocyte chemoattractant protein-1 and its receptor chemokine receptor 2 in human crescentic glomerulonephritis," *Journal of the American Society of Nephrology*, vol. 11, no. 12, pp. 2231–2242, 2000.

[54] M. Urushihara, N. Ohashi, K. Miyata, R. Satou, O. W. Acres, and H. Kobori, "Addition of angiotensin II Type 1 receptor blocker to CCR2 antagonist markedly attenuates crescentic glomerulonephritis," *Hypertension*, vol. 57, no. 3, pp. 586–593, 2011.

[55] T. Wada, K. Matsushima, and K. I. Kobayashi, "Monocyte chemoattractant protein-1: does it play a role in diabetic nephropathy?" *Nephrology Dialysis Transplantation*, vol. 18, no. 3, pp. 457–459, 2003.

[56] S. Kato, V. A. Luyckx, M. Ots et al., "Renin-angiotensin blockade lowers MCP-1 expression in diabetic rats," *Kidney International*, vol. 56, no. 3, pp. 1037–1048, 1999.

[57] C. Zoja, D. Corna, D. Rottoli et al., "Effect of combining ACE inhibitor and statin in severe experimental nephropathy," *Kidney International*, vol. 61, no. 5, pp. 1635–1645, 2002.

[58] Y. M. Chen, M. I. Hu-Tsai, S. L. Lin, T. J. Tsai, and B. S. Hsieh, "Expression of CX3CL1/fractalkine by mesangial cells in vitro and in acute anti-Thy1 glomerulonephritis in rats," *Nephrology Dialysis Transplantation*, vol. 18, no. 12, pp. 2505–2514, 2003.

Hindawi Publishing Corporation
Journal of Biomedicine and Biotechnology
Volume 2012, Article ID 541245, 7 pages
doi:10.1155/2012/541245

Research Article

Nuclear Expression of a Mitochondrial DNA Gene: Mitochondrial Targeting of Allotopically Expressed Mutant ATP6 in Transgenic Mice

David A. Dunn and Carl A. Pinkert

Department of Pathobiology, College of Veterinary Medicine, Auburn University, 212 Samford Hall, Auburn, AL 36849, USA

Correspondence should be addressed to Carl A. Pinkert, cap@auburn.edu

Received 10 January 2012; Revised 13 April 2012; Accepted 16 April 2012

Academic Editor: Oreste Gualillo

Nuclear encoding of mitochondrial DNA transgenes followed by mitochondrial targeting of the expressed proteins (allotopic expression; AE) represents a potentially powerful strategy for creating animal models of mtDNA disease. Mice were created that allotopically express either a mutant (A6M) or wildtype (A6W) *mt-Atp6* transgene. Compared to non-transgenic controls, A6M mice displayed neuromuscular and motor deficiencies (wire hang, pole, and balance beam analyses; $P < 0.05$), no locomotor differences (gait analysis; $P < 0.05$) and enhanced endurance in Rota-Rod evaluations ($P < 0.05$). A6W mice exhibited inferior muscle strength (wire hang test; $P < 0.05$), no difference in balance beam footsteps, accelerating Rota-Rod, pole test and gait analyses; ($P < 0.05$) and superior performance in balance beam time-to-cross and constant velocity Rota-Rod analyses ($P < 0.05$) in comparison to non-transgenic control mice. Mice of both transgenic lines did not differ from non-transgenic controls in a number of bioenergetic and biochemical tests including measurements of serum lactate and mitochondrial MnSOD protein levels, ATP synthesis rate, and oxygen consumption ($P > 0.05$). This study illustrates a mouse model capable of circumventing *in vivo* mitochondrial mutations. Moreover, it provides evidence supporting AE as a tool for mtDNA disease research with implications in development of DNA-based therapeutics.

1. Introduction

Throughout mitochondrial evolution, gene transfer from the mitochondrial compartment to the nucleus has been an ongoing process [1]. Through AE, this phenomenon is replicated in the laboratory. AE gene therapy was postulated as a strategy for correcting diseases involving mitochondrial DNA (mtDNA) mutation [2, 3] and as a means to overcome the scarcity of animal models for diseases caused by mitochondrial DNA mutations [4, 5]. AE was shown to occur in cultured cells [6–9] and in somatic tissues following delivery via viral vector [10, 11]. Here, we report the first germline competent transgenic model of AE.

Transversion of T to G at position 8993 of the human mitochondrial genome causes substitution of arginine for a conserved leucine in residue 156 (L156R) of the mitochondrial encoded MT-ATP6 gene [12]. This gives rise to Neuropathy, Ataxia and Retinitis Pigmentosa (NARP) [13], and Maternally Inherited Leigh Syndrome (MILS) [14] disease states. Expression of a recoded mutated *Atp6* in mice was postulated to bring about mitochondrial and functional deficits similar to those seen in human patients. To test this hypothesis, two versions of a nuclear-coded mouse *Atp6* gene element were expressed in transgenic mice. Our initial transgenic mouse model coded for the protein sequence of the wild-type murine *Atp6*. The second model encoded the same sequence with the exception of amino acid 156 where leucine was replaced with an arginine residue. Mitochondrial physiology and motor function were assessed in resultant transgenic lineages.

2. Materials and Methods

2.1. Gene Synthesis. Two forms of the nuclear-coded mitochondrial *Atp6* gene were synthesized *de novo*. Gene

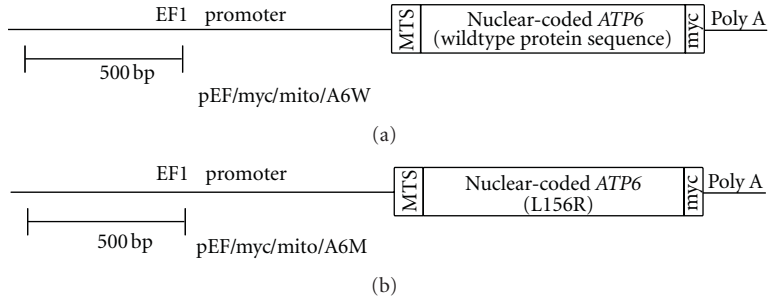

Figure 1: Schematic representation of AE DNA constructs. High-level transcription is driven by the human EF1α promoter. Protein-coding elements include the N-terminal mitochondrial transport signal of human cytochrome oxidase VIII, nuclear-coded wild-type (a) or mutant (b) mouse Atp6 gene sequence and a C-terminal myc epitope tag.

synthesis was performed using a three-step polymerase chain reaction (PCR)-based technique [15]. *Atp6* genes were synthesized coding for murine wild-type and mutated amino acid sequences (L156R) using nuclear codons. Oligonucleotides/primers (25nt) spanned forward and reverse sequences to be synthesized.

2.2. Plasmid Cloning/Transgenic Mouse Production. Synthesized *Atp6* DNAs were cloned in frame into the pEF/ *myc*/ mito plasmid (Invitrogen). Elements in this expression system include the promoter for human EF-1α [16], the mitochondrial targeting sequence from the human cytochrome c oxidase subunit VIII gene[17], and an in-frame 3′ myc epitope tag [18] (Figure 1). This gave rise to two plasmids, pEF/myc/mito/A6W and pEF/myc/mito/A6M procedures for generating transgenic mice were as described [19]. A6M and A6W transgenic mice were produced on C57BL/6 and B6(B6SJLF1) genetic backgrounds, respectively. Mice were genotyped by PCR analysis; forward and reverse primers were 5′tggccattccactatggg3′and 5′gatggctggcaactagaagg3′; expected amplification product size was 473 bp. All mouse procedures were approved by the Auburn University Institutional Animal Care and Use Committee.

2.3. Transmission Electron Microscopy. Electron microscopy was performed to analyze mitochondrial localization of allotopically expressed ATP6. Anaesthetized mice were perfused with 3% paraformaldehyde and 0.2% glutaraldehyde. Striatum was diced into 1-2 mm pieces and fixed in the same perfusion solution for 30–40 min. Tissue was rinsed, dehydrated in a graded ethanol series, and embedded in LR White Medium Grade Resin (Electron Microscopy Sciences). Immune labeling of sections utilized 1 : 4000 rabbit polyclonal anti-myc antibody (Abcam) with 1 : 100 donkey anti-rabbit Ultrasmall gold (Aurion) (diameter of average gold cluster <0.8 nm) as secondary label. R-Gent SE-EM (Aurion) was utilized for silver enhancement of samples.

2.4. Motor Assays. Forty mice were subjected to all motor tests. Groups of 5 males and 5 females were hemizygous A6M and nontransgenic (C57BL/6), hemizygous A6W and nontransgenic (B6(B6SJL)). All neuromuscular and motor tests followed a paradigm outlined earlier [20] and as detailed below. Motor-testing analyses were initiated at weaning (21 days of age) and progressed until completion in the order described below. All neuromuscular and motor tests were performed blinded as to the genotype of the mouse being tested. Motor testing commenced with the wire hang test, followed by the balance beam test, constant velocity Rota-Rod, accelerating Rota-Rod, pole test, and gait test.

2.5. Wire Hang Test. Neuromuscular strength was measured using a wire hang test [20]. Latency to fall was recorded with a maximum time of 240 sec. Experimental data collection began immediately without mouse training sessions. Twelve trials were completed for each mouse consisting of four trials per day over a three-day period; each trial was separated by at least 20 min.

2.6. Balance Beam Test. Motor coordination was tested using a balance beam [21]. Six beams of different sizes included three square beams with 28, 12, and 5 mm widths and three round beams with 27, 17, and 11 mm diameters. Data were collected in two trials for each of the six beams. Latency to cross the beam into the escape box and footslips was recorded.

2.7. Rota-Rod Test. Two analyses were performed using a Rota-Rod apparatus [20]. In the first analysis, mice ran on the Rota-Rod at a constant rotational velocity of 36 RPM for a maximum of 240 sec. In the second, rotational velocity gradually increased from 5 to 40 RPM over a period of 300 sec. In both analyses, latency to fall was measured. Data collection proceeded over a three-day period with four trials performed each day separated by 30 min intervals.

2.8. Pole Test. Motor coordination was evaluated with a pole test apparatus [20]. Mice were placed head-up near the top of the pole. Latency to turn 180 degrees and reach the base of the 50 cm pole was measured with a maximum time of 240 sec. Data collection continued over the course of three days with four trials performed each day separated by 15 min intervals.

2.9. Gait Analysis. Gait was assessed as described [21]. Nontoxic paint was applied to paws, and the mice were allowed to run the length of a 50 cm chute at a 30° incline into an escape box. Distances between footfalls were measured.

2.10. Biochemical Assays. Following motor testing, all mice were subjected to a series of biochemical tests. ATP synthesis and respirometry assays were performed the same day as mitochondrial isolation; remaining mitochondria and sera were frozen for lactate and SOD measurements. Mitochondrial isolation and ATP synthesis and respirometry tests were performed on 10 groups of four mice each. Each group contained one A6M hemizygous, one A6M nontransgenic, one A6W hemizygous, and one A6W nontransgenic mouse. A6M transgenic and wild-type mice were euthanized and samples taken at a mean age of 58.7 ± 1.3 and 57.8 ± 1.6 weeks, and at 28.9 ± 5.3 and 46.0 ± 3.3 weeks for A6W transgenic and wild-type mice, respectively.

2.11. Mitochondrial Isolation. Mitochondria were isolated from whole brain, heart, and gastrocnemius muscle as previously reported [22].

2.12. Oxygen Consumption. Aerobic respiration of isolated mitochondria was measured using MitoXpress A65N-1 (Luxcel) [23] in 96 well plates with an Infinite M200 plate reader (Tecan). 100 μg mitochondria were incubated with 12.5 mM of glutamate and malate (States II and III) and 1.65 mM ADP (State III only) in a total volume of 100 μL. State II values were obtained by measuring oxygen consumption in the absence of ADP; State III was measured with ADP present. Respiratory control ratio (RCR) values were calculated by dividing State III values by State II values.

2.13. ATP Synthesis Assay. ATP production rate was measured using the chemiluminescent ATP-consuming reaction of Luciferase-Luciferin [24]. ATP consumption values were calculated by comparing luminescence of a standard ATP concentration curve to luminescent kinetics in the experimental reaction.

2.14. MnSOD Protein Levels. Protein measurements of manganese superoxide dismutase (MnSOD, SOD2) were generated with a SOD2 Protein Quantity Microplate Assay Kit (MitoSciences) ELISA.

2.15. Serum Lactate Assay. Lactate was measured in serum of all experimental mice using the Lactate Colorimetric Assay Kit (Abcam). All samples were measured in duplicate.

2.16. Statistical Analyses. All statistical analyses were performed using SAS software (SAS Institute). Hazard ratios (HRs) with 95% confidence intervals were generated for all measurements that produced censored values (wire hang, balance beam time, Rota-Rod and pole measurements) by proportional hazards regression analysis using PROC PHREG. Analysis of gait measurements was performed with repeated measures modeling using PROC MIXED. P values of gait measurements were manually corrected using the Bonferroni method. Odds ratios (OR) were calculated with 95% confidence intervals for balance beam slips analyses with logistic regression using PROC LOGISTIC. t-test analyses of oxygen consumption, ATP synthesis, MnSOD and lactate measurements were performed using Proc t-test. All data subjected to t-test analysis were presented as mean ± SE.

3. Results and Discussion

Two synthesized, nuclear-coded ATP6 genes were each cloned into vectors containing a high-level constitutive EF-1α promoter, mitochondrial transport signal, myc epitope tag, and polyadenylation signal (Figure 1).

The A6M expression construct was injected into 263 C57BL/6 and 97 B6(B6SJLF1) embryos from which 3 C57BL/6 and 7 B6(B6SJLF1) transgenic founder mice were derived. The A6W expression construct was injected into 112 C57BL/6 and 78 B6(B6SJLF1) embryos from which 0 C57BL/6 and 5 B6(B6SJLF1) transgenic founder mice resulted. One line of transgenic mice for each construct was selected for further characterization based on transgene expression and fertility in founder transgenic mice.

Allotopically expressed proteins from both A6M and A6W lineages were found to colocalize with mitochondria in electron micrographs of striatum sections (Figure 2). Thus, nuclear expression of a mitochondrial gene can result in mitochondrial localization of the cytoplasmically translated protein.

A6M and A6W mice were compared to nontransgenic control mice in a series of neuromuscular and motor assays (Table 1). In wire hang testing, A6M and A6W mice did not perform as well as nontransgenic control mice (A6M: $P = 0.0008$; A6W: $P = 0.002$). Analysis of the time to cross balance beams into an escape box showed that A6M mice performed inferior to nontransgenic controls ($P = 0.0004$), while A6W mice displayed superior performance compared to control mice $P = 0.0067$. Analysis of foot slips in balance beam testing indicated a greater degree of slips by A6M mice than control mice ($P = 0.0191$), but no differences were seen in A6W mice ($P = 0.6305$). A6M and A6W mice both outperformed their respective controls in Rota-Rod testing at a constant rotational velocity (A6M: $P < 0.0001$; A6W: $P = 0.0002$). A6M animals displayed superior performance in accelerating Rota-Rod analyses ($P < 0.0001$) while A6W mice were not different from their nontransgenic counterparts ($P = 0.72$). In the pole test, A6M mice did not perform as well as controls ($P = 0.022$) and A6W mice were not different than controls ($P = 0.46$). Gait analyses did not detect any gait differences in either transgenic line (Bonferroni-corrected P values range from 0.36 to 1.0 over several measures).

Of the parameters measured in this group of tests (wire hang, beam time, beam slips, constant Rota-Rod, accelerating Rota-Rod, pole test, gait), A6M mice displayed performance inferior to control mice in four out of seven tests while A6W mice displayed inferior performance to their controls in a single analysis. Additionally, both A6M and

Table 1: Motor and biochemical analyses of A6M and A6W transgenic mice. Hazard and odds ratios are expressed with 95% confidence intervals (95% CI) and P values. Biochemical data are expressed as mean ± standard error of the mean (SE).

	A6M	A6W
Wirehang hazard ratio (95% CI)	HR: 0.54 (0.376–0.770) $P = 0.0008$	HR: 0.424 (0.246–0.731) $P = 0.002$
BB slips/crossing odds ratio (95% CI)	OR: 0.12 (0.021–0.709) $P = 0.0191$	OR: 0.68 (0.141–3.276) $P = 0.6305$
BB time hazard ratio (95% CI)	HR: 1.72 (1.274–2.309) $P = 0.0004$	HR: 0.67 (0.506–0.896) $P = 0.0067$
Constant Rota-Rod hazard ratio (95% CI)	HR: 2.28 (1.722–3.030) $P < 0.0001$	HR: 2.09 (1.414–3.097) $P = 0.0002$
Accelerating Rota-Rod hazard ratio (95% CI)	HR: 2.37 (1.589–3.523) $P < 0.0001$	HR: 1.09 (0.681–1.739) $P = 0.72$
Poletest hazard ratio (95% CI)	HR: 1.50 (1.156–1.941) $P = 0.0022$	HR: 1.10 (0.860–1.399) $P = 0.46$
Gait		
LF-LF	$P = 1.0$	$P = 1.0$
LF-LR	$P = 1.0$	$P = 1.0$
LF-RF	$P = 1.0$	$P = 1.0$
LR-LR	$P = 1.0$	$P = 1.0$
LR-RR	$P = 1.0$	$P = 1.0$
RF-RF	$P = 1.0$	$P = 1.0$
RF-RR	$P = 1.0$	$P = 1.0$
RR-RR	$P = 0.36$	$P = 1.0$
Brain state II (nmol O_2/min/mg protein ± SE)	Transgenic: 10.1 ± 1.2 Nontransgenic: 8.9 ± 1.9 $P = 0.6094$	Transgenic: 7.5 ± 0.7 Nontransgenic: 8.5 ± 0.8 $P = 0.3149$
Heart state II (nmol O_2/min/mg protein ± SE)	Transgenic: 20.2 ± 1.3 Nontransgenic: 21.5 ± 1.6 $P = 0.5291$	Transgenic: 21.1 ± 1.3 Nontransgenic: 21.1 ± 1.2 $P = 0.9634$
Skeletal muscle state II (nmol O_2/min/mg protein ± SE)	Transgenic: 14.5 ± 1.7 Nontransgenic: 16.3 ± 1.8 $P = 0.4672$	Transgenic: 15.4 ± 1.3 Nontransgenic: 14.6 ± 1.2 $P = 0.6687$
Brain state III (nmol O_2/min/mg protein ± SE)	Transgenic: 24.2 ± 2.7 Nontransgenic: 23.1 ± 1.2 $P = 0.7128$	Transgenic: 20.3 ± 1.1 Nontransgenic: 24.0 ± 2.2 $P = 0.1508$
Heart state III (nmol O_2/min/mg protein ± SE)	Transgenic: 31.4 ± 2.0 Nontransgenic: 33.1 ± 3.0 $P = 0.5965$	Transgenic: 31.6 ± 2.1 Nontransgenic: 32.8 ± 1.9 $P = 0.6910$
Skeletal muscle state III (nmol O_2/min/mg protein ± SE)	Transgenic: 35.1 ± 3.5 Nontransgenic: 34.7 ± 4.0 $P = 0.9438$	Transgenic: 34.4 ± 3.7 Nontransgenic: 31.0 ± 2.6 $P = 0.5882$
Brain respiratory control ratio	Transgenic: 2.48 ± 0.18 Nontransgenic: 3.19 ± 0.41 $P = 0.1458$	Transgenic: 2.84 ± 0.21 Nontransgenic: 3.01 ± 0.41 $P = 0.7192$
Heart respiratory control ratio	Transgenic: 1.57 ± 0.08 Nontransgenic: 1.53 ± 0.05 $P = 0.6707$	Transgenic: 1.51 ± 0.06 Nontransgenic: 1.58 ± 0.11 $P = 0.5530$
Skeletal muscle respiratory control ratio	Transgenic: 2.59 ± 0.26 Nontransgenic: 2.16 ± 0.12 $P = 0.1595$	Transgenic: 2.24 ± 0.17 Nontransgenic: 2.20 ± 0.11 $P = 0.8709$

Table 1: Continued.

	A6M	A6W
Brain ATP synthesis (nmol/min/mg protein)	Transgenic: 60 ± 2.0 Nontransgenic: 64 ± 6.7 $P = 0.5991$	Transgenic: 65 ± 7.9 Nontransgenic: 62 ± 4.9 $P = 0.7143$
Heart ATP synthesis (nmol/min/mg protein)	Transgenic: 64 ± 10.8 Nontransgenic: 58 ± 5.7 $P = 0.6006$	Transgenic: 68 ± 8.3 Nontransgenic: 65 ± 4.7 $P = 0.7549$
Skeletal muscle ATP synthesis (nmol/min/mg protein)	Transgenic: 36 ± 2.9 Nontransgenic: 40 ± 3.6 $P = 0.4167$	Transgenic: 38 ± 2.1 Nontransgenic: 37 ± 2.3 $P = 0.6902$
Brain MnSOD protein levels (arbitrary colorimetric values)	Transgenic: 4.6 ± 0.66 Nontransgenic: 5.2 ± 0.47 $P = 0.4098$	Transgenic: 5.4 ± 1.11 Nontransgenic: 4.2 ± 0.39 $P = 0.3514$
Heart MnSOD protein levels arbitrary colorimetric values)	Transgenic: 3.7 ± 0.11 Nontransgenic: 4.0 ± 0.15 $P = 0.2691$	Transgenic: 4.6 ± 0.33 Nontransgenic: 4.2 ± 0.13 $P = 0.2569$
Skeletal muscle MnSOD protein levels (arbitrary colorimetric values)	Transgenic: 5.1 ± 0.93 Nontransgenic: 5.0 ± 0.57 $P = 0.9361$	Transgenic: 3.9 ± 0.35 Nontransgenic: 3.9 ± 0.46 $P = 0.9590$
Serum lactate (mM)	Transgenic: 11.2 ± 0.83 Nontransgenic: 12.5 ± 0.83 $P = 0.2073$	Transgenic: 9.6 ± 0.51 Nontransgenic: 11.6 ± 0.73 $P = 0.0370$

LF: left front; LR: left rear; RF: right front; RR: right rear.

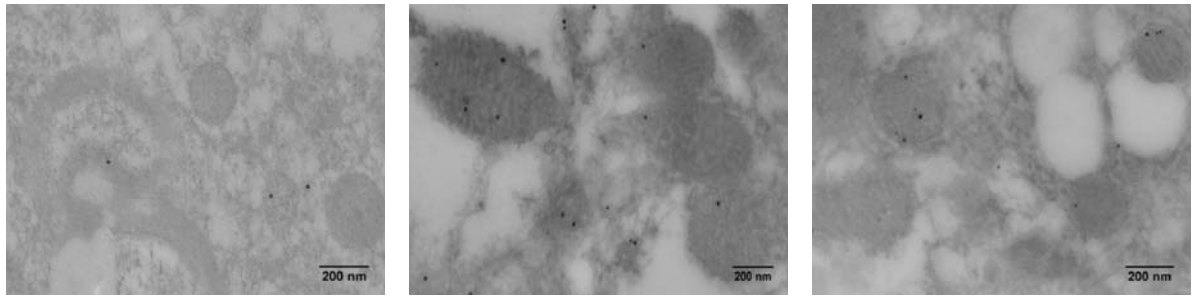

Figure 2: Mitochondrial localization of allotopically expressed ATP6 in brain sections of nontransgenic, A6M and A6W mice. The small amount of cytosolic nonmitochondrial staining is not unexpected as proteins are cytoplasmically translated prior to mitochondrial translocalization.

A6W mice displayed enhanced performance in two measures in comparison to their controls. The superior performance of A6M mice in all Rota-Rod analyses, while surprising, might be explained by differences in what is measured in each test on a physiological or tissue level. This discrepancy of A6M Rota-Rod results versus the other tests suggests that further study and characterization of the functional consequences of allotopic expression of mitochondrial genes is warranted.

A6M transgenic and wild-type mice were euthanized and samples taken at a mean age of 58.7 ± 1.3 and 57.8 ± 1.6 weeks ($P = 0.667$), and at 28.9 ± 5.3 and 46.0 ± 3.3 ($P = 0.014$) weeks for A6W transgenic and wild-type mice. Mitochondria from brain, heart and muscle tissues, and serum from the same mice that underwent motor testing were collected and subjected to a series of biochemical and physiological tests (Table 1). In oxygen utilization studies, State II, III, and RCR measurements showed no difference between mitochondria from A6M and A6W mice and their respective controls ($P > 0.05$). The rate of ATP synthesis in mitochondria isolated from A6M and A6W mice did not differ from that of mitochondria from nontransgenic control mice ($P > 0.05$). Protein levels of MnSOD in mitochondria also did not differ between either transgenic line and its respective control ($P > 0.05$). Serum concentrations of lactic acid were

not different between A6M mice and nontransgenic control mice ($P = 0.297$), but A6W hemizygous mice had lower lactate concentrations than nontransgenic control mice ($P = 0.037$). Dissimilarities in A6W serum lactate concentrations might be due to differences in age at time of euthanasia.

The absence of detectable differences in mitochondrial function between transgenic mice and their nontransgenic counterparts was somewhat surprising in light of the clear differences seen in motor function in A6M mice. These discrepancies may reflect a reduction of stress due to the lag time between the end of motor tests and commencement of mitochondrial isolation. Alternatively, levels of allotopically expressed L156R ATP6 protein in mitochondria might vary during an individual's lifespan such that differences in ATP synthesis that are undetectable in adult mice are of sufficient magnitude in fetal and/or postnatal development to cause a change in developmental trajectory that results in the functional differences observed. Future experiments on mice that undergo motor analysis and functional strain immediately prior to biochemical analysis might yield different results. The experiments reported here using genetically defined mice might yield different results with modified genetic and/or environmental variables.

4. Conclusion

While mtDNA mutations are primary etiologic agents in mitochondrial disease, pathogenic phenotypes are intensified or attenuated by numerous secondary factors including background mtDNA sequence [25], nuclear genetic and environmental influences [26]. The utility of the transgenic approach in allotopic expression of mitochondrial genes is shown here to be successful in delivery of protein derived from a nuclear transcript to mitochondria. Phenotypic characterization of mice carrying a mutant *ATP6* yielded mixed results. In some tests, functional motor deficiencies similar to those seen in human NARP patients were seen, while enhanced performance was observed in others.

The results of these experiments have implications for the potential future use of allotopic expression as a strategy for gene therapy. Nuclear expression of one or more mitochondrial genes in a clinical setting could improve mitochondrial function in the context of mitochondrial disease. This modeling might also provide an effective method for protecting the 13 genes encoded on the mitochondrial genome from the oxidative damage that results from normal aging, age-related neurodegenerative diseases and other pathological states shown to have mitochondrial involvement.

Acknowledgments

The authors thank M. H. Irwin, M. V. Cannon, and K. Parameshwaran for helpful discussion and critical project reviews, S. Agnew, L. Buchanan, J. DeFoor, C. Goracke, R. McFarlin, P. Rubinstein, M. Isaacson, A. Parnell, C. Shafferman, S. Widick, and E. Zimmer for assistance with motor assays, and K. Wolfe for assistance with electron microscopy. This work was supported in part by grants from the MitoCure Foundation, National Institutes of Health (NIH) (HD053037 and RR16286), National Science Foundation (NSF) (EPS-0447675), the Alabama Agricultural Experiment Station, and Auburn University.

References

[1] J. N. Timmis, M. A. Ayliffe, C. Y. Huang, and W. Martin, "Endosymbiotic gene transfer: organelle genomes forge eukaryotic chromosomes," *Nature Reviews Genetics*, vol. 5, no. 2, pp. 123–135, 2004.

[2] S. DiMauro and M. Mancuso, "Mitochondrial diseases: therapeutic approaches," *Bioscience Reports*, vol. 27, no. 1–3, pp. 125–137, 2007.

[3] D. S. Kyriakouli, P. Boesch, R. W. Taylor, and R. N. Lightowlers, "Progress and prospects: gene therapy for mitochondrial DNA disease," *Gene Therapy*, vol. 15, no. 14, pp. 1017–1023, 2008.

[4] H. Cwerman-Thibault, J. A. Sahel, and M. Corral-Debrinski, "Mitochondrial medicine: to a new era of gene therapy for mitochondrial DNA mutations," *Journal of Inherited Metabolic Disease*, vol. 34, no. 2, pp. 327–344, 2011.

[5] D. A. Dunn, M. V. Cannon, M. H. Irwin, and C. A. Pinkert, "Animal models of human mitochondrial DNA mutations," *Biochimica et Biophysica Acta*, vol. 1820, no. 5, pp. 601–607, 2011.

[6] D. P. Gearing and P. Nagley, "Yeast mitochondrial ATPase subunit 8, normally a mitochondrial gene product, expressed in vitro and imported back into the organelle," *The EMBO Journal*, vol. 5, no. 13, pp. 3651–3655, 1986.

[7] G. Manfredi, J. Fu, J. Ojaimi et al., "Rescue of a deficiency in ATP synthesis by transfer of MTATP6, a mitochondrial DNA-encoded gene, to the nucleus," *Nature Genetics*, vol. 30, no. 4, pp. 394–399, 2002.

[8] Y. Shidara, K. Yamagata, T. Kanamori et al., "Positive contribution of pathogenic mutations in the mitochondrial genome to the promotion of cancer by prevention from apoptosis," *Cancer Research*, vol. 65, no. 5, pp. 1655–1663, 2005.

[9] S. J. Zullo, W. T. Parks, M. Chloupkova et al., "Stable transformation of CHO cells and human NARP cybrids confers oligomycin resistance (olir) following transfer of a mitochondrial DNA-encoded olir ATPase6 gene to the nuclear genome: a model system for mtDNA gene therapy," *Rejuvenation Research*, vol. 8, no. 1, pp. 18–28, 2005.

[10] X. Qi, L. Sun, A. S. Lewin, W. W. Hauswirth, and J. Guy, "The mutant human ND4 subunit of complex I induces optic neuropathy in the mouse," *Investigative Ophthalmology & Visual Science*, vol. 48, no. 1, pp. 1–10, 2007.

[11] J. Guy, X. Qi, R. D. Koilkonda et al., "Efficiency and safety of AAV-mediated gene delivery of the human ND4 complex I subunit in the mouse visual system," *Investigative Ophthalmology & Visual Science*, vol. 50, no. 9, pp. 4205–4214, 2009.

[12] I. J. Holt, A. E. Harding, R. K. Petty, and J. A. Morgan-Hughes, "A new mitochondrial disease associated with mitochondrial DNA heteroplasmy," *American Journal of Human Genetics*, vol. 46, no. 3, pp. 428–433, 1990.

[13] P. Makela-Bengs, A. Suomalainen, A. Majander et al., "Correlation between the clinical symptoms and the proportion of mitochondrial DNA carrying the 8993 point mutation in the NARP syndrome," *Pediatric Research*, vol. 37, no. 5, pp. 634–639, 1995.

[14] F. M. Santorelli, S. Shanske, A. Macaya, D. C. DeVivo, and S. DiMauro, "The mutation at nt 8993 of mitochondrial DNA is a common cause of Leigh's syndrome," *Annals of Neurology*, vol. 34, no. 6, pp. 827–834, 1993.

[15] L. Young and Q. Dong, "Two-step total gene synthesis method," *Nucleic Acids Research*, vol. 32, no. 7, article e59, 2004.

[16] R. Rizzuto, A. W. Simpson, M. Brini, and T. Pozzan, "Rapid changes of mitochondrial Ca^{2+} revealed by specifically targeted recombinant aequorin," *Nature*, vol. 358, no. 6384, pp. 325–327, 1992.

[17] D. W. Kim, T. Uetsuki, Y. Kaziro, N. Yamaguchi, and S. Sugano, "Use of the human elongation factor 1α promoter as a versatile and efficient expression system," *Gene*, vol. 91, no. 2, pp. 217–223, 1990.

[18] G. I. Evan, G. K. Lewis, G. Ramsay, and J. M. Bishop, "Isolation of monoclonal antibodies specific for human c-myc proto-oncogene product," *Molecular and Cellular Biology*, vol. 5, no. 12, pp. 3610–3616, 1985.

[19] C. A. Pinkert, *Transgenic Animal Technology: A Laboratory Handbook*, Academic Press, San Diego, Calif, USA, 2002.

[20] T. Karl, R. Pabst, and S. von Hörsten, "Behavioral phenotyping of mice in pharmacological and toxicological research," *Experimental and Toxicologic Pathology*, vol. 55, no. 1, pp. 69–83, 2003.

[21] R. J. Carter, L. A. Lione, T. Humby et al., "Characterization of progressive motor deficits in mice transgenic for the human Huntington's disease mutation," *Journal of Neuroscience*, vol. 19, no. 8, pp. 3248–3257, 1999.

[22] I. A. Trounce, Y. L. Kim, A. S. Jun, and D. C. Wallace, "Assessment of mitochondrial oxidative phosphorylation in patient muscle biopsies, lymphoblasts, and transmitochondrial cell lines," *Methods in Enzymology*, vol. 264, pp. 484–509, 1996.

[23] Y. Will, J. Hynes, V. I. Ogurtsov, and D. B. Papkovsky, "Analysis of mitochondrial function using phosphorescent oxygen-sensitive probes," *Nature Protocols*, vol. 1, no. 6, pp. 2563–2572, 2007.

[24] C. Vives-Bauza, L. Yang, and G. Manfredi, "Assay of mitochondrial ATP synthesis in animal cells and tissues," *Methods in Cell Biology*, vol. 80, pp. 155–171, 2007.

[25] M. D'Aurelio, C. Vives-Bauza, M. M. Davidson, and G. Manfredi, "Mitochondrial DNA background modifies the bioenergetics of NARP/MILS ATP6 mutant cells," *Human Molecular Genetics*, vol. 19, no. 2, Article ID ddp503, pp. 374–386, 2010.

[26] D. C. Wallace, "Bioenergetics and the epigenome: interface between the environment and genes in common diseases," *Developmental Disabilities Research Reviews*, vol. 16, no. 2, pp. 114–119, 2010.

Hindawi Publishing Corporation
Journal of Biomedicine and Biotechnology
Volume 2012, Article ID 460841, 7 pages
doi:10.1155/2012/460841

Methodology Report

Development of Animal Model for Studying Deep Second-Degree Thermal Burns

Danielle dos Santos Tavares Pereira,[1] Maria Helena Madruga Lima-Ribeiro,[2] Nicodemos Teles de Pontes-Filho,[3] Ana Maria dos Anjos Carneiro-Leão,[2] and Maria Tereza dos Santos Correia[1,4]

[1] *Programa de Pós-Graduação em Ciências Biológicas, Universidade Federal de Pernambuco, 50670-901 Recife, PE, Brazil*
[2] *Programa de Pós-Graduação em Biociência Animal, Universidade Federal Rural de Pernambuco, 52171-900 Recife, PE, Brazil*
[3] *Departamento de Patologia, Universidade Federal de Pernambuco, 50670-901 Recife, PE, Brazil*
[4] *Departamento de Bioquímica, Centro de Ciências Biológicas, Universidade Federal de Pernambuco, 50670-901 Recife, PE, Brazil*

Correspondence should be addressed to Danielle dos Santos Tavares Pereira, dstpereira@yahoo.com.br

Received 9 January 2012; Revised 9 March 2012; Accepted 13 March 2012

Academic Editor: Monica Fedele

Thermal lesions were produced in 12 male Wistar rats, positioning a massive aluminum bar 10 mm in diameter (51 g), preheated to 99°C ± 2°C/10 min. on the back of each animal for 15 sec. After 7, 14, 21, and 28 days, animals were euthanized. The edema intensity was mild, with no bubble and formation of a thick and dry crust from the 3rd day. The percentage of tissue shrinkage at 28 days was 66.67 ± 1.66%. There was no sign of infection, bleeding, or secretion. Within 28 days reepithelialization was incomplete, with fibroblastic proliferation and moderate fibrosis and presence of modeled dense collagen fibers. It is concluded that the model established is applicable in obtaining deep second-degree thermal burns in order to evaluate the healing action of therapeutic agents of topical use.

1. Introduction

Burns are tissue lesions from thermal origin for exposure to flames, hot surfaces and liquids, extreme cold, chemicals, radiation, or friction [1]. Even with improved prognosis [2] and progress in the use of biological skin substitutes [3], burns are an important cause of mortality [4].

Burns are classified depending on the lesion severity into superficial or first degree, when lesion is restricted to the epidermis or skin causing redness; partial thickness or second degree that can be superficial when reaching the epidermis and superficial dermis, showing hypersensitivity and pain, or deep when it extends to the deepest layer of the dermis and may have reduced sensitivity with red and/or white coloration of the tissue; full-thickness or third degree when lesion involves the subcutaneous layer, with no sensitivity and white coloring [5].

The use of animals as experimental models in different areas of biological research was encouraged by Claude Bernard [6], who around 1865, described in his paper entitled "Introduction to the Study of Experimental Medicine" the use of animals as a model for study and transposition into human physiology. Experimental models are essential in mammals when studying on burns. There are literature reports on the use of rabbits [7], pigs [8], dogs [9], rats [10], and mice [11] as models in the study of burns.

The healing of skin lesions induces the burn-injured tissue inflammation, edema, and hypertrophic and unsightly scars [12]. Thus, the choice of a topical agent or the type of coverage to be used in treating burns should be conducted based on the assessment of lesion characteristics and evidence reported in the specific literature. These products must have features such as antimicrobial or bacteriostatic activity, absence of toxicity and hypersensitivity, compliance, reduced healing time, and cost/benefit [13]. However, many of the methods used in healing injuries caused by burns are controversial [14].

In this context, the objective of this study was to establish an experimental protocol for induction of deep second-degree thermal lesions in Wistar male rats to obtain clinical and histopathologic data that will facilitate understanding of results concerning the evolution of the healing action of topical therapeutic agents.

2. Materials and Methods

2.1. Animals. The experiment was conducted at the Department of Experimental Surgery, Federal University of Pernambuco, using albino Wistar male rats (*Rattus norvegicus*) weighing 250 ± 50 g, kept in individual cages of polypropylene measuring 30 × 20 × 19 cm and controlled lighting conditions (12 h light/dark photoperiod), temperature (24 ± 2°C), receiving water, and food (Labina) ad libitum. The experimental procedure was approved by the ethics committee on animal experimentation of the Federal University of Pernambuco (Case no. 23076.015015/2009-31).

2.2. Thermal Burn Experimental Model. Initially, 12 animals were weighed and intramuscularly preanesthetized with atropine sulfate (0.04 mg/kg) and 10 minutes after subjected to anesthetic combination of 10% ketamine (90 mg/kg) and 2% xylazine (10 mg/kg) intramuscularly [15, 16]. With the animal properly anesthetized trichotomy of back was performed and antisepsis with 1% polyvinylpyrrolidone iodine. Thermal injuries were made with a solid aluminum bar 10 mm in diameter (Figure 1(a)), previously heated in boiling water and so that the temperature reached 100°C measured with a thermometer. The bar is maintained in contact with the animal skin on the dorsal proximal region for 15 sec (Figure 1(b)). The pressure exerted on the animal skin corresponded to the mass of 51 g of aluminum bar used in the burn induction. Immediately after the procedure, analgesia with dipyrone sodium (40 mg/kg) was performed intramuscularly, being maintained for three consecutive days sodium dipyrone at 200 mg/kg orally administered in the drinking water supplied to animals.

2.3. Clinical Evaluation. The clinical course of skin lesions by burns was evaluated for 28 consecutive days based on the following aspects: blistering, swelling, redness, crust, bleeding, secretion, granulation tissue, and scar tissue.

The wound retraction was evaluated using a caliper in 7, 14, 21, and 28 days after burn induction. Wound contraction was expressed as reduction in percentage of original wound size. % wound contraction on day X = [(area on day 0 − open area on day X)/area on day 0] × 100 [17].

2.4. Microbiological Evaluation. Microbiological evaluation was carried out using "swabs" in the injury area at the moment of surgery and respective days of biopsies. This sample was transferred to a Petri dish of 20 × 150 mm containing nutrient agar medium in a laminar flow chamber. After 24 h incubation, plates inoculated in triplicate for each sample were evaluated. This routine evaluation was performed to evaluate the degree of contamination of injuries.

(a) (b)

Figure 1: Experimental model of second-degree thermal burn in male Wistar rats. (a) Solid aluminum bar of 10 mm in diameter and 51 g used in the induction of thermal burns by direct heat transference. (b) Proximal dorsal region chosen for burn induction.

2.5. Histological Analysis. At the preestablished times for biopsy (7, 14, 21, and 28 days after burn induction), three animals randomly selected underwent anesthesia combination of 10% ketamine (90 mg/kg) and 2% xylazine (10 mg/kg), intramuscularly [15, 16] for tissue samples collection. Euthanasia was performed by excessive doses of sodium pentobarbital intraperitoneally (100 mg/kg) [18].

Tissue samples were immediately fixed by immersion in 4% formaldehyde (v/v) prepared in PBS (0.01 M, pH 7.2), followed by routine histological processing paraffin embedding, microtomy with 4 μm cuts, and Masson's trichrome staining. Histological study was performed by comparative descriptive analysis of the experimental groups in binocular optical microscope (Zeiss-Axiostar model) where were evaluated the evolution of skin healing after thermal trauma.

The histological analysis was performed by independent pathologist who was experienced in the examination of burn wound specimens, in the following ways: (1) inflammatory response, characterized by the presence of polymorphonuclear leukocytes (PNM), (2) granular tissue, characterized by the presence of fibroblasts, myofibroblasts, and neovascularization, (3) fibrosis, characterized by the density of collagen fibers identified by the intensity of blue color observed under optical microscopy due to staining by Masson's trichrome. A score was made for all parameters evaluated : − = absent, + = mild presence, ++ = moderate presence, and +++ = strong presence.

Figure 2: Clinical evolution observed in the experimental model of deep second-degree thermal burns in male Wistar rats. (a) Animal's skin after shaving. (b) Thermal lesion obtained with 10 mm diameter bar, with presence of mild edema. (c) Injured tissue on day 7 after burn induction, presence of thin and dry crust with homogeneous staining and discreet detachment on the edges. (d) Damaged tissue on day 14 after burn induction, presence of granulation tissue in the center of the lesion with a second discreet crust and formation of scar tissue at the edge. (e) Injured tissue on day 21 after the burn induction, discreet presence of granulation tissue with the presence of scar tissue. (f) Injured tissue at day 28 after burn induction, tissue with incomplete healing.

2.6. Statistical Analysis. Data were analyzed using nonparametric tests. To detect differences between groups, the Kruskal-Wallis was used. All results were expressed as mean values for group ± standard deviation and analyzed considering $P < 0.05$ as statistically significant.

3. Results and Discussion

3.1. Study Design. This experimental model was established to standardize thermal burn injuries in order to obtain injuries with the same size and depth degree. The choice of Wistar rats due to these animals shows a great ease of handling, accommodation and resistance to surgical aggressions, and infectious processes, with low mortality [19, 20]. However, the choice of male rats is due to variations in hormonal cycles in females that could intervene in the process of tissue repair [21]. The result of clinical evaluation showed no signs of infection, secretion, bleeding, or death in both groups. If wounds are not well treated, they can be infected. Infected wounds heal more slowly, reepithelisation is more prolonged, and there is also the risk of systemic infection [22].

Shaving the back of the animals was performed by manual traction of hair (Figure 2(a)) thus preventing secondary skin lesions that often occurs by the use of laminated devices [23]. The option to induce only one burning

Table 1: Clinical parameters evaluated in the experimental model of deep second degree thermal burns in male Wistar rats.

Time	Animal	Clinical signs of the experimental model			
		Edema	Hyperemia	Crust	Scar tissue
7th day	1	+	+	*	−
	2	+	−	*	−
	3	+	−	*	−
14th day	1	−	+	−	+
	2	+	−	−	+
	3	−	−	−	+
21st day	1	−	−	−	+++
	2	−	−	−	+++
	3	−	−	−	+++
28th day	1	−	−	−	++
	2	−	−	−	+
	3	−	−	−	+

The intensity of clinical signs was scored as −: absent; *: present, +: mild, ++: moderate, +++: strong.

in the dorsal-proximal aimed at preventing the animal itself could reach the burn so that altering the outcome of the clinical evaluation of lesions. The use of individual aluminum bar for each animal in the experimental group is important in reducing the interval between the induction of a burn and another within the same group, thus avoiding large variations in the assessment of healing time. The size of lesions showed uniform average distribution of 10 ± 1 mm in diameter (Figure 2(b)). Similar studies by Heredero and colleagues [20] and Meyer and Silva [24] revealed that it is not possible to perform a perfectly uniform burn in all experimental rats.

According to Vale [25], the burn depth depends on the intensity of the thermal agent, generator or heat transmitter and time of contact with the tissue, which is the determinant of the aesthetic and functional result of the burn. Medeiros et al. [26] caused thermal burns by using 5 cm^2 aluminum plate heated to 130°C, which were pressed into the skin of the back for 5 seconds. However, this method can generate lesions with different depths depending on the pressure during the procedure. In our study, the pressure was equivalent to the mass of the aluminum bar (51 g) there being no interference by researcher, thus ensuring the reproducibility of thermal injuries.

The standardization of procedures, systematization, and organization of knowledge about the interrelationships of models is necessary to provide more reliable knowledge advance [27]. The most common method for obtaining second-degree thermal burns uses hot water as heat transfer agent. Khorasani et al. [28] induced second-degree thermal burns on the back of rats using submersion in hot water (90°C) for 6 seconds. In this experiment, 10% body surface of the animal was injured producing lesions of variable size. According to Orgaes et al. [23], burns when reaching 26% to 30% of total body surface area of these mice cause mortality

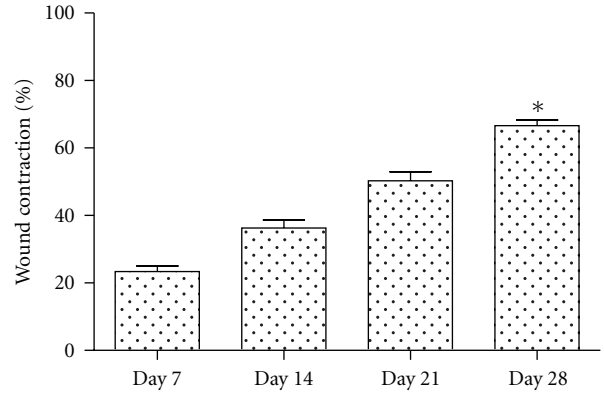

Figure 3: Contraction area percentage of deep second-degree thermal burns in the experimental model in male Wistar rats. $n = 3$. Values are mean ± SEM. $^*P < 0.05$.

rates of 40% after three days, 52.5% after 7 days, 57.5% after 15 days, and 62.5% after 25 days.

3.2. Macroscopic Evaluation. Results of this study revealed thermal burns white in color, painful, with no bubbles, mild edema until the 3rd day after injury (Figure 2(b)). Similar definition is reported by [29, 30] that describes the deep second-degree burns and injuries that have pale color with pain in lower intensity compared to superficial second-degree burn. In our evaluation variation of the degree of hyperemia in the first three days of experiment that changed from slight to absent was observed (Table 1). The formation of a thick and dry crust was observed from day 3 after burn induction. Signs of the scar tissue formation at the edge of the lesion were observed from day 14 (Figure 2(d)).

The burn healing occurs by second intention, which is a slow process with high risk of infection, producing scar retraction, which depending on the area of injury can cause extensive scarring and consequently high cost in treatment [31]. The contraction of skin lesions occurs centripetally fromthe injury edges being caused by the action of myofibroblasts present at the site. In turn, myofibroblasts may promote lesion retraction from 50 to 70% of original size [32]. The percentage of lesion contraction at the end of the experiment was 66.67 ± 1.66%. Values obtained in this study are similar to those published by Zohdi and colleagues [33], who observed 72.75 ± 1.8% of reduction in control rats treated with hydrogel without drug (placebo) at 28 days of study (Figure 3).

According to Mandelbaum and colleagues [34], the mechanism of tissue repair is the integration of dynamic cellular and molecular processes involving biochemical and physiological phenomena aiming at ensuring tissue restoration. For this reason, only the clinical evaluation of a burn injury does not provide information on the evolution degree of tissue healing, being of fundamental importance of the histopathologic evaluation of these lesions.

3.3. Microscopic Evaluation. The histopathological findings confirmed the acquisition of deep second-degree burns based

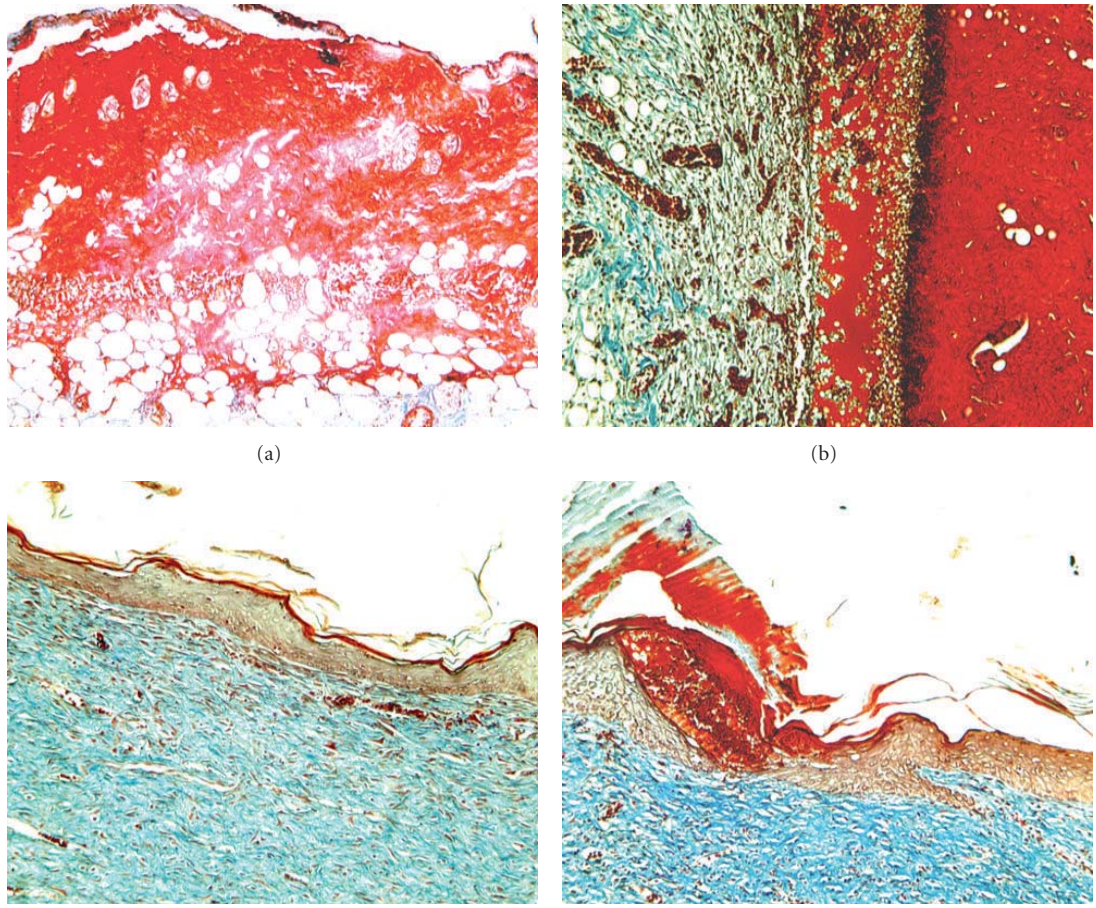

Figure 4: Histopathological aspects of deep second-degree thermal burns. Masson's trichrome staining. 100x Magnification. (a) Animal showing thin crust and epithelial tissue with complete destruction of dermis and epidermis and hypodermis maintenance at the 7th day after the thermal lesion induction. (b) Animal at day 14, with crust and tissue reepithelialization, showing collagen, not modeled and slight fibrosis. (c) Animal at day 21, tissue repithelialization showing intense fibroblastic proliferation with the presence of dense collagen, not modeled and moderate fibrosis. (d) Animal at day 28, with incomplete tissue repithelialization, moderate fibroblastic proliferation, presence of modeled dense collagen mesh, and moderate fibrosis.

on the observation of total autolysis of both the dermis and epidermis, without reaching the hypodermis. These data are consistent with reports of several authors who characterize it as deep second-degree burn injuries that cause partial or total destruction of nerve endings, hair follicles, and sweat glands [25, 35, 36].

Thermal injury was observed on the 7th day and extensive inflammatory exudate featuring an intense inflammatory reaction. Inngjerdinger et al. [22] describe in their study the occurrence in the control group, treated with saline solution, an acute inflammatory process on the 6th day of evaluation. By day 14 the inflammatory response was classified as moderate with presence of macrophages, progressing to discreet at day 21. By day 28 signs of inflammatory response in the animals evaluated was not observed (Table 2).

Tissue still presented a complete destruction of the dermis and epidermis and maintenance of the hypodermis (Figure 4(a)) on the 7th day after lesion induction. Histopathology section of the burned skin of control animals on 5th day showed denuded epidermis, diffuse infiltration of plasma cells, lymphocytes, and polymorphs [37]. After 14 days the histopathological evaluation revealed moderate autolysis of the tissue, with discrete neovascularization and fibroblast proliferation, with loose collagen fibers, not modeled with mild fibrosis and crust absence (Figure 4(b)). Yaman and colleagues [38] confirm the presence of crust formed by remnants of necrotic tissue and infiltration of mononuclear cells on the 4th day of experimentation in the control group. The crust detachment was only observed by these authors on the 14th day of study.

By day 21 we observed the absence of autolysis, discrete neovascularization and intense fibroblastic proliferation, with dense collagen, not modeled and moderate fibrosis (Figure 4(c)). By the end of the experiment at 28 days, histological observations showed incomplete reepithelialization of the injured tissue with autolysis and absent neovascularization, showing moderate fibroblastic proliferation and

Table 2: Histopathological analysis on the degree of inflammatory intensity, presence of granulation tissue, and fibrosis in the skin after deep second-degree thermal burn. Samples were obtained on days 7, 14, 21, and 28 after burn wound induction.

Time	Animal	Inflammatory response	Granulation tissue	Fibrosis
7th day	1	+++	+	−
	2	+++	+	−
	3	+++	+	−
14th day	1	+	++	+
	2	++	+++	+
	3	++	+++	+
21st day	1	+	+	+
	2	+	+	++
	3	+	++	++
28th day	1	−	−	++
	2	−	−	++
	3	−	−	++

Intensity of the evaluated parameters was scored as −: absent, +: mild presence, ++: moderate presence; +++: strong presence.

fibrosis with the presence of modeled dense collagen fibers (Figure 4(d)).

Wound healing includes number of stages like clotting, inflammation, granulation, fibrosis, arrangement of collagen with spasm of wound, and epithelization. The time required for complete healing of deep second-degree burns, without the application of specific therapeutic agents, can be three to six weeks or more, and these burns will leave a scar tissue that may hypertrophy and contract itself [29, 30].

4. Conclusion

In this new model of second-degree thermal burns, injuries are easy to create and easily reproducible. There are similarities with the human second-degree burns in clinical and pathologic aspects. Thus, the animal model presented in this study is applicable in evaluating the use of therapeutic agents in the healing evolution of deep second-degree burns.

References

[1] S. A. Jorge and S. R. P. E. Dantas, *Abordagem Multiprofissional do Tratamento de Feridas*, Atheneu, São Paulo, Brazil, 2003.

[2] J. P. Barret and D. N. Herndon, "Modulation of inflammatory and catabolic responses in severely burned children by early burn wound excision in the first 24 hours," *Archives of Surgery*, vol. 138, no. 2, pp. 127–132, 2003.

[3] M. Ramos-E-Silva and M. C. Ribeiro de Castro, "New dressings, including tissue-engineered living skin," *Clinics in Dermatology*, vol. 20, no. 6, pp. 715–723, 2002.

[4] R. L. Sheridan, M. I. Hinson, M. H. Liang et al., "Long-term outcome of children surviving massive burns," *Journal of the American Medical Association*, vol. 283, no. 1, pp. 69–73, 2000.

[5] M. F. Rangel and A. P. J. T. Pereira, "Atendimento inicial e definitivo do grande queimado," *Jornal Brasileiro de Medicina*, vol. 92, no. 2, pp. 20–22, 2007.

[6] C. Bernard, "An introduction to the study of experimental medicine (1865)," In: Images from the history of medicine division, *National Library of Medicine*, http://www.ihm.nlm.nih.gov.

[7] K. Bashkaran, E. Zunaina, S. Bakiah, S. A. Sulaiman, K. Sirajudeen, and V. Naik, "Anti-inflammatory and antioxidant effects of Tualang honey in alkali injury on the eyes of rabbits: experimental animal study," *BMC Complementary and Alternative Medicine*, vol. 11, article 90, 2011.

[8] A. J. Singer, D. Hirth, S. A. McClain, and R. A. Clark, "Lack of agreement between gross visual and histological assessment of burn reepithelialization in a porcine burn model," *Journal of Burn Care and Research*, vol. 33, no. 2, pp. 286–290, 2012.

[9] S. Hu, J. W. Che, and Y. J. Tian, "Effect of oral fluid resuscitation on pulmonary vascular permeability and lung water content in burn dogs in shock stage," *Zhonghua Shao Shang Za Zhi*, vol. 25, no. 3, pp. 184–187, 2009 (Chinese).

[10] P. Campelo, M. W. Campelo, G. A. Britto, A. P. Ayala, S. B. Guimarães, and P. R. Vasconcelos, "An optimized animal model for partial and total skin thickness burns studies," *Acta Cirúrgica Brasileira*, vol. 26, no. 1, pp. 38–42, 2011.

[11] A. Asai, Y. Tsuda, M. Kobayashi, T. Hanafusa, D. N. Herndon, and F. Suzuki, "Pathogenic role of macrophages in intradermal infection of methicillin-resistant *Staphylococcus aureus* in thermally injured mice," *Infection and Immunity*, vol. 78, no. 10, pp. 4311–4319, 2010.

[12] V. Kumar, A. K. Abbas, N. Fausto, and J. Aster, *Robbins & Cotran Pathologic Basis of Disease*, WB Saunders, Philadelphia, Pa, USA, 8th edition, 2010.

[13] E. Ferreira, R. Lucas, L. A. Rossi, and D. Andrade, "Treatment of the burned patient: a review of the literature," *Revista da Escola de Enfermagem da USP*, vol. 37, no. 1, pp. 44–51, 2003.

[14] B. S. Atiyeh, S. N. Hayek, and S. W. Gunn, "New technologies for burn wound closure and healing—review of the literature," *Burns*, vol. 31, no. 8, pp. 944–956, 2005.

[15] F. Massone, *Anestesiologia Veterinária: Farmacologia e Técnicas*, Guanabara Koogan, Rio de Janeiro, Brazil, 2nd edition, 1994.

[16] E. V. Hillyer and K. E. Quesenberry, *Ferrets, Rabbits and Rodents: Clinical Medicine and Surgery*, WB Sounders, New York, NY, USA, 1997.

[17] M. S. Kumar, R. Sripriya, H. V. Raghavan, and P. K. Sehgal, "Wound healing potential of *Cassia fistula* on infected albino rat model," *Journal of Surgical Research*, vol. 131, no. 2, pp. 283–289, 2006.

[18] R. R. de Lucca, S. R. Alexandre, T. Marques, N. L. Souza, J. L. Merusse, and S. P. Neves, *Manual Para Técnicos em Bioterismo*, Winner Graph, São Paulo, Brazil, 1996.

[19] F. B. Marchini, D. M. F. S. Martins, D. C. Teves, and M. J. Simões, "Efeito do óleo de rosa mosqueta na cicatrização de feridas abertas," *Revista Paulista de Medicina*, vol. 106, no. 6, article 356, 1988.

[20] F. X. S. Heredero, C. Hamann, J. M. O. Martin, C. R. Arias, and S. C. Menchero, "Experimental burn models," *Annals of Burns and Fire Disasters*, vol. 9, no. 2, pp. 96–97, 1996.

[21] D. C. Teves, A. C. V. Cabral, M. J. Simões, and J. R. L. Kulay, "Biologia das reparações teciduais," *Jornal Brasileiro de Medicina*, vol. 50, pp. 39–44, 1986.

[22] K. Inngjerdinger, C. S. Nergard, D. Diallo, P. P. Monoro, and B. S. Paulsin, "An ethnopharmacological survey of plants used for wound healing in Dongoland, Mali, West Africa," *Journal of Ethnopharmacology*, vol. 92, pp. 233–244, 2004.

[23] F. A. F. S. Orgaes, M. C. Lyra, O. F. Rodrigues Jr., and H. A. Gonella, "Estudo histopatológico do uso de heparina tópica em queimaduras por escaldo em ratos," *Revista Brasileira de Cirurgia Plástica*, vol. 22, no. 1, pp. 39–44, 2007.

[24] T. N. Meyer and A. L. Silva, "A standard burn model using rats," *Acta Cirúrgica Brasileira*, vol. 14, no. 4, 1999.

[25] E. C. S. Vale, "Primeiro atendimento em queimaduras: a abordagem do dermatologista," *Anais Brasileiros de Dermatologia*, vol. 80, no. 1, pp. 9–19, 2005.

[26] A. C. Medeiros, A. M. O. Ramos, A. M. Dantas Filho, R. C. F. Azevedo, and F. L. F. B. Araújo, "Tratamento tópico de queimaduras do dorso de ratos com ácido hialurônico," *Acta Cirúrgica Brasileira*, vol. 14, no. 4, 1999.

[27] D. J. Fagundes and M. O. Taha, "Modelo animal de doença: critérios de escolha e espécies de animais de uso corrente," *Acta Cirúrgica Brasileira*, vol. 19, no. 1, pp. 59–65, 2004.

[28] G. Khorasani, S. J. Hosseinimehr, P. Zamani, M. Ghasemi, and A. Ahmadi, "The effect of saffron (*Crocus sativus*) extract for healing of second-degree burn wounds in rats," *The Keio Journal of Medicine*, vol. 57, no. 4, pp. 190–195, 2008.

[29] J. S. Tecklin, *Fisioterapia Pediátrica*, Artmed, Porto Alegre—Rio Grande do Sul, Brazil, 3rd edition, 2002.

[30] R. M. Johnson and R. Richard, "Partial-thickness burns: identification and management," *Advances in Skin & Wound Care*, vol. 16, no. 4, pp. 178–187, 2003.

[31] C. O. M. Coelho, C. M. F. Rezende, and A. P. M. Tenório, "Contração de feridas após cobertura com substitutos temporários de pele," *Ciência Rural*, vol. 29, no. 2, pp. 297–303, 1999.

[32] S. F. Swaim, S. H. Hinkle, and D. M. Bradley, "Wound contraction: basic and clinical factors," *Compendium on Continuing Education for the Practicing Veterinarian*, vol. 23, no. 1, pp. 20–33, 2001.

[33] R. M. Zohdi, Z. A. B. Zakaria, N. Yusof, N. M. Mustapha, and M. N. Abdullah, "Gelam (*Melaleuca* spp.) honey-based hydrogel as burn wound dressing," *Evidence-Based Complementary and Alternative Medicine*, vol. 2012, Article ID 843025, 7 pages, 2012.

[34] S. R. Mandelbaum, E. P. di Santis, and M. H. Mandelbaum, "Cicatrização: conceitos atuais e recursos auxiliares—parte I," *Anais Brasileiros de Dermatologia*, vol. 78, no. 4, pp. 393–410, 2003.

[35] O. S. Lima, F. S. Lima Verde, and O. S. Lima Filho, "Queimados: alterações metabólicas, fisiopatologia, classificação e interseções com o tempo de jejum," in *Medicina Perioperatória*, vol. 91, pp. 803–815, Sociedade de Anestesiologia do Estado do Rio de Janeiro, 91. Capítulo, Rio de Janeiro, Brazil, 2006.

[36] J. M. Mélega, *Cirurgia Plástica—Fundamentos e Arte: Princípios Gerais*, Guanabara Koogan, Rio de Janeiro, Brazil, 1st edition, 2002.

[37] P. K. Chandran and R. Kuttan, "Effect of *Calendula officinalis* flower extract on acute phase proteins, antioxidant defense mechanism and granuloma formation during thermal burns," *Journal of Clinical Biochemistry and Nutrition*, vol. 43, no. 2, pp. 58–64, 2008.

[38] I. Yaman, A. S. Durmus, S. Ceribasi, and M. Yaman, "Efects of *Nigella sativa* and silver sulfadiazine on burn wound healing in rats," *Veterinarni Medicina*, vol. 55, no. 12, pp. 619–624, 2010.

Hindawi Publishing Corporation
Journal of Biomedicine and Biotechnology
Volume 2012, Article ID 817341, 12 pages
doi:10.1155/2012/817341

Review Article

Think Small: Zebrafish as a Model System of Human Pathology

J. R. Goldsmith[1] and Christian Jobin[1,2,3]

[1] *Department of Pharmacology, University of North Carolina, Chapel Hill, NC 27599, USA*
[2] *Department of Medicine, University of North Carolina, Chapel Hill, NC 27599, USA*
[3] *Department of Microbiology and Immunology, University of North Carolina, Chapel Hill, NC 27599, USA*

Correspondence should be addressed to Christian Jobin, job@med.unc.edu

Received 9 January 2012; Accepted 12 March 2012

Academic Editor: Andrea Vecchione

Although human pathologies have mostly been modeled using higher mammal systems such as mice, the lower vertebrate zebrafish has gained tremendous attention as a model system. The advantages of zebrafish over classical vertebrate models are multifactorial and include high genetic and organ system homology to humans, high fecundity, external fertilization, ease of genetic manipulation, and transparency through early adulthood that enables powerful imaging modalities. This paper focuses on four areas of human pathology that were developed and/or advanced significantly in zebrafish in the last decade. These areas are (1) wound healing/restitution, (2) gastrointestinal diseases, (3) microbe-host interactions, and (4) genetic diseases and drug screens. Important biological processes and pathologies explored include wound-healing responses, pancreatic cancer, inflammatory bowel diseases, nonalcoholic fatty liver disease, and mycobacterium infection. The utility of zebrafish in screening for novel genes important in various pathologies such as polycystic kidney disease is also discussed.

1. Introduction

Investigators have long utilized reductionist systems and animal models to mimic and study basic processes regulating cellular biology, organ function, and host homeostasis. While much work has been accomplished and continues to be undertaken in higher mammalian systems such as mice, rats, and rabbits, important discoveries have also been made using invertebrate systems such as *Caenorhabditis elegans* and *Drosophila melanogaster*. For example, RNA interference technology was first discovered in *C. elegans* [1], as was the initial caspase enzyme, caspase-1 (ced-3 in *C. elegans*) [2]. Similarly, it was in Drosophila melanogaster that the innate signaling Toll-like receptors (TLRs) were first identified via the discovery of the Toll gene, as was its linkage to the nuclear factor kappa-light-chain-enhancer of activated B cells (NF-κB) signaling cascade [3]. In the last ~15 years, there has been a growing appreciation for the vertebrate organism *Danio rerio* (zebrafish) as a tool to study human disease [4]. As opposed to *C. elegans* and *Drosophila melanogaster*, zebrafish is a vertebrate organism with physiological and anatomical characteristics of its higher organism counterparts (see Figure 1 for a diagram of larval zebrafish anatomy), while maintaining the ease of use of a lower organism. The characteristics of zebrafish that make them desirable tools for the study of embryogenesis/development also make them useful for the study of human pathologies. Zebrafish have a fully mapped genome (http://www.sanger.ac.uk/Projects/D_rerio/), which has significant homology with the human genome, including noncoding regions (~60 per gene globally across all genes) [5] suggesting that numerous genes involved in human diseases could be matched in the zebrafish genome. Reverse (morpholino knock-down, Targeting Induced Local Lesions in Genome—TILLING [6]) and forward genetic (mutagenesis, transgenic) approaches are well established and commonly used to manipulate and characterize zebrafish gene function.

Zebrafish are highly fecund and breed rapidly; a pair of zebrafish produces over 100 embryos per clutch that are usable for larval experiments as early as 3 days post fertilization (dpf). These larvae are transparent through 7 dpf, and this can be extended to up to 9–14 dpf with the addition of the melanocyte inhibitor phenylthiourea. Moreover, the

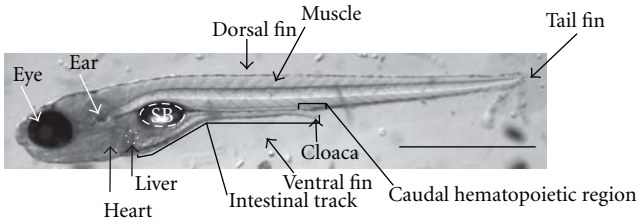

Figure 1: Diagram of zebrafish anatomy. A representative image of a transparent, 6 dpf larvae captured with brightfield microscopy. Organs and anatomical features are denoted in the figure. SB: swim bladder. Scale bar is 1 mm.

recent generation of transparent adult zebrafish such as the *Casper* line adds new imaging possibilities [7]. The transparency of zebrafish, in conjunction with sophisticated utilization of fluorescent technology to mark signaling proteins or cellular entities, allows for powerful time-lapse imaging of biological and disease processes. Additionally, the vertebrate zebrafish has many features commonly found in mammals, including an innate immune system composed of neutrophils, NK cells, and monocyte/macrophages with functionality by 48 hours post fertilization (hpf) [8, 9] and an adaptive immune system that is fully functional at 4–6 weeks post fertilization [10]. The adaptive immune system is highly analogous to that of mammals, with T cells and B cells that have Rag-dependent V(D)J recombination (reviewed extensively in [9]). Finally, the zebrafish research community benefits from an up-to-date database of techniques, genetic strains, and other useful resources at http://zfin.org/.

In this paper, we focus our discussion on larval and adult zebrafish models that recapitulate human diseases, focusing on four separate branches of pathology: wound healing/restitution, gastrointestinal disease, microbe-host interactions, and genetic diseases and drug screens.

2. Wound Healing/Restitution

Wound healing represents a critical biological response of injured tissues and organs. Events causing epithelial injury and barrier breakdown initiate a biological response known as "restitution", which is aimed at resealing the damaged region and reestablishing host homeostasis. This "wound healing" response involves migration of epithelial cells toward the injured regions as well as epithelial cell proliferation to replenish the cell pool. Understanding the cellular and molecular mechanisms regulating this response could have profound translational impact for patients suffering from chronic inflammation, ischemia/hypoxia, burn injury, and cancer. The powerful imaging modalities available to zebrafish researchers alongside their ease of genetic manipulation make this vertebrate system an ideal model for studying wound healing response to various injuries [11]. Additionally, the ability of zebrafish to regenerate both limbs and cardiac tissue [12] makes them a powerful animal model for understanding the molecular mechanisms involved in regenerative signaling.

The most popular zebrafish injury model is the larval tail wounding model, where a segment of the tail fin is resected. Using this injury model with transgenic zebrafish expressing EGFP under the transcriptional controlled of the neutrophil-specific myeloperoxidase (MPO) promoter—*Tg*(*BACmpx:GFP*)*i114*—investigators studied real-time neutrophil chemotaxis to the site of injury [13]. In this study, they observed retrograde chemotaxis of neutrophils toward the vasculature alongside where injury resolution was observed, suggesting for the first time that retrograde chemotaxis may play an important role in the resolution phase of the inflammatory response [13]. To determine the function of the reactive oxygen species H_2O_2 in the wound healing response, investigators injected mRNA encoding for the hydrogen peroxide sensor HyPer to one-cell stage developing zebrafish embryos [14]. Upon tail wounding of 3 dpf larvae, the HyPer sensor demonstrated increased H_2O_2 production along a gradient decreasing away from the wound site, which signaled leukocyte chemotaxis to the injured location [11]. Using pharmacological and morpholino blockade, the authors showed that generation of the H_2O_2 gradient is dependent on the activity of the dual oxidase (duox) gene. This HyPer reporter system has also been utilized in the study of neuronal regeneration, an important area of study for the treatment of many human diseases. H_2O_2 produced by injured keratinocytes was shown to induce somatosensory axonal regeneration in zebrafish. Similar to the tail fin wounding model, neuronal regeneration required activation of *duox* [15]. Moreover, H_2O_2 administration promoted axonal regeneration following neuronal injury, even without accompanying keratinocyte injury [15]. These results expand the understanding of posttraumatic nerve injury and subsequent loss of limb function in humans. The healing-enhancing properties of H_2O_2 have since been extended to studies in both rabbits [16] and horses [17] as well as one reported case study in a human patient [18].

Beyond cutaneous wounds, zebrafish have been used for the ability to regenerate cardiac tissue. Unlike mammals, which form scars and do not regenerate cardiac tissue following injury, zebrafish are able to fully regenerate their heart within 2 months after 20% ventricular resection [19]. This ability for zebrafish to overcome scar formation requires activation of Mps1, a mitotic checkpoint kinase [19]. Additionally, cardiac regeneration involves upregulation of wound healing genes and proliferative factors including *apoeb, vegcf*, and *granulina* (all of which have human analogs) and likely activation of platelet-derived growth factor B signaling [20]. Cardiac regeneration studies in zebrafish could produce novel paradigms and identify unique pathways/targets with profound translational impact for patients suffering from ischemic heart disease.

3. Gastrointestinal Diseases

The zebrafish gastrointestinal system is highly homologous to that of mammals, containing a liver, pancreas, gall bladder, and a linearly segmented intestinal track with absorptive and secretory functions [21, 22]. The intestinal epithelium displays proximal-distal functional specification and

Table 1: Zebrafish gastrointestinal models of pathology.

Model	Mechanism of pathology	Human relevancy/key features	Key references
Pan-GI neoplasias	Heterozygotic APC mutation	APC mutations drive spontaneous and genetic intestinal adenocarcinomas.	Haramis et al., 2006 [24]
Hepatocellular carcinoma	Thioacetamide ± HCV-core-protein-zebrafish	Human genetic overlap. Rising prevalence of HCV-driven HCC in humans.	Lam and Gong, 2006 [25] Rekha et al., 2008 [26]
Pancreatic cancer	Transgenic *ptf1a*-KRAS zebrafish	Recapitulates hedgehog signaling aberrations found in humans. Elucidates a potential cellular origin for pancreatic cancers.	Park et al., 2008 [27]
Inflammatory bowel disease	TNBS in the media of zebrafish larvae	Model inflammatory and goblet cell hypertrophy. Responds to bacterial status and IBD medications.	Flemming et al., 2010 [28] Oehlers et al., 2011 [29]
Inflammatory bowel disease	Oxazolone enema in adult zebrafish	Goblet cell depletion and eosinophil infiltration. Responds to antibiotic therapy.	Brugman et al., 2009 [30]
NAFLD	Mutation in a novel gene: *foigr*^{hi1532b}. Alternative model involves chemical induction with thioacetamide	Large lipid filled hepatocytes and cellular apoptosis; pathology linked to ER stress responses. Alternative model generates a fatty liver and hepatocyte apoptosis.	Cinaroglu et al., 2011 [31] Amali et al., 2006 [32] (alternative model)
Alcoholic liver disease	2% ethanol to the water of 4 dpf zebrafish for 32 days	Hepatomegaly and steatosis, with upregulation of genes involved in toxic alcohol metabolism. Model is sensitive to sterol regulatory binding protein, important in human disease.	Passeri et al., 2009 [33]

Abbreviations: GI: gastrointestinal; APC: adenomatous polyposis coli; HCV: hepatitis C virus; TNBS: 2,4,6-trinitrobenzene sulfonic acid; IBD: inflammatory bowel diseases; NAFLD: nonalcoholic fatty liver disease; ER: endoplasmic reticulum.

contains many of same epithelial cell lineages found in mammals including absorptive enterocytes, goblet cells, and enteroendocrine cells [21, 22]. Enterocytes have a basolateral nuclei and form tight junctions, apical microvilli, and an intestinal brush border [23]. In the last decade, numerous gastrointestinal pathologies have been modeled in the zebrafish, as summarized in Table 1.

Interestingly, a forward genetic mutagenesis screen (*N*-ethyl-*N*-nitrosourea (ENU), see section five) generated zebrafish mutants that develop spontaneous intestinal, pancreatic, and hepatic neoplasias [24]. These mutants were later found to be heterozygotic for a truncated form of APC, thereby leading to accumulation of nuclear β-catenin and increased expression of downstream genes such as *cmyc* and *axin2* [24]. Adding the carcinogen 7, 12-dimethylbenz[a]anthracene to these mutant zebrafish increases the frequency of tumor development. Since germline-truncated APC mutations in both humans [34, 35] and mice [36] result in the spontaneous development of a large numbers of intestinal polyps, the APC zebrafish model could be useful in genetic, drug screening, and toxicology studies.

There are roughly 24,000 new cases of hepatocellular carcinoma (HCC) annually in the United States, resulting in over 18,000 deaths per year [37]. Worldwide, the disease incidence can be as much as 30-fold higher due to the increased prevalence of hepatitis infections [38]; globally estimated 564,000 new cases occur per year, accounting for 5.6% of all human cancers [38], and resulting in similar rates of mortality as seen in the USA [38]. Oncogenomic profiling of liver tumors showed a significant overlap between human and zebrafish in 132 genes [25]. These genes included those involved in β-catenin and Ras-MAPK signaling pathways as well as genes implicated in cellular adhesion, apoptosis, and liver-specific metabolism found in both organisms [25]. HCC can be induced in zebrafish with the liver toxin thioacetamide, resulting in HCC-related pathology within 12 weeks of exposure. The timeline of thioacetamide-induced HCC could be significantly accelerated (6 versus 12 weeks) by using transgenic fish expressing the hepatitis C virus (HCV) core protein (HCP-transgenic fish) [26]. The increasing prevalence of HCC in humans has been attributed to the rise of HCV infection [39], in particular through the oncogenic action of the HCV core protein [40], making this model particularly relevant to human disease.

Pancreatic cancer represents the fourth most common cause of cancer-related mortality in the western world, likely due to limited diagnostic tools and inability to survey the disease. Exocrine pancreatic cells are responsible for more

than 95% of pancreatic cancer [37]. The cell population in the pancreas that gives rise to human exocrine pancreatic cancer remains unknown and investigators have turned to zebrafish models to investigate this important question. Transgenic zebrafish were generated using a bacterial artificial chromosome (BAC) approach that expressed EGFP-KRAS fusion protein under the control of the zebrafish pancreatic locus *ptf1a* (*Tg*(*pft1a:EGFP-Hsa.KRAS*^{G12V})*jh7* [27]. Using these fish, investigators found that while normal pancreatic cell progenitors differentiated normally, KRAS-transgenic fish had blocked cellular differentiation, producing a pool of undifferentiated progenitors that progressed to invasive pancreatic cancer over a course of 3 to 9 months. These cancer cells also had increased expression of multiple hedgehog genes (*shh*, *dhh*, *ihha*, *ihhb*) as well as the downstream hedgehog targets *Ptc2*, *ptc1*, and *gli1*. This aberrant signaling pattern seen in these pancreatic tumor cells was also typical of human pancreatic cancer [27]. This zebrafish model established for the first time that oncogenic exocrine pancreatic progenitor cells could be the cellular origin for pancreatic cancer.

Outside of cancer models, one area of gastrointestinal disease that has received significant attention in recent years is the development of zebrafish models of Inflammatory Bowel Disease (IBD). In humans, IBD is the result of dysregulated interactions between a genetically susceptible host and their commensal gut microbiota [41–43]. IBD is primarily a disease of the Western world; it affects 1.4 million Americans and there is no cure for the disease [44]. Outside of North America, similar disease burdens are seen in Europe but are ~3-fold lower in Asia and the Middle East, with the exception of Japan [45]. Pharmacological treatment centers around the use of anti-inflammatories and immunosuppressants, and surgical management of the disease is also possible though not always curative [46]. Numerous chemicals and genetic approaches are currently used by the IBD research community to study this pathology. These models mimic various aspects of the disease, such as disrupted barrier function and impaired innate and adaptive immune responses [47, 48]. Among the chemical models, the hapten oxazolone has been used for studies of acute intestinal inflammation. This murine model consists of rectal administration of a single dose of oxazolone dissolved in ethanol, resulting in an acute colitis lasting up to 10 days, with peak inflammation at 2 days post administration in mice [49]. The model is characterized by a strong Th2-dependent immune response that can be abrogated by IL-4 neutralizing antibodies and has similar characteristics to human ulcerative colitis [48].

Investigators have tried to adapt the hapten oxazolone model of colitis to adult zebrafish. Brugman et al. showed intestinal epithelial damage and goblet cell depletion in oxazolone-treated fish within 5 hours of treatment, which lasts for up to 7 days [30]. This was accompanied by eosinophil infiltration into the intestine with increased *il1b*, *tnf*, and *il10* gene production compared to untreated zebrafish. The inflammatory phenotype was reduced by the administration of the gram-positive-specific antibiotic vancomycin, suggesting a role for commensal bacteria in the inflammatory process of this model. The main constraint of this model is the need to use adult, nontransparent zebrafish which severely limits imaging capability. In addition, the need to rectally administer each individual zebrafish with oxazolone represents a technical challenge.

The hapten 2,4,6-trinitrobenzene sulfonic acid (TNBS) is another popular mammalian model of colitis characterized by a Th1-driven immune response [48] that is used for the study of both acute and chronic intestinal inflammation. In the acute model, TNBS is dissolved in ethanol and rectally administered in a single dose, while the chronic model can have multiple administrations weekly over a period of months [50]. The ethanol is responsible for disrupting the intestinal barrier while the TNBS serves to activate the immune system [48]. Two research groups have developed a larval model of colitis by exposing 3 dpf zebrafish for 3–5 days to TNBS in the fish media [28, 29]. Using the MPO reporter strain (*Tg*(*BACmpx:GFP*)*i114*) these investigators noticed neutrophil infiltration throughout the zebrafish [13], gut-specific increases in *il1b* expression, altered intestinal lipid metabolism, goblet cell hypertrophy, and intestinal shortening. This larval TNBS model presents several advantages, including a dose-dependent phenotype, a sensitivity to antibiotics treatment, and a response to anti-inflammatory agents (5-ASA and prednisolone) widely used to treat human IBD [29]. However, the intestinal histopathologies are poorly characterized in this model. In addition, the inflammatory component appears mostly to be nonintestine specific. Furthermore, no intestinal epithelial cell damage is observed histologically [29], suggesting a lack of significant intestinal injury. Finally, it is unclear how a hapten could cause an inflammatory reaction in larvae missing a functional adaptive immune system.

We have recently established a model of epithelial injury in zebrafish using the NSAID glafenine [51]. Administration of glafenine to 5 dpf zebrafish for 12 hours results in a dramatic increase in intestinal epithelial cell apoptosis. This intestinal-specific apoptotic response is mediated by induction of endoplasmic reticulum (ER) stress and is accompanied by attenuation of the unfolded protein response (UPR) coupled to an improper activation of downstream UPR mediators such *atf6* and *s-xbp1*. Interestingly, loss of XBP1 in IECs results in the development of spontaneous enterocolitis in mice [52] and polymorphisms of this gene are associated with human IBD [53].

Chronic liver disease is responsible for over 25,000 deaths annually in the United States and represents the tenth leading cause of death, with a prevalence of over 5.5 million patients in 1998 [54] and that has since been estimated to affect up to 30% of the US population [55]. In the UK, the picture is grimmer, as it is the fifth leading cause of death [56]. Nonalcoholic fatty liver disease (NAFLD) is a highly prevalent form of severe chronic liver disease, affecting 3% of all adults in America [57]. It also has significant associated mortality, with a 5-year survival of 67% and 10-year survival of 59% [57]. Additionally, up to one-third of all Americans have some level of NAFLD [56]. Outside of the USA, where obesity is less prevalent, rates are also increasing. In Italy, which is traditionally considered low risk, an incidence of NAFLD of 20–25% of the population

has been recently been reported [56]. In China and Japan, the disease incidence has been reported at 15% and 14% of the population, respectively [56]. There is no identifiable cause of NAFLD, but the pathology is linked to obesity, diabetes, and hyperlipidemia. Treatment involves managing these complex etiologies, and pharmacological therapies specific for NAFLD are not available for these patients [57]. Consequently, significant work has been invested to develop reliable zebrafish larvae models of liver pathology that could be easily utilized for drug targeting and screening.

The most characterized zebrafish model of NAFLD involved a forward genetic screen using viral insertion and screening for hepatomegaly. In the case of the NAFLD model, a 172 bp gene trap cassette was found to be inserted in the intron between exons 11 and 12 of the recently discovered zebrafish gene *foie gras* (*foigr*) [58], which results in a frame shift mutation, and generation of a stop codon. This mutation ($foigr^{hi1532b}$) results in the development of steatosis (fatty liver disease) resembling human NAFLD, characterized by large lipid filled hepatocytes and cellular apoptosis in larvae as young as 5 dpf [58]. However, the exact function of this gene, which is highly conserved across species including humans, is not yet determined. Further studies with the *foigr* mutant have shown that the apoptosis observed involves increased ER stress and is regulated in part through the UPR gene *atf6*. Morpholino blockade of *atf6* ameliorates liver injury during chronic ER stress in the *foigr* mutants [31]. However, *atf6* blockade potentiates steatosis during acute ER stress induced by the toxin tunicamycin [31], suggesting that *atf6* may have variable effects in different phases (acute/chronic) of liver injury. Hepatic steatosis has also been induced in zebrafish larvae using thioacetamide [32]. Investigators have showed that administration of 0.025% thioacetamide into the fish media at 3 dpf resulted in liver damage by 5 dpf, characterized by increased accumulation of fatty droplets, hepatocyte apoptosis, and upregulation of apoptotic genes such as *bad, bax, p-38a, caspase-3* and *8*, and *jnk-1*. Overall, the availability of NAFLD zebrafish models is burgeoning, and they are poised to be screened for pharmacological compounds that could for the first time effectively treat this disease.

Alcoholic fatty liver disease (ALD) is estimated to be involved in over 50% of all deaths due to liver failure secondary to liver cirrhosis, but accurate estimates for prevalence are unavailable [54]. Binge drinking leads to transient fatty liver disease, but chronic alcohol consumption can lead to fibrosis, cirrhosis, and steatohepatitis [59]. An ALD model has also been developed in zebrafish with administration of 2% ethanol to the water of 4 dpf zebrafish for 32 days. This regimen results in hepatomegaly and steatosis, alongside upregulation of hepatic *cyp2e1*, *sod*, and *bip* gene expression—indicating hepatotoxic metabolism of the ethanol [33]. Importantly, ethanol-induced steatosis was prevented by morpholino blockade of the sterol regulatory binding protein (Srebps). Because Srebps activation is important in chronic alcoholic liver disease [33] in humans, the zebrafish ALD model could be utilized to identify new therapeutic mechanisms and to screen for therapeutic agents.

4. Microbe-Host Interactions

The ability to generate germ-free and gnotobiotic zebrafish [60] has led to an increasing interest in understanding cellular and molecular mechanisms of microbial-host interactions using zebrafish. Microbial-host interactions have received significant interested in recent years and have been implicated in a wide variety of human diseases, including CRC [61], IBD [42, 43], obesity and diabetes [62], intestinal healing [63], irritable bowel syndrome [64], and inflammatory nociception [65]. Zebrafish are host to gram-positive and gram-negative bacteria, mycobacteria, protozoa, and viruses [66], also allowing for their use as a model for infectious diseases. In most cases, microorganisms associated with these pathologies are not intrinsically pathogenic but are rather part of the normal, commensal biota. The organ exposed to the highest amount of microorganisms in the human body is the gastrointestinal (GI) tract, especially the distal ileum and colon. Because of the high prevalence of bacteria and bacterial products in the GI tract, investigators have studied mechanisms controlling homeostasis in the face of such highly antigenic materials. The zebrafish GI tract also harbors the highest concentration of bacteria and as such represents an interesting model to study bacterial/host interactions.

Bacteria and their associated products such as DNA, RNA, and membrane structures (peptidoglycans, LPS—lipopolysaccharide) are typically detected by a series of innate sensors that are evolutionary conserved. A survey of the zebrafish genome has identified numerous innate sensors from the TLR and the Nod-like receptor family as well as their associated signaling pathways [67]. An almost complete set of TLRs (TLR1-5, 7-9, 21 [68]) exist in zebrafish, as do the intracellular sensors Nod1 and Nod2 [69]. Associated innate signaling proteins have also been identified in zebrafish such as myeloid differentiation primary response gene (MyD88) [68, 70], TIR domain-containing adaptor inducing IFN-β (TRIF) [71], and NF-κB [72, 73].

The most studied bacterial product is arguably the gram-negative-derived LPS. In mammals, LPS is detected by TLR4, in association with the coreceptors MD2 and CD-14 [74]. Once engaged, TLR4 recruits the adapter protein Myd88 or TRIF to propagate the signal to NF-κB [75] and the interferon responsive factor (IRF) 3, respectively [76]. This signaling cascade plays a critical role in host response to microbes and microbial products. As in humans, high doses of LPS are toxic to zebrafish [77]. Studies using commensal and germ-free zebrafish established that intestinal alkaline phosphatase (*iap*), known to detoxify the endotoxic lipid moiety A of LPS in mammals, is induced following microbial colonization [77]. Knockout of *iap* resulted in excessive intestinal neutrophil infiltration, a process involving functional *myd88* and *tnfr* as determined by morpholino blockade [77].

Another important TLR system is TLR5, which detects flagellin and activates various signaling pathways including NF-κB [74]. Similarly to mammals, zebrafish detect flagellin (*Salmonella* derived in these experiments) to induce multiple matrix metalloproteinase genes as well as the inflammatory markers *il1b, il8, ifn,* and *cxcl-C1c* [78]. Morpholino blockade

showed that flagellin-induced *Il1b* and metalloproteinase 9 (*mmp9*) were *myd88* dependent whereas *ifn* and *il8* were activated through another signaling system [78].

The functions of some of these TLR downstream signaling adaptors have also been studied in zebrafish. Both red and green transgenic Myd88 reporter strains such as *Tg*(*myd88:EGFP*)*z163* and *Tg*(*myd88-DsRED2*)*z164* have been developed [70]. These strains have been crossed to both macrophage (*Tg*(*lyz:DsRED2*)*nz50* [79]) and neutrophil (*Tg*(BAC*mpx:GFP*)*i114* [13]) reporter strains to monitor myd88 signaling. Studies with these dual-reporter fish demonstrated that MyD88 colocalized with both macrophages and neutrophils and that these *myd88*-expressing leukocytes migrated to wound sites and were involved in bacterial phagocytosis [70].

Another downstream mediator of LPS signaling, acting independently of MyD88, is TRIF. While zebrafish TRIF shares only 32% homology with the human protein, like in mammalian systems it can induce IFN and NF-κB luciferase-reporter responses as seen using an overexpression system in human HEK293T cells [71]. Interestingly TRIF-dependent gene induction through the TLR4 pathway was found to be nonfunctional in experiments with adult zebrafish stimulated with LPS [71]; however, this is to be expected given that zebrafish TLR4 paralogues (*tlr4a* and *tlr4b*) do not recognize LPS [80, 81].

Outside of the TLRs, the intracellular sensors Nod1 and Nod2 are critical innate signaling systems in mammals. Importantly, Nod2 was the first innate signaling molecule to be genetically linked to Crohn's disease susceptibility [82]. The exact protective role of Nod proteins in mammals is not fully understood but defective bacterial killing appears to be an important factor [82–84]. Both *nod1* and *nod2* genes are expressed in IECs and neutrophils of zebrafish. Functional studies using morpholino blockade showed that Nod2 plays an important role in setting host antimicrobial properties [69]. Interestingly, Nod1 or Nod2 depletion resulted in increased susceptibility to *Salmonella* infection in a zebrafish embryonic infection model [69]. This study suggests that the antimicrobial properties of Nod2 are conserved in zebrafish.

As mentioned previously, NF-κB signaling is an important effector pathway downstream of numerous innate sensor systems [85]. Colonization of germ-free NF-κB; EGFP reporter zebrafish *Tg*(*NFkB:EGFP*)^{nc1} with a commensal microbiota induced NF-κB activation and expression of NF-κB target genes including *complement factor b* (*cfb*) and *serum amyloid a* (*saa*) in intestinal as well as in extraintestinal tissues of the GI tract [86]. Activation of NF-κB signaling in zebrafish indicates an important role of this transcription factor in maintaining host homeostasis that is conserved across species. The ability to longitudinally study NF-κB activation in a cell-type specific fashion in response to various microbial stimuli makes the zebrafish a powerful system to decipher complex host-microbe interaction. Overall, the recent development of the aforementioned technologies makes the study of microbial-host interactions in zebrafish a burgeoning area of research.

Response to infection is another area of microbial-host interaction that has received significant attention in zebrafish. The most studied and prominent zebrafish infectious model is the *M. marinum* model, which is highly analogous to the human infectious agent *M. tuberculosis*, the etiologic agent for Tuberculosis (TB). TB is a growing epidemic worldwide, with over 83 million cases reported between 1990 and 1999, resulting in over 3 million deaths annually [87]. Many strains of the infectious bacteria are becoming drug resistant, resulting in an increase in global disease burden, including in the Unites States [88]. Finding new drugs to combat the ongoing threat of TB is consequently essential, as the disease can no longer be contained with current medications [89]. Coincubation of *M. marinum* with 5 hpf embryos results in the formation of macrophage-driven granulomas within 5 dpf [90], a hallmark of TB pathology. *In vivo* imaging and macrophage depletion showed that granulomas, traditionally thought to be a host-protective mechanism, may in fact be a source of early TB tissue dissemination by passing *M. marinum* into uninfected macrophages during phagocytosis [91, 92]. Consequently, this system has provided novel insights into the pathological mechanisms of TB infection and its interactions with the host immune system and is poised to be used as a drug screen to identify novel anti-TB compounds.

Other pathogens have also been studied in zebrafish. These include *S. aureus*, *S. pyogenes*, and *S. typhimurium*. These and other infectious models in zebrafish have recently been reviewed in detail by Meeker and Trede [9]. Although very informative, these studies were not performed using a natural route of infection but rather by using direct delivery (injection) into embryos at various developmental stages. However, oral gavage technology in larvae would likely improve the physiological relevance of infectious models perform in zebrafish. Another limitation of zebrafish infection models is the difference in host temperature; zebrafish and their natural pathogens exist at a temperature of 28°C, while many human-relevant pathogens are only infectious at 37°C [9]. Finally, there is some evolutionary divergence in TLR signaling that must be taken into account when working with this organism. Specifically, in contrast to mammals, LPS is not sensed by zebrafish TLR4 and the sensor negatively regulates MyD88 signaling [80]. Despite these limitations, zebrafish remain a powerful tool for studying microbe-host interactions [67].

5. Genetic Diseases and Drug Screens

Because of their high fecundity, transparency, and ease of imaging, zebrafish are particularly well suited for genetic screening approaches. Forward and reverse genetic approaches can be undertaken to generate new zebrafish phenotypes and identify new genes of interest with potential relevance to human disease phenotypes. Zebrafish disease models can also be screened in a cost- and time-effective manner to discover disease-suppressing compounds. Using a whole organism is a particularly appealing aspect of zebrafish-based screens, since complex cell-cell and organ-organ interactions are kept intact.

There are two main approaches to forward-genetic screens in zebrafish that have been undertaken thus far. The

first involves exposing males to the mutagen ethylnitrosourea (ENU) and then screening for a phenotype [93, 94] shared by all mutants, such as renal cysts or heart failure. ENU is an alkylating agent that typically induces A → T base transversions. Zebrafish are relatively resistant to the ENU toxic side effects, allowing for higher dosages and thus increased rates of mutation [95]. An alternative mutagenesis approach employs random retroviral insertion [96, 97]. While this retroviral method is only one-ninth as efficient at generating a mutation as the ENU approach, it circumvents the need for positional cloning by tagging each insertion event, saving significant screening effort once a phenotype is found.

Duchenne muscular dystrophy (DMD) affects 1 in 3500 males and causes progressive muscle degeneration that can lead to death. DMD *is the result of mutations in the sarcolemmal protein* dystrophin located on the X-chromosome [98]. During an ENU screen of zebrafish [94], a mutation referred to as *sapje* [99] was discovered. This mutation was later found to be located in the zebrafish Duchenne muscular dystrophy (*dmd*) gene and causes progressive muscular degeneration in zebrafish larvae [100]. Electron microscopy showed that muscular degeneration was the result of failure to form proper muscle attachments at the myotendinous junction. This pathological mechanism was hypothesized to occur in mammals but was lacking concrete evidence, making the zebrafish a novel system for studying the pathophysiology of this devastating disease.

The most common form of heritable polycystic kidney disease (PKD) is autosomal dominant PKD. This disease affects more than 1 in 1000 live births and approximately 10% of patients with PKD will require kidney transplant due to renal failure [101]. PKD has been linked to defects in primary cilia formation and function in humans [101]. This disease has also been successfully modeled in zebrafish by using retroviral insertion mutagenesis and screening for cystic kidneys in 5 dpf larvae [102]. The screen discovered 12 genes whose loss formed cysts in the glomerular-tubular region, including two already associated with human disease (*vhnf1* and *pkd2*), demonstrating genetic and phenotypic homology between humans and zebrafish. Three of the 10 remaining genes are homologues of *Chlamydomonas* (a genus of green algae) genes, which encode components of intraflagellar transport particles involved in cilia formation [102], but have yet to be analyzed in human PKD patients. The other 7 genes discovered provide completely novel targets for studying the underlying genetics and mechanisms of PKD, as many of the genes that can result in PKD remain unidentified in humans [101].

Dilated cardiomyopathy (DCM) is the cause of at least half of the 5.8 million heart failure cases in the USA, typically resulting from prior heart damage due to a myocardial infarction or an infection [103]. Worldwide, DCM is the leading indicator for heart transplant [104], with incidences to be as high as 9.6 per 100,000 person-years in Europe [104] and China [105]. DCM results in poor heart function that eventually leads to death [103]. ENU zebrafish screens discovered numerous fish with cardiac abnormalities [93, 106, 107]. Two of these mutants, *sih* and *pickwickm171*, were found to have dilated hearts with thin walls and defective contractility [108, 109]. Further analysis showed that the *sih* (silent heart) mutants had a mutation in cardiac troponin T gene [108], while the *pickwickm171* mutants had a mutation in the *titin* gene [109]. Since both of these genes are known to be important in human DCM, these mutants zebrafish represent interesting and complementary models to study this pathology.

All of the aforementioned models demonstrate that forward genetic screens in zebrafish can generate specific phenotypes that are highly homologous to human diseases. Further analysis of these mutants almost invariability leads to the identification of a gene with high homology and relevance to corresponding human disease.

Targeted, reverse genetic approaches are also quite successful in generating models of disease, especially if a homolog exists between the human gene(s) driving the disease and the zebrafish. One disease that has recently been modeled in zebrafish using a reverse-genetic approach is Hutchinson-Gilford progeria syndrome (HGPS), a rare (1 : 4,000,000 people) premature senescence syndrome that generally results from sporadic mutations that disrupts conversion of prelamin A to mature lamin A [110]. HGPS patients have markedly aberrant development characterized by lipodystrophy, osteolysis that is most pronounced in the cranium, and coronary dysfunction [110]. The mean life expectancy for patients with HGPS is less than 13 years. In zebrafish, investigators were able to use a combination of directed loss of function mutations and morpholino knockdowns of prelamin and progerin to generate zebrafish that were able to live to adulthood (though with shortened lifespans). These fish had both phenotypic and molecular signs of early senescence, including lipodystrophy, aberrant musculature and craniofacial skeletal structure, increased cellular apoptosis, and cell-cycle arrest [111]. These phenotypic manifestations align remarkably well with those seen in human HGPS, demonstrating a proof of concept for reverse genetic approaches to developing zebrafish models of human diseases.

Some of the mutants generated during forward-genetic screens have been subsequently subjected to drug screening methodologies. The ability to rapidly and easily image large numbers of developing zebrafish makes them highly tractable as a preclinical system for drug screens [112]. A prototypical example of drug screening in mutant zebrafish discovered with the ENU forward-genetic approaches involves the *gridlock* (*grl*) mutant. The *grl* mutant lacks blood flow to the posterior trunk and tail due to a localized block in caudal blood flow at the base of the dorsal aorta [113]. This model has many characteristics similar to the human congenital disease coarctation of the aorta, making it of significant clinical interest. Coarctation of the aorta involves narrowing of the aorta that affects 1 in 2,500 live births [114]. It is the fifth most common form of congenital heart defect, and without surgical treatment the mean age of survival is only 31 years of age [114]. Surgical intervention can prevent early death, but significant morbidity, usually in the form of hypertension, can persist and results in decreased life expectancy [114]. Unfortunately, no clear etiology of the

disease exists, and the *grl* model in zebrafish is the best animal model currently in existence for the study of this disease [114].

The *grl* zebrafish has a hypomorphic mutation in the *hey2* gene, a basic helix-loop-helix protein involved in aortic development [115]. Gene titration studies using morpholino technology demonstrated that dose-dependent loss of this gene results in ablation of progressively larger sections of the aorta and expansion of the contiguous region of vein [116]. A pharmacological screen, assessing restoration of blood flood and survival of larvae using bright-field microscopy, found that two structurally related compounds (GS3999 and GS4012, unknown targets) promoted activation of the vascular endothelial growth factor (VEGF) pathway and were able to rescue the phenotype [117]. Another unrelated screen found that phosphoinositide-3-kinase (PI3K) inhibitors were also able to rescue the phenotype by driving VEGF activation [118]. This included the uncharacterized flavone GS4898, a structurally similar compound to the PI3K inhibitor LY294002, and the PI3K inhibitor wortmannin. This work also demonstrated for the first time that ERK signaling in embryos drives aortic differentiation, while activation of PI3K signaling produces a venous fate. These findings have since been recapitulated in a murine system and have provided new insights into arterial morphogenesis [119] as well as generated some of the first insights into the underlying mechanisms behind coarctation of the aorta in humans.

A pair of robust screens has also been performed to evaluate compounds known to induce prolonged QT intervals in humans in the hopes of developing a preclinical cardiac toxicity screen. Cardiac QT elongation, which can cause the fatal heart arrhythmia known as Torsade de Pointes, is required to be evaluated in clinical drug trials [120] and thus these screens are of great clinical importance. Two such screens to evaluate bradycardia, atrioventricular blockade and arrhythmias in zebrafish have been performed thus far [121, 122]. In the first study 100 biologically active compounds were screened and 18 of the 23 that caused arrhythmias in humans were also positive in the zebrafish, while postscreen analysis showed that poor absorption explained 4 out of 5 of the false-negatives [122]. Additionally, the combination of erythromycin and cisapride was also positive during screening while each drug alone was not, recapitulating a known drug-drug interaction that causes arrhythmias in humans. Consequently, the zebrafish hold significant promise to be used as a screen to evaluate new drugs for their potential to generate this serious and often fatal side effect.

6. Overall Limitations

The use of zebrafish as a model organism for studying human disease is a relatively new and emerging field of research. Consequently, the number of available zebrafish strains and facilities that house zebrafish is much smaller than for well-developed model higher vertebrate organisms such as the mouse. Additionally, very few validated zebrafish reagents such as antibodies and cell lines are available to the research community. This significantly curtails the in-depth investigation of molecular and cellular details implicated in a given phenotypes.

Zebrafish also have numerous duplicate genes [123], which significantly complicate generation of knockout strains using either forward or reverse-genetic approaches. Forward-genetic approaches that disrupt one gene copy likely will not disrupt the second copy, and duplicate genes also make targeted knockout strategies more difficult as both copies must be deleted. Additionally, while the zebrafish genome has been fully sequenced, the annotation is still limited and more of a work in progress. Furthermore comparative genomic analyses between zebrafish and the human or murine genome counterparts have yet to be performed.

Zebrafish also have environmental conditions that differ substantially from humans. They must be raised in water with specific ionic concentrations and temperature (28°C). Consequently, some water-insoluble small molecules cannot be administered to zebrafish because carrier solvents (such as EtOH or DMSO) would reach toxic levels before solubility is achieved. Additionally, since drugs are administered directly to the fish media, bathing the entire fish in the test compound can result in nondesired toxic side effects. An example in our hands was the attempt to use dextran sodium sulfate (DSS) to induce colitis in larval zebrafish. At concentrations as low as 0.01% (v/v) the surfactant properties of the DSS choked the gills of the zebrafish, resulting in their death before an intestine-specific effect could be observed (Goldsmith and Jobin, unpublished observation). As discussed in a previous section, the development of an oral gavage approach could circumvent this important limitation.

7. Perspectives

Animal models have been used since the inception of medical research. For most models of human disease, the preferred and most utilized animal system of human disease is overwhelmingly the murine system. Despite the tremendous gain of knowledge provided by using murine experimental systems, the long gestation time (18–20 days) and sexual maturation rate (6–8 weeks) combined with high cost of housing and breeding represent significant limitations. Furthermore, experiments with mice are labor intensive and not particularly well suited for high-throughput screening. These limitations have spurred the need to develop other model organisms that could be used to provide initial gene or drug targets information before beginning investigations in more expensive systems.

Transparent, larval zebrafish models have the potential to fill this important niche in the study of human disease, enabling rapid, physiologically relevant *in vivo* screening. The transparent nature of zebrafish also allows for real-time imaging of pathogenesis, which has already provided key insights into the molecular mechanisms of metastasis [124–127] and tuberculosis dissemination [90–92]. The recent advent of the *Casper* fish promises to extend the imaging capacity beyond larvae to adult fish, permitting studies in fish with a functional adaptive immune system. The zebrafish has already demonstrated profound bench-to-bedside power, as evidenced by the rapid translation time

(~2-years) from the initial reports of the role of H_2O_2 in neutrophil chemotaxis during wound healing in zebrafish [11] to the first utilizations of such knowledge in human patients [18].

The zebrafish remains a relatively underdeveloped model organism with large amounts of untapped potential. As more is understood about the comparative genome, anatomy, and physiology of zebrafish to that of humans, the relevance and utility of this vertebrate model will only grow and provide a powerful complement to the murine system. Two decades of research has demonstrated the power and relevancy of the zebrafish in modeling human disease. Its unique properties make it an ideal *in vivo* system for initial use in the interrogation of a given pathology before translating the observations made in the model organism to more expensive murine systems.

References

[1] A. Fire, S. Xu, M. K. Montgomery, S. A. Kostas, S. E. Driver, and C. C. Mello, "Potent and specific genetic interference by double-stranded RNA in caenorhabditis elegans," *Nature*, vol. 391, no. 6669, pp. 806–811, 1998.

[2] J. Yuan, S. Shaham, S. Ledoux, H. M. Ellis, and H. R. Horvitz, "The C. elegans cell death gene ced-3 encodes a protein similar to mammalian interleukin-1β-converting enzyme," *Cell*, vol. 75, no. 4, pp. 641–652, 1993.

[3] G. K. Hansson and K. Edfeldt, "Toll to be paid at the gateway to the vessel wall," *Arteriosclerosis, Thrombosis, and Vascular Biology*, vol. 25, no. 6, pp. 1085–1087, 2005.

[4] B. A. Barut and L. I. Zon, "Realizing the potential of zebrafish as a model for human disease," *Physiological Genomics*, vol. 2000, no. 2, pp. 49–51, 2000.

[5] J. T. Shin, J. R. Priest, I. Ovcharenko et al., "Human-zebrafish non-coding conserved elements act *in vivo* to regulate transcription," *Nucleic Acids Research*, vol. 33, no. 17, pp. 5437–5445, 2005.

[6] C. B. Moens, T. M. Donn, E. R. Wolf-Saxon, and T. P. Ma, "Reverse genetics in zebrafish by TILLING," *Briefings in Functional Genomics and Proteomics*, vol. 7, no. 6, pp. 454–459, 2008.

[7] R. M. White, A. Sessa, C. Burke et al., "Transparent adult zebrafish as a tool for in vivo transplantation analysis," *Cell Stem Cell*, vol. 2, no. 2, pp. 183–189, 2008.

[8] G. J. Lieschke, A. C. Oates, M. O. Crowhurst, A. C. Ward, and J. E. Layton, "Morphologic and functional characterization of granulocytes and macrophages in embryonic and adult zebrafish," *Blood*, vol. 98, no. 10, pp. 3087–3096, 2001.

[9] N. D. Meeker and N. S. Trede, "Immunology and zebrafish: spawning new models of human disease," *Developmental and Comparative Immunology*, vol. 32, no. 7, pp. 745–757, 2008.

[10] B. Novoa and A. Figueras, *zebrafish: Model for the Study of Inflammation and the Innate Immune Response to Infectious Diseases: Current Topics in Innate Immunity II*, Springer, New York, NY, USA, 2012.

[11] P. Niethammer, C. Grabher, A. T. Look, and T. J. Mitchison, "A tissue-scale gradient of hydrogen peroxide mediates rapid wound detection in zebrafish," *Nature*, vol. 459, no. 7249, pp. 996–999, 2009.

[12] A. Raya, C. M. Koth, D. Büscher et al., "Activation of Notch signaling pathway precedes heart regeneration in zebrafish," *Proceedings of the National Academy of Sciences of the United States of America*, vol. 100, supplement 1, pp. 11889–11895, 2003.

[13] J. R. Mathias, B. J. Perrin, T. X. Liu, J. Kanki, A. T. Look, and A. Huttenlocher, "Resolution of inflammation by retrograde chemotaxis of neutrophils in transgenic zebrafish," *Journal of Leukocyte Biology*, vol. 80, no. 6, pp. 1281–1288, 2006.

[14] V. V. Belousov, A. F. Fradkov, K. A. Lukyanov et al., "Genetically encoded fluorescent indicator for intracellular hydrogen peroxide," *Nature Methods*, vol. 3, no. 4, pp. 281–286, 2006.

[15] S. Rieger and A. Sagasti, "Hydrogen peroxide promotes injury-induced peripheral sensory axon regeneration in the zebrafish skin," *PLoS Biology*, vol. 9, no. 5, Article ID e1000621, 2011.

[16] Q. Pan, W. Y. Qiu, Y. N. Huo, Y. F. Yao, and M. F. Lou, "Low levels of hydrogen peroxide stimulate corneal epithelial cell adhesion, migration, and wound healing," *Investigative Ophthalmology and Visual Science*, vol. 52, no. 3, pp. 1723–1734, 2011.

[17] T. Toth, H. Brostrom, V. Baverud et al., "Evaluation of LHP(1% hydrogen peroxide) cream versus petrolatum and untreated controls in open wounds in healthy horses: a randomized, blinded control study," *Acta Veterinaria Scandinavica*, vol. 53, p. 45, 2011.

[18] J. Weiss, F. J. Winkelman, A. Titone, and E. Weiss, "Evaluation of hydrogen peroxide as an intraprocedural hemostatic agent in manual dermabrasion," *Dermatologic Surgery*, vol. 36, no. 10, pp. 1601–1603, 2010.

[19] K. D. Poss, L. G. Wilson, and M. T. Keating, "Heart regeneration in zebrafish," *Science*, vol. 298, no. 5601, pp. 2188–2190, 2002.

[20] C. L. Lien, M. Schebesta, S. Makino, G. J. Weber, and M. T. Keating, "Gene expression analysis of zebrafish heart regeneration," *PLoS Biology*, vol. 4, no. 8, p. e260, 2006.

[21] A. N. Y. Ng, T. A. de Jong-Curtain, D. J. Mawdsley et al., "Formation of the digestive system in zebrafish: III. Intestinal epithelium morphogenesis," *Developmental Biology*, vol. 286, no. 1, pp. 114–135, 2005.

[22] K. N. Wallace, S. Akhter, E. M. Smith, K. Lorent, and M. Pack, "Intestinal growth and differentiation in zebrafish," *Mechanisms of Development*, vol. 122, no. 2, pp. 157–173, 2005.

[23] H. William, I. Detrich, M. Westerfield, and L. Zon, *The zebrafish: Cellular and Developmental Biology*, Academic Press, New York, NY, USA, 2011.

[24] A. P. G. Haramis, A. Hurlstone, Y. van der Velden et al., "Adenomatous polyposis coli-deficient zebrafish are susceptible to digestive tract neoplasia," *EMBO Reports*, vol. 7, no. 4, pp. 444–449, 2006.

[25] S. H. Lam and Z. Gong, "Modeling liver cancer using zebrafish: a comparative oncogenomics approach," *Cell Cycle*, vol. 5, no. 6, pp. 573–577, 2006.

[26] R. D. Rekha, A. A. Amali, G. M. Her et al., "Thioacetamide accelerates steatohepatitis, cirrhosis and HCC by expressing HCV core protein in transgenic zebrafish Danio rerio," *Toxicology*, vol. 243, no. 1-2, pp. 11–22, 2008.

[27] S. W. Park, J. M. Davison, J. Rhee, R. H. Hruban, A. Maitra, and S. D. Leach, "Oncogenic KRAS induces progenitor cell expansion and malignant transformation in zebrafish," *Gastroenterology*, vol. 134, no. 7, pp. 2080–2090, 2008.

[28] A. Fleming, J. Jankowski, and P. Goldsmith, "In vivo analysis of gut function and disease changes in a zebrafish larvae model of inflammatory bowel disease: a feasibility study," *Inflammatory Bowel Diseases*, vol. 16, no. 7, pp. 1162–1172, 2010.

[29] S. H. Oehlers, M. V. Flores, K. S. Okuda, C. J. Hall, K. E. Crosier, and P. S. Crosier, "A chemical enterocolitis model in zebrafish larvae that is dependent on microbiota and responsive to pharmacological agents," *Developmental Dynamics*, vol. 240, no. 1, pp. 288–298, 2011.

[30] S. Brugman, K. Y. Liu, D. Lindenbergh-Kortleve et al., "Oxazolone-induced enterocolitis in zebrafish depends on the composition of the intestinal microbiota," *Gastroenterology*, vol. 137, no. 5, pp. 1757–67, 2009.

[31] A. Cinaroglu, C. Gao, D. Imrie, and K. C. Sadler, "Activating transcription factor 6 plays protective and pathological roles in steatosis due to endoplasmic reticulum stress in zebrafish," *Hepatology*, vol. 54, no. 2, pp. 495–508, 2011.

[32] A. A. Amali, R. D. Rekha, C. J. F. Lin et al., "Thioacetamide induced liver damage in zebrafish embryo as a disease model for steatohepatitis," *Journal of Biomedical Science*, vol. 13, no. 2, pp. 225–232, 2006.

[33] M. J. Passeri, A. Cinaroglu, C. Gao, and K. C. Sadler, "Hepatic steatosis in response to acute alcohol exposure in zebrafish requires sterol regulatory element binding protein activation," *Hepatology*, vol. 49, no. 2, pp. 443–452, 2009.

[34] J. Groden, A. Thliveris, W. Samowitz et al., "Identification and characterization of the familial adenomatous polyposis coli gene," *Cell*, vol. 66, no. 3, pp. 599–600, 1991.

[35] K. W. Kinzler, M. C. Nilbert, L. K. Su et al., "Identification of FAP locus genes from chromosome 5q21," *Science*, vol. 253, no. 5020, pp. 661–665, 1991.

[36] L. K. Su, K. W. Kinzler, B. Vogelstein et al., "Multiple intestinal neoplasia caused by a mutation in the murine homolog of the APC gene," *Science*, vol. 256, no. 5057, pp. 668–670, 1992.

[37] A. Jemal, R. Siegel, J. Xu, and E. Ward, "Cancer statistics, 2010," *CA Cancer Journal for Clinicians*, vol. 60, no. 5, pp. 277–300, 2010.

[38] F. X. Bosch, J. Ribes, M. Díaz, and R. Cléries, "Primary liver cancer: worldwide incidence and trends," *Gastroenterology*, vol. 127, no. 5, supplement 1, pp. S5–S16, 2004.

[39] H. B. El-Serag, J. A. Davila, N. J. Petersen, and K. A. McGlynn, "The continuing increase in the incidence of hepatocellular carcinoma in the United States: an update," *Annals of internal medicine*, vol. 139, no. 10, pp. 817–823, 2003.

[40] M. N. Lee, E. Y. Jung, H. J. Kwun et al., "Hepatitis C virus core protein represses the p21 promoter through inhibition of a TGF-β pathway," *Journal of General Virology*, vol. 83, no. 9, pp. 2145–2151, 2002.

[41] T. Karrasch and C. Jobin, "Wound healing responses at the gastrointestinal epithelium: a close look at novel regulatory factors and investigative approaches," *Zeitschrift fur Gastroenterologie*, vol. 47, no. 12, pp. 1221–1229, 2009.

[42] R. B. Sartor, "Microbial influences in inflammatory bowel diseases," *Gastroenterology*, vol. 134, no. 2, pp. 577–594, 2008.

[43] R. B. Sartor and M. Muehlbauer, "Microbial host interactions in IBD: implications for pathogenesis and therapy," *Current Gastroenterology Reports*, vol. 9, no. 6, pp. 497–507, 2007.

[44] E. V. Loftus, "Clinical epidemiology of inflammatory bowel disease: incidence, prevalence, and environmental influences," *Gastroenterology*, vol. 126, no. 6, pp. 1504–1517, 2004.

[45] N. A. Molodecky, I. S. Soon, D. M. Rabi et al., "Increasing incidence and prevalence of the inflammatory bowel diseases with time, based on systematic review," *Gastroenterology*, vol. 142, no. 1, pp. 46–54, 2012.

[46] A. B. Pithadia and S. Jain, "Treatment of Inflammatory Bowel Disease (IBD)," *Pharmacological Reports*, vol. 63, no. 3, pp. 629–642, 2011.

[47] M. Saleh and C. O. Elson, "Experimental inflammatory bowel disease: insights into the host-microbiota dialog," *Immunity*, vol. 34, no. 3, pp. 293–302, 2011.

[48] S. Wirtz, C. Neufert, B. Weigmann, and M. F. Neurath, "Chemically induced mouse models of intestinal inflammation," *Nature Protocols*, vol. 2, no. 3, pp. 541–546, 2007.

[49] M. Boirivant, I. J. Fuss, A. Chu, and W. Strober, "Oxazolone colitis: a murine model of T helper cell type 2 colitis treatable with antibodies to interleukin 4," *Journal of Experimental Medicine*, vol. 188, no. 10, pp. 1929–1939, 1998.

[50] S. Fichtner-Feigl, W. Strober, E. K. Geissler, and H. J. Schlitt, "Cytokines mediating the induction of chronic colitis and colitis-associated fibrosis," *Mucosal Immunology*, vol. 1, supplement 1, pp. S24–S27, 2008.

[51] J. R. Goldsmith, J. F. Rawls, and C. Jobin, "The neuropeptide DALDA protects against NSAID-induced acute intestinal injury in zebrafish larvae," *Gastroenterology*, vol. 140, no. 5, p. S-474, 2011.

[52] A. Kaser, A. H. Lee, A. Franke et al., "XBP1 links ER stress to intestinal inflammation and confers genetic risk for human inflammatory bowel disease," *Cell*, vol. 134, no. 5, pp. 743–756, 2008.

[53] A. Kaser, E. Martínez-Naves, and R. S. Blumberg, "Endoplasmic reticulum stress: implications for inflammatory bowel disease pathogenesis," *Current Opinion in Gastroenterology*, vol. 26, no. 4, pp. 318–326, 2010.

[54] W. R. Kim, R. S. Brown, N. A. Terrault, and H. El-Serag, "Burden of liver disease in the United States: summary of a workshop," *Hepatology*, vol. 36, no. 1, pp. 227–242, 2002.

[55] M. Lazo and J. M. Clark, "The epidemiology of nonalcoholic fatty liver disease: a global perspective," *Seminars in Liver Disease*, vol. 28, no. 4, pp. 339–350, 2008.

[56] R. Williams, "Global challenges in liver disease," *Hepatology*, vol. 44, no. 3, pp. 521–526, 2006.

[57] B. A. Neuschwander-Tetri and S. H. Caldwell, "Nonalcoholic steatohepatitis: summary of an AASLD Single Topic Conference," *Hepatology*, vol. 37, no. 5, pp. 1202–1219, 2003.

[58] K. C. Sadler, A. Amsterdam, C. Soroka, J. Boyer, and N. Hopkins, "A genetic screen in zebrafish identifies the mutants *vps18*, *nf2* and foie gras as models of liver disease," *Development*, vol. 132, no. 15, pp. 3561–3572, 2005.

[59] C. S. Lieber, "Alcoholic fatty liver: its pathogenesis and mechanism of progression to inflammation and fibrosis," *Alcohol*, vol. 34, no. 1, pp. 9–19, 2004.

[60] L. N. Pham, M. Kanther, I. Semova, and J. F. Rawls, "Methods for generating and colonizing gnotobiotic zebrafish," *Nature Protocols*, vol. 3, no. 12, pp. 1862–1875, 2008.

[61] J. M. Uronis and C. Jobin, "Microbes and colorectal cancer: is there a relationship?" *Current Oncology*, vol. 16, no. 4, pp. 22–24, 2009.

[62] R. E. Ley, "Obesity and the human microbiome," *Current Opinion in Gastroenterology*, vol. 26, no. 1, pp. 5–11, 2010.

[63] C. D. Packey and M. A. Ciorba, "Microbial influences on the small intestinal response to radiation injury," *Current Opinion in Gastroenterology*, vol. 26, no. 2, pp. 88–94, 2010.

[64] C. Rousseaux, X. Thuru, A. Gelot et al., "Lactobacillus acidophilus modulates intestinal pain and induces opioid and cannabinoid receptors," *Nature Medicine*, vol. 13, no. 1, pp. 35–37, 2007.

[65] F. A. Amaral, D. Sachs, V. V. Costa et al., "Commensal microbiota is fundamental for the development of inflammatory pain," *Proceedings of the National Academy of Sciences of the United States of America*, vol. 105, no. 6, pp. 2193–2197, 2008.

[66] A. M. van der Sar, B. J. Appelmelk, C. M. J. E. Vandenbroucke-Grauls, and W. Bitter, "A star with stripes: zebrafish as an infection model," *Trends in Microbiology*, vol. 12, no. 10, pp. 451–457, 2004.

[67] M. Kanther and J. F. Rawls, "Host-microbe interactions in the developing zebrafish," *Current Opinion in Immunology*, vol. 22, no. 1, pp. 10–19, 2010.

[68] C. Jault, L. Pichon, and J. Chluba, "Toll-like receptor gene family and TIR-domain adapters in Danio rerio," *Molecular Immunology*, vol. 40, no. 11, pp. 759–771, 2004.

[69] S. H. Oehlers, M. V. Flores, C. J. Hall, S. Swift, K. E. Crosier, and P. S. Crosier, "The inflammatory bowel disease (IBD) susceptibility genes NOD1 and NOD2 have conserved antibacterial roles in zebrafish," *Disease Models & Mechanisms*, vol. 4, no. 6, pp. 832–841, 2011.

[70] C. Hall, M. V. Flores, A. Chien, A. Davidson, K. Crosier, and P. Crosier, "Transgenic zebrafish reporter lines reveal conserved Toll-like receptor signaling potential in embryonic myeloid leukocytes and adult immune cell lineages," *Journal of Leukocyte Biology*, vol. 85, no. 5, pp. 751–765, 2009.

[71] S. Fan, S. Chen, Y. Liu et al., "Zebrafish TRIF, a Golgi-localized protein, participates in IFN induction and NF-κB activation," *Journal of Immunology*, vol. 180, no. 8, pp. 5373–5383, 2008.

[72] R. G. Correa, T. Matsui, V. Tergaonkar, C. Rodriguez-Esteban, J. C. Izpisua-Belmonte, and I. M. Verma, "Zebrafish IκB kinase 1 negatively regulates NF-κB activity," *Current Biology*, vol. 15, no. 14, pp. 1291–1295, 2005.

[73] R. G. Correa, V. Tergaonkar, J. K. Ng, I. Dubova, J. C. Izpisua-Belmonte, and I. M. Verma, "Characterization of NF-κB/IκB proteins in zebra fish and their involvement in notochord development," *Molecular and Cellular Biology*, vol. 24, no. 12, pp. 5257–5268, 2004.

[74] R. Medzhitov, "Toll-like receptors and innate immunity," *Nature Reviews Immunology*, vol. 1, no. 2, pp. 135–145, 2001.

[75] S. Janssens and R. Beyaert, "A universal role for MyD88 in TLR/IL-1R-mediated signaling," *Trends in Biochemical Sciences*, vol. 27, no. 9, pp. 474–482, 2002.

[76] S. E. Doyle, S. A. Vaidya, R. O'Connell et al., "IRF3 mediates a TLR3/TLR4-specific antiviral gene program," *Immunity*, vol. 17, no. 3, pp. 251–263, 2002.

[77] J. M. Bates, J. Akerlund, E. Mittge, and K. Guillemin, "Intestinal alkaline phosphatase detoxifies lipopolysaccharide and prevents inflammation in zebrafish in response to the gut microbiota," *Cell Host and Microbe*, vol. 2, no. 6, pp. 371–382, 2007.

[78] O. W. Stockhammer, A. Zakrzewska, Z. Hegedûs, H. P. Spaink, and A. H. Meijer, "Transcriptome profiling and functional analyses of the zebrafish embryonic innate immune response to salmonella infection," *Journal of Immunology*, vol. 182, no. 9, pp. 5641–5653, 2009.

[79] C. Hall, M. Flores, T. Storm, K. Crosier, and P. Crosier, "The zebrafish lysozyme C promoter drives myeloid-specific expression in transgenic fish," *BMC Developmental Biology*, vol. 7, article 42, 2007.

[80] M. P. Sepulcre, F. Alcaraz-Pérez, A. López-Muñoz et al., "Evolution of lipopolysaccharide (LPS) recognition and signaling: fish TLR4 does not recognize LPS and negatively regulates NF-κB activation," *Journal of Immunology*, vol. 182, no. 4, pp. 1836–1845, 2009.

[81] C. Sullivan, J. Charette, J. Catchen et al., "The gene history of zebrafish tlr4a and tlr4b is predictive of their divergent functions," *Journal of Immunology*, vol. 183, no. 9, pp. 5896–5908, 2009.

[82] J. P. Hugot, M. Chamaillard, H. Zouali et al., "Association of NOD2 leucine-rich repeat variants with susceptibility to Crohn's disease," *Nature*, vol. 411, no. 6837, pp. 599–603, 2001.

[83] L. Eckmann and M. Karin, "NOD2 and Crohn's disease: Loss or gain of function?" *Immunity*, vol. 22, no. 6, pp. 661–667, 2005.

[84] E. Noguchi, Y. Homma, X. Kang, M. G. Netea, and X. Ma, "A Crohn's disease-associated NOD2 mutation suppresses transcription of human IL10 by inhibiting activity of the nuclear ribonucleoprotein hnRNP-A1," *Nature Immunology*, vol. 10, no. 5, pp. 471–479, 2009.

[85] T. Karrasch and C. Jobin, "NF-κB and the intestine: friend or foe?" *Inflammatory Bowel Diseases*, vol. 14, no. 1, pp. 114–124, 2008.

[86] M. Kanther, X. Sun, M. Mhlbauer et al., "Microbial colonization induces dynamic temporal and spatial patterns of NF-κB activation in the zebrafish digestive tract," *Gastroenterology*, vol. 141, no. 1, pp. 197–207, 2011.

[87] P. J. Dolin, M. C. Raviglione, and A. Kochi, "Global tuberculosis incidence and mortality during 1990–2000," *Bulletin of the World Health Organization*, vol. 72, no. 2, pp. 213–220, 1994.

[88] D. L. Cohn, F. Bustreo, and M. C. Raviglione, "Drug-resistant tuberculosis: review of the worldwide situation and the WHO/IUATLD global surveillance project," *Clinical Infectious Diseases*, vol. 24, supplement 1, pp. S121–S130, 1997.

[89] N. R. Gandhi, P. Nunn, K. Dheda et al., "Multidrug-resistant and extensively drug-resistant tuberculosis: a threat to global control of tuberculosis," *The Lancet*, vol. 375, no. 9728, pp. 1830–1843, 2010.

[90] J. M. Davis, H. Clay, J. L. Lewis, N. Ghori, P. Herbomel, and L. Ramakrishnan, "Real-time visualization of mycobacterium-macrophage interactions leading to initiation of granuloma formation in zebrafish embryos," *Immunity*, vol. 17, no. 6, pp. 693–702, 2002.

[91] H. Clay, J. M. Davis, D. Beery, A. Huttenlocher, S. E. Lyons, and L. Ramakrishnan, "Dichotomous role of the macrophage in early mycobacterium marinum infection of the zebrafish," *Cell Host and Microbe*, vol. 2, no. 1, pp. 29–39, 2007.

[92] J. M. Davis and L. Ramakrishnan, "The role of the granuloma in expansion and dissemination of early tuberculous infection," *Cell*, vol. 136, no. 1, pp. 37–49, 2009.

[93] W. Driever, L. Solnica-Krezel, A. F. Schier et al., "A genetic screen for mutations affecting embryogenesis in zebrafish," *Development*, vol. 123, pp. 37–46, 1996.

[94] P. Haffter, M. Granato, M. Brand et al., "The identification of genes with unique and essential functions in the development of the zebrafish, Danio rerio," *Development*, vol. 123, pp. 1–36, 1996.

[95] G. J. Lieschke and P. D. Currie, "Animal models of human disease: zebrafish swim into view," *Nature Reviews Genetics*, vol. 8, no. 5, pp. 353–367, 2007.

[96] A. Amsterdam, S. Burgess, G. Golling et al., "A large-scale insertional mutagenesis screen in zebrafish," *Genes and Development*, vol. 13, no. 20, pp. 2713–2724, 1999.

[97] A. Amsterdam, R. M. Nissen, Z. Sun, E. C. Swindell, S. Farrington, and N. Hopkins, "Identification of 315 genes essential for early zebrafish development," *Proceedings of the National Academy of Sciences of the United States of America*, vol. 101, no. 35, pp. 12792–12797, 2004.

[98] A. E. H. Emery, "The muscular dystrophies," *The Lancet*, vol. 359, no. 9307, pp. 687–695, 2002.

[99] M. Granato, F. J. M. van Eeden, U. Schach et al., "Genes controlling and mediating locomotion behavior of the zebrafish embryo and larva," *Development*, vol. 123, pp. 399–413, 1996.

[100] D. I. Bassett, R. J. Bryson-Richardson, D. F. Daggett, P. Gautier, D. G. Keenan, and P. D. Currie, "Dystrophin is required for the formation of stable muscle attachments in the zebrafish embryo," *Development*, vol. 130, no. 23, pp. 5851–5860, 2003.

[101] A. C. M. Ong and D. N. Wheatley, "Polycystic kidney disease—the ciliary connection," *The Lancet*, vol. 361, no. 9359, pp. 774–776, 2003.

[102] Z. Sun, A. Amsterdam, G. J. Pazour, D. G. Cole, M. S. Miller, and N. Hopkins, "A genetic screen in zebrafish indentifies cilia genes as a principal cause of cystic kidney," *Development*, vol. 131, no. 16, pp. 4085–4093, 2004.

[103] R. E. Hershberger, A. Morales, and J. D. Siegfried, "Clinical and genetic issues in dilated cardiomyopathy: a review for genetics professionals," *Genetics in Medicine*, vol. 12, no. 11, pp. 655–667, 2010.

[104] S. Rakar, G. Sinagra, A. Di Lenarda et al., "Epidemiology of dilated cardiomyopathy. A prospective post-mortem study of 5252 necropsies," *European Heart Journal*, vol. 18, no. 1, pp. 117–123, 1997.

[105] H. Jiang and J. Ge, "Epidemiology and clinical management of cardiomyopathies and heart failure in China," *Heart*, vol. 95, no. 21, pp. 1727–1731, 2009.

[106] J. N. Chen, P. Haffter, J. Odenthal et al., "Mutations affecting the cardiovascular system and other internal organs in zebrafish," *Development*, vol. 123, pp. 293–302, 1996.

[107] D. Y. R. Stainier, B. Fouquet, J. N. Chen et al., "Mutations affecting the formation and function of the cardiovascular system in the zebrafish embryo," *Development*, vol. 123, pp. 285–292, 1996.

[108] A. J. Sehnert, A. Huq, B. M. Weinstein, C. Walker, M. Fishman, and D. Y. R. Stainier, "Cardiac troponin T is essential in sarcomere assembly and cardiac contractility," *Nature Genetics*, vol. 31, no. 1, pp. 106–110, 2002.

[109] X. Xu, S. E. Meiler, T. P. Zhong et al., "Cardiomyopathy in zebrafish due to mutation in an alternatively spliced exon of titin," *Nature Genetics*, vol. 30, no. 2, pp. 205–209, 2002.

[110] R. C. M. Hennekam, "Hutchinson-Gilford progeria syndrome: review of the phenotype," *American Journal of Medical Genetics A*, vol. 140, no. 23, pp. 2603–2624, 2006.

[111] E. Koshimizu, S. Imamura, J. Qi et al., "Embryonic senescence and laminopathies in a progeroid zebrafish model," *PLoS One*, vol. 6, no. 3, Article ID e17688, 2011.

[112] C. Parng, W. L. Seng, C. Semino, and P. McGrath, "Zebrafish: a preclinical model for drug screening," *Assay and Drug Development Technologies*, vol. 1, no. 1, pp. 41–48, 2002.

[113] B. M. Weinstein, D. L. Stemple, W. Driever, and M. C. Fishman, "Gridlock, a localized heritable vascular patterning defect in the zebrafish," *Nature Medicine*, vol. 1, no. 11, pp. 1143–1147, 1995.

[114] D. Kenny and Z. M. Hijazi, "Coarctation of the aorta: from fetal life to adulthood," *Cardiology Journal*, vol. 18, no. 5, pp. 487–495, 2011.

[115] M. C. Fishman, "gridlock, an HLH gene required for assembly of the aorta in zebrafish," *Science*, vol. 287, no. 5459, pp. 1820–1824, 2000.

[116] T. P. Zhong, S. Childs, J. P. Leu, and M. C. Fishman, "Gridlock signalling pathway fashions the first embryonic artery," *Nature*, vol. 414, no. 6860, pp. 216–220, 2001.

[117] R. T. Peterson, S. Y. Shaw, T. A. Peterson et al., "Chemical suppression of a genetic mutation in a zebrafish model of aortic coarctation," *Nature Biotechnology*, vol. 22, no. 5, pp. 595–599, 2004.

[118] C. C. Hong, Q. P. Peterson, J. Y. Hong, and R. T. Peterson, "Artery/vein specification is governed by opposing phosphatidylinositol-3 kinase and MAP kinase/ERK signaling," *Current Biology*, vol. 16, no. 13, pp. 1366–1372, 2006.

[119] B. Ren, Y. Deng, A. Mukhopadhyay et al., "ERK1/2-Akt1 crosstalk regulates arteriogenesis in mice and zebrafish," *Journal of Clinical Investigation*, vol. 120, no. 4, pp. 1217–1228, 2010.

[120] D. M. Roden, "Drug-induced prolongation of the QT interval," *The New England Journal of Medicine*, vol. 350, no. 10, pp. 1013–1022, 2004.

[121] U. Langheinrich, G. Vacun, and T. Wagner, "Zebrafish embryos express an orthologue of HERG and are sensitive toward a range of QT-prolonging drugs inducing severe arrhythmia," *Toxicology and Applied Pharmacology*, vol. 193, no. 3, pp. 370–382, 2003.

[122] D. J. Milan, T. A. Peterson, J. N. Ruskin, R. T. Peterson, and C. A. MacRae, "Drugs that induce repolarization abnormalities cause bradycardia in zebrafish," *Circulation*, vol. 107, no. 10, pp. 1355–1358, 2003.

[123] I. G. Woods, P. D. Kelly, F. Chu et al., "A comparative map of the zebrafish genome," *Genome Research*, vol. 10, no. 12, pp. 1903–1914, 2000.

[124] J. Etchin, J. P. Kanki, and A. T. Look, "Zebrafish as a model for the study of human cancer," *Methods in Cell Biology*, vol. 105, pp. 309–337, 2011.

[125] L. M. J. Lee, E. A. Seftor, G. Bonde, R. A. Cornell, and M. J. C. Hendrix, "The fate of human malignant melanoma cells transplanted into zebrafish embryos: assessment of migration and cell division in the absence of tumor formation," *Developmental Dynamics*, vol. 233, no. 4, pp. 1560–1570, 2005.

[126] K. Stoletov, V. Montel, R. D. Lester, S. L. Gonias, and R. Klemke, "High-resolution imaging of the dynamic tumor cell-vascular interface in transparent zebrafish," *Proceedings of the National Academy of Sciences of the United States of America*, vol. 104, no. 44, pp. 17406–17411, 2007.

[127] J. M. Topczewska, L. M. Postovit, N. V. Margaryan et al., "Embryonic and tumorigenic pathways converge via Nodal signaling: role in melanoma aggressiveness," *Nature Medicine*, vol. 12, no. 8, pp. 925–932, 2006.

Hindawi Publishing Corporation
Journal of Biomedicine and Biotechnology
Volume 2012, Article ID 346761, 7 pages
doi:10.1155/2012/346761

Review Article

Advancement in the Development of Models for Hepatitis C Research

Wendy C. Carcamo[1] and Cuong Q. Nguyen[2, 3]

[1] *Department of Oral Biology, University of Florida, 1395 Center Drive, Gainesville, FL 32610, USA*
[2] *Center for Orphan Autoimmune Disorders, College of Dentistry, University of Florida, Gainesville, FL 32610, USA*
[3] *Department of Infectious Diseases and Pathology, University of Florida, 2015 SW 16th Avenue, Gainesville, Florida 32608-00881, USA*

Correspondence should be addressed to Cuong Q. Nguyen, nguyen@pathology.ufl.edu

Received 18 January 2012; Accepted 2 April 2012

Academic Editor: Andrea Vecchione

Hepatitis C virus (HCV) is a pandemic disease affecting an estimated 180 million individuals worldwide and infecting each year another ~3-4 million people making HCV a global public health issue. HCV is the main cause for chronic hepatitis, cirrhosis, and hepatocellular carcinoma. In the United States, HCV-related chronic liver disease is a leading cause of liver transplantation. Despite significant improvements in antiviral drugs, only ~50% of treated patients with HCV have viral clearance after treatment. Showing unique species specificity, HCV has a narrow range of potential hosts infecting only chimpanzees and humans. For decades, the chimpanzee model has been the only and instrumental primate for studying HCV infection; however, availability, economic, and ethical issues make the chimpanzee an unsuitable animal model today. Thus, significant research has been devoted to explore different models that are suitable in studying the biology of the virus and application in the clinical research for developing efficient and tolerable treatments for patients. This review focuses on experimental models that have been developed to date and their findings related to HCV.

1. Introduction

Hepatitis C virus (HCV) is a small positive sense single-stranded RNA virus that causes acute and chronic hepatitis C in humans [1, 2]. HCV is one of the major causative agents of liver disease worldwide, with more than 180 million people infected [2, 3]. It is estimated that 3-4 million people are newly infected each year [2]. In the United States, hepatitis-C-related chronic liver disease is a leading cause of liver transplantation and causes thousands of deaths annually [4]. Although therapeutic options are improving, viral clearance fails in about 80% of infected patients, resulting in a chronic viral disease [5]. In 4–20% of patients with chronic hepatitis C, liver cirrhosis develops within 20 years, with 1–5% of these patients developing hepatocellular carcinoma (HCC). Persistent HCV infections are facilitated by the ability of virus to incorporate adaptive mutations in the host and exist as genetically distinct quasispecies. Moreover, the persistent infection may also result from the ability of the virus to disrupt host defense by blocking phosphorylation and function of interferon regulatory factor-3 (IRF-3), an antiviral signaling molecule [6]. Unlike for hepatitis A and B, there is no vaccine to prevent HCV infection; therefore, current treatment is a combination therapy of pegylated interferon-alpha (IFN-α) and ribavirin, which results in sustained clearance of serum HCV-RNA. However, this treatment is only efficacious in approximately 50% of patients [7–9]. Several host factors, such as age, stage of liver fibrosis, body mass index (BMI), liver steatosis, insulin resistance, ethnicity, and IL28B single nucleotide polymorphisms, as well as viral genotype, can potentially influence the treatment outcome [10, 11]. For instance, patients with HCV genotypes 2 and 3 respond more favorably to treatment than patients with genotype 1 and 4 [12]. Therefore, new antiviral compounds that are more efficacious and better-tolerated need to be developed.

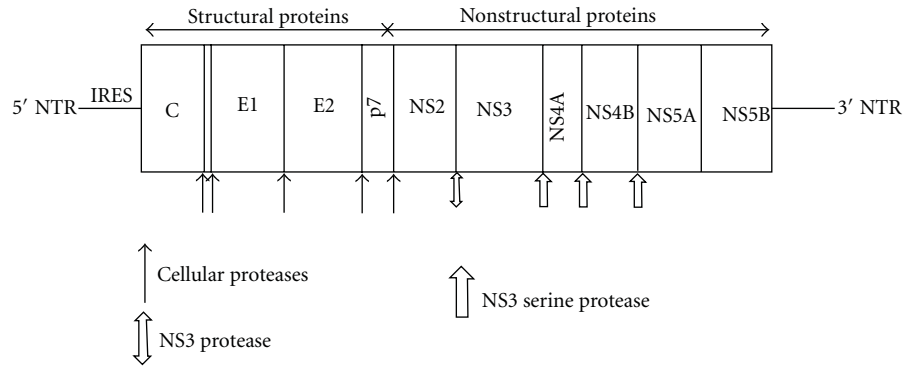

Figure 1: HCV genome and polyprotein cleavage products. A schematic representation of the HCV genome indicating the structural and nonstructural regions, including the 5′ and 3′ NTRs. The polyprotein cleavage products are drawn within. The cleavage site and the corresponding protease are indicated (arrows).

One of the biggest challenges in developing and implementing therapy for HCV infection is finding the appropriate models to examine the translational capability. The focus of this review emphasizes the biological importance of the virus and discusses a number of relevant *in vitro* and *in vivo* small animal models that are used for preclinical evaluations prior to translating to clinical trials in humans.

2. HCV and Its Life Cycle

HCV was originally referred to as non-A non-B Hepatitis (NANB). In 1989, a major breakthrough in HCV research was discovered in which the complete sequence of the viral genome was identified and cloned by Choo and collaborators [13]. HCV is the only member of the *Hepacivirus* genus that belongs to the *Flaviviridae* family [14, 15]. Structural analysis of the virus revealed that the genetic material is surrounded by a protective nucleocapside, composed mainly of the protein core (C), and further protected by a lipid envelope [16]. The lipid envelope contains two major glycoproteins, envelope protein 1 (E1) and E2, that are embedded in the envelope [17]. The genome consists of a single open-reading frame (ORF), that is, ~9,600 nucleotides long, which is made into a single polyprotein (3,010 or 3,033 amino acids) product (Figure 1) [18, 19]. The HCV genome is flanked by two nontranslated regions (NTRs), which are essential in the replication and synthesis of viral proteins. Viral and cellular proteases mediate the processing of the polyprotein into structural (core, E1, E2, and p7) and nonstructural proteins (NS2, NS3, NS4A, NS4B, NS5A, and NS5B) as illustrated in Figure 1 [20–22]. The HCV life cycle is entirely cytoplasmic and replication occurs mainly in hepatocytes, but the virus may also replicate in peripheral blood mononuclear cells (PBMCs). The virus enters the host cells through a complex interaction between virions and cell surface molecules CD81, LDL receptor, scavenger receptor class B type 1 (SR-B1), Claudin-1, and Occludin [23–26]. Recent studies by Ray et al. and Sainz et al. have identified Niemann-Pick C1-like 1 (NPC1L1) cholesterol absorption receptor as a new HCV entry factor [27, 28]. Once inside the cell, the virus takes over the intracellular machinery to replicate [29]. Due to its high-mutation rate caused by the virus' RNA-dependent RNA polymerase (NS5B), which lacks 3′-5′ exonuclease activity [30], HCV is considered a quasispecies composed of 6 genotypes with several subtypes [12]. The eleven genotypes have differences in geographic distribution, disease progression, and response to therapy. Genotypes 1, 2, and 3 are distributed worldwide, with genotypes 1a and 1b accounting for 60% of global infections. In the United States, genotypes 1a and 2b are more commonly encountered.

3. Development of Animal Models Used to Study HCV

HCV infects only humans and chimpanzees. Although the virus was discovered more than 20 years ago using molecular biological methods and the entire genome of the virus sequenced, acquiring further knowledge of the virus has been hampered by the lack of a small animal model. Much of the understanding of HCV replication has been based on subgenomic and genomic replicon systems developed by Bartenschlager and colleagues, described below [31]. Viruses are obligate intracellular parasites that require a permissive host cell in order to study replication. Therefore, development of a suitable small animal is critical in understanding the pathogenesis of the virus, establishing a relevant translational platform for therapeutic methods, and developing effective vaccines. The following describes various models used to study the pathogenicity of HCV and its applicable progression into *in vivo* models, which are summarized in Table 1.

4. Cell-Based or *In Vitro* Models

Viral infection and propagation requires specific host factors that are mainly expressed in highly differentiated cells. To mimic the host factors in an *in vitro* system, development of a cell-based model is essential. A number of cell-based models have been established; however, most of them have yielded limited success. Poor reproducibility and low levels of HCV replication mainly contribute to the shortfall of these models. Furthermore, highly sensitive techniques are needed

Table 1: *In vitro* and *in vivo* models to study HCV.

In Vitro	*In Vivo*
Human fetal Hepatocytes	Chimpanzee
Chimpanzee Hepatocytes	Tree Shrew (*Tupaias* sp.)
Human Hepatocytes	Chimeric mouse model
Peripheral Blood Mononuclear Cells (PBMCs)	Humanized mouse model
HepG2	
HuH-7	
Li23	
HEp3B	
PH5CH	
MOLT-4	
MT-2	
B-Cell Daudi	

for transcript and protein detection. Strand-specific real-time-polymerase chain reaction (rt-PCR) was used to detect minus-strand RNA intermediates during HCV replication; however, due to false priming, this technique is not reliable. As a result, several other genetic and biological indicators are refined and employed to show viral replication such as detection of plus-strand RNA, inhibition of viral replication using IFN-α or antisense oligonucleotides, transmission of cell culture grown HCV to naïve cells, detection of viral antigens by immunofluorescences, and the long-term propagation of HCV [22].

4.1. Primary Cell Lines. Primary cell lines obtained from humans and chimpanzees have been used to study HCV infection. Cultivation of HCV in tissue culture was achieved by Iacovacci et al. in which primary fetal human hepatocytes were injected with sera isolated from patients with HCV. Although, these studies demonstrated an increase in copy number of the minus-strand RNA [32, 33], the total efficiency after 24 days was low, expressing a maximum of 20,000 copies of RNA in 10^6 cells. Following a similar strategy as used by Iacovacci, Lanford et al. demonstrated a rapid increase in positive-strand RNA from days 1 to 4 and sustained constant levels of transcripts using primary hepatocytes from chimpanzees [34]. Using strand-specific rt-PCR, the authors detected minus-strand RNA replication intermediates, which indicate that the virus is undergoing replication within the hepatocytes. In addition, they showed that primary liver cells obtained from baboons could not be used to cultivate the virus. This observation supports the concept that HCV is quite species selective and has a narrow range of hosts. In 1999, Rumin et al. developed specific tissue culture conditions that could support the culturing of primary human hepatocytes for 4 months, without any morphogenic changes [35]. Although they were able to detect increasing levels of RNA during the 3 months of culturing, the efficiency had many uncontrollable parameters such as the infectivity of the sera and the quality of the hepatocytes. In addition to the potential to infect hepatocytes, HCV has also been shown to replicate in PBMCs, indicating its ability to replicate in extrahepatic cells [35]. Consistent with this observation, HCV has been reported to replicate within PBMCs isolated from chronically infected patients. Cribier et al. reported detection of viral RNA 28 days after infecting a mixture of white blood cells (obtained from 10 donors) that were infected *in vitro* with high-titer serum [36]. However, the levels and quality of RNA were similar to those reported in hepatocytes.

4.2. Nonprimary Cell Lines. The most critical shortfalls in culturing primary cell lines have been the availability and the technical challenges associated with culturing these cells *in vitro*. As a result, tremendous efforts have been made in developing a nonprimary cell line that is able to mimic physiological hepatocytes. Although a number of cell lines have been tested to show persistent replication, the most extensive studies have been conducted with the non-neoplastic cell line PH5CH, which was obtained from a human hepatocyte immortalized with the simian virus 40 large T antigen. Two important studies by Ikeda et al. and Kato et al. have shown that HCV plus-strand RNA can be detected more than 100 days after infection with HCV [37, 38]. In addition, they determined that only certain variants, variants in the hypervariable region 1 (HVR1) of the E2 protein, could infect and replicate in PH5CH cells. More importantly, these two groups demonstrated that infected PH5CH cells treated with IFN-α showed significant loss of plus-strand RNA of the virus; thereby, it can serve as an ideal *in vitro* platform to examine potential therapeutic molecules.

In addition to nonneoplastic cell lines, human B- and T-cell lines have been used as *in vitro* model to study HCV infection. Mizutani et al. using the T-cell line MT2 isolated a clone containing HCV RNA after 200 days postinfection [39]. Moreover, T- and B-cell lines; HPB-Ma and Daudi, respectively, have been shown to sustain virus propagation lasting for more than one year [40]. A study by Shimizu et al. has demonstrated that supernatant from HCV infected Daudi cells exhibited remarkable infectious capacity in chimpanzee [41]. HCV RNA was detected in the chimpanzee serum after 5 weeks postinfection, however, the levels of HCV replication in the infected animal were low and gradually disappeared after 25 weeks postinfection.

5. Transfected Cell Lines

5.1. Cloned HCV Genomes. Generation of clones from the HCV genome has permitted the genetic analysis of a variety of different aspects in the HCV life cycle. Introduction of cloned virus genome is superior to infection using HCV infected patient serum because the clone is well defined and can be generated in high quantities. Studies by Dash et al. and Yoo et al. have shown that transfecting HepG2 and HuH-7, respectively, with truncated HCV genomes that lacked the 3′ NTR were able to maintain extended culture infected with HCV [42, 43]. However, the usage of this truncated genome contradicts the finding that the 3′ NTR is essential for replicating *in vivo* [44, 45]. In addition, this method is not

useful in infecting chimpanzee with HCV producing cells, unlike other transfected cell methods.

5.2. Subgenomic Replicons. In 1999, Bartenschlager et al. developed a system that consisted of subgenomic replicons of HCV that could replicate autonomously in hepatic cell cultures [31, 46]. To obtain the subgenomic replicons, they isolated sera from patients infected with HCV and purified the viral genome. Complementary DNA was synthesized and amplified; therefore, the final clones selected contained the complete genome including the 5′ and 3′ NTR, which was stably expressed in the pCR2.1 expression vector containing a T7 promoter. The final replicon contained a gene resistant to neomycin and the region encoding the structural proteins was eliminated. The structural proteins were removed from this replicon because it was previously observed that for several plus-strand RNA viruses did not require the structural proteins for RNA replication [47–49]. This replicon was able to replicate itself within the cell; however, it was not capable of producing infectious viruses. In addition, this replicon was able to reproduce in HuH-7 cells with high efficiency and for an extended period of time [50]. Studies have also been conducted to determine if certain mutations improve replication. It was determined that mutations in the NS5a region and in the NS4b region increase replication more than 1,000 times [51, 52].

Subgenomes of other genotypes of HCV have been shown to be efficient in maintaining high infectious potential and long-term *in vitro* culture, for example, genotype 2a clone isolated from a Japanese patient with a rare case of fulminant hepatitis C, designated as JFH-1 (Japanese fulminant hepatitis C). The data have indicated the isolate could replicate in HuH-7 cells without the requirements for adaptive mutations that were required for previous isolates [53]. HuH-7 cells infected with cloned JFH-1 genomes produced viruses (designated as HCVcc for cell culture derived HCV) that were capable of infecting naïve HuH-7 cells [54]. In addition, the virus particles could be neutralized with a monoclonal antibody against the viral glycoprotein E2 [55]. The study was the first *in vitro* experiment that showed the complete lifecycle of HCV. More importantly, virus obtained from the cell culture was highly infectious *in vivo* by readily infecting chimpanzees [54, 56] as well as immunodeficient mice with partial human livers (chimeric mice) described later [56].

In addition to HuH-7 cells supporting propagation of HCVcc, additional cell lines have been developed. Human hepatoma Li23-derived cells were found to possess the necessary components required for HCV RNA replication and persistent production of infectious HCV [57]. Similar expression levels of HCV entry factors were observed between Li23- and HuH-7-derived cells, suggesting that certain factors are necessary for infectivity and propagation of HCVcc. Recent studies have shown that expression of a liver-specific microRNA, miR-122, in HEp3B cells can propagate HCVcc [58]. A lentiviral vector expressing miR-122 was placed in HEp3B cells at comparable levels with HuH-7 cells, which lead to the production of infectious particles. The levels were comparable to those observed in HuH-7-infected cells. Shimakami et al. have shown that miR-122 forms a complex with Ago2 to protect and stabilize HCV RNA from 5′ exonuclease activity of the host mRNA decay machinery [59]. This finding may explain why expression of miR-122 in HEp3B cells can support HCV propagation.

6. Animal Model

6.1. Chimpanzees. The chimpanzee animal model (*Pan troglodytes*) is currently the only established animal or primate model for HCV infection. The chimpanzee model for HCV infection was instrumental in the initial studies of non-A, non-B hepatitis, including observations on the clinical course of infection, determination of the physical properties of the virus, and eventual cloning of the HCV nucleic acid [60]. The chimpanzee model has been invaluable in demonstrating that the cDNA clones of HCV developed from HCV strains of genotypes 1a, 1b, and 2a were infectious. In addition, using this primate model that is evolutionarily close and associated with humans has provided important insight regarding the etiology of liver disease caused by HCV. The chimpanzee has provided evidence that infection with HCV did not provide complete protective immunity when challenged with homologous or heterologous viral strains [61, 62]. As a result, it has been difficult to design effective vaccines against the virus, even though chimpanzees have allowed for the identification of important viral genetic elements. Several studies have identified the importance of the active sites of various enzymatic functions as well as the role of the p7 protein. Thus, chimpanzees are certainly one of the ideal models to study the pathogenesis of the HCV and serve as a great model for translation research; however, it is quite a challenge to work with this model due to limited availability, the costs associated with acquiring and maintaining the animal for scientific research, and public resistance.

6.2. Tupaias. The tree shrew, *Tupaias* (T. belangeri chinensis), was previously shown to be susceptible to the hepatitis B virus [63, 64]. Xie et al. have demonstrated that *Tupaia* were susceptible to HCV infection [65]. However, persistent HCV infection could not be established and only 25% of infected animals developed transient or intermittent viremia. In addition, *Tupaia* must undergo severe immunosuppression before they can be infected with HCV. However, sera or plasmas obtained from patients with HCV were able to infect primary Tupaia hepatocyte cultures [66]. The authors demonstrated that the hepatocytes could produce infectious viruses that were capable of infecting naïve hepatocytes. Sequence analysis of cloned *Tupaia* cDNA revealed a high degree of homology between *Tupaia* and human CD81 large extracellular loops (LELs), suggesting CD81 aids in viral entry. In addition, the study indicated that viral entry can also occur through receptors other than CD81 since cellular binding of E2 and anti-CD81 antibodies or soluble CD81-LEL could not inhibit HCV infection.

6.3. Chimeric Human Liver Mouse Model. By genetically manipulating the uPA transgenic mouse, Mercer et al. have generated a chimeric mouse model with human hepatocytes.

This was done by transplanting normal human hepatocytes into severe combined immunodeficiency (SCID) mice carrying a plasminogen activator transgene [67]. The human hepatocytes transplanted were able to integrate into the parenchyma and repopulate the diseased mouse liver without losing their metabolic functions. Successfully generated chimeric mice exhibited prolonged infection with high viral titers following inoculation with HCV and HBV isolated from human serum. In addition, the authors have demonstrated that the model was able to exhibit horizontal transmission in which HCV can be transmitted from one infected animal to another. Since the mice were immunodeficient, they were not appropriate models to study HCV pathogenesis, although they were useful in assessing the activity of antiviral compounds, specifically the effect of IFN-α, HCV protease inhibitors and cyclophilin inhibitor DEBIO-025 on virus propagation and infectivity [68]. Moreover, this chimeric mouse model has been used to show that neutralizing antibodies can prevent an HCV infection *in vivo* [69].

6.4. Genetically Humanized Mouse Model. Studies by Ploss et al. have previously shown that CD81 and occludin (OCLN) were the minimum human factors required for HCV uptake by rodent cells [70]. To determine these human factors for efficient HCV infection, the authors constructed recombinant adenovirus expressing human CD81, scavenger receptor type B class 1 (SCARB1), claudin 1 (CLDN1), and OCLN. Inoculating mice with these human factors expressed in adenoviral vector was sufficient for HCV infection [71]. Furthermore, the authors employed a bicistronic HCV genome expressing CRE recombinase (Bi-nlsCre-Jc1FLAG2, abbreviated HCV-CRE), which activates a loxP-flanked luciferase reporter in Rosa26-Fluc mice. The mice were infected with the HCV-CRE and the mice that were expressing all four transgenes had luciferase signal that peaked at 72 hours postinfection. Interestingly, only animals that expressed both human CD81 and OCLN displayed 6–10 fold increase in virus infection. In addition, they were also able to show that SCARB1 is a legitimate HCV entry factor. This system allows for the studies of HCV coreceptor biology *in vivo* and evaluation of passive immunization strategies. This, therefore, represents the first immunocompetent small animal model for HCV study.

7. Conclusions

Although, great strides in small animal models for the study of HCV have been made in the past decades, HCV remains a global public health issue. In past years, advancements have been made *in vitro* and *in vivo* models for the study of hepatitis C, in particular, the chimeric and genetically humanized mouse models, which have provided a platform to study new antiviral treatments and evaluate immunization strategies. With the advent of autoantibodies recognizing structural proteins found in HCV patients, both *in vitro* and *in vivo* models could provide an important foundation for the discovery of novel biomarkers for prognosis and treatment [72, 73]. With new insights on HCV biology obtained from *in vitro* models and the ability to infect animals with active immune systems, it should be possible to develop new therapies and possibly a vaccine for HCV.

Acknowledgments

This work was supported by the Sjögren's Syndrome Foundation, PHS Grant K99/R00 DE018958, grant from the NIDCR (CQN). W. C. Carcamo is supported by Bridges to Doctorate, University of Florida Graduate School and University of Florida Alumni Graduate.

References

[1] J. H. Hoofnagle, "Course and outcome of hepatitis C," *Hepatology*, vol. 36, no. 5, supplement 1, pp. S21–S29, 2002.

[2] "National Institutes of Health Consensus Development Conference Statement: management of hepatitis C 2002 (June 10–12, 2002)," *Gastroenterology*, vol. 123, no. 6, pp. 2082–2099, 2002.

[3] H. J. Alter and L. B. Seeff, "Recovery, persistence, and sequelae in hepatitis C virus infection: a perspective on long-term outcome," *Seminars in Liver Disease*, vol. 20, no. 1, pp. 17–35, 2000.

[4] M. Charlton, "Hepatitis C infection in liver transplantation," *American Journal of Transplantation*, vol. 1, no. 3, pp. 197–203, 2001.

[5] L. B. Seeff, "Natural history of hepatitis C," *Hepatology*, vol. 26, no. 3, supplement 1, pp. 21S–28S, 1997.

[6] E. Foy, K. Li, C. Wang et al., "Regulation of interferon regulatory factor-3 by the hepatitis C virus serine protease," *Science*, vol. 300, no. 5622, pp. 1145–1148, 2003.

[7] M. W. Fried, M. L. Shiffman, K. Rajender Reddy et al., "Peginterferon alfa-2a plus ribavirin for chronic hepatitis C virus infection," *New England Journal of Medicine*, vol. 347, no. 13, pp. 975–982, 2002.

[8] S. J. Hadziyannis, H. Sette, T. R. Morgan et al., "Peginterferon-α2a and ribavirin combination therapy in chronic hepatitis C: a randomized study of treatment duration and ribavirin dose," *Annals of Internal Medicine*, vol. 140, no. 5, pp. 346–I67, 2004.

[9] M. P. Manns, J. G. McHutchison, S. C. Gordon et al., "Peginterferon alfa-2b plus ribavirin compared with interferonalfa-2b plus ribavirin for initial treatment of chronic hepatitis C: a randomised trial," *Lancet*, vol. 358, no. 9286, pp. 958–965, 2001.

[10] A. Kau, J. Vermehren, and C. Sarrazin, "Treatment predictors of a sustained virologic response in hepatitis B and C," *Journal of Hepatology*, vol. 49, no. 4, pp. 634–651, 2008.

[11] K. R. Smith, V. Suppiah, K. O'Connor et al., "Identification of improved IL28B SNPs and haplotypes for prediction of drug response in treatment of hepatitis C using massively parallel sequencing in a cross-sectional European cohort," *Genome Medicine*, vol. 3, no. 8, p. 57, 2011.

[12] P. Simmonds, J. Bukh, C. Combet et al., "Consensus proposals for a unified system of nomenclature of hepatitis C virus genotypes," *Hepatology*, vol. 42, no. 4, pp. 962–973, 2005.

[13] Q. L. Choo, G. Kuo, A. J. Weiner, L. R. Overby, D. W. Bradley, and M. Houghton, "Isolation of a cDNA clone derived from a blood-borne non-A, non-B viral hepatitis genome," *Science*, vol. 244, no. 4902, pp. 359–362, 1989.

[14] G. M. Lauer and B. D. Walker, "Hepatitis C virus infection," *New England Journal of Medicine*, vol. 345, no. 1, pp. 41–52, 2001.

[15] L. B. Dustin and C. M. Rice, "Flying under the radar: the immunobiology of hepatitis C," *Annual Review of Immunology*, vol. 25, pp. 71–99, 2007.

[16] S. Rosenberg, "Recent advances in the molecular biology of Hepatitis C virus," *Journal of Molecular Biology*, vol. 313, no. 3, pp. 451–464, 2001.

[17] A. O. De Beeck and J. Dubuisson, "Topology of hepatitis C virus envelope glycoproteins," *Reviews in Medical Virology*, vol. 13, no. 4, pp. 233–241, 2003.

[18] N. Kato, "Genome of human hepatitis C virus (HCV): gene organization, sequence diversity, and variation," *Microbial and Comparative Genomics*, vol. 5, no. 3, pp. 129–151, 2000.

[19] K. I. Ohba, M. Mizokami, J. Y. N. Lau, E. Orito, K. Ikeo, and T. Gojobori, "Evolutionary relationship of hepatitis C, pesti-, flavi-, plantviruses, and newly discovered GB hepatitis agents," *FEBS Letters*, vol. 378, no. 3, pp. 232–234, 1996.

[20] F. Penin, J. Dubuisson, F. A. Rey, D. Moradpour, and J. M. Pawlotsky, "Structural biology of hepatitis C virus," *Hepatology*, vol. 39, no. 1, pp. 5–19, 2004.

[21] V. Lohmann, J. O. Koch, and R. Bartenschlager, "Processing pathways of the hepatitis C virus proteins," *Journal of Hepatology, Supplement*, vol. 24, supplement 2, pp. 11–19, 1996.

[22] R. Bartenschlager and V. Lohmann, "Replication of hepatitis C virus," *Journal of General Virology*, vol. 81, no. 7, pp. 1631–1648, 2000.

[23] M. J. Evans, T. Von Hahn, D. M. Tscherne et al., "Claudin-1 is a hepatitis C virus co-receptor required for a late step in entry," *Nature*, vol. 446, no. 7137, pp. 801–805, 2007.

[24] B. Bartosch and F. L. Cosset, "Cell entry of hepatitis C virus," *Virology*, vol. 348, no. 1, pp. 1–12, 2006.

[25] L. Cocquerel, C. Voisset, and J. Dubuisson, "Hepatitis C virus entry: potential receptors and their biological functions," *Journal of General Virology*, vol. 87, no. 5, pp. 1075–1084, 2006.

[26] I. Kohaar, A. Ploss, E. Korol et al., "Splicing diversity of the human OCLN gene and its biological significance for hepatitis C virus entry," *Journal of Virology*, vol. 84, no. 14, pp. 6987–6994, 2010.

[27] K. Ray, "Hepatitis: NPC1L1 identified as a novel HCV entry factor," *Nature Reviews Gastroenterology and Hepatology*, vol. 9, no. 3, 124.

[28] B. Sainz Jr, N. Barretto, D. N. Martin et al., "Identification of the Niemann-Pick C1-like 1 cholesterol absorption receptor as a new hepatitis C virus entry factor," *Nature Medicine*, vol. 18, no. 2, pp. 281–285, 2012.

[29] B. D. Lindenbach and C. M. Rice, "Unravelling hepatitis C virus replication from genome to function," *Nature*, vol. 436, no. 7053, pp. 933–938, 2005.

[30] N. Pavio and M. M. C. Lai, "The hepatitis C virus persistence: how to evade the immune system?" *Journal of Biosciences*, vol. 28, no. 3, pp. 287–304, 2003.

[31] R. Bartenschlager, "Hepatitis C virus replicons: potential role for drug development," *Nature Reviews Drug Discovery*, vol. 1, no. 11, pp. 911–916, 2002.

[32] S. Iacovacci, A. Manzin, S. Barca et al., "Molecular characterization and dynamics of hepatitis C virus replication in human fetal hepatocytes infected in vitro," *Hepatology*, vol. 26, no. 5, pp. 1328–1337, 1997.

[33] S. Iacovacci, M. Sargiacomo, I. Parolini, A. Ponzetto, C. Peschle, and G. Carloni, "Replication and multiplication of hepatitis C virus genome in human foetal liver cells," *Research in Virology*, vol. 144, no. 4, pp. 275–279, 1993.

[34] R. E. Lanford, C. Sureau, J. R. Jacob, R. White, and T. R. Fuerst, "Demonstration of in vitro infection of chimpanzee hepatocytes with hepatitis C virus using strand-specific RT/PCR," *Virology*, vol. 202, no. 2, pp. 606–614, 1994.

[35] S. Rumin, P. Berthillon, E. Tanaka et al., "Dynamic analysis of hepatitis C virus replication and quasispecies selection in long-term cultures of adult human hepatocytes infected in vitro," *Journal of General Virology*, vol. 80, no. 11, pp. 3007–3018, 1999.

[36] B. Cribier, C. Schmitt, A. Bingen, A. Kirn, and F. Keller, "In vitro infection of peripheral blood mononuclear cells by hepatitis C virus," *Journal of General Virology*, vol. 76, no. 10, pp. 2485–2491, 1995.

[37] M. Ikeda, K. Sugiyama, T. Mizutani et al., "Human hepatocyte clonal cell lines that support persistent replication of hepatitis C virus," *Virus Research*, vol. 56, no. 2, pp. 157–167, 1998.

[38] N. Kato, M. Ikeda, T. Mizutani et al., "Replication of hepatitis C virus in cultured non-neoplastic human hepatocytes," *Japanese Journal of Cancer Research*, vol. 87, no. 8, pp. 787–792, 1996.

[39] T. Mizutani, N. Kato, M. Ikeda, K. Sugiyama, and K. Shimotohno, "Long-term human T-cell culture system supporting hepatitis C virus replication," *Biochemical and Biophysical Research Communications*, vol. 227, no. 3, pp. 822–826, 1996.

[40] N. Nakajima, M. Hijikata, H. Yoshikura, and Y. K. Shimizu, "Characterization of long-term cultures of hepatitis C virus," *Journal of Virology*, vol. 70, no. 5, pp. 3325–3329, 1996.

[41] Y. K. Shimizu, H. Igarashi, T. Kiyohara et al., "Infection of a chimpanzee with hepatitis C virus grown in cell culture," *Journal of General Virology*, vol. 79, no. 6, pp. 1383–1386, 1998.

[42] B. J. Yoo, M. J. Selby, J. Choe et al., "Transfection of a differentiated human hepatoma cell line (Huh7) with in vitro-transcribed hepatitis C virus (HCV) RNA and establishment of a long- term culture persistently infected with HCV," *Journal of Virology*, vol. 69, no. 1, pp. 32–38, 1995.

[43] S. Dash, A. B. Halim, H. Tsuji, N. Hiramatsu, and M. A. Gerber, "Transfection of HepG2 cells with infectious hepatitis C virus genome," *American Journal of Pathology*, vol. 151, no. 2, pp. 363–373, 1997.

[44] M. Yanagi, M. S. Claire, S. U. Emerson, R. H. Purcell, and J. Bukh, "In vivo analysis of the 3′ untranslated region of the hepatitis C virus after in vitro mutagenesis of an infectious cDNA clone," *Proceedings of the National Academy of Sciences of the United States of America*, vol. 96, no. 5, pp. 2291–2295, 1999.

[45] A. A. Kolykhalov, K. Mihalik, S. M. Feinstone, and C. M. Rice, "Hepatitis C virus-encoded enzymatic activities and conserved RNA elements in the 3' nontranslated region are essential for virus replication in vivo," *Journal of Virology*, vol. 74, no. 4, pp. 2046–2051, 2000.

[46] V. Lohmann, F. Körner, J. O. Koch, U. Herian, L. Theilmann, and R. Bartenschlager, "Replication of subgenomic hepatitis C virus RNAs in a hepatoma cell line," *Science*, vol. 285, no. 5424, pp. 110–113, 1999.

[47] S. E. Behrens, C. W. Grassmann, H. J. Thiel, G. Meyers, and N. Tautz, "Characterization of an autonomous subgenomic pestivirus RNA replicon," *Journal of Virology*, vol. 72, no. 3, pp. 2364–2372, 1998.

[48] P. Liljestrom and H. Garoff, "A new generation of animal cell expression vectors based on the Semliki Forest virus replicon," *Bio/Technology*, vol. 9, no. 12, pp. 1356–1361, 1991.

[49] A. A. Khromykh and E. G. Westaway, "Subgenomic replicons of the flavivirus Kunjin: construction and applications," *Journal of Virology*, vol. 71, no. 2, pp. 1497–1505, 1997.

[50] T. Pietschmann, V. Lohmann, G. Rutter, K. Kurpanek, and R. Bartenschlager, "Characterization of cell lines carrying self-replicating hepatitis C virus RNAs," *Journal of Virology*, vol. 75, no. 3, pp. 1252–1264, 2001.

[51] N. Krieger, V. Lohmann, and R. Bartenschlager, "Enhancement of hepatitis C virus RNA replication by cell culture-adaptive mutations," *Journal of Virology*, vol. 75, no. 10, pp. 4614–4624, 2001.

[52] V. Lohmann, F. Körner, A. Dobierzewska, and R. Bartenschlager, "Mutations in hepatitis C virus RNAs conferring cell culture adaptation," *Journal of Virology*, vol. 75, no. 3, pp. 1437–1449, 2001.

[53] T. Kato, T. Date, M. Miyamoto et al., "Efficient replication of the genotype 2a hepatitis C virus subgenomic replicon," *Gastroenterology*, vol. 125, no. 6, pp. 1808–1817, 2003.

[54] T. Wakita, T. Pietschmann, T. Kato et al., "Production of infectious hepatitis C virus in tissue culture from a cloned viral genome," *Nature Medicine*, vol. 11, no. 7, pp. 791–796, 2005.

[55] B. D. Lindenbach, M. J. Evans, A. J. Syder et al., "Virology: complete replication of hepatitis C virus in cell culture," *Science*, vol. 309, no. 5734, pp. 623–626, 2005.

[56] B. D. Lindenbach, P. Meuleman, A. Ploss et al., "Cell culture-grown hepatitis C virus is infectious in vivo and can be recultured in vitro," *Proceedings of the National Academy of Sciences of the United States of America*, vol. 103, no. 10, pp. 3805–3809, 2006.

[57] N. Kato, K. Mori, K. I. Abe et al., "Efficient replication systems for hepatitis C virus using a new human hepatoma cell line," *Virus Research*, vol. 146, no. 1-2, pp. 41–50, 2009.

[58] H. Kambara, T. Fukuhara, M. Shiokawa et al., "Establishment of a novel permissive cell line for the propagation of hepatitis C virus by expression of microRNA miR122," *Journal of Virology*, vol. 86, no. 3, pp. 1382–1393, 2012.

[59] T. Shimakami, D. Yamane, R.K. Jangra et al., "Stabilization of hepatitis C virus RNA by an Ago2-miR-122 complex," *Proceedings of the National Academy of Sciences of the United States of America*, vol. 109, no. 3, pp. 941–946, 2012.

[60] J. Bukh, "A critical role for the chimpanzee model in the study of hepatitis C," *Hepatology*, vol. 39, no. 6, pp. 1469–1475, 2004.

[61] P. Farci, H. J. Alter, S. Govindarajan et al., "Lack of protective immunity against reinfection with hepatitis C virus," *Science*, vol. 258, no. 5079, pp. 135–140, 1992.

[62] A. M. Prince, B. Brotman, T. Huima, D. Pascual, M. Jaffery, and G. Inchauspe, "Immunity in hepatitis C infection," *Journal of Infectious Diseases*, vol. 165, no. 3, pp. 438–443, 1992.

[63] R. Q. Yan, J. J. Su, D. R. Huang, Y. C. Gan, C. Yang, and G. H. Huang, "Human hepatitis B virus and hepatocellular carcinoma II. Experimental induction of hepatocellular carcinoma in tree shrews exposed to hepatitis B virus and aflatoxin B1," *Journal of Cancer Research and Clinical Oncology*, vol. 122, no. 5, pp. 289–295, 1996.

[64] E. Walter, R. Keist, B. Niederöst, I. Pult, and H. E. Blum, "Hepatitis B virus infection of tupaia hepatocytes in vitro and in vivo," *Hepatology*, vol. 24, no. 1, pp. 1–5, 1996.

[65] Z. C. Xie, J. I. Riezu-Boj, J. J. Lasarte et al., "Transmission of hepatitis C virus infection to tree shrews," *Virology*, vol. 244, no. 2, pp. 513–520, 1998.

[66] X. Zhao, Z. Y. Tang, B. Klumpp et al., "Primary hepatocytes of Tupaia belangeri as a potential model for hepatitis C virus infection," *Journal of Clinical Investigation*, vol. 109, no. 2, pp. 221–232, 2002.

[67] D. F. Mercer, D. E. Schiller, J. F. Elliott et al., "Hepatitis C virus replication in mice with chimeric human livers," *Nature Medicine*, vol. 7, no. 8, pp. 927–933, 2001.

[68] P. Meuleman and G. Leroux-Roels, "The human liver-uPA-SCID mouse: a model for the evaluation of antiviral compounds against HBV and HCV," *Antiviral Research*, vol. 80, no. 3, pp. 231–238, 2008.

[69] T. Vanwolleghem, J. Bukh, P. Meuleman et al., "Polyclonal immunoglobulins from a chronic hepatitis C virus patient protect human liver-chimeric mice from infection with a homologous hepatitis C virus strain," *Hepatology*, vol. 47, no. 6, pp. 1846–1855, 2008.

[70] A. Ploss, M. J. Evans, V. A. Gaysinskaya et al., "Human occludin is a hepatitis C virus entry factor required for infection of mouse cells," *Nature*, vol. 457, no. 7231, pp. 882–886, 2009.

[71] M. Dorner, J. A. Horwitz, J. B. Robbins et al., "A genetically humanized mouse model for hepatitis C virus infection," *Nature*, vol. 474, no. 7350, pp. 208–212, 2011.

[72] W. C. Carcamo, M. Satoh, H. Kasahara et al., "Induction of cytoplasmic rods and rings structures by inhibition of the CTP and GTP synthetic pathway in mammalian cells," *PLoS ONE*, vol. 6, no. 12, Article ID e29690, 2011.

[73] G. Covini, W. C. Carcamo, E. Bredi, C. A. von Muhlen, M. Colombo, and E. K. Chan, "Cytoplasmic rods and rings autoantibodies developed during pegylated interferon and ribavirin therapy in patients with chronic hepatitis C," *Antiretroviral Therapy*. In press.

Hindawi Publishing Corporation
Journal of Biomedicine and Biotechnology
Volume 2012, Article ID 692609, 11 pages
doi:10.1155/2012/692609

Review Article

Animal Models of Glaucoma

Rachida A. Bouhenni,[1] Jeffrey Dunmire,[1] Abby Sewell,[1] and Deepak P. Edward[2, 3]

[1] *Department of Ophthalmology, Summa Health System, Akron, OH 44304, USA*
[2] *Wilmer Eye Institute, Johns Hopkins University, Baltimore, MD 21210, USA*
[3] *Research Department, King Khaled Eye Specialist Hospital, P.O. Box 7191, Riyadh 11462, Saudi Arabia*

Correspondence should be addressed to Deepak P. Edward, deepak.edward@gmail.com

Received 16 January 2012; Revised 27 February 2012; Accepted 29 February 2012

Academic Editor: Monica Fedele

Glaucoma is a heterogeneous group of disorders that progressively lead to blindness due to loss of retinal ganglion cells and damage to the optic nerve. It is a leading cause of blindness and visual impairment worldwide. Although research in the field of glaucoma is substantial, the pathophysiologic mechanisms causing the disease are not completely understood. A wide variety of animal models have been used to study glaucoma. These include monkeys, dogs, cats, rodents, and several other species. Although these models have provided valuable information about the disease, there is still no ideal model for studying glaucoma due to its complexity. In this paper we present a summary of most of the animal models that have been developed and used for the study of the different types of glaucoma, the strengths and limitations associated with each species use, and some potential criteria to develop a suitable model.

1. Introduction

Glaucoma is a leading cause of blindness and visual impairment worldwide affecting 70 million people [1]. It is a devastating disorder that leads to retinal ganglion cell (RGC) degeneration, visual field loss, and, eventually, blindness. To date, over 3 million Americans suffer from glaucoma, with another 100,000 patients being diagnosed each year [1, 2]. Although efforts and research in the field of glaucoma are substantial, its pathophysiology is not completely understood.

Animal models have greatly improved our understanding of the causes and progression of human diseases and have proven to be a useful tool for discovering targets for therapeutic drugs. However, several diseases remain incurable because not all models used for studying these diseases mimicked the human disorders completely.

In glaucoma, a wide variety of animal models of different species have been used to study the disease [3, 4]. These included large animals such as monkeys [5], dogs and cats [6, 7], pigs [8], and small animals such as rodents [9]. Glaucoma in these animals was either spontaneous or induced. Although these models have provided valuable information about the disease, they all had drawbacks and glaucoma remains incurable.

Several types of glaucoma have been described. These have been broadly classified as acute and chronic, secondary and primary. In general, glaucoma in humans is classified into three major types: Primary Open Angle Glaucoma (POAG), Primary Angle Closure Glaucoma (PACG), and Primary Congenital Glaucoma (PCG) with POAG being the most common type in most populations [10]. Although the final common pathway of tissue damage in all types of glaucoma is the axonal damage that manifests as optic nerve (ON) atrophy, causing progressive visual field defects that eventually lead to blindness, each type of glaucoma may be caused by a different mechanism. Elevated intraocular pressure (IOP) is a common thread that connects most forms of glaucoma and is a major risk factor for the disease. In this paper, we describe a wide variety of the animal species that have been developed and used to study the different types of glaucoma and outline their features, unique strengths and limitations, as well as some potential criteria to develop a suitable model.

Table 1: Summary of the animal models commonly used for glaucoma research.

Glaucoma type	Animal	Model mode, mechanism	Reference
POAG	Monkey	Spontaneous inheritance	[11]
		Laser photocoagulation of entire TM, reduced outflow by PAS	[12–17]
		Intracameral injection of latex microspheres, TM blockage	[18]
		Intracameral injection of autologous fixed red blood cells, TM blockage	[19, 20]
	Dog	Spontaneous inheritance	[21, 22]
	Mouse	Transgenic, Myoc mutation	[23, 24]
		Transgenic, alpha-1 subunit of collagen type I	[25, 26]
	Rat	Topical application of dexamethasone	[27]
	Zebrafish	Transgenic, *bug eye* mutant	[28, 29]
		Transgenic, *Irp2* mutation	[30]
		Transgenic, *wdr36* mutation	[31]
	Rabbit	Subconjunctival injection of betamethasone	[32–34]
		Posterior chamber injection of α-chymotrypsin, TM blockage	[35–37]
	Sheep	Topical application of prednisolone	[38–40]
	Cow	Topical application of prednisolone	[41, 42]
	Birds	Light-induced, reduced outflow facility	[43–45]
PACG	Dog	Spontaneous inheritance	[46–53]
	Turkey	Spontaneous inheritance	[54]
	Rat	Episcleral vein injection of saline, obstruction of outflow	[55]
		Injection of polystyrene microbeads or hyaluronic acid, TM blockage	[56, 57]
		Cauterization of episcleral veins, reduced outflow by PAS	[58]
		Ligation of episcleral veins, obstruction of outflow	[59]
		Laser photocoagulation of translimbal region, reduced outflow by PAS	[60]
	Mouse	Transgenic, *Vav2*/*Vav3* knockout	[61]
		Laser photocoagulation of episcleral veins, reduced outflow by PAS	[62, 63]
		Cauterization of episcleral veins, reduced outflow by PAS	[64]
	Rabbit	Water loading, decreased outflow facility	[65, 66]
		Laser photocoagulation of TM, obstruction of outflow	[67–69]
PCG	Rabbit	Spontaneous inheritance	[70–75]
	Rat	Spontaneous inheritance, WAG strain	[76, 77]
		Spontaneous inheritance, RCS strain	[78, 79]
	Cat	Spontaneous inheritance	[6, 21, 80, 81]
	Mouse	Transgenic, *Cyp1b1* mutation	[82–84]
		Transgenic, *Cyp1b1* and Tyr mutations	[85]
	Quail	Spontaneous inheritance, al mutant	[86, 87]
Normal tension	Mouse	Transgenic, *Glast* or *Eaac1* mutation	[88]
Autoimmune	Rat	Immunization against HSP27 and HSP60, RGC loss	[89, 90]
Pigmentary	Mouse	DBA/2J strain, Gpnmb, and Tyrp1 mutation	[91–93]

TM: trabecular meshwork; PAS: peripheral anterior synechiae; RGC: retinal ganglion cell.

1.1. Primary Open Angle Glaucoma (POAG). POAG is the most common form of glaucoma in most populations. More than 20 genetic loci have been reported for POAG but only three causative genes have been identified to date (Myocilin, Optineurin, and WDR36) [94]. POAG is characterized by elevated IOP and acquired loss of RGCs and atrophy of the ON [10]. Animal models (spontaneous and induced) that have been used to study POAG (Table 1), and provided valuable information about the disease are described below.

1.1.1. Monkeys. Glaucoma in monkeys was first described in 1993, when a group of rhesus monkeys at the Cayo Santiago monkey colony in Puerto Rico examined for potential diseases in the posterior segment of the eye were found to have both low and high (> or =22 mmHg) tension POAG [11]. POAG in the rhesus monkey was found to be of maternal inheritance in more than 40% of the animals demonstrating increased IOP. Affected animals exhibit a loss of RGCs, excavation of the ON, and electrophysiological evidence of damage to the retinal peripheral field.

Experimental monkey models have also been developed for the study of POAG. Gaasterland and Kupfer developed an experimental monkey model using argon laser photocoagulation [12]. They used a modified Koeppe-type

goniolens to laser the entire circumference of the trabecular meshwork (TM) which resulted in IOP elevation in 70% of the animals. The IOP range was between 24 and 50 mmHg after the 4th treatment and remained elevated for 25 days. Histopathologic specimens from eyes with elevated IOP and ON cupping showed selective loss of RGCs and thinning of the nerve fiber layer compared with specimens from untreated controls suggesting that glaucoma was achieved. Several studies after that used the monkey model to describe the functional and anatomic changes that occur within the eye and ON in an effort to understand the reasons that lead to elevated IOP [13–17]. Other experimental monkey models of chronic IOP elevation were developed by Weber and Zelenak using latex microspheres [18] and Quigley and Addicks using autologous fixed red blood cells [19, 20]. Another model that develops acute elevation of IOP was also used to study the mechanism of ON damage [95].

The close phylogeny and high homology of the monkey with humans makes it an excellent model for studying glaucoma. Monkeys have retinal and ON anatomy that is almost identical to humans. Unfortunately, monkeys are very expensive, their availability is limited, and they are difficult to handle. Experiments using monkeys require highly experienced teams and special housing facilities, making them beyond the reach of many research laboratories.

1.1.2. Dogs. In 1981, Gelatt et al. described an inherited POAG in the beagles bred in their laboratory [21]. The condition appeared to be autosomal recessive. Elevation of IOP (30 to 40 mmHg) in this model developed bilaterally at 1-2 years of age, tonographic recordings, and constant pressure perfusions indicated a reduction in the aqueous humor outflow. Gonioscopically, the disease had two phases: open iridocorneal angle during the onset and the first 2–4 years of the disease and closed iridocorneal angles associated with lens subluxation and displacement from the anterior vitreous patellar fossa. The animal also exhibited cupping and atrophy of the optic disc, buphthalmia, cataract formation, vitreous syneresis, and eventually phthisis bulbi. This model was recently used in a genome wide SNP array study to map the disease genes and led to the identification of the metalloproteinase ADAMTS10 as a candidate gene for POAG [22].

The advantage of using this model and dogs in general in glaucoma research is the spontaneous inheritance of the disease without congenital anomalies and the availability of the genome sequence. Dogs have relatively large eyes but can be aggressive and difficult to handle in the laboratory. Also, anatomically, dogs have an intrascleral plexus, rather than a Schlemm's canal; this difference may be minor but can be a limitation and their availability may be limited.

1.1.3. Mice. A mouse strain expressing the Tyr423His myocilin point mutation corresponding to the human MYOC Tyr437His mutation was developed to study POAG [23, 24]. Myocilin is one of the causative genes of POAG in humans [96] and has been extensively studied. At 18 months of age, the myocilin model demonstrated loss of ~20% of the RGCs in the peripheral retina, axonal degeneration in the ON, detachment of the endothelial cells of the trabecular meshwork (TM), and moderate and persistent elevation of IOP (2 mmHg higher than normal) [23].

Another transgenic mouse strain with a targeted mutation in the gene for the $\alpha 1$ subunit of collagen type I has also been developed to study POAG. This model demonstrated open angles, progressive ON axonal loss, and gradual elevation of IOP suggesting an association between IOP regulation and fibrillar collagen turnover [25, 26].

There are several advantages of using mice in glaucoma research. These include the high degree of conservation between mice and human genomes, enabling genetic manipulation by altering the mouse genome, and the ability to breed the animals as desired. In addition, they are inexpensive and easy to house and handle, their eyes are easy to obtain, and the sample number for studies can be large. The disadvantages of the mouse model in glaucoma are the absence of the lamina cribrosa in the ON, the very small size of the globe which makes it hard to access clinically, and the availability of specific models may be limited.

1.1.4. Rats. A glaucoma rat model, induced by topical application of dexamethasone, was also developed to study the expression of myocilin. Although IOP was elevated after 2 weeks of treatment, the protein and mRNA levels of myocilin in the TM and around Schlemm's canal in the treated eyes were not different from those of the controls suggesting that myocilin may not be directly linked to ocular hypertension [27].

Similar to mice, rats have many advantages. In contrast to other nonprimate models, the rat shares similar anatomical [97, 98] and developmental [99, 100] characteristics of the anterior chamber, especially in the aqueous outflow pathway, with the human. Therefore, results obtained from the rat are expected to mimic changes that occur in the human. In addition, there is reasonable IOP elevation as retinal and ON changes are similar to those seen in humans. Also, reduction of IOP in response to glaucoma medications has been described but the medication effects were not all identical to those observed in humans [101]. Furthermore, rats are easier to maintain in the laboratory and similar to mice they enable genetic manipulation and can be used in large numbers.

1.1.5. Zebrafish. Transgenic teleost Danio rerio (zebrafish) models have been developed for studying glaucoma [102, 103]. The *bug eye* mutant that was developed by Simon et al. shows RGC death and high IOP [28, 29]. The mutant develops buphthalmia shortly after sexual maturation and an average IOP of 32.9 ± 16.2 mmHg compared to that in the wild type (14.7 ± 3.6 mmHg). This model was recently used in a study that led to the identification of a mutation in the low-density lipoprotein receptor-related protein 2 (*Lrp2*) that is important for myopia and other risk factors for glaucoma [30]. The *lrp2* mutant exhibited a phenotype that included high IOP, enlarged eyes, decreased retinal neurons, activation of RCG stress genes, and ON pathology. Another zebrafish glaucoma model, the *wdr36* mutant that was developed by Skarie and Link, was used to characterize the *wdr36*

function [31]. This model, however, was only developed to study the function of *wdr36*, as it did not show a typical glaucoma phenotype [31].

The zebrafish model has received attention for its usefulness in studying glaucoma and other human diseases [104, 105] because of its short generation times and a well-supported genomic infrastructure. It allows the combination of forward and reverse genetic approaches in order to identify critical genetic interactions required for normal and pathological events. This model would be ideal for studying developmental changes in glaucoma such as those occurring in PCG. It is easily adapted to laboratory settings and can be maintained in a relatively small space. The fish typically reaches sexual maturity in 3 to 4 months, and a breeding pair can produce more than 200 fertilized eggs per mating. Fertilization is external, and the egg and embryo are transparent, which makes it easy to visualize the changes with a regular dissecting microscope. The fish develops quickly, and all major organ systems are formed by 24 hrs after fertilization. Mutagenesis in zebrafish is performed by gamma ray and chemical approaches. The fish also enables haploid screens and diploidization, transgenesis, and forward and reverse genetic approaches which make it an attractive model for genetic manipulations of the visual system.

1.1.6. Other POAG Models. Administration of glucocorticosteroids can lead to the development of ocular hypertension and POAG through a reduction in aqueous humor outflow [106, 107]. Models using steroid-induced ocular hypertension have been developed in many animals such as rabbits, bovine, and sheep [32–34, 38–42]. A topical application of prednisolone acetate induced IOP elevation in 100% of bovine and sheep (from 16-17 mmHg to 30–35 mmHg and from 11.2 mmHg in to 23.2 mmHg in bovine and sheep, resp.). IOP in these animals returned to normal when the treatment was discontinued. In rabbits, injection of betamethasone subconjunctivally or α-chymotrypsin into the posterior chamber also resulted in elevated IOP that lasted for 7 weeks [35–37]. The consistency and robustness of the IOP response and the low cost of maintaining the animals developed using steroids (rats, rabbit, sheep, and cows) compared to primates are all advantages of this model. However, the prolonged topical corticosteroid treatment required to achieve glaucoma can cause significant adverse effects such as cataracts and corneal ulcers.

Avians. Light induced avian models of POAG have also been described [43, 44]. IOP in these models appeared to be responsive to several antiglaucoma drugs [45]. At 8-9 weeks of age, the chicks had significantly enlarged eyes and an IOP that was slightly lower (13.79 v. 16.46 mmHg; $P < 0.05$). At this age, the aqueous outflow was markedly reduced but no change in aqueous inflow could be demonstrated. By 18 to 20 weeks the glaucomatous eyes were further enlarged and the IOP was higher (mean IOP 29.85 v. 22.27 mmHg; $P < 0.05$). Birds may be easy to handle in the laboratory and are not expensive. This model could be potentially valuable for studying the effect of glaucoma medications on IOP.

1.2. Primary Angle Closure Glaucoma (PACG). Similar to POAG, PACG is characterized by elevated IOP, damage to the ON, and visual field loss. The iris in PACG obstructs the TM, whereas in POAG the TM is open and unobstructed [108]. There are several animal models that have been developed for the study of PACG (Table 1), some of these are congenital such as dogs and turkeys, and some are induced such as mice and rats.

1.2.1. Dogs. Glaucoma in dogs has been identified in Beagles, Cockers, Wirehaired Fox Terrier, Sealyham Terriers, and Basset Hounds [46–51] and was described in the late 1960s by veterinary ophthalmologists. Glaucoma in most species of dogs is of the closed angle type. Dogs may also have congenital, primary, or secondary glaucoma [52]. It is a rare condition and is caused by abnormalities in the aqueous humor outflow pathways and mimics congenital glaucoma in humans. Puppies generally present young (3–6 months of age) with an acute onset of buphthalmia and corneal edema with IOP reaching about 40 mmHg at 18 months. It may be unilateral and bilateral and may be associated with other ocular anomalies [53]. Since the disease is rare in dogs and the genotype and phenotype of glaucoma have not been well characterized, this model has not been used to study angle closure or congenital glaucoma.

1.2.2. Turkeys. An inherited eye disease leading to secondary angle closure glaucoma was also described in a slate line of domestic turkeys (Meleagris gallopavo) [54]. The disease was progressive and the model demonstrated buphthalmia, low-grade aqueous cell, and flare associated with progressive posterior synechiae formation resulting in papillary block and iris bombe. IOP in this model was significantly increased and was associated with an increase in corneal diameter. This model is good for studying angle closure glaucoma; however, its availability may be limited.

1.2.3. Mice. Genetically manipulated Vav2/Vav3-deficient mice were also described and found to have elevated IOP, which eventually manifests as buphthalmos [61]. Loss of Vav2 and Vav3 expression in these mice is associated with changes in the iridocorneal angle, which leads to chronic angle closure. The elevation of IOP is accompanied by selective loss of RGCs and optic nerve head (ONH) excavation. The characteristics that make this model useful for glaucoma research are as follows: (1) the elevated IOP occurs spontaneously in these mice and does not require the ocular manipulation necessary in induced models, (2) the frequency of the ocular phenotype is high and onset occurs at a relatively young age, and (3) ocular hypotensives commonly used to treat human glaucoma show efficacy in lowering IOP in this model. The most significant advantage of this mouse glaucoma model is that the deleted genes, Vav2 and Vav3, are well-focused targets that have been studied for over 20 years, providing a useful starting point for further investigation of the potential molecular mechanisms underlying this phenotype.

1.2.4. Additional PACG Models. A wide variety of rat and mouse models have been developed to study the effect of elevated IOP on the ON and RGC degeneration. Though these models were primarily developed to study retinal IOP-related posterior segment damage, the histopathological examination showed varying degrees of angle closure. IOP elevation has been induced by a number of techniques that include the use of hypertonic saline injection into the episcleral veins, cauterization or ligation of episcleral veins, or laser photocoagulation of the perilimbal region.

(1) Rats. Episcleral vein saline injections of Brown Norway rats resulted in sustained IOP elevations after 4 weeks in 45% of rats with 35% developing sustained elevations after subsequent injections [55]. Of those having sustained elevations, the mean IOP change from baseline ranged from 7 to 28 mmHg. IOP change of 10 to 20 mmHg for more than 3 weeks or greater than 20 mmHg for over 1 week resulted in total involvement of the ON with occasional axons that appeared morphologically normal. Electron micrographs of eyes from this model showed axons within damaged nerves which were frequently swollen associated with accumulation of vesicles, dense bodies, and swollen mitochondria providing histological evidence of glaucoma. Additional models using fluorescent polystyrene microbeads and hyaluronic acid injections have also been developed [56, 57]. These models showed a significant IOP elevation and glaucomatous damage in the retina. Wistar rats injected with a solution of microbeads demonstrated an IOP of 29.7 mmHg that remained stable for 13 days and resulted in an axon density that was 16% lower than that in the control groups [56]. Wistar rats receiving weekly injections of hyaluronic acid had elevated IOP in the low 20 s for the duration of the 10 weeks. Eyes enucleated after 10 weeks showed significant loss of RGCs [57].

When cauterization of episcleral veins of Wistar rats was used [58], an IOP elevation from 13.2 mmHg to 53 mmHg was noted. There was an increase of 2.3-fold above the mean normal IOP at 2.5 months, whereas ligation of the episcleral veins increased IOP from 20.2 mmHg to 27.7 mmHg after one week and IOP elevation persisted for 7 months in 40.8% of animals [59]. Further ligation was needed in 59.2% of animals for induced persistent IOP elevation. At 24 weeks there was a 35% reduction in the RGC number compared with control retinas. Intracameral India Ink injection resulted in a dark circle along the circumference of the limbus. Translimbal photocoagulation of the darkened area raised IOP to greater than 25 mmHg after 3 laser treatments; however, further laser treatments were necessary to maintain IOP $>$ 20 mmHg during the course of the study. The thickness of the nerve fiber layer decreased in the glaucomatous eyes and the surface nerve fiber layer and prelaminar region of the ON were considerably atrophic. Another study using translimbal photocoagulation with a diode laser (with laser settings of 0.7 seconds and 0.4 Watts) that was aimed at either the TM and episcleral veins or only the TM of Wistar rats yielded an elevated IOP and subsequent glaucomatous damage which included RGC loss and abnormal outflow channels in the anterior chamber [60]. Peak IOP was 49.0 mmHg in the combination group and 34 mmHg in the TM only group. IOP remained elevated for 3 weeks for both methods and there was axonal loss with both methods.

As mentioned previously, rats are easy and more economical to maintain, and a large number can be treated in one day by one person reducing the cost associated with additional personnel. However, similar to other induced animal models, the technique may need multiple sessions to achieve IOP elevation. Although IOP elevation is achieved, the response to induction of glaucoma may be inconsistent. The hypertonic saline model is likely to be the most consistent model but is technically difficult to perform and has mainly been used in Brown Norway rats. The IOP elevation in all these models is sustained for a period of 2–6 weeks.

(2) Mice. Other mouse models that have been developed to study PACG included those developed by photocoagulation of the episcleral vessels [62, 63, 109] and episcleral vein cauterization [64]. These models exhibited elevated IOP for up to 4 weeks, loss of RGCs, and damage of RGC axons. Translimbal-photocoagulation-treated eyes of Black Swiss mice reached a maximum IOP of 39.6 mmHg with IOP elevation being statistically significant compared with controls for up to 6 weeks [109], whereas in photocoagulation of episcleral- and limbal-vein-treated Albino CD1 mice eyes had doubling of their IOP within 4 hours [62]. IOP in these models remained stable through the second postoperative day (27.6 mmHg) but returned to baseline after one week. At day fourteen after treatment, there was a 42% loss of RGCs. When C57BL/6J mice were treated in a similar fashion as described previously, during the first four weeks after laser treatment, the mean IOP was 20 mmHg compared with 13 mmHg before treatment. Two weeks after laser photocoagulation, the percentage of RCG lost in treated eyes of these mice with elevated IOP compared to untreated controls was about 17% and at 4 weeks, and the death rate was 22.4% [63]. Using fluorescent polystyrene microbeads injection in C57BL/6 mice as well, a consistent 30% elevation in IOP that persisted for more than 3 weeks was achieved using 1 single injection [56].

(3) Rabbits. Rabbit models for angle closure glaucoma were also created by either water loading [65, 66] or argon laser energy applied to the TM [67–69]. Both pigmented and albino rabbits were used in these studies. Although elevated IOP and buphthalmia were achieved in these animals, these models all had drawbacks. For example, in the water loading models, the damage produced included the whole eye and the IOP rise was of insufficient duration (1 hr) and caused selective loss of RGCs. In the laser-induced glaucoma models, the IOP elevation lasted for a few weeks but it was hard to achieve a successful model because of the structure of the iridocorneal angle, which is different from that of humans. The longest IOP elevation was reported in the α-chymotrypsin-injected models.

1.3. Primary Congenital Glaucoma. Primary Congenital Glaucoma (PCG) is an autosomal recessive disease caused

by an abnormal development of the anterior chamber angle. PCG has been linked to several genetic loci. *CYP1B1* and *LTBP2* are the only genes in which mutations are currently known. However, the role that these genes play in the pathophysiology of PCG and development of the anterior chamber is not known. An assortment of spontaneous glaucoma models has been described in different animal species (Table 1). These included rabbits, dogs, monkeys, mice, rats, cats, and albino quails. The study of these models has provided valuable information on the pathophysiology of glaucoma as it relates to changes in the anterior chamber angle, the ON, and the retina but the mechanisms leading to these changes are still elusive.

1.3.1. Rabbits. Spontaneous Congenital Glaucoma in rabbits was first described in 1886 by Schloesser [70]. However, research with this model did not advance until the 1960s when Kolker et al. [73], Hanna et al. [72], and Fox et al. [71] described a group of albino New Zealand rabbits that spontaneously exhibited congenital abnormalities in the development of the anterior chamber. The abnormalities included loss or compression of the iris pillars (pectinate ligaments) and posterior displacement or poor development of the aqueous plexus. Additional findings include dilated or compressed intertrabecular spaces, disorganization of trabecular lamellae, decreased trabecular endothelial cells, and a loss of trabecular endothelial cell-to-cell associations. Others have reported the replacement of the angular meshwork (the trabecular meshwork-like structure in rabbits) with abundant extracellular matrix (ECM), basal-lamina like material, and unidentified round cells just beneath the aqueous plexus [74, 75]. The anterior chamber angle dysgenesis in the rabbit appears to be secondary to an alteration in the differentiation and maintenance of the structural integrity of the angular meshwork. Some of these changes bear resemblance to angle changes seen in PCG in humans [72]. The interest in studying this model decreased in the 1990s when other genetic models of glaucoma became available.

Many studies have indicated that glaucoma in rabbits is most likely autosomal recessive with incomplete penetrance (semi lethal) [72]. It typically manifests in the first 6 months and is associated with variable IOP elevation, enlarged cloudy corneas, and elongated globes. The outflow facility is decreased, suggesting a defect in the outflow pathway, which correlates with the reported histological findings. RGC loss and cupping of the optic nerve were also observed in these rabbits. The phenotypic similarities between rabbits and human patients with congenital glaucoma include the age of onset, IOP elevation, and buphthalmia. In addition, the rabbit eye is also relatively large, which makes it a good model for eye research. However, there are some limitations that make this animal unsuitable for glaucoma research. These include differences in the structure of the trabecular meshwork and aqueous outflow pathways between the human and the rabbit making it difficult to make direct correlations between the developmental changes in the anterior chamber angle in both species. In addition, IOP levels in the buphthalmic rabbit were found to decrease with age. IOP was found to be comparable to normal (18–20 mmHg) until about 5 months of age, followed by intermittent elevation into the 30 mmHg range. A decrease in outflow facility precedes the elevation of IOP. The IOP elevation among animals is variable (20–30 mmHg) up to about 18 months of age; then it decreases to near the normal range between 24 and 48 months. The cause of IOP reduction to normal levels despite decreased outflow facility is unclear. The genome sequence of the rabbit was recently made available at http://www.ncbi.nlm.nih.gov/projects/genome/guide/rabbit/. This will help identify the genetic defects that cause glaucoma. The biggest disadvantage of this model is its limited availability from commercial vendors. This model has recently been used to study the protein changes in the aqueous humor and has provided valuable information about proteomics and the histopathological changes seen in the anterior chamber of this rabbit, although a *CYP1B1* mutation could not be identified in this model [110].

1.3.2. Rats. Congenital glaucoma in rats was first described in 1926 by Addison and How [76], and in 1974, Young et al. also reported a spontaneous occurrence of buphthalmos in a colony of WAG inbred rats [77]. The condition in the latter appeared to be inherited but no completely satisfactory mode of inheritance was given. These reports were followed by another one in 1975 by Heywood [78]. Recently, an RCS-rdy$^-$ rat model that develops glaucoma spontaneously was also described [78, 79]. The mutant animals had either a unilateral or bilateral enlargement of the globes with an IOP that ranged from 25 to 45 mmHg, as compared to control values of 12–16 mmHg. The IOP increased significantly with age to reach a value of 35 ± 7.3 at 12–18 months of age. The animals also had decreased number of RGCs with age as well as atrophic ONHs. The anterior chamber was narrow and the iridocorneal angle was open. These rats were used in other studies in glaucoma research and yielded valuable information about RGC loss [111].

1.3.3. Cats. Feline glaucoma is a rare condition. It has been described in Burmese cats [80], domestic cats [6], and Siamese cats [21, 81]. Examination of the Siamese cats revealed bilateral mild-to-moderate buphthalmos and moderate elevation in IOP, which was as high as 31.6 mmHg. Clinical features identified in these cats were similar to those seen in human PCG, though details such as IOP levels and clinical course were not described in these reports. Structurally, these cats had prominent, elongated ciliary processes, Haab's striae, and lens subluxation. Gonioscopic examination revealed open or slightly narrowed iridocorneal angles, with mild pectinate ligament dysplasia and sparse prominent iris processes. Histological examination of Burmese cat eyes revealed loss of RGC, corneal edema, and multifocal breaks in Descemet's membrane [112]. Similar to rabbits, the cat eyes are relatively larger making them attractive for use in glaucoma research. However, no further reports were published describing clinical, pathological, and genetic characterization of the disease in cats.

1.3.4. Mice. A knockout model with *Cyp1b1* has also been developed to simulate PCG where *CYP1B1* mutations are the predominant cause of PCG in humans in some populations [82]. *Cyp1b1*-deficient mice exhibit abnormalities in their ocular drainage structure and TM that are similar to those reported in human PCG patients [83]. However, other studies generated a *Cyp1b1*-null mouse that revealed no evidence of glaucoma, and the animals were not blind [84]. A mouse model with mutations in both *Cyp1b1* and *Tyr* (tyrosinase) was also developed. Studies using this model showed that the anterior segment developmental pathway involves a tyrosinase and that the *Tyr* mutation modifies the phenotype associated with inheritance of mutant orthologs of *Cyp1b1* and *Foxc1,* which both have been shown to cause PCG in humans [85]. Although results are contradictory, studies using this model could lead to understanding the abnormalities seen in the ocular drainage and the structure of the TM. Similar to the buphthalmic rabbit described previously, *CYP1B1* mutation could be specific to the human PCG only which makes this model and other PCG animal models not suitable for studying the genetics in this disease.

1.3.5. Albino Quails. The albino quail model of glaucoma (*al* mutant) was described in 1986 by Takatsuji et al. [86]. The *al* mutation is sex-linked semilethal recessive of known penetrance. The gene mutation has not been described. The bird exhibited enlargement of the eye, RGC degeneration, cupping of the optic disc, and cataract with retinal histopathological features similar to those in animals with experimentally induced or spontaneous glaucoma. Loss of RGCs was similar to human [87]. The *al* mutant quails show significantly higher IOP at 6 months of age. The iridocorneal angle is initially open but eventually closes in later stages of the disease [86]. The mutant bird would be a good model to study glaucoma, as it is easy to maintain and to handle in a laboratory. However, the cornea of these birds is very small and IOP measurement may be challenging, although a tonopen can be used. In addition, availability of the albino quail is also limited.

1.4. Other Types of Glaucoma

1.4.1. Normal Tension Glaucoma. Normal Pressure or Normal Tension Glaucoma (NTG) is a condition where the clinical features are largely identical to those seen in POAG except the IOP, which, in affected patients, is below the statistically normal upper limit (21 mmHg). The pathophysiology of RGC degeneration and ON damage in NTG remains unclear. A number of factors have been implicated as potential mechanisms of RGC degeneration. Some of these include poor blood flow to the ON, genetic mutations, and vascular spasm [113–115]. To explore the possible pathways of RGC degeneration, genetically modified mice with normal IOP have been utilized as models of NTG as described below.

Because glutamate excitotoxicity and oxidative stress have been implicated in RGC death, mice deficient in the glutamate transporter genes *Glast* or *Eaac1* have been developed as models for normal tension glaucoma. These mice demonstrate RGC and ON degeneration without IOP elevation [88] suggesting that these transporters play important roles in preventing RGC degeneration by keeping the extracellular glutamate concentration below the neurotoxic level and maintaining the glutathione levels in Müller cells by synthesizing and transporting glutamate into the cells. Glutamate is the substrate for glutathione synthesis. This model was used to investigate ASK1 deficiency on neural cell death [116]. ASK1 is a mitogen-activated protein kinase (MAPK) kinase kinase and has an important role in stress-induced RGC apoptosis. The authors found that loss of ASK1 had no effects on the production of glutathione or malondialdehyde in the retina or on IOP. Tumor-necrosis-factor-(TNF-) induced activation of p38 MAPK and the production of inducible nitric oxide synthase were suppressed also in ASK1-deficient Müller glial cells and RGCs which suggested that ASK1 activation is involved in NTG.

1.4.2. Autoimmune Glaucoma. Several reports have suggested that an autoimmune response is one possible mechanism of RGC degeneration in normal pressure glaucoma [117]. To test this hypothesis, some studies have examined serum samples from glaucoma patients to look for autoantibodies and have found increased levels of heat shock protein 27 (HSP27) and heat shock protein 60 (HSP60). HSP27 and HSP60 immunization in the Lewis rat induced RGC degeneration and axonal loss 1–4 months later in a pattern similar to human glaucoma [89], suggesting the role of these proteins in the development of glaucoma. The models also showed IOP-independent RGC loss and changes in serum antibody patterns [90]. Experimental autoimmune glaucoma offers a valuable tool to examine the diverse roles of the immune system in glaucoma. It may also facilitate the identification of treatment strategies to prevent pressure-independent RGC degeneration as it may occur in select patients with glaucoma. However, depending on the animal used, limitations can be encountered such as the size of the eye, the cost of the animal, and the anatomical similarities of the animal's eye to that of the human.

1.4.3. Pigmentary Glaucoma. The DBA/2J mouse, which develops a progressive increase of IOP, was recognized in 1978 [118]. The glaucoma in this strain is caused by iris abnormalities related to recessive mutations in two genes, glycosylated protein nmb (*Gpnmb*) and tyrosinase-related protein 1 (*Tyrp1*) [91, 92]. Both mutations show incomplete penetrance. Therefore, only about 70% of animals develop glaucoma [93]. The mechanism of glaucoma is related to iris atrophy, pigment dispersion, and development of peripheral anterior synechiae leading to angle closure. IOP elevation in the DBA/2J mouse is seen at 8 months of age and remains until death. The mouse develops pigment dispersion which precedes iris atrophy, anterior synechiae, and elevated IOP. These changes are accompanied by retinal and ON changes consistent with glaucoma. The disease progresses with increasing age similar to glaucoma in humans [92, 118]. However, there appears to be a closed angle component to

the glaucoma unlike in humans where pigmentary glaucoma is of an open angle form. Although this model has been extensively studied, there is one limitation that makes this model not ideal for studying glaucoma: The elevated IOP phenotype is not primary, but secondary due to the systemic pigment dispersion syndrome with the associated mutations in the *Gpnmb* and *Tyrp1* loci [91, 92]. In addition, mice with spontaneous glaucoma other than the DBA/2J, such as the DBA/2 and DBA/2NNia, are difficult to obtain commercially.

2. Conclusion

This paper describes most of the animal models utilized in glaucoma research to date. These animal models have provided valuable information about certain aspects of the disease process but the search for models that address knowledge gaps in specific forms of glaucoma must continue. The validity of each of these models depends upon the degree of similarity to the human condition as well as considerations of the model being economical and practical. Since the mechanisms of glaucoma differ among animal models, data obtained from a particular model should not be generalized and should be interpreted within the context of that model. The animal model used should be selected based on the experimental needs and the hypothesis being tested. For example, genetically induced models might be preferable to investigate the effects of elevated IOP on the ocular tissues over prolonged periods without the superimposed effects of experimental procedures or inflammation whereas spontaneously occurring large animal models such as monkeys, dogs, rabbit, and the recently described pig [8] offer a unique opportunity to collect data by using instrumentation identical to that used in human patients with glaucoma. Experimentally induced models have the advantage of studying some of the changes in glaucoma over a short period of time. However, sophisticated equipment and trained personnel to induce glaucoma are often needed. In addition, glaucoma induction can be somewhat unpredictable. These models may be useful in testing responses to medications. It is likely that genetic models developed to address specific hypotheses will provide valuable information on the pathophysiology of the various types and aspects of glaucoma and potentially lead to the discovery of new therapeutic targets.

References

[1] H. Quigley and A. T. Broman, "The number of people with glaucoma worldwide in 2010 and 2020," *British Journal of Ophthalmology*, vol. 90, no. 3, pp. 262–267, 2006.

[2] B. Thylefors, A. D. Négrel, R. Pararajasegaram, and K. Y. Dadzie, "Available data on blindness (update 1994)," *Ophthalmic epidemiology*, vol. 2, no. 1, pp. 5–39, 1995.

[3] K. N. Gelatt, "Animal models for glaucoma," *Investigative Ophthalmology and Visual Science*, vol. 16, no. 7, pp. 592–596, 1977.

[4] E. Vecino, "Animal models in the study of the glaucoma: past, present and future," *Archivos de la Sociedad Espanola de Oftalmologia*, vol. 83, no. 9, pp. 517–519, 2008.

[5] C. A. Rasmussen and P. L. Kaufman, "Primate glaucoma models," *Journal of Glaucoma*, vol. 14, no. 4, pp. 311–314, 2005.

[6] D. E. Brooks, "Glaucoma in the dog and cat," *Veterinary Clinics of North America—Small Animal Practice*, vol. 20, no. 3, pp. 775–797, 1990.

[7] U. Dietrich, "Feline glaucomas," *Clinical Techniques in Small Animal Practice*, vol. 20, no. 2, pp. 108–116, 2005.

[8] J. Ruiz-Ederra, M. García, M. Hernández et al., "The pig eye as a novel model of glaucoma," *Experimental Eye Research*, vol. 81, no. 5, pp. 561–569, 2005.

[9] I. H. Pang and A. F. Clark, "Rodent models for glaucoma retinopathy and optic neuropathy," *Journal of Glaucoma*, vol. 16, no. 5, pp. 483–505, 2007.

[10] H. A. Quigley, "Open-angle glaucoma," *New England Journal of Medicine*, vol. 328, no. 15, pp. 1097–1106, 1993.

[11] W. W. Dawson, D. E. Brooks, G. M. Hope et al., "Primary open angle glaucomas in the rhesus monkey," *British Journal of Ophthalmology*, vol. 77, no. 5, pp. 302–310, 1993.

[12] D. Gaasterland and C. Kupfer, "Experimental glaucoma in the rhesus monkey," *Investigative Ophthalmology*, vol. 13, no. 6, pp. 455–457, 1974.

[13] H. A. Quigley, R. M. Sanchez, and G. R. Dunkelberger, "Chronic glaucoma selectively damages large optic nerve fibers," *Investigative Ophthalmology and Visual Science*, vol. 28, no. 6, pp. 913–920, 1987.

[14] Y. Glovinsky, H. A. Quigley, and G. R. Dunkelberger, "Retinal ganglion cell loss is size dependent in experimental glaucoma," *Investigative Ophthalmology and Visual Science*, vol. 32, no. 3, pp. 484–491, 1991.

[15] Y. Glovinsky, H. A. Quigley, and M. E. Pease, "Foveal ganglion cell loss is size dependent in experimental glaucoma," *Investigative Ophthalmology and Visual Science*, vol. 34, no. 2, pp. 395–400, 1993.

[16] H. A. Quigley and R. M. Hohman, "Laser energy levels for trabecular meshwork damage in the primate eye," *Investigative Ophthalmology & Visual Science*, vol. 24, no. 9, pp. 1305–1307, 1983.

[17] C. B. Toris, G. L. Zhan, Y. L. Wang et al., "Aqueous humor dynamics in monkeys with laser-induced glaucoma," *Journal of Ocular Pharmacology and Therapeutics*, vol. 16, no. 1, pp. 19–27, 2000.

[18] A. J. Weber and D. Zelenak, "Experimental glaucoma in the primate induced by latex microspheres," *Journal of Neuroscience Methods*, vol. 111, no. 1, pp. 39–48, 2001.

[19] H. A. Quigley and E. M. Addicks, "Chronic experimental glaucoma in primates. I. Production of elevated intraocular pressure by anterior chamber injection of autologous ghost red blood cells," *Investigative Ophthalmology and Visual Science*, vol. 19, no. 2, pp. 126–136, 1980.

[20] H. A. Quigley and E. M. Addicks, "Chronic experimental glaucoma in primates. II. Effect of extended intraocular pressure elevation on optic nerve head and axonal transport," *Investigative Ophthalmology and Visual Science*, vol. 19, no. 2, pp. 137–152, 1980.

[21] K. N. Gelatt, G. G. Gum, and R. M. Gwin, "Animal model of human disease. Primary open angle glaucoma. Inherited primary open angle glaucoma in the beagle," *American Journal of Pathology*, vol. 102, no. 2, pp. 292–295, 1981.

[22] J. Kuchtey, L. M. Olson, T. Rinkoski et al., "Mapping of the disease locus and identification of ADAMTS10 as a candidate gene in a canine model of primary open angle Glaucoma," *PLoS Genetics*, vol. 7, no. 2, Article ID e1001306, 2011.

[23] V. Senatorov, I. Malyukova, R. Fariss et al., "Expression of mutated mouse myocilin induces open-angle glaucoma in transgenic mice," *Journal of Neuroscience*, vol. 26, no. 46, pp. 11903–11914, 2006.

[24] Y. Zhou, O. Grinchuk, and S. I. Tomarev, "Transgenic mice expressing the Tyr437His mutant of human myocilin protein develop glaucoma," *Investigative Ophthalmology and Visual Science*, vol. 49, no. 5, pp. 1932–1939, 2008.

[25] F. Mabuchi et al., "Optic nerve damage in mice with a targeted type I collagen mutation," *Investigative Ophthalmology & Visual Science*, vol. 45, no. 6, pp. 1841–1845, 2004.

[26] M. Aihara, J. D. Lindsey, and R. N. Weinreb, "Ocular hypertension in mice with a targeted type I collagen mutation," *Investigative Ophthalmology and Visual Science*, vol. 44, no. 4, pp. 1581–1585, 2003.

[27] K. Sawaguchi, Y. Nakamura, Y. Nakamura, H. Sakai, and S. Sawaguchi, "Myocilin gene expression in the trabecular meshwork of rats in a steroid-induced ocular hypertension model," *Ophthalmic Research*, vol. 37, no. 5, pp. 235–242, 2005.

[28] S. W. John, R. S. Smith, B. D. Perkins et al., "Characterization of the zebrafish bug eye mutation, exploring a genetic model for pressure-induced retinal cell death," *Investigative Ophthalmology & Visual Science*, vol. 44, E- Abstract 1125, 2003.

[29] J. M. Stujenske, J. E. Dowling, and F. Emran, "The bugeye mutant zebrafish exhibits visual deficits that arise with the onset of an enlarged eye phenotype," *Investigative Ophthalmology & Visual Science*, vol. 52, no. 7, pp. 4200–4207, 2011.

[30] K. N. Veth, J. R. Willer, R. F. Collery et al., "Mutations in zebrafish Lrp2 result in adult-onset ocular pathogenesis that models myopia and other risk factors for glaucoma," *PLoS Genetics*, vol. 7, no. 2, Article ID e1001310, 2011.

[31] J. M. Skarie and B. A. Link, "The Primary open-angle glaucoma gene WDR36 functions in ribosomal RNA processing and interacts with the p53 stress-response pathway," *Human Molecular Genetics*, vol. 17, no. 16, pp. 2474–2485, 2008.

[32] L. Bonomi, S. Perfetti, and E. Noya, "Experimental corticosteroid ocular hypertension in the rabbit," *Albrecht von Graefes Archiv fur Klinische und Experimentelle Ophthalmologie*, vol. 209, no. 2, pp. 73–82, 1978.

[33] U. Ticho, M. Lahav, S. Berkowitz, and P. Yoffe, "Ocular changes in rabbits with corticosteroid-induced ocular hypertension," *British Journal of Ophthalmology*, vol. 63, no. 9, pp. 646–650, 1979.

[34] D. C. Wood, D. Sweet, I. Contaxis, and J. Van Dolah, "Response of rabbits to corticosteroids. II. Influence of topical therapy on lens, aqueous humor, serum and urine composition," *American Journal of Ophthalmology*, vol. 63, no. 4, pp. 849–856, 1967.

[35] P. Chee and D. I. Hamasaki, "The basis for chymotrypsin-induced glaucoma.," *Archives of Ophthalmology*, vol. 85, no. 1, pp. 103–106, 1971.

[36] M. Best, A. Z. Rabinovitz, and S. Masket, "Experimental alphachymotrypsin glaucoma," *Annals of Ophthalmology*, vol. 7, no. 6, pp. 803–810, 1975.

[37] S. Lessell and T. Kuwabara, "Experimental alpha-chymotrypsin glaucoma.," *Archives of Ophthalmology*, vol. 81, no. 6, pp. 853–864, 1969.

[38] O. A. Candia, R. Gerometta, J. C. Millar, and S. M. Podos, "Suppression of corticosteroid-induced ocular hypertension in sheep by anecortave," *Archives of Ophthalmology*, vol. 128, no. 3, pp. 338–343, 2010.

[39] R. Gerometta, M. G. Spiga, T. Borrás, and O. A. Candia, "Treatment of sheep steroid-induced ocular hypertension with a glucocorticoid-inducible MMP1 gene therapy virus," *Investigative Ophthalmology and Visual Science*, vol. 51, no. 6, pp. 3042–3048, 2010.

[40] R. Gerometta, S. M. Podos, J. Danias, and O. A. Candia, "Steroid-induced ocular hypertension in normal sheep," *Investigative Ophthalmology and Visual Science*, vol. 50, no. 2, pp. 669–673, 2009.

[41] O. Y. Tektas, C. M. Hammer, J. Danias et al., "Morphologic changes in the outflow pathways of bovine eyes treated with corticosteroids," *Investigative Ophthalmology and Visual Science*, vol. 51, no. 8, pp. 4060–4066, 2010.

[42] R. Gerometta, S. M. Podos, O. A. Candia et al., "Steroid-induced ocular hypertension in normal cattle," *Archives of Ophthalmology*, vol. 122, no. 10, pp. 1492–1497, 2004.

[43] J. K. Lauber, "Light-induced avain glaucoma as an animal model for human primary glaucoma," *Journal of Ocular Pharmacology*, vol. 3, no. 1, pp. 77–100, 1987.

[44] A. Kinnear, J. K. Lauber, and T. A. S. Boyd, "Genesis of light induced avian glaucoma," *Investigative Ophthalmology*, vol. 13, no. 11, pp. 872–875, 1974.

[45] J. K. Lauber, M. A. McLaughlin, and G. C. Y. Chiou, "Timolol and pilocarpine are hypotensive in light-induced avian glaucoma," *Canadian Journal of Ophthalmology*, vol. 20, no. 4, pp. 147–152, 1985.

[46] C. L. Martin and M. Wyman, "Glaucoma in the Basset Hound.," *Journal of the American Veterinary Medical Association*, vol. 153, no. 10, pp. 1320–1327, 1968.

[47] H. M. Whigham, D. E. Brooks, S. E. Andrew, K. N. Gelatt, D. T. Strubbe, and D. J. Biros, "Treatment of equine glaucoma by transscleral neodymium:yttrium aluminum garnet laser cyclophotocoagulation: a retrospective study of 23 eyes of 16 horses," *Veterinary Ophthalmology*, vol. 2, no. 4, pp. 243–250, 1999.

[48] L. G. Lovekin, "Primary Glaucoma in Dogs," *Journal of the American Veterinary Medical Association*, vol. 145, pp. 1081–1091, 1964.

[49] W. G. Magrane, "Canine glaucoma. II. Primary classification," *Journal of the American Veterinary Medical Association*, vol. 131, no. 8, pp. 372–374, 1957.

[50] M. Wyman and K. Ketring, "Congenital glaucoma in the basset hound: a biologic model," *Transactions of the American Academy of Ophthalmology and Otolaryngology*, vol. 81, no. 4, pp. OP645–OP652, 1976.

[51] K. N. Gelatt et al., "Glaucoma in the beagle," *Transactions of the American Academy of Ophthalmology and Otolaryngology*, vol. 81, no. 4, pp. OP636–OP644, 1976.

[52] K. N. Gelatt et al., "Clinical manifestations of inherited glaucoma in the beagle," *Investigative Ophthalmology & Visual Science*, vol. 16, no. 12, pp. 1135–1142, 1977.

[53] S. Reinstein, A. Rankin, and R. Allbaugh, "Canine glaucoma: pathophysiology and diagnosis," *Compendium: Continuing Education For Veterinarians*, vol. 31, no. 10, pp. 450–453, 2009.

[54] A. W. De Kater, R. Smyth, R. C. Rosenquist, and D. L. Epstein, "The Slate turkey: a model for secondary angle closure glaucoma," *Investigative Ophthalmology and Visual Science*, vol. 27, no. 12, pp. 1751–1754, 1986.

[55] J. C. Morrison, C. G. Moore, L. M. H. Deppmeier, B. G. Gold, C. K. Meshul, and E. C. Johnson, "A rat model of chronic pressure-induced optic nerve damage," *Experimental Eye Research*, vol. 64, no. 1, pp. 85–96, 1997.

[56] R. M. Sappington et al., "The microbead occlusion model: a paradigm for induced ocular hypertension in rats and mice," *Investigative Ophthalmology & Visual Science*, vol. 51, no. 1, pp. 207–216, 2009.

[57] M. C. Moreno, H. J. Aldana Marcos, J. O. Croxatto et al., "A new experimental model of glaucoma in rats through intracameral injections of hyaluronic acid," *Experimental Eye Research*, vol. 81, no. 1, pp. 71–80, 2005.

[58] S. R. Shareef, E. Garcia-Valenzuela, A. Salierno, J. Walsh, and S. C. Sharma, "Chronic ocular hypertension following episcleral venous occlusion in rats," *Experimental Eye Research*, vol. 61, no. 3, pp. 379–382, 1995.

[59] S. Yu, T. Tanabe, and N. Yoshimura, "A rat model of glaucoma induced by episcleral vein ligation," *Experimental Eye Research*, vol. 83, no. 4, pp. 758–770, 2006.

[60] H. Levkovitch-Verbin, H. A. Quigley, K. R. G. Martin, D. Valenta, L. A. Baumrind, and M. E. Pease, "Translimbal laser photocoagulation to the trabecular meshwork as a model of glaucoma in rats," *Investigative Ophthalmology and Visual Science*, vol. 43, no. 2, pp. 402–410, 2002.

[61] K. Fujikawa, T. Iwata, K. Inoue et al., "VAV2 and VAV3 as candidate disease genes for spontaneous glaucoma in mice and humans," *PLoS One*, vol. 5, no. 2, Article ID e9050, 2010.

[62] C. T. Fu and D. Sretavan, "Laser-induced ocular hypertension in albino CD-1 mice," *Investigative Ophthalmology and Visual Science*, vol. 51, no. 2, pp. 980–990, 2010.

[63] R. L. Gross, J. Ji, P. Chang et al., "A mouse model of elevated intraocular pressure: retina and optic nerve findings," *Transactions of the American Ophthalmological Society*, vol. 101, pp. 163–171, 2003.

[64] J. Ruiz-Ederra and A. S. Verkman, "Mouse model of sustained elevation in intraocular pressure produced by episcleral vein occlusion," *Experimental Eye Research*, vol. 82, no. 5, pp. 879–884, 2006.

[65] T. O. McDonald, J. W. Hodges, A. R. Borgmann, and F. E. Leaders, "The water-loading test in rabbits. A method to detect potential ocular hypotensive drugs.," *Archives of Ophthalmology*, vol. 82, no. 3, pp. 381–384, 1969.

[66] R. M. Thorpe and A. E. Kolker, "A tonographic study of water loading in rabbits.," *Archives of Ophthalmology*, vol. 77, no. 2, pp. 238–243, 1967.

[67] T. Gherezghiher, W. F. March, R. E. Nordquist, and M. C. Koss, "Laser-induced glaucoma in rabbits," *Experimental Eye Research*, vol. 43, no. 6, pp. 885–894, 1986.

[68] B. Johnson, P. House, W. Morgan, X. Sun, and D. Y. Yu, "Developing laser-induced glaucoma in rabbits," *Australian and New Zealand Journal of Ophthalmology*, vol. 27, no. 3-4, pp. 180–183, 1999.

[69] R. J. Seidehamel and K. W. Dungan, "Characteristics and pharmacologic utility of an intraocular pressure (IOP) model in unanesthetized rabbits," *Investigative Ophthalmology*, vol. 13, no. 4, pp. 319–322, 1974.

[70] C. V. Schloesser, "Acutes Secundar-Glaucom beim Kaninchen," *Zeitschrift für Vergleichende Augenheilkunde*, vol. 35, no. 4, pp. 232–233, 1886.

[71] R. R. Fox, D. D. Crary, E. J. Babino, and B. Sheppard, "Buphthalmia in the rabbit: pleiotropic effects of the (bu) gene and a possible explanation of mode of gene action," *Journal of Heredity*, vol. 60, no. 4, pp. 206–212, 1969.

[72] B. L. Hanna, P. B. Sawin, and L. B. Sheppard, "Recessive buphthalmos in the rabbit," *Genetics*, vol. 47, pp. 519–529, 1962.

[73] A. E. Kolker, R. A. Moses, M. A. Constant, and B. Becker, "The development of glaucoma in rabbits," *Investigative ophthalmology*, vol. 2, pp. 316–321, 1963.

[74] A. Ueno, A. Tawara, T. Kubota, Y. Ohnishi, H. Inomata, and A. S. Solomon, "Histopathological changes in iridocorneal angle of inherited glaucoma in rabbits," *Graefe's Archive for Clinical and Experimental Ophthalmology*, vol. 237, no. 8, pp. 654–660, 1999.

[75] P. A. Knepper, D. G. McLone, W. Goossens, T. Vanden Hoek, and R. G. Higbee, "Ultrastructural alterations in the aqueous outflow pathway of adult buphthalmic rabbits," *Experimental Eye Research*, vol. 52, no. 5, pp. 525–533, 1991.

[76] W. H. F. Addison and H. W. How, "Congenital hypertrophy of the eye in an albino rat," *The Anatomical Record*, vol. 32, no. 4, pp. 271–277, 1926.

[77] C. Young, M. F. W. Festing, and K. C. Barnett, "Buphthalmos (congenital glaucoma) in the rat," *Laboratory Animals*, vol. 8, no. 1, pp. 21–31, 1974.

[78] R. Heywood, "Glaucoma in the rat," *British Veterinary Journal*, vol. 131, no. 2, pp. 213–221, 1975.

[79] R. Naskar and S. Thanos, "Retinal gene profiling in a hereditary rodent model of elevated intraocular pressure," *Molecular Vision*, vol. 12, pp. 1199–1210, 2006.

[80] E. C. G. M. Hampson, R. I. E. Smith, and M. E. Bernays, "Primary glaucoma in Burmese cats," *Australian Veterinary Journal*, vol. 80, no. 11, pp. 672–680, 2002.

[81] G. J. McLellan, D. M. Betts, K. Sigle, and S. Grozdanic, "Congenital glaucoma in the siamese cat—a novel spontaneous animal model for glaucoma research," *Investigative Ophthalmology & Visual Science*, vol. 46: E-Abstract 134, 1995.

[82] B. A. Bejjani, R. A. Lewis, K. F. Tomey et al., "Mutations in CYP1B1, the gene for cytochrome P4501B1, are the predominant cause of primary congenital glaucoma in Saudi Arabia," *American Journal of Human Genetics*, vol. 62, no. 2, pp. 325–333, 1998.

[83] M. Sarfarazi and I. Stoilov, "Molecular genetics of primary congenital glaucoma," *Eye*, vol. 14, no. 3B, pp. 422–428, 2000.

[84] J. T. M. Buters, S. Sakai, T. Richter et al., "Cytochrome P450 CYP1B1 determines susceptibility to 7,12-dimethylbenz[a]anthracene-induced lymphomas," *Proceedings of the National Academy of Sciences of the United States of America*, vol. 96, no. 5, pp. 1977–1982, 1999.

[85] R. T. Libby, R. S. Smith, O. V. Savinova et al., "Modification of ocular defects in mouse developmental glaucoma models by tyrosinase," *Science*, vol. 299, no. 5612, pp. 1578–1581, 2003.

[86] K. Takatsuji et al., "Animal model of closed angle glaucoma in albino mutant quails," *Investigative Ophthalmology & Visual Science*, vol. 27, no. 3, pp. 396–400, 1986.

[87] K. Takatsuji et al., "Selective loss of retinal ganglion cells in albino avian glaucoma," *Investigative Ophthalmology & Visual Science*, vol. 29, no. 6, pp. 901–909, 1988.

[88] T. Harada, C. Harada, K. Nakamura et al., "The potential role of glutamate transporters in the pathogenesis of normal tension glaucoma," *Journal of Clinical Investigation*, vol. 117, no. 7, pp. 1763–1770, 2007.

[89] M. B. Wax, G. Tezel, J. Yang et al., "Induced autoimmunity to heat shock proteins elicits glaucomatous loss of retinal ganglion cell neurons via activated T-cell-derived fas-ligand," *Journal of Neuroscience*, vol. 28, no. 46, pp. 12085–12096, 2008.

[90] S. C. Joachim et al., "Complex antibody profile changes in an experimental autoimmune glaucoma animal model," *Investigative Ophthalmology & Visual Science*, vol. 50, no. 10, pp. 4734–4742, 2009.

[91] B. Chang, R. S. Smith, N. L. Hawes et al., "Interacting loci cause severe iris atrophy and glaucoma in DBA/2J mice," *Nature Genetics*, vol. 21, no. 4, pp. 405–409, 1999.

[92] M. G. Anderson, R. S. Smith, N. L. Hawes et al., "Mutations in genes encoding melanosomal proteins cause pigmentary glaucoma in DBA/2J mice," *Nature Genetics*, vol. 30, no. 1, pp. 81–85, 2002.

[93] R. T. Libby, M. G. Anderson, I. H. Pang et al., "Inherited glaucoma in DBA/2J mice: pertinent disease features for studying the neurodegeneration," *Visual Neuroscience*, vol. 22, no. 5, pp. 637–648, 2005.

[94] B. J. Fan, D. Y. Wang, D. S. C. Lam, and C. P. Pang, "Gene mapping for primary open angle glaucoma," *Clinical Biochemistry*, vol. 39, no. 3, pp. 249–258, 2006.

[95] H. A. Quigley, R. W. Flower, E. M. Addicks, and D. S. McLeod, "The mechanism of optic nerve damage in experimental acute intraocular pressure elevation," *Investigative Ophthalmology and Visual Science*, vol. 19, no. 5, pp. 505–517, 1980.

[96] J. H. Fingert, E. M. Stone, V. C. Sheffield, and W. L. M. Alward, "Myocilin glaucoma," *Survey of Ophthalmology*, vol. 47, no. 6, pp. 547–561, 2002.

[97] E. Van Der Zypen, "Experimental morphological study on structure and function of the filtration angle of the rat eye," *Ophthalmologica*, vol. 174, no. 5, pp. 285–298, 1977.

[98] T. Daimon, M. Kazama, Y. Miyajima, and M. Nakano, "Immunocytochemical localization of thrombomodulin in the aqueous humor passage of the rat eye," *Histochemistry and Cell Biology*, vol. 108, no. 2, pp. 121–131, 1997.

[99] Ch. Reme, B. Aeberhard, and U. Urner, "The development of the chamber angle in the rat eye. Morphological characteristics of developmental stages," *Graefe's Archive for Clinical and Experimental Ophthalmology*, vol. 220, no. 3, pp. 139–153, 1983.

[100] P. Nucci, G. Tredici, M. P. Manitto, G. Pizzini, and R. Brancato, "Neuron-specific enolase and embryology of the trabecular meshwork of the rat eye: an immunohistochemical study," *International Journal of Biological Markers*, vol. 7, no. 4, pp. 253–255, 1992.

[101] I. H. Pang, W. H. Wang, and A. F. Clark, "Acute effects of glaucoma medications on rat intraocular pressure," *Experimental Eye Research*, vol. 80, no. 2, pp. 207–214, 2005.

[102] C. McMahon, E. V. Semina, and B. A. Link, "Using zebrafish to study the complex genetics of glaucoma," *Comparative Biochemistry and Physiology C*, vol. 138, no. 3, pp. 343–350, 2004.

[103] B. A. Link, M. P. Gray, R. S. Smith, and S. W. M. John, "Intraocular pressure in zebrafish: comparison of inbred strains and identification of a reduced melanin mutant with raised IOP," *Investigative Ophthalmology and Visual Science*, vol. 45, no. 12, pp. 4415–4422, 2004.

[104] B. A. Barut and L. I. Zon, "Realizing the potential of zebrafish as a model for human disease," *Physiological Genomics*, vol. 2000, no. 2, pp. 49–51, 2000.

[105] P. Goldsmith, H. Baier, and W. A. Harris, "Two zebrafish mutants, ebony and ivory, uncover benefits of neighborhood on photoreceptor survival," *Journal of Neurobiology*, vol. 57, no. 3, pp. 235–245, 2003.

[106] R. Jones and D. J. Rhee, "Corticosteroid-induced ocular hypertension and glaucoma: a brief review and update of the literature," *Current Opinion in Ophthalmology*, vol. 17, no. 2, pp. 163–167, 2006.

[107] J. P. Kersey and D. C. Broadway, "Corticosteroid-induced glaucoma: a review of the literature," *Eye*, vol. 20, no. 4, pp. 407–416, 2006.

[108] A. L. Coleman, "Glaucoma," *Lancet*, vol. 354, no. 9192, pp. 1803–1810, 1999.

[109] M. Aihara, J. D. Lindsey, and R. N. Weinreb, "Experimental mouse ocular hypertension: establishment of the model," *Investigative Ophthalmology and Visual Science*, vol. 44, no. 10, pp. 4314–4320, 2003.

[110] D. P. Edward and R. Bouhenni, "Anterior segment alterations and comparative aqueous humor proteomics in the buphthalmic rabbit," *Transactions of the American Ophthalmological Society*, vol. 109, pp. 66–114, 2011.

[111] Z. Gatzioufas, P. Charalambous, B. Seitz et al., "Cholinergic inhibition by botulinum toxin in a rat model of congenital glaucoma raises intraocular pressure," *British Journal of Ophthalmology*, vol. 92, no. 6, pp. 826–831, 2008.

[112] S. Jacobi and R. R. Dubielzig, "Feline primary open angle glaucoma," *Veterinary Ophthalmology*, vol. 11, no. 3, pp. 162–165, 2008.

[113] M. B. Wax, "The case for autoimmunity in glaucoma," *Experimental Eye Research*, vol. 93, no. 2, pp. 187–190, 2010.

[114] J. Caprioli and A. L. Coleman, "Blood pressure, perfusion pressure, and glaucoma," *American Journal of Ophthalmology*, vol. 149, no. 5, pp. 704–712, 2010.

[115] M. B. Shields, "Normal-tension glaucoma: is it different from primary open-angle glaucoma?" *Current Opinion in Ophthalmology*, vol. 19, no. 2, pp. 85–88, 2008.

[116] C. Harada, K. Namekata, X. Guo et al., "ASK1 deficiency attenuates neural cell death in GLAST-deficient mice, a model of normal tension glaucoma," *Cell Death and Differentiation*, vol. 17, no. 11, pp. 1751–1759, 2010.

[117] I. Maruyama, M. Nakazawa, and H. Ohguro, "Autoimmune mechanisms in molecular pathology of glaucomatous optic neuropathy," *Nippon Ganka Gakkai Zasshi*, vol. 105, no. 4, pp. 205–212, 2001.

[118] S. W. John and al. et, "Essential iris atrophy, pigment dispersion, and glaucoma in DBA/2J mice," *Investigative Ophthalmology & Visual Science*, vol. 39, no. 6, pp. 951–962, 1998.

Hindawi Publishing Corporation
Journal of Biomedicine and Biotechnology
Volume 2012, Article ID 718617, 13 pages
doi:10.1155/2012/718617

Review Article

Dextran Sodium Sulphate Colitis Mouse Model: Traps and Tricks

Martina Perše and Anton Cerar

Institute of Pathology, Medical Experimental Centre, Medical Faculty, University of Ljubljana, Zaloška 4, 1105 Ljubljana, Slovenia

Correspondence should be addressed to Martina Perše, martina.perse@mf.uni-lj.si

Received 9 December 2011; Accepted 5 March 2012

Academic Editor: Oreste Gualillo

Inflammatory bowel disease (IBD) is a complex multifactorial disease of unknown etiology. Thus, dozens of different animal models of IBD have been developed in past decades. Animal models of IBD are valuable and indispensable tools that provide a wide range of options for investigating involvement of various factors into the pathogenesis of IBD and to evaluate different therapeutic options. However, the dextran sulphate sodium (DSS-) induced colitis model has some advantages when compared to other animal models of colitis. It is well appreciated and widely used model of inflammatory bowel disease because of its simplicity. It has many similarities to human IBD, which are mentioned in the paper. In spite of its simplicity and wide applicability, there are also traps that need to be taken into account when using DSS model. As demonstrated in the present paper, various factors may affect susceptibility to DSS-induced lesions and modify results.

1. Introduction

Inflammatory bowel disease (IBD) is a complex multifactorial disease [1–3]. It commonly refers to ulcerative colitis (UC) and Crohn's disease (CD), the two chronic conditions that involve inflammation of the intestine. IBD is common in developed countries, with up to 1 in 200 of individuals of Northern European region affected by these disease [4]. Patients with IBD present several clinically challenging problems for physicians. Despite recent advances in treatment, there remains a need for a safe, well-tolerated therapy with a rapid onset, and increased capacity for maintaining long-term remission [5].

In past decades, dozens of different animal models of IBD have been developed. These models can be broadly divided into spontaneous colitis models, inducible colitis models, genetically modified models, and adoptive transfer models [6–8]. Although these models do not represent the complexity of human disease, they are valuable and indispensable tools that provide a wide range of options for investigating involvement of various factors into the pathogenesis of IBD and evaluate different therapeutic options. Chemically induced murine models of intestinal inflammation are one of the most commonly used models because they are simple to induce, the onset, duration, and severity of inflammation are immediate and controllable. Both dextran sulphate sodium (DSS) and trinitrobenzene sulfonic acid (TNBS-) induced colitis are well-established animal models of mucosal inflammation that have been used for over 2 decades in the study of IBD pathogenesis and preclinical studies [6–8]. The DSS-induced colitis model has some advantages when compared to other animal models of colitis. For example, an acute, chronic, or relapsing model can be produced easily by changing the concentration of administration of DSS (and cycle in rats and other strains of mice). Moreover, dysplasia that resembles the clinical course of human UC occurs frequently in the chronic phase of DSS-induced colitis. DSS-induced model for studying colitis-associated carcinogenesis has been recently reviewed by others [9, 10]. Furthermore, studies that validated DSS model by using different therapeutic agents for human IBD show that DSS-induced colitis can be used as a relevant model for the translation of mice data to human disease [11]. Thus, the aim of the present paper is to give a concise introduction of different factors that may be involved in the patogenesis of DSS-induced colitis and need to be taken into account when using this model. At the same time few aspects of applicability and further investigation of this model are mentioned.

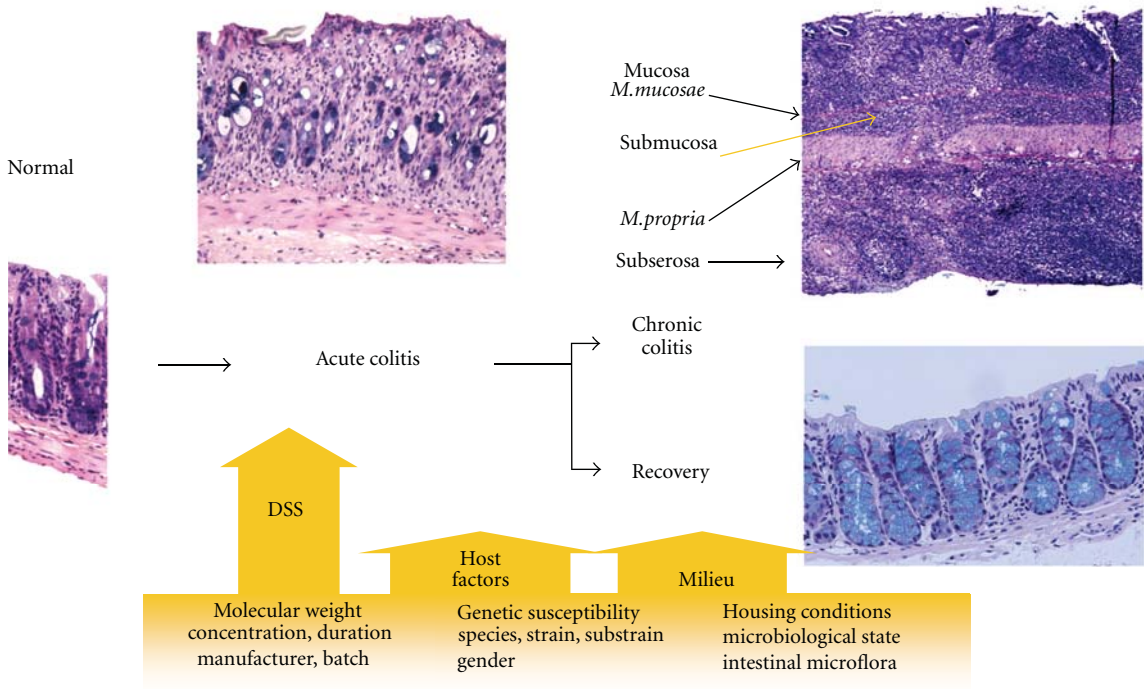

Figure 1: Schematic simplified representation of various factors that can influence the susceptibility, onset, severity, and responsiveness to DSS-induced colitis.

2. Induction of DSS Colitis

First report on the use of DSS dates back in the year 1985, when Ohkusa et al. published their investigation on DSS-induced colitis in hamsters [12]. Thereafter, DSS colitis was induced also in mice [13]. Today there are numerous studies using DSS-induced colitis model to investigate pathogenesis of colitis and different factors affecting colitis. Colitis is induced by addition of DSS to drinking water. Depending on the concentration, the duration, and frequency of DSS administration, the animals may develop acute or chronic colitis or even colitis-induced dysplastic lesions. Mice show differential susceptibilities and responsiveness to DSS-induced colitis. The varying responses to DSS appear to be dependent on not only DSS (concentration, molecular weight, duration of DSS exposure, manufacturer, and batch) but also genetic (strain and substrain, gender) and microbiological (microbiological state and intestinal flora) factors of animal, which are disscussed in the present paper (Figure 1). Colitis onset and severity may vary with many of these factors. Stress can be one of them [14]. Differences in the DSS susceptibility do not correlate with differences in the consumption of DSS-supplemented water [15]. However, there is a need to monitor DSS consumption, especially when animals are exposed to different therapeutic strategies that may lower consumption of DSS (increased fluid intake or thirst) [16].

3. The Molecular Weight of DSS

DSS is sulfated polysaccharide with a highly variable molecular weight, ranging from 5 kDa to up to 1400 kDa. It was found that the molecular weight of DSS is very important factor in the induction of colitis [17] or colitis-induced dysplastic lesions (carcinogenicity) [18]. The severity of colitis [17] and carcinogenic activity [18] differs with the administration of DSS at different molecular weights (i.e., 5 kDa, 40 kDa, and 500 kDa). The most severe colitis in BALB/c mice was observed when mice were treated with DSS of 40 kDa molecular weight, while mice treated with DSS of 5 kDa developed milder form of colitis. Mice treated with DSS of 500 kDa had no lesions in the large bowel [17]. Similarly, carcinogenic activity in colon was induced by DSS of 54 kDa, while DSS of larger (520 kDa) or smaller (9.5 kDa) molecular weights induced no carcinogenic activity [18]. Examination of uptake and tissue distribution of DSS by histochemical techniques showed that failure in the induction of colitis with 500 kDa DSS is due to its high molecular weight that prevents passage of the molecule through the mucosal membrane [17]. Molecular weight of DSS can affect location of colitis as well. Mice treated with 40 kDa DSS developed most severe diffuse colitis in the middle and distal third of the large bowel, while mice treated with 5 kDa DSS developed relatively patchy lesions mainly in the cecum and upper colon [17].

3.1. Uptake and Tissue Distribution of DSS. The histochemical analyses of uptake and tissue distribution of DSS at 40 kDa molecular weight demonstrated that DSS penetrates the mucosal membrane in the intestine. One day after DSS treatment small amounts of DSS were found in macrophages in large bowel and mesenteric lymph nodes and in the liver Kupffer cells. At day 3 DSS was noticed in a few macrophages

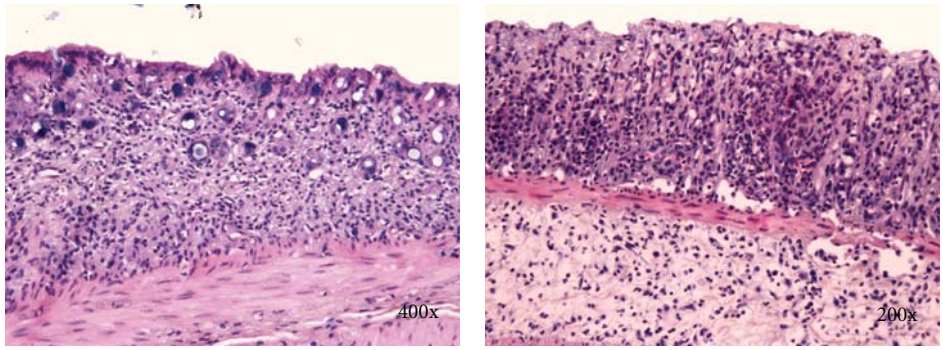

(a) (b)

Figure 2: (a) Disappearance of crypts. (b) Erosion and phlegmonous inflammation of mucosa and submucosa. Kreyberg trichrom stain (acid mucopolysaccharides are stained blue). C57BL/6JOlaHsd female mice are exposed to 3% DSS solution for 5 days followed by drinking water for 7 days.

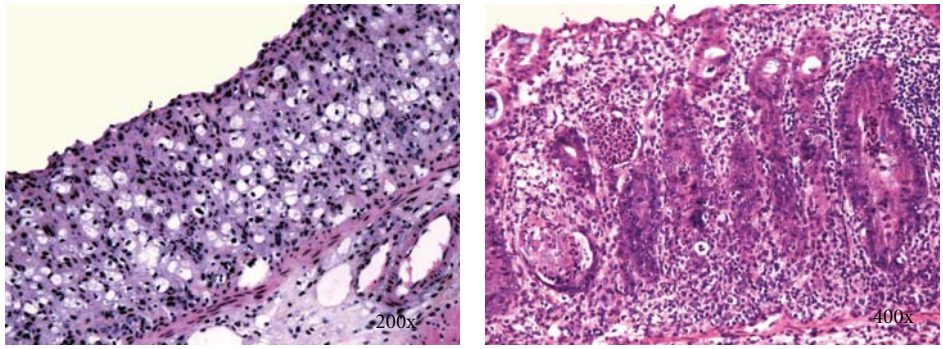

(a) (b)

Figure 3: (a) Vacuolar hydropic degeneration of cells. (b) Epithelial necrosis, cryptitis, and crypt abscesses. Kreyberg trichrom stain (acid mucopolysaccharides are stained blue). C57BL/6JOlaHsd female mice exposed to 3% DSS solution for 5 days followed by drinking water for 21 days.

in the spleen and 7 days after the start of 5 day DSS treatment in the kidney and in a few macrophages in the small intestine. DSS was seen in the liver Kupffer cells even 8 weeks after DSS removal [19]. During chronic phase of DSS colitis, considerable amounts of DSS were also found in the spleen [20]. In other organs and tissues (for instance brain, lung, heart, thymus, stomach, and duodenum), DSS was not observed [19]. Major excretion routes of DSS are urine and feces. Thus, presence of DSS in the epithelial cells of the proximal renal tubules after 7 days of DSS treatment is an indication of the excretion process of absorbed DSS [19]. DSS is resistant to degradation by intestinal microflora or the effects of different pH conditions (4.0–7.5) and anaerobic incubation [21].

4. Clinical and Histological Features of DSS-Induced Colitis

Clinical and histopathological features of DSS-colitis reflect those seen in human IBD. Acute colitis is usually induced by continuous administration of 2–5% DSS for short period (4–9 days). Chronic colitis may be induced by continuous treatment of low concentrations of DSS or cyclical administration of DSS. For instance, 4 cycles of DSS treatment for 7 days followed by 10 days of water (Table 4). Clinical manifestation of DSS colitis in acute phase may include weight loss, diarrhea, occult blood in stools, piloerection, anaemia, and eventually death. However, clinical manifestations in chronic phase of colitis usually do not reflect severity of inflammation or histologic features found in large bowel.

Histological changes in DSS-induced colitis can be classified as acute (early) and chronic (advanced). Typical histological changes of acute DSS-colitis are mucin depletion, epithelial degeneration, and necrosis leading to disappearance of epithelial cells (Figure 2(a)). The latter is accompanied by neutrophils infiltration of lamina propria and submucosa, cryptitis, crypt abscesses (Figures 3(b) and 4), and phlegmonous inflammation in mucosa and submucosa (Figure 2(b)). Usually also shallow erosions appear (Figure 2(b)). Rarely there is a vacuolar hydropic degeneration of cells (Figure 3(a)). Transepithelial migration of neutrophils into mucosal epithelium is termed cryptitis. Migration of numerous neutrophils through mucosal epithelium into crypt lumen results in the formation of crypt abscess. Cryptitis and crypt abscesses are common histological feature of human IBD but rarely reported in DSS-induced colitis

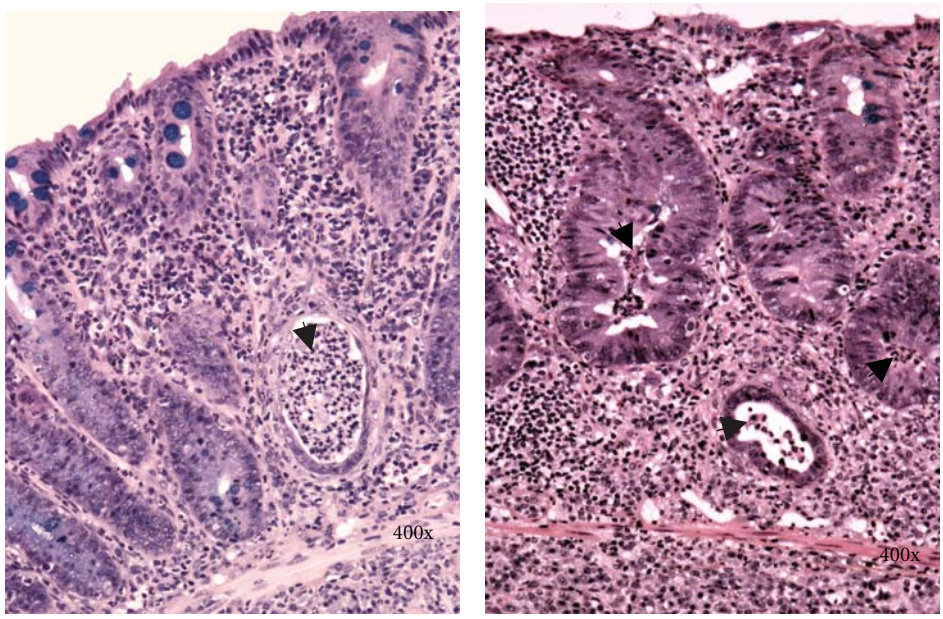

(a) (b)

Figure 4: Arrows denote crypt abscesses (neutrophils) in the lumen of crypts. Kreyberg trichrom stain (acid mucopolysaccharides are stained blue). C57BL/6JOlaHsd male mice are exposed to 3% DSS solution for 5 days followed by drinking water for (a) 7 days and (b) 28 days.

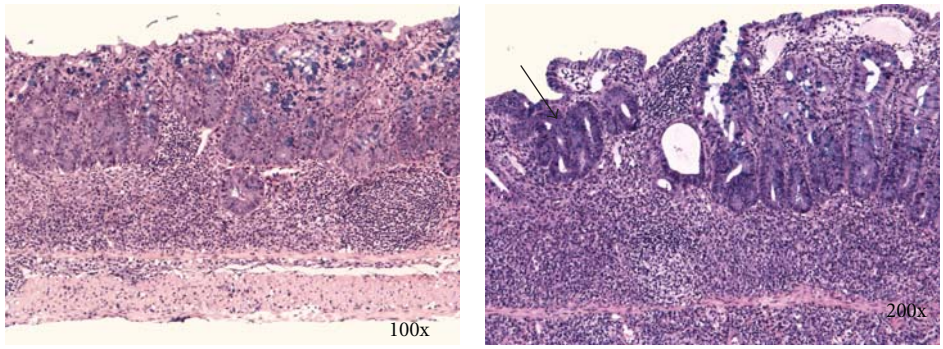

(a) (b)

Figure 5: (a) Mononuclear leucocytes infiltration, crypt architectural disarray, and deep mucosal lymphocytosis. (b) Focally there is a moderate epithelial regeneratory atypia simulating dysplasia (arrow). Kreyberg trichrom stain (acid mucopolysaccharides are stained blue). C57BL/6JOlaHsd male mice are exposed to 3% DSS solution for 5 days followed by drinking water for 28 days.

using haematoxylin-eosin staining method [22]. In contrast, we found cryptitis and crypt abscesses in half of DSS-treated C57BL/6JOlaHsd mice, while in BALB/cAnNHsd mice cryptitis was rarely observed (unpublished data). However, we used Kreyberg-Jareg trichrom staining method that differentially stains acid mucopolysaccharides blue and thus contributes to better distinction between normal and aberrant mucosa. Interestingly, the presence of neutrophils in the epithelial lining of colon mucosa (cryptitis) and in the lumen of crypts (crypt abscess) was reported in DSS-treated C57BL/6OlaHsd mice when investigators used immunofluorescent staining against neutrophils [23].

Chronic changes appear few weeks after DSS application. They consist of mononuclear leucocytes infiltration, crypt architectural disarray (Figure 5(a)), increasing the distance (widening of the gap) between crypt bases and muscularis mucosa, deep mucosal lymphocytosis (Figure 4(a)), and transmural inflammation (Figure 6). It is widely believed that transmural inflammation is infrequent feature of DSS-induced colitis. In contrast, we observed transmural inflammation in C57BL/6JOlaHsd mice as well as in BALB/cAnNHsd mice, consonant with observation by Melgar et al. [22]. Moreover, in chronic colitis of C57BL/6JOlaHsd mice we even observed transmural inflammation with lymphoid follicles (Figure 6(b)), which is histological feature of Crohn's disease and was until now not observed in DSS colitis model.

Rarely reported characteristic change is also reepithelisation of rectal and distal colonic erosions by squamous epithelium that evidently originates from anal squamous

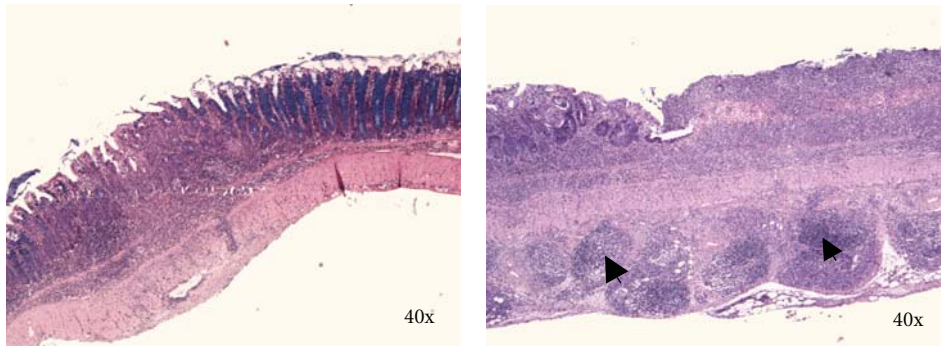

(a) (b)

Figure 6: (a) Focal transmural chronic colitis (skip lesion). C57BL/6JOlaHsd female mice are exposed to 3% DSS solution for 5 days followed by drinking water for 28 days. (b) Transmural inflammation with lymphoid follicles in subserosa (arrows) and chronic erosion. C57BL/6JOlaHsd female mice are exposed to 3% DSS solution for 9 days followed by drinking water for 28 days. Kreyberg trichrom stain (acid mucopolysaccharides are stained blue).

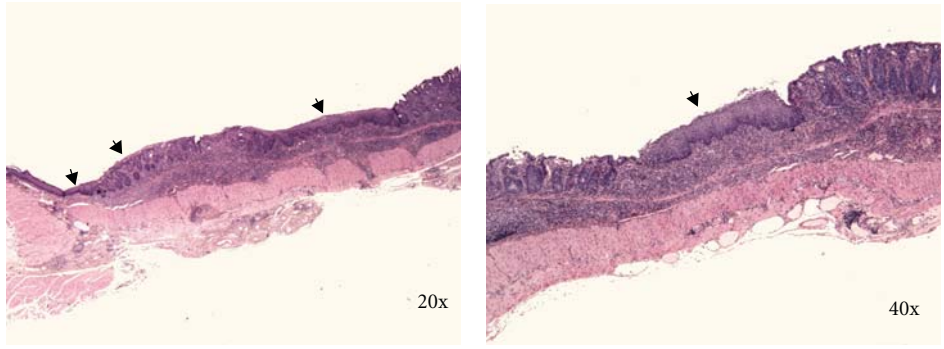

(a) (b)

Figure 7: (a) and (b) reepithelisation of rectal and distal colonic erosion by squamous epithelium (arrows). C57BL/6JOlaHsd male mice are exposed to 3% DSS solution for 5 days followed by drinking water for 7 days. Kreyberg trichrom stain (acid mucopolysaccharides are stained blue).

mucosa (Figure 7). In some slides islands of squamous epithelium are found surrounded by colonic mucosa proximally and distally, but in most cases with deeper sections there appeared a continuity of squamous epithelium distally, suggesting an irregular shape of a squamous cell regenerate. Focally sometimes there is a moderate epithelial regeneratory atypia simulating dysplasia (Figure 5(b)). Most frequently it is found at the edge of chronic erosions.

We observed reepithelisation of distal part of colon as early as day 5 of DSS treatment in C57BL/6JOlaHsd but not in BALB/cAnNHsd mice. According to our experience reepithelisation of distal colon with squamous epithelium is frequent observation in C57BL/6JOlaHsd mice 1–4 weeks after DSS removal. The distance of reepithelisation with squamous epithelium that we measured under microscope ranged from 0.5–6.5 mm of colon length.

Histological changes seen in mouse DSS-induced colitis are the features of IBD in man, some of them of ulcerative colitis (regular rectal localization) and some of Crohn's disease (transmural inflammation with disseminated lymphoid follicles, focal lesions) [24, 25].

Besides all in Figure 1, mentioned factors that affect features of DSS-induced colitis preparation of tissues for histological examination may also be one of the reasons for discrepancy among studies. According to our experience as well as recommendation of other investigators [15] longitudinal sections as well as at least few sections of the same slide at intermediate distance of not less than 0.1 mm may better reflect the actual damage of DSS colitis than cross sections because of the patchy nature of DSS-induced lesions. In addition, the choice of staining method may also affect histological observations. For instance, cryptitis, crypt abscesses as well as squamous reepithelisation are easier to diagnose in sections stained with Kreyberg-Jareg method than hematoxylin-eosin method.

5. The Role of Intestinal Flora in the Pathogenesis of DSS-Induced Colitis

Intestinal microflora and their products have been implicated in the pathogenesis of human IBD [2, 26–28] and in several animal models [29]. The importance of the intestinal flora is directly supported by studies of some murine models where colitis is not observed when they are maintained in a gnotobiotic state but rapidly emerges

Table 1: Susceptibility to DSS-induced colitis among inbred strains (adapted from [15]).

	Cecum	Proximal colon	Middle colon	Distal colon
DBA/2J	BC	—	A	A
NON/LtJ	AB	—	A	A
NON.H2^{g7}	AB	—	AB	AB
129/SvPas	A	—	AB	B
NOD-scid	D	A	AB	BC
C57BL/6J	BC	A	B	BC
C3H/HeJ	D	A	AB	C
NOD/LtJ	CD	—	B	BC
C3H/HeJBir	D	A	AB	C

Strains that do not share the same letter in a column have significat differences in histological score for particular part of the colon after DSS administration. Letter A denotes the lowest histological score, while D denotes the highest histological score observed among the strains. — denotes no changes found in the colon (normal mucosa).

when they are reconstituted with bacteria that are considered normal constituents of luminal flora (explained in detail by Nell et al. [29]). It has been demonstrated that intestinal flora is implicated in the pathogenesis of DSS colitis in mice as well. First who suggested contribution of colonic bacteria or their products in the development of colitis in this model were Okayasu et al. [13]. They observed increased numbers of Enterobacteriaceae, Bacteroidaceae, and Clostridium spp. in the colons of mice affected by DSS colitis [13]. Another suggestion in this direction was given by Hans et al. [30], who reported that treatment with antibiotics reduced infiltration of granulocytes in the mucosa and improved histological signs of DSS colitis in acute phase [30]. The role of commensal bacteria and innate immunity in the development of intestinal inflammation has been further demonstrated by Hudcovic et al. [31]. When DSS-treated immunocompetent BALB/c and immunodeficient SCID mice (lacking T and B lymphocytes) were maintained under conventional conditions, both strains developed substantial changes in the colon mucosa. BALB/c mice showed complete loss of the surface epithelium and severe infiltration of inflammatory cells. To evaluate susceptibility to DSS colitis in gnotobiotic conditions BALB/c and SCID mice were transferred into isolators for germ-free rearing by special gnotobiological techniques. Interestingly, BALB/c and SCID mice reared in germ-free conditions (lacking any intestinal microflora) developed only minor signs of mucosal inflammation after DSS treatment [31]. This finding indicates that the presence of microflora facilitates the inflammation in DSS-induced colitis. Similar findings were observed by Kitajima et al. [32]. They used IQI/Jic mice maintained in germ-free conditions and their littermates that were conventionalized with feces obtained from SPF BALB/c mice three weeks before DSS administration. Histopathological findings revealed that IQI/Jic mice under germ-free conditions had no lesions indicative of colitis in the large intestine 3 days after 5% DSS treatment, while IQI/Jic mice in conventional conditions developed focal erosions in the large bowel, mostly in the cecum and proximal colon. Interestingly, when both groups of mice were treated with 1% DSS for 14 days, mice under germ-free conditions developed slight inflammatory cell infiltration and edema in the lamina propria of the cecum and proximal colon and sever ulcerations, hemorrhages with frequent thrombi, and slight inflammatory cell infiltration in the distal colon. In the large bowel of IQI/Jic mice in conventional conditions only focal lesions of slight inflammatory cells infiltration and edema in mucosa along the whole large bowel were observed [32]. These findings demonstrate firstly that mucosal destruction caused by DSS occurs without the involvement of intestinal microflora and secondly that intestinal microflora may play an important modifying role in the susceptibility and responsiveness to DSS-induced damage of epithelial cells. The role of intestinal microflora in DSS-induced colitis is further investigated in mice deficient for different toll-like receptors (TLR), which function as sensors of microbial infection and are critical for the initiation of inflammatory and immune defence responses [33].

6. The Role of Genetic Factors in the Pathogenesis of DSS-Induced Colitis

Similar to IBD in humans [3], genetic factors play important role in DSS-induced colitis. Differences in susceptibility and responsiveness to DSS-induced colitis among inbred strains and substrains of mice have been identified. A quantitative histological analysis of DSS-induced colitis in nine mouse strains using a standardized protocol (3.5% DSS of 36–45 kDa molecular weight for 5 days) demonstrated major differences in DSS responsiveness among strains [15]. C3H/HeJ, NOD/Ltj, and NOD-scid inbred strains are very susceptible to DSS-induced lesions, which develop in severe form mostly in the cecum. 129/SvPas and DBA/2J inbred mice are less susceptible to DSS-induced lesions and show various degrees of susceptibility to DSS, depending upon anatomical site as schematically demonstrated in the Table 1. Interestingly, severity of DSS-induced lesions in most inbred strains increased from proximal to the distal colon. A greater susceptibility to DSS-induced colonic but not cecal lesions was observed in male mice [15].

Stevceva et al. [35] demonstrated that C3H mice are more susceptible to DSS colitis than CBA/H and BALB/c. C3H mice developed severe colitis with severe inflammatory

Table 2: Differentially expressed genes in acute phase of DSS colitis that had been previously associated with human IBD [34].

Gene	Name	Expression	Gene	Name	Expression
Cytokine			*Genes involved in tissue remodeling*		
IL-6	Interleukin-6	↑ 2.6	*Mmp3*	Stromelysin 1	↑ 22.5
IL-16	Interleukin-16	↓ 2.7	*Mmp14*	Membrane type 1 MMP	↑ 2.1
IL-22	Interleukin-22	↑ 2.4	*Timp1*	Tissue inhibitor of metalloproteinase 1	↑ 3.6
Chemokine			*Regenerating islet-derived genes*		
CCL2	JE (human:MCP-1)	↑ 1.8	*Reg3γ*	Regenerating islet-derived 3γ	↑ 14.0
CCL3	MIP-1α	↑ 3.3	*Pap*	Pancreatitis-associated protein	↑ 79.1
CCL11	Eotaxin	↑ 3.3	*S-100a9*	S-100 calcium-binding protein A9 (calgranulin B)	↑ 14.0
CXCL1	KC (hu: GROα)	↑ 2.9	*Prostaglandin metabolism*		
CXCL5	LIX (hu: ENA-78)	↑ 6.6	*Ptgs2*	Prostaglandin-endoperoxidase synthase 2 (COX-2)	↑ 4.1

Colitis was induced in 8 wk female BALB/c mice that received 3% DSS for 7 days and were sacrificed on day 7. ↑: significantly increased expression by denoted factor, ↓: significantly decreased expression by denoted factor.

response predominantly involving ascending (proximal) colon and cecum, while CBA/H and BALB/c mice developed severe colitis mostly in distal colon. BALB/c mice, which are frequently used strain in DSS-colitis, are also less susceptible to DSS as IQI/Jic [32] or C57BL/6 [22]. The differences in the susceptibility to DSS-induced lesions were either due to genetic differences in the ability of the mucosa to withstand inflammatory damage, differences in the ability to limit the inflammatory response, or both. Melgar et al. [22] demonstrated differences in the progression of DSS colitis between two commonly used strains. After DSS withdrawal (one cycle), BALB/c mice recovered of DSS colitis, while in C57BL/6 mice colitis progressed into chronic phase [22]. The genetic factors contributing to DSS susceptibility in mice are unknown. Interestingly, some strains of mice are able to limit and eliminate DSS-induced inflammatory response in colon, while inflammatory process in C57BL/6 mice can not be repared but progresses into chronic form of colitis [22]. This indicates that genetic factors are importantly involved into regulations of inflammatory response, which is of great interest for further research.

7. Pathogenesis of DSS-Induced Colitis

It is widely accepted that DSS is toxic to colonic epithelial cells and causes defects in the epithelial barrier integrity, whereby increasing the colonic mucosal permeability to allow permeation of large molecules such as DSS. The mechanism of how DSS passes through the mucosal epithelial cells (transcellularly or paracellularly mediated via tight junctions) remains uncertain. First changes related to DSS were observed after 1 day of DSS treatment. These changes were loss of one of the components of tight junction complex [36, 37] zonula occludens-1 (ZO-1) [38] and significantly increased expression of proinflammatory cytokines (TNF-α, IL-1β, IFN-γ, IL-10, and IL-12) in the colon [39]. By day 3 of DSS treatment significant increase in permeability to Evan's blue was observed [38]. At this time first histological changes in the colonic mucosa in the form of basal crypts loss and increased inflammatory cells infiltration can be seen. In acute phase of DSS colitis the impairment of epithelial barrier function is associated with loss and redistribution of the tight junction proteins such as occludin, ZO-1 [38], claudin-1, -3, -4, and -5 and an increased epithelial apoptotic ratio [40]. Altered expression of tight junction proteins and increased epithelial apoptosis were reported also in human IBD. It was proposed that imbalance between apoptosis and proliferation causes relevant leaks in the epithelial barrier. This is supported by the finding that both increased apoptosis and decreased proliferation of the epithelium take place in the acute phase of DSS colitis [41]. The single layered intestinal epithelium is a physical and immunological barrier that prevents direct contact of the intestinal mucosa with the luminal microbiota.

As evidenced by the amelioration of inflammation in germ-free animals and in mice treated with antibiotics [27, 30, 31], DSS-induced breakdown of mucosal epithelial barrier function allows the entry of luminal antigens and microorganisms into the mucosa resulting in overwhelming inflammatory response.

Microarray analysis of the gene expression revealed that 173 genes were differentially and significantly expressed in the colon of DSS-treated mice by a factor of two or more when compared to control mice. Fifteen were previously associated with IBD in humans (shown in Table 2) [34]. Intestinal Na^+-related transporters/channels and their regulatory proteins (NHE1,3, β-ENaC, and NHERF1,2) have been found to be downregulated in mouse colon in acute phase of DSS colitis and in mucosal biopsies from IBD patients (UC or CD) in active phase of disease [44].

7.1. Inflammatory Response and Mediators Involved in the Pathogenesis of DSS Colitis . Numerous inflammatory mediators have been implicated in the pathogenesis of human IBD. These include cytokines, eicosanoids, reactive oxygen species, nitric oxide, and complement system activation products [45–48]. Similarly, DSS-induced colitis is associated with the upregulation of different cytokines, chemokines, nitric oxide [49, 50], and inducible nitric oxide synthase (iNOS) [51]. Changes in production of inflammatory mediators in DSS-treated mice were investigated during different phases of colitis, in the serum and/or colon and by

Table 3: Profile of inflammatory mediators in different phases of DSS-induced colitis in mice.

Tissue/method	Analytes measured	acute DSS colitis	chronic DSS colitis	Mouse strain	ref.
		7 days of DSS treatment			
Colon/RT PCR	IL-1, IL-4, IL-10, IL-12, IFNγ, TNFα	↑ IL-1, IL-10, IL-12, ↑ IFN-γ, TNFα	—	BALB/c	[42]
		5 days of DSS treatment	*5 days of DSS followed by 28 days of water*		
Colon/ELISA, MSI	IL-1α, IL-1β, IL-12 p40, IL-12 p70, IL-17, IL-6, G-CSF, IL-18	↑ IL-1α, IL-1β, IL-12 p40, ↑ IL-12 p70, IL-17, IL-6, ↑ G-CSF	↑ IL-1α, IL-1β, IL-12 p40, ↑ IL-12 p70, IL-17, IL-6, ↑ G-CSF	C57BL/6J	[22]
		↑ IL-1α, IL-1β, IL-6, ↑ IL-18, G-CSF	↑ IL-12 p40	BALB/c	[22]
		5 days of DSS treatment	*5 days of DSS followed by 7 days of water*		
Colon/RT PCR	TNF-α, IL-1β, IL-6, IL-10, IL-12, IFN-γ, KC, MIP-2	↑ TNF-α, IL-1β, IL-6, ↑ IL-10, IL-12, IFN-γ, ↑ KC, MIP-2	↑ TNF-α, IL-1β, IL-6, IL-10, ↑ IL-12, IFN-γ, KC, MIP-2	C57BL/6J	[39]
		7 days of DSS treatment	*4 cycles of 7days of DSS followed by 10 days of water*		
Serum/MSI	IL-1β, IL-2, IL-4, IL-5, IL-6, IL-10, IL-12, IL-17, IFN-γ, TNF-α, GM-CSF, IP-10, KC, MCP-1, MIG, MIP-1α	↑ IL-6, IL-17, TNF-α, KC	↑ IL-6, IFN-γ, IL-4, IL-10		[43]
Colon/Western	IL-6, IL-12, IL-23, IL-17, IFN-γ	↑ IL-6, IFN-γ, IL-17	↑ IL-6	C57BL/6J	[43]

RT PCR: real-time PCR; MSI: multiplex sandwich immunoassay; IFN-γ: interferone gama; IL: interleukine; GM-CSF: granulocyte-macrophage colony-stimulating factor; IP-10: interferon-inducible protein; KC: keratinocyte-derived chemokine; MCP-1: monocyte chemoattractant protein; MIG: monokine induced by IFN-γ; MIP-1α: macrophage inflammatory protein; TNF-α: tumor necrosis factor alpha.

different methods (shown in Table 3). Increased expression of different inflammatory mediators (TNF-α, IL-1β, IFN-γ, IL-10, and IL-12) was observed as early as the first day of DSS treatment [39]. The production of these inflammatory mediators increased progressively during DSS treatment. Different profile of inflammatory mediators in acute and chronic phase of DSS colitis was demonstrated. Acute inflammation in DSS colitis converts to a predominant Th2-mediated inflammatory response in the chronic state (lower levels of TNF-α, IL-17, and KC and elevated levels of IL-6, IFN-γ, and IL-4, IL-10) [43]. Progressive upregulation in the transcripts for Th1 cytokines (IL-12, IFN-γ, IL-1, and TNF-α) was observed with increasing dosage of DSS [42]. Different cytokine profile in chronic phase of DSS colitis was found between BALB/c and C57BL/6J mice, which reflected the severity of inflammation or infiltration of inflammatory cells in the colon found histologically [22].

These inflammatory mediators not only play a role in the pathogenesis of DSS-induced colitis but are important as intervention targets against colitis as excellently described by Kawada et al. [52]. Cytokine profile in DSS colitis correlates with clinical and histological parameters as well as barrier properties. Different expression depending on strain and phase of colitis provides this model as a useful tool to dissect the role of these cytokines in the induction of inflammation and recovery from it.

Recently comprehensive study of mucosal and systemic immune responses in C57BL/6OlaHsd mice exposed to 3% DSS for 6 days has been performed using immunofluorescent staining and flow cytometry analyses. It has been shown that adaptive immune responses in this mouse strain are induced during both acute and chronic phase of colitis in all organs tested, that are, colon, spleen, and mesenteric lymph nodes as early as day 1 of DSS treatment until the end (i.e., day 25) [23]. Interplay of neutrophils, dendritic cells, macrophages, and T and B cells among spleen, mesenteric lymph nodes, and colon in DSS-treated C57BL/6OlaHsd mice in temporal fashion is schematically represented in Figure 8.

8. Geneticaly Modified Mice and DSS Treatment

DSS-induced colitis is nowadays frequently used in genetically engineered mice (GEM), to study basic immunologic mechanisms of IBD and to elucidate the role of particular deleted ($^{-/-}$) or inserted (Tg) gene in the pathogenesis of the colitis.

Toll-like receptors (TLR) are critical receptors and signal transducers for structurally conserved pathogen-associated molecular patterns of bacterial cell components (such as lipopolysaccharide) that provoke innate immune responses by stimulating macrophages/dendritic cells to produce proinflammatory cytokines. It has been shown that mice deficient for different TLR (TLR2, TLR4) or other molecules, which are implicated in signaling via TLR such as myeloid differential protein (MyD88), are very susceptible

Table 4: Genetically engineered mouse models in the pathogenesis of DSS colitis.

GEM model	Background (breeder)	Age gender N	MS	MW of DSS	DSS treatment	End	S	Ref
$TLR2^{-/-}$								
$TLR4^{-/-}$								
$TLR2/4^{-/-}$	C57BL/10ScSn	$N = 10$–12	nr	40 kDa	3.5% for 7 days	Day 8	↑	[53]
		5–8 wks						
$TLR4^{-/-}$	C57BL/6J	Male, female			2.5% for 5 days	Day 5		
$MyD88^{-/-}$	(Jax)	$N = 5$-6	nr	36–50 kDa	2.5% for 5/7 days	Day 12/14	↑	[54]
$TLR2^{-/-}$								
$TLR4^{-/-}$	F2							
$MyD88^{-/-}$	129/SvJ × C57BL/6		SPF	40 kDa	2% for 7 days	Day 0–28	↑	[33]
		8 wks						
		Male			1.2% for 8 days			
$MyD88^{-/-}$	nr	$N = 10$	SPF	50 kDa	2.5% for 8 days	Day 8	↑	[55]
		10 wks						
	C57BL/6	Male						[56, 57]
$IL\text{-}18^{Tg}$	(nr)	$N = 20$	SPF	50 kDa	2% for 8 days	Day 12	↑	
					3 cycles of			
	C57BL/6	7–9 wks			2% for 5 days +	Day 5		
$IL\text{-}15^{-/-}$	(Taconic)	$N = 11$	nr	36–50 kDa	5 days of water	Day 25	↓	[58]
	C57BL/6J	Male, female						
$TNF\text{-}\alpha^{-/-}$	(Shimizu, Japan)	$N = 15$	nr	8 kDa	4.5% for 7 days	Day 7	↑	[51]
		8–10 wks						
		Male						
$MRP1^{-/-}$	FVB	$N = 8$	SC	40 kDa	3% for 7days	Day 7	↑	[59]
	C57BL/6	8-9 wks				Day 4, 7		
$Mtgr1^{-/-}$	(nr)	Male, female	nr	40–50 kDa	3% for 4days	Wk 6, 10	↑	[60]
		7-8 wks						
	C57BL/6	Male, female			3% for 5 days			
$SOCS\text{-}1^{+/-}$	(nr)	$N = 14$	SPF	36–50 kDa	(4% for 7 days)	Day 14	↑	[61]
					5 cycles of			
	C57BL/6J	8–12 wk			2% for 7 days +			
$IRF\text{-}1^{-/-}$	(Jax)	$N = 15$	nr	40 kDa	7 days of water	Wk 10	↑	[62]
		8–10 wk						
		Female						
$PPAR\gamma^{\Delta IEpC}$	nr	$N = 20$	nr	35–40 kDa	2.5% for 7 days	Day 7	↑	[63]
	C57BL/6J							
$PPAR\gamma^{\Delta CD4+}$	(nr)	$N = 34$	nr	36–44 kDa	2.5% for 7 days	Day 0,2,7	↑	[64]
	C57BL/6							
$TPH1^{-/-}$	(Taconic)	$N = 10$	nr	40 kDa	5% for 5 days	Day 5	↓	[65]
$Bk2R^{-/-}$	C57BL/6	8–12 wk					ns	
$C3^{-/-}$	(Jax)	$N = 8$	nr	36–40 kDa	3% for 10 days	Day 10	↓	[45]
	C57BL/6	Male, female						
$iNOS^{-/-}$	(Jax)	$N = 5$	nr	40 kDa	2.5% for 9 days	Day 3,9	↓	[49, 50]
$eNOS^{-/-}$							↓	
$nNOS^{-/-}$	129/Sv × C57BL/6	Male, female					↑	
$e/nNOS^{-/-}$	(Jax)	$N = 5$	nr	40 kDa	2.5% for 9 days	Day 3,9	ns	[49]

Table 4: Continued.

GEM model	Background (breeder)	Age gender N	MS	MW of DSS	DSS treatment	End	S	Ref
		5–10 wks						
	C57BL/6	Female						
APN$^{-/-}$	(nr)	N = 5–7	nr	40 kDa	2% for 5 days	Day 5,10	↓	[66]
		8–10 wks						
	C57BL/6J	Male						
APN$^{-/-}$	(Clea Japan)	N = 11	SPF	36–50 kDa	0.5% for 15 days	Day 15	↑	[67]
Vhl$^{\Delta F/F}$						Day 5	↑	
Hif-1$\alpha^{\Delta F/F}$		6–8 wk			2.5% or 5% for	1 year	ns	
Arnt$^{\Delta F/F}$	nr	nr	nr	35–40 kDa	5 days		ns	[68]

GEM: genetically engineered mice, N: number of mice pre group, MS: microbiological state, MW: molecular weight, S: susceptibility to DSS in comparison to wild-type mice (mice of the same strain without deletion), ↓: significantly lower, SFP: specific pathogen-free conditions, SC: standard conditions, ns: nonsignificant, nr: not reported, ↑: significantly higher, wk: week, TLR: toll-like receptor, MyD88: myeloid differential protein, IL: interleukine, MRP: multi drug resistant protein, Mtgr: myeloid translocation gene related-1, SOCS: suppressor of cytokine signaling, IRF: Interferon regulatory factor, PPAR: peroxisome proliferator-activated receptor, TPH: tryptophan hydroxylase, Bk2R: bradykinin type 2 receptor, C3: complement, APN: adiponectine, Vhl: von Hippel-Lindau tumor suppressor protein, Hif: hypoxia-inducible factor, Arnt: aryl hydrocarbon nuclear translocator.

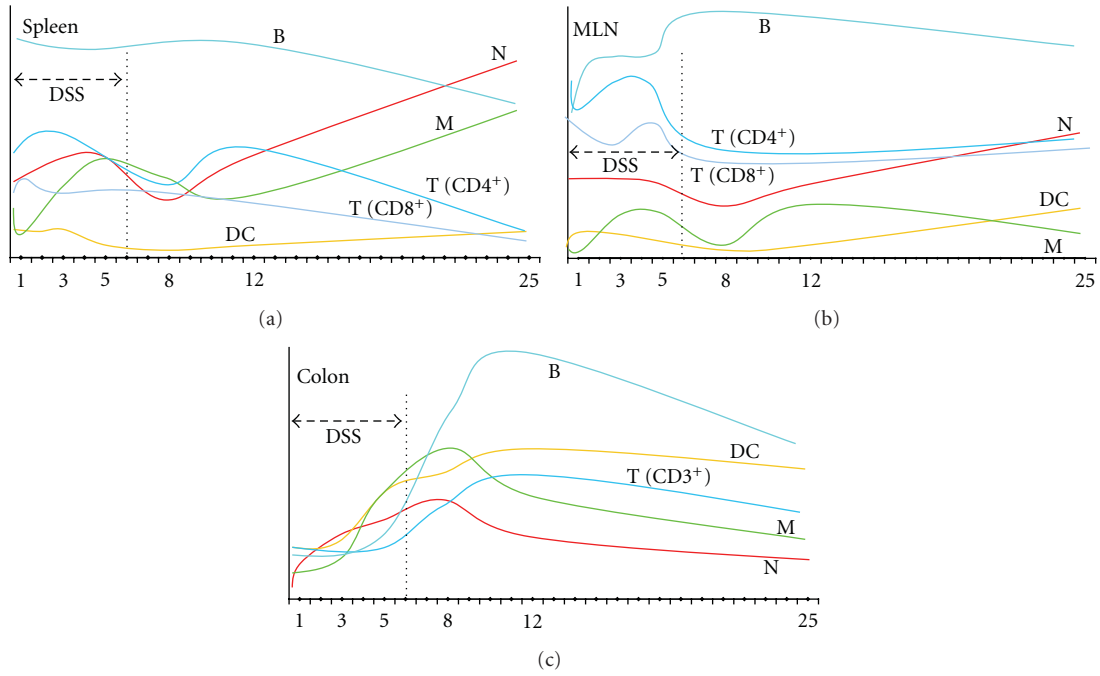

Figure 8: Schematic representation of mucosal (colon) and systemic (spleen, MLN) immune responses in C57BL/6OlaHsd mice exposed to 3% DSS for 6 days followed by water for 19 days. Measurements were made on day 0, 1, 3, 5, 8, 12, and 25 as denoted by numbers. Schematic representation is based on results obtained by Hall et al. [23]. MLN: mesenteric lymph nodes, N: neutrophils, M: macrophages, DC: dendritic cells, T: T cells, B: B cells.

to DSS colitis, indicating important protective role of these molecules in colitis [33, 53–55]. Overproduction of IL-18 or deletion of TNF-α has been shown to exacerbate DSS colitis [51, 56]. On the other hand mice deficient for IL-15 showed reduced susceptibility to DSS colitis [58]. Mice deficit for IL-12 developed mild DSS colitis, while mice deficit for IL-18 developed severe colitis associated with high lethality [69]. Deletion of suppressor of cytokine signaling-1 (SOCS-1), which is a negative feedback molecule for cytokine signaling, increased susceptibility to DSS colitis, suggesting that SOCS-1 plays preventive role in the development of DSS-induced colitis in mice by inhibiting IFN-γ/STAT1 signaling [61]. Interferon regulatory factor-1 (IRF-1) is a transcription factor stimulated by IFN-γ and TNF-α that binds to the promoter region of inflammation-related genes, such as IFN-α, IFN-β, and iNOS. It is expressed in lymphocytes, monocytes, and a wide variety of other cell types, including enterocytes. Mice lacking IRF-1 transcription factor developed significantly increased DSS-induced colonic dysplasia [62]. Tryptophan hydroxylase-1 (TPH1) catalyzes the rate-limiting step in the synthesis of 5-hydroxytryptamine (5-HT) from tryptophan. It is an

important enteric mucosal signaling molecule influencing gut physiology (motor and secretory function) following inflammation and is considered important in maintaining intestinal homeostasis. However, mice lacking TPH1 had significantly reduced susceptibility to DSS colitis [65].

Taken together, GEM treated with DSS are valuable model to test different molecules, which are involved in the mediation of inflammation such as cytokines (IL-12, IL-15, IL-18, TNF-α), nitric oxides (iNOS, eNOS, and nNOS), complement system activation products or other molecules involved in signaling of inflammation (SOCS-1, IRF-1), to further identify bacterial factors involved in maintaining intestinal homeostasis (TLR, MyD88), to investigate the role of particular factor when totally deleted or deleted only in particular types of cells such as intestinal, (PPAR$\gamma^{\Delta IEpC}$; Vhl$^{\Delta F/F}$; Hif-1$\alpha^{\Delta F/F}$; Arnt$^{\Delta F/F}$) or CD4+ T cells (PPAR$\gamma^{\Delta CD4+}$) and to test therapeutic interventions based upon inhibition of particular gene expression strategies (TPH1, APN, and MRP1). In the Table 4 susceptibility to DSS-induced colitis in mice deficient for a particular gene is shown. Mouse background, gender, microbiological state, molecular weight of DSS, and DSS treatment, factors that importantly affect DSS colitis and need to be taken into account in designing investigation or evaluating results, are also stated.

9. Conclusion

DSS-induced model is simple to induce and not expensive, which makes it one of the most commonly used model of IBD to study various aspects of IBD such as pathogenesis, genetic predisposition to IBD, immune mechanisms, and role of microflora in the pathogenesis of IBD as well as bowel malignancy secondary to IBD. As demonstrated above, various factors may affect susceptibility to DSS and modify results. Representative examples of how important can be all mentioned details are studies where two groups of researchers investigated the role of adiponectine in DSS colitis. Both groups used in their studies the same mice model (mice with APN deletion) exposed to DSS treatment. They observed quite opposite results [66, 67]. It is thus advisable to state and describe all details and conditions that may affect the DSS susceptibility.

Acknowledgment

This work was in part supported by ARRS (Slovenian Research Agency, Program P3-0054).

References

[1] R. B. Sartor and M. Muehlbauer, "Microbial host interactions in IBD: implications for pathogenesis and therapy," *Current Gastroenterology Reports*, vol. 9, no. 6, pp. 497–507, 2007.

[2] R. B. Sartor, "Microbial influences in inflammatory bowel diseases," *Gastroenterology*, vol. 134, no. 2, pp. 577–594, 2008.

[3] R. J. Xavier and D. K. Podolsky, "Unravelling the pathogenesis of inflammatory bowel disease," *Nature*, vol. 448, no. 7152, pp. 427–434, 2007.

[4] C. S. Gismera and B. S. Aladren, "Inflammatory bowel diseases: a disease (s) of modern times? Is incidence still increasing?" *World Journal of Gastroenterology*, vol. 14, no. 36, pp. 5491–5498, 2008.

[5] L. J. Zhu, X. Yang, and X. Q. Yu, "Anti-TNF-alpha therapies in systemic lupus erythematosus," *Journal of Biomedicine and Biotechnology*, vol. 2010, Article ID 465898, 8 pages, 2010.

[6] M. Neurath, I. Fuss, and W. Strober, "TNBS-colitis," *International Reviews of Immunology*, vol. 19, no. 1, pp. 51–62, 2000.

[7] S. Wirtz and M. F. Neurath, "Mouse models of inflammatory bowel disease," *Advanced Drug Delivery Reviews*, vol. 59, no. 11, pp. 1073–1083, 2007.

[8] S. Wirtz, C. Neufert, B. Weigmann, and M. F. Neurath, "Chemically induced mouse models of intestinal inflammation," *Nature Protocols*, vol. 2, no. 3, pp. 541–546, 2007.

[9] R. M. De, E. Massi, M. L. Poeta et al., "The AOM/DSS murine model for the study of colon carcinogenesis: from pathways to diagnosis and therapy studies," *Journal of Carcinogenesis*, vol. 10, article 9, 2011.

[10] M. Kanneganti, M. Mino-Kenudson, and E. Mizoguchi, "Animal models of colitis-associated carcinogenesis," *Journal of Biomedicine and Biotechnology*, vol. 2011, Article ID 342637, 23 pages, 2011.

[11] S. Melgar, L. Karlsson, E. Rehnstrom et al., "Validation of murine dextran sulfate sodium-induced colitis using four therapeutic agents for human inflammatory bowel disease," *International Immunopharmacology*, vol. 8, no. 6, pp. 836–844, 2008.

[12] T. Ohkusa, "Production of experimental ulcerative colitis in hamsters by dextran sulfate sodium and changes in intestinal microflora," *Nihon Shokakibyo Gakkai Zasshi*, vol. 82, no. 5, pp. 1327–1336, 1985.

[13] I. Okayasu, S. Hatakeyama, M. Yamada, T. Ohkusa, Y. Inagaki, and R. Nakaya, "A novel method in the induction of reliable experimental acute and chronic ulcerative colitis in mice," *Gastroenterology*, vol. 98, no. 3, pp. 694–702, 1990.

[14] S. Melgar, K. Engstrom, A. Jagervall, and V. Martinez, "Psychological stress reactivates dextran sulfate sodium-induced chronic colitis in mice," *Stress*, vol. 11, no. 5, pp. 348–362, 2008.

[15] M. Mahler, I. J. Bristol, E. H. Leiter et al., "Differential susceptibility of inbred mouse strains to dextran sulfate sodium-induced colitis," *American Journal of Physiology*, vol. 274, no. 3, part 1, pp. G544–G551, 1998.

[16] T. Vowinkel, T. J. Kalogeris, M. Mori, C. F. Krieglstein, and D. N. Granger, "Impact of dextran sulfate sodium load on the severity of inflammation in experimental colitis," *Digestive Diseases and Sciences*, vol. 49, no. 4, pp. 556–564, 2004.

[17] S. Kitajima, S. Takuma, and M. Morimoto, "Histological analysis of murine colitis induced by dextran sulfate sodium of different molecular weights," *Experimental Animals*, vol. 49, no. 1, pp. 9–15, 2000.

[18] I. Hirono, K. Kuhara, T. Yamaji, S. Hosaka, and L. Golberg, "Carcinogenicity of dextran sulfate sodium in relation to its molecular weight," *Cancer Letters*, vol. 18, no. 1, pp. 29–34, 1983.

[19] S. Kitajima, S. Takuma, and M. Morimoto, "Tissue distribution of dextran sulfate sodium (DSS) in the acute phase of murine DSS-induced colitis," *Journal of Veterinary Medical Science*, vol. 61, no. 1, pp. 67–70, 1999.

[20] H. S. Cooper, S. N. Murthy, R. S. Shah, and D. J. Sedergran, "Clinicopathologic study of dextran sulfate sodium experimental murine colitis," *Laboratory Investigation*, vol. 69, no. 2, pp. 238–249, 1993.

[21] S. Kitajima, M. Morimoto, and E. Sagara, "A model for dextran sodium sulfate (DSS)-induced mouse colitis: bacterial degradation of DSS does not occur after incubation with mouse cecal contents," *Experimental Animals*, vol. 51, no. 2, pp. 203–206, 2002.

[22] S. Melgar, A. Karlsson, and E. Michaelsson, "Acute colitis induced by dextran sulfate sodium progresses to chronicity in C57BL/6 but not in BALB/c mice: correlation between symptoms and inflammation," *American Journal of Physiology*, vol. 288, no. 6, pp. G1328–G1338, 2005.

[23] L. J. Hall, E. Faivre, A. Quinlan, F. Shanahan, K. Nally, and S. Melgar, "Induction and activation of adaptive immune populations during acute and chronic phases of a murine model of experimental colitis," *Digestive Diseases and Sciences*, vol. 56, no. 1, pp. 79–89, 2011.

[24] I. Talbot, A. Price, and M. Salto-Tellez, *Biopsy Pathology in Colorectal Disease*, Hadder Arnol, 2nd edition, 2007.

[25] C. M. Fenoglio-Preiser, A. W. Noffsinger, G. N. Stemmermann, P. E. Lantz, and P. G. Isaacson, *Gastrointestinal Pathology*, LWW, 3rd edition, 2008.

[26] H. Tlaskalova-Hogenova, R. Stepankova, T. Hudcovic et al., "Commensal bacteria (normal microflora), mucosal immunity and chronic inflammatory and autoimmune diseases," *Immunology Letters*, vol. 93, no. 2-3, pp. 97–108, 2004.

[27] H. Tlaskalova-Hogenova, L. Tuckova, R. Stepankova et al., "Involvement of innate immunity in the development of inflammatory and autoimmune diseases," *Annals of the New York Academy of Sciences*, vol. 1051, pp. 787–798, 2005.

[28] S. Prakash, C. Tomaro-Duchesneau, S. Saha, and A. Cantor, "The gut microbiota and human health with an emphasis on the use of microencapsulated bacterial cells," *Journal of Biomedicine and Biotechnology*, vol. 2011, Article ID 981214, 12 pages, 2011.

[29] S. Nell, S. Suerbaum, and C. Josenhans, "The impact of the microbiota on the pathogenesis of IBD: lessons from mouse infection models," *Nature Reviews Microbiology*, vol. 8, no. 8, pp. 564–577, 2010.

[30] W. Hans, J. Scholmerich, V. Gross, and W. Falk, "The role of the resident intestinal flora in acute and chronic dextran sulfate sodium-induced colitis in mice," *European Journal of Gastroenterology and Hepatology*, vol. 12, no. 3, pp. 267–273, 2000.

[31] T. Hudcovic, R. Stepankova, J. Cebra, and H. Tlaskalova-Hogenova, "The role of microflora in the development of intestinal inflammation: acute and chronic colitis induced by dextran sulfate in germ-free and conventionally reared immunocompetent and immunodeficient mice," *Folia Microbiologica*, vol. 46, no. 6, pp. 565–572, 2001.

[32] S. Kitajima, M. Morimoto, E. Sagara, C. Shimizu, and Y. Ikeda, "Dextran sodium sulfate-induced colitis in germ-free IQI/Jic mice," *Experimental Animals*, vol. 50, no. 5, pp. 387–395, 2001.

[33] S. Rakoff-Nahoum, J. Paglino, F. Eslami-Varzaneh, S. Edberg, and R. Medzhitov, "Recognition of commensal microflora by toll-like receptors is required for intestinal homeostasis," *Cell*, vol. 118, no. 2, pp. 229–241, 2004.

[34] A. A. te Velde, F. de Kort, E. Sterrenburg et al., "Comparative analysis of colonic gene expression of three experimental colitis models mimicking inflammatory bowel disease," *Inflammatory Bowel Diseases*, vol. 13, no. 3, pp. 325–330, 2007.

[35] L. Stevceva, P. Pavli, G. Buffinton, A. Wozniak, and W. F. Doe, "Dextran sodium sulphate-induced colitis activity varies with mouse strain but develops in lipopolysaccharide-unresponsive mice," *Journal of Gastroenterology and Hepatology*, vol. 14, no. 1, pp. 54–60, 1999.

[36] N. Ichikawa-Tomikawa, K. Sugimoto, S. Satohisa, K. Nishiura, and H. Chiba, "Possible Involvement of tight junctions, extracellular matrix and nuclear receptors in epithelial differentiation," *Journal of Biomedicine and Biotechnology*, vol. 2011, Article ID 253048, 10 pages, 2011.

[37] P. Laprise, "Emerging role for epithelial polarity proteins of the crumbs family as potential tumor suppressors," *Journal of Biomedicine and Biotechnology*, vol. 2011, Article ID 868217, 9 pages, 2011.

[38] L. S. Poritz, K. I. Garver, C. Green, L. Fitzpatrick, F. Ruggiero, and W. A. Koltun, "Loss of the tight junction protein ZO-1 in dextran sulfate sodium induced colitis," *Journal of Surgical Research*, vol. 140, no. 1, pp. 12–19, 2007.

[39] Y. Yan, V. Kolachala, G. Dalmasso et al., "Temporal and spatial analysis of clinical and molecular parameters in dextran sodium sulfate induced colitis," *PLoS One*, vol. 4, no. 6, Article ID e6073, 2009.

[40] R. Mennigen, K. Nolte, E. Rijcken et al., "Probiotic mixture VSL#3 protects the epithelial barrier by maintaining tight junction protein expression and preventing apoptosis in a murine model of colitis," *American Journal of Physiology*, vol. 296, no. 5, pp. G1140–G1149, 2009.

[41] Y. Araki, K. Mukaisyo, H. Sugihara, Y. Fujiyama, and T. Hattori, "Increased apoptosis and decreased proliferation of colonic epithelium in dextran sulfate sodium-induced colitis in mice," *Oncology Reports*, vol. 24, no. 4, pp. 869–874, 2010.

[42] B. Egger, M. Bajaj-Elliott, T. T. MacDonald, R. Inglin, V. E. Eysselein, and M. W. Büchler, "Characterisation of acute murine dextran sodium sulphate colitis: cytokine profile and dose dependency," *Digestion*, vol. 62, no. 4, pp. 240–248, 2000.

[43] P. Alex, N. C. Zachos, T. Nguyen et al., "Distinct cytokine patterns identified from multiplex profiles of murine DSS and TNBS-induced colitis," *Inflammatory Bowel Diseases*, vol. 15, no. 3, pp. 341–352, 2009.

[44] S. Sullivan, P. Alex, T. Dassopoulos et al., "Downregulation of sodium transporters and NHERF proteins in IBD patients and mouse colitis models: potential contributors to IBD-associated diarrhea," *Inflammatory Bowel Diseases*, vol. 15, no. 2, pp. 261–274, 2009.

[45] F. Lu, S. M. Fernandes, and A. E. Davis III, "The role of the complement and contact systems in the dextran sulfate sodium-induced colitis model: the effect of C1 inhibitor in inflammatory bowel disease," *American Journal of Physiology*, vol. 298, no. 6, pp. G878–G883, 2010.

[46] P. López, C. Gutiérrez, and A. Suárez, "IL-10 and TNFalpha genotypes in SLE," *Journal of Biomedicine and Biotechnology*, vol. 2010, Article ID 838390, 11 pages, 2010.

[47] B. Marshall and S. Swain, "Cytotoxic CD4 T cells in antiviral immunity," *Journal of Biomedicine and Biotechnology*, vol. 2011, Article ID 954602, 8 pages, 2011.

[48] P. K. Yadav, C. Chen, and Z. Liu, "Potential role of NK cells in the pathogenesis of inflammatory bowel disease," *Journal of Biomedicine and Biotechnology*, vol. 2011, Article ID 348530, 6 pages, 2011.

[49] P. L. Beck, R. Xavier, J. Wong et al., "Paradoxical roles of different nitric oxide synthase isoforms in colonic injury," *American Journal of Physiology*, vol. 286, no. 1, pp. G137–G147, 2004.

[50] P. L. Beck, Y. Li, J. Wong et al., "Inducible nitric oxide synthase from bone marrow-derived cells plays a critical role in regulating colonic inflammation," *Gastroenterology*, vol. 132, no. 5, pp. 1778–1790, 2007.

[51] Y. Naito, T. Takagi, O. Handa et al., "Enhanced intestinal inflammation induced by dextran sulfate sodium in tumor

necrosis factor-alpha deficient mice," *Journal of Gastroenterology and Hepatology*, vol. 18, no. 5, pp. 560–569, 2003.

[52] M. Kawada, A. Arihiro, and E. Mizoguchi, "Insights from advances in research of chemically induced experimental models of human inflammatory bowel disease," *World Journal of Gastroenterology*, vol. 13, no. 42, pp. 5581–5593, 2007.

[53] M. M. Heimesaat, A. Fischer, B. Siegmund et al., "Shift towards pro-inflammatory intestinal bacteria aggravates acute murine colitis via toll-like receptors 2 and 4," *PLoS One*, vol. 2, no. 7, article e662, 2007.

[54] M. Fukata, K. S. Michelsen, R. Eri et al., "Toll-like receptor-4 is required for intestinal response to epithelial injury and limiting bacterial translocation in a murine model of acute colitis," *American Journal of Physiology*, vol. 288, no. 5, pp. G1055–G1065, 2005.

[55] A. Araki, T. Kanai, T. Ishikura et al., "MyD88-deficient mice develop severe intestinal inflammation in dextran sodium sulfate colitis," *Journal of Gastroenterology*, vol. 40, no. 1, pp. 16–23, 2005.

[56] T. Hoshino, Y. Kawase, M. Okamoto et al., "Cutting edge: IL-18-transgenic mice: in vivo evidence of a broad role for IL-18 in modulating immune function," *Journal of Immunology*, vol. 166, no. 12, pp. 7014–7018, 2001.

[57] T. Ishikura, T. Kanai, K. Uraushihara et al., "Interleukin-18 overproduction exacerbates the development of colitis with markedly infiltrated macrophages in interleukin-18 transgenic mice," *Journal of Gastroenterology and Hepatology*, vol. 18, no. 8, pp. 960–969, 2003.

[58] K. Yoshihara, T. Yajima, C. Kubo, and Y. Yoshikai, "Role of interleukin 15 in colitis induced by dextran sulphate sodium in mice," *Gut*, vol. 55, no. 3, pp. 334–341, 2006.

[59] H. T. Ten, P. Drillenburg, J. Wijnholds, A. A. te Velde, and S. J. H. van Deventer, "Differential susceptibility of multidrug resistance protein-1 deficient mice to DSS and TNBS-induced colitis," *Digestive Diseases and Sciences*, vol. 47, no. 9, pp. 2056–2063, 2002.

[60] J. A. Martinez, C. S. Williams, J. M. Amann et al., "Deletion of mtgr1 sensitizes the colonic epithelium to dextran sodium sulfate-induced colitis," *Gastroenterology*, vol. 131, no. 2, pp. 579–588, 2006.

[61] J. Horino, M. Fujimoto, F. Terabe et al., "Suppressor of cytokine signaling-1 ameliorates dextran sulfate sodium-induced colitis in mice," *International Immunology*, vol. 20, no. 6, pp. 753–762, 2008.

[62] E. E. Mannick, R. L. Cote, J. R. Schurr et al., "Altered phenotype of dextran sulfate sodium colitis in interferon regulatory factor-1 knock-out mice," *Journal of Gastroenterology and Hepatology*, vol. 20, no. 3, pp. 371–380, 2005.

[63] M. Adachi, R. Kurotani, K. Morimura et al., "Peroxisome proliferator activated receptor γ in colonic epithelial cells protects against experimental inflammatory bowel disease," *Gut*, vol. 55, no. 8, pp. 1104–1113, 2006.

[64] A. J. Guri, S. K. Mohapatra, W. T. Horne, R. Hontecillas, and J. Bassaganya-Riera, "The role of T cell PPAR gamma in mice with experimental inflammatory bowel disease," *BMC Gastroenterology*, vol. 10, article 60, 2010.

[65] J. E. Ghia, N. Li, H. Wang et al., "Serotonin has a key role in pathogenesis of experimental colitis," *Gastroenterology*, vol. 137, no. 5, pp. 1649–1660, 2009.

[66] R. Fayad, M. Pini, J. A. Sennello et al., "Adiponectin deficiency protects mice from chemically induced colonic inflammation," *Gastroenterology*, vol. 132, no. 2, pp. 601–614, 2007.

[67] T. Nishihara, M. Matsuda, H. Araki et al., "Effect of adiponectin on murine colitis induced by dextran sulfate sodium," *Gastroenterology*, vol. 131, no. 3, pp. 853–861, 2006.

[68] Y. M. Shah, S. Ito, K. Morimura et al., "Hypoxia-inducible factor augments experimental colitis through an mif-dependent inflammatory signaling cascade," *Gastroenterology*, vol. 134, no. 7, pp. 2036–2048, 2008.

[69] H. Takagi, T. Kanai, A. Okazawa et al., "Contrasting action of IL-12 and IL-18 in the development of dextran sodium sulphate colitis in mice," *Scandinavian Journal of Gastroenterology*, vol. 38, no. 8, pp. 837–844, 2003.

Hindawi Publishing Corporation
Journal of Biomedicine and Biotechnology
Volume 2012, Article ID 587590, 8 pages
doi:10.1155/2012/587590

Review Article

Posterior Circulation Stroke: Animal Models and Mechanism of Disease

Tim Lekic[1] and Chizobam Ani[2]

[1] *Division of Physiology, Department of Basic Science, Loma Linda University School of Medicine, 11041 Campus Street, Risley Hall, CA 92354, USA*
[2] *Department of Family Medicine, Charles Drew University of Medicine and Science, Los Angeles, CA 90059-2518, USA*

Correspondence should be addressed to Tim Lekic, tlekic@llu.edu

Received 10 January 2012; Revised 6 March 2012; Accepted 12 March 2012

Academic Editor: Andrea Vecchione

Posterior circulation stroke refers to the vascular occlusion or bleeding, arising from the vertebrobasilar vasculature of the brain. Clinical studies show that individuals who experience posterior circulation stroke will develop significant brain injury, neurologic dysfunction, or death. Yet the therapeutic needs of this patient subpopulation remain largely unknown. Thus understanding the causative factors and the pathogenesis of brain damage is important, if posterior circulation stroke is to be prevented or treated. Appropriate animal models are necessary to achieve this understanding. This paper critically integrates the neurovascular and pathophysiological features gleaned from posterior circulation stroke animal models into clinical correlations.

1. Introduction

The posterior circulation is an understudied brain region that is affected by stroke. When translational research progresses to clinical trials, most trials will enroll very few or completely exclude posterior stroke patients [1–5]. Though posterior circulation strokes are too uncommon in many population centers to achieve sufficient numbers, other studies try to control for the heterogeneity between the anterior and posterior circulations [6, 7]. This leads to evidence-based guidelines which may not sufficiently represent some important spectrums of stroke. For these reasons, experimental animal models could be a useful tool to address emerging posterior circulation treatment strategies [8]. In this paper, we will integrate clinical features with animal models in describing characteristics of posterior circulation strokes, including the neurovascular features, and pathophysiology mechanisms founded from these experimental models.

2. Hemodynamic Posterior Circulation

The posterior circulation originates from the paired vertebral arteries and a single basilar artery, to supply the inferior thalamus, occipital lobes, midbrain, cerebellum, and brainstem. At the pontomedullary junction, the vertebral arteries fuse to form the basilar artery, which then courses along the ventral aspect of the pons and mesencephalon [9]. From the basilar artery, dorsolateral (circumferential) superficial vessels branch out to the lateral sides and course toward the cerebellum, while deep (paramedian) branches perforate directly into the brainstem, along the ventral aspect. The basilar artery terminates at the mesencephalic cistern, with perforator branches to parts of the diencephalon, and bifurcation into the paired posterior cerebral arteries (PCAs). The PCAs course laterally to combine with the posterior communicating arteries (PComAs) and then continue to supply parts of the occipital and temporal cortices. The circumferential, paramedian, and other perforator branches are called terminal vascular branches, which lack collateral flow and may potentiate focal ischemia during vertebrobasilar vessel occlusions. The pontine paramedian and the lateral cerebellar circumferential branches are the most common sites of hemorrhage. Several clinical syndromes (Table 1) are described for posterior circulation vascular injuries [10, 11].

Vascular reserve within the basilar circulation includes bidirectional flow through the AICA, PICA, and cer-ebellar leptomeninges [12, 13]. The leptomeningeal interconnec-

Table 1: Posterior circulation syndromes and associated brain region, clinical signs.

Syndrome(s)	Vessel(s)	Brain region(s)	Contralateral sign(s)	Ipsilateral sign(s)
None	VA, PICA	Cerebellum	None	Truncal, leg, and gait ataxia/dystaxia
Medial medullary, Wallenberg	ASA, VA, PICA	Caudal Medulla	Any sensory input loss hemiplegia	Horner's syndrome, tongue weakness, dysphagia, hoarseness, loss of facial sensation, nystagmus, vertigo, ataxia
Locked-in, Foville, Millard-Gubler, Marie-foix	BA, AICA	Pons	Loss of pain or temperature sensation, hemiplegia	Facial or lateral gaze weakness, dysarthria, hemiplegia, ataxia
Parinaud, Benedikt, Weber, Claude	PCA	Midbrain	Tremor, hemiplegia, motor deficit, cerebellar ataxia	Paralysis of gaze and accommodation, fixed pupils, CNIII palsy
Dejerine-Roussy	PCA	Thalamus	Pain syndrome, any sensory input loss	None
Balint, Anton	PCA	Occipital, Temporal lobes	Vision loss, blindness denial	Vision and eye movement loss, misinterpretation of visual objects, blindness denial, loss of visual-motor coordination

VA: vertebral artery; PICA: posterior inferior cerebellar artery; ASA: anterior spinal artery; BA: basilar artery; AICA: anterior inferior cerebellar artery; PCA: posterior cerebral artery; CNIII: cranial nerve three.

tions between cerebellar arteries are similar to the cerebral pial network and can reverse blood flow back through the tributaries of the basilar artery [14]. Outside the posterior circulation, the direction of blood flow can be reversed through hemodynamic connections between PComA (posterior communicating artery), first PCA segment, and carotid circulation [14]. Increased PComA vessel luminal size is directly proportional to improved patient outcome after basilar artery and first segmental PCA occlusions [15]. Patients with PComAs greater than 1 mm in diameter have less ischemic injury during carotid territory occlusions [16]. During basilar artery occlusion, PComAs reverse blood flow through the basilar bifurcation, PCA, and SCA (quadrigeminal plate) [14]. However, individual variations in arterial anatomy and the collateral circulation are common (asymmetric or single vertebral arteries, SCA and AICA branching variants, small PComAs) and these can narrow the basilar artery, diminishing vascular reserve, and leading to a greater incidence and severity of stroke [14–18].

3. Transient Posterior Brain Injury

Around ten years ago (vertebrobasilar), transient ischemic attack (TIA) was defined as follows: "a brief episode of neurologic dysfunction caused by focal brain ischemia, with clinical symptoms typically lasting less than one hour, and without evidence of acute infarction" [19]. VTIAs are half the duration of carotid territory TIAs [10] and generally perceived by clinicians as having a more benign course [20–25]. Consequently, VTIA patients receive less clinical investigation and treatment [26–28]. However, a systematic review of sixteen-thousand patients found no differences between carotid and vertebrobasilar TIAs, in the rate of stroke, death, or disability [26]. In fact, VTIAs are more likely to convert into full-on strokes during the acute-phase, and a third will have a stroke within 5 years [29, 30].

4. Ischemic Posterior Brain Injury

One-quarter of all ischemic strokes are located in the vertebrobasilar (VB) territory [31, 32]. These are usually caused by thrombi/emboli and rarely from vertebral artery dissection of C1-2 vertebral level trauma [10]. Patients with large vessel (basilar artery or intracranial VA) occlusions affecting the brainstem tend to have a worse prognosis while small lacunar occlusions generally do well, so long as cardiorespiratory centers are intact ([6]; clinical features are summarized in Table 1).

Patient outcomes after VB ischemic stroke have been somewhat the subject of debate. The Oxfordshire Community Stroke Project [31] prospectively followed 129 patients and found a 14% mortality and 18% major disability rate, while the New England Medical Centre Posterior Circulation Registry (NEMC-PCR) [33] found a 4% (death) and 18% (disability) rate, with a prospective study of 407 patients. For basilar artery occlusion (BAO), the most severe form of VB ischemic stroke, a systematic analysis of 10 published case series and 344 patients, reported an overall death or dependency rate of 76% [34], while the NEMC-PCR study with 87 patients reported poor outcomes in 28–58% of patients [35].

5. Hemorrhagic Posterior Brain Injury

One-fifth of all intracerebral hemorrhage (ICH) occurs in the cerebellum or brainstem [36, 37]. Brainstem hemorrhages have a 65% mortality rate and around 40% after cerebellar hemorrhage [38–40]. Prolonged endovascular cerebrovascular damage from uncontrolled hypertension leads to arteriosclerotic and amyloid angiopathic changes, vessel fragility, and rupture at the deep cerebellar vessels or brainstem basilar (paramedian) branches [37, 41]. Less common relations to occurrence are cancer, coagulopathy, or vascular anomalies (arterial-venous malformations, aneurysms,

cavernomas, and dural arteriovenous fistulas) [37, 41]. For most patients, supportive care is the only treatment rendered, since surgery is only available for one-quarter of hospitalized cerebellar hemorrhage patients, and the brainstem is not surgically accessible [42–45]. Mechanisms of infratentorial hemorrhage have never been studied and to this end we have developed animal models using collagenase to address this brain hemorrhage subpopulation [46, 47].

6. Animal Studies

Experimental models are available to study ischemic posterior circulation stroke [48]. Many animal studies of anterior circulation ischemic stroke have demonstrated impaired autoregulation after ischemic stroke. The extent of which would depend on occlusion duration and extent of reperfusion hyperemia [49–51]. These mechanisms warrant further study—this can be achieved using available animal models of posterior circulation stroke. Under experimental conditions, the standardized progressive hypotension in rats showed that autoregulatory kinetics remained intact at the cerebrum, while a progressive loss of autoregulatory efficacy in the cerebellum [52]. As a next step, however, changes in mean arterial blood pressure (MABP) and CO_2 levels (in cats) while measuring blood flow (hydrogen clearance method) in the cerebrum, cerebellum, and spinal cord found greater susceptibility to pressure-dependant ischemia in the cerebrum and spinal cord than cerebellum, which was relatively resistant [53].

Corroborative studies [54] used transcranial Doppler methods for comparing blood flow in supratentorial and infratentorial brain compartments during increasing intracranial pressures, in the rabbit experimental model. Essentially, the maximum vasomotor activity amplitude of occurred 30 seconds later in the basilar artery, compared with the carotids. Such reports demonstrate that delays are present in the effect of intracranial pressure upon hindbrain microvascular tone. Using a canine experimental model of permanent occlusion to posterior cerebral artery perforators [55] with the ability to monitor cerebral blood flow (autoregulation) and carbon dioxide reactivity, in response to induced hypotension/hypertension, it was found that cerebral cortex maintained autoregulation and carbon dioxide reactivity, while thalamic autoregulation was maintained in hypotension, but not during episodic hypertension. On the other hand, the midbrain retained marked impaired autoregulation and carbon dioxide reactivity. Such findings reveal differential brain vulnerability following permanent vascular occlusions. In essence, animal studies indicate that brainstem nuclei decompensated compared to forebrain regions, despite abundant amounts of posterior collateral circulation.

The animal model of bilateral carotid ligation using spontaneously hypertensive rats showed impaired autoregulation in the cerebrum [56]. However, the addition of stepwise drops in mean arterial pressures caused impairment of cerebellar autoregulation as well. Hypothetically, it is possible that vulnerability to hypotension in areas distant from the stroke ictus is modulated by alpha-adrenoceptor (vasoconstrictive) neurons responding to cerebral (transtentorial) hypertension signals [57]. The collateral vascular compensation may be a function of age, since bilateral carotid occlusion causes greater dependence upon basilar flow in adult rats, compared to dependence upon extracerebral midline collaterals in younger experimental animals [58].

7. Animal Models: Vascular Responses to Stroke

Experimental studies reveal that similar cerebrovascular mechanisms are found after ischemic and hemorrhagic stroke [59]. Normally, cerebrovascular autoregulation maintains optimal brain tissue perfusion through arterial constriction/dilation in response to local levels of CO_2 and systemic variations of blood pressures (MABP) [60]. Human stroke leads to damaged cerebral autoregulation capacity and greater dependence upon systemic arterial pressure [61–63] occurring after both carotid and vertebrobasilar-based vascular territories [62, 64]. This impairment is recognized as an important mechanism of secondary brain injury and edema formation, following human ischemic stroke [65] and intracerebral hemorrhage [66]. There is a rationale behind the tight hemodynamic and respiratory control in the intensive care units.

Animal studies show that the vertebrobasilar vessels have a greater capacity to mechanically vasodilate and vasoconstrict compared to carotid-based vasculature, suggesting greater dynamic autoregulatory ability [67–69]. This may be a mechanism enabling the hindbrain to divert blood flow to the carotid system during cerebrovascular strain, since drops in total brain perfusion lead to proportionally greater diminished flow across the basilar compared to the middle-cerebral artery [70]. When systemic CO_2 and blood pressure changes are superimposed upon permanent posterior cerebral artery occlusion, in dogs, this showed graded autoregulatory decompensation caudally from the supratentorial region to the brainstem, while carotid-based autoregulation was preserved [55]. Experiments in rats show cerebral sparing, while systemic hypotension causes progressive decline in cerebellar autoregulatory kinetics, and carotid autoregulatory kinetics remain intact [52]. The impairment of cerebellar autoregulation also occurs after bilateral carotid ligation in spontaneously hypertensive rats [57]. Conversely, the combination of hypocapnia with systemic hypotension, in cats, caused greater ischemic susceptibility in cortical brain-regions compared with the cerebellum [53]. Cerebellar autoregulatory kinetics may, therefore, accommodate CO_2 fluctuation more favorably, in the face of hypoperfusion, while drops in arterial pressures, without systemic CO_2 change, would affect the cerebellum more severely [52].

In most species, the cerebellum and brainstem have an abundance of white matter tracts. Magnetic resonance imaging (MRI) perfusion and diffusion studies in humans have determined white matter to have an infarction threshold of 20 mL/100 g/minute, while gray matter can sustain flow down to infarctions starting at 12 mL/100 g/minute [71].

A greater density of white matter tracts in the hindbrain would imply greater vulnerability to ischemic injury. Therefore the viability of brainstem cardiorespiratory centers during periods of severe systemic hypotension, global cerebral ischemia, and cardiac arrest will necessitate further study.

8. Animal Models: Neural Consequences from Stroke

Animal models show that ischemic interruption of cerebral blood flow leads to hypoxic and anoxic brain injury, increased neuronal excitability, and cell death [72]. Reperfusion injury further augments this damage through free radial production and mitochondrial dysfunction [73, 74] and similar mechanisms are at play after hemorrhagic stroke also [59]. Neurons in the CA1 hippocampal region are particularly vulnerable to ischemia; yet, experimentally, these cells are more resistant to damage than several areas of the hindbrain [75, 76]. Electrophysiological studies after hypoxic injury have shown greater neuronal excitability in the hypoglossal (CNXII) and dorsal vagal motor (DVMN) cranial nuclei of the brainstem compared to hippocampal CA1 regions [76]. Animal models show that anoxia of the hypoglossal nucleus will have both greater initial injury and impaired recovery compared with these temporal lobe neurons [77]. In vitro simulation of ischemic reperfusion injury, using cell cultures of oxygen-glucose deprivation followed by reoxygenation (OGD-R), showed greater free-radical injury (lipid peroxidation) and mitochondrial impairment in cerebellar cells compared to cerebral cortical cell culture [78]. Experiments comparing cerebellum with brainstem injury, after vertebral arterial occlusions in gerbils, showed greatest amount of cell death near regions controlling coordination and balance (cerebellar interpositus and lateral vestibular nuclei), while brainstem cardiorespiratory areas remain relatively more intact [75]. The scattered mosaic nature of brainstem nuclei means that this is not simply a redistribution of blood flow and is likely a feature of the neuronal environment, and this deserves further study.

Experimental studies reveal significant cerebellar fastigial nuclei (FN) involvement in the regulation of blood pressure and flow [79–81]. This occurs via integration of autonomic signals from vestibular and cerebellar Purkinje neurons [82, 83]. FN also modulate the function of adjacent medullary structures and autonomic spinal intermediolateral column neurons [84, 85]. In primates, these nuclei interconnect with vestibular (lateral and inferior), reticular (lateral, paramedian, and gigantocellular), and cervical spinal anterior gray neurons [86]. Animal models demonstrate that electrical stimulation of the FN leads to pressor responses with tachycardia, as mediated by fibers passing through, or very close to, the FN, while chemical activation causes a depressor response, with bradycardia via intrinsic FN neuronal activity [87–89]. Taken together, cerebellar fastigial nuclei serve important cardiovascular functions, the manner of which is of significant clinical interest, since cerebellar injury in association with cardiopulmonary consequences is a common occurrence [90–93].

Neurons of the area postrema (AP) also contribute to cardiovascular regulation [94–97]. Biochemically, the cell-surface receptors of circulating molecules: angiotensin II (AT1), and vasopressin (V1), are expressed within this brain region [98–100]. Here, the angiotensin II neurohormone can reset the baroreflex to higher blood pressure levels through indirect interactions with the nucleus of the solitary tract and interconnections within the medulla [101–103]. These nuclei can also modulate the cardiovascular regulatory effects of other neuropeptides—such as vasopressin. While this homeostatic effector readily binds somatic V2 type receptors, causing peripheral vasoconstriction, V1 receptor binding-interactions within the area postrema will paradoxically enhance baroreflex sensitivity towards activation at lower threshold pressure set-points [104–106]. All together, these pathways help keep the balance of complex cerebrovascular systems.

9. Development and Gender

Young children exhibit sex differences in the autoregulatory capacity between anterior and posterior circulations. Female children, ages 4–8 years, have higher flow velocities for both the middle cerebral and basilar arteries, while both sexes exhibit greater flow velocity in the middle cerebral compared to basilar arteries [107]. Later, autoregulatory capacities begin to emerge with females (10–16 years old) having greater capacity in the basilar artery than males, but males having the advantage of greater MCA autoregulatory index [108]. Up through adolescence, however, females continue to have higher flow velocities (compared to males) for both the middle cerebral and basilar arteries. This may indicate a gender-specific ability to handle an occlusive thrombus in the hindbrain. Further studies are needed to understand these gender differences.

10. Conclusion

The hindbrain injury pathogenesis, prevention, and treatment remain largely unknown, and animal models may be necessary to achieve this understanding. Furthermore, injury to this area can be particularly devastating. This brain region may have less innate neurovascular protective mechanisms and greater amount of cell death and injury in comparison to supratentorial strokes. Significant experimental study has been done for posterior circulation stroke. Future studies can choose from an array of animal models, to test interventions for reversing the mechanisms of injury in this brain region. The strength of this paper is related to the comprehensive nature of the information presented. In limitation, future reports will need to further critically appraise the reported data in the context of available evidence.

Acknowledgment

The authors wish to thank Professor John H. Zhang for his constant and consistent support and encouragement throughout the years.

References

[1] M. A. Foulkes, P. A. Wolf, T. R. Price, J. P. Mohr, and D. B. Hier, "The stroke data bank: design, methods, and baseline characteristics," *Stroke*, vol. 19, no. 5, pp. 547–554, 1988.

[2] W. M. Clark, S. Wissman, G. W. Albers, J. H. Jhamandas, K. P. Madden, and S. Hamilton, "Recombinant tissue-type plasminogen activator (Alteplase) for ischemic stroke 3 to 5 hours after symptom onset. The ATLANTIS Study: a randomized controlled trial. Alteplase Thrombolysis for Acute Noninterventional Therapy in Ischemic Stroke," *Journal of the American Medical Association*, vol. 282, no. 21, pp. 2019–2026, 1999.

[3] W. Hacke, M. Kaste, C. Fieschi et al., "Intravenous thrombolysis with recombinant tissue plasminogen activator for acute hemispheric stroke: the European Cooperative Acute Stroke Study (ECASS)," *Journal of the American Medical Association*, vol. 274, no. 13, pp. 1017–1025, 1995.

[4] A. D. Mendelow and A. Unterberg, "Surgical treatment of intracerebral haemorrhage," *Current Opinion in Critical Care*, vol. 13, no. 2, pp. 169–174, 2007.

[5] W. M. Clark, G. W. Albers, K. P. Madden, and S. Hamilton, "The rtPA (alteplase) 0- to 6-hour acute stroke trial, part A (A0276g): results of a double-blind, placebo-controlled, multicenter study. Thromblytic therapy in acute ischemic stroke study investigators," *Stroke*, vol. 31, no. 4, pp. 811–816, 2000.

[6] M. Macleod, "Current issues in the treatment of acute posterior circulation stroke," *CNS Drugs*, vol. 20, no. 8, pp. 611–621, 2006.

[7] M. R. Macleod, S. M. Davis, P. J. Mitchell et al., "Results of a multicentre, randomised controlled trial of intra-arterial urokinase in the treatment of acute posterior circulation lschaemic stroke," *Cerebrovascular Diseases*, vol. 20, no. 1, pp. 12–17, 2005.

[8] T. Lekic, P. R. Krafft, J. S. Coats, A. Obenaus, J. Tang, and J. H. Zhang, "Infratentorial strokes for posterior circulation folks: clinical correlations for current translational therapeutics," *Translational Stroke Research*, vol. 2, no. 2, pp. 144–151, 2011.

[9] H. Duvemoy, *Human Brain Stem Vessels*, Springer, Berlin, Germany, 1999.

[10] L. Worthley and A. W. Holt, "Acute ischaemic stroke: part II. The vertebrobasilar circulation," *Critical care and Resuscitation*, vol. 2, no. 2, pp. 140–145, 2000.

[11] A. Ferbert, H. Bruckmann, and R. Drummen, "Clinical features of proven basilar artery occlusion," *Stroke*, vol. 21, no. 8, pp. 1135–1142, 1990.

[12] E. de Oliveira, H. Tedeschi, A. Rhoton, and D. Peace, "Microsurgical anatomy of the posterior circulation: vertebral and basilar arteries," in *Neurovascular Surgery*, L. Carter, R. Spetzler, and M. Hamilton, Eds., pp. 25–34, McGraw-Hill, New York, NY, USA, 1995.

[13] J. R. Lister, A. L. Rhoton Jr., T. Matsushima, and D. A. Peace, "Microsurgical anatomy of the posterior inferior cerebellar artery," *Neurosurgery*, vol. 10, no. 2, pp. 170–199, 1982.

[14] M. Bergui, P. Cerrato, and G. B. Bradac, "Stroke attributable to acute basilar occlusion," *Current Treatment Options in Neurology*, vol. 9, no. 2, pp. 126–135, 2007.

[15] G. K. Steinberg, C. G. Drake, and S. J. Peerless, "Deliberate basilar or vertebral artery occlusion in the treatment of intracranial aneurysms. Immediate results and long-term outcome in 201 patients," *Journal of Neurosurgery*, vol. 79, no. 2, pp. 161–173, 1993.

[16] D. F. Schomer, M. P. Marks, G. K. Steinberg et al., "The anatomy of the posterior communicating artery as a risk factor for ischemic cerebral infarction," *The New England Journal of Medicine*, vol. 330, no. 22, pp. 1565–1570, 1994.

[17] V. Ganesan, W. K. Chong, T. C. Cox, S. J. Chawda, M. Prengler, and F. J. Kirkham, "Posterior circulation stroke in childhood: risk factors and recurrence," *Neurology*, vol. 59, no. 10, pp. 1552–1556, 2002.

[18] S. Chaturvedi, T. G. Lukovits, W. Chen, and P. B. Gorelick, "Ischemia in the territory of a hypoplastic vertebrobasilar system," *Neurology*, vol. 52, no. 5, pp. 980–983, 1999.

[19] G. W. Albers, L. R. Caplan, J. D. Easton et al., "Transient ischemic attack—proposal for a new definition," *The New England Journal of Medicine*, vol. 347, no. 21, pp. 1713–1716, 2002.

[20] F. H. McDowell, J. Potes, and S. Groch, "The natural history of internal carotid and vertebral-basilar artery occlusion," *Neurology*, vol. 11, no. 4, part 2, pp. 153–157, 1961.

[21] J. E. Olsson, R. Muller, and S. Bernell, "Long term anticoagulant therapy for TIAs and minor strokes with minimum residuum," *Stroke*, vol. 7, no. 5, pp. 444–451, 1976.

[22] T. M. Turney, W. M. Garraway, and J. P. Whisnant, "The natural history of hemispheric and brainstem infarction in Rochester, Minnesota," *Stroke*, vol. 15, no. 5, pp. 790–794, 1984.

[23] D. K. Ziegler and R. S. Hassanein, "Prognosis in patients with transient ischemic attacks," *Stroke*, vol. 4, no. 4, pp. 666–673, 1973.

[24] J. Marshall, "The natural history of transient ischaemic cerebro-vascular attacks," *The Quarterly Journal of Medicine*, vol. 33, pp. 309–324, 1964.

[25] J. Sivenius, P. J. Riekkinen, P. Smets, M. Laakso, and A. Lowenthal, "The European stroke prevention study (ESPS): results by arterial distribution," *Annals of Neurology*, vol. 29, no. 6, pp. 596–600, 1991.

[26] E. Floßmann and P. M. Rothwell, "Prognosis of vertebrobasilar transient ischaemic attack and minor stroke," *Brain*, vol. 126, no. 9, pp. 1940–1954, 2003.

[27] A. Culebras, C. S. Kase, J. C. Masdeu et al., "Practice guidelines for the use of imaging in transient ischemic attacks and acute stroke: a report of the Stroke Council, American Heart Association," *Stroke*, vol. 28, no. 7, pp. 1480–1497, 1997.

[28] P. J. Martin, "Vertebrobasilar ischaemia," *Monthly Journal of the Association of Physicians*, vol. 91, no. 12, pp. 799–811, 1998.

[29] J. C. Wehman, R. A. Hanel, C. A. Guidot, L. R. Guterman, and L. N. Hopkins, "Atherosclerotic occlusive extracranial vertebral artery disease: indications for intervention, endovascular techniques, short-term and long-term results," *Journal of Interventional Cardiology*, vol. 17, no. 4, pp. 219–232, 2004.

[30] C. R. Hornig, C. Lammers, T. Buttner, O. Hoffmann, and W. Dorndorf, "Long-term prognosis of infratentorial transient ischemic attacks and minor strokes," *Stroke*, vol. 23, no. 2, pp. 199–204, 1992.

[31] J. Bamford, P. Sandercock, M. Dennis, J. Burn, and C. Warlow, "Classification and natural history of clinical identifiable subtypes of cerebral infarction," *The Lancet*, vol. 337, no. 8756, pp. 1521–1526, 1991.

[32] J. Bogousslavsky, G. Van Melle, and F. Regli, "The lausanne stroke registry: analysis of 1,000 consecutive patients with first stroke," *Stroke*, vol. 19, no. 9, pp. 1083–1092, 1988.

[33] T. A. Glass, P. M. Hennessey, L. Pazdera et al., "Outcome at 30 days in the new England medical center posterior circulation

registry," *Archives of Neurology*, vol. 59, no. 3, pp. 369–376, 2002.

[34] P. J. Lindsberg and H. P. Mattle, "Therapy of basilar artery occlusion: a systematic analysis comparing intra-arterial and intravenous thrombolysis," *Stroke*, vol. 37, no. 3, pp. 922–928, 2006.

[35] B. Voetsch, L. D. DeWitt, M. S. Pessin, and L. R. Caplan, "Basilar artery occlusive disease in the New England Medical Center Posterior Circulation Registry," *Archives of Neurology*, vol. 61, no. 4, pp. 496–504, 2004.

[36] M. L. Flaherty, D. Woo, M. Haverbusch et al., "Racial variations in location and risk of intracerebral hemorrhage," *Stroke*, vol. 36, no. 5, pp. 934–937, 2005.

[37] G. R. Sutherland and R. N. Auer, "Primary intracerebral hemorrhage," *Journal of Clinical Neuroscience*, vol. 13, no. 5, pp. 511–517, 2006.

[38] M. L. Flaherty, M. Haverbusch, P. Sekar et al., "Long-term mortality after intracerebral hemorrhage," *Neurology*, vol. 66, no. 8, pp. 1182–1186, 2006.

[39] K. Balci, T. Asil, M. Kerimoglu, Y. Celik, and U. Utku, "Clinical and neuroradiological predictors of mortality in patients with primary pontine hemorrhage," *Clinical Neurology and Neurosurgery*, vol. 108, no. 1, pp. 36–39, 2005.

[40] M. D. Hill, F. L. Silver, P. C. Austin, and J. V. Tu, "Rate of stroke recurrence in patients with primary intracerebral hemorrhage," *Stroke*, vol. 31, no. 1, pp. 123–127, 2000.

[41] A. I. Qureshi, S. Tuhrim, J. P. Broderick, H. H. Batjer, H. Hondo, and D. F. Hanley, "Spontaneous intracerebral hemorrhage," *The New England Journal of Medicine*, vol. 344, no. 19, pp. 1450–1460, 2001.

[42] S. Tuhrim, "Intracerebral hemorrhage—improving outcome by reducing volume?" *The New England Journal of Medicine*, vol. 358, no. 20, pp. 2174–2176, 2008.

[43] O. Adeoye, D. Woo, M. Haverbusch et al., "Surgical management and case-fatality rates of intracerebral hemorrhage in 1988 and 2005," *Neurosurgery*, vol. 63, no. 6, pp. 1113–1117, 2008.

[44] J. Morioka, M. Fujii, S. Kato et al., "Surgery for spontaneous intracerebral hemorrhage has greater remedial value than conservative therapy," *Surgical Neurology*, vol. 65, no. 1, pp. 67–72, 2006.

[45] M. E. Fewel, B. G. Thompson, and J. T. Hoff, "Spontaneous intracerebral hemorrhage: a review," *Neurosurgical Focus*, vol. 15, no. 4, article E1, 2003.

[46] T. Lekic, W. Rolland, R. Hartman et al., "Characterization of the brain injury, neurobehavioral profiles, and histopathology in a rat model of cerebellar hemorrhage," *Experimental Neurology*, vol. 227, no. 1, pp. 96–103, 2011.

[47] T. Lekic, J. Tang, and J. H. Zhang, "A rat model of pontine hemorrhage," *Acta Neurochirurgica, Supplementum*, no. 105, pp. 135–137, 2008.

[48] T. Lekic and J. H. Zhang, "Posterior circulation stroke and animal models," *Frontiers in Bioscience*, vol. 13, no. 5, pp. 1827–1844, 2008.

[49] J. C. Drummond, Y. S. Oh, D. J. Cole, and H. M. Shapiro, "Phenylephrine-induced hypertension reduces ischemia following middle cerebral artery occlusion in rats," *Stroke*, vol. 20, no. 11, pp. 1538–1544, 1989.

[50] M. J. Cipolla, A. L. McCall, N. Lessov, and J. M. Porter, "Reperfusion decreases myogenic reactivity and alters middle cerebral artery function after focal cerebral ischemia in rats," *Stroke*, vol. 28, no. 1, pp. 176–180, 1997.

[51] L. Olah, C. Franke, W. Schwindt, M. Hoehn, and M. Fisher, "CO_2 reactivity measured by perfusion MRI during transient focal cerebral ischemia in rats," *Stroke*, vol. 31, no. 9, pp. 2236–2244, 2000.

[52] S. Merzeau, M. P. Preckel, B. Fromy, G. Lefthériotis, and J. L. Saumet, "Differences between cerebral and cerebellar autoregulation during progressive hypotension in rats," *Neuroscience Letters*, vol. 280, no. 2, pp. 103–106, 2000.

[53] M. Sato, G. Pawlik, and W. D. Heiss, "Comparative studies of regional CNS blood flow autoregulation and responses to CO_2 in the cat. Effects of altering arterial blood pressure and $PaCO_2$ on rCBF of cerebrum, cerebellum, and spinal cord," *Stroke*, vol. 15, no. 1, pp. 91–97, 1984.

[54] J. M. de Bray, F. Tranquart, J. L. Saumet, M. Berson, and L. Pourcelot, "Cerebral vasodilation capacity: acute intracranial hypertension and supra- and infra- tentorial artery velocity recording," *Clinical Physiology*, vol. 14, no. 5, pp. 501–512, 1994.

[55] S. Matsumoto, S. Kuwabara, and K. Moritake, "Effects of cerebrovascular autoregulation and CO_2 reactivity in experimental localized brainstem infarction," *Neurological Research*, vol. 22, no. 2, pp. 197–203, 2000.

[56] O. Shiokawa, S. Sadoshima, K. Kusuda, Y. Nishimura, S. Ibayashi, and M. Fujishima, "Cerebral and cerebellar blood flow autoregulations in acutely induced cerebral ischemia in spontaneously hypertensive rats—transtentorial remote effect," *Stroke*, vol. 17, no. 6, pp. 1309–1313, 1986.

[57] O. Shiokawa, S. Sadoshima, K. Fujii, H. Yao, and M. Fujishima, "Impairment of cerebellar blood flow autoregulation during cerebral ischemia in spontaneously hypertensive rats," *Stroke*, vol. 19, no. 5, pp. 615–622, 1988.

[58] M. Choy, V. Ganesan, D. L. Thomas et al., "The chronic vascular and haemodynamic response after permanent bilateral common carotid occlusion in newborn and adult rats," *Journal of Cerebral Blood Flow and Metabolism*, vol. 26, no. 8, pp. 1066–1075, 2006.

[59] G. Xi, R. F. Keep, and J. T. Hoff, "Mechanisms of brain injury after intracerebral haemorrhage," *Lancet Neurology*, vol. 5, no. 1, pp. 53–63, 2006.

[60] S. S. Kety and C. F. Schmidt, "The effects of altered arterial tensions of carbon dioxide and oxygen on cerebral blood flow and cerebral oxygen consumption of normal young men," *The Journal of Clinical Investigation*, vol. 27, no. 4, pp. 484–492, 1948.

[61] P. J. Eames, M. J. Blake, S. L. Dawson, R. B. Panerai, and J. F. Potter, "Dynamic cerebral autoregulation and beat to beat blood pressure control are impaired in acute ischaemic stroke," *Journal of Neurology Neurosurgery and Psychiatry*, vol. 72, no. 4, pp. 467–472, 2002.

[62] S. L. Dawson, R. B. Panerai, and J. F. Potter, "Serial changes in static and dynamic cerebral autoregulation after acute ischaemic stroke," *Cerebrovascular Diseases*, vol. 16, no. 1, pp. 69–75, 2003.

[63] S. Schwarz, D. Georgiadis, A. Aschoff, and S. Schwab, "Effects of body position on intracranial pressure and cerebral perfusion in patients with large hemispheric stroke," *Stroke*, vol. 33, no. 2, pp. 497–501, 2002.

[64] S. L. Dawson, M. J. Blake, R. B. Panerai, and J. F. Potter, "Dynamic but not static cerebral autoregulation is impaired in acute ischaemic stroke," *Cerebrovascular Diseases*, vol. 10, no. 2, pp. 126–132, 2000.

[65] C. Dohmen, B. Bosche, R. Graf et al., "Identification and clinical impact of impaired cerebrovascular autoregulation in patients with malignant middle cerebral artery infarction," *Stroke*, vol. 38, no. 1, pp. 56–61, 2007.

[66] J. Diedler, M. Sykora, A. Rupp et al., "Impaired cerebral vasomotor activity in spontaneous intracerebral hemorrhage," *Stroke*, vol. 40, no. 3, pp. 815–819, 2009.

[67] H. Ito, I. Yokoyama, H. Iida et al., "Regional differences in cerebral vascular response to P_aCO_2 changes in humans measured by positron emission tomography," *Journal of Cerebral Blood Flow and Metabolism*, vol. 20, no. 8, pp. 1264–1270, 2000.

[68] W. Hida, Y. Kikuchi, S. Okabe, H. Miki, H. Kurosawa, and K. Shirato, "CO_2 response for the brain stem artery blood flow velocity in man," *Respiration Physiology*, vol. 104, no. 1, pp. 71–75, 1996.

[69] M. Reinhard, Z. Waldkircher, J. Timmer, C. Weiller, and A. Hetzel, "Cerebellar autoregulation dynamics in humans," *Journal of Cerebral Blood Flow and Metabolism*, vol. 28, no. 9, pp. 1605–1612, 2008.

[70] L. Garbin, F. Habetswallner, and A. Clivati, "Vascular reactivity in middle cerebral artery and basilar artery by transcranial Doppler in normals subjects during hypoxia," *Italian Journal of Neurological Sciences*, vol. 18, no. 3, pp. 135–137, 1997.

[71] M. S. Bristow, J. E. Simon, R. A. Brown et al., "MR perfusion and diffusion in acute ischemic stroke: human gray and white matter have different thresholds for infarction," *Journal of Cerebral Blood Flow and Metabolism*, vol. 25, no. 10, pp. 1280–1287, 2005.

[72] N. Fujiwara, H. Higashi, K. Shimoji, and M. Yoshimura, "Effects of hypoxia on rat hippocampal neurones in vitro," *Journal of Physiology*, vol. 384, pp. 131–151, 1987.

[73] T. Back, "Pathophysiology of the ischemic penumbra—revision of a concept," *Cellular and Molecular Neurobiology*, vol. 18, no. 6, pp. 621–638, 1998.

[74] F. Facchinetti, V. L. Dawson, and T. M. Dawson, "Free radicals as mediators of neuronal injury," *Cellular and Molecular Neurobiology*, vol. 18, no. 6, pp. 667–682, 1998.

[75] R. Hata, M. Matsumoto, T. Hatakeyama et al., "Differential vulnerability in the hindbrain neurons and local cerebral blood flow during bilateral vertebral occlusion in gerbils," *Neuroscience*, vol. 56, no. 2, pp. 423–439, 1993.

[76] D. F. Donnelly, C. Jiang, and G. G. Haddad, "Comparative responses of brain stem and hippocampal neurons to O_2 deprivation: in vitro intracellular studies," *American Journal of Physiology*, vol. 262, no. 5, pp. L549–L554, 1992.

[77] J. P. O'Reilly, C. Jiang, and G. G. Haddad, "Major differences in response to graded hypoxia between hypoglossal and neocortical neurons," *Brain Research*, vol. 683, no. 2, pp. 179–186, 1995.

[78] A. Scorziello, C. Pellegrini, L. Forte et al., "Differential vulnerability of cortical and cerebellar neurons in primary culture to oxygen glucose deprivation followed by reoxygenation," *Journal of Neuroscience Research*, vol. 63, no. 1, pp. 20–26, 2001.

[79] L. O. Lutherer, B. C. Lutherer, and K. J. Dormer, "Bilateral lesions of the fastigial nucleus prevent the recovery of blood pressure following hypotension induced by hemorrhage or administration of endotoxin," *Brain Research*, vol. 269, no. 2, pp. 251–257, 1983.

[80] M. Miura and D. J. Reis, "Cerebellum: a pressor response elicited from the fastigial nucleus and its efferent pathway in brainstem," *Brain Research*, vol. 13, no. 3, pp. 595–599, 1969.

[81] F. Xu, T. Zhou, T. Gibson, and D. T. Frazier, "Fastigial nucleus-mediated respiratory responses depend on the medullary gigantocellular nucleus," *Journal of Applied Physiology*, vol. 91, no. 4, pp. 1713–1722, 2001.

[82] N. Doba and D. J. Reis, "Role of the cerebellum and the vestibular apparatus in regulation of orthostatic reflexes in the cat," *Circulation Research*, vol. 40, no. 4, pp. 9–18, 1974.

[83] B. J. Yates, "Vestibular influences on the autonomic nervous system," *Annals of the New York Academy of Sciences*, vol. 781, pp. 458–373, 1996.

[84] M. M. Caverson, J. Ciriello, and F. R. Calaresu, "Direct pathway from cardiovascular neurons in the ventrolateral medulla to the region of the intermediolateral nucleus of the upper thoracic cord: an anatomical and electrophysiological investigation in the cat," *Journal of the Autonomic Nervous System*, vol. 9, no. 2-3, pp. 451–475, 1983.

[85] R. A. Dampney, A. K. Goodchild, L. G. Robertson, and W. Montgomery, "Role of ventrolateral medulla in vasomotor regulation: a correlative anatomical and physiological study," *Brain Research*, vol. 249, no. 2, pp. 223–235, 1982.

[86] R. R. Batton, A. Jayaraman, D. Ruggiero, and M. B. Carpenter, "Fastigial efferent projections in the monkey: an autoradiographic study," *Journal of Comparative Neurology*, vol. 174, no. 2, pp. 281–305, 1977.

[87] K. Chida, C. Iadecola, M. D. Underwood, and D. J. Reis, "A novel vasodepressor response elicited from the rat cerebellar fastigial nucleus: the fastigial depressor response," *Brain Research*, vol. 370, no. 2, pp. 378–382, 1986.

[88] K. Chida, C. Iadecola, and D. J. Reis, "Lesions of rostral ventrolateral medulla abolish some cardio- and cerebrovascular components of the cerebellar fastigial pressor and depressor responses," *Brain Research*, vol. 508, no. 1, pp. 93–104, 1990.

[89] T. J. Parry and J. C. McElligott, "Kainic administration in the fastigial nucleus produces differential cardiovascular effects in awake and anesthetized rats," *Brain Research*, vol. 635, no. 1-2, pp. 27–36, 1994.

[90] M. L. Chen, M. B. Witmans, M. A. Tablizo et al., "Disordered respiratory control in children with partial cerebellar resections," *Pediatric Pulmonology*, vol. 40, no. 1, pp. 88–91, 2005.

[91] P. M. Macey, L. A. Henderson, K. E. Macey et al., "Brain morphology associated with obstructive sleep apnea," *American Journal of Respiratory and Critical Care Medicine*, vol. 166, no. 10, pp. 1382–1387, 2002.

[92] R. Kumar, P. M. Macey, M. A. Woo, J. R. Alger, T. G. Keens, and R. M. Harper, "Neuroanatomic deficits in congenital central hypoventilation syndrome," *Journal of Comparative Neurology*, vol. 487, no. 4, pp. 361–371, 2005.

[93] M. A. Woo, P. M. Macey, G. C. Fonarow, M. A. Hamilton, and R. M. Harper, "Regional brain gray matter loss in heart failure," *Journal of Applied Physiology*, vol. 95, no. 2, pp. 677–684, 2003.

[94] P. Ylitalo, H. Karppanen, and M. K. Paasonen, "Is the area postrema a control centre of blood pressure?" *Nature*, vol. 247, no. 5435, pp. 58–59, 1974.

[95] M. D. Joy and R. D. Lowe, "Evidence that the area postrema mediates the central cardiovascular response to angiotensin II," *Nature*, vol. 228, no. 5278, pp. 1303–1304, 1970.

[96] C. J. Price, T. D. Hoyda, and A. V. Ferguson, "The area postrema: a brain monitor and integrator of systemic autonomic state," *Neuroscientist*, vol. 14, no. 2, pp. 182–194, 2008.

[97] S. Sisó, M. Jeffrey, and L. González, "Sensory circumventricular organs in health and disease," *Acta Neuropathologica*, vol. 120, no. 6, pp. 689–705, 2010.

[98] R. Gerstberger and F. Fahrenholz, "Autoradiographic localization of V1 vasopressin binding sites in rat brain and kidney," *European Journal of Pharmacology*, vol. 167, no. 1, pp. 105–116, 1989.

[99] Z. Lenkei, M. Palkovits, P. Corvol, and C. Llorens-Cortès, "Expression of angiotensin type-1 (AT1) and type-2 (AT2) receptor mRNAs in the adult rat brain: a functional neuroanatomical review," *Frontiers in Neuroendocrinology*, vol. 18, no. 4, pp. 383–439, 1997.

[100] J. Huang, Y. Hara, J. Anrather, R. C. Speth, C. Iadecola, and V. M. Pickel, "Angiotensin II subtype 1A (AT1A) receptors in the rat sensory vagal complex: subcellular localization and association with endogenous angiotensin," *Neuroscience*, vol. 122, no. 1, pp. 21–36, 2003.

[101] J. W. Osborn, G. D. Fink, A. F. Sved, G. M. Toney, and M. K. Raizada, "Circulating angiotensin II and dietary salt: converging signals for neurogenic hypertension," *Current Hypertension Reports*, vol. 9, no. 3, pp. 228–235, 2007.

[102] S. McMullan, A. K. Goodchild, and P. M. Pilowsky, "Circulating angiotensin II attenuates the sympathetic baroreflex by reducing the barosensitivity of medullary cardiovascular neurones in the rat," *Journal of Physiology*, vol. 582, no. 2, pp. 711–722, 2007.

[103] B. Xue, H. Gole, J. Pamidimukkala, and M. Hay, "Role of the area postrema in angiotensin II modulation of baroreflex control of heart rate in conscious mice," *American Journal of Physiology*, vol. 284, no. 3, pp. H1003–H1007, 2003.

[104] R. Oikawa, Y. Nasa, R. Ishii et al., "Vasopressin V1A receptor enhances baroreflex via the central component of the reflex arc," *European Journal of Pharmacology*, vol. 558, no. 1–3, pp. 144–150, 2007.

[105] T. A. Koshimizu, Y. Nasa, A. Tanoue et al., "V1a vasopressin receptors maintain normal blood pressure by regulating circulating blood volume and baroreflex sensitivity," *Proceedings of the National Academy of Sciences of the United States of America*, vol. 103, no. 20, pp. 7807–7812, 2006.

[106] B. F. Cox, M. Hay, and V. S. Bishop, "Neurons in area postrema mediate vasopressin-induced enhancement of the baroreflex," *American Journal of Physiology*, vol. 258, no. 6, part 2, pp. H1943–H1946, 1990.

[107] N. Tontisirin, S. L. Muangman, P. Suz et al., "Early childhood gender differences in anterior and posterior cerebral blood flow velocity and autoregulation," *Pediatrics*, vol. 119, no. 3, pp. e610–e615, 2007.

[108] M. S. Vavilala, M. S. Kincaid, S. L. Muangman, P. Suz, I. Rozet, and A. M. Lam, "Gender differences in cerebral blood flow velocity and autoregulation between the anterior and posterior circulations in healthy children," *Pediatric Research*, vol. 58, no. 3, pp. 574–578, 2005.

Hindawi Publishing Corporation
Journal of Biomedicine and Biotechnology
Volume 2012, Article ID 201689, 4 pages
doi:10.1155/2012/201689

Review Article

Cytokines and VEGF Induction in Orthodontic Movement in Animal Models

M. Di Domenico,[1] F. D'apuzzo,[2] A. Feola,[1] L. Cito,[3] A. Monsurrò,[2] G. M. Pierantoni,[4] L. Berrino,[5] A. De Rosa,[2] A. Polimeni,[6] and L. Perillo[2]

[1] *Department of General Pathology, Second University of Naples, Via L. De Crecchio 7, 80138 Naples, Italy*
[2] *Department of Oral Pathology, Orthodontics and Oral Surgery, Institute of Biochemistry, Second University of Naples, Via L. De Crecchio 6, 80138 Naples, Italy*
[3] *INT-CROM, "Pascale Foundation" National Cancer Institute - Cancer Research Center, Via Ammiraglio Bianco, 83013 Mercogliano, Italy*
[4] *Department of Cellular and Molecular Biology and Pathology, Faculty of Medicine of Naples, University of Naples "Federico II," Via Pansini 5, 80131 Naples, Italy*
[5] *Department of Experimental Medicine, Second University of Naples, Via L. De Crecchio 7, 80138 Naples, Italy*
[6] *Department of Oral and Maxillofacial Sciences, University of Rome "La Sapienza", Viale Regina Elena 287/A, 00161 Rome, Italy*

Correspondence should be addressed to M. Di Domenico, marina.didomenico@unina2.it

Received 29 December 2011; Revised 13 March 2012; Accepted 14 March 2012

Academic Editor: Monica Fedele

Orthodontics is a branch of dentistry that aims at the resolution of dental malocclusions. The specialist carries out the treatment using intraoral or extraoral orthodontic appliances that require forces of a given load level to obtain a tooth movement in a certain direction in dental arches. Orthodontic tooth movement is dependent on efficient remodeling of periodontal ligament and alveolar bone, correlated with several biological and mechanical responses of the tissues surrounding the teeth. A periodontal ligament placed under pressure will result in bone resorption whereas a periodontal ligament under tension results in bone formation. In the primary stage of the application of orthodontic forces, an acute inflammation occurs in periodontium. Several proinflammatory cytokines are produced by immune-competent cells migrating by means of dilated capillaries. In this paper we summarize, also through the utilization of animal models, the role of some of these molecules, namely, interleukin-1β and vascular endothelial growth factor, that are some proliferation markers of osteoclasts and osteoblasts, and the macrophage colony stimulating factor.

1. Orthodontic Movement and Inflammation

Orthodontic movement is correlated with an inflammatory process, that, in concert with the mechanical responses of periodontal and oral tissues, is essential for achieving tooth movement clinically. Early effects of orthodontic forces are of physical [1] and biological nature, and they involve extracellular matrix and cells of the alveolar bone, periodontal ligament, blood vessels, and neural elements. As consequence, many changes occur in these structures and various molecules are produced or inducted, as well as cytokines, growth factors, colony-stimulating factors, and neurotransmitters [2]. The first stages before the orthodontic force application are characterized by an acute inflammatory response. In the periodontium this process involves the vasodilatation of capillaries which allows the migration of leucocytes in the periodontal tissue, where they are induced by biochemical signals to synthesize and to secrete several proinflammatory cytokines and chemokines, growth factors and enzymes.

Orthodontic appliances impose forces on the teeth with a predetermined direction, and tooth movement occurs through different phases. The biological responses of hard tissue to mechanical loadings around the tooth are different between a tension area and a compression area (Figure 1). Mechanical forces are transduced to the cells triggering the biologic response by means of an aseptic transitory inflammatory process that involves several inflammatory

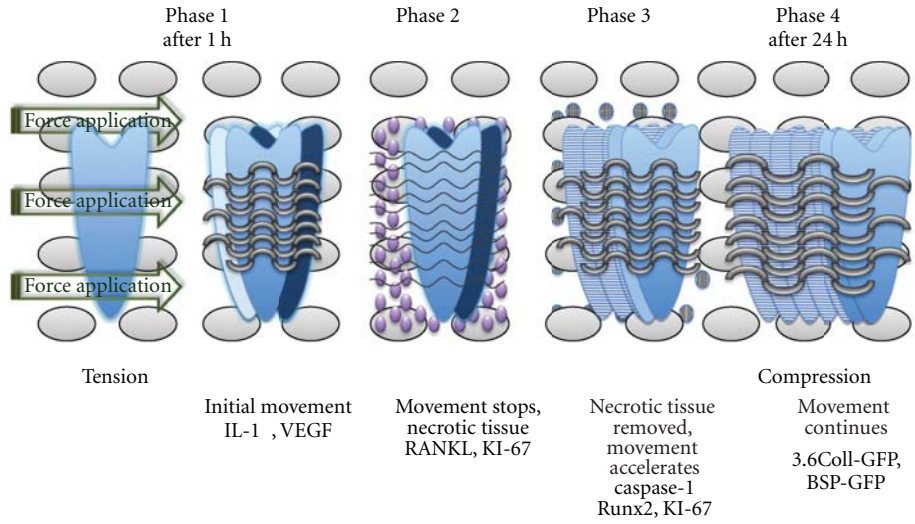

Figure 1: Phases of tooth movement associated with the application of orthodontic forces.

mediators. This succession of local events is the base for achieving the remodeling of the parodontium, so to allow the tooth movement [3].

The following paragraphs of the paper are intended to focus on the role of various chemical and cellular factors primarily present after the application of orthodontic forces.

The goal of this paper is to provide to orthodontic clinicians and educators some basic information and the summary of some updated studies about the correlation between tooth movement and inflammatory process. Understanding of these molecular phenomena is crucial to share the notion that orthodontic tooth movement is "the biologic response to interference in the physiologic equilibrium of the dentofacial complex by an externally applied force" [4].

1.1. Interleukine-1β Induction at Primary Stage of Orthodontic Tooth Movement. Cytokine expression in the rat periodontal ligament at the initial stage of orthodontic tooth movement has been investigated to evaluate the change of periodontal ligament. Interleukin (IL)-1β is one of the most abundant cytokines in the periodontal environment during the initial stage of orthodontic tooth movement because of its direct implications in alveolar bone resorption induced in the pressure side by mechanical loading [5].

IL-1β takes part in the survival, fusion, and activation of osteoclasts and exerts an important role since the amount of tooth movement correlates with the efficiency of bone remodeling in the alveolar process [6]. Higher levels of expression of inflammatory cytokines and of their respective receptors had been shown after an inducted inflammatory process by perforating the buccal cortical plate of orthodontically treated rats. The concentration of IL-1β mRNA in the rats' periodontal ligament is increased within 3 h after orthodontic force loading, particularly on pressure side [7]. The soft tissues surrounding the teeth are involved in orthodontic tooth shift such as the hard tissues, periodontal ligament, and alveolar bone, and changes in gingival contour always follow tooth movement. After the application of mechanical loadings, IL-1β mRNA in pressure side gingival is significantly increased in a rat model under orthodontic treatment [8].

IL-1β can bind two types of receptors, IL-1RI and IL-1RII [9]. Only the former is examined in this context [10, 11] since the latter acts only as a "decoy" target for the cytokine. The particular function as proinflammatory cytokine of IL-1β has been demonstrated by the administration of exogenous interleukin (IL)-1 receptor antagonist (IL-1Ra) in mice undergoing orthodontic treatment [12]. The level of IL-1β decreased by 66% in mice treated with IL-Ra therapy, and this associated with a reduction of the number of osteoclasts in the pressure side of periodontal tissues after histological characterization, and with a less rate of tooth displacement. These results showed that IL-1Ra has an anti-inflammatory role that leads to a downregulation of the orthodontic tooth movement.

The production of IL-1β is inducted from the processing and the activation of a pro-IL-1β by a protease, the caspase-1. Indeed, an apoptosis process occurs in conjunction with the inflammatory one that eliminates the hyalinized periodontal tissue formed during the early stages of orthodontic movement. Caspase-1 is the most important mediator of inflammation and apoptosis responses, activated by inflammatory signals as alterations in the intracellular ionic milieu. In a rat model under orthodontic treatment, caspase-1 expression is increased, and the level of caspase-1 changes with different temporal phases of orthodontic tooth movement [13]. If the local orthodontic application of force is excessive, or else if in the body there is an hyper-expression of caspase-1 by a kind of diseases like rheumatoid arthritis, an irreversible root resorption and a deformation of periodontal tissues might appear. Researchers propose that, because of the primary role of caspase-1 in inflammatory response due to orthodontic tooth movement, a method to preserve the structure of periodontal ligament may be the administration of the inhibitors of caspase-1 activity such as VX-765 [14] and Pralnacasan [15].

1.2. VEGF Localization during Orthodontic Tooth Movement in Animal Models. Vascular endothelial growth factor is the primary mediator of angiogenesis and it increases vascular permeability. This cytokine is involved in tissue neoformation that is strictly correlated with the presence of blood vessels. During orthodontic tooth movement, compressive forces induce angiogenesis of periodontal ligament together with the role of mediator of the VEGF. The localization of VEGF was analyzed in vivo in rat periodontal tissues during experimental tooth movement. In this analysis, 15 male Wistar rats were used. A compressive force at 150 mN was applied by means of a uniform standardized compressive spring placed between the right and left upper first molars in each rat's mouths. The maxillary bone was removed by the animals and it was analyzed with immunohistochemical staining. In the experimental animals, VEGF immunoreactivity was in vascular endothelial cells, osteoblasts, osteoclasts in resorption lacunae, in fibroblasts adjacent to hyalinized tissue, a local necrotic area in compressed zone, and in mononuclear cells in periodontal tissues from the animals [16]. VEGF mRNA was also detected in fibroblasts and osteoblasts in tension area of mice periodontal ligament during experimental tooth orthodontic movement [17]. The protocol included 10 mice, divided between experimental and control animals, and provided the analysis of premaxillary bone frontal sections [18]. Therefore, VEGF exerts a fundamental role in remodeling periodontal ligament and is also involved in bone resorption and formation.

1.3. Relation among Some Markers of Bone Cell Proliferation and M-CSF with Orthodontic Movement. There are other studies that examine a variety of proliferation markers expressed during orthodontic tooth movement. For instance, the high presence of the antigen KI-67, nuclear protein associated with cellular proliferation and ribosomal RNA transcription, and of RANKL, a key factor for osteoclast differentiation and activation [19, 20], indicates the recruitment of osteoclasts in compression areas [21], whereas, the expression of Runx2, a transcription factor associated with osteoblast differentiation, shows the increase of differentiated osteoblasts in tension areas [6]. In other studies, researchers analyzed the collagen type 1 (3.6Col1) and the bone sialoprotein (BSP) in periodontal ligament, using transgenic mice containing transgenes of these promoters fused with green fluorescent proteins (GFP), and they discovered that 3.6Col1-GFP and BSP-GFP cells have an increase on the tension side of the periodontal ligament [22, 23].

Another important role in tooth movement is played by the macrophage colony-stimulating factor (M-CSF), an early osteoclast differentiation factor, that increases the rate of osteoclastic recruitment and differentiation [24].

In particular, optimal dosages of M-CSF correlated with measurable changes in tooth movement and gene expression, providing potential for clinical studies in accelerating tooth movement.

2. Rats as Models for Orthodontic Movement

Up to now, a large number of studies in various species of animals, such as cats, dogs, and rats, have been done to enlighten the biological response to periodontal ligament. Rats are the most used animals for studying tooth movement, even if there are advantages and disadvantages [25]. Among the disadvantages, it must be remembered that the alveolar bone of rats is more dense than in humans, and there are no osteons. Indeed, the osteoid tissue along the alveolar bone surface in rats is less, their bone extracellular matrix has a few mucopolysaccharides, and, finally, the calcium concentration is more controlled by intestinal absorption. Disparities have been reported also in the arrangement of the peritoneal fibers and in the supporting structures, as in the root formations, which seem to be faster. Notwithstanding these disadvantages, rats are considered a good model to study orthodontic tooth movement. Indeed, they are relatively inexpensive, the histological preparation of their material is easier than other animals, and transgenic strains are almost exclusively developed in small rodents.

Clinical studies show that there are different phases in tooth movement. The application of force during orthodontic tooth movement results in bone resorption by osteoclasts and deposition by osteoblasts on the pressure and tension sides of the periodontal ligament. Recent studies in mice demonstrate that preosteoclasts, and not monocytes, may be recruited to the periodontal ligament during orthodontic tooth movement, and these cells may be targeted for acceleration of tooth movement.

3. Concluding Remarks

Knowledge regarding the biological mechanisms involved in orthodontic tooth movement appears to be of considerable importance for orthodontists that may modulate mechanoresponses and inflammatory process, accelerating or decelerating tooth movement, by adding various exogenous substances, taking also in consideration the condition of health of each orthodontically treated subject.

Acknowledgment

The authors thank R. De Lucia for her support in the drafting of the paper.

References

[1] V. Krishnan and Z. Davidovitch, "On a path to unfolding the biological mechanisms of orthodontic tooth movement," *Journal of Dental Research*, vol. 88, no. 7, pp. 597–608, 2009.

[2] V. Krishnan, "Cellular, molecular, and tissue-level reactions to orthodontic force," *American Journal of Orthodontics and Dentofacial Orthopedics*, vol. 129, no. 4, pp. 469.e1–469.e32, 2006.

[3] T. P. Garlet, U. Coelho, J. S. Silva, and G. P. Garlet, "Cytokine expression pattern in compression and tension sides of the periodontal ligament during orthodontic tooth movement in humans," *European Journal of Oral Sciences*, vol. 115, no. 5, pp. 355–362, 2007.

[4] W. R. Proffit, "Biologic basis of orthodontic therapy," in *Contemporary Orthodontics*, W. R. Proffit and H. W. Fields, Eds., Mosby, St. Louis, Mo, USA, 3rd edition, 2000.

[5] A. Bletsa, E. Berggreen, and P. Brudvik, "Interleukin-1 and tumor necrosis factor-α expression during the early phases of orthodontic tooth movement in rats," *European Journal of Oral Sciences*, vol. 114, no. 5, pp. 423–429, 2006.

[6] C. C. Teixeira, E. Khoo, J. Tran et al., "Cytokine expression and accelerated tooth movement," *Journal of Dental Research*, vol. 89, no. 10, pp. 1135–1141, 2010.

[7] S. Baba, N. Kuroda, C. Arai, Y. Nakamura, and T. Sato, "Immunocompetent cells and cytokine expression in the rat periodontal ligament at the initial stage of orthodontic tooth movement," *Archives of Oral Biology*, vol. 56, no. 5, pp. 466–473, 2011.

[8] T. Y. Lee, K. J. Lee, and H. S. Baik, "Expression of IL-1,MMP-9 and TIMP-1 on the pressure side of gingiva under orthodontic loading," *Angle Orthodontist*, vol. 79, no. 4, pp. 733–739, 2009.

[9] J. H. Kim, H. M. Jin, K. Kim et al., "The mechanism of osteoclast differentiation induced by IL-1," *Journal of Immunology*, vol. 183, no. 3, pp. 1862–1870, 2009.

[10] L. R. Iwasaki, J. E. Haack, J. C. Nickel, R. A. Reinhardt, and T. M. Petro, "Human interleukin-1b and interleukin-1 receptor antagonist secretion and velocity of tooth movement," *Archives of Oral Biology*, vol. 46, no. 2, pp. 185–189, 2001.

[11] L. R. Iwasaki, J. R. Chandler, D. B. Marx, J. P. Pandey, and J. C. Nickel, "IL-1 gene polymorphisms, secretion in GCF, and speed of human tooth orthodontic movement," *Orthodontics and Craniofacial Research*, vol. 12, no. 2, pp. 129–140, 2009.

[12] J. T. Salla, S. R. A. Taddei, C. M. Queiroz-Junior et al., "The effect of IL-1 receptor antagonist on orthodontic tooth movement in mice," *Archives of Oral Biology*, vol. 57, no. 5, pp. 519–524, 2012.

[13] X. Yan, J. Chen, Y. Hao, Y. Wang, and L. Zhu, "Changes of caspase-1 after the application of orthodontic forces in the periodontal tissues of rats," *Angle Orthodontist*, vol. 79, no. 6, pp. 1126–1132, 2009.

[14] J. Stack, K. Beaumont, P. D. Larsen et al., "IL-converting enzyme/caspase-1 inhibitor VX-765 blocks the hypersensitive response to an inflammatory stimulus in monocytes from familial cold autoinflammatory syndrome patients," *Journal of Immunology*, vol. 175, no. 4, pp. 2630–2634, 2005.

[15] K. Rudolphi, N. Gerwin, N. Verzijl, P. van der Kraan, and W. van den Berg, "Pralnacasan, an inhibitor of interleukin-1β converting enzyme, reduces joint damage in two murine models of osteoarthritis," *Osteoarthritis and Cartilage*, vol. 11, no. 10, pp. 738–746, 2003.

[16] A. Miyagawa, M. Chiba, H. Hayashi, and K. Igarashi, "Compressive force induces VEGF production in periodontal tissues," *Journal of Dental Research*, vol. 88, no. 8, pp. 752–756, 2009.

[17] M. Kaku, M. Motokawa, Y. Tohma et al., "VEGF and M-CSF levels in periodontal tissue during tooth movement," *Biomedical Research*, vol. 29, no. 4, pp. 181–187, 2008.

[18] M. Kaku, S. Kohno, T. Kawata et al., "Effects of vascular endothelial growth factor on osteoclast induction during tooth movement in mice," *Journal of Dental Research*, vol. 80, no. 10, pp. 1880–1883, 2001.

[19] T. Kim, A. Handa, J. Iida, and S. Yoshida, "RANKL expression in rat periodontal ligament subjected to a continuous orthodontic force," *Archives of Oral Biology*, vol. 52, no. 3, pp. 244–250, 2007.

[20] M. Yamaguchi, "RANK/RANKL/OPG during orthodontic tooth movement," *Orthodontics and Craniofacial Research*, vol. 12, no. 2, pp. 113–119, 2009.

[21] P. J. Brooks, D. Nilforoushan, M. F. Manolson, C. A. Simmons, and S. G. Gong, "Molecular markers of early orthodontic tooth movement," *Angle Orthodontist*, vol. 79, no. 6, pp. 1108–1113, 2009.

[22] F. Uribe, Z. Kalajzic, J. Bibko et al., "Early effects of orthodontic forces on osteoblast differentiation in a novel mouse organ culture model," *Angle Orthodontist*, vol. 81, no. 2, pp. 284–291, 2011.

[23] C. Olson, F. Uribe, Z. Kalajzic et al., "Orthodontic tooth movement causes decreased promoter expression of collagen type-1, bone sialoprotein and alpha-smooth muscle actin in the periodontal ligament," *Orthodontic Craniofacial Research*, vol. 15, pp. 52–61, 2012.

[24] P. J. Brooks, A. F. Heckler, K. Wei, and S. G. Gong, "M-CSF accelerates orthodontic tooth movement by targeting preosteoclasts in mice," *Angle Orthodontist*, vol. 81, no. 2, pp. 277–283, 2011.

[25] Y. Ren, J. C. Maltha, and A. M. Kuijpers-Jagtman, "The rat as a model for orthodontic tooth movement—a critical review and a proposed solution," *European Journal of Orthodontics*, vol. 26, no. 5, pp. 483–490, 2004.

Hindawi Publishing Corporation
Journal of Biomedicine and Biotechnology
Volume 2012, Article ID 298657, 20 pages
doi:10.1155/2012/298657

Review Article

The Current State of Knowledge of Hepatic Ischemia-Reperfusion Injury Based on Its Study in Experimental Models

M. Mendes-Braz,[1] M. Elias-Miró,[2] M. B. Jiménez-Castro,[2] A. Casillas-Ramírez,[2] F. S. Ramalho,[1] and C. Peralta[2,3]

[1] *Departamento de Patologia e Medicina Legal, Faculdade de Medicina, Universidade de Sao Paulo, 14040-900 Ribeirão Preto, SP, Brazil*
[2] *Institut d'lnvestigacions Biomèdiques August Pi i Sunyer (IDIBAPS), 08036 Barcelona, Spain*
[3] *Centro de Investigación Biomédica en Red de Enfermedades Hepáticas y Digestivas, 08036 Barcelona, Spain*

Correspondence should be addressed to C. Peralta, cperalta@clinic.ub.es

Received 1 December 2011; Accepted 23 February 2012

Academic Editor: Oreste Gualillo

The present review focuses on the numerous experimental models used to study the complexity of hepatic ischemia/reperfusion (I/R) injury. Although experimental models of hepatic I/R injury represent a compromise between the clinical reality and experimental simplification, the clinical transfer of experimental results is problematic because of anatomical and physiological differences and the inevitable simplification of experimental work. In this review, the strengths and limitations of the various models of hepatic I/R are discussed. Several strategies to protect the liver from I/R injury have been developed in animal models and, some of these, might find their way into clinical practice. We also attempt to highlight the fact that the mechanisms responsible for hepatic I/R injury depend on the experimental model used, and therefore the therapeutic strategies also differ according to the model used. Thus, the choice of model must therefore be adapted to the clinical question being answered.

1. Introduction

Ischemia-reperfusion (I/R) injury is a phenomenon in which cellular damage in a hypoxic organ is accentuated following the restoration of oxygen delivery [1–3]. In the liver, this form of injury was recognized as a clinically important pathological disorder by Toledo-Pereyra et al. in 1975 during studies of experimental liver transplantation (LT). However, it was not until the mid-1980s that the term reperfusion injury was generally used in the literature on LT [2]. I/R injury is an important cause of liver damage occurring during surgical procedures including hepatic resections and LT [4–6]. The shortage of organs has led centers to expand their criteria for the acceptance of marginal grafts that exhibit poor tolerance to I/R [7]. Some of these include the use of organs from older donors and grafts such as small-for-size or steatotic livers. However, I/R injury is the underlying cause of graft dysfunction in marginal organs [7]. Indeed, the use of steatotic livers for transplantation is associated with an increased risk of primary nonfunction or dysfunction after surgery [8]. In addition, the occurrence of postoperative liver failure after hepatic resection in a steatotic liver exposed to normothermic ischemia has been reported [9]. Therefore, minimizing the adverse effects of I/R injury could improve outcomes in steatotic liver surgery, increasing the number of patients who successfully recover from major liver surgery.

Animal models of cold and warm hepatic I/R are valuable tools for understanding the physiopathology of hepatic I/R injury and discovering novel therapeutic targets and drugs. Some of the mechanisms and cell types involved in hepatic I/R injury are described below.

The lack of oxygen in hepatocytes during ischemia causes ATP depletion and alterations in H^+, Na^+, and Ca^{2+} homeostasis that activate hydrolytic enzymes and impair cell volume regulation leading to the swelling of sinusoidal endothelial cells (SECs) and Kupffer cells (KCs) [10]. This fact, together with the imbalance between nitric oxide (NO) and endothelin production, contributes to the narrowing of the

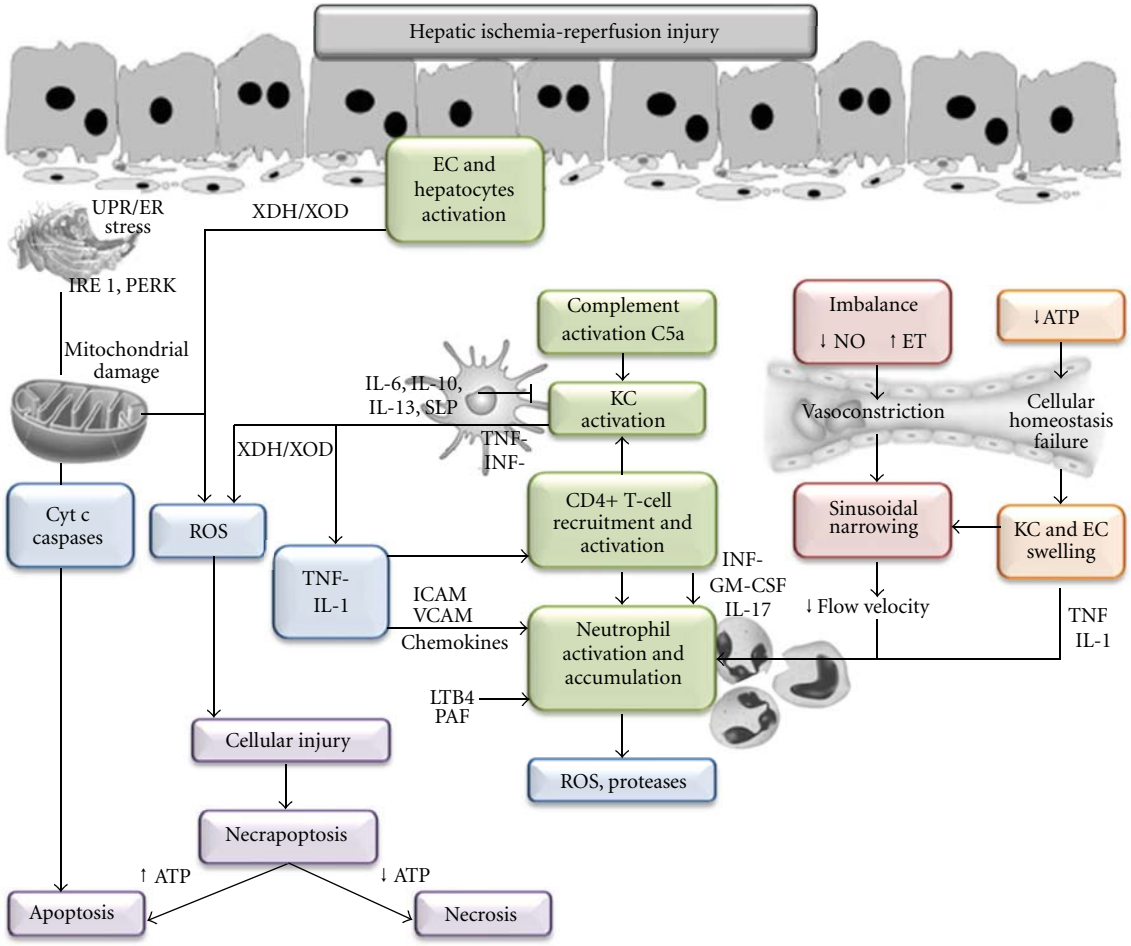

Figure 1: Mechanisms involved in hepatic ischemia-reperfusion injury. EC, endothelial cell; ET, endothelin; UPR/ER, unfolded protein response/endoplasmic reticulum; IRE1, inositol-requiring enzyme 1; PERK, PKR-like ER kinase; SLP, secretory leukocyte protease inhibitor; ICAM, intracellular cell adhesion molecule; VCAM, vascular cell adhesion molecule; GM-CSF, granulocyte-macrophage colony-stimulating factor; IL, interleukin; INF, interferon; TNF, tumor necrosis factor; PAF, platelet-activating factor; LTB4, leucotriene B4; KC, Kupffer cell; X/XOD, xanthine/xanthine oxidase; Cyt c: cytochrome c.

sinusoidal lumen and thus to microcirculatory dysfunction (Figure 1). Capillary narrowing also contributes to hepatic neutrophil accumulation [11]. Concomitantly, the activation of KCs releases reactive oxygen species (ROS) and proinflammatory cytokines, including tumour necrosis factor-alpha (TNF-α) and interleukin-1 (IL-1) [12]. Similar to their production in KCs, ROS can derive from mitochondria and the xanthine dehydrogenase/xanthine oxidase (XDH/XOD) pathway in activated SEC and hepatocytes. Cytokines release through the induction of adhesion molecules (intercellular cell adhesion molecule and vascular cell adhesion molecule), and chemokines promote neutrophil activation and accumulation, thereby contributing to the progression of parenchymal injury by releasing ROS and proteases [1, 3, 12]. In addition, IL-1 and TNF-α recruit and activate CD4+ T lymphocytes, which produce granulocyte-macrophage colony-stimulating factor, interferon gamma and TNF-β (Figure 1). These cytokines amplify KC activation and TNF-α and IL-1 secretion and promote neutrophil recruitment and adherence into the liver sinusoids [13, 14]. Platelet-activating factor can prime neutrophils for superoxide generation, whereas leukotriene B4 contributes to the amplification of the neutrophil response [1, 3].

2. Experimental Models

The speed of human studies is slow, the majority of human tissues are not routinely accessible for research purposes, and there is a very limited opportunity for interventional studies. Although scientific research has always relied on the use of cell cultures, information that is obtained through *in vitro* studies can be extrapolated to biomedical research only when analyzed within a complex organism with metabolic functioning. Therefore, one avenue holding tremendous potential in the search for therapies against I/R damage is the use of intact living systems, in which complex biological processes can be examined. There are many advantages of animal studies: large numbers of animals (especially rodents)

can be bred and studied, interventional studies can be performed, and established and emerging tools for targeted manipulation of gene expression levels provide insight into the function of mediators in hepatic I/R injury.

Comparison of the results of animal studies and their extrapolation to human beings is feasible, but with limitations. Among the primary obstacles are differences in hypothermia and ischemia tolerance, differences in the anatomy of the livers of various species and subspecies, differences between and within the experimental models used, and differences in the modes of administration, dosage, and metabolic breakdown of the drugs under investigation. Thus, it is very important to choose the animal species and the experimental model and to standardize the protocol according to the clinical question under study.

2.1. Choice of the Animal Model. The species used for experimental investigation of hepatic I/R injury range from mice to pigs. Small animals such as mice and rats are exceptionally useful because they are easy to manage, present minimal logistical, financial, or ethical problems, and provide the potential for genetic alterations (e.g., transgenic and knockout animals). However, an important drawback is that the results of studies performed in small animals are of limited applicability to human beings due to their varying size and anatomy of the liver and their faster metabolism [15]. Large animals such as pigs, sheep, and dogs exhibit greater similarity in their anatomy and physiology to human beings. Thus, they are more suited for the study of problems of direct clinical relevance. However, their use is restricted by serious logistical and financial difficulties and often by ethical concerns. Furthermore, the technical possibilities of blood and tissue processing are extremely restricted because of the limited availability of immunological tools for use in large animal species [15].

When selecting an animal species, the age and sex of the animals should be considered. Depending on the duration of ischemia, young (35–50 g) and older rats (250–400 g) exhibit significant differences in their hepatic microcirculation [16]. A mature rat weighing more than 250 g (14–16 weeks old) is the most suitable because younger rats can present technical problems, whereas older rats are more prone to respiratory infections and fat accumulation. Sex selection also affects experimental results, as hormone levels in female animals are dependent on the estrous cycle, which certainly affects the ischemia tolerance of the liver. For instance, a study demonstrated that after normothermic liver ischemia, male rats were less sensitive to reperfusion injury than female rats [17].

Considering the relevancy of hepatic steatosis in surgery, experimental models of hepatic I/R injury in the presence of steatosis have been developed. However, the mechanisms involved in hepatic I/R injury, as it will be described in following sections, are different depending on the method used to induce steatosis. The different models of steatosis include (1) induced genetic models such as db/db and ob/ob mice and fa/fa rats, (2) animals fed diets with high levels of saturated fat and/or carbohydrates and/or proteins, (3) animals fed diets deficient in methyl groups (choline, methionine, folates), and (4) animals fed modified high-fat diets (lower methionine and choline and higher-fat content) [18].

2.2. Standardization of the Experiment. The induction of I/R injury must be performed under standardized experimental conditions. Of primary importance are the conditions under which the animals are kept such as adequate acclimatization time, maintenance under climatized conditions with 12 h light/12 h darkness, and standardized diets. The anesthetic method and postoperative analgesic regimen must also be standardized. When choosing the anesthetic and analgesic procedures, possible interactions with liver metabolism must be considered. Attention must be paid to adequate monitoring of blood pressure, heart rate, and body temperature.

3. Normothermic Ischemia

3.1. Global Hepatic Ischemia with Portocaval Decompression. The model of global liver ischemia with portal decompression ideally simulates the clinical situation of warm ischemia after the Pringle maneuver for liver resection and LT. The first successful shunt operation in humans was performed by Vidal in 1903 [19]. Blakemore was one of the first workers to report successful portal-systemic anastomosis in rats working principally with endothelium-lined tubes [20]. Burnett et al. modified this technique to form a portocaval shunt [21]. In 1959 Bernstein and Cheiker developed the portosystemic shunt that conducted the portal blood after functional hepatectomy into one of the iliac veins [22]. In small animals, in addition to many other shunt techniques such as the portofemoral shunt and the mesentericocaval shunt via the jugular vein, in 1995, Spiegel et al. developed the splenocaval shunt [23] (Figure 2). In large animals, on the contrary, a portofemorojugular bypass is frequently employed [24].

3.2. Global Liver Ischemia with Spleen Transposition. Bengmark et al. developed this model in 1970 for the surgical treatment of portal hypertension [25]. In 1981 Meredith and Wade presented a rat model that by transposition of the spleen produced a portosystemic shunt in the anhepatic rat [26]. A small incision is made in the left hypochondrium. After transposition of the spleen into a subcutaneous pouch, adequate portosystemic anastomoses arise after 2-3 weeks (Figure 3). Reversal of blood flow in the splenic vein, induced by the transposition, stimulates angiogenesis. In the second step 2 weeks later, the surgeon performs a median laparotomy and temporary occlusion of the hepatoduodenal ligament. This decompression by spleen transposition does not require microsurgical technique and is therefore easy to perform [27]. Two-to-three weeks postoperatively, the spleen will have been encapsulated without any signs of bleeding or inflammation (Figure 3). One disadvantage of this model is the long time lapse (3 weeks) until the formation of adequate portosystemic collaterals. Not until this point in time are the collaterals sufficiently large to take over portal vein flow

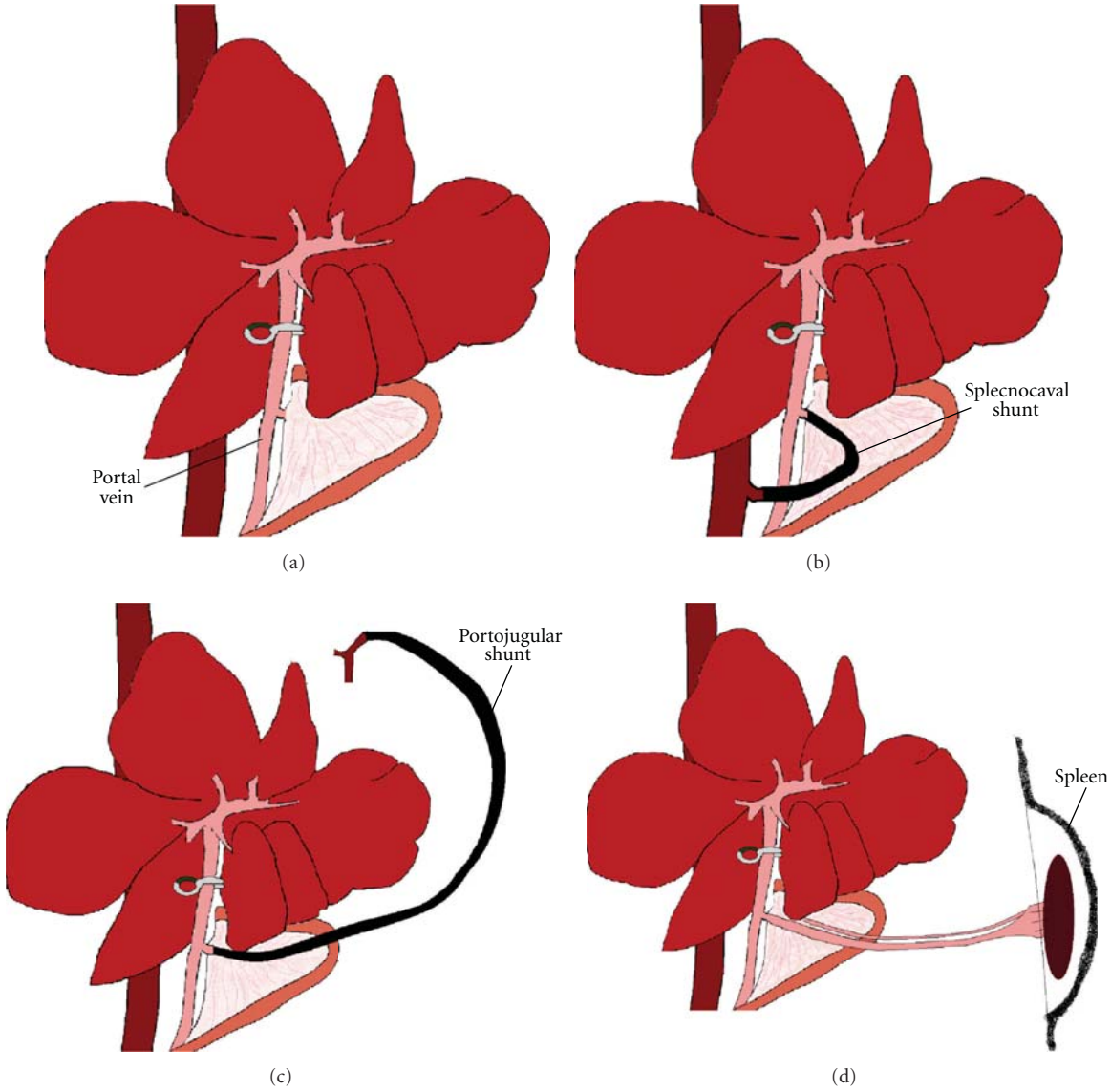

Figure 2: Models of global normothermic liver ischemia. (a) Pringle maneuver. (b) Splecnocaval shunt. (c) Portojugular shunt. (d) Spleen transposition.

completely. Furthermore, it is uncertain how the changes in hepatic inflow will react upon the collaterals [28].

3.3. Partial Liver Ischemia. In 1982, Yamauchi et al. and Hasselgren et al. described a model of hepatic ischemia [29, 30]. In this technique, ischemia is induced by occlusion of the hepatic artery, the portal vein, and the bile duct of the left and median lobes. An extracorporeal shunt is not necessary because blood flow continues through the right and caudal liver lobes. This model of 70% partial ischemia has been widely used in experimental studies of hepatic I/R [31, 32]. Additionally, a experimental model of 30% partial liver ischemia has been used in which blood supply to the right lobe of the liver is interrupted by occlusion at the level of the hepatic artery and portal vein [11, 33].

It is known that, in clinical situations, partial hepatectomy under I/R is usually performed to control bleeding during parenchymal dissection. Therefore, the use of a experimental model including both hepatic regeneration and I/R injury is advisable to simulate the clinical situation of selective or hemihepatic vascular occlusion for liver resections. In experimental model, after resection of left hepatic lobe, a microvascular clamp is placed across the portal triad supplying the median lobe (30%). Congestion of the bowel is avoided during the clamping period by preserving the portal flow through the right and caudate lobes. At the end of ischemia time, the right lobe and caudate lobes are resected, and reperfusion of the median lobe is achieved by releasing the clamp. This model of hepatic resection does not require any portal decompression and also

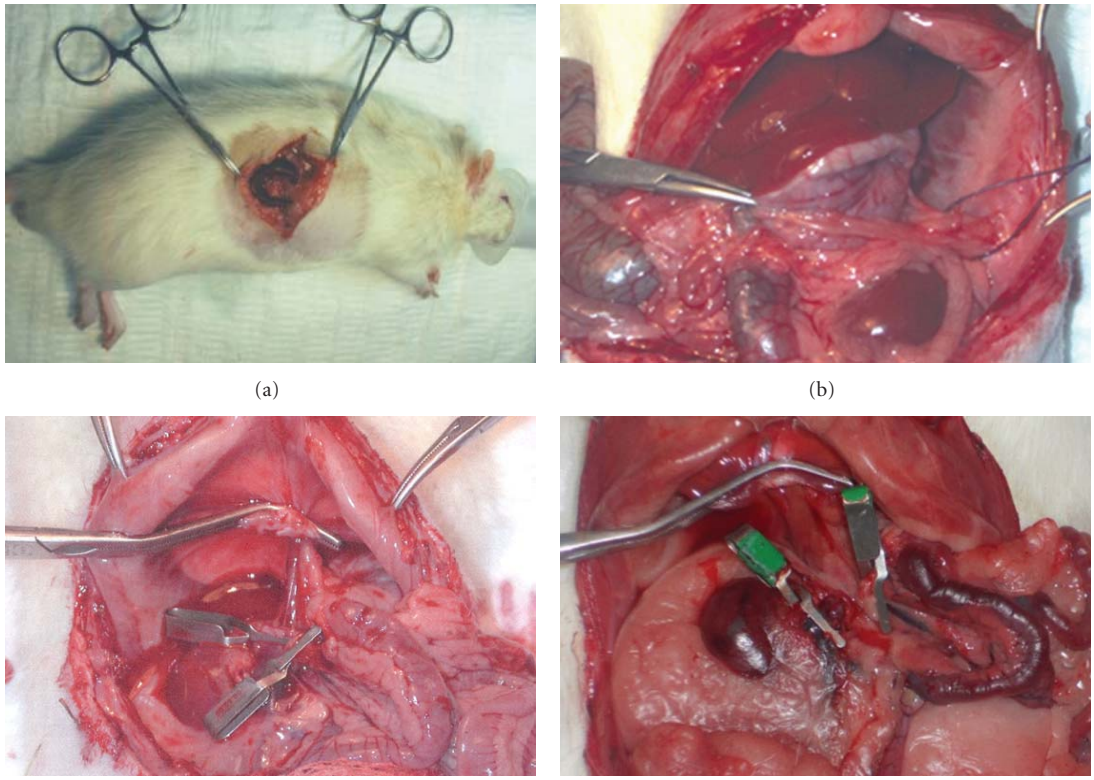

(a) (b) (c) (d)

Figure 3: (a) Transposition of the spleen to the subcutaneous tissue in the left hypochondrium. (b) Abdominal cavity after three weeks of the transposition of the spleen. (c) Anhepatic phase in recipient with SPS. No intestinal congestion is observed secondary to clamping of different vessels. (d) Anhepatic phase in recipient without SPS. Intestinal congestion is observed secondary to clamping of the different vessels.

fulfills certain important criteria such as reversibility, good reproducibility, and simple performance [34, 35].

4. Liver Transplantation

LT in larger laboratory animals such as dogs and pigs is technically easier. However, the rat has become the most important subject for experimental LT because of, among other factors, the availability of genetically defined animals [36].

Orthotopic liver transplantation (OLT) is a common yet complex microsurgical technique. OLT in mice is technically very difficult, even without reconstruction of the hepatic artery. By contrast, OLT in rats is technically accessible, producing more clinically relevant and reliable data [37]. The development of clinically relevant OLT models in rats [37] has advanced clinical knowledge in LT. These experimental models facilitate the study of new preservation methods, tolerance induction, rejection mechanisms, and novel immunosuppressor therapies [38].

OLT in rats was first reported in 1973 using hand-suture techniques [39], and a modified model without hepatic artery reconstruction and temporal shunt of the portojugular venovenous bypass was documented in 1975 [40]. However, these models were not widely used due to the prolonged surgical time and technical demand. With the cuff method being introduced in 1979 by Kamada and Calne [41], OLT in rats without hepatic artery reconstruction became globally accepted [37].

The donor operation, including the harvesting and preparation of the donor liver, is usually performed according to the procedure described by Kamada and Calne [41]. After arterial and portal perfusion, the suprahepatic vena cava is dissected free from the diaphragmatic ring, and the intrathoracic vena cava is transected. The aorta is cut around the celiac axis to form the aortic patch. Finally, the inferior vena cava, the portal vein, and the bile duct are cut, and the graft is placed in a cold preservation solution [42] (Figure 4). OLT is then performed by suture or mechanical microvascular anastomoses. Sutured vascular anastomosis reduces the incidence of thrombosis but takes a long time to perform. Suprahepatic vena cava anastomosis is performed by the continuous suturing technique. Then, portal vein and infrahepatic vena cava anastomosis is performed in the same manner. Hepatic artery reconstruction in rat LT can prevent bile duct ischemia and preserve the structure of the liver [43]. Several techniques of rearterialization by suture have been proposed [42, 43], the best being the aortic segment anastomosis technique [42]. After rearterialization,

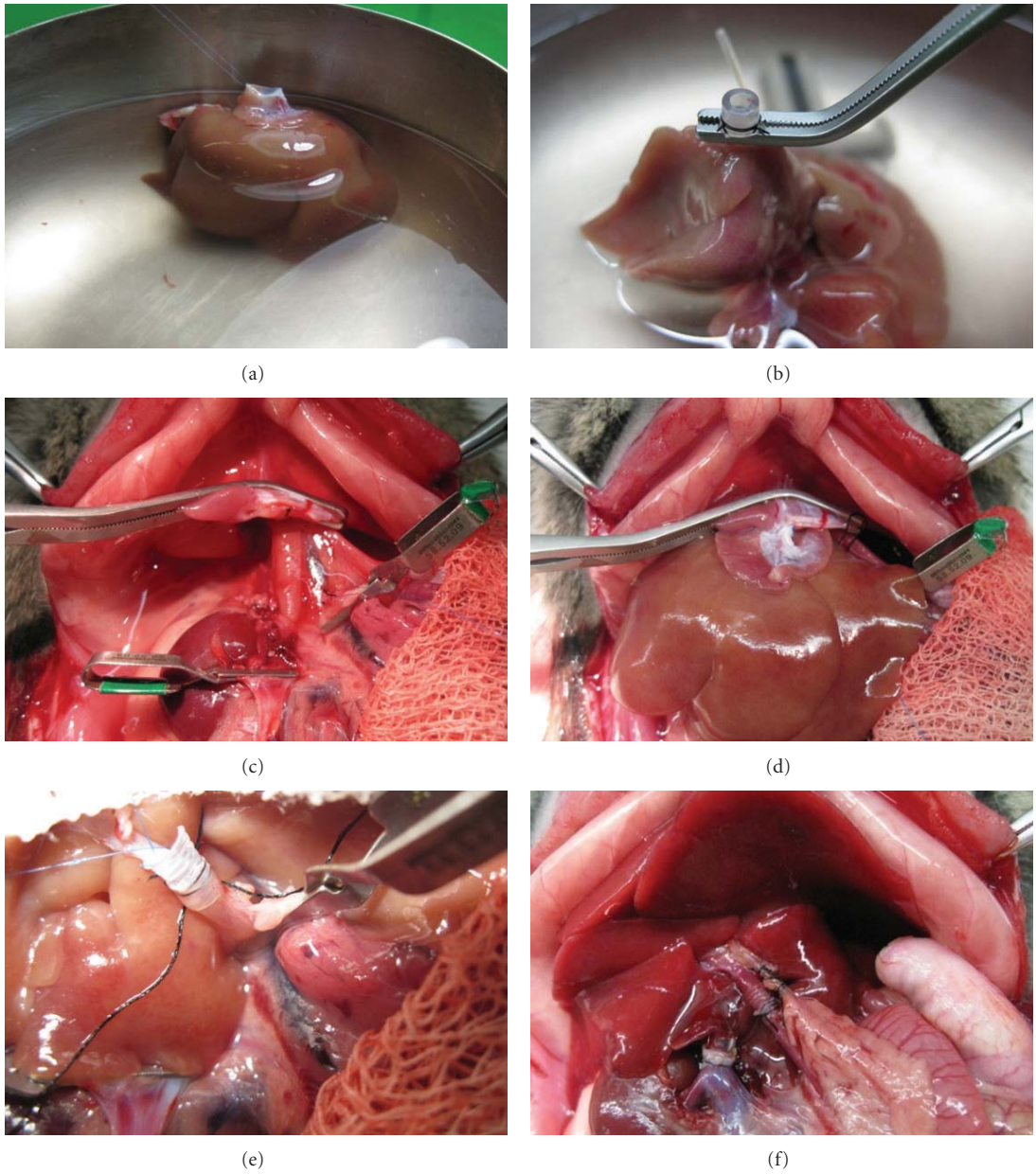

Figure 4: Liver transplantation procedure. (a) Suprahepatic cava vein prepared for the anastomosis. (b) Inferior vein cava cuff attachment. (c) Anhepatic phase in the recipient rat. (d) Anastomosis of suprahepatic cava vein by continuous suture. (e) Portal vein anastomosis through the cuff method. (f) Anastomosis of the bile duct.

the common bile duct is anastomosed. OLT by hand-sewn microanastomosis is a very useful method because this technique comes closest to the techniques used in human transplantation surgery [42]. Alternatively, livers can be satisfactorily allografted in rats by using the rapid cuff-ligature technique for anastomosis [41, 42]. In the simplified technique, the donor hepatic artery can be ligated because it will not be anastomosed [38]. A mechanical microvascular anastomosis for OLT in the rat using a quick-linker technique that significantly reduces the warm ischaemia time has recently been proposed [44].

In an attempt to expand the size of the donor pool, a number of surgical techniques have been developed over the past 15 years, including split LT and living donor LT [45]. One of the benefits of reduced-size grafts from living donors is a graft of good quality with a short ischemic time, this latter being possible because live donor procurements can be electively timed with the recipient procedure. Conversely, the major concern over the application of living-related LT for adults is graft-size disparity. Small grafts require posterior regeneration to restore the liver/body ratio. It is well known that I/R significantly reduces liver regeneration after hepatectomy [46]. Thus, the identification and subsequent modulation of mechanism that are involved in liver injury and regeneration might favor the recovery and functioning of the transplanted organ.

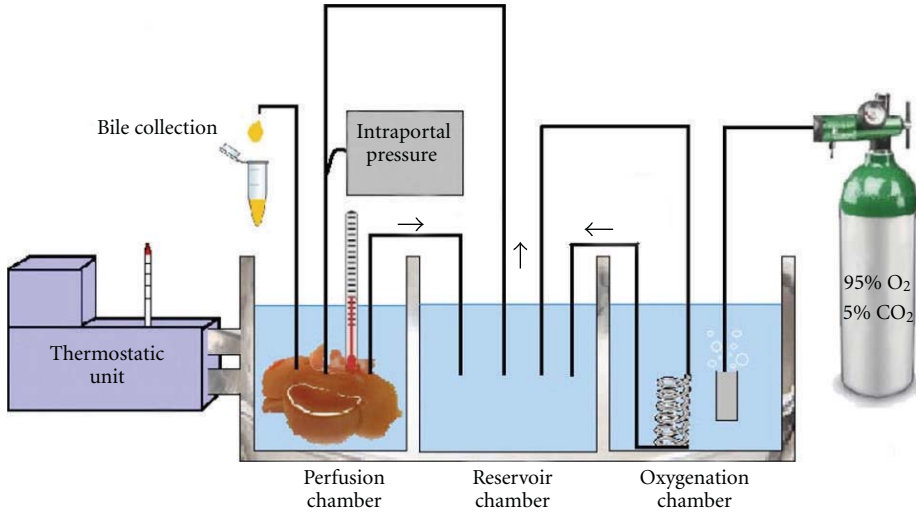

Figure 5: Illustrative representation of machine reperfusion.

To mimic some of the pathophysiological events that occur during such clinical situations, several experimental models of reduced-size LT have been developed. For example, OLT with the implantation of liver grafts that approximated 30%–70% of the normal mass of a rat liver has been performed. Graft size is important for normal liver function and host survival [45]. It has been reported that 100% of recipient rats that were implanted with 40%, 50%, 60%, or 70% of the liver survived regardless of the duration of preservation. This suggests that graft sizes of 40% or greater are sufficient to meet the metabolic demands of the recipients. The transplantation of a graft of 30% of the normal liver mass provides an extreme model of hepatic reduction that presumably stimulated a maximal regenerative response [45].

Three possibilities exist with respect to the timing of the graft reduction: in the donor before perfusion, in the container (*ex situ*), or in the recipient after reperfusion. If the reduction is done *in vivo* prior to the removal of the donor liver, then two concerns exist (1) excessive bleeding might stimulate systemic responses that could alter the liver and (2) the immediate phase of the regeneration response could be initiated in the donor animal. The second choice, *ex situ* reduction, can be done without the risk of damaging the graft by manipulation or affecting anastomosis after reperfusion. Finally, resection of the graft after implantation in the recipient adds surgical stress and the risk of bleeding [47].

5. Optimizing the Graft

5.1. Static Organ Preservation. The introduction of the University of Wisconsin (UW) solution by Belzer and Southard for static cold storage was a breakthrough and remains the conventional method of preservation. Reduction of metabolic activity (by cooling) is the major principle of organ preservation [48, 49]. Using this method, however, organs undergo injury at several consecutive stages: warm ischemia prior to preservation, cold preservation injury, ischemic rewarming during surgical implantation, and reperfusion injury [49]. Only a few studies have demonstrated the optimization of graft function and survival with modification of static preservation. It is doubtful that considerable improvements in organ preservation and especially in the rescue of marginal organs will be possible as long as the strategy is based on static principles [48]. The improvements in UW preservation solution are summarized in Table 1.

5.2. Machine Perfusion. Machine liver perfusion has emerged with promising data over the past decade because it has significant potential in graft preservation and even more potential in graft optimization when the use of marginal organs is the objective.

Compared with simple cold storage (SCS), machine perfusion (Figure 5) confers many anticipated advantages such as the following: (1) provision of continuous circulation and better preservation of the microcirculation, (2) continuous nutrient and oxygen delivery to fulfill the organ's metabolic demands, (3) removal of metabolic waste products and toxins, (4) opportunity to assess organ viability, (5) improved clinical outcomes via improved immediate graft function rates, (6) prolonged preservation time without increased preservation damage, (7) administration of cytoprotective and immunomodulating substances, and (8) lower graft dysfunction incidence, shorter hospital stays, and better graft survival rates [50].

5.3. Normothermic Machine Perfusion. Normothermic machine perfusion (NMP) maintains and mimics normal *in vivo* liver conditions and function during the entire period of preservation, thus avoiding hypothermia and hypoxia and minimizing preservation injury [48, 50].

Schön et al. [51] studied NMP to preserve pig livers for transplantation and to rescue them from warm ischemia in a model of donor after cardiac death (DCD). Short (5 h) or prolonged (20 h) NMP preservation is superior to SCS

Table 1: Pharmacological treatments to protect liver against ischemia/reperfusion. AMP; activated protein kinase, AMPK; heme oxygenase-1, HO-1; interleukin, IL; nitric oxide, NO; peroxisome proliferator-activated receptor-α, PPAR-α; peroxisome proliferator-activated receptor (PPAR) γ, PPAR-γ; reactive oxygen species, ROS; tumour necrosis factor TNF;. xanthine dehydrogenase/xanthine oxidase, XDH/XOD.

Pharmacological therapy Liver transplantation and warm hepatic ischemia				
Drug	Specie	Experimental model	Ischemic time	Effect
Chlorpromazine (Ca2+ channel antagonist)	Rat	Liver transplantation	24 h	↑ ATP, ↓ mitochondrial dysfunction and alterations in lipid metabolism
Tauroursodeoxy-cholate	Rat	Liver transplantation Warm ischemia + hepatectomy	8 h 1 h	↓ Endoplasmic reticulum stress
Cbz-Val-Phe methyl ester (calpain inhibitor)	Rat	Liver transplantation	24, 40 h	↓ Calpain activation and SEC apoptotic
Tocopherol (antioxidant)	Rat	Liver transplantation Warm ischemia	5 h 45, 90 min	↓ Lipid peroxidation, ↓ SEC damage and microcirculatory disturbances
Glutathione (antioxidant)	Rat	Warm ischemia Liver transplantation	60, 90 min 24 h	↓ Microcirculatory disturbances, ↑ detoxification of ROS,
SOD (antioxidant)	Rat	Warm ischemia Liver transplantation	45 min and 1 h 8 h	↓ Microcirculatory disturbances and leukocyte accumulation
Allopurinol (XOD inhibitor)	Rat, Mice	Liver transplantation Warm ischemia	8, 16 h 30, 60 min	↓ Oxidative stress
Bucillamine (antioxidant)	Rat	Liver transplantation	24 h	↓ Oxidative stress
AMPK activators	Rat	Warm ischemia	90 min	↑ NO, and ATP
Adenosine	Rat	Warm ischemia	90 min	↑ NO
N-acetylcysteine (glutathione precursor)	Rat	Liver transplantation	24 h	↓ Microcirculatory disturbances
L-arginine (NO precursor)	Rat	Liver transplantation Warm ischemia	18 h 45 min	↑ ATP, ↑ NO, ↓neutrophil accumulation
Spermine NONOate (NO donor)	Rat	Warm ischemia	60, 90 min	↓ IL-1α and oxidative stress
FK 409 (NO donor)	Rat	Liver transplantation	80 min	↓ SEC damage, ↓ IL-1 ↑ HSP, and IL-10
EHNA (adenosine deaminase inhibitor)	Rat	Liver transplantation	24, 44 h	↑ Interstitial adenosine, ↓ leukocytes rolling and microcirculatory disturbances
CGS-21680 (adenosine A2 receptor agonist)	Rat	Liver transplantation	30 h	↓ SEC killing, ↑ cAMP
Anti-TNF antiserum	Rat	Liver transplantation Warm ischemia	6, 24 h 90 min	↓ TNF and leukocyte accumulation
FR167653 (IL-1β and TNFα suppressor)	Rat	Liver transplantation	48 h	↓ TNF and IL1-α and Kupffer cell activation
IL-10	Rat	Warm ischemia	60 min	↓ IL-1 and oxidative stress
Anti-ICAM-1	Rat	Liver transplantation Warm ischemia	24 h 1 h	↓ Adherence of leukocytes in postsinusoidal venules
PSGL-1 (P-selectin blocker)	Rat	Liver transplantation	6 h	↓ Neutrophil infiltration, ↓ INFγ, TNFα and iNOS
CS1 peptides (FN-α4β1 interaction blocker)	Rat	Liver transplantation	4 h	↓ Neutrophil and lymphocyte T infiltration, ↓ TNFα and iNOS
sCR1 (complement inhibitor)	Rat	Liver transplantation	24 h	↓ Microcirculatory disturbances, ↓ leukocyte adhesion
Sodium ozagrel (thromboxane synthase inhibitor)	Pig	Liver transplantation	8 h	↓ ET-1
Glycine (Kupfer cell modulator)	Rat	Liver transplantation	24 h	↓ TNFα and neutrophil accumulation

Table 1: Continued.

Pharmacological therapy Liver transplantation and warm hepatic ischemia				
Drug	Specie	Experimental model	Ischemic time	Effect
$GdCl_3$ (Kupffer cell blocker)	Rat	Liver transplantation	24 h	↓ TNFα and neutrophil accumulation,
Z-DEVD-FMK (caspase 3 and 7 inhibitor)	Rat	Liver transplantation	16 h	↓ Apoptosis, ↑ microvascular perfusion and Bcl-2
Cobalt-protoporphyrin IX (HO-1 inducer)	Rat	Liver transplantation	6 h	↓ T-cell and macrophages infiltration
ANP (vasodilating peptide)	Rat	Liver transplantation	24 h	↓ Apoptosis, ↑ PI3K/Akt
Hemin (HO-1 inducer)	Rat	Liver transplantation	6 h	↑ Bcl-2
Cerulenin (fatty acid synthase inhibitor)	Mice	Warm ischemia Liver transplantation	15 min 80 min	↓ UCP2, ↑ ATP
Doxorubicin (heat shock proteins inducer)	Rat	Liver transplantation	48 h	↓ TNFα, MIP-2 and NF B
Catalase and derivatives	Mice	Warm ischemia	30 min	↓ Oxidative stress
Rosiglitazone (PPAR-α agonist)	Rat	Warm ischemia	30, 60, 90 min	↑ Autophagy, ↓ cytokines
Apocynin (NAPH oxidase inhibitor)	Mice	Warm ischemia	30 min	↓ Oxidative stress
TBC-1269 (PAN selectin)	Mice	Warm ischemia	90 min	↓ Inflammatory response, ↓ ERK 1/2
Melatonin (hormone)	Rat	Warm ischemia	40 min	↓ IKK and JNK pathways
Ascorbate (ROS scavenger)	Rat	Warm ischemia	30 min	↓ Apoptosis
FK506 (Immunosuppressant)	Rat	Warm ischemia	60, 90 min	↓ TNF
Gabexate mesilate (Protease inhibitor)	Rat	Warm ischemia	60 min	↓ Leukocyte activation, ↓ TNFα
OP-2507 (Analogue of prostacyclin)	Rat	Warm ischemia	60 min	↓ Microcirculatory disturbances
WY-14643 (PPAR-α agonist)	Rat	Warm ischemia	60 min	↓ Inflammatory cytokines, ↓oxidative stress
α-Lipoic acid (Antioxidant)	Rat	Warm ischemia	90 min	↓ Apoptosis, ↑ liver regeneration
Sirolimus (Immunossupressant)	Rat	Warm ischemia + hepatectomy	60 min	↓ Linfocytes
IL-1ra (IL-1 receptor antagonist)	Rat	Warm ischemia + hepatectomy	90 min	↓ TNF and oxidative stress
FK 3311 (Cox-2 Inhibitor)	Dog	Warm ischemia	60 min	↓ Cox-2, ↓ neutrophil infiltration

for normal and ischemically damaged livers, respectively [50]. The NMP circuit dually perfuses 1.5 L of autologous heparinized blood at physiological pressures, which allows hepatic blood flow autoregulation. Prostacyclin, taurocholic acid, and essential amino acids are infused continuously. Apart from logistics, one potential drawback of NMP is the mandatory use of oxygen carriers if blood is not available [50]. Perhaps the only weakness is that SCS prior to NMP revokes its beneficial effect. Therefore, immediately after cardiac asystole, normothermic perfusion in the donor should be installed, as described by Fondevila et al. [52], for the preservation of livers from uncontrolled DCD.

The use of non-heart-beating donors (NHBDs) as a source of liver grafts for transplantation has long been debated. The concept of normothermic recirculation in the context of NHBDs was first developed by García-Valdecasas and Fondevila [53]. With 4 h of NMP, hepatic damage incurred during 90 min of cardiac arrest can be reverted, achieving 100% graft survival after 5 days of postransplant followup. These results offer the hope that NMP will be able to increase the clinical applicability of NHBD LT over that offered by traditional cold storage [53].

5.4. Hypothermic Machine Perfusion. For decades, cooling down organs to cold temperatures allowed successful organ transplantation within a limited period. The first and most prominent difference between SCS and (oxygenated) hypothermic machine perfusion (HMP) is the restoration of the tissue's energy charge and glycogen content while preventing ATP depletion [50]. In 1990, Pienaar et al. [54]

reported that seven of eight dogs survived after LT with HMP preservation for 72 h and a similar outcome after 48 h of SCS.

There is a substantial body of research, predominantly in rodents, demonstrating improved preservation by providing oxygen to livers [55]. Nevertheless, clear guidelines towards target values/ranges for oxygen levels regarding the optimal duration of oxygenation during HMP are lacking. HMP can also be applied at the end of the cold storage period, which is attractive for logistical reasons. The disadvantage here is the time-dependent increase in vascular resistance, bearing the risk of damage to the sinusoidal endothelium [48].

5.5. Subnormothermic Machine Perfusion. Subnormothermic machine perfusion (SNMP) preservation lies between HMP and NMP, but it remained relatively unexplored until recently despite holding promising applications [56]. In an isolated rat liver perfusion model, SNMP enhanced the functional integrity of steatotic livers compared with SCS findings. Organ-protecting properties mediated by decreasing the temperature to a 20–28°C have been observed previously. SNMP avoids some of the downsides of hypothermia while maintaining mitochondrial function, and it may circumvent the logistical restraints of NMP [50].

6. Factors to Be Considered before the Selection of an Experimental Model of Hepatic I/R

Many investigators have used rodent models of warm (*in situ*) liver I/R to mimic some of the pathophysiological events that occur during LT. Although a great deal of useful information has been generated from these studies, an overriding question remains: Are the mechanisms responsible for transplant-mediated liver injury and dysfunction the same as those that have been reported for warm liver I/R injury? The answer is yes and no; that is, some of the mechanisms are similar, but many are dissimilar. It is important to make a distinction between the different types of ischemia, because there already is some controversy regarding the pathophysiological mechanisms depending on the type of ischemia (cold or normothermic), and it should be considered that the type of ischemia, the extent and time of ischemia, the type of liver submitted to I/R, and the presence of liver regeneration, all lead to differences in the pathophysiological mechanisms of hepatic I/R. These are discussed below to provide the reader with a guide to select the appropriate experimental model of hepatic I/R depending on the aims being pursued.

6.1. Relevance of the Duration of Hepatic Ischemia. The severity of hepatocyte damage depends on duration of ischemia. Depending on the objectives of the research, it is important to consider a specific ischemia duration. In other words, if you want to study the mechanisms involved in hepatic I/R injury or the protective mechanisms of a drug, it is more appropriate to use a duration of ischemia associated with high survival. If the purpose is to study the relevance of a drug in hepatic I/R injury, then it is advisable to assess survival, and, therefore, it is more adequate to use experimental models in which the ischemic period is associated with low survival. These observations are based on the following data reported in the literature. It appears that short periods (60 min) of warm ischemia result in reversible cell injury, in which liver oxygen consumption returns to control levels when oxygen is resupplied after ischemia. Reperfusion after more prolonged periods of warm ischemia (120–180 min) results in irreversible cell damage. These observations agree with a previous report on rat liver subjected to I/R, indicating a cellular endpoint for hepatocytes after 90 min of ischemia [57]. In human LT, a long ischemic period is a predicting factor for posttransplantation graft dysfunction, and some transplantation groups hesitate to transplant liver grafts preserved for more than 10 h [58]. Some studies in experimental models of LT indicate that cold ischemia for 24 h induces low survival at 24 h after LT. However, LT, following shorter ischemic periods, may also result in primary organ dysfunction. For animals subjected to 8 h of cold ischemia, an ischemic period associated with high survival, histological examination of the livers at 24 h after LT revealed multifocal and extensive areas of hepatocyte coagulative necrosis with neutrophil infiltration and hemorrhage [10, 59].

The mechanisms of hepatic I/R injury are also different depending on the duration of hepatic ischemia. For instance, to clarify the importance of XDH/XOD versus mitochondria, it should be considered that there are differences in the experimental models evaluated, including the duration of ischemia. Along these lines, XDH/XOD plays a crucial role in hepatic I/R injury only in conditions under which significant conversion of XDH to XOD occurs (80–90% of XOD) such as 16 h of cold ischemia. However, this ROS generation system does not appear to be crucial for shorter ischemic periods such as 6 h of cold ischemia [59]. Thus, even after prolonged periods of ischemia during which a significant conversion of XDH to XOD occurs, these enzymes may only play a minor role compared to mitochondria [60]. Similarly, in assessing the relative contribution of intracellular versus vascular oxidant stress to hepatic I/R injury, it should also be noted that oxidative stress in hepatocytes and the stimulatory state of KCs after I/R depend on the duration of ischemia and may also differ between ischemia at 4°C and that at 37°C, which probably leads to different developmental mechanisms of liver damage [13].

6.2. Relevance of the Extent of Hepatic Ischemia. Another factor to consider before selecting the experimental model of hepatic I/R is the percentage of hepatic ischemia applied. It is known that the extent of hepatic injury as well as the hepatic I/R mechanisms, including the recovery of blood flow and energy charge during hepatic reperfusion, is dependent on the extent of ischemia—whether total or partial (70%) hepatic ischemia is applied [34, 35]. This fact could be explained by the stealing phenomenon. In contrast to 100% hepatic ischemia, during ischemia in the left and median lobes, the flow is shunted via the right lobes and following the release of the occlusion of the left and median lobes, a significant amount of shunting via the right lobes will

continue during reperfusion until vascular resistance in the postischemic lobes decreases. This occurs because blood flows through the path of least resistance. The reasons for this may be cellular swelling endothelial, stasis, or other changes. Thus, the recovery of blood flow and hepatic perfusion of the preischemic lobe is later in the case of 70% hepatic ischemia than in 100% hepatic ischemia [61]. In line with these observations, the benefits of some drugs such as ATP–MgCl2 were dependent on the extent of hepatic ischemia used [30, 62].

6.3. Relevance of the Type of Liver Submitted to I/R. A variety of clinical factors including starvation, graft age, and steatosis have been studied in different experimental models of hepatic I/R because of the relevance of these factors in clinical practice. These factors enhance liver susceptibility to I/R injury, further increasing the patient risks related to reperfusion injury [13].

6.3.1. Starvation. In clinical LT, starvation of the donor, due to prolonged intensive care unit hospitalization or the lack of adequate nutritional support, increases the incidence of hepatocellular injury and primary nonfunction [63]. Fasting exacerbates I/R injury because the low content of glycogen stores results in more rapid ATP depletion during ischemia [64]. In addition, fasting causes alterations in tissue antioxidant defenses, accelerates the conversion of XDH to XOD during hypoxia and induces mitochondrial alterations [63].

Considering these observations, an artificial nutritional support may represent a new approach for the prevention of reperfusion injury in fasted livers [65]. On the contrary, fasting has been reported to improve organ viability and survival [66], as it reduces phagocytosis and the generation of TNF-α [66]. To understand these apparent contradictory results, it is important to consider the different experimental conditions in these investigations. A beneficial effect of high glycogen content can mainly be expected under conditions of long preservation times and long periods of warm ischemia. Under these conditions, high metabolic reserves of the liver may attenuate ischemic cell injury and preserve defense functions against cytotoxic mediators of KCs. Conversely, short ischemic periods require lower metabolic reserves, and the extent of KC activation can be the dominant factor in early graft injury [10].

6.3.2. Age. A number of distinct age-related alterations have been identified in the hepatic inflammatory response to hepatic I/R [10, 67]. Under warm hepatic ischemia, mature adult mice had greatly increased neutrophil function, increased intracellular oxidant levels, and decreased mitochondrial function compared with the findings in young adult mice. These alterations contributed to the increased liver injury after I/R observed in mature adult mice compared with that in young adult mice. The results obtained in an experimental model of isolated perfused liver indicate that, during reperfusion, livers obtained from old rats generate a lower amount of oxyradicals than livers from young rats. This fact could be explained by the lower KC activity, the reduction of liver blood flow, and the impaired functions and structural alterations observed in the livers of old rats [68]. In fact, in hepatocytes from mature adult mice, delayed activation of nuclear factor kappa B (NF B) in response to TNF-α and virtually no production of macrophage inflammatory protein 2 have been detected, which may be due to an age-related defect in hepatocytes [10, 67].

6.3.3. Steatosis. The first step to minimize the adverse effects of I/R in steatotic livers is a full understanding of the mechanisms involved in I/R injury in these marginal organs [10]. This can be achieved only with the selection of an appropriate method to induce steatosis in livers undergoing I/R. It is well known that the mechanisms involved in hepatic I/R injury are different depending on the type of liver (nonsteatotic versus steatotic livers). In addition to the impairment of microcirculation, mitochondrial ROS generation dramatically increases during reperfusion in steatotic livers [69–71]. Results obtained under warm hepatic ischemia indicate that apoptosis is the predominant form of hepatocyte death in the ischemic nonsteatotic liver, whereas the steatotic livers develop massive necrosis after an ischemic insult [72]. Steatotic livers differed from nonsteatotic livers in their response to the unfolded protein response and endoplasmic reticulum stress since inositol-requiring enzyme 1 and PKR-like ER kinase were weaker in the presence of steatosis [73]. Decreased ATP production and dysfunction of regulators of apoptosis, such that Bcl-2, Bcl-xL and Bax have been proposed to explain the failure of apoptosis in steatotic livers. Differences were also observed when we analyzed the role of the renin-angiotensin system, as the nonsteatotic grafts exhibited higher angiotensin (Ang)-II levels than steatotic grafts whereas steatotic grafts exhibited higher Ang-(1–7) levels [74]. Moreover, reduced retinol-binding protein 4 and increased peroxisome proliferator-activated receptor gamma (PPAR)-γ levels were observed in steatotic livers compared to nonsteatotic livers [75]. The vulnerability of steatotic livers subjected to warm ischemia is also associated with increased adiponectin, oxidative stress, and IL-1 levels and a reduced ability to generate IL-10 and PPAR-α [31, 76].

It should be considered that there are differences in the mechanisms involved in hepatic I/R injury depending on the method used to induce steatosis. In contrast with other experimental models of steatosis, both dietary high fat and alcohol exposure induced the production of superoxide dismutase (SOD)/catalase-insensitive ROS, which may be involved in the mechanism of steatotic liver failure after OLT [77]. Neutrophils have been involved in the increased vulnerability of steatotic livers to I/R injury, especially in alcoholic steatotic livers. However, neutrophils do not account for the differentially greater injury in nonalcoholic steatotic livers during the early or late hours of reperfusion. Similarly, the role of TNF in the vulnerability of steatotic livers to I/R injury may be dependent on the type of steatosis [4, 78].

6.4. Relevance of Regeneration in Experimental Models of Hepatic I/R. It is known that different experimental models

trigger different responses when a common mechanism or the same drug is investigated. This situation is witnessed when analyzing liver injury in models of I/R with or without hepatectomy. This situation is illustrated by Ramalho et al. [34] regarding the loss of protection of Ang-II receptor antagonists against liver damage in conditions of partial hepatectomy under I/R compared with the study of I/R without hepatectomy, in which Ang-II receptor antagonists reduced hepatic damage. These different results could not be explained by differences in the dose or frequency of drug administration but rather by differences in surgical conditions (percentage of hepatic ischemia and the presence or absence of hepatectomy). In the model of I/R without hepatectomy [32], the blood supply to the left and median liver lobes (70% hepatic mass) was interrupted, and the other hepatic lobes remained intact. However, in partial hepatectomy under I/R, only blood supply to the remnant liver (30% hepatic mass) was interrupted and the other hepatic lobes were excised [34]. It is well known that the mechanisms of hepatic damage are different depending on the percentage of hepatic mass that is deprived of blood [10, 61, 62]. In addition, the inherent mechanisms of hepatic damage derived from the extensive removal of hepatic mass should be considered [34].

In line with the data above mentioned, ischemic preconditioning (IP) (a surgical strategy that exert benefits in hepatic I/R) reduced XDH/XOD in nonreduced liver grafts during cold ischemia [72] whereas IP did not induce changes in this ROS generating system in reduced-size liver grafts [46]. In contrast to the conditions of I/R without hepatectomy [79], hepatic regeneration was not correlated to the ATP levels of the remaining liver in small-for-size liver grafts [46]. The reduction in TNF release following hepatic I/R induced by IP has been previously reported in cold ischemia conditions without hepatectomy [72]. However, IP did not modify the levels of TNF in reduced-size liver grafts after transplantation [46].

7. Strategies Applied in Experimental Models of Hepatic I/R

7.1. Pharmacological Treatment. Numerous experimental studies have focused on the developing pharmacological strategies aimed at inhibiting the harmful effects of I/R [13, 59, 73, 76, 79–88]. Some of these studies are summarized in Table 1. However, none of these treatments has managed to prevent hepatic I/R injury. The possible side effects of some drugs may frequently limit their use in human LT [13]. For example, idiosyncratic liver injury in humans is documented for chlorpromazine, pernicious systemic effects have been described for NO donors, allopurinol therapy can cause hematological changes and gadolinium can induce coagulation disorders [13]. Some case reports of acute hepatotoxicity attributed to rosiglitazone have been published [89]. High dose of resveratrol aggravated liver injury [90]. The development of therapeutic strategies that utilize the protective effect of heme oxygenase-1 induction is hampered by the fact that most pharmacological inducers of this enzyme perturb organ function by themselves [91].

Pharmacological treatment-derived difficulties must also be considered. In this regard, SOD and glutathione exhibit inadequate delivery to intracellular sites of ROS action [92]. The administration of anti-TNF antibodies does not effectively protect against hepatic I/R injury, and this finding has been related to the failure of complete TNF-α neutralization locally [93]. Although this also occurs in nonsteatotic livers, modulating I/R injury in steatotic livers poses a greater problem. Differences in the action mechanisms between steatotic and nonsteatotic livers mean that therapies that are effective in nonsteatotic livers may prove useless in the presence of steatosis, and the effective drug dose may differ between the two liver types. Findings such as these must be considered when applying pharmacological strategies in the same manner to steatotic and nonsteatotic livers because the effects may be very different. For example, caspase inhibition, a highly protective strategy in nonsteatotic livers, had no effect on hepatocyte injury in steatotic livers [70]. Moreover, whereas in an LT experimental model, an NO donor reduced oxidative stress in nonsteatotic livers, the same dose increased the vulnerability of steatotic grafts to I/R injury [94]. Furthermore, there may be drugs that would only be effective in steatotic livers. This was the case of compounds such as cerulenin, which reduce UCP-2 expression in steatotic livers [95, 96] and carnitine [97].

Further investigations are required to optimize some treatments because long-term therapy (more of 10 days) appears to be necessary to exert the desired effects [98]. However, there are obvious difficulties concerning the feasibility of long-term drug administration in some I/R processes, in particular, LT from cadaveric donors, because this is an emergency procedure in which there is very little time to pretreat the donor with drugs.

7.2. Preservation Solutions

7.2.1. Additives in Preservation Solutions. The inclusion of some components in the UW solution has been both advocated and criticized. For instance, adenosine has been added to the UW solution as a substrate for the generation of adenine nucleotides. However, simplified variants of the UW solution in which adenosine was omitted were demonstrated to have similar or even higher protective potential during cold liver storage. Another limitation of the UW solution is that some of its constituent compounds (allopurinol, lactobionate) do not offer very good protection because they are not present at a suitable concentration and encounter problems in reaching their site of action [13, 99].

A number of ingredients, which have been summarized in Table 2, have been introduced into UW solution in experimental models of hepatic cold ischemia [13, 100–106]. However, none of these modifications to the UW solution composition have found their way into routine clinical practice. For instance, studies aimed at enriching the UW solution with caspase inhibitors revealed that this prevents SEC apoptosis, but such inhibitors have little effect

Table 2: Additives to UW solution to protect liver against ischemia/reperfusion. Nitric oxide, NO; platelet-activating factor, PAF; sinusoidal endothelial cells, SEC.

Additives to UW solution Liver transplantation			
Drug	Specie	Ischemic time	Effect
Ruthenium red (mitochondrial Ca^{2+} uniporter inhibitor)	Rat	24 h	↓ Mitocondrial dysfunction
OP-4183 (PGI2 analogue)	Rat	24 h	↓ Oxidative stress
SAM (ATP precursor)	Rat	24 h	↓ Oxidative stress
Trifluoperazine (calmodulin inhibitor)	Dog	24 h	↓ Microcirculatory dysturbances
Sodium nitroprusside (NO donor)	Rat	24, 48 h	↓ Microcirculatory dysturbances
E5880 (PAF antagonist)	Pig	8 h	↓ Microcirculatory dysturbances
FR167653 (p38 inhibitor)	Rat	30 h	↓ Microcirculatory dysturbances
EGF, IGF-1, NGF-α	Pig	18 h	↑ ATP
LY294002 (PI3K inhibitor)	Rat	3, 7, 9, 24 h	↓ Apoptosis
IDN-1965 (caspase inhibitors)	Rat	24, 30 h	↓ Apoptosis
8br-cAMP and 8br-cGMP (nucleotide analogs)	Rat	24 h	↓ NFα and neutrophil accumulation,
GSNO (NO donor)	Rat	48 h	↓ SEC damage
Pifithrin-alpha (p53 inhibitor)	Rat	24, 48 h	↓ Apoptosis
OP-4183 (PGI2 analogue)	Rat	24 h	↓ Oxidative stress
Tauroursodeoxy-cholate	Rat	2 h	↓ Endoplasmic reticulum stress

on necrosis [14]. Along these lines, the addition of precursors for ATP resynthesis such as S-adenosyl methyltransferase resulted in poor initial ATP recovery during liver reperfusion [107].

7.2.2. Use of Perfluorochemicals in Preservation Solutions. Perfluorochemicals (PFC) are hydrocarbons, in which all or most of the hydrogen atoms have been replaced with fluorine [108]. The most interesting property of PFC is a very high capacity for dissolving respiratory and other nonpolar gases. A negligible O_2-binding constant of PFC allows them to release O_2 more effectively than hemoglobin into the surrounding tissue (acts as an oxygen-supplying agent) [109]. PFC differs from hemoglobin preparations in that it is a totally synthetic compound formed on a liquid hydrocarbon base. In contrast to hemoglobin, oxygen is not chemically bound to the PFC carrier. Unlike hemoglobin, acidosis, alkalosis, and temperature seem to have no or little effect on the oxygen delivery of PFC, allowing this compound to be used effectively during cold storage of organs [110].

Since the 1980s, PFC has been used intravenously as an "artificial blood" [111]. Several small animal studies have reported the beneficial effects of liver perfusion with PFC emulsions. PFC was first used for liver graft preservation in 1980 by Kamada et al. [112] which perfused the livers of rat with a PFC Fluosol (FC-43)-based solution for up to 25 hr, demonstrating good survival rates after transplantation and beneficial effect of PFCs [111, 112]. By using a similar rat model, Tamaki et al. [113] showed that liver perfusion using a combination of hemaccel-isotonic citrate solution with FC-43 could prolong liver preservation for up to 48 hr. In another liver rodent model, perfusion with a PFC emulsion was also found to protect against nonparenchymal cell injury [114]. Nonetheless, these techniques were not translated successfully to the porcine liver with a report of increased intravascular resistance during perfusion [115]. In this report the authors concluded that possible causes related to the high instability of the PFC-based solution, causing complement activation leading to an increased leucocyte adhesion and further macromolecules or that the perfusion technique itself caused injury (a strong vasoconstriction caused by the inflow of cold PDF-UW emulsion) [115, 116]. In recenting study, used oxycyte, a PFC added to UW solution can be beneficial after cardiac death liver graft preservation in a rat model [111]. In such study, after cardiac arrest, livers were flushed and preserved during 8 h in preoxygenated UW solution containing Oxycyte. The authors show that the primary mechanism of action is due to PFC's ability to carry high amounts of O_2 along with rapid dissociation in the tissue. This can help to minimize organ injury after prolonged hypoxia. A possible secondary mechanism of this O_2 action is suppression of hypoxia-induced apoptosis mediated through a mitochondrial pathway. PFC also appears to activate downregulation or reversal of gene activation responsible

Table 3: Gene therapy to protect liver againts ischemia/reperfusion. Heme oxygenase-1, HO-1; interleukin-13, IL-13; small interference RNA, siRNA; superoxide dismutase, SOD; tumour necrosis factor TNF.

Gene therapy Liver transplantation and warm hepatic ischemia				
Drug	Specie	Experimental model	Ischemic time	Effect
Bag-1 (adenoviral transfer)	Rat	Liver transplantation	24 h	↓ TNFα, ↓neutrophil infiltration, ↓ microcirculatory disturbances
Bcl-2 gene (adenoviral transfer)	Rat	Liver transplantation	16 h	↓ Apoptosis
Cu/Zn-SOD gene (adenoviral transfer)	Rat	Liver transplantation	24 h	↓ Oxidative stress
HO-1 gene (adenoviral transfer)	Rat	Liver transplantation	4 h	↓ Macrophage infiltration, ↓ apoptosis
IL-13 (adenoviral transfer)	Rat	Liver transplantation	24 h	↓ Proinflammatory cytokines, ↓ liver neutrophil recruitment
Adiponectin (siRNA)	Rat	Warm ischemia	1 h	↓ Oxidative stress
ASMase (siRNA)	Mice	Warm ischemia + hepatectomy	90 min	↓ Ceramide, ↓ apoptosis
Caspase 3 (siRNA)	Mice	Warm ischemia	90 min	↓ Apoptosis
Caspase 8 (siRNA)	Mice	Warm ischemia	90 min	↓ Apoptosis
SOD gene (adenoviral transfer)	Rat	Warm ischemia	1 h	↓ Oxidative stress
IL-13 (adenoviral transfer)	Rat	Warm ischemia	30 min	↓ Proinflammatory cytokine, ↓ neutrophil recruitment

for apoptosis [111]. Although the benefits of preoxygenated PFC have been reported on liver preservation, their effects on reperfusion injury were not evaluated in that study. In fact, the possibility that preoxygenated PFC exacerbates the reactive oxygen species during reperfusion should not be discarded. In fact, previous studies indicate that the use of gaseous oxygen, applied to the livers during the storage period via the caval vein was only effective in improving hepatic viability upon reperfusion when antioxidants were added to the UW rinse solution [117].

7.3. Gene Therapy. Advances in molecular biology have provided new opportunities to reduce liver I/R injury using gene therapy [13, 14, 31, 80, 118–120] (see Table 3). However, the experimental data indicate that there are a number of problems inherent in gene therapy, such as vector toxicity, difficulties in increasing transfection efficiencies and protein expression at the appropriate time and site, and the problem of obtaining adequate mutants (in the case of NF B) due to the controversy regarding NF B activation [121, 122]. Although nonviral vectors (such as naked DNA and liposomes) are likely to present fewer toxic or immunological problems, they suffer from inefficient gene transfer [122]. In addition, LT is an emergency procedure in most cases, which leaves very little time to pretreat the donor with genetic approaches.

7.4. Surgical Strategies. The response of hepatocyte to ischemia never ceases to surprise. In fact, contrary to what might be expected, the induction of consecutive periods of ischemia in the liver does not induce an additive effect in terms of hepatocyte lesions. IP based on brief periods of ischemia followed by a short interval of reperfusion prior to a prolonged ischemic stress protects the liver against I/R injury by regulating different cell types and multiple mechanisms such as energy metabolism, microcirculatory disturbances, leukocyte adhesion, KC activation, proinflammatory cytokine release, oxidative stress, apoptosis, and necrosis [13, 80] (Table 4). This is an advantage in relation with the use of drugs that exerts its action on a specific mechanism.

The benefits of IP observed in experimental models of hepatic warm and cold ischemia [80, 123] prompted human trials of IP. To date, IP has been successfully applied in human liver resections in both steatotic and nonsteatotic livers. The effectiveness of IP in hepatic surgery was first reported by Clavien et al. in 2003 [124], preliminary clinical studies have reported the benefits of IP in LT [125, 126], and additional randomized clinical studies are necessary to confirm whether this surgical strategy can be commonly used in clinical liver surgery.

8. Conclusion and Perspectives

From the data obtained in experimental models of hepatic I/R, we can state that I/R injury is a multifaceted and intriguing phenomenon that probably cannot be reduced to a single pathway. The increasing use of marginal donors in major liver surgery and the fact that these organs are more susceptible to ischemia highlight the need for further research directed at the mechanisms of I/R injury. However, the mechanisms by which metabolic changes due to age or steatosis affect I/R injury and subsequently influence protective strategies are poorly understood. Whether liver machine perfusion will find its way into widespread clinical application remains uncertain. Machine perfusion has been criticized for its complicated logistics (e.g., portability) and for possibly damaging the organ and vital structures such as

Table 4: Ischemic preconditioning as a surgical strategy to protect livers against ischemia/reperfusion. Interleukin-10, IL-10; interleukin-1β, IL-1β; nitric oxide, NO; endothelin, ET; reactive oxygen species, ROS; peroxisome proliferator-activated receptor-α, PPAR-α; peroxisome proliferator-activated receptor (PPAR) γ, PPAR-γ; xanthine dehydrogenase/xanthine oxidase, XDH/XOD; superoxide dismutase, SOD; reduced glutathione, GSH; tumour necrosis factor TNF; heme oxygenase-1, HO-1; heat-shock protein 72, HSP72; protein kinase C, PKC; AMP-activated protein kinase, AMPK; renin-angiotensin system, RAS.

Surgical strategy-ischemic preconditioning Liver transplantation and warm hepatic ischemia			
Specie	Experimental model	Ischemic time	Effects
Rat	Liver transplantation	16, 24, 30 h	
Rat	Liver transplantation (steatotic liver)	4 h	
Mice	Warm ischemia	75, 120 min	
Mice	Warm ischemia (old mice)	60 min	
Mouse	Warm ischemia (cirrohtic liver)	60, 75 min	
Rat	Warm ischemia	30, 60, 90, 120 min	
Rat	Warm ischemia (old rat)	45 min	
Rat	Warm ischemia (steatotic liver)	45, 60, 75 min	
Rat	Warm ischemia + hepatectomy	30, 45, 60, 90 min	
Pig	Warm ischemia + hepatectomy	120 min	

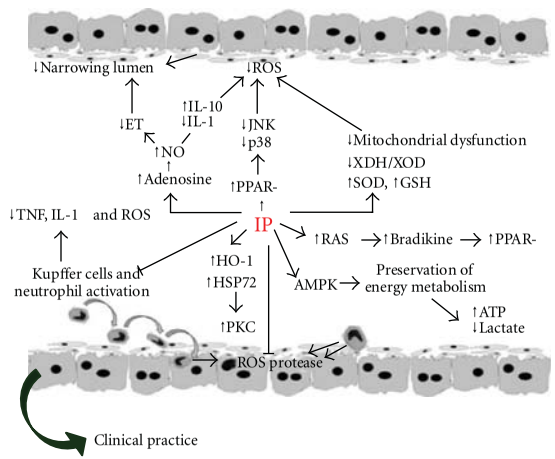

the endothelium. On the contrary, NMP fulfils all ideal organ preservation criteria by avoiding hypoxia and hypothermia. Responses to the strategies aimed at reducing hepatic I/R injury might depend on the surgical procedure and type of liver. Whether the pharmacological approaches presented in this review can be translated into treatments for human disease remains unknown, but further research is required to optimize the treatments. Surgical strategies such as IP affect multiple aspects of IR injury, whereas pharmacological approaches often affect only a few mediators and might have systemic side effects. Only a full appraisal of the mechanisms involved in hepatic I/R using experimental models will permit the design of new protective strategies in clinical liver surgery.

Acknowledgments

The author thank Bioscience Writers for revising the English text. M. Mendes-Braz is in receipt of a fellowship from CAPES Foundation, Ministry of Education of Brazilia, Brasília. MB. Jiménez-Castro is in receipt of a fellowship from SETH Foundation (Sociedad Española de Transplante Hepatico) Spain. This research was supported by the *Ministerio de Ciencia e Innovación* (project Grant BFU2009-07410) Madrid, Spain; the ACC1Ó (project Grant VALTEC08-2-0033) Barcelona, Spain.

References

[1] H. Jaeschke, "Mechanisms of reperfusion injury after warm ischemia of the liver," *Journal of Hepatobiliary & Pancreatic Surgery*, vol. 5, no. 4, pp. 402–408, 1998.

[2] N. C. Teoh and G. C. Farrell, "Hepatic ischemia reperfusion injury: pathogenic mechanisms and basis for hepatoprotection," *Journal of Gastroenterology and Hepatology*, vol. 18, no. 8, pp. 891–902, 2003.

[3] H. Jaeschke, "Molecular mechanisms of hepatic ischemia-reperfusion injury and preconditioning," *American Journal of Physiology, Gastrointestinal and Liver Physiology*, vol. 284, no. 1, pp. G15–G26, 2003.

[4] A. Serafin, J. Rosello-Catafau, N. Prats, C. Xaus, E. Gelpi, and C. Peralta, "Ischemic preconditioning increases the tolerance of fatty liver to hepatic ischemia-reperfusion injury in the rat," *American Journal of Pathology*, vol. 161, no. 2, pp. 587–601, 2002.

[5] P. A. Clavien, P. R. C. Harvey, and S. M. Strasberg, "Preservation and reperfusion injuries in liver allografts: an overview and synthesis of current studies," *Transplantation*, vol. 53, no. 5, pp. 957–978, 1992.

[6] C. Huguet, A. Gavelli, P. A. Chieco et al., "Liver ischemia for hepatic resection: where is the limit?" *Surgery*, vol. 111, no. 3, pp. 251–259, 1992.

[7] R. W. Busuttil and K. Tanaka, "The utility of marginal donors in liver transplantation," *Liver Transplantation*, vol. 9, no. 7, pp. 651–663, 2003.

[8] R. J. Ploeg, A. M. D'Alessandro, S. J. Knechtle et al., "Risk factors for primary dysfunction after liver transplantation—a multivariate analysis," *Transplantation*, vol. 55, no. 4, pp. 807–813, 1993.

[9] K. E. Behrns, G. G. Tsiotos, N. F. DeSouza, M. K. Krishna, J. Ludwig, and D. M. Nagorney, "Hepatic steatosis as a potential risk factor for major hepatic resection," *Journal of Gastrointestinal Surgery*, vol. 2, no. 3, pp. 292–298, 1998.

[10] M. Massip-salcedo, J. Roselló-Catafau, J. Prieto, M. A. Avíla, and C. Peralta, "The response of the hepatocyte to ischemia," *Liver International*, vol. 27, no. 1, pp. 6–16, 2007.

[11] C. Peralta, D. Closa, G. Hotter, E. Gelpí, N. Prats, and J. Roselló-Catafau, "Liver ischemic preconditioning is mediated by the inhibitory action of nitric oxide on endothelin," *Biochemical and Biophysical Research Communications*, vol. 229, no. 1, pp. 264–270, 1996.

[12] A. B. Lentsch, A. Kato, H. Yoshidome, K. M. McMasters, and M. J. Edwards, "Inflammatory mechanisms and therapeutic strategies for warm hepatic ischemia/reperfusion injury," *Hepatology*, vol. 32, no. 2, pp. 169–173, 2000.

[13] A. Casillas-Ramírez, I. B. Mosbah, F. Ramalho, J. Roselló-Catafau, and C. Peralta, "Past and future approaches to ischemia-reperfusion lesion associated with liver transplantation," *Life Sciences*, vol. 79, no. 20, pp. 1881–1894, 2006.

[14] N. Selzner, H. Rudiger, R. Graf, and P. A. Clavien, "Protective strategies against ischemic injury of the liver," *Gastroenterology*, vol. 125, no. 3, pp. 917–936, 2003.

[15] E. E. Abdo, J. E. M. Cunha, P. Deluca, A. M. M. Coelho, T. Bacchella, and M. C. C. Machado, "Protective effect of n2-mercaptopropionylglycine on rats and dogs liver during ischemia/reperfusion process," *Arquivos De Gastroenterologia*, vol. 40, no. 3, pp. 177–180, 2003.

[16] A. M. Yahanda, C. N. Paidas, and M. G. Clemens, "Susceptibility of hepatic microcirculation to reperfusion injury: a comparison of adult and suckling rats," *Journal of Pediatric Surgery*, vol. 25, no. 2, pp. 208–213, 1990.

[17] A. Gasbarrini, G. Addolorato, C. Di Campli et al., "Gender affects reperfusion injury in rat liver," *Digestive Diseases and Sciences*, vol. 46, no. 6, pp. 1305–1312, 2001.

[18] M. Varela-Rey, N. Embade, U. Ariz, S. C. Lu, J. M. Mato, and M. L. Martínez-Chantar, "Non-alcoholic steatohepatitis and animal models: understanding the human disease," *International Journal of Biochemistry and Cell Biology*, vol. 41, no. 5, pp. 969–976, 2009.

[19] M. Vidal, "Traitement chirurgical des ascites," *La Presse Médicale*, vol. 11, pp. 747–749, 1903.

[20] A. Blakemore and J. Lord, "The technic of using vitallium tubes in establishing portacaval shunts for portal hypertension," *Annals of Surgery*, vol. 122, no. 4, pp. 449–475, 1945.

[21] W. E. Burnett, G. P. Rosemond, J. K. Weston, and R. R. Tyson, "Studies of hepatic response to changes in blood supply," *Surgical Forum*, pp. 147–153, 1951.

[22] D. Bernstein and S. Cheiker, "Simple technique for portocaval shunt in the rat," *Journal of Applied Physiology*, vol. 14, no. 3, pp. 467–470, 1959.

[23] H. U. Spiegel, C. Bremer, C. Boin, and M. Langer, "Reduction of hepatic reperfusion injury by indomethacin-mediated vasoconstriction: a rat model with temporary splenocaval shunt," *Journal of Investigative Surgery*, vol. 8, no. 5, pp. 363–369, 1995.

[24] D. Uhlmann, B. Armann, G. Gaebel et al., "Endothelin a receptor blockade reduces hepatic ischemia/reperfusion injury after warm ischemia in a pig model," *Journal of Gastrointestinal Surgery*, vol. 7, no. 3, pp. 331–339, 2003.

[25] S. Bengmark, B. Börjesson, T. Olin, S. Sakuma, and J. Vosmic, "Subcutaneous transposition of the spleen–an experimental study in the rat," *Scandinavian Journal of Gastroenterology, Supplement*, vol. 7, pp. 175–179, 1970.

[26] C. G. Meredith and D. N. Wade, "A model of portal-systemic shunting in the rat," *Clinical and Experimental Pharmacology & Physiology*, vol. 8, pp. 651–652, 1981.

[27] S. Omokawa, Y. Arai, H. Saito et al., "A simple experimental model of total hepatectomy, hepatic ischemia and extrahepatic portal obstruction in rats using splenic transposition," *Japanese Journal of Surgery*, vol. 21, no. 1, pp. 50–56, 1991.

[28] S. Suzuki, S. Nakamura, T. Sakaguchi et al., "Pathophysiological appraisal of a rat model of total hepatic ischemia with an extracorporeal portosystemic shunt," *Journal of Surgical Research*, vol. 80, no. 1, pp. 22–27, 1998.

[29] H. Yamauchi, I. Baca, and U. Mittmann, "Postischemic liver damage in rats: effect of some therapeutic interventions on survival rate," *Tohoku Journal of Experimental Medicine*, vol. 138, no. 1, pp. 63–70, 1982.

[30] P. O. Hasselgren, E. Jennische, J. Fornander, and A. Hellman, "No beneficial effect of atp-mgcl2 on impaired transmembrane potential and protein synthesis in liver ischemia," *Acta Chirurgica Scandinavica*, vol. 148, no. 7, pp. 601–607, 1982.

[31] M. Massip-Salcedo, M. A. Zaouali, S. Padrissa-Altés et al., "Activation of peroxisome proliferator-activated receptor-α inhibits the injurious effects of adiponectin in rat steatotic liver undergoing ischemia-reperfusion," *Hepatology*, vol. 47, no. 2, pp. 461–472, 2008.

[32] A. Casillas-Ramirez, M. Amine-Zaouali, M. Massip-Salcedo et al., "Inhibition of angiotensin ii action protects rat steatotic livers against ischemia-reperfusion injury," *Critical Care Medicine*, vol. 36, no. 4, pp. 1256–1266, 2008.

[33] C. Peralta, R. Bartrons, L. Riera et al., "Hepatic preconditioning preserves energy metabolism during sustained ischemia," *American Journal of Physiology, Gastrointestinal and Liver Physiology*, vol. 279, no. 1, pp. G163–G171, 2000.

[34] F. S. Ramalho, I. Alfany-Fernandez, A. Casillas-Ramirez et al., "Are angiotensin ii receptor antagonists useful strategies in steatotic and nonsteatotic livers in conditions of partial hepatectomy under ischemia-reperfusion?" *Journal of Pharmacology and Experimental Therapeutics*, vol. 329, no. 1, pp. 130–140, 2009.

[35] M. Selzner, C. A. Camargo, and P. A. Clavien, "Ischemia impairs liver regeneration after major tissue loss in rodents: protective effects of interleukin-6," *Hepatology*, vol. 30, no. 2, pp. 469–475, 1999.

[36] H. U. Spiegel and D. Palmes, "Surgical techniques of orthotopic rat liver transplantation," *Journal of Investigative Surgery*, vol. 11, no. 2, pp. 83–96, 1998.

[37] T. Hori, J. H. Nguyen, X. Zhao et al., "Comprehensive and innovative techniques for liver transplantation in rats: a surgical guide," *World Journal of Gastroenterology*, vol. 16, no. 25, pp. 3120–3132, 2010.

[38] M. A. Aller, M. Mendez, M. P. Nava, L. Lopez, J. L. A. Arias, and J. Arias, "The value of microsurgery in liver research," *Liver International*, vol. 29, no. 8, pp. 1132–1140, 2009.

[39] S. Lee, A. C. Charters, J. G. Chandler, and M. J. Orloff, "A technique for orthotopic liver transplantation in the rat," *Transplantation*, vol. 16, no. 6, pp. 664–669, 1973.

[40] S. Lee, A. C. Charters, and M. J. Orloff, "Simplified technic for orthotopic liver transplantation in the rat," *American Journal of Surgery*, vol. 130, no. 1, pp. 38–40, 1975.

[41] N. Kamada and R. Y. Calne, "Orthotopic liver transplantation in the rat. technique using cuff for portal vein anastomosis and biliary drainage," *Transplantation*, vol. 28, no. 1, pp. 47–50, 1979.

[42] J. P. Hölzen, D. Palmes, M. Langer, and H. U. Spiegel, "Microsurgical training curriculum for learning kidney and liver transplantation in the rat," *Microsurgery*, vol. 25, no. 8, pp. 614–623, 2005.

[43] Y. Ma, G. D. Wang, Z. Y. Guo, Z. G. Guo, X. S. He, and G. H. Chen, "Surgical techniques of arterialized orthotopic liver transplantation in rats," *Chinese Medical Journal*, vol. 120, no. 21, pp. 1914–1917, 2007.

[44] G. Oldani, M. Maestri, A. Gaspari et al., "A novel technique for rat liver transplantation using quick linker system: a preliminary result," *Journal of Surgical Research*, vol. 149, no. 2, pp. 303–309, 2008.

[45] H. Urakami, Y. Abe, and M. B. Grisham, "Role of reactive metabolites of oxygen and nitrogen in partial liver transplantation: lessons learned from reduced-size liver ischaemia and reperfusion injury," *Clinical and Experimental Pharmacology and Physiology*, vol. 34, no. 9, pp. 912–919, 2007.

[46] R. Franco-Gou, C. Peralta, M. Massip-Salcedo, C. Xaus, A. Serafín, and J. Roselló-Catafau, "Protection of reduced-size liver for transplantation," *American Journal of Transplantation*, vol. 4, no. 9, pp. 1408–1420, 2004.

[47] T. Omura, N. L. Ascher, and J. C. Emond, "Fifty-percent partial liver transplantation in the rat," *Transplantation*, vol. 62, no. 2, pp. 292–293, 1996.

[48] O. De Rougemont, K. Lehmann, and P. A. Clavien, "Preconditioning, organ preservation, and postconditioning to prevent ischemia-reperfusion injury to the liver," *Liver Transplantation*, vol. 15, no. 10, pp. 1172–1182, 2009.

[49] T. Vogel, J. G. Brockmann, and P. J. Friend, "Ex-vivo normothermic liver perfusion: an update," *Current Opinion in Organ Transplantation*, vol. 15, no. 2, pp. 167–172, 2010.

[50] D. Monbaliu and J. Brassil, "Machine perfusion of the liver: past, present and future," *Current Opinion in Organ Transplantation*, vol. 15, no. 2, pp. 160–166, 2010.

[51] M. R. Schön, O. Kollmar, S. Wolf et al., "Liver transplantation after organ preservation with normothermic extracorporeal perfusion," *Annals of Surgery*, vol. 233, no. 1, pp. 114–123, 2001.

[52] C. Fondevila, A. J. Hessheimer, A. Ruiz et al., "Liver transplant using donors after unexpected cardiac death: novel preservation protocol and acceptance criteria," *American Journal of Transplantation*, vol. 7, no. 7, pp. 1849–1855, 2007.

[53] J. C. García-Valdecasas and C. Fondevila, "In-vivo normothermic recirculation: an update," *Current Opinion in Organ Transplantation*, vol. 15, no. 2, pp. 173–176, 2010.

[54] B. H. Pienaar, S. L. Lindell, T. Van Gulik, J. H. Southard, and F. O. Belzer, "Seventy-two-hour preservation of the canine liver by machine perfusion," *Transplantation*, vol. 49, no. 2, pp. 258–260, 1990.

[55] K. Vekemans, Q. Liu, J. Brassil, M. Komuta, J. Pirenne, and D. Monbaliu, "Influence of flow and addition of oxygen during porcine liver hypothermic machine perfusion," *Transplantation Proceedings*, vol. 39, no. 8, pp. 2647–2651, 2007.

[56] M. Vairetti, A. Ferrigno, F. Carlucci et al., "Subnormothermic machine perfusion protects steatotic livers against preservation injury: a potential for donor pool increase?" *Liver Transplantation*, vol. 15, no. 1, pp. 20–29, 2009.

[57] B. Gonzalez-Flecha, J. C. Cutrin, and A. Boveris, "Time course and mechanism of oxidative stress and tissue damage in rat liver subjected to in vivo ischemia-reperfusion," *Journal of Clinical Investigation*, vol. 91, no. 2, pp. 456–464, 1993.

[58] E. Klar, M. Angelescu, C. Zapletal, T. Kraus, M. Bredt, and C. Herfarth, "Definition of maximum cold ischemia time without reduction of graft quality in clinical liver transplantation," *Transplantation Proceedings*, vol. 30, no. 7, pp. 3683–3685, 1998.

[59] L. Fernandez, N. Heredia, L. Grande et al., "Preconditioning protects liver and lung damage in rat liver transplantation: role of xanthine/xanthine oxidase," *Hepatology*, vol. 36, no. 3, pp. 562–572, 2002.

[60] H. Jaeschke and J. R. Mitchell, "Mitochondria and xanthine oxidase both generate reactive oxygen species in isolated perfused rat liver after hypoxic injury," *Biochemical and Biophysical Research Communications*, vol. 160, no. 1, pp. 140–147, 1989.

[61] H. Hayashi, I. H. Chaudry, M. G. Clemens, and A. E. Baue, "Hepatic ischemia models for determining the effects of atp-mgcl2 treatment," *Journal of Surgical Research*, vol. 40, no. 2, pp. 167–175, 1986.

[62] I. H. Chaudry, M. G. Clemens, M. Ohkawa, S. Schleck, and A. E. Baue, "Restoration of hepatocellular function and blood flow following hepatic ischemia with atp-$MgCl_2$," *Advances in Shock Research*, vol. 8, pp. 177–186, 1982.

[63] M. Stadler, V. Nuyens, L. Seidel, A. Albert, and J. G. Boogaerts, "Effect of nutritional status on oxidative stress in an ex vivo perfused rat liver," *Anesthesiology*, vol. 103, no. 5, pp. 978–986, 2005.

[64] R. Cywes, P. D. Greig, J. R. Sanabria et al., "Effect of intraportal glucose infusion on hepatic glycogen content and degradation, and outcome of liver transplantation," *Annals of Surgery*, vol. 216, no. 3, pp. 235–247, 1992.

[65] M. Domenicali, G. Vendemiale, G. Serviddio et al., "Oxidative injury in rat fatty liver exposed to ischemia-reperfusion is modulated by nutritional status," *Digestive and Liver Disease*, vol. 37, no. 9, pp. 689–697, 2005.

[66] H. N. Sankary, A. Chong, P. Foster et al., "Inactivation of kupffer cells after prolonged donor fasting improves viability of transplanted hepatic allografts," *Hepatology*, vol. 22, no. 4 I, pp. 1236–1242, 1995.

[67] T. Okaya, J. Blanchard, R. Schuster et al., "Age-dependent responses to hepatic ischemia/reperfusion injury," *Shock*, vol. 24, no. 5, pp. 421–427, 2005.

[68] A. Gasbarrini, P. Pasini, B. Nardo et al., "Chemiluminescent real time imaging of post-ischemic oxygen free radicals formation in livers isolated from young and old rats," *Free Radical Biology and Medicine*, vol. 24, no. 2, pp. 211–216, 1998.

[69] S. Ijaz, W. Yang, M. C. Winslet, and A. M. Seifalian, "Impairment of hepatic microcirculation in fatty liver," *Microcirculation*, vol. 10, no. 6, pp. 447–456, 2003.

[70] M. Selzner, H. A. RüDiger, D. Sindram, J. Madden, and P. A. Clavien, "Mechanisms of ischemic injury are different in the steatotic and normal rat liver," *Hepatology*, vol. 32, no. 6, pp. 1280–1288, 2000.

[71] P. Caraceni, M. Domenicali, G. Vendemiale et al., "The reduced tolerance of rat fatty liver to ischemia reperfusion is associated with mitochondrial oxidative injury," *Journal of Surgical Research*, vol. 124, no. 2, pp. 160–168, 2005.

[72] L. Fernández, E. Carrasco-Chaumel, A. Serafín et al., "Is ischemic preconditioning a useful strategy in steatotic liver transplantation?" *American Journal of Transplantation*, vol. 4, no. 6, pp. 888–899, 2004.

[73] I. Ben Mosbah, I. Alfany-Fernández, C. Martel et al., "Endoplasmic reticulum stress inhibition protects steatotic and non-steatotic livers in partial hepatectomy under ischemia-reperfusion," *Cell Death and Disease*, vol. 1, no. 7, article no. e52, 2010.

[74] I. Alfany-Fernandez, A. Casillas-Ramirez, M. Bintanel-Morcillo et al., "Therapeutic targets in liver transplantation: angiotensin ii in nonsteatotic grafts and angiotensin-(1-7) in steatotic grafts," *American Journal of Transplantation*, vol. 9, no. 3, pp. 439–451, 2009.

[75] A. Casillas-Ramírez, I. Alfany-Fernández, M. Massip-Salcedo et al., "Retinol-binding protein 4 and peroxisome proliferator-activated receptor-γ in steatotic liver transplantation," *Journal of Pharmacology and Experimental Therapeutics*, vol. 338, no. 1, pp. 143–153, 2011.

[76] A. Serafin, J. Rosello-Catafau, N. Prats, E. Gelpi, J. Rodes, and C. Peralta, "Ischemic preconditioning affects interleukin release in fatty livers of rats undergoing ischemia/reperfusion," *Hepatology*, vol. 39, no. 3, pp. 688–698, 2004.

[77] W. Gao, H. D. Connor, J. J. Lemasters, R. P. Mason, and R. G. Thurman, "Primary nonfunction of fatty livers produced by alcohol is associated with a new, antioxidant-insensitive free radical species," *Transplantation*, vol. 59, no. 5, pp. 674–679, 1995.

[78] S. Yamada, T. Iida, T. Tabata et al., "Alcoholic fatty liver differentially induces a neutrophil-chemokine and hepatic necrosis after ischemia-reperfusion in rat," *Hepatology*, vol. 32, no. 2, pp. 278–288, 2000.

[79] C. Peralta, R. Bartrons, A. Serafin, C. Blazquez, M. Guzman, N. Prats et al., "Adenosine monophosphate–activated protein kinase mediates the protective effects of ischemic preconditioning on hepatic ischemia-reperfusion injury in the rat," *Hepatology*, vol. 34, no. 2, pp. 278–288, 2000.

[80] R. Bahde and H. U. Spiegel, "Hepatic ischaemia-reperfusion injury from bench to bedside," *British Journal of Surgery*, vol. 97, no. 10, pp. 1461–1475, 2010.

[81] T. Shin, S. Kuboki, N. Huber et al., "Activation of peroxisome proliferator-activated receptor-γ during hepatic ischemia is age-dependent," *Journal of Surgical Research*, vol. 147, no. 2, pp. 200–205, 2008.

[82] T. Akahori, M. Sho, K. Hamada et al., "Importance of peroxisome proliferator-activated receptor-γ in hepatic ischemia/reperfusion injury in mice," *Journal of Hepatology*, vol. 47, no. 6, pp. 784–792, 2007.

[83] D. Sindram, V. Kohli, J. F. Madden, and P. A. Clavien, "Calpain inhibition prevents sinusoidal endothelial, cell apoptosis in the cold ischemic rat liver," *Transplantation*, vol. 68, no. 1, pp. 136–140, 1999.

[84] Y. H. Tian, T. Schäfer, A. Sckell, and M. K. Schilling, "Adenosine deaminase inhibition attenuates reperfusion low flow and improves graft survival after rat liver transplantation," *Transplantation*, vol. 69, no. 11, pp. 2277–2281, 2000.

[85] M. Arai, R. G. Thurman, and J. J. Lemasters, "Contribution of adenosine a2 receptors and cyclic adenosine monophosphate to protective ischemic preconditioning of sinusoidal endothelial cells against storage/reperfusion injury in rat livers," *Hepatology*, vol. 32, no. 2, pp. 297–302, 2000.

[86] F. Amersi, X. D. Shen, C. Moore et al., "Fibronectin-$\alpha 4\beta 1$ integrin-mediated blockade protects genetically fat zucker rat livers from ischemia/reperfusion injury," *American Journal of Pathology*, vol. 162, no. 4, pp. 1229–1239, 2003.

[87] T. G. Lehmann, T. A. Koeppel, M. Kirschfink et al., "Complement inhibition by soluble complement receptor type 1 improves microcirculation after rat liver transplantation," *Transplantation*, vol. 66, no. 6, pp. 717–722, 1998.

[88] I. Yokoyama, T. Kobayashi, M. Negita et al., "Liberation of vasoactive substances and its prevention with thromboxane a2 synthase inhibitor in pig liver transplantation," *Transplant International*, vol. 9, no. 1, pp. 76–81, 1996.

[89] H. Reynaert, A. Geerts, and J. Henrion, "Review article: the treatment of non-alcoholic steatohepatitis with thiazolidinediones," *Alimentary Pharmacology and Therapeutics*, vol. 22, no. 10, pp. 897–905, 2005.

[90] S. Hassan-Khabbar, C. H. Cottart, D. Wendum et al., "Postischemic treatment by trans-resveratrol in rat liver ischemia-reperfusion: a possible strategy in liver surgery," *Liver Transplantation*, vol. 14, no. 4, pp. 451–459, 2008.

[91] R. Schmidt, "Hepatic organ protection: from basic science to clinical practice," *World Journal of Gastroenterology*, vol. 16, no. 48, pp. 6044–6045, 2010.

[92] M. M. R. Polyak, B. O. Arrington, S. Kapur, W. T. Stubenbord, and M. Kinkhaswala, "Glutathione supplementation during cold ischemia does not confer early functional advantage in renal transplantation," *Transplantation*, vol. 70, no. 1, pp. 202–205, 2000.

[93] C. Peralta, L. Fernandez, J. Panes, N. Prats, M. Sans, J. Pique et al., "Preconditioning protects against systemic disorders associated with hepatic ischemia-reperfusion through blockade of tumor necrosis factor-induced P-selectin upregulation in the rat," *Hepatology*, vol. 33, no. 1, pp. 100–113, 2001.

[94] E. Carrasco-Chaumel, J. Roselló-Catafau, R. Bartrons et al., "Adenosine monophosphate-activated protein kinase and nitric oxide in rat steatotic liver transplantation," *Journal of Hepatology*, vol. 43, no. 6, pp. 997–1000, 2005.

[95] K. D. Chavin, R. N. Fiorini, S. Shafizadeh et al., "Fatty acid synthase blockade protects steatotic livers from warm ischemia reperfusion injury and transplantation," *American Journal of Transplantation*, vol. 4, no. 9, pp. 1440–1447, 2004.

[96] K. D. Chavin, S. Yang, H. Z. Lin et al., "Obesity induces expression of uncoupling protein-2 in hepatocytes and promotes liver atp depletion," *Journal of Biological Chemistry*, vol. 274, no. 9, pp. 5692–5700, 1999.

[97] K. Yonezawa, R. H. Tolba, A. Wetter, Y. Yamamoto, Y. Yamaoka, and T. Minor, "L-carnitine could not improve hepatic warm ischemia-reperfusion injury despite ameliorated blood flow," *Journal of Surgical Research*, vol. 125, no. 1, pp. 16–22, 2005.

[98] F. Hong, S. Radaeva, H. N. Pan, Z. Tian, R. Veech, and B. Gao, "Interleukin 6 alleviates hepatic steatosis and ischemia/reperfusion injury in mice with fatty liver disease," *Hepatology*, vol. 40, no. 4, pp. 933–941, 2004.

[99] E. J. Pesonen, N. Linder, K. O. Raivio et al., "Circulating xanthine oxidase and neutrophil activation during human liver transplantation," *Gastroenterology*, vol. 114, no. 5, pp. 1009–1015, 1998.

[100] C. D. Anderson, G. Upadhya, K. D. Conzen et al., "Endoplasmic reticulum stress is a mediator of posttransplant injury in severely steatotic liver allografts," *Liver Transplantation*, vol. 17, no. 2, pp. 189–200, 2011.

[101] T. Maeda, N. Murase, V. Subbotin et al., "Analogs of cyclic nucleotides in rat liver preservation," *Transplantation*, vol. 66, no. 7, pp. 844–851, 1998.

[102] A. B. Quintana, H. L. Lenzi, L. L. Almada et al., "Effect of s-nitrosoglutathione (gsno) added to the university of wisconsin solution (UW): ii) functional response to cold preservation/reperfusion of rat liver," *Annals of Hepatology*, vol. 1, no. 4, pp. 183–191, 2002.

[103] X. L. Li, K. Man, K. T. Ng, C. K. Sun, C. M. Lo, and S. T. Fan, "The influence of phosphatidylinositol 3-kinase/akt pathway on the ischemic injury during rat liver graft preservation," *American Journal of Transplantation*, vol. 5, no. 6, pp. 1264–1275, 2005.

[104] A. M. El-Gibaly, C. Scheuer, M. D. Menger, and B. Vollmar, "Improvement of rat liver graft quality by pifithrin-α-mediated inhibition of hepatocyte necrapoptosis," *Hepatology*, vol. 39, no. 6, pp. 1553–1562, 2004.

[105] S. Natori, M. Selzner, K. L. Valentino et al., "Apoptosis of sinusoidal endothelial cells occurs during liver preservation injury by a caspase-dependent mechanism," *Transplantation*, vol. 68, no. 1, pp. 89–96, 1999.

[106] S. Ambiru, K. Uryuhara, S. Talpe et al., "Improved survival of orthotopic liver allograft in swine by addition of trophic factors to university of wisconsin solution," *Transplantation*, vol. 77, no. 2, pp. 302–319, 2004.

[107] K. Vajdová, R. Graf, and P. A. Clavien, "Atp-supplies in the cold-preserved liver: a long-neglected factor of organ viability," *Hepatology*, vol. 36, no. 6, pp. 1543–1552, 2002.

[108] S. Matsumoto and Y. Kuroda, "Perfluorocarbon for organ preservation before transplantation," *Transplantation*, vol. 74, no. 12, pp. 1804–1809, 2002.

[109] Y. Fujino, "Two-layer cold storage method for pancreas and islet cell transplantation," *World Journal of Gastroenterology*, vol. 16, no. 26, pp. 3235–3238, 2010.

[110] J. Lakey, T. Tsujimura, A. Shapiro, and Y. Kuroda, "Preservation of the human pancreas before islet isolation usging a two-layer (UW solution-perfluorochemical) cold storage method," *Tranplantation*, vol. 74, no. 12, pp. 1809–1811, 2002.

[111] D. Bezinover, S. Ramamoorthy, T. Uemura et al., "Use of a third-generation perfluorocarbon for preservation of rat DCD liver grafts," submitted to *Journal of Surgical Research*.

[112] N. Kamada, R. Y. Calne, D. G. D. Wight, and J. G. Lines, "Orthotopic rat liver transplantation after long-term preservation by continuous perfusion with fluorocarbon emulsion," *Transplantation*, vol. 30, no. 1, pp. 43–48, 1980.

[113] T. Tamaki, N. Kamada, D. G. Wight, and D. E. Pegg, "Successful 48-hour preservation of the rat liver by continuous hypothermic perfusion with haemaccel-isotonic citrate solution," *Transplantation*, vol. 43, no. 4, pp. 468–471, 1987.

[114] H. Shiki, Y. Ku, Y. Kuroda, and Y. Saito, "The effect of oxygen supply in continuos cold perfusion of the rat liver using perfluorochemical emulsion-parenchymal and nonparenchymal cell injuries evaluated with trypan blue perfusion/fixation techniques," *Nihon Geka Gakkai Zasshi*, vol. 94, no. 9, pp. 1033–1042, 1993.

[115] E. Klar, T. Kraus, P. Reuter et al., "Oxygenated perfusion for liver preservation: a perfluorodecalin-uw emulsion is not feasible," *Transplantation Proceedings*, vol. 30, no. 7, pp. 3707–3710, 1998.

[116] S. A. Hosgood and M. L. Nicholson, "The role of perfluorocarbon in organ preservation," *Transplantation*, vol. 89, no. 10, pp. 1169–1175, 2010.

[117] T. Minor and M. Kötting, "Gaseous oxygen for hypothermic preservation of predamaged liver grafts: fuel to cellular homeostasis or radical tissue alteration?" *Cryobiology*, vol. 40, no. 2, pp. 182–186, 2000.

[118] C. Fan, R. M. Zwacka, and J. F. Engelhardt, "Therapeutic approaches for ischemia/reperfusion injury in the liver,"

Journal of Molecular Medicine, vol. 77, no. 8, pp. 577–592, 1999.

[119] L. Llacuna, M. Marí, C. Garcia-Ruiz, J. C. Fernandez-Checa, and A. Morales, "Critical role of acidic sphingomyelinase in murine hepatic ischemia-reperfusion injury," *Hepatology*, vol. 44, no. 3, pp. 561–572, 2006.

[120] J. L. Contreras, M. Vilatoba, C. Eckstein, G. Bilbao, J. Anthony Thompson, and D. E. Eckhoff, "Caspase-8 and caspase-3 small interfering rna decreases ischemia/reperfusion injury to the liver in mice," *Surgery*, vol. 136, no. 2, pp. 390–400, 2004.

[121] M. L. Chaisson, J. T. Brooling, W. Ladiges, S. Tsai, and N. Fausto, "Hepatocyte-specific inhibition of nf- b leads to apoptosis after tnf treatment, but not after partial hepatectomy," *Journal of Clinical Investigation*, vol. 110, no. 2, pp. 193–202, 2002.

[122] N. Somia and I. M. Verma, "Gene therapy: trials and tribulations," *Nature Reviews Genetics*, vol. 1, no. 2, pp. 91–99, 2000.

[123] K. K. Desai, G. S. Dikdan, A. Shareef, and B. Koneru, "Ischemic preconditioning of the liver: a few perspectives from the bench to bedside translation," *Liver Transplantation*, vol. 14, no. 11, pp. 1569–1577, 2008.

[124] P. A. Clavien, M. Selzner, H. A. Rudiger, R. Graft, Z. Kadry, V. Rousson et al., "A prospective randomized study in 100 consecutive patients undergoing major liver resection with versus without ischemic preconditioning," *Annals of Surgery*, vol. 238, no. 6, pp. 843–850, 2003.

[125] D. Azoulay, M. Del Gaudio, P. Andreani et al., "Effects of 10 minutes of ischemic preconditioning of the cadaveric liver on the graft's preservation and function: the ying and the yang," *Annals of Surgery*, vol. 242, no. 1, pp. 133–139, 2005.

[126] W. Jassem, S. V. Fuggle, L. Cerundolo, N. D. Heaton, and M. Rela, "Ischemic preconditioning of cadaver donor livers protects allografts following transplantation," *Transplantation*, vol. 81, no. 2, pp. 169–174, 2006.

Hindawi Publishing Corporation
Journal of Biomedicine and Biotechnology
Volume 2012, Article ID 896162, 5 pages
doi:10.1155/2012/896162

Research Article

Effect of Colic Vein Ligature in Rats with Loperamide-Induced Constipation

Flavia Neri,[1,2] Giuseppe Cavallari,[1,2] Matvey Tsivian,[1,2] Elisa Bianchi,[1,2] Rita Aldini,[2] Monica Cevenini,[2] Elena Guidetti,[2] Gian Luca Piras,[2] Milena Pariali,[2] and Bruno Nardo[1,2]

[1] *Department of General Surgery and Transplantation, S. Orsola-Malpighi Hospital, University of Bologna, 40126 Bologna, Italy*
[2] *Center for Applied Biomedical Research (CRBA), S. Orsola-Malpighi Hospital, University of Bologna, 40126 Bologna, Italy*

Correspondence should be addressed to Giuseppe Cavallari, giuseppe.cavallari3@unibo.it

Received 29 November 2011; Revised 6 February 2012; Accepted 20 February 2012

Academic Editor: Monica Fedele

Introduction. Medical treatment in chronic constipation is not always successful. Surgery is indicated in unresponsive selected severe cases. This study presents the distal venous colic ligation in rat as a novel surgical approach. *Materials and Methods*. 16 rats (study group) were evaluated in 3 phases of 6 days each: A (normal conditions), B (loperamide-induced constipation), and C (colic vein legation) and compared with rats treated in phase C with PEG 4,000 (control group). Blood biochemical and physiological parameters, daily fecal water content (FWC), and histological analysis were performed in all study phases. *Results*. No biochemical and physiological parameters changes were observed. FWC decreased in phase B and increased in phase C in both groups with a grow up to 2.3-fold in study group compared to control ($P < 0.0001$). Moreover, in study group, a high number of colonic goblet cells were detected (phase C versus phase B: $P < 0.001$) while no differences were registered in control. *Conclusion*. By ligature of the colic vein in constipated rats, an increase in FWC and goblet cells higher than in PEG treated rats was detected. The described surgical procedure appeared effective, simple, and safe; further studies in animal models, however, are necessary to assess its clinical applicability.

1. Introduction

A consensus definition of constipation was reached in the ROME conference held in 1992 with a further revision in 2001 [1]. Two or more of the following symptoms, present in the previous 3 months, were considered diagnostic for constipation: symptom onset at least 6 months before diagnosis; straining during at least 25% of defecations; lumpy or hard stools in at least 25% of defecations; sensation of incomplete evacuation for at least 25% of defecations; sensation of anorectal obstruction/blockage for at least 25% of defecations; manual maneuvers to facilitate at least 25% of defecations; fewer than 3 defecations/week [1].

For its high prevalence constipation represents also an extensive economical burden in terms of general and specialistical medical care due to diagnostic procedures, hospitalization, and therapy [2, 3]. The pathogenesis of chronic constipation is often unclear; in only about 10% of cases some metabolic or structural etiological conditions are identified [4]. Generally, each patient's complaint is different, making it difficult to understand the problem and find appropriate therapeutic measures. Lifestyle changes are not often successful, and different types of laxatives are usually necessary. Pharmacological treatment is the first therapeutical choice for constipation and surgery is only reserved as the last option when conservative treatments have failed, and therefore it should be limited to refractory constipation, in most cases due to mixed conditions [1]. Colon resection, in particular, seems to have beneficial effects in some cases of inertia coli [5]. Although the great effort in identifying the best treatment options for patients affected by chronic constipation, the results are often still partial and unsatisfactory [1–6].

In the attempt to address this issue we took inspiration from our direct clinical experience [7]. In that occasion we treated a 25-year-old women with acute liver failure for intoxication from tetracycline, through the arterialization of the portal vein. In particular, with the aim to increase the

oxygenation of the blood coming to the liver through the portal system, a branch of the inferior mesenteric artery was connected to the inferior mesenteric vein. At long-term follow-up, the patient referred a reversal of the chronic constipation that she had always experienced before. We hypothesized that the physiopathological mechanism for the resolution of constipation was that the ligation of the inferior mesenteric vein, performed to allow the anastomosis between the arterial and the venous splanchnic system, by impairing the colic vein drainage, must decrease the reabsorption of the luminal solute and water, increasing the colonic water content.

Loperamide is a synthetic opioid agonist, able to induce a constipation in animal model by extension of the evacuation time [8], inhibition of colonic peristalsis [9], and reduction of colonic mucus [10]. In order to better characterize the correlation between colic vein congestion and improved fecal transit, the aim of this study was to evaluate the effect of the colic vein ligature in rat with loperamide-induced constipation.

2. Materials and Methods

2.1. Animals and Constipation Induction. In our study we used 25 male Sprague-Dawley rats (Charles River Laboratories, Calco, Italy) weighing about 400 g/b.w.: 16 rats were enrolled in study group and 9 in control group. All animal procedures were approved by the local committee for care and use of laboratory animals of the University of Bologna and performed according to Italian governmental and international guidelines on animal experimentation. Constipation in rats was induced by injection of loperamide (Sigma-Aldrich) at the dose of 0.15 mg/100 g twice a day subcutaneously.

2.2. Study Design. The animals were subjected to a three study phases. The first phase (A; from day 1 to 6) was the control period, useful to collect the basal physical parameters of each animal. The second phase (B; from day 6 to 12) was the period of loperamide-induced constipation. In the third phase (C; from day 12 to 18) loperamide was continued and animals of study group underwent colic vein ligation (Figure 1), while animals of control group were administered PEG 4,000 (Sigma-Aldrich) (250 mg/kg/day). The equivalent dose for the drug to be administered to rat could not be calculated by the usual formula corrected for the ratio of human serum albumin Kg/rat serum albumin Kg [11], due to the very poor intestinal absorption of PEG 4,000 (from 0.05 and 2.5%). Since this formula cannot apply to drugs with little or no intestinal absorption, we chose a dose which was 50% of the minimal dose inducing toxic effects, such as severe diarrhoea and tremor, obtained by the previous evaluation of the clinical effect of the drug in a dose-response curve from 100 mg/kg/day to 1000 mg/kg/day in a cohort of healthy rats (data non reported). To perform a histological comparative analysis of the colic mucosa in the different study phases, 4 of the 16 animals used were sacrificed at the end of phase A, 4 at the end of phase B, and 8 at the end of phase C. Three animals of the control group were similarly sacrificed at the end of each phase. Biochemical, physiological, and histological parameters of the animals were evaluated through the three sequential phases, for a total of 18 days.

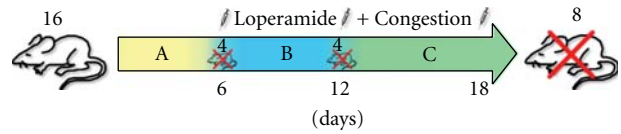

Figure 1: Study group design.

2.3. Biochemical and Physiological Parameters. We assessed serum osmolarity and concentration of proteins, sodium, and chloride. The analysis was performed at the end of the three study phases (A, B, and C).

The physiological parameters daily evaluated in our study were body weight, food and water intake, urine volume, weight of wet, and dry fecal pellets. These parameters were collected every morning at the same time in order to minimize the physiological variables. The procedure of feces drying was performed with UNIVAPOR vacuum concentrator. The fecal samples were let to dry for 24 hours at room temperature obtaining a complete removal of water and other volatile substances. The water content of the fecal pellet was calculated as the difference between the wet and dry weights of the pellet.

2.4. Histology. The colic mucosa of all the animals was examined using periodic acid-Shiff (PAS) staining to detect the presence of the intracellular mucus, identifying the number of goblet cells. For this experiment a standard PAS staining protocol was adopted; after deparaffinization and hydratation to water, the slides were oxidized in 0.5% periodic acid solution for 5 minutes, then rinsed in distilled water and placed in Schiff reagent for 15 minutes. Afterwards the slides were washed under tap water for 5 minutes and then counterstained in Mayer's hematoxylin for 1 minute before the dehydration and the placement of the mounting medium and coverslip. The slides were then analyzed under an optical microscope, and the number of PAS positive cells in the crypts of colic epithelium among the different groups was counted: three fields per slide at a magnification of 20X, three slides per animal.

2.5. Surgical Procedure. The animals were anesthetized through intraperitoneal injection of xylazine-tiletamine-zolazepam (Zoletil, Virbac) at the dose of 0.1 mL/100 g. A median xipho-pubic incision was performed in order to expose the abdominal organs and the intestinal vessels. The colic vein was identified at the inferior edge of the pancreas and ligated and cut under microscope visualization (Figure 2). After the procedure an immediate colic venous congestion was observed below the ligation. The abdominal wall was then closed in two layers.

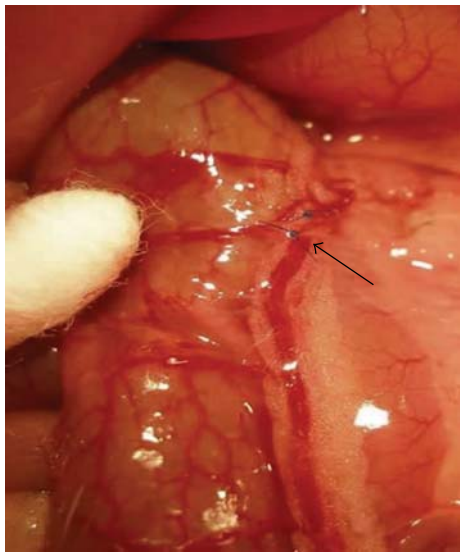

Figure 2: Ligation and cut of the colic vein.

3. Results

3.1. Biochemical and Physiological Parameters

Study Group. No significant differences of the biochemical parameters evaluated were detected at the end of each of the three phases of the study. Concerning physiological parameters, the body weight was substantially unchanged during the three phases of the study: 424 ± 12, 432 ± 10, 403 ± 7 g/b.w. respectively for phases A, B, and C. Food and water intake remained constant in each phase; the mean daily food intake value was 20.2, 23, and 19.6 g, respectively, in phase A, B, and C. The volume of urine produced was unchanged during phase A and B with a mean of 13 mL ±1 and increased slightly to 15 mL ±1 during phase C. The weight of total daily fecal production also remained constant around 7.5 g/day.

Concerning fecal water content, the mean water content in the feces decreased from 49.4 ± 0.7% (phase A) to 47.1 ± 0.8% after induction of constipation with loperamide (phase B). After the surgical procedure the water content of the feces increased to 51.4 ± 1%, that was significantly higher compared to the constipated rats (phase C versus phase B; $P < 0.0001$). A similar trend was observed concerning the water content of the single fecal pellet, that was reduced from 59.7 ± 0.8% (phase A) to 55.0 ± 0.7% (phase B) and increased after the colic vein ligation to 62.6 ± 0.9% (phase C versus phase B: $P < 0.0001$).

Control Group. No significant differences were found at the end of each period in the biochemical parameters. As for the physiological parameters, the body weight was not significantly changed (420 ± 15, 438 ± 28, 407 ± 20 g/b.w., resp., during phase A, B, and C). Daily food intake was not different in the three phases; the daily water intake was increased in phase C with respect to both phases A and B, but not significantly. The urine volume produced was also similar in the three phases. The daily fecal weight was increased, but not significantly in phase C: 7.5 ± 0.5, 7.1 ± 0.4 and 8.0 ± 0.2 g/day, respectively, for phase A, B, and C. The fecal content of water was reduced from phase A (49.7 ± 0.6%) to phase B (46.7 ± 0.5%). After the laxative assumption, the water content of feces increased to 48.5 ± 0.9%; (phase C versus phase B; $P < 0.0001$). Similarly, the water content of the single fecal pellet was, respectively, 59.2 ± 0.8, 54.3 ± 0.8 and 58.0 ± 0.7% in the three phases (phase C versus phase B; $P < 0.0001$). No case of diarrhoea was registered both in study and control group.

3.2. Histology. We did not detect any signs of inflammation or alteration of the colic mucosa in the animals sacrificed at the different study time points, neither in the colic vein ligation group nor in the control group. However a mild mucosal edema was noticed in the animals sacrificed after ligation of the colic vein (Figure 3). The average number of PAS-positive cells detected in the crypts of colic epithelium of study group rats, was respectively, 177 ± 2 in phase A, 144 ± 2 in phase B and 211 ± 2 cells/hpf in phase C (phase C versus phase B: $P < 0.001$).

In the control group, no difference was found in the histological parameters, and the average number of PAS positive cell was not significantly different in the three study phases.

4. Discussion

Chronic constipation is an important worldwide issue which affects almost 25% of the western population [2]. The general goal of all medical treatments for constipation is to increase fecal water content by retention of intraluminal water, increase of intestinal secretion, or shortening of intestinal transit. However in some cases these treatments are ineffective [1]. Once every medical therapeutical option has failed, surgery can be proposed as a last remedy to a selected and limited category of patients [5]. Slow transit constipation, which is unresponsive to high doses of laxatives, is considered the consequence of chronic intestinal pseudoobstruction, a rare and severe neuropathic disorder presenting with impaired gastrointestinal propulsion and bowel obstruction, without any lesion occluding the gut lumen. Patients suffering from this disease can view the surgical approach as the last option to their condition; as any surgical treatment, complication rate could be high [5]. Research for new therapeutical strategies addressing this issue is therefore strongly encouraged.

The present investigation was prompted by the observation of bowel function normalization, following arterialization of the portal vein in a patient with acute liver failure, who had previously complained of severe constipation. The report of cases of portal hypertension due to a splenic arteriovenous fistula with symptoms of diarrhea [12, 13] confirmed us in the concept that intestinal congestion can decrease water absorption in the colon and increase the watery content of stools, thus improving the symptoms.

In this setting we focused on evaluating the effect of the surgically induced colic vein congestion on chronic

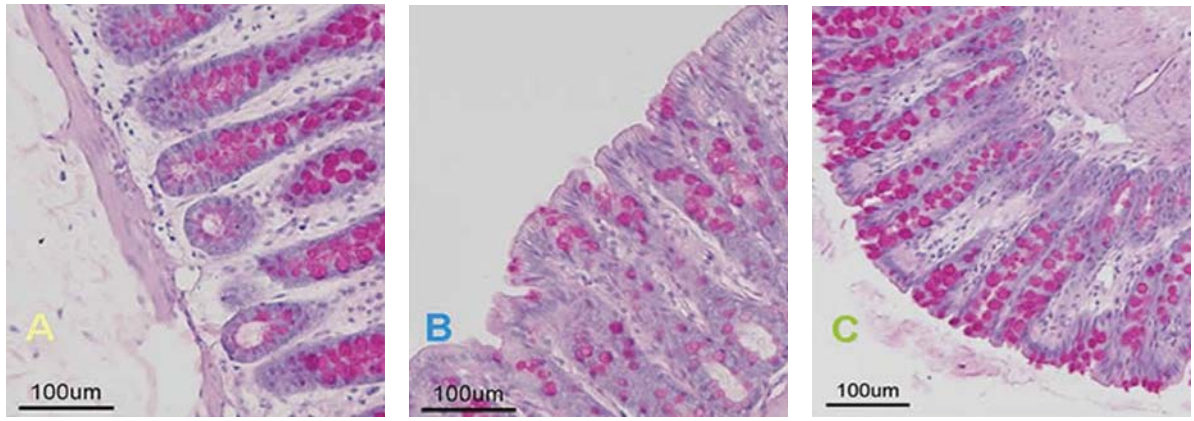

(a) (b) (c)

Figure 3: Histological images of the colic mucosa of study group animals sacrificed in the three different phases.

constipation. We employed a model of pharmacological constipation induced by loperamide (Sigma-Aldrich) [10] which can resemble the chronic functional constipation, presenting less daily fecal excretion, lower water content, and thinner mucus of fecal pellets [14]. The gastrointestinal functionality of the rats was observed in terms of quantity and water content of fecal pellets at basal condition, after loperamide injection and after surgical procedure. We did not observe a difference in the amount of feces in the three phases of the study. However, we did notice a trend of increase in water content of fecal pellets in animals treated with colic vein ligation compared to the basal and constipation phases. The results were higher than in the PEG 4,000 treatment control group, thus showing that colic vein ligation has more potent laxative effect in loperamide-induced constipation than PEG 4,000. The osmotic force for colonic fluid excretion of PEG 4,000 has already been documented [15], and the results obtained by the two different methods provide a sort of clinical validation of the present surgical model, demonstrating the "laxative like" effect of the colic vein ligation. The control group, however, did not represent a refractory constipation model, and the colic vein ligation should be preferred over the noninvasive pharmacological treatment limited to cases of medical treatment failure. Loperamide has shown to reduce the amount of mucus secreted by colic mucosa [10]; in the present investigation, we have demonstrated that the colic vein ligation can increase the amount of mucus in the colic mucosa and reverse the loperamide effect. We observed a statistically significant increase in PAS positive cells, containing mucus, in the groups of animals after colic vein ligation compared to the basal and constipated groups, suggesting that this surgical technique produces a laxative effect and alleviates the symptoms of loperamide-induced constipation. Since loperamide inhibits intestinal water secretion, as seen in human jejunum [16], it is possible that this mechanism should be compensated by the inhibition of water reabsorption in the colon, induced by the colic vein ligature with a resultant net fluid increase in the lumen.

The described procedure in rats with pharmacologically induced constipation showed to be easy and reproducible without negative apparent side effects or histologically detectable damages. These positive results prompt the development of additional experimental studies to better characterize the physiopathological mechanism beneath the observed improvement of constipation and to confirm the efficacy and safety of this surgical model in the long term and in large size animals, as swines. This step, which is crucial for the clinical translation of this research, would allow a better understanding of the effect of this procedure on a gastrointestinal system more similar to the human one. Once assessed and verified the efficacy of this therapy on other preclinical animal models, a laparoscopic approach could be applied as well, allowing to perform the procedure through minimally invasive surgery.

5. Conclusions

The present paper reports a tentative of surgical approach to constipation by colic vein ligation. The described procedure in rats with pharmacologically induced constipation showed to be effective, easy, and reproducible without negative apparent side effects or histologically detectable damages. These positive results prompt the development of additional experimental studies to better characterize the physiopathological mechanism beneath the observed improvement of constipation and to confirm the efficacy and safety of this surgical model in the long term and in large size animals. If these studies will confirm and fortify our preliminary results, the surgical procedure described could be considered as a valid option for selected categories of patients suffering from chronic constipation refractory to medical therapy. To this end, it is critically important that translational medical research bridges the gap between findings in basic science and data in the clinical setting.

References

[1] P. Deepak and E. D. Ehrenpreis, "Constipation," *Dis Mon*, vol. 57, pp. 511–517, 2011.

[2] P. D. R. Higgins and J. F. Johanson, "Epidemiology of constipation in North America: a systematic review," *American Journal of Gastroenterology*, vol. 99, no. 4, pp. 750–759, 2004.

[3] K. A. Nyrop, O. S. Palsson, R. L. Levy et al., "Costs of health care for irritable bowel syndrome, chronic constipation, functional diarrhoea and functional abdominal pain," *Alimentary Pharmacology and Therapeutics*, vol. 26, no. 2, pp. 237–248, 2007.

[4] G. F. Longstreth, W. G. Thompson, W. D. Chey, L. A. Houghton, F. Mearin, and R. C. Spiller, "Functional bowel disorders," *Gastroenterology*, vol. 130, no. 5, pp. 1480–1491, 2006.

[5] K. C. W. Hsiao, S. W. Jao, C. C. Wu, T. Y. Lee, H. J. Lai, and J. C. Kang, "Hand-assisted laparoscopic total colectomy for slow transit constipation," *International Journal of Colorectal Disease*, vol. 23, no. 4, pp. 419–424, 2008.

[6] American College of Gastroenterology Chronic Constipation Task Force, "An evidence-based approach to the management of chronic constipation in North America," *The American Journal of Gastroenterology*, vol. 100, supplement 1, pp. S1–S4, 2005.

[7] B. Nardo, R. Montalti, L. Puviani et al., "Portal vein arterialization in a patient with acute liver failure [1]," *Transplantation*, vol. 79, no. 7, pp. 851–852, 2005.

[8] K. Yamada and Y. Onoda, "Comparison of the effects of T-1815, yohimbine and naloxone on mouse colonic propulsion," *Journal of Smooth Muscle Research*, vol. 29, no. 2, pp. 47–53, 1993.

[9] Y. Sohji, K. Kawashima, and M. Shimizu, "Pharmacological studies of loperamide, an anti-diarrheal agent. II. Effects on peristalsis of the small intestine and colon in guinea pigs," *Folia Pharmacologica Japonica*, vol. 74, no. 1, pp. 155–163, 1978.

[10] A. Shimotoyodome, S. Meguro, T. Hase et al., "Decreased colonic mucus in rats with loperamid einduced constipation," *Comparative Biochemistry and Physiology A*, vol. 126, no. 2, pp. 203–212, 2000.

[11] S. Reagan-Shaw, M. Nihal, and N. Ahmad, "Dose translation from animal to human studies revisited," *The FASEB Journal*, vol. 22, no. 3, pp. 659–661, 2008.

[12] M. Orrego, H. E. Vargas, V. Balan et al., "Portal hypertension due to a splenic arteriovenous fistula: a case report," *Digestive Diseases and Sciences*, vol. 51, no. 6, pp. 1113–1116, 2006.

[13] J. H. Schmidt, R. J. Howard, M. A. Herrera, and I. F. Hawkins, "Splenic arteriovenous fistula with portal hypertension, ascites, and diarrhea," *Southern Medical Journal*, vol. 81, no. 5, pp. 670–672, 1988.

[14] Z. H. Yang, H. J. Yu, A. Pan et al., "Cellular mechanisms underlying the laxative effect of flavonol Naringenin on rat constipation model," *PLoS One*, vol. 3, no. 10, Article ID e3348, 2008.

[15] R. de Giorgio, R. Cestari, R. Corinaldesi et al., "Use of macrogol 4000 in chronic constipation," *European Review for Medical and Pharmacological Sciences*, vol. 15, no. 8, pp. 960–966, 2011.

[16] S. Hughes, N. B. Higgs, and L. A. Turnberg, "Loperamide has antisecretory activity in the human jejunum in vivo," *Gut*, vol. 25, no. 9, pp. 931–935, 1984.

Hindawi Publishing Corporation
Journal of Biomedicine and Biotechnology
Volume 2012, Article ID 961461, 7 pages
doi:10.1155/2012/961461

Research Article

What Sequences on High-Field MR Best Depict Temporal Resolution of Experimental ICH and Edema Formation in Mice?

Mingchang Li,[1,2] Reza M. Akhavan-Sharif,[3] Robert M. Friedlander,[1,4] Rose Du,[1] and Ruth Thiex[1,5]

[1] *Department of Neurosurgery, Brigham and Women's Hospital, Harvard Medical School, Boston, MA 02115, USA*
[2] *Department of Neurosurgery, The Second Affiliated Hospital of Guangzhou Medical University, Guangzhou 510260, China*
[3] *Department of Radiology, Beth Israel Deaconess Medical Center, Boston, MA 02115, USA*
[4] *Department of Neurological Surgery, University of Pittsburgh Medical Center, Pittsburgh, PA 15213, USA*
[5] *Division of Endovascular Neurosurgery and Interventional Neuroradiology, Departments of Radiology and Neurosurgery, Brigham and Women's Hospital, Harvard Medical School, Boston, MA 02115, USA*

Correspondence should be addressed to Ruth Thiex, ruth.thiex@post.rwth-aachen.de

Received 3 January 2012; Accepted 27 February 2012

Academic Editor: Oreste Gualillo

Background and Purpose. Pilot study to examine the use of T1-, T2-, and T2*-weighted images for evaluating hematoma size and extent of edema in mouse brain at high field. *Methods*. Following collagenase-induced intracerebral hemorrhage, nine mice were imaged at 4.7 T using T1-, T2-, and T2*-weighted images for hematoma and edema quantitation on days 1, 3, 10, and 21 after surgery. Values were compared with morphometric analysis of cryosections at the time of final MR imaging. *Results*. For hematoma quantitation, the Spearman correlation coefficient (r) between T1 signal change and histology was 0.70 ($P < 0.04$) compared with $r = 0.61$ ($P < 0.09$) for T2*. The extent of perihematomal edema formation on cryosections was well reflected on T2 with $r = 0.73$ ($P < 0.03$). *Conclusions*. Within the limits of our pilot study, MR imaging on 4.7 T appears to approximate the temporal changes in hematoma and edema sizes in murine ICH well, thus laying the groundwork for longitudinal studies on hematoma resorption and edema formation.

1. Introduction

In humans, intracerebral hemorrhage (ICH) causes secondary damage in the brain through the induction of cerebral edema and perihematomal injury [1, 2]. Perihematomal edema with mass effect is an almost universal complication of ICH, elaborated over several days after the initial insult. Glutamate release, bioenergetic failure, inflammation, and apoptosis play a key role in the pathogenesis of secondary injury [3, 4]. In animal models of ICH, molecular and cellular studies also indicate that hemorrhage induces inflammation, apoptotic cell death, and progressive tissue destruction in perihematomal tissue [5–7].

Various knockout mice have been bred to study the gene expression of the pro-oxidants heme [8] and ferrous iron [9], proteolytic enzymes such as metalloproteinases [10], thrombin [10], and inducible nitric oxide synthase [11], as well as leucocyte adhesion molecules (CD18) [12] in the perihematomal area. Their genetic variability has turned the mouse into a key study animal for intracerebral hemorrhage despite the small size of its brain. The hematoma is either induced by stereotactic injection of collagenase or autologous blood into the basal ganglia. Longitudinal studies of hematoma kinetics in mice are sparse and generally use one modality only [13]. The purpose of our pilot study was (i) to develop T1-and T2-weighted MRI protocols for high-resolution studies of mouse brain in vivo which allow for the identification of hematoma and edema, and (ii) to perform a direct comparison of hematoma and edema volumes on MRI with morphometric studies on cryosections. Serial MR imaging would allow longitudinal studies of the temporal and spatial evolution of intracerebral hemorrhages and perihematomal injury. That would not only substantially reduce the amount of animals needed, but also better depict

the time-dependent action mechanism of various pathogenetic factors.

2. Materials and Methods

2.1. Animals. C57BL/6 mice (Jackson Laboratories, Bar Harbor, ME, USA) were maintained in the Department of Laboratory Animal Research at Harvard Medical School with access to food and water ad libitum. All experiments were performed in accordance to the National Institutes of Health guide for the care and use of laboratory animals as well as the institutional guidelines established by the Institutional Animal Care and Use Committee (IACUC) at Harvard Medical School.

2.2. Intracerebral Hemorrhage Model. The procedure of hematoma induction was previously described [14–17]. A total of 11 male adult mice, 10–12 weeks of age, with a body weight of 20–30 g, were used. Mice were anesthetized by intraperitoneal injection of 0.5 mg/g body weight of avertin (tribromoethanol, Sigma-Aldrich, St. Louis, MO, USA). To induce hemorrhage, mice were injected with 0.075U collagenase type VII-s (Sigma-Aldrich, St. Louis, MO, USA) in 500 nL saline into the left caudate putamen using the following stereotactic coordinates: 0.5 mm posterior, 3.0 mm lateral to the bregma, and 4.0 mm in depth. Collagenase was infused over 2 minutes using a stereotaxic injector (Stoelting, Wood Dale, IL, USA) and the 1 μL-syringe (Hamilton, Reno, NV) stayed in place for 10 minutes to prevent reflux.

2.3. MRI Setup. This study was performed in 2 parts. In part 1, two mice underwent MR imaging 2, 8, and 24 hours after collagenase injection to define the best early time points for MR imaging. In part 2, nine mice were subjected to an imaging schedule from days 1 ($n = 9$), 3 ($n = 7$), 10 ($n = 5$), and 21 ($n = 2$) based on the different phases of edema (hyperacute, acute, subacute, chronic) that bear their own pathophysiology. Animals were evaluated using a modified 28-point neurological scoring system before isoflurane anesthesia for the MR [14]. The test included body symmetry, gait, climbing, circling behaviours, front limb asymmetry, and compulsory circling. Each point was graded from 0 to 4, establishing a maximum deficit score of 24. MR imaging was performed with a high-field 4.7 Tesla MR scanner (Biospin, Bruker, Germany) at the Center for Basic MR Research at Beth Israel Deaconess Medical Center. Anesthesia was induced with 2% isoflurane and maintained with 1.6% isoflurane in 100% O_2 via an MR-compatible nose cone apparatus to minimize motion artifacts. Mice were positioned headfirst and prone inside a plexiglass "cradle" with respiratory monitoring and a constant flow of isoflurane delivered directly to the nose of the mouse. This method bypasses intubation of the vulnerable trachea. The magnet compatible apparatus allows a precise and reproducible fixation of the head at the center of the Bruker linear birdcage radiofrequency coil with an inner diameter of 22 mm. After the isoflurane administration was discontinued, mice were monitored until awake from anesthesia.

2.4. MRI Parameters. T1- and T2-weighted images were acquired at a 256×256 matrix and a $2.56 \times 2.56\,cm^2$ field of view. A relaxation enhancement (RARE) sequence was used for both T1-weighted (echo time/relaxation time [TE/TR] = 12/500, RARE factor = 1) and T2-weighted (TE/TR = 75/2000, RARE factor = 12) imaging. T2*-weighted imaging parameters were TE = 14 ms, TR = 1500 ms, FOV = $2.56 \times 2.56\,cm^2$, and FA = 30°, matrix 128×128. In all acquisitions, 9 axial slices with 1 mm thickness were obtained. Hematoma size was determined from T1 and T2* images, and T2 images were used for edema quantification. The measurements were performed by an examiner blinded to the exam date using a computer-assisted image analysis program (ImageJ, NIH, available at website http://rsb.info.nih.gov/ij/). The values for hematoma and edema volumes were compared with those determined from cryosections.

2.5. Histology. Following final MR imaging, brains were removed, placed in 4% paraformaldehyde and cryoprotected in 30% sucrose for 3 days at 4°C before they were frozen. Coronal sections of 20 μm-thickness were taken at 300 μm intervals over the rostral-caudal extent of the lesion. Sections were stained with Luxol Fast Blue and cresyl violet according to previously published protocols [15, 17, 18]. Hematoma and edema volumes were measured by digitally analyzing stained sections with ImageJ. Lesion volumes (mm^3) were computed as running sums of lesion area multiplied by the thickness of each section (300 μm) over the extent of the lesion expressed as an orthogonal projection [19].

2.6. Statistical Analysis. Given the small sample size at different examination dates, the correlation coefficient (Spearman coefficient) for non-parametric correlations and two-tailed p values at a confidence interval CI = 95% were analyzed using one-way ANOVA.

3. Results

3.1. MR Appearance of Hematoma and Edema. In two animals, MR imaging was performed as early as 2 hours after hematoma induction, and the hematoma was observed as a focal hypointensity on T1-, T2-, and T2*-weighted images. The hematoma remained stable without any evidence of expansion when scanned again 8 hours and 24 hours following collagenase injection (Figure 1).

In mice with serial MR imaging up to 72 hours, 10 and 21 days, the predominantly low-signal hematoma within the left caudate/putamen in T1-, T2-, and T2*-weighted images were consistent with deoxyhemoglobin and intracellular methemoglobin after 24 hours. The signal converted to predominantly high intensity at 72 hours to 10 days on T2-weighted RARE spin-echo images, consistent with extracellular methemoglobin (Figure 2). The initially hypointense hematoma on T1-weighted images became hyperintense on days 3 and 10. Even on T2*-weighted images, the signal of the hematoma core became hyperintense at 10 days. On day 21, a low-signal streak was left at the site of the former space-occupying hematoma on T1-, T2-, and T2*-weighted images (Figures 3 and 4).

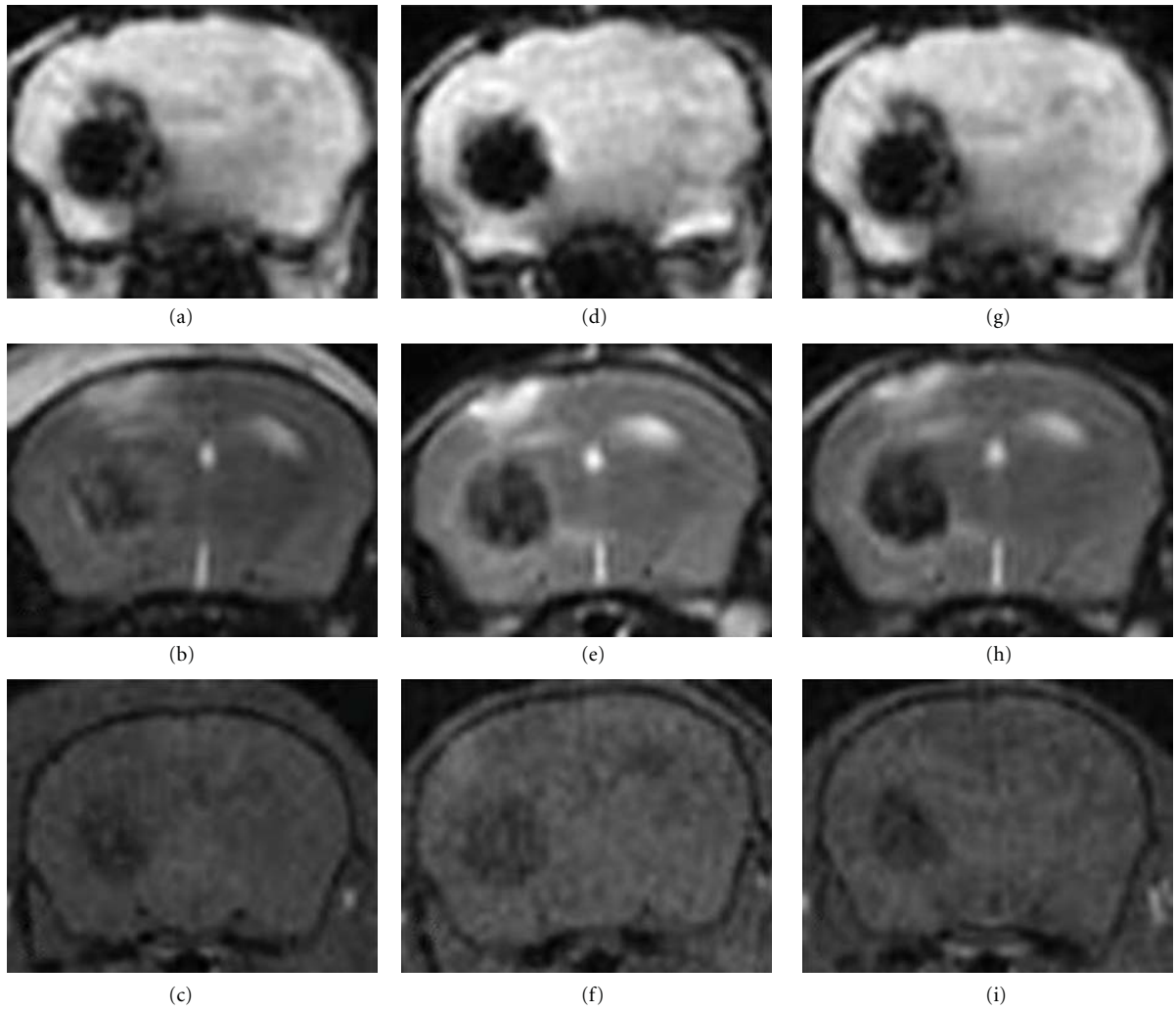

Figure 1: MR tomographic images on 4.7 T using T2*- (a, d, and g), T2- (b, e, and h), and T1-weighted images (c, f, and i) in a mouse 2 (a–c), 8 (d–f), and 24 hours (g–i) after stereotactic collagenase injection. The hematoma appears hypointense on T1 as early as 2 hours after collagenase injection and does not change in signal intensity and homogeneity over the first 24 hours. The blooming effect of T2*-weighted sequences makes the hematoma appear larger and needs referencing with T1- and T2-weighted images. T2-weighted images reveal a rim of hyperintensity surrounding the hypointense core as early as 8 hours. There is no evidence of hematoma enlargement over the first 24 hours.

3.2. Quantification of Hematoma and Edema Volumes. Table 1 illustrates the mean hematoma sizes on T1- and T2*-weighted images and the mean edema sizes on T2 on day 1 for nine mice, on day 3 for seven mice, on day 10 for four mice, and for the remainder ($n = 2$) on day 21. After final imaging, the equivalent hematoma and edema volumes were compared with the hematoma and edema areas on histology as also shown in Table 1. The Spearman correlation coefficient between hematoma volume on T2*-weighted images and histology was $r = 0.61$ ($P < 0.09$) over all times points, thus not reaching statistical significance. The Spearman correlation coefficient between hematoma volume on T1 and histology, however, was statistically significant $r = 0.7$ ($P < 0.04$). So was the coefficient for edema volume on T2 and histology on all examination dates with $r = 0.73$ ($P < 0.03$).

4. Discussion

Ongoing research in intracerebral hemorrhage and the prospects of therapy have raised the need for a noninvasive method to investigate ICH in rodent models. The quantification of hematoma volume is currently based on spectrophotometry assays [8, 20], histomorphometry on stained brain slices [15], or computer-assisted outlining of brain slices [20], thus excluding follow-up measurements during the disease progression and for the evaluation of novel therapeutic interventions. The same accounts for edema volumetry that uses brain water content measurements [11, 16, 17], blood-brain barrier permeability for Evans blue dye on histology [11], or hemispheric enlargement [8] for quantitation. Among the biological imaging techniques, magnetic resonance imaging (MRI) constitutes an excellent tool for

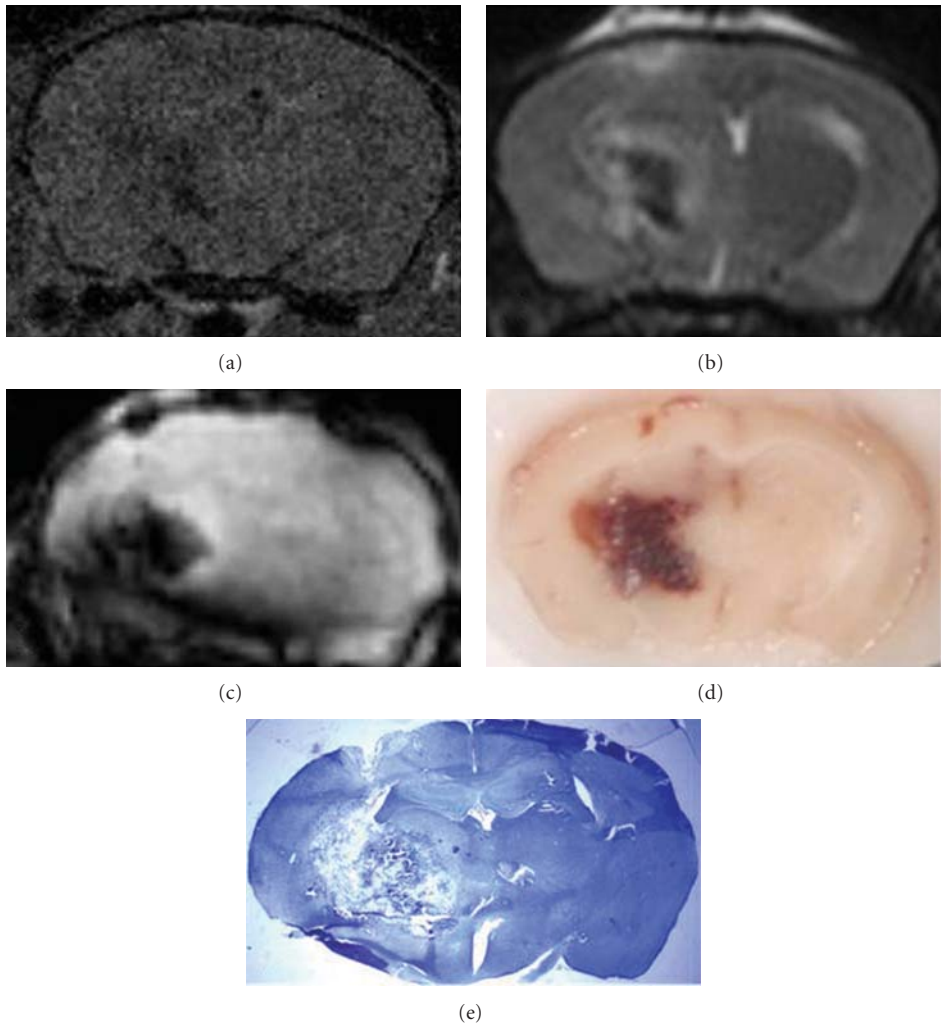

Figure 2: T1- (a), T2- (b), and T2*- (c) weighted images in a mouse 24 hours after hematoma induction reveal a hypointensity that matched well with the hematoma size found on frozen section (d) and cryostat section stained with Luxol Fast Blue and cresyl violet [×10] (e). Again, T2*-weighted images need referencing with T1- and T2-weighted images for hematoma quantitation. Of note is an artefact on the left to midventral surface (c).

Table 1: MR volumetry and histology.

Study dates	Mean hematoma size ± SD on T1 in mm^3	Mean hematoma size ± SD on T2* in mm^3	Mean edema size ± SD on T2 in mm^3	Mean edema size ± SD on T2 in mm^3 for euthanized mice	Mean edema size ± SD on histology in mm^3 for euthanized mice	Median neurological score (0–24)
Day 1	14.0 ± 3.4	13.4 ± 3.4	11.1 ± 5.6	16.0 ± 4.0	10.6 ± 1.5	4
Day 3	7.4 ± 3.8	8.0 ± 4.4	8.9 ± 3.4	12.2 ± 1.3	27.2 ± 2.2	2
Day 10	6.1 ± 3.4	6.9 ± 3.5	1.6 ± 0.8	1.4 ± 0.6	1.5 ± 1.6	0
Day 21	3.4 ± 3.1	4.3 ± 0.9	0.8 ± 1.1	0.8 ± 1.1	0.1 ± 0.1	0

neuroimaging in rats [21] and pigs [22, 23]. Owing to the variety of knockout genotypes in mice, repeated studies of the same animal are important research tools to study hematoma and edema evolution in a longitudinal fashion. Previous MRI studies of the mouse brain have either been postmortem imaging of excised specimen with a near-microscopic spatial resolution [24, 25] or in vivo studies with a high in-plane resolution at the expense of a much poorer section thickness [26].

At high magnetic fields, the ratio between surface and volume in the head is important because of the presence of high susceptibility effects and poor magnetic field homogeneity in the whole head. Even with optimization of the shimming procedure and a reduction in TR, it was not

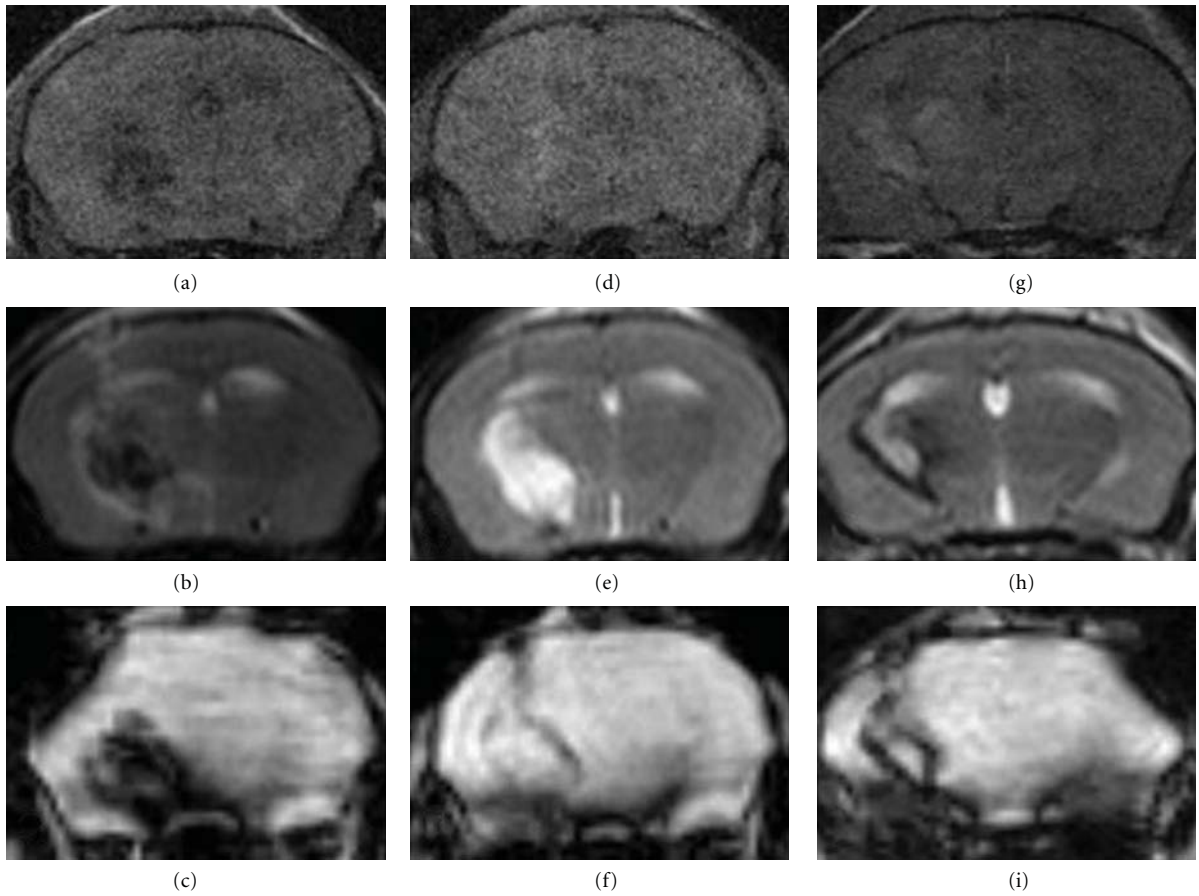

Figure 3: Temporal evolution of hematoma and edema after day 1 (a, b, and c), day 3 (d, e, and f), and day 10 (g, h, and i). On T1-weighted images, the hyperintense hematoma on day 1 (a) gradually changes to a hyperintense core over 10 days (c). On T2-weighted images, the core of the hematoma becomes hyperintense within 3 days (e) and develops a hypointense ring on day 10 (h) representing cavitation. The latter could also be discerned on T2*-weighted images on day 10 (i).

possible to suppress this artifact completely. For T1-weighted sequence, the echo time was minimized to remove any T2 weighting and minimize susceptibility artifacts at air/tissue interfaces. In T2-weighted sequence, a RARE factor of 12 increased the effective echo time and reduced the scan time. The echo time in T2* sequence was optimized to provide adequate signal-to-noise ratio while maximizing the contrast for measurement of hematoma.

A review of the literature revealed only two reports [13, 27] with murine experimental ICH and quantitation of hematoma size on T2* [13] alone or T2-weighted images [27]. Given these extremely limited data on the changes in signal intensities in the course of hematoma resorption and the lack of data for edema formation, we undertook this study to describe the signal characteristics of hematoma resorption and edema evolution in mice over time.

In our pilot study, we show for the first time that intracerebral hemorrhages appear hypointense on T1 at high field strength as early as 2 hours after the ictus. Although less well demarcated compared to T2* images, the hematoma remained discernable on T1 in the course of hematoma resorption. Hematoma volumes on T1 correlated well with those on histology ($P < 0.04$). T2 images approximated edema size well in the acute to chronic phase of edema formation in mice when compared with histology ($P < 0.03$). Van der Weerd et al. [28] had found T2-weighted images useful for quantitation of lesion volume 24 hours after stroke in a MCAO model. As our results indicate, T2* changes do not correlate with hematoma volumes on histology. That might be due to blooming artifacts that render the suitability of T2* images for quantification of hematoma at this field strength questionable [13]. Knight et al. [29] assessed the evolution of intracerebral hemorrhage in rats by MRI estimates of T2 relaxation time and hematoma-induced changes in cerebral blood flow and blood-brain barrier permeability over 14 days using a 7-Tesla, 20-cm bore magnet. The lesion core and adjacent rim were identified by windowing of T2 values and changed in a consistent manner over time. The MRI and histological estimates of tissue loss were well correlated.

Despite the novel approach for following the temporal and spatial resolutions of intracerebral hemorrhages in mice by high field MR imaging, our pilot study has several limitations. The small number of animals at different examination dates precludes subgroup analysis. The high costs for experimental MR imaging at high field are a major drawback to

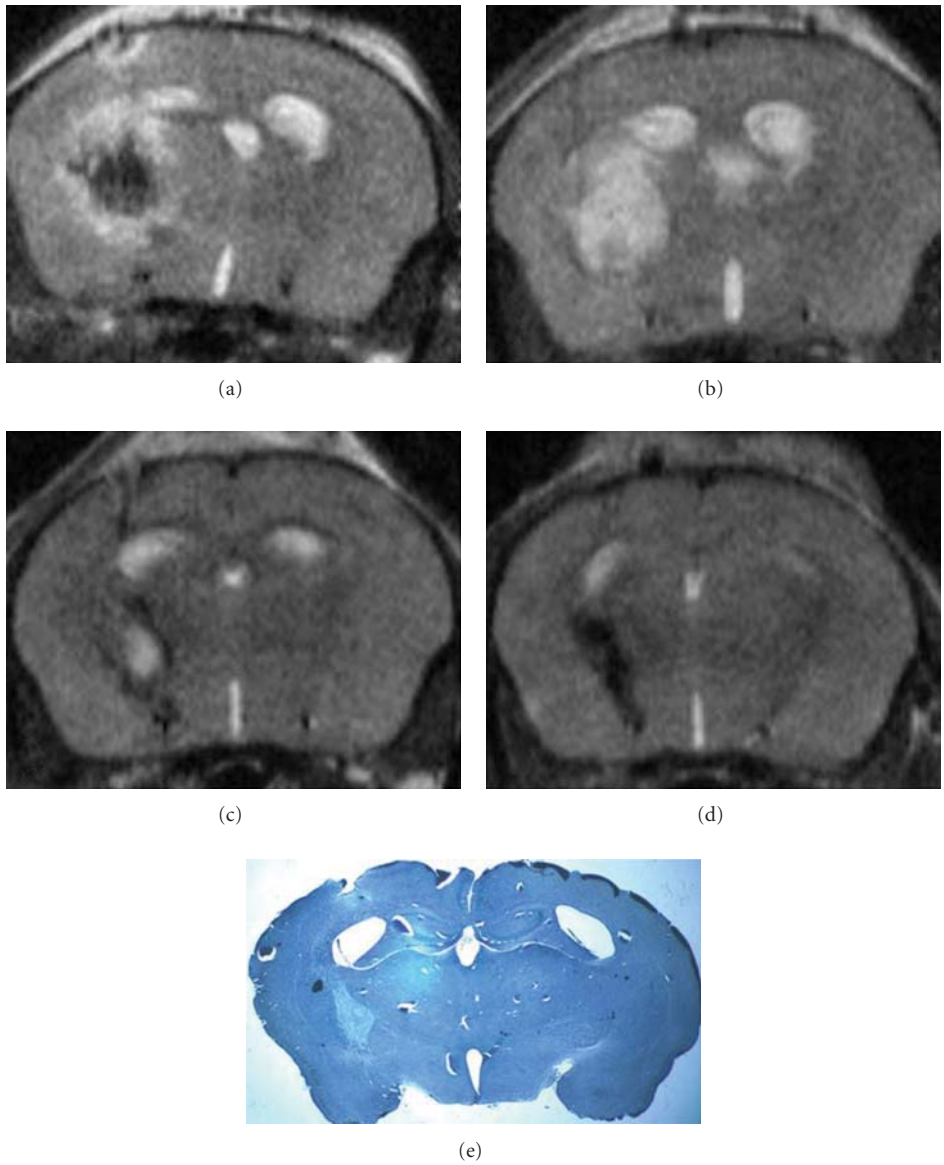

Figure 4: T2-weighted RARE spin-echo images at 24 hours (a) show predominantly low-signal hematoma within the left caudate/putamen, consistent with deoxyhemoglobin and intracellular methemoglobin. At 72 hours (b), there is conversion to predominantly high-signal, consistent with extracellular methemoglobin. In the course of hematoma resorption, the core hyperintensity (c) subsequently transforms to a hypointense gliotic scar at 21 days (d). The cryostat section stained with Luxol Fast Blue and cresyl violet [×10] (e) also well delineates the gliotic scar.

large study groups. The reproducibility of the murine ICH model used in our study that was pioneered by Clark et al. [14] made it one of the principal models of murine ICH [11, 12, 15–17, 30]. It mimics the pathogenetic mechanism of vessel wall rupture leading to intracerebral hemorrhage. Theoretical concerns that bacterial collagenase might induce an inflammatory response, independent of that elicited by parenchymal blood, have not been confirmed for the activation of microglia in cell cultures after the addition of collagenase at various concentrations [16]. Whether the morphological substrate of what we depict as hyperintensity on T2-weighted images exclusively represents edema, remains questionable. Alternate techniques imply the injection of autologous blood into the striatum [8, 10], but lack the pathophysiologic event of vessel rupture.

5. Conclusions

Repetitive multimodal MRI scanning at 4.7 T in mice with collagenase-induced ICH allows studying the individual kinetics of signal intensities underlying hematoma resolution and edema formation in a noninvasive manner. That would allow studying a wide range of therapeutic treatments in a longitudinal fashion in mice.

Acknowledgment

This paper was supported by National Nature Science Foundation of China (81171112, MC Li).

References

[1] A. I. Qureshi, S. Tuhrim, J. P. Broderick, H. H. Batjer, H. Hondo, and D. F. Hanley, "Spontaneous intracerebral hemorrhage," *The New England Journal of Medicine*, vol. 344, no. 19, pp. 1450–1460, 2001.

[2] G. Xi, R. F. Keep, and J. T. Hoff, "Mechanisms of brain injury after intracerebral haemorrhage," *The Lancet Neurology*, vol. 5, no. 1, pp. 53–63, 2006.

[3] C. M. Miller, P. M. Vespa, D. L. McArthur, D. Hirt, and M. Etchepare, "Frameless stereotactic aspiration and thrombolysis of deep intracerebral hemorrhage is associated with reduced levels of extracellular cerebral glutamate and unchanged lactate pyruvate ratios," *Neurocritical Care*, vol. 6, no. 1, pp. 22–29, 2007.

[4] J. Castillo, A. Davalos, J. Alvarez-Sabin et al., "Molecular signatures of brain injury after intracerebral hemorrhage," *Neurology*, vol. 58, no. 4, pp. 624–629, 2002.

[5] T. D. Ardizzone, A. Lu, K. R. Wagner, Y. Tang, R. Ran, and F. R. Sharp, "Glutamate receptor blockade attenuates glucose hypermetabolism in perihematomal brain after experimental intracerebral hemorrhage in rat," *Stroke*, vol. 35, no. 11, pp. 2587–2591, 2004.

[6] K. R. Wagner, "Modeling intracerebal hemorrhage: glutamate, nuclear factor-kappa B signaling and cytokines," *Stroke*, vol. 38, no. 2, pp. 753–758, 2007.

[7] S. T. Carmichael, P. M. Vespa, J. L. Saver et al., "Genomic profiles of damage and protection in human intracerebral hemorrhage," *Journal of Cerebral Blood Flow and Metabolism*, vol. 28, no. 11, pp. 1860–1875, 2008.

[8] J. Wang, J. Fields, and S. Dore, "The development of an improved preclinical mouse model of intracerebral hemorrhage using double infusion of autologous whole blood," *Brain Research*, vol. 1222, pp. 214–221, 2008.

[9] R. F. Regan, M. Chen, Z. Li, X. Zhang, L. Benvenisti-Zarom, and J. Chen-Roetling, "Neurons lacking iron regulatory protein-2 are highly resistant to the toxicity of hemoglobin," *Neurobiology of Disease*, vol. 31, no. 2, pp. 242–249, 2008.

[10] M. Xue, M. D. Hollenberg, and V. W. Yong, "Combination of thrombin and matrix metalloproteinase-9 exacerbates neurotoxicity in cell culture and intracerebral hemorrhage in mice," *Journal of Neuroscience*, vol. 26, no. 40, pp. 10281–10291, 2006.

[11] D. W. Kim, S. H. Im, J. Y. Kim, D. E. Kim, G. T. Oh, and S. W. Jeong, "Decreased brain edema after collagenase-induced intracerebral hemorrhage in mice lacking the inducible nitric oxide synthase gene: laboratory investigation," *Journal of Neurosurgery*, vol. 111, no. 5, pp. 995–1000, 2009.

[12] E. Titova, C. G. Kevil, R. P. Ostrowski et al., "Deficiency of CD18 gene reduces brain edema in experimental intracerebral hemorrhage in mice," *Acta Neurochirurgica, Supplementum*, no. 105, pp. 85–87, 2008.

[13] S. Illanes, W. Zhou, S. Heiland, Z. Markus, and R. Veltkamp, "Kinetics of hematoma expansion in murine warfarin-associated intracerebral hemorrhage," *Brain Research*, vol. 1320, pp. 135–142, 2010.

[14] W. Clark, L. Gunion-Rinker, N. Lessov, and K. Hazel, "Citicoline treatment for experimental intracerebral hemorrhage in mice," *Stroke*, vol. 29, no. 10, pp. 2136–2140, 1998.

[15] R. Thiex, L. Mayfrank, V. Rohde, J. M. Gilsbach, and S. A. E. Tsirka, "The role of endogenous versus exogenous tPA on edema formation in murine ICH," *Experimental Neurology*, vol. 189, no. 1, pp. 25–32, 2004.

[16] J. Wang, A. D. Rogove, A. E. Tsirka, and S. E. Tsirka, "Protective role of tuftsin fragment 1–3 in an animal model of intracerebral hemorrhage," *Annals of Neurology*, vol. 54, no. 5, pp. 655–664, 2003.

[17] J. Wang and S. E. Tsirka, "Tuftsin fragment 1–3 is beneficial when delivered after the induction of intracerebral hemorrhage," *Stroke*, vol. 36, no. 3, pp. 613–618, 2005.

[18] S. Geisler, H. Heilmann, and R. W. Veh, "An optimized method for simultaneous demonstration of neurons and myelinated fiber tracts for delineation of individual trunco- and palliothalamic nuclei in the mammalian brain," *Histochemistry and Cell Biology*, vol. 117, no. 1, pp. 69–79, 2002.

[19] J. J. Ohab, S. Fleming, A. Blesch, and S. T. Carmichael, "A neurovascular niche for neurogenesis after stroke," *Journal of Neuroscience*, vol. 26, no. 50, pp. 13007–13016, 2006.

[20] C. Foerch, K. Arai, G. Jin et al., "Experimental model of warfarin-associated intracerebral hemorrhage," *Stroke*, vol. 39, no. 12, pp. 3397–3404, 2008.

[21] B. Orakcioglu, K. Becker, O. W. Sakowitz, A. Unterberg, and P. D. Schellinger, "Serial diffusion and perfusion MRI analysis of the perihemorrhagic zone in a rat ICH model," *Acta Neurochirurgica, Supplementum*, no. 103, pp. 15–18, 2008.

[22] R. Thiex, W. Kuker, H. D. Muller et al., "The long-term effect of recombinant tissue-plasminogen-activator (rt-PA) on edema formation in a large-animal model of intracerebral hemorrhage," *Neurological Research*, vol. 25, no. 3, pp. 254–262, 2003.

[23] R. Thiex, J. Weis, T. Krings et al., "Addition of intravenous N-methyl-D-aspartate receptor antagonists to local fibrinolytic therapy for the optimal treatment of experimental intracerebral hemorrhages," *Journal of Neurosurgery*, vol. 106, no. 2, pp. 314–320, 2007.

[24] H. Benveniste, K. Kim, L. Zhang, and G. A. Johnson, "Magnetic resonance microscopy of the C57BL mouse brain," *NeuroImage*, vol. 11, no. 6 I, pp. 601–611, 2000.

[25] R. F. Kooy, M. Verhoye, V. Lemmon, and A. van der Linden, "Brain studies of mouse models for neurogenetic disorders using *in vivo* magnetic resonance imaging (MRI)," *European Journal of Human Genetics*, vol. 9, no. 3, pp. 153–159, 2001.

[26] S. Xu, E. K. Jordan, W. Li et al., "In vivo three-dimensional MR microscopy of mice with chronic relapsing experimental autoimmune encephalomyelitis after treatment with insulin-like growth factor-I," *The American Journal of Neuroradiology*, vol. 19, no. 4, pp. 653–658, 1998.

[27] M. L. James, P. M. Sullivan, C. D. Lascola, M. P. Vitek, and D. T. Laskowitz, "Pharmacogenomic effects of apolipoprotein e on intracerebral hemorrhage," *Stroke*, vol. 40, no. 2, pp. 632–639, 2009.

[28] L. van der Weerd, M. F. Lythgoe, R. A. Badin et al., "Neuroprotective effects of HSP70 overexpression after cerebral ischaemia—an MRI study," *Experimental Neurology*, vol. 195, no. 1, pp. 257–266, 2005.

[29] R. A. Knight, Y. Han, T. N. Nagaraja et al., "Temporal MRI assessment of intracerebral hemorrhage in rats," *Stroke*, vol. 39, no. 9, pp. 2596–2602, 2008.

[30] T. Nakamura, G. Xi, Y. Hua, T. Schallert, J. T. Hoff, and R. F. Keep, "Intracerebral hemorrhage in mice: model characterization and application for genetically modified mice," *Journal of Cerebral Blood Flow and Metabolism*, vol. 24, no. 5, pp. 487–494, 2004.

Hindawi Publishing Corporation
Journal of Biomedicine and Biotechnology
Volume 2012, Article ID 758169, 7 pages
doi:10.1155/2012/758169

Review Article

MicroRNAs and Induced Pluripotent Stem Cells for Human Disease Mouse Modeling

Chingiz Underbayev, Siddha Kasar, Yao Yuan, and Elizabeth Raveche

Department of Pathology and Laboratory Medicine, University of Medicine and Dentistry of New Jersey, 185 South Orange Avenue, MSB C512, Newark, NJ 07103, USA

Correspondence should be addressed to Elizabeth Raveche, raveches@umdnj.edu

Received 10 December 2011; Accepted 14 February 2012

Academic Editor: Monica Fedele

Human disease animal models are absolutely invaluable tools for our understanding of mechanisms involved in both physiological and pathological processes. By studying various genetic abnormalities in these organisms we can get a better insight into potential candidate genes responsible for human disease development. To this point a mouse represents one of the most used and convenient species for human disease modeling. Hundreds if not thousands of inbred, congenic, and transgenic mouse models have been created and are now extensively utilized in the research labs worldwide. Importantly, pluripotent stem cells play a significant role in developing new genetically engineered mice with the desired human disease-like phenotype. Induced pluripotent stem (iPS) cells which represent reprogramming of somatic cells into pluripotent stem cells represent a significant advancement in research armament. The novel application of microRNA manipulation both in the generation of iPS cells and subsequent lineage-directed differentiation is discussed. Potential applications of induced pluripotent stem cell—a relatively new type of pluripotent stem cells—for human disease modeling by employing human iPS cells derived from normal and diseased somatic cells and iPS cells derived from mouse models of human disease may lead to uncovering of disease mechanisms and novel therapies.

1. Human Disease Mouse Models

Model organisms such as fruit flies, zebrafish, and mice have provided great insights into gene function in humans because they are easy to grow and genetically manipulate in the laboratory setting. By evaluating different mutations in these organisms, one can identify candidate genes that lead to disease in humans and develop models to better understand human disease pathogenesis [1]. The mouse is an ideal model organism for human disease. Not only they are physiologically similar to humans, but a large genetic reservoir of potential models of human disease has been accumulated through the generation of radiation- or chemically induced mutant loci. Multiple technological advances have dramatically advanced our skills to create mouse models of human diseases. High-resolution genetic and physical linkage maps of the mouse genome have greatly facilitated the identification and cloning of mouse disease genes. Furthermore, transgenic approaches allowed us to ectopically express or make germline mutations in virtually any gene in the mouse genome by using homologous recombination in embryonic stem (ES) cells [2, 3]. Inbred, congenic and transgenic strains are widely used in current research labs as very valuable tools to investigate human diseases pathogenesis and develop new effective therapeutical strategies.

2. Embryonic Stem (ES) and Induced Pluripotent Stem (iPS) Cells

Pluripotency is the ability of a cell to give rise to progeny representing all types of cells in an organism [4]. Murine embryonic stem cells derived from inner cell mass (ICM) of the embryo exhibit two remarkable features in culture. First, under certain conditions, they can be propagated indefinitely as a stable self-renewing population where every cell undergoes symmetrical division. This immortalized phenotype allows ES cells to be cultured over extended periods of time. Upon differentiation, this feature is lost and progeny undergoes cellular aging (Hayflick limit) as has

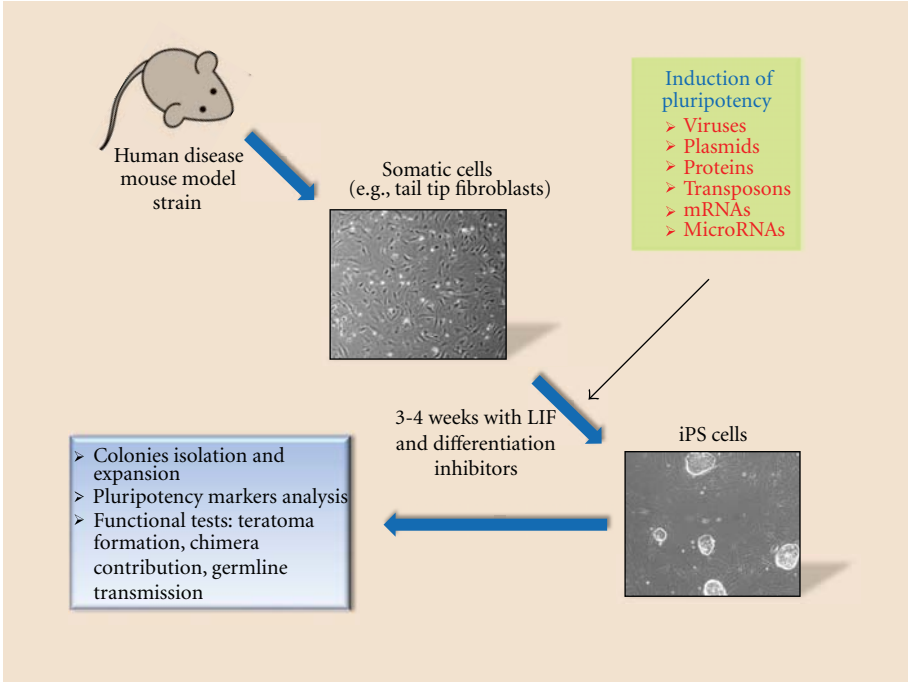

Figure 1: Generation of induced pluripotent stem cells from mouse model somatic cells.

been previously documented for all other nontransformed primary cells [5]. A second feature is that, during culture, ES cells retain their pluripotency and can differentiate into the same range of cell types as those seen in the embryo from ICM. The value of ES cells is partly due to their amenability to extensive gene manipulation. Homologous recombination between genomic and the exogenous DNA is a very inefficient and rare process, but it takes place in ES cells with relatively higher efficiency than it does in other cell types [4]. Gene targeting by homologous recombination in ES cells has improved our ability to study many biological processes [3]. Since ES cells contribute to all tissues upon injection into a recipient blastocyst, including the germline [6, 7] modification in an ES cell genome can be transmitted, by the breeding of ES cell/wild-type chimaeras, to generate mice containing the desired mutations in all cells. In this way mice with a variety of modifications such as null and point mutations, chromosomal rearrangements and large deletions have been generated. In addition, it is possible to target reporter genes under the control of specific promoters to study gene expression patterns in different cell types. Furthermore, the ability of ES cells to differentiate in vitro to many different mature somatic cell types, in combination with purification of the cell of interest by methods such as directed differentiation and lineage selection, opens up the opportunity to use these mature cell types for various basic and therapeutical applications [3]. Unfortunately, not every mouse model is permissive for true ES cells derivation. This makes it harder to investigate gene function and pathogenesis in those strains. With the advent of iPS technology this issue has been overcome.

In 2006, Takahashi and Yamanaka initially reported the direct reprogramming of murine embryonic fibroblasts (MEFs) to pluripotent stem cells by introducing four transcription factors [8]. Those factors, namely, *Oct4*, *Sox2*, *Klf4,* and c*Myc,* that are important for self-renewal of embryonic stem cells (ESCs) have been shown to reprogram both mouse and human somatic cells into ESC-like pluripotent cells (Figure 1). Since then, a large number of laboratories have derived induced pluripotent stem cells from somatic cells, and many important advances have been made [9–15]. Most importantly these iPS cells have shown properties very similar to the ones of ES cells such as pluripotency markers expression, teratoma formation, chimeras contribution, and germline transmission. Moreover, the critical advantages of iPS cells over ES cells now seem to be obvious. First of all iPS cells are being generated from the autologous recipient thus obviating the graft-versus-host problem in transplantation settings. The second benefit pertains to the ethical concerns. Unlike in the past, one can now generate ES-like iPS cells from human skin fibroblasts or hair-follicle cells without the need to resort to the human ES cell lines and potentially (in the future) apply them to the therapeutic and/or basic science approaches [13].

3. Making Use of iPS Cells for Human Disease Modeling

For the human disease animal modeling iPS cell technology opened the way to even wider spectrum of available mouse model strains. In 2009, Zhao et al. reported the generation of all-iPS-derived viable, fertile live-born progeny by tetraploid complementation [16] which further proved them to be useful for the development of transgenic mice strains with desired gene defects homologous to those seen in human pathology.

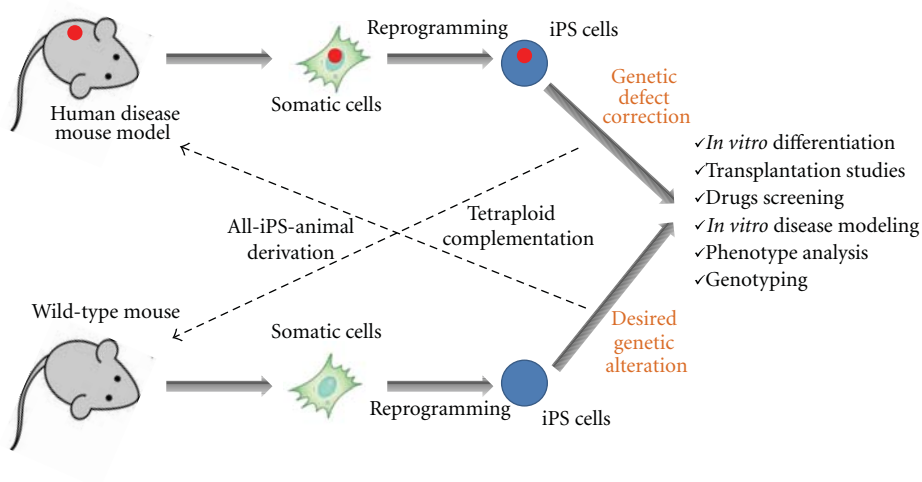

Figure 2: Mouse induced pluripotent stem cells applications for human disease mouse modeling.

At present, with this valuable tool in hand one can take literally any human disease mouse strain somatic cells (e.g., tail tip fibroblasts) and induce pluripotent stem cells from them. These disease-specific iPS cells can be further used to explore given disease mechanisms both in vitro and in vivo. (Figure 2). For example, human chronic lymphocytic leukemia (CLL) (CD5+ B-cell malignancy) mouse model—New Zealand Black mouse—exhibits a defect in the miR-15a/16–1 gene on chromosome 14 which results in decreased levels of these microRNAs, which is also seen in more than 50% of CLL patients [17]. Unfortunately, this mouse strain is refractory to true ES cells derivation which makes it difficult to study the role of this microRNA gene defect in B-cell development both in vitro and in vivo. In our lab, we were able to successfully generate NZB iPS cells from spleen stromal cells. Now they can be used as subjects for gene targeting (correcting miR-15a/16–1 mutation and deletion) followed by in vitro differentiation towards B-lineage. This would help find out what role this particular gene defect plays in B-cell lymphogenesis and how its correction might alleviate malignant clonal expansion. Furthermore, NZB iPS cells with corrected miR-15a defect could be differentiated into hematopoietic stem cells (HSCs) followed by their adoptive transfer into appropriate recipients in order to observe the effect of gene correction on CLL development in vivo.

Another way to utilize iPS cells to study human diseases in animal models is xenograft transplantation assay. In this case iPS cells would be generated from patient's somatic cells (Figure 3), differentiated into desired type of cells (e.g., HSC), and transplanted into immunodeficient murine recipients. In a recent report, Yao et al. [18] have demonstrated a generation of human iPS cells with zinc-finger nuclease, mediated disruption of CCR5 locus which is known to be a coreceptor for HIV entry. These patient-specific iPS cells can now be differentiated into HSC and transplanted into animal recipients to study the role of CCR5 in HIV infection development in vivo. In another work, Lee et al. have used human iPS-derived neural stem cells (NSCs) in a mouse intracranial human glioma xenograft model [19]. In this case, iPS-derived NSCs have been used as cellular vehicles for targeted anticancer gene therapy since they will home to the brain. As a proof of principle, Hanna and colleagues have taken advantage of autologous iPS cells derived from humanized mouse model of sickle cells anemia to correct human sickle hemoglobin allele by gene-specific targeting followed by their differentiation into hematopoietic stem cells and transplantation into irradiated recipients [20]. It has been shown that mice could be rescued from disease progression after transplantation. This work has underlined the benefits of iPS technology for the combined gene and cell therapy approach to study human disease in animal models. It is needless to say that currently various labs worldwide use patient-specific iPS cells for animal modeling both in vitro and in vivo. Such pathological conditions as Huntington disease, amyotrophic lateral sclerosis, spinal muscular dystrophy, Gaucher disease type III, Down syndrome, type 1 diabetes, Parkinson's disease, β-thalassemia, and hepatic failure have been investigated using iPS cells generation [20–29].

4. MicroRNAs

MicroRNAs (miRs) are small noncoding RNAs which are known to be critical for the expression control of more than a third of all protein coding genes [30] by means of binding to the 3′ untranslated region (UTR) of target mRNAs via an imperfect match to repress their translation and/or stability [31]. They have been implicated in the regulation of many biological processes, including the stem cells self-renewal and pluripotency [32–34]. MiRNAs are generated from precursor transcripts—primary miRNAs (pri-miRNAs)—that are first processed in the nucleus into an intermediate pre-miRNAs by the complex of enzymes containing Drosha and DGCR8 proteins [35–37]. The pre-miRNAs are then transported by the exportin 5-RanGTP shuttle into the cytoplasm, in which they are further processed by Dicer, into mature miRNAs [38]. In ES cells a set of microRNAs (including miR-302 and miR-17–92 clusters) closely interfere with the

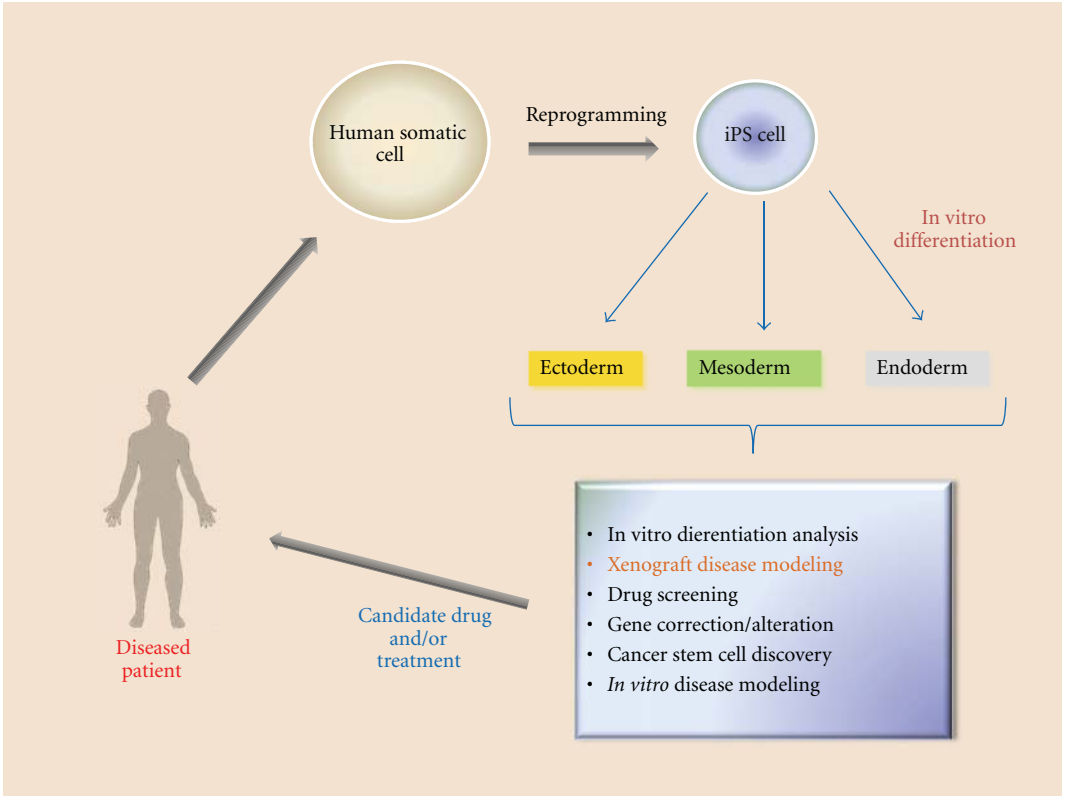

Figure 3: Human induced pluripotent stem cells applications for human disease mouse models.

key pluripotency factors such as Oct4, Sox2, and Nanog [39, 40] thereby preventing them from differentiation and controlling their proper self-renewal potential [41]. Xu et al. have demonstrated miR-145 to control the expression of Oct4, Sox2, and Klf4 and repress self-renewal of human ES cells [42]. On the other hand, c-Myc has been reported to repress miRNAs such as miR-21, let-7a, and miR-29a during reprogramming [43]. Tissue-specific miRNAs often play important roles in normal tissues and organ formation [44, 45]. More importantly for the current review, microRNAs proved to be effective tools for the iPS generation. In particular, inhibition of miR-21, let-7a, or mir-29a has been shown to enhance the reprogramming efficiency [43]. Alternatively, overexpression of the miR302/367 cluster has been shown to rapidly and efficiently reprogram both mouse and human somatic cells to iPS state without any exogenous transcription factors delivery through Oct4 gene expression activation and the suppression of Hdac2 [46]. MicroRNA gene expression profiling in human ES cells revealed specific miR-signatures of elevated expression of miR-302 cluster, miR-200 family members as well as miR-520 cluster [47]. This might imply the possibility of them to be used as tools to increase the efficiency of iPS generation without any exogenous interventions into the genomic DNA of the host cells and serve as additional iPS quality control markers. Conversely, as the regulators of gene expression microRNAs could be used to drive patient-specific iPS cells down the specific cells lineage in vitro in order to produce the required cell type to be studied [48].

Another promise that microRNAs are holding is the development of microRNA-based gene targeting for the temporal gene-of-interest silencing [49]. For instance, aberrant expression of Pax5 (also known as BSAP), a critical regulator of B-cell development, is known to correlate with aggressive subsets of B-cell non-Hodgkin lymphoma [50]. It has been previously shown that overexpression of miR-15a/16 reduces endogenous c-Myb levels and compromises Pax5 function [51]. Now one can produce iPS cells from Pax5-affected non-Hodgkin lymphoma patient and apply in vitro B-cell differentiation protocol along with miR-15a/16–1 delivery to evaluate lymphomagenesis in the mouse xenograft model. Potentially, the similar approach could be employed for the discovery of leukemia (or more commonly cancer) stem cells [52]. Finally, miRs can be used as biomarkers of human disease progression in mouse model settings. Overall diagram of microRNA application for mouse modeling is shown in Figure 4.

5. Conclusion

The importance of disease mouse models and their impact on medical research is hard to overestimate. Therefore the value of animal modeling is very critical for our understanding of human disease and development of new effective approaches to therapy. Induced pluripotent stem cells hold a great promise for both basic and applied science and open the road for many more opportunities for human disease research. Coupled with the use of fine-tune regulators

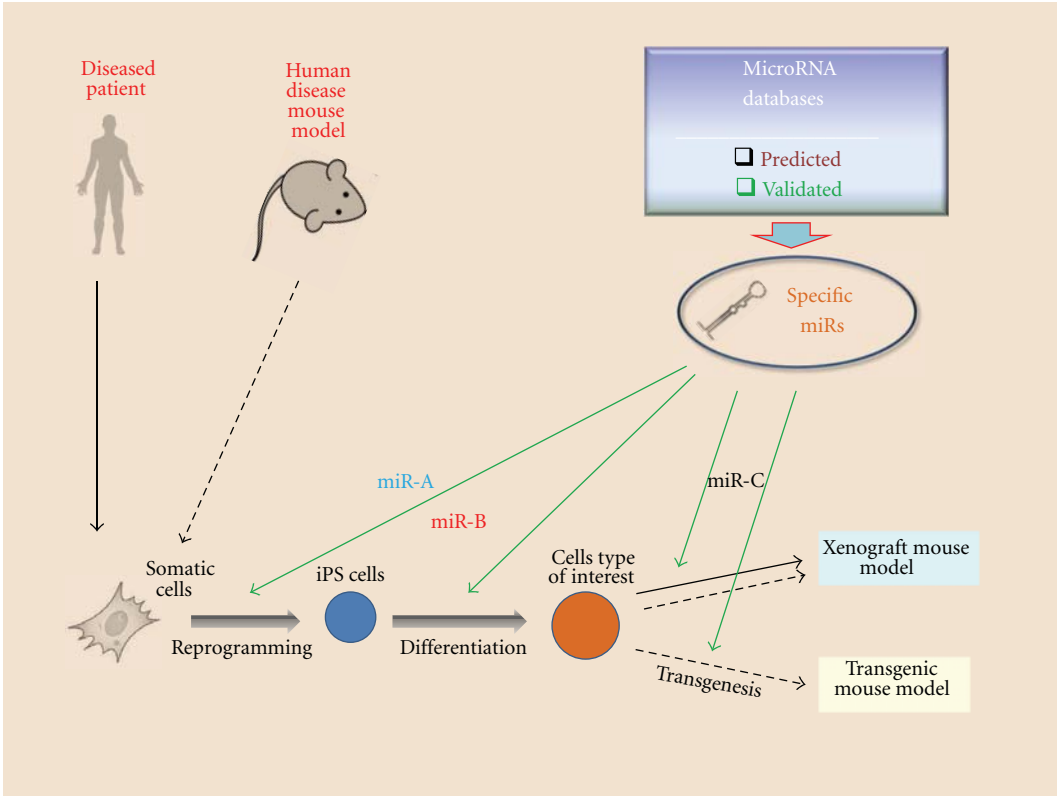

Figure 4: MicroRNA applications for iPS-mediated human disease mouse models.

of gene expression, microRNAs, and mouse modeling they have a promising potential for subsequent discoveries and new therapies development in the complex field of human pathology.

References

[1] N. L. Washington, M. A. Haendel, C. J. Mungall, M. Ashburner, M. Westerfield, and S. E. Lewis, "Linking human diseases to animal models using ontology-based phenotype annotation," *PLoS Biology*, vol. 7, no. 11, Article ID e1000247, 2009.

[2] M. A. Bedell, N. A. Jenkins, and N. G. Copeland, "Mouse models of human disease. Part I: techniques and resources for genetic analysis in mice," *Genes and Development*, vol. 11, no. 1, pp. 1–10, 1997.

[3] L. Hook, C. O'Brien, and T. Allsopp, "ES cell technology: an introduction to genetic manipulation, differentiation and therapeutic cloning," *Advanced Drug Delivery Reviews*, vol. 57, no. 13, pp. 1904–1917, 2005.

[4] H. Niwa, "Mouse ES cell culture system as a model of development," *Development Growth and Differentiation*, vol. 52, no. 3, pp. 275–283, 2010.

[5] S. Ohtsuka and S. Dalton, "Molecular and biological properties of pluripotent embryonic stem cells," *Gene Therapy*, vol. 15, no. 2, pp. 74–81, 2008.

[6] A. Bradley, M. Evans, M. H. Kaufman, and E. Robertson, "Formation of germ-line chimaeras from embryo-derived teratocarcinoma cell lines," *Nature*, vol. 309, no. 5965, pp. 255–256, 1984.

[7] E. Robertson, A. Bradley, M. Kuehn, and M. Evans, "Germline transmission of genes introduced into cultured pluripotential cells by retroviral vector," *Nature*, vol. 323, no. 6087, pp. 445–448, 1986.

[8] K. Takahashi and S. Yamanaka, "Induction of pluripotent stem cells from mouse embryonic and adult fibroblast cultures by defined factors," *Cell*, vol. 126, no. 4, pp. 663–676, 2006.

[9] K. Okita, M. Nakagawa, H. Hyenjong, T. Ichisaka, and S. Yamanaka, "Generation of mouse induced pluripotent stem cells without viral vectors," *Science*, vol. 322, no. 5903, pp. 949–953, 2008.

[10] M. Stadtfeld, M. Nagaya, J. Utikal, G. Weir, and K. Hochedlinger, "Induced pluripotent stem cells generated without viral integration," *Science*, vol. 322, no. 5903, pp. 945–949, 2008.

[11] T. Seki, S. Yuasa, M. Oda et al., "Generation of induced pluripotent stem cells from human terminally differentiated circulating T cells," *Cell stem cell*, vol. 7, no. 1, pp. 11–14, 2010.

[12] M. Wernig, A. Meissner, R. Foreman et al., "In vitro reprogramming of fibroblasts into a pluripotent ES-cell-like state," *Nature*, vol. 448, no. 7151, pp. 318–324, 2007.

[13] J. Zou, M. L. Maeder, P. Mali et al., "Gene Targeting of a Disease-Related Gene in Human Induced Pluripotent Stem and Embryonic Stem Cells," *Cell Stem Cell*, vol. 5, no. 1, pp. 97–110, 2009.

[14] M. I. Lai, W. Y. Wendy-Yeo, R. Ramasamy et al., "Advancements in reprogramming strategies for the generation of induced pluripotent stem cells," *Journal of Assisted Reproduction and Genetics*, vol. 28, no. 4, pp. 291–301, 2011.

[15] K. Takahashi, "Direct reprogramming 101," *Development Growth and Differentiation*, vol. 52, no. 3, pp. 319–333, 2010.

[16] X. Y. Zhao, W. Li, Z. Lv et al., "IPS cells produce viable mice through tetraploid complementation," *Nature*, vol. 461, no. 7260, pp. 86–90, 2009.

[17] E. Salerno, B. J. Scaglione, F. D. Coffman et al., "Correcting miR-15a/16 genetic defect in New Zealand Black mouse model of CLL enhances drug sensitivity," *Molecular Cancer Therapeutics*, vol. 8, no. 9, pp. 2684–2692, 2009.

[18] Y. Yao, B. Nashun, T. Zhou et al., "Generation of CD34+ cells from CCR5-disrupted human embryonic and induced pluripotent stem cells," *Human Gene Therapy*, vol. 23, no. 2, pp. 238–242, 2012.

[19] E. X. Lee, D. H. Lam, C. Wu et al., "Glioma gene therapy using induced pluripotent stem cell derived neural stem cells," *Molecular Pharmaceutics*, vol. 8, no. 5, pp. 1515–1524, 2011.

[20] J. Hanna, M. Wernig, S. Markoulaki et al., "Treatment of sickle cell anemia mouse model with iPS cells generated from autologous skin," *Science*, vol. 318, no. 5858, pp. 1920–1923, 2007.

[21] J. T. Dimos, K. T. Rodolfa, K. K. Niakan et al., "Induced pluripotent stem cells generated from patients with ALS can be differentiated into motor neurons," *Science*, vol. 321, no. 5893, pp. 1218–1221, 2008.

[22] A. D. Ebert, J. Yu, F. F. Rose et al., "Induced pluripotent stem cells from a spinal muscular atrophy patient," *Nature*, vol. 457, no. 7227, pp. 277–280, 2009.

[23] I. H. Park, N. Arora, H. Huo et al., "Disease-specific induced pluripotent stem cells," *Cell*, vol. 134, no. 5, pp. 877–886, 2008.

[24] F. Soldner, D. Hockemeyer, C. Beard et al., "Parkinson's disease patient-derived induced pluripotent stem cells free of viral reprogramming factors," *Cell*, vol. 136, no. 5, pp. 964–977, 2009.

[25] L. Ye, J. C. Chang, C. Lin, X. Sun, J. Yu, and Y. W. Kan, "Induced pluripotent stem cells offer new approach to therapy in thalassemia and sickle cell anemia and option in prenatal diagnosis in genetic diseases," *Proceedings of the National Academy of Sciences of the United States of America*, vol. 106, no. 24, pp. 9826–9830, 2009.

[26] M. Wernig, J. P. Zhao, J. Pruszak et al., "Neurons derived from reprogrammed fibroblasts functionally integrate into the fetal brain and improve symptoms of rats with Parkinson's disease," *Proceedings of the National Academy of Sciences of the United States of America*, vol. 105, no. 15, pp. 5856–5861, 2008.

[27] Q. Zhou, J. Brown, A. Kanarek, J. Rajagopal, and D. A. Melton, "In vivo reprogramming of adult pancreatic exocrine cells to β-cells," *Nature*, vol. 455, no. 7213, pp. 627–632, 2008.

[28] I. S. Behbahan, Y. Duan, A. Lam et al., "New approaches in the differentiation of human embryonic stem cells and induced pluripotent stem cells toward hepatocytes," *Stem Cell Reviews and Reports*, vol. 7, no. 3, pp. 748–759, 2011.

[29] S. Asgari, M. Moslem, K. Bagheri-Lankarani, B. Pournasr, M. Miryounesi, and H. Baharvand, "Differentiation and transplantation of human induced pluripotent stem cell-derived hepatocyte-like cells," *Stem Cell Reviews and Reports*. In press.

[30] S. K. Mallanna and A. Rizzino, "Emerging roles of microRNAs in the control of embryonic stem cells and the generation of induced pluripotent stem cells," *Developmental Biology*, vol. 344, no. 1, pp. 16–25, 2010.

[31] T. M. Rana, "Illuminating the silence: understanding the structure and function of small RNAs," *Nature Reviews Molecular Cell Biology*, vol. 8, no. 1, pp. 23–36, 2007.

[32] C. Melton, R. L. Judson, and R. Blelloch, "Opposing microRNA families regulate self-renewal in mouse embryonic stem cells," *Nature*, vol. 463, no. 7281, pp. 621–626, 2010.

[33] Y. Tay, J. Zhang, A. M. Thomson, B. Lim, and I. Rigoutsos, "MicroRNAs to Nanog, Oct4 and Sox2 coding regions modulate embryonic stem cell differentiation," *Nature*, vol. 455, no. 7216, pp. 1124–1128, 2008.

[34] Y. M. S. Tay, W. L. Tam, Y. S. Ang et al., "MicroRNA-134 modulates the differentiation of mouse embryonic stem cells, where it causes post-transcriptional attenuation of Nanog and LRH1," *Stem Cells*, vol. 26, no. 1, pp. 17–29, 2008.

[35] Y. Lee, C. Ahn, J. Han et al., "The nuclear RNase III Drosha initiates microRNA processing," *Nature*, vol. 425, no. 6956, pp. 415–419, 2003.

[36] Y. Lee, K. Jeon, J. T. Lee, S. Kim, and V. N. Kim, "MicroRNA maturation: stepwise processing and subcellular localization," *EMBO Journal*, vol. 21, no. 17, pp. 4663–4670, 2002.

[37] Y. Zeng and B. R. Cullen, "Sequence requirements for micro RNA processing and function in human cells," *RNA*, vol. 9, no. 1, pp. 112–123, 2003.

[38] V. K. Gangaraju and H. Lin, "MicroRNAs: key regulators of stem cells," *Nature Reviews Molecular Cell Biology*, vol. 10, no. 2, pp. 116–125, 2009.

[39] A. Marson, S. S. Levine, M. F. Cole et al., "Connecting microRNA genes to the core transcriptional regulatory circuitry of embryonic stem cells," *Cell*, vol. 134, no. 3, pp. 521–533, 2008.

[40] K. D. Wilson, S. Venkatasubrahmanyam, F. Jia, N. Sun, A. J. Butte, and J. C. Wu, "MicroRNA profiling of human-induced pluripotent stem cells," *Stem Cells and Development*, vol. 18, no. 5, pp. 749–757, 2009.

[41] Y. Wang, R. Medvid, C. Melton, R. Jaenisch, and R. Blelloch, "DGCR8 is essential for microRNA biogenesis and silencing of embryonic stem cell self-renewal," *Nature Genetics*, vol. 39, no. 3, pp. 380–385, 2007.

[42] N. Xu, T. Papagiannakopoulos, G. Pan, J. A. Thomson, and K. S. Kosik, "MicroRNA-145 regulates OCT4, SOX2, and KLF4 and represses pluripotency in human embryonic stem cells," *Cell*, vol. 137, no. 4, pp. 647–658, 2009.

[43] C. S. Yang, Z. Li, and T. M. Rana, "microRNAs modulate iPS cell generation," *RNA*, vol. 17, no. 8, pp. 1451–1460, 2011.

[44] K. N. Ivey, A. Muth, J. Arnold et al., "MicroRNA regulation of cell lineages in mouse and human embryonic stem cells," *Cell Stem Cell*, vol. 2, no. 3, pp. 219–229, 2008.

[45] Y. Zhao, E. Samal, and D. Srivastava, "Serum response factor regulates a muscle-specific microRNA that targets Hand2 during cardiogenesis," *Nature*, vol. 436, no. 7048, pp. 214–220, 2005.

[46] F. Anokye-Danso, C. M. Trivedi, D. Juhr et al., "Highly efficient miRNA-mediated reprogramming of mouse and human somatic cells to pluripotency," *Cell Stem Cell*, vol. 8, no. 4, pp. 376–388, 2011.

[47] J. Ren, P. Jin, E. Wang, F. M. Marincola, and D. F. Stroncek, "MicroRNA and gene expression patterns in the differentiation of human embryonic stem cells," *Journal of Translational Medicine*, vol. 7, article 20, 2009.

[48] L. R. Saunders et al., "miRNAs regulate SIRT1 expression during mouse embryonic stem cell differentiation and in adult mouse tissues," *Aging*, vol. 2, no. 7, pp. 415–431, 2010.

[49] C. C. Lan, I. U. S. Leong, D. Lai, and D. R. Love, "Disease modeling by gene targeting using MicroRNAs," *Methods in Cell Biology*, vol. 105, pp. 419–436, 2011.

[50] L. Krenacs, A. W. Himmelmann, L. Quintanilla-Martinez et al., "Transcription factor B-cell-specific activator protein (BSAP) is differentially expressed in B cells and in subsets of B-cell lymphomas," *Blood*, vol. 92, no. 4, pp. 1308–1316, 1998.

[51] E. Y. Chung, M. Dews, D. Cozma et al., "c-Myb oncoprotein is an essential target of the dleu2 tumor suppressor microRNA cluster," *Cancer Biology and Therapy*, vol. 7, no. 11, pp. 1758–1764, 2008.

[52] P. H. Gunaratne, "Embryonic stem cell MicroRNAs: defining factors in induced pluripotent (iPS) and cancer (CSC) stem cells?" *Current Stem Cell Research and Therapy*, vol. 4, no. 3, pp. 168–177, 2009.

Hindawi Publishing Corporation
Journal of Biomedicine and Biotechnology
Volume 2012, Article ID 125384, 11 pages
doi:10.1155/2012/125384

Review Article

Animal Model of Dermatophytosis

Tsuyoshi Shimamura,[1,2] Nobuo Kubota,[1] and Kazutoshi Shibuya[2,3]

[1] *R&D Laboratories, POLA Pharma Inc, 560 Kashio-cho, Totsuka-ku, Yokohama 244-0812, Japan*
[2] *Department of Surgical Pathology, Toho University School of Medicine, 6-11-1 Omori-Nishi, Ota-Ku, Tokyo 143-8541, Japan*
[3] *Department of Dermatology, Peking University First Hospital, Beijing 100034, China*

Correspondence should be addressed to Kazutoshi Shibuya, kaz@med.toho-u.ac.jp

Received 9 December 2011; Revised 8 February 2012; Accepted 13 February 2012

Academic Editor: Monica Fedele

Dermatophytosis is superficial fungal infection caused by dermatophytes that invade the keratinized tissue of humans and animals. Lesions from dermatophytosis exhibit an inflammatory reaction induced to eliminate the invading fungi by using the host's normal immune function. Many scientists have attempted to establish an experimental animal model to elucidate the pathogenesis of human dermatophytosis and evaluate drug efficacy. However, current animal models have several issues. In the present paper, we surveyed reports about the methodology of the dermatophytosis animal model for tinea corporis, tinea pedis, and tinea unguium and discussed future prospects.

1. Introduction

Superficial mycoses affect 20% to 25% of the world's population, and the incidence is increasing [1]. However, the mechanisms of the characteristic pathology, the mechanisms of host protection against infection, and the reason for intractable tinea pedis have not been clarified. Thus, experiments to elucidate these questions regarding dermatophytosis are needed using an animal model that closely resembles human pathology.

However, the suggestion has been made that the model of experimental infection on the backs of animals was insufficient to clarify the pathology of tinea corporis and tinea pedis because the site of infection was as severe as in kerion celsi, and the treatment duration was limited due to spontaneous healing within 4 weeks after infection [2]. Concerning onychomycosis, tinea unguium research in humans has not progressed due to the inability to biopsy nails. And the pathogenesis and the invasion have not been fully understood. Thus, there are few reports of a model of onychomycosis because of the difficulty in setting up a model.

In this paper, we surveyed the reported animal models of tinea corporis, tinea pedis, and tinea unguium and will discuss the future direction of research to establish a dermatophytosis animal model with high reproducibility for human dermatophytosis.

2. Animal Model of Tinea Corporis

Tinea corporis in humans is mainly caused by *Trichophyton rubrum*, *Trichophyton mentagrophytes*, and *Microsporum canis* and take several clinical forms but commonly present as classic ringworm [3]. Ringworm of the body is usually observed on the trunk, shoulders, or limbs, and occasionally the face (excluding the beard area). The infection may range from mild to severe, commonly appearing as annular, scaly patches with sharply marginated, raised erythematous vesicular borders [4].

The efforts to establish an animal model of tinea corporis began with the first report by Bloch in 1908 [5]. Sakai et al. [6] were the first to report of animal studies evaluating the efficacy of tinea corporis, and the research became the basis for the tinea corporis model. Subsequently, many research studies have been reported an animal model of tinea corporis since 1962. To reproduce dermatophytosis in humans, the examination of methods using animal models mainly focused on animal species, fungal selection, and the condition of the infection (occlusion or open condition with or without abrasion) of the skin.

2.1. Animal Species. The tinea corporis model has been reported in a variety of different animals, such as cockscomb

[7], germ-free guinea pigs [8], grafting guinea pig skin onto congenitally athymic mice [9], mice [10], nude rats [11, 12], rabbits [13], chickens [13], humans [14–16], and guinea pigs [6, 7, 9, 10, 12, 13, 17–60].

According to reports of *T. mentagrophytes* on cockscomb and guinea pigs [7], the skin of guinea pigs showed a greater resemblance to human skin; however, cockscomb was more suitable than the skin of guinea pigs for fungal growth. Nonetheless, topical treatment of cockscomb with drugs is difficult, especially a fluid excipient.

In germfree guinea pigs infected with *T. mentagrophytes*, forming serious ulcers took twice the time as healing compared with conventionally reared guinea pigs. Cutaneous reinfection of germfree guinea pigs with *T. mentagrophytes* was protracted. However, the lesions healed in about the same time as the primary infection in conventionally reared guinea pigs. These reactions were considered cell-mediated hypersensitivity similar to contact dermatitis [8]. Thus, no advantage was gained in using germfree guinea pigs as the animal model for tinea corporis because tinea corporis in humans shows no spontaneous healing.

The *in vivo* model using nude mice xenografted with guinea pig skin showed well-grown dermatophytosis on the xenograft but not on nude mouse skin [9]. On the other hand, *T. mentagrophytes* could be cultured from the skin of nude rats (*rnu*/*rnu*) for 90 days and euthymic rats (*rnu*/+) for 35 days [11]. In these studies, the same strain of *T. mentagrophytes* ATCC18748 was used. Thus, this difference in the infection period between nude mice and nude rats was not due to the organism. We suggest that this difference involved the different structures of the skin. Fujita [61] reported that hairless guinea pigs whose skin resembled human hair-bearing skin could be induced to show clinical signs similar to human hair-bearing skin lesions and suggested that the difference in the skin structure, especially the density of hair and the thickness of the horny cell layer, affected the establishment of the infection.

Infectivity of two strains of human origin, *Trichophyton quinckeanum* NCPF309 and *T. mentagrophytes* MRL 81/889, were evaluated in seven inbred strain mice: BALB/c, AKR, C3H, DBA/2, (CBA×DBA/2)F_1, CBA, and C57BL/6 [10]. As a result, variations were noted in susceptibility in different inbred mice strains, and BALB/c mice showed greater susceptibility to the infection from both fungal strains.

Ringworm lesions developed in rabbits infected with *T. mentagrophytes* B32663 (dog origin) after intravenous administration in the same manner as lesions that developed after percutaneous administration [13].

In experimental infections of humans [15], *T. mentagrophytes* ATCC18748 was applied to the ankles followed by 4-day-continuous occlusion. The time course of the disease was described in fine details as follows. (1) During the first 2 days following removal of the occlusive patches, no signs of infection were present. (2) Erythema, edema, and small vesicles appeared and the degree of inflammation steadily increased from the 3rd to the 10th days. (3) The lesions enlarged to fill nearly the entire area originally overlain by the occlusive patch from the 11th to the 22nd days. (4) The erythema and edema were replaced by scaling, and discrete follicular infections became apparent from the 23rd to the 45th days. (5) Finally, the infections healed spontaneously from the 46th to the 90th days. Furthermore, the volar surface of the forearm was infected using the same method. Pathological changes were the same as the lesions on the ankles. However, the whole infection period was shortened, and the lesions finally healed spontaneously within 60 days. The sustainability of lesions may involve the skin structure as well as immunity because involvement of immunity on sustainability of the disease in nude rats (*rnu*/*rnu*) was clear from the difference in the duration of complete healing using euthymic rats (*rnu*/+) [11].

Guinea pigs have been widely used as a model due to reproducibility, high susceptibility, and its easy handling. However, different studies have been attempted because of the suggestion that there were defects wherein the clinical signs and the course of the pathology have not been similar to that of humans [62].

2.2. Selection of Fungi. In the preparation of a guinea pig model, the following fungi were examined: *T. mentagrophytes*, *Trichophyton mentagrophytes* var. *quinckeanum* (mice, *T. mentagrophytes* is synonymous), *Trichophyton mentagrophytes* var. *granulosum* (rodents, now designated *Trichophyton interdigitale*), *Trichophyton mentagrophytes* var. *mentagrophytes* (now designated *T. interdigitale*), *Trichophyton mentagrophytes* var. *erinacei* (hedgehog), *Trichophyton verrucosum* (cattle, horse), *T. rubrum* (anthropophilic), *Trichophyton tonsurans* (anthropophilic), *Trichophyton asteroids*, *Trichophyton violaceum* (anthropophilic), *Trichophyton concentricum* (anthropophilic), *M. canis*, *Microsporum gypseum*, *Microsporum pesicolor*, *Candida albicans*, and *Epidermophyton floccosum*. In general, zoophilic dermatophytes are more pathogenic to laboratory animals than anthropophilic strains [63, 64]. Thus, *T. mentagrophytes* and *M. canis* were specially used for the study of susceptibility to infection [2, 61, 63].

2.3. Pre- and Posttreatment. In addition to the selection of fungi, pre- or posttreatment included occlusion and abrasion [23, 34, 37, 38, 42, 47, 51, 56]. Each occlusion method after inoculation of fungi was reported as follows: covered with ointment [56], covered by a sheet of polyethylene film with an impermeable plastic tape for 24 hr [34], moistened gauze pad with Teflon between 24 hr and 72 hr [38, 39, 42], covered with a glass fiber filter [37], or covered with a chamber [51]. The occlusion method was suitable for the tinea corporis model because it was closer to natural infection and achieved high reproducibility [61]. On the other hand, Kerbs et al. reported that the occlusive method had not been implemented in the guinea pig model with *T. mentagrophytes* ATCC18748 because occlusion treatment weakened the infection [42]. Furthermore, Saunte et al. [51] suggested that inoculation under occlusion showed no advantage in the establishment of experimental infections. In consideration of these reports, we should consider the need for occlusion to infect fungi according to the procedure and fungal strains.

While there are some reports using nonabraded skin without occlusion [44, 53, 55], abraded skin was used in

many experiments to secure a high infection rate. The methods of abrading back skin include the use of sandpaper [22, 23, 25, 31, 33, 45, 47, 48, 54, 58], a roughened pestle [40, 41], a steel brush [50], pumice stone [17], shaving [51, 57, 59], and tape stripping [21, 26–30, 32, 35, 36, 46, 51, 52]. The abrasion techniques using sandpaper, a roughened pestle, and a pumice stone are simple and easy; however, such techniques may lead to skin wounds such as an ulcer, which subsequently can be confused with lesions produced during dermatophyte infections [51]. Meanwhile, shaving and tape stripping avoids the problem of creating ulcers by an artificial procedure and can make the skin equally and superficially traumatized prior to inoculation [51]. In addition, Saunte et al. stated that pretreatment, such as shaving with a razor or tape stripping, did not influence the nature of the infection by *M. canis* [51].

2.4. Inoculation Size. An animal model using the occlusion method without abrasion may be made with a small amount of fungi (100 spores/3.8 cm^2) [39, 42]. One report stated that the optimal conditions for dermatophytosis in guinea pigs were found to be an inoculum of 10^7 fungal cells applied to abraded skin without occlusion and that of 10^8 fungal cells induced severe lesions [47]. In almost all cases, the inoculum of 10^7 fungal cells was applied to the area of infection made by dermatophytosis *in vivo* by all kinds of abrasion methods without occlusion.

2.5. Preparation Method of Tinea Corporis in Guinea Pigs Model. The typical methods of infection using *T. mentagrophytes* are described below, which summarized the results from a survey of the literature.

The nonocclusion method involved removing the back hair of guinea pigs from the entire surface of the skin with electric hair clippers and then preparing the inoculation site. Next, the skin was abraded by applying and removing adhesive tape three or four times, shaving the infection area using a razor, or abrasion with sandpaper, a roughened pestle, a steel brush, or a pumice stone. After pre-treatment to create an abrasion, the skin was inoculated by applying a volume of 50–100 μL of *T. mentagrophytes* 10^6 cells/mL. However, the application volume must be changed according to the area.

The occlusion method involved applying 100 cells/site to a section of the skin to induce an infection [39, 42] and did not include the abrasion procedure [2]. The duration of occlusion was set from 24 hr to 72 hr [34, 37–39, 51].

2.6. Pathology of Tinea Corporis in Guinea Pig Model. The pathophysiologic changes over time as a model of infection in the guinea pig showed that the normal evolution of dermatophytosis may be clearly divided into four phases [63]: incubation phase, spreading phase, inflammation phase, and healing or cleaning phase extending from days 25 to 60. The length of each phase depends on the mode of infection, fungal species, and strain [63].

Fujita [61] described the pathophysiology of changes over time focusing on the biological responses of guinea pigs infected with *T. mentagrophytes* as the tinea corporis model. Briefly, erythema and red papules appeared between 4 and 6 days after inoculation, and then the reaction to trichophytin was positive between 7 and 8 days. This positive reaction to trichophytin indicated the establishment of cellular immunity to *T. mentagrophytes*. Therefore, the erythema and papules gradually increased in size and then fused together. The lesions that climaxed at 14-15 days showed infiltrative plaque-like erythema with thick scale and crusts. Subsequently, these eruptions gradually disappeared and almost healed spontaneously within 4 weeks after inoculation. Another report by Koga [64] described the pathophysiologic changes over time as almost the same as stated above. Furthermore, Koga reported histopathological changes in detail: no findings except slight acanthosis thought to be formed by abrasion on the 3rd day after inoculation. Fungal elements were only confirmed in the horny cell layer of the epidermis and epithelium of the follicular infundibulum. Acanthosis and hyperkeratosis were noted over the entire surface of the skin, and vasodilatation and inflammatory cell infiltration in the upper layer of the dermis were observed on the 7th day. In addition, there was a large amount of hyphae in the horny cell layer of the epidermis. On the 14th day, spongiosis was observed along with severe inflammatory cell infiltration in the dermis, however, hyphae were present only in the follicles and not in the horny cell layer of the epidermis. This disappearance of hyphae in the horny cell layer of the epidermis was understood as a result of exclusion by increased skin turnover. In addition, hyphae in the follicles were excluded before and after the 20th day as part of spontaneous healing.

2.7. Evaluation of Treatment and Prophylaxis by Tinea Corporis Model. The tinea corporis animal model was used to estimate the efficacy of antifungal agents like bifonazole [21, 22, 25, 26, 35, 46, 52], clotrimazole [22, 23, 25, 35, 37, 40, 46, 52], miconazole [37, 44], tolnaftate [12, 22, 25, 37, 40], griseofulvin [28, 29, 37, 40, 65], ketoconazole [12, 18, 20, 29, 37, 40], omoconazole [32, 36], terbinafine [26, 29, 40, 41, 47, 48, 50, 58, 65], econazole [40], butenafine [22, 23, 33], naftifine [22], itraconazole [20, 27, 41, 50, 51, 59, 65], amorolfine [21, 65], sertaconazole [44], saperconazole [24], latoconazole [25], fluconazole [27, 28, 31, 41, 65], SCH 39304 [31, 54], lanoconazole [30, 33, 48], mupirocin [18], laudamonium [17], KP-103 [33], neticonazole [33], R126638 [59], voriconazole [57], ciclopirox [58], pramiconazole [50], luliconazole [48], and *Astragalus verus* Olivier [45].

In general, the timing of the start with oral or topical administration of antifungal agents is when the primary lesion begins to occur in each model or experiment. In most cases, the time is from 3–5 days after infection. In a recent study, Ghannoum et al. [47] started oral treatment of terbinafine on the day of infection considering pharmacokinetics. That is, the start of oral therapy with terbinafine was set to allow the drug to be absorbed by the gastrointestinal tract and to reach the tissue by the time the infection was established.

The prophylaxis effect of antifungal agents was evaluated in the tinea corporis model. There was a wide range in the start of administration between 5 days before infection and

30 minutes after infection [12, 17, 22, 41, 59]. A clear rationale for when to start administration has not been described in detail in these reports. However, the start of administration and the duration of treatment should be set to consider the local skin pharmacokinetics of the drug. Although relapse after treatment was reported [33], examinations have not often been conducted because of spontaneous healing in the guinea pigs.

3. Animal Model of Tinea Pedis

The feet, especially the soles and toe webs, are the most frequent site of tinea pedis in humans. The most common clinical manifestation is intertriginous dermatitis, which presents with maceration, peeling, and fissuring in the spaces between the fourth and fifth toes. Another common presentation is the chronic, squamous, hyperkeratotic type in which fine silvery scales cover the pinkish skin of the soles, heels, and sides of the foot (moccasin foot). An acute inflammatory condition characterized by the formation of vesicles, pustules, and sometimes bullae is most frequently caused by *T. mentagrophytes*. The more chronic agents of tinea pedis is caused by *T. rubrum*, *T. mentagrophytes* var. *interdigitale*, and *E. floccosum* [4].

Fujita and Matsuyama reported an animal model of tinea pedis using a paper disk [66]. Meanwhile, Uchida and Yamaguchi reported another animal model using a sheer adhesive bandage [67]. These two animal models of tinea pedis in guinea pigs are superior because they showed clinical and histopathological nonspontaneous healing similar to human hyperkeratotic tinea pedis.

3.1. Selection of Fungi. In the first report on the establishment of an animal model, Fujita and Matsuyama examined the methodology in the fungal selection of *T. mentagrophytes* strains using the paper disk method, anthropophilic or zoophilic, and arthroconidia or microconidia [66]. As a result, no clear difference was noted between arthroconidia and microconidia by $MFID_{50}$ (50% minimal foot infectious dose). In the histopathological examination, both the anthropophilic and zoophilic strains infected the horny cell layer, and the fungal invasions apparently continued for 6 months. Furthermore, the zoophilic strain infected a deeper layer than the anthropophilic strain. Thus, the zoophilic strain is thought to be more suitable for the animal model than the anthropophilic strain.

3.2. Inoculation Size. No reports discussed a direct comparison using inoculation size in each animal model. Thus, we surveyed previously published reports using *T. mentagrophytes* TIMM2789 (SM-110), which was selected most often for the tinea pedis model.

The inoculation sizes in the paper disk method ranged from 5×10^4 to 5×10^6 fungal cells/planta [66, 68–72]. In the bandage method, inoculation size was only 1×10^7 fungal cells/planta in all reports [67, 72–77]. However, even if either method was selected, inoculum concentrations applied to the animal should be considered in the concept of the experiment described in the next section.

3.3. Duration of Infection and Treatment. The determination of the infection period can be divided into two major concepts. One is the concept of an infinitely close association with human pathology in order to accurately predict the clinical effects in humans. Another concept is that it should be evaluated easily and quickly as a screening method for candidate drugs. In the former, because it has been reported that it took more than 26 weeks to spread over the sole [66], the drug treatment was started 2 or 3 weeks after inoculation [73–76]. In this case, the duration of drug treatment had been set from 2 weeks to 4 weeks followed by the clinical application period. In the latter case, the drug treatment was started from 3 days after inoculation, and the duration of treatment was for 3 or 7 days [71, 72]. In addition, the duration of being fixed by paper disk or bandage on the planta pedis was 3 or 7 days in both cases.

3.4. Preparation Method of Tinea Pedis. The paper disk method involved two types of paper disks, with or without aluminum foil. A paper disk with aluminum foil was covered with a piece of aluminum foil on one side (1.5 mm thick by 8 mm in diameter), while the other side held the inoculum suspension. Any type of disc was wetted with 50 μL of the inoculum suspension and then fixed on the planta pedis of the guinea pig foot with elastic adhesive tape. The disc was removed on the 3rd or the 7th day after infection.

The bandage method was as follows. Sheer Adhesive Bandages (Band-Aid; Johnson & Johnson Co., Ltd., Tokyo, Japan) were wetted with 100 μL of the inoculum suspension (1×10^8 conidia/mL) and then fixed on the sole of an animal's foot with elastic adhesive tape. The Sheer Adhesive Bandages were removed on the 3rd or the 7th day after infection.

3.5. Pathology of Tinea Pedis Model. A detailed histopathological examination of the guinea pig model was reported by Fujita and Matsuyama [66]. With the anthropophilic strain *T. mentagrophytes* NTM-105, the infecting fungi were observed in the upper two-thirds of the horny cell layer. Vertical invasions to the deeper part of the horny cell layer next to the granular layer were not observed at any time. Thus, infection was superficial, and no inflammatory response was induced. The growing fungi spread horizontally in the horny cell layer, and all parts of the plantar side of the foot were infected. Clinical signs of erythema, hyperkeratosis, and desquamation were absent. Such a silent infection persisted throughout the observation period for 1 year.

In contrast to the anthropophilic strain *T. mentagrophytes*, the zoophilic strain *T. mentagrophytes* SM-110 invaded the whole horny cell layer, and infecting fungi were observed just above the granular layer. Vasodilatation in the dermal papillae was noted. Two weeks after inoculation, strong inflammatory responses were induced. Spongiosis and vesicle formation were characteristic changes in the

epidermis. Infiltrations of mononuclear and polymorphonuclear cells were recognized under the vesicles and in the perivascular areas. Exocytosis of these cells into the spongiotic epidermis was also present. However, the strong inflammatory response subsided rapidly within a week, and mild responses persisted thereafter. Three weeks after inoculation, massive growth of fungi in the hair follicles and cellular infiltration became prominent in the skin of the dorsal foot area. Clinically, severe signs of indurated erythema and formation of thick scale and crust developed. All fungi were recovered by culture from the infected feet throughout the observation period for 6 months.

Although the anthropophilic strain *T. mentagrophytes* NTM-105 had spread only in a small area during 3 weeks, the infected area steadily spread to an approximately 19 mm radius at 13 weeks after inoculation. By contrast, the zoophilic strain *T. mentagrophytes* SM-110 spread rapidly at first, reaching sites approximately 8 mm from the point of inoculation within 4 weeks, but the subsequent rate of spread was much slower. Although the two strains spread differently, most areas of the plantar part were infected in 26 weeks.

3.6. Evaluation of Treatment with Tinea Pedis Model. Antifungal efficacy in the tinea pedis animal model was evaluated with different antifungals, such as butenafine [73, 78, 79], latoconazole [25, 80], naftifine [78], tolnaftate [25, 76, 78, 80], clotrimazole [25, 76, 78, 80], bifonazole [25, 74, 78–80], terbinafine [67, 71–73], griseofulvin [67], lanoconazole [70–72, 81], omoconazole [74], miconazole [75], NND-502 (luliconazole) [72, 77], a combination drug of 0.2% pyrrolnitrin and 0.4% clotrimazole [75], variotin [76], phenyl-11-iodo-10-undecynoate [76], siccanin [76], KP-103 [81], and neticonazole [81]. Ohmi et al. compared antifungal efficacy with two animal models, tinea corporis and tinea pedis, using the same antifungal agents [80]. They suggested that the conventional tinea corporis model produced on the back of guinea pigs was sensitive to treatment with several major topical antifungal agents, such as clotrimazole, bifonazole, and tolnaftate, probably because of spontaneous healing during the experimental period. However, the tinea pedis model was much more resistant to treatment with these drugs. The mycological cure rate of bifonazole 1% cream in this report was 70%. In the clinical report, that of bifonazole 1% cream for 4 weeks was 49.6% [82]. Thus, it is possible to compare the efficacy of each drug in tinea pedis model; however, it may not accurately reflect the clinical effectiveness yet due to the difference of mycological cure rate between human and animal.

3.7. Evaluation of Relapse by Tinea Pedis Model. The relapse after drug treatment was examined in the tinea pedis model, which would not have healed spontaneously, unlike the tinea corporis animal model, using the antifungal agents, such as butenafine [73, 79], bifonazole [79], terbinafine [73], KP-103 [81], neticonazole [81], lanoconazole [81], and NND-502 (luliconazole) [77]. The relapse of dermatophytosis, which is highly dependent on environmental factors, is difficult to determine accurately in clinical practice. Thus, verification of relapse using an animal model is very important research.

4. Animal Model of Tinea Unguium

Invasion of the nail plate by a dermatophyte is referred to as tinea unguium in humans. There are two main types of nail involvement: invasive subungual (distal and proximal) and superficial white mycotic infection (leukonychia trichophytica). *T. rubrum* and *T. mentagrophytes*, respectively, are the most common dermatophytes of this infection [4].

There are few reports of the animal model of tinea unguium. One study used guinea pigs [73, 83], and the other used rabbits [84]. This section describes the two animal models.

4.1. Animal Model of Tinea Unguium in Guinea Pigs. Uchida et al. reported that *T. mentagrophytes* could infect the nail when the tinea pedis model in guinea pigs would extend the duration of the experiment [73]. Subsequently, the tinea unguium model, which was modified by the above model, was reported and evaluated drug efficacy [83]. The method and the evaluation results of drug efficacy in tinea unguium using guinea pigs were as follows.

The arthrospores of *T. mentagrophytes* SM-110 were suspended, and the suspension was adjusted to give a concentration of 10^8 spores/mL. Two paper disks were immersed by the fungal suspension and applied between the toes of the hind paw (between the second third toes and between the third and fourth toes) with a foam pad, then fixed with adhesive elastic tape (day 0 after infection). The disks were removed on day 21 after infection. The antifungal treatment, topical KP-103, amorolfine, and terbinafine and oral terbinafine, started on day 60 after infection when the invasion of *T. mentagrophytes* SM-110 into the nail was confirmed; treatment continued for 30 consecutive days. The therapeutic efficacy of tinea unguium was evaluated by the culture method to avoid the drug carryover effects by using dialyzed samples that have been digested by enzymes. In the result, topical amorolfine and topical or oral terbinafine were ineffective even in terms of reducing the fungal burden. In contrast, topical KP-103 significantly reduced the fungal burden in the infected nails compared with the burdens found in the vehicle- and oral-terbinafine-treated groups.

This model was able to evaluate drug efficacy by two administration routes, oral and topical. Furthermore, this model can prevent drug carryover in the recovery culture and assess the pure viability of the fungi. However, this evaluation method is applicable only to water-soluble drugs. Thus, further consideration in the case of lipid-soluble drugs is necessary.

4.2. Animal Model of Tinea Unguium in Rabbits. We established an animal model using rabbits with confirmed fungi in the deep layer of the nail under an immunosuppressive condition [84]. In this section, we describe the method and results of the drug efficacy of our model.

In some preliminary studies, three points were concluded: first, microconidia were more suitable than arthroconidia with regard to infection rate; second, the postinfection period from the end of infection to nail sampling was needed to maintain high infection rates; and third, administration of an immunosuppressant was essential to make *T. mentagrophytes* invade the nail to establish a reproducible infection. Subsequently, we performed experiments aimed at setting the suitable postinfection period, and the protocol for this experiment was as follows.

The nails of rabbits were immunosuppressed with injections of methylprednisolone acetate intramuscularly prior to application of 0.2 mL of fungal suspension (10^8 microconidia/mL) of *T. mentagrophytes* TIMM2789 at a site between the lunula and the proximal nail fold. The nail plates of the first-to-third toes of the hind paw were wrapped together with a gauze patch and finger cot, and 0.5 mL of sterile water was injected into the finger cot to produce a culture environment around the nail that was seemed suitable for fungal growth. This condition was maintained for the duration of the infection for 2 weeks with no other intervention. The finger cot and the gauze patch were removed after 2 weeks of exposure, and this condition was maintained during for 0, 2, or 6 weeks without finger cot and gauze patch; this was termed the postinfection period. After each postinfection period was completed, the animals were sacrificed, and the nails were removed from the paw and treated histopathologically.

In the results, some of the infected nails became cloudy on gross appearance, which was similar to the findings with human onychomycosis. With a longer postinfection period, these findings were fully confirmed. On histopathological examination, hyphae of *T. mentagrophytes* penetrated the nail plate, and some invading fungi reached the nail bed. The infection rate in the sample at 0, 2, and 6 weeks after infection was 57%, 87%, and 93%, respectively. In addition, fungi proliferated and moved distally into the nail plate depending on the duration of infection. The presence of subungual abscess with associated necrosis of the epithelium of the nail bed or matrix was confirmed near the fungi in the nail plate. Above all, a high infection rate was obtained by 2 weeks inoculation with microconidia of *T. mentagrophytes* TIMM2789 and postinfection periods of more than 2 weeks were required.

Subsequently, the experiment for drug efficacy was confirmed for the topical antifungal agents, 8% ciclopirox nail lacquer and 5% amorolfine nail lacquer, using this model. The therapeutic period was set as 4 weeks after a 2-week infection period. The animals in the untreated control group underwent the process of infection and removal of the material used for this process, but they were not exposed to the test agents. The next day after the last treatment, the animals were sacrificed and the nails were removed from the paw for histopathological and microbiological examinations. In the microbiological examination, the infected nail intended for evaluation using culture recovery was cut into 10 pieces in cross-sections, and each nail piece was cultured on Sabouraud dextrose agar for 2 weeks at 28°C. A nail piece that had confirmed fungal growth was assessed as culture positive, and a nail with more than one culture-positive piece was considered fungus positive.

In the results of microbiological examination, a statistically significantly lower rate of culture positivity was found in the 5% amorolfine nail lacquer group for comparing the infection rate to that in both the control and 8% ciclopirox nail lacquer groups. Additionally, when the rate of culture positivity in the drug-treated groups was subtracted from that in the nontreated group, the differences were 54.2% on 5% amorolfine nail lacquer and 8.3% on 8% ciclopirox nail lacquer. This figure was similar in the clinical reports [85–87].

This is the first report of fungal behavior in the nail plate in an experimental animal model of onychomycosis. Our experimental animal model succeeded in encouraging *T. mentagrophytes* to invade the deeper layers of the nail plate. The findings in our model were similar to the clinical diagnoses of the proximal subungual type (PSO). Furthermore, the efficacy of this model was close to the clinical cure rate. Further research using this model may be able to clarify the pathogenesis of onychomycosis and contribute to the development of drugs that match the clinical efficacy.

5. Approach to Accurately Evaluate the Antifungal Agent *In Vivo*

Thus, animal models have been introduced to simulate human skin diseases, as well as changes in disease, and have presented different ideas for antifungal evaluation. It is also necessary to accurately evaluate the therapeutic effects that have been provided to create an environment in various pathological ways [88–90].

In evaluating the effectiveness of antifungal agents in samples from animals and humans, it is necessary to pay attention to the fact that the new medium can attenuate the effects of antifungal agents remaining in the skin sections as has been reported in *in vitro* experiments [88], as well as the culture results that have been reported in human skin sections [89]. In addition, methods have been reported to evaluate the effects of antifungal agents in accordance with the size of the expanding growth of fungal colonies [90]. Contributions have been made in the determination of *in vivo* effects of antifungal agents in combination with the previous medium has been suggested. Already a new method against onychomycosis was proposed by Nakashima et al. [91]. This approach is expected to be useful for evaluating the preliminary antifungal effect.

6. Immunology

An understanding of the defense mechanism of humans with regard to a fungus is very important in order to create a dermatophytosis animal model that shows high reproducibility of human disease. The major problem faced by animal models is the occurrence of spontaneous healing, which does not occur in humans.

Dermatophyte colonization on the human skin is characteristically limited to the dead keratinized tissue of the

stratum corneum and results in a mild or intense inflammatory reaction. The fungi invade the horny layer which lacks a specific immune system to combat the infection are eliminated by skin turnover with subsequent desquamation. Nevertheless, both humoral and cell-mediated reactions and specific and nonspecific host defense mechanisms respond and eventually eliminate the fungus.

Detailed research on the relationship between fungi and immunity has been reviewed by Weitzman and Summerbell [4]. Briefly described below: (1) keratinases and glycopeptides are known as the two major classes of dermatophyte antigens. Keratinases, produced by the dermatophytes to enable skin invasion, elicit delayed-type hypersensitivity (DTH) responses when injected intradermally into the skin of animals. The protein portion of the glycopeptides preferentially stimulates cell-mediated immunity (CMI), whereas the polysaccharide portion preferentially stimulates humoral immunity. However, antibodies produced by humoral immunization do not help eliminate the infection since the highest level of antibodies is found in those patients with chronic infections. Rather, the development of CMI, which is correlated with DTH, is usually associated with a clinical cure and ridding the stratum corneum of the offending dermatophyte. (2) Infections by anthropophilic fungi like *T. rubrum* often elicit less of an inflammatory response and are less likely to elicit an intense DTH response than infections caused by geophilic or zoophilic dermatophytes which characteristically evoke an intense inflammatory reaction. Much of this inflammation is produced by the activated lymphocytes and macrophages which are involved in the DTH reaction to the trichophytin glycopeptides. (3) Enhanced proliferation of the skin in response to the inflammation may be the final mechanism that removes the fungus from the skin by epidermal desquamation. (4) Mannan, a glycoprotein component of the fungal cell wall, may suppress the inflammatory response especially in atopic or other persons susceptible to the mannan-induced suppression of CMI. Incubation of purified *T. rubrum* mannan (TRM) inhibited the lymphocyte proliferation response to mitogens and various antigenic stimuli. TRM also inhibits keratinocyte proliferation, thus slowing epidermal turnover and allowing for a more persistent chronic infection. (5) Chronic dermatophytosis may be caused by the anthropophilic form of *T. mentagrophytes*, *T. mentagrophytes* var. *interdigitale* (*T. interdigitale*). Primary chronic trichophytosis may be associated with defective phagocytosis of peripheral blood leukocytes and that this defect is probably caused by the fungus itself.

Keywords to note are keratinases, glycopeptides, CMI, DTH, Mannan, phagocytosis of peripheral blood leukocytes, and skin turnover. Thus, the factors of fungi such as keratinase and glycopeptides including Mannan induce human CMI which is specially correlated with DTH, phagocytosis of peripheral blood leukocytes, and inhibition of skin turnover. In other words, the loss or decrease of these host's defense mechanisms lead to unsuccessful elimination of the fungi and may cause chronic dermatophytosis. We suggest that future experiments will be required on the relationship between fungi and immunity to overcome the challenges of the current animal model.

7. Animal Ethics

Because reproduction of human pathophysiology is hardly difficult in an *in vitro* experiment, the experiments using animals are necessary for the elucidation of unknown pathogenesis and the development of significant drugs for patients. For now, animals will undergo invasive procedures and may bleed for several weeks after surgical intervention or another way in order to make a model of dermatophytosis which must be essentially regarded as a category of chronic inflammation. Thus, we will have to plan an experiment that should follow the spirit of the 3Rs: reduction, refinement, and replacement [92]. All experimental designs should be reviewed by the Institutional Animal Care and Use Committees (IACUC) to determine whether the protocol follows the experiment facility guidelines or national guidelines [93].

8. Conclusion and Future Prospects

Using the main dermatophytosis animal model for tinea corporis, tinea pedis, and tinea unguium to elucidate the pathophysiology of human dermatophytosis and to evaluate antifungal agent efficacy, various experiments have been conducted. Reports of the tinea corporis model have been most published as comparisons of other dermatophytosis models; however, a satisfactory model has not been reported with regard to reproducibility and usefulness in the evaluation of drug efficacy because of spontaneous healing. Thus, antifungal efficacy may be estimated as greater than the actual effect. For nonspontaneous healing, the tinea pedis model has been said that the best model for dermatophytosis. This model confirmed that drug efficacy was dependent on MIC values. On the other hand, intractable tinea pedis is observed in humans. The pathology of intractable tinea pedis cannot be reproduced in this model, yet. The eradication of onychomycosis is important because onychomycosis causes the recurrence of tinea pedis or the spread of infection. However, there is no animal model that can reproduce all types of tine unguium in humans.

These difficulties in the establishment of a dermatophytosis animal model are thought to be attributed to the differences between animals and humans: the skin structure, immune system, and causative fungi. The differences in the skin structure, such as the thickness of the epidermis and horny cell layer and the number of follicles, may determine whether fungi can attach to the skin surface because experimentally infection was performed on the xenografted guinea pig skin but not on the skin of xenograft nude mice. Complex immune functions against organisms through fungal attachment are activated in order to eliminate fungi by CMI involved in DTH and skin turnover. Thus, the spontaneous healing observed in the animal model is the host's normal response. Considering the situation that many challenges remain in animal models, however, the loss or decrease in normal immune functions may be necessary in order to create a reproducible animal model. The characteristics of the causative organisms are important in the animal model because the causes to be eliminated are antigens against metabolic products by fungi and a part of the fungus itself.

With the rapid development of molecular biology in recent years has come the gradual expansion of genetic studies of *Trichophyton* spp. [94]. This body of research will enable the transformation of fungi. The creation of a transformed strain that causes lesions similar to humans, but also leads to understanding human disease, can lead to proper verification of the drug effect.

Acknowledgments

The authors would like thank Dr. Majima. This work was supported by the Health Science Research Grants for Research on Emerging and Re-emerging Infectious Diseases (H22-Shinkou-Ippan-8 and H23-Shinkou-Ippan-018), Measures for Intractable Diseases (H20-nannchi-ippann-35) from the Ministry of Health, Labor and Welfare of Japan; a grant from the Strategic Basis on Research Grounds for Non-governmental Schools at Heisei 20th from the Ministry of Education, Culture, Sports, Science and Technology of Japan to K. S; a grant from the Strategic Research Foundation Grant-Aided Project for Private Schools at Heisei 23th from Ministry of Education, Culture, Sports, Science and Technology of Japan, 2011-2015. K. Shibuya received research grants from Pfizer Inc., Janssen Pharmaceutical K. K., and Dainippon Sumitomo Pharma Co. The authors declare that they have no competing interests.

References

[1] B. Havlickova, V. A. Czaika, and M. Friedrich, "Epidemiological trends in skin mycoses worldwide," *Mycoses*, vol. 52, no. 1, p. 95, 2009.

[2] S. Fujita, "Animal models of dermatomycoses in recent years," *Japanese Journal of Medical Mycology*, vol. 38, no. 1, pp. 33–37, 1997.

[3] S. J. Rupke, "Fungal skin disorders," *Primary Care*, vol. 27, no. 2, pp. 407–421, 2000.

[4] I. Weitzman and R. C. Summerbell, "The dermatophytes," *Clinical Microbiology Reviews*, vol. 8, no. 2, pp. 240–259, 1995.

[5] B. Bloch, "Zur lehre von den dermatomykosen," *Archives of Dermatological Research*, vol. 93, no. 1-2, pp. 157–220, 1908.

[6] S. Sakai, T. kada, G. Saito, N. Muraoka, and Y. Takahashi, "Studies on chemotherapy of trichophyton infection. 1. Antifungal properties of halogen phenol esters," *Journal of the Scientific Research Institute*, vol. 46, pp. 113–117, 1952.

[7] R. Sulzmann, W. Weuffen, and A. Kramer, "Testing of antimycoticly active substances on the model of experimental cockscomb dermatophytosis. 3. Comparative histological studies of mycosis foci of the cockscomb and of the back skin of the guinea pig," *Mykosen*, vol. 14, no. 1, pp. 15–18, 1971.

[8] F. Green III and E. Balish, "Trichophyton mentagrophytes dermatophytosis in germfree guinea pig," *Journal of Investigative Dermatology*, vol. 75, no. 6, pp. 476–480, 1980.

[9] F. Green III, K. W. Lee, and E. Balish, "Chronic T. Mentagrophytes dermatophytosis of guinea pig skin grafts on nude mice," *Journal of Investigative Dermatology*, vol. 79, no. 2, pp. 125–129, 1982.

[10] R. J. Hay, R. A. Calderon, and M. J. Collins, "Experimental dermatophytosis: the clinical and histopathologic features of a mouse model using Trichophyton quinckeanum (mouse favus)," *The Journal of Investigative Dermatology*, vol. 81, no. 3, pp. 270–274, 1983.

[11] F. Green, J. K. Weber, and E. Balish, "The thymus dependency of acquired resistance to Trichophyton mentagrophytes dermatophytosis in rats," *Journal of Investigative Dermatology*, vol. 81, no. 1, pp. 31–38, 1983.

[12] J. Weber and E. Balish, "Antifungal therapy of dermatophytosis in guinea pigs and congenitally athymic rats," *Mycopathologia*, vol. 90, no. 1, pp. 47–54, 1985.

[13] J. Van Cutsem and P. A. Janssen, "Experimental systemic dermatophytosis," *Journal of Investigative Dermatology*, vol. 83, no. 1, pp. 26–31, 1984.

[14] A. G. Knight, "A review of experimental human fungus infections," *Journal of Investigative Dermatology*, vol. 59, no. 4, pp. 354–358, 1972.

[15] J. H. Reinhardt, A. M. Allen, D. Gunnison, and W. A. Akers, "Experimental human Trichophyton mentagrophytes infections," *Journal of Investigative Dermatology*, vol. 63, no. 5, pp. 419–422, 1974.

[16] H. Nakajima, "The pathophysiology and defense mechanism against superficial and subcutaneous fungal infection," *Japanese Journal of Medical Mycology*, vol. 46, no. 1, pp. 5–9, 2005.

[17] A. Treiber, W. Pittermann, and H. C. Schuppe, "Efficacy testing of antimycotic prophylactics in an animal model," *International Journal of Hygiene and Environmental Health*, vol. 204, no. 4, pp. 239–243, 2001.

[18] R. O. Nicholas, V. Berry, P. A. Hunter, and J. A. Kelly, "The antifungal activity of mupirocin," *The Journal of Antimicrobial Chemotherapy*, vol. 43, no. 4, pp. 579–582, 1999.

[19] G. Maestrone, S. Sadek, and M. Mitrovic, "Lesions of dermatophytosis in quinea pigs treated with triamcinolone acetonide: an animal model," *American Journal of Veterinary Research*, vol. 34, no. 6, pp. 833–836, 1973.

[20] K. Uchida, H. Yamaguchi, and K. Shibuya, "The therapeutic effects of itraconazole, a new triazole antifungal agent, for experimental fungal infections," *Japanese Journal of Antibiotics*, vol. 44, no. 5, pp. 588–599, 1991.

[21] K. Uchida, A. Matsuzaka, and H. Yamaguchi, "Therapeutic effect of amorolfine on experimental dermatophytosis," *The Japanese Journal of Antibiotics*, vol. 44, no. 9, pp. 1020–1031, 1991.

[22] T. Arika, M. Yokoo, T. Hase, T. Maeda, K. Amemiya, and H. Yamaguchi, "Effects of butenafine hydrochloride, a new benzylamine derivative, on experimental dermatophytosis in guinea pigs," *Antimicrobial Agents and Chemotherapy*, vol. 34, no. 11, pp. 2250–2253, 1990.

[23] T. Arika, T. Hase, and M. Yokoo, "Anti-Trichophyton mentagrophytes activity and percutaneous permeation of butenafine in guinea pigs," *Antimicrobial Agents and Chemotherapy*, vol. 37, no. 2, pp. 363–365, 1993.

[24] K. P. Fu, D. M. Isaacson, J. Lococo, B. Foleno, and J. Hilliard, "In vitro and in vivo antidermatophytic activity of saperconazole a new fluorinated triazole," *Drugs under Experimental and Clinical Research*, vol. 18, no. 11-12, pp. 443–446, 1992.

[25] H. Oka, Y. Niwano, T. Ohmi, T. Tanake, M. Uchida, and H. Yamaguchi, "Therapeutic efficacy of latoconazole in formulations of clinical use on experimental dermatophytosis in guinea pigs," *Arzneimittel-Forschung/Drug Research*, vol. 42, no. 3, pp. 345–349, 1992.

[26] K. Uchida and H. Yamaguchi, "Therapeutic efficacy of terbinafine creams, a new allylamine antimycotic, in guinea pig dermatophytosis model," *Japanese Journal of Medical Mycology*, vol. 32, no. 4, pp. 333–342, 1991.

[27] K. Nagino, H. Shimohira, M. Ogawa, K. Uchida, and H. Yamaguchi, "Comparison of the therapeutic efficacy of oral doses of fluconazole and itraconazole in a guinea pig model of dermatophytosis," *Journal of Infection and Chemotherapy*, vol. 6, no. 1, pp. 41–44, 2000.

[28] K. Nagino, H. Shimohira, M. Ogawa, K. Uchida, and H. Yamaguchi, "Comparison of the therapeutic efficacy of oral doses of fluconazole and griseofulvin in a guinea pig model of dermatophytosis," *Journal of Antibiotics*, vol. 53, no. 2, pp. 207–210, 2000.

[29] K. Uchida and H. Yamaguchi, "Therapeutic efficacy of oral administration of terbinafine in guinea pig trichophytosis model," *Japanese Journal of Medical Mycology*, vol. 34, no. 4, pp. 485–491, 1993.

[30] Y. Niwano, T. Tabuchi, K. Kanai, H. Hamaguchi, K. Uchida, and H. Yamaguchi, "Therapeutic efficacy of lanoconazole ointment in guinea pig model of tinea corporis, a comparative study with ointment and cream preparations," *Japanese Journal of Antibiotics*, vol. 48, no. 1, pp. 150–154, 1995.

[31] R. M. Parmegiani, D. Loebenberg, A. Cacciapuoti et al., "Sch 39304, a new antifungal agent: oral and topical treatment of vaginal and superficial infections," *Journal of Medical and Veterinary Mycology*, vol. 31, no. 3, pp. 239–248, 1993.

[32] T. Hashiguchi, A. Ryu, T. Itoyama, K. Uchida, and H. Yamaguchi, "Study of the effective dose of a topical antifungal agent, omoconazole nitrate, on the basis of percutaneous pharmacokinetics in guinea-pigs and mice," *Journal of Pharmacy and Pharmacology*, vol. 49, no. 8, pp. 757–761, 1997.

[33] Y. Tatsumi, M. Yokoo, T. Arika, and H. Yamaguchi, "KP-103, a novel triazole derivative, is effective in preventing relapse and successfully treating experimental interdigital tinea pedis and tinea corporis in guinea pigs," *Microbiology and Immunology*, vol. 46, no. 7, pp. 425–432, 2002.

[34] H. Tagami, S. Watanabe, and S. Ofuji, "Trichophytin contact sensitivity in guinea pigs with experimental dermatophytosis induced by a new inoculation method," *Journal of Investigative Dermatology*, vol. 61, no. 4, pp. 237–241, 1973.

[35] K. Uchida, S. Yamashita, and H. Yamaguchi, "Therapeutic effect of bifonazole, a topical imidazole antimycotic agent, on experimental Trichophyton mentagrophytes infection," *Chemotherapy*, vol. 32, no. 11, pp. 842–854, 1984.

[36] K. Uchida and H. Yamaguchi, "Oxiconazole nitrate, a new imidazole-antimycotic: evaluation of antifungal activity in vivo," *Chemotherapy*, vol. 32, no. 9, pp. 585–601, 1984.

[37] M. E. Valiant and B. M. Frost, "An experimental model for evaluation of antifungal agents in a Trichophyton mentagrophytes infection of guinea pigs," *Chemotherapy*, vol. 30, no. 1, pp. 54–60, 1984.

[38] J. H. Greenberg, R. D. King, S. Krebs, and R. Field, "A quantitative dermatophyte infection model in the guinea pig: a parallel to the quantitated human infection model," *Journal of Investigative Dermatology*, vol. 67, no. 6, pp. 704–708, 1976.

[39] S. Kerbs, J. Greenberg, and K. Jesrani, "Temporal correlation of lymphocyte blastogenesis, skin test responses and erythema during dermatophyte infections," *Clinical and Experimental Immunology*, vol. 27, no. 3, pp. 526–530, 1977.

[40] G. Petranyi, J. G. Meingassner, and H. Mieth, "Activity of terbinafine in experimental fungal infections of laboratory animals," *Antimicrobial Agents and Chemotherapy*, vol. 31, no. 10, pp. 1558–1561, 1987.

[41] H. Mieth, I. Leitner, and J. G. Meingassner, "The efficacy of orally applied terbinafine, itraconazole and fluconazole in models of experimental trichophytoses," *Journal of Medical and Veterinary Mycology*, vol. 32, no. 3, pp. 181–188, 1994.

[42] S. Kerbs and A. M. Allen, "Effect of occlusion on Trichophyton mentagrophytes infections in guinea pigs," *Journal of Investigative Dermatology*, vol. 71, no. 5, pp. 301–304, 1978.

[43] F. Green III, J. W. Anderson, and E. Balish, "Cutaneous basophil hypersensitivity and contact sensitivity after cutaneous Trichophyton mentagrophytes infection," *Infection and Immunity*, vol. 29, no. 2, pp. 758–767, 1980.

[44] C. Palacin, A. Sacristan, and J. A. Ortiz, "In vivo activity of sertaconazole in experimental dermatophytosis in guinea pigs," *Arzneimittel-Forschung A*, vol. 42, no. 5, pp. 714–718, 1992.

[45] A. Mikaeili, M. Modaresi, I. Karimi, H. Ghavimi, M. Fathi, and N. Jalilian, "Antifungal activities of astragalus verus olivier. against trichophyton verrucosum on in vitro and in vivo guinea pig model of dermatophytosis," *Mycoses*. In press.

[46] H. Yamaguchi and K. Uchida, "In vivo activity of bifonazole in guinea pigs: its characteristic features and comparison with clotrimazole," *Dermatologica*, vol. 169, supplement 1, pp. 33–45, 1984.

[47] M. A. Ghannoum, M. A. Hossain, L. Long, S. Mohamed, G. Reyes, and P. K. Mukherjee, "Evaluation of antifungal efficacy in an optimized animal model of Trichophyton mentagrophytes-dermatophytosis," *Journal of Chemotherapy*, vol. 16, no. 2, pp. 139–144, 2004.

[48] M. A. Ghannoum, L. Long, H. G. Kim, A. J. Cirino, A. R. Miller, and P. Mallefet, "Efficacy of terbinafine compared to lanoconazole and luliconazole in the topical treatment of dermatophytosis in a guinea pig model," *Medical Mycology*, vol. 48, no. 3, pp. 491–497, 2010.

[49] X. J. Chen, Y. N. Shen, G. X. Lü, and W. D. Liu, "Establishing an experimental guinea pig model of dermatophytosis using Trichophyton rubrum," *Acta Academiae Medicinae Sinicae*, vol. 30, no. 5, pp. 599–602, 2008.

[50] K. de Wit, C. Paulussen, A. Matheeussen, K. van Rossem, P. Cos, and L. Maes, "In vitro profiling of pramiconazole and in vivo evaluation in Microsporum canis dermatitis and Candida albicans vaginitis laboratory models," *Antimicrobial Agents and Chemotherapy*, vol. 54, no. 11, pp. 4927–4929, 2010.

[51] D. M. Saunte, J. P. Hasselby, A. Brillowska-Dabrowska et al., "Experimental guinea pig model of dermatophytosis: a simple and useful tool for the evaluation of new diagnostics and antifungals," *Medical Mycology*, vol. 46, no. 4, pp. 303–313, 2008.

[52] K. Uchida and H. Yamaguchi, "Assessment of in vivo activity of bifonazole against dermatophytic infection in guinea pigs on the basis of the amount of a specific fungal cell wall component chitin in the infected skin," *Dermatologica*, vol. 169, supplement 1, pp. 47–50, 1984.

[53] Z. Hussin and J. M. Smith, "Vaccination procedures and the infectivity of dermatophyte lesions," *Mycopathologia*, vol. 81, no. 2, pp. 71–76, 1983.

[54] L. Wearley, B. Antonacci, A. Cacciapuoti et al., "Relationship among physicochemical properties, skin permeability, and topical activity of the racemic compound and pure enantiomers of new antifungal," *Pharmaceutical Research*, vol. 10, no. 1, pp. 136–140, 1993.

[55] N. Chittasobhon and J. M. Smith, "The production of experimental dermatophyte lesions in guinea pigs," *Journal of Investigative Dermatology*, vol. 73, no. 2, pp. 198–201, 1979.

[56] A. F. Bonk, L. Friedman, and V. J. Derbes, "Experimental dermatophytosis," *The Journal of Investigative Dermatology*, vol. 39, pp. 281–286, 1962.

[57] D. M. Saunte, F. Simmel, N. Frimodt-Moller et al., "In vivo efficacy and pharmacokinetics of voriconazole in an animal model of dermatophytosis," *Antimicrobial Agents and Chemotherapy*, vol. 51, no. 9, pp. 3317–3321, 2007.

[58] M. A. Ghannoum, L. Long, and W. R. Pfister, "Determination of the efficacy of terbinafine hydrochloride nail solution in the topical treatment of dermatophytosis in a guinea pig model," *Mycoses*, vol. 52, no. 1, pp. 35–43, 2009.

[59] F. Odds, J. Ausma, F. Van Gerven et al., "In vitro and in vivo activities of the novel azole antifungal agent R126638," *Antimicrobial Agents and Chemotherapy*, vol. 48, no. 2, pp. 388–391, 2004.

[60] H. Yamaguchi and K. Uchida, "Once daily administration of terbinafine to guinea-pigs with experimental dermatophytosis," *Clinical and Experimental Dermatology*, vol. 14, no. 2, pp. 108–109, 1989.

[61] S. Fujita, "Conditions required for successful experimental dermatophytosis and its histopathogenesis," *Japanese Journal of Medical Mycology*, vol. 33, no. 2, pp. 115–125, 1992.

[62] K. Uchida and H. Yamaguchi, "Preclinical therapeutic evaluation of agents for treating dermatophytosis," *Japanese Journal of Medical Mycology*, vol. 37, no. 4, pp. 199–205, 1996.

[63] J. Van Cutsem, "Animal models for dermatomycotic infections," *Current Topics in Medical Mycology*, vol. 3, pp. 1–35, 1989.

[64] H. Koga, "Animal model for superficial mycosis," *Japanese Journal of Medical Mycology*, vol. 50, no. 2, pp. 84–89, 2009.

[65] A. Polak, "Combination of amorolfine with various antifungal drugs in dermatophytosis," *Mycoses*, vol. 36, no. 1-2, pp. 43–49, 1993.

[66] S. Fujita and T. Matsuyama, "Experimental tinea pedis induced by non-abrasive inoculation of Trichophyton mentagrophytes arthrospores on the plantar part of a guinea pig foot," *Journal of Medical and Veterinary Mycology*, vol. 25, no. 4, pp. 203–213, 1987.

[67] K. Uchida and H. Yamaguchi, "Effectiveness of oral treatment with terbinafine in a guinea pig model of tinea pedis," *Japanese Journal of Antibiotics*, vol. 47, no. 10, pp. 1401–1406, 1994.

[68] S. Fujita, T. Matsuyama, and Y. Sato, "Experimental tinea pedis in guinea pig feet—scanning electron microscopic and histological study of the infection," *Japanese Journal of Medical Mycology*, vol. 29, no. 3, pp. 163–168, 1988.

[69] S. Fujita, Y. Kaneko, Y. Sato, and T. Matsuyama, "Invasiveness of infecting fungi and tissue response in experimental tinea pedis in guinea pigs," *Japanese Journal of Medical Mycology*, vol. 30, no. 4, pp. 233–240, 1989.

[70] Y. Niwano, T. Tabuchi, K. Kanai, H. Hamaguchi, K. Uchida, and H. Yamaguchi, "Therapeutic efficacy of lanoconazole ointment in guinea pig model of tinea pedis, in comparison with that of cream preparations," *Japanese Journal of Antibiotics*, vol. 47, no. 9, pp. 1192–1195, 1994.

[71] Y. Niwano, T. Tabuchi, K. Kanai, H. Hamaguchi, K. Uchida, and H. Yamaguchi, "Short-term topical therapy of experimental tinea pedis in guinea pigs with lanoconazole, a new imidazole antimycotic agent," *Antimicrobial Agents and Chemotherapy*, vol. 39, no. 10, pp. 2353–2355, 1995.

[72] Y. Niwano, N. Kuzuhara, H. Kodama, M. Yoshida, T. Miyazaki, and H. Yamaguchi, "In vitro and in vivo antidermatophyte activities of NND-502, a novel optically active imidazole antimycotic agent," *Antimicrobial Agents and Chemotherapy*, vol. 42, no. 4, pp. 967–970, 1998.

[73] K. Uchida, M. Kudoh, and H. Yamaguchi, "A study on effectiveness of treatment and prevention of relapse using topical administration of terbinafine in a guinea pig model for tinea pedis," *The Japanese Journal of Antibiotics*, vol. 47, no. 10, pp. 1407–1412, 1994.

[74] T. Itoyama, K. Uchida, H. Yamaguchi, and S. Fujita, "Therapeutic effects of omoconazole nitrate on experimental tinea pedis, an intractable dermatophytosis, in guinea-pigs," *Journal of Antimicrobial Chemotherapy*, vol. 40, no. 3, pp. 441–444, 1997.

[75] K. Uchida and H. Ymaguchi, "Therapeutic efficacy of a topical antifungal solution preparation formulated with pyrrolnitrin and clotrimazole in combination (Pyroace) in guinea pig model of tinea pedis," *Japanese Journal of Antibiotics*, vol. 52, no. 1, pp. 68–74, 1999.

[76] H. Yamaguchi, K. Uchida, T. Tanaka, and T. Yamaguchi, "Therapeutic efficacy of a topical tolnaftate preparation in guinea pig model of tinea pedis," *The Japanese Journal of Antibiotics*, vol. 54, no. 6, pp. 323–330, 2001.

[77] K. Uchida, T. Tanaka, and H. Yamaguchi, "Achievement of complete mycological cure by topical antifungal agent NND-502 in guinea pig model of tinea pedis," *Microbiology and Immunology*, vol. 47, no. 2, pp. 143–146, 2003.

[78] T. Arika, M. Yokoo, T. Maeda, K. Ameniya, and H. Yamaguchi, "Effects of butenafine hydrochloride, a new benzylamine derivative, on experimental tinea pedis in guinea pigs," *Antimicrobial Agents and Chemotherapy*, vol. 34, no. 11, pp. 2254–2255, 1990.

[79] T. Arika, M. Yokoo, and H. Yamaguchi, "Topical treatment with butenafine significantly lowers relapse rate in an interdigital tinea pedis model in guinea pigs," *Antimicrobial Agents and Chemotherapy*, vol. 36, no. 11, pp. 2523–2525, 1992.

[80] T. Ohmi, S. Konaka, M. Uchida, and H. Yamaguchi, "Antifungal activity of the new agent latoconazole in two tinea models," *Arzneimittel-Forschung/Drug Research*, vol. 41, no. 8, pp. 847–851, 1991.

[81] Y. Tatsumi, M. Yokoo, T. Arika, and H. Yamaguchi, "In vivo fungicidal effect of KP-103 in a guinea pig model of interdigital tinea pedis determined by using a new method for removing the antimycotic carryover effect," *Microbiology and Immunology*, vol. 46, no. 7, pp. 433–439, 2002.

[82] S. Watanabe, H. Takahashi, T. Nishikawa et al., "A comparative clinical study between 2 weeks of luliconazole 1% cream treatment and 4 weeks of bifonazole 1% cream treatment for tinea pedis," *Mycoses*, vol. 49, no. 3, pp. 236–241, 2006.

[83] Y. Tatsumi, M. Yokoo, H. Senda, and K. Kakehi, "Therapeutic efficacy of topically applied KP-103 against experimental tinea unguium in guinea pigs in comparison with amorolfine and terbinafine," *Antimicrobial Agents and Chemotherapy*, vol. 46, no. 12, pp. 3797–3801, 2002.

[84] T. Shimamura, N. Kubota, S. Nagasaka, T. Suzuki, H. Mukai, and K. Shibuya, "Establishment of a novel model of onychomycosis in rabbits for evaluation of antifungal agents," *Antimicrobial Agents and Chemotherapy*, vol. 55, no. 7, pp. 3150–3155, 2011.

[85] J. Lauharanta, "Comparative efficacy and safety of amorolfine nail lacquer 2% versus 5% once weekly," *Clinical and Experimental Dermatology, Supplement*, vol. 17, no. 1, pp. 41–43, 1992.

[86] D. Reinel and C. Clarke, "Comparative efficacy and safety of amorolfine nail lacquer 5% in onychomycosis, once-weekly versus twice-weekly," *Clinical and Experimental Dermatology, Supplement*, vol. 17, no. 1, pp. 44–49, 1992.

[87] A. K. Gupta and W. S. Joseph, "Ciclopirox 8% nail lacquer in the treatment of onychomycosis of the toenails in the United States," *Journal of the American Podiatric Medical Association*, vol. 90, no. 10, pp. 495–501, 2000.

[88] T. Nakashima, A. Nozawa, T. Ito, T. Majima, and H. Yamaguchi, "Development of a new medium useful for the recovery of dermatophytes from clinical specimens by minimizing the carryover effect of antifungal agents," *Microbiology and Immunology*, vol. 46, no. 2, pp. 83–88, 2002.

[89] M. Adachi and S. Watanabe, "Evaluation of combined deactivators-supplemented agar medium (CDSAM) for recovery of dermatophytes from patients with tinea pedis," *Medical Mycology*, vol. 45, no. 4, pp. 347–349, 2007.

[90] T. Majima, S. Masui, K. Uchida, and H. Yamaguchi, "A novel mycological analysis valuable for evaluating therapeutic efficacy of antimycotics against experimental dermatophytosis in guinea pigs," *Mycoses*, vol. 48, no. 2, pp. 108–113, 2005.

[91] T. Nakashima, A. Nozawa, T. Ito, and T. Majima, "Experimental tinea unguium model to assess topical antifungal agents using the infected human nail with dermatophyte in vitro," *Journal of Infection and Chemotherapy*, vol. 8, no. 4, pp. 331–335, 2002.

[92] W. M. S. Russell and R. L. Burch, *The Principles of Humane Experimental Technique*, Methuen & Co., London, UK, 1959.

[93] Institute of Laboratory Animal Resources-National Research Council, *Guide for the Care and Use of Laboratory Animals*, National Academy Press, Washington, DC, USA, 8th edition, 2011.

[94] T. Yamada, "Molecular approach to pathology of and immunity against dermatophytes," *Japanese Journal of Medical Mycology*, vol. 49, no. 4, pp. 293–297, 2008.

Hindawi Publishing Corporation
Journal of Biomedicine and Biotechnology
Volume 2012, Article ID 728178, 8 pages
doi:10.1155/2012/728178

Research Article

Proteomic Characterization of a Mouse Model of Familial Danish Dementia

Monica Vitale,[1,2] Giovanni Renzone,[3] Shuji Matsuda,[4] Andrea Scaloni,[3] Luciano D'Adamio,[4] and Nicola Zambrano[1,2]

[1] *Dipartimento di Biochimica e Biotecnologie Mediche, Università degli Studi di Napoli Federico II, 80131 Napoli, Italy*
[2] *CEINGE Biotecnologie Avanzate, 80145 Napoli, Italy*
[3] *Proteomics and Mass Spectrometry Laboratory, ISPAAM, National Research Council, 80147 Napoli, Italy*
[4] *Department of Microbiology and Immunology, Albert Einstein College of Medicine, Bronx, NY 10462, USA*

Correspondence should be addressed to Nicola Zambrano, zambrano@unina.it

Received 30 December 2011; Accepted 2 February 2012

Academic Editor: Monica Fedele

A dominant mutation in the *ITM2B/BRI2* gene causes familial Danish dementia (FDD) in humans. To model FDD in animal systems, a knock-in approach was recently implemented in mice expressing a wild-type and mutant allele, which bears the FDD-associated mutation. Since these FDD_{KI} mice show behavioural alterations and impaired synaptic function, we characterized their synaptosomal proteome via two-dimensional differential in-gel electrophoresis. After identification by nanoliquid chromatography coupled to electrospray-linear ion trap tandem mass spectrometry, the differentially expressed proteins were classified according to their gene ontology descriptions and their predicted functional interactions. The Dlg4/Psd95 scaffold protein and additional signalling proteins, including protein phosphatases, were revealed by STRING analysis as potential players in the altered synaptic function of FDD_{KI} mice. Immunoblotting analysis finally demonstrated the actual downregulation of the synaptosomal scaffold protein Dlg4/Psd95 and of the dual-specificity phosphatase Dusp3 in the synaptosomes of FDD_{KI} mice.

1. Introduction

Familial Danish Dementia (FDD) is a neurodegenerative disease characterized by early cataracts, deafness, progressive ataxia, and dementia. Patients with FDD show diffuse brain atrophy and widespread amyloid angiopathy. In FDD, neurofibrillary tangles (NFTs) are the major histological finding in the hippocampus [1–3]. FDD is an autosomal dominant disease caused by the accumulation of the amyloidogenic C-terminal 34 amino acid peptide of BRI2. BRI2, a product of the *ITM2B/BRI2* gene, is a type II transmembrane protein of unknown function. Physiologically, BRI2 is cleaved at the C-terminus by furin endoprotease, producing a 23-amino acid soluble C-terminal fragment [2]. FDD is caused by a decamer duplication in the 3′ region of the *ITM2B/BRI2* gene. This mutation produces a longer 34 amino acid C-terminal fragment that accumulates as amyloid [4, 5].

FDD and Alzheimer's disease (AD) share neuropathological features, including amyloid deposition and neurodegeneration in the central nervous system [6–8]. The mature form of BRI2 is able to reduce accumulation of the Aβ peptide [9–12] while APP catabolites, including Aβ, were significantly increased in the brain of FDD patients [13]. The interaction between these two amyloidogenic proteins (BRI2 and APP) can be relevant for the design of new therapeutic strategies for FDD and AD.

To model FDD pathogenesis in animals, several mouse lines have been generated and analyzed so far [14], which include transgenic mice expressing wild-type [15] or mutant [16, 17] BRI2 proteins, as well as *ITM2B/BRI2* gene knock-out mice [10] or *ITM2B/BRI2* knock-in mutant mice [18]. The transgenic mice overexpressing the FDD-associated mutation of human *ITM2B/BRI2* partially recapitulated the main histopathological features of FDD; they indeed developed cerebral amyloid angiopathy, parenchymal amyloid deposition, and neuroinflammation [14, 16]. Age-dependent deposition of Danish amyloid peptide was also observed in the brain of a second transgenic model, with associated angiopathy and microhemorrhage, neuritic dystrophy, and neuroinflammation [17]. In this model, deposition of

the Danish peptide also accelerated Tau pathology in a double transgenic model with mutant *ITM2B/BRI2* and *Tau* (P301S) constructs.

To study the pathogenesis of FDD in the absence of potential artifacts due to transgenic overexpression of the mutant protein, a refined mouse model has been recently generated, which is based on a knock-in approach where the exon 6 of the murine *ITM2B/BRI2* gene was substituted for by a mutant sequence carrying the human FDD mutation [18]. The analysis of FDD_{KI} mouse model, carrying a mutant and a wild-type *ITM2B/BRI2* allele, has shown that the Danish mutation causes impaired synaptic plasticity and deficits in hippocampal memory, in the absence of cerebral deposits and lesions [19]. A similar scenario applies to a Familial British Dementia (FBD) knock-in model, in which the dominant, mutant *ITM2B/BRI2* allele responsible for FBD is associated to memory deficits and loss of BRI2 function, without the histopathological alterations typical to neurodegenerative disorders [20]. In agreement with the previously reported function of BRI2 in the stabilization of APP holoprotein [9, 12], FDD_{KI} mice also show decreased BRI2 protein levels and increased levels of APP catabolites [19]; the latter evidence recapitulated the occurrence of increased APP metabolites in the brain of an FDD patient [13]. The functional link between *ITM2B/BRI2* and *APP* genes is also strongly supported by the genetic suppression of memory and synaptic dysfunctions in FDD_{KI} mice by *APP* haplodeficiency [19] or inhibition of APP cleavage by β-secretase [20]. The functional association between *ITM2B/BRI2* and *APP* genes strongly supports the participation of the encoded proteins to synaptic dysfunction. Accordingly, decreased levels of BRI2/APP complexes have been observed in the synaptic membranes of FDD_{KI} mice [19].

In this paper, we profiled the expression pattern of synaptosomal proteins in the FDD_{KI} mouse model, via differential expression analysis based on two-dimensional differential in-gel electrophoresis (2D-DIGE) in combination with tandem mass spectrometry. Our validated results showed decreased representation of the synaptosomal scaffold protein Psd95/Dlg4 and of the Dusp3 phosphatase in the FDD_{KI} synaptosomes.

2. Materials and Methods

2.1. Mice, Preparation of Synaptosomal Extracts, and 2D-DIGE Analysis. Mice were handled according to the Ethical Guidelines for Treatment of Laboratory Animals of the Albert Einstein College of Medicine. The procedures were described and approved in animal protocol number 200404. FDD_{KI} mice were on a C57BL/6J background. Crude synaptosomal fractions containing both membrane and soluble synaptosomal proteins were obtained from three biological replicates each of wild-type (C57BL/6J) or FDD_{KI} mice, as described in [13]. Briefly, mouse brain homogenates in Hepes-sucrose buffer (20 mM Hepes/NaOH pH 7.4, 1 mM EDTA, 1 mM EGTA, and 0.25 M sucrose) supplemented with protease and phosphatase inhibitors (wt/vol = 10 mg tissue/100 mL buffer) were centrifuged at 800 ×g for 10 min, at 4°C. The supernatant (S1, total brain extract) was separated into supernatant (S2) and pellet (P2) by centrifugation at 9,200 ×g for 15 min, at 4°C. P2 fractions, representing the crude synaptosomal fractions, were resuspended in 7 M urea, 2 M thiourea, 4% CHAPS to extract the whole synaptosomal content, then precipitated in acetone/methanol (8 : 1, v : v) for 16 h, at −20°C, and finally recovered by centrifugation at 16,000 ×g for 30 min, at 4°C. The synaptosomal proteins were resuspended in 7 M urea, 2 M thiourea, 4% CHAPS, and 30 mM Tris-HCl; protein concentration was determined by using the Bradford method (Bio-Rad). Before labelling, the pH of the samples was adjusted to pH 8.5 with HCl solutions; each labelling reaction was performed in a 10 μL volume with 50 μg of the synaptosomal proteins, in the presence of 400 pmol of Cy2-, Cy3-, or Cy5-dyes (minimal labelling dyes, GE Healthcare). A dye-swapping strategy was used to label samples; accordingly, two samples from wild-type synaptosomal extracts were labelled with Cy3, while the third was labelled with Cy5; in a complementary manner, two samples from FDD_{KI} extracts were labelled with Cy5, and the third was labelled with Cy3. Three mixtures of the 6 samples (50 μg each) were also labelled with Cy2 dye, as the internal standard required for the 2D-DIGE procedure. The labelling was performed for 30 min, at 0°C, in the dark, and was chased by the addition of 1 mM lysine. Three sample mixtures, made of appropriate Cy3- and Cy5-labeled pairs and a Cy2-labeled control, were supplemented with 1% (v/v) IPG buffer, pH 3–10 NL (GE Healthcare), 1.4% (v/v) DeStreak reagent (GE Healthcare), and 0.2% (w/v) DTT to a final volume of 450 μL in 7 M urea, 2 M thiourea, and 4% CHAPS. The mixtures (150 μg of total protein content) were used to passively hydrate the immobilized pH gradient IPG gel strips (24 cm, pH 3–10 NL) for 16 h, at 20°C. Isoelectric focusing (IEF) was carried out with an IPGphor II apparatus (GE Healthcare) up to 75,000 V/h, at 20°C (current limit set to 50 μA per strip). The strips were equilibrated in 6 M urea, 2% SDS, 20% glycerol, and 0.375 M Tris-HCl (pH 8.8), for 15 min, in the dark, in the presence of 0.5% (w : v) DTT, and then in the presence of 4.5% (w/v) iodoacetamide in the same buffer, for additional 15 min. Equilibrated IPG stripss were transferred onto 12% polyacrylamide gels, within low-fluorescence glass plates (ETTAN-DALT 6 system, GE Healthcare). The second-dimension SDS-PAGE was performed by using a DALT II electrophoresis unit (GE Healthcare) at 2 W/gel for 12 h. Gels were scanned with a Typhoon 9400 variable mode imager (GE Healthcare), using appropriate excitation/emission wavelengths for Cy2 (488/520 nm), Cy3 (532/580 nm), and Cy5 (633/670 nm). Images were acquired in the Image-Quant software (GE Healthcare) and analyzed by using the DeCyder 6.0 software (GE Healthcare). A DeCyder differential in-gel-analysis (DIA) module was used for spot detection and pairwise comparison of each sample (Cy3 and Cy5) to the Cy2, mixed standard present in each gel. The DeCyder biological variation analysis (BVA) module was then used to simultaneously match all of the protein-spot maps from the gels, and to calculate average abundance ratios and P values across the triplicate sets of samples (Student's t-test).

For preparative protein separations, 500 μg of unlabeled protein samples from pooled, wild-type, and FDD_{KI} synaptosomal samples were used for passive hydration of 24 cm strips for the first gel dimension (pH 3–10 NL IPG strips, GE Healthcare). The first and second dimension runs were carried out as described above. After 2-DE, gels were fixed and stained with SyproRuby fluorescent stain (Invitrogen). After spot matching with the master gel from the analytical step in the BVA module of DeCyder software, a pick list was generated for spot picking by a robotic picker (Ettan spot picker, GE Healthcare).

2.2. Protein Identification and Bioinformatic Analysis. Spots from 2-DE were excised from gels, minced and washed with water. Proteins were *in-gel* reduced, S-alkylated, and digested with trypsin, as previously reported [21]. Protein digests were subjected to a desalting/concentration step on μZipTipC18 pipette tips (Millipore Corp., Bedford, MA, USA) and then analyzed by nanoLC-ESI-LIT-MS/MS using a LTQ XL mass spectrometer (ThermoFinnigan, USA) equipped with Proxeon nanospray source connected to an Easy-nanoLC (Proxeon, Denmark) [21, 22]. Peptide mixtures were separated on an Easy C_{18} column (10×0.075 mm, 3 μm) (Proxeon) using a gradient of acetonitrile containing 0.1% formic acid in aqueous 0.1% formic acid; acetonitrile ramped from 5% to 35% over 15 min and from 35% to 95% over 2 min, at a flow rate of 300 nL/min. Spectra were acquired in the range m/z 400–2000. Acquisition was controlled by a data-dependent product ion-scanning procedure over the three most abundant ions, enabling dynamic exclusion (repeat count 2 and exclusion duration 1 min). The mass isolation window and collision energy were set to *m/z* 3 and 35%, respectively. MASCOT software package version 2.2.06 (Matrix Science, UK) [23] was used to identify spots unambiguously from a nonredundant sequence database (all taxa UniProtKB 2010/01/09). NanoLC-ESI-LIT-MS/MS data were searched by using a mass tolerance value of 2 Da for precursor ion and 0.8 Da for MS/MS fragments, trypsin as proteolytic enzyme, a missed cleavages maximum value of 2 and Cys carbamidomethylation, and Met oxidation as fixed and variable modification, respectively. Candidates with more than 2 assigned peptides with an individual MASCOT score >25, both corresponding to $P < 0.05$ for a significant identification, were further evaluated by the comparison with their calculated mass and pI values, using the experimental values obtained from 2-DE.

Search for functional interaction between proteins identified by MS analysis was performed using the String v. 8.3 database (http://string83.embl.de/) [24]. Gene ontology classification of the identified proteins was performed through the web-accessible DAVID (v 6.7) annotation system (http://david.abcc.ncifcrf.gov/home.jsp) [25, 26]. Briefly, the identified proteins were converted into RefSeq-protein identifiers through the DAVID Gene ID conversion tool; the new list was then submitted to functional annotation clustering.

2.3. Antibodies and Western Blotting. Western blot analysis was used to validate differential expression data obtained by proteomic analysis. Triplicate synaptosomal samples from wild-type and FDD_{KI} mice were separated on 10% polyacrylamide gels by SDS-PAGE and then blotted on PVDF membranes (GE Healthcare). Filters were blocked in PBS containing 5% nonfat dry milk and incubated with 1 : 250 dilutions of the different primary antibodies, obtained from Santa Cruz Biotechnology, except for $\alpha-$tubulin (DM1A; Sigma) antibody. Appropriate secondary IgG horseradish peroxidase conjugated was used as secondary antibody (Southern Biotechnology); bands were visualised by the ECL kit (GE Healthcare).

3. Results and Discussion

3.1. Differentially Expressed Proteins in Synaptosomes of FDD_{KI} Mice. In order to characterize the synaptosomal proteome of the available mouse model of FDD, we used the differential in-gel electrophoresis approach (2D-DIGE), which was applied to synaptosomal extracts from wild-type and FDD_{KI} mice. Indeed, three biological replicates of synaptosomal preparations from wild-type and FDD_{KI} mice were generated for protein extraction and fluorescence labelling with Cy-dyes. Analysis of the 2D-DIGE images, according to the DeCyder bioinformatic software, allowed us to detect about 2,000 matched protein spots within the three gels. We performed a quantitative and statistical analysis under parameters defined as relative expression ratio in FDD_{KI} versus WT mice of >1.25 for protein spots upregulated and of <−1.25 for protein spots downregulated, with a P value <0.05. We found that twelve spots appeared to be deregulated (circled in Figure 1(a)); in particular, four protein spots were upregulated, whereas eight protein spots were downregulated, in FDD_{KI} versus WT mice.

In order to identify the differentially expressed proteins, the spots of interest were matched to the corresponding ones from a preparative gel stained with fluorescent stain SyproRuby (yellow circles in Figure 1(b)), which were then individually excised, digested with trypsin, and finally identified by nanoLC-ESI-LIT-MS/MS analysis, as detailed in Methods. Table 1 summarizes the relative spot expression ratios in FDD_{KI} versus WT mice as well as the mass spectrometry data for the corresponding identified proteins.

3.2. Functional Classification of the Identified Proteins. In order to find relevant proteins among the multiple identifications obtained by proteomic analysis, we subjected the list of the 13 proteins from Table 1 to bioinformatic analysis in the String database, which integrates interaction data from several bioinformatic sources and provides information about physical and functional, known and predicted interactions of genes and their products [24] (Figure 2). String analysis showed that Dlg4 protein is directly linked to 4 additional proteins, namely Ppp3ca, Hspa8, Atp6v1a, and Gnb1. The evidences responsible for those functional associations are mainly experimental (purple line), and reflect protein-protein interactions [27–29]. Indeed, Dlg4, also known as post-synaptic density protein 95 (Psd95), contributes to the organization of multiprotein complexes at the postsynaptic

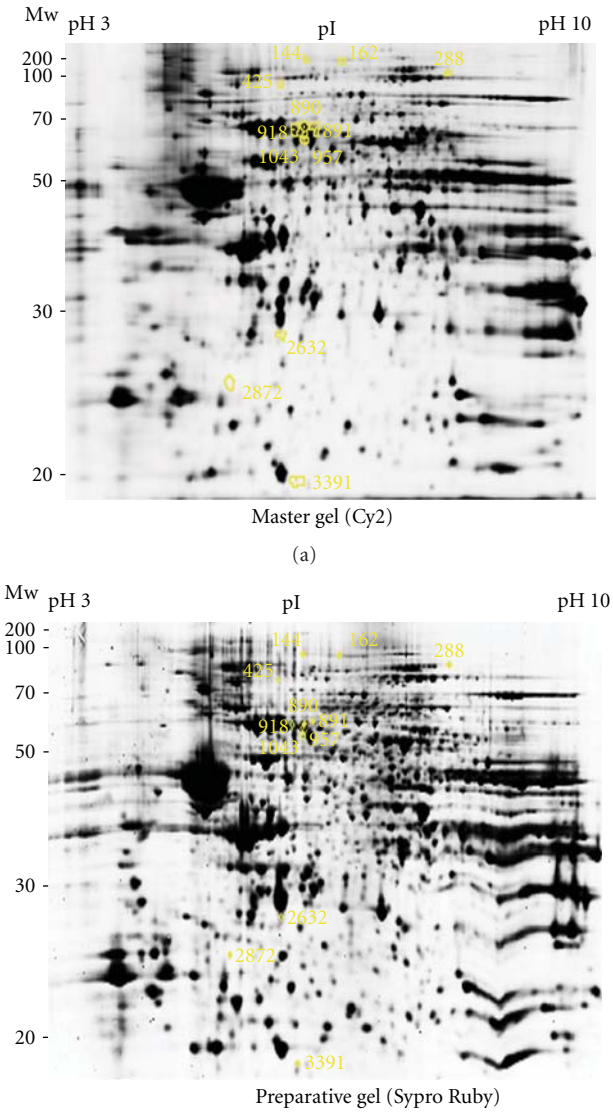

Figure 1: 2-DE map of the differentially expressed protein spots. The figure shows the position on the master (a) and on the preparative (b) gels of the 12 deregulated spots, according to the differential expression analysis of proteins from wild-type and FDD_{KI} mouse synaptosomes. In (a), the deregulated spots are surrounded by a yellow border; matched spots within the preparative gel (b) are highlighted by a yellow circle, which also denotes the picking surface for the robotic spot picker. The representative image reported in (a) shows the Cy2-labelled proteins on the scanned master gel; protein spots in (b) were visualized by Sypro Ruby fluorescent staining. Mw: molecular weight; pI: isoelectric point.

contact zone, via its multiple protein interaction domains. This molecular network is made of receptors (i.e., NMDA and AMPA receptors), small signalling proteins (i.e., Ras-GAP), cell adhesion and cytoskeletal proteins, as well as protein kinases (i.e., CaMKII), thus organizing receptors and signal transduction molecules at the synaptic contact zone [30, 31]. On its own, Gnb1 is also tightly connected to Gnb2; indeed, the two proteins are the beta 1 and beta 2 components of heterotrimeric G protein complexes, respectively. These proteins share a high protein sequence identity (>90%) in mouse, in fact they were coidentified in spot 2632 (Table 1). Additional associations involving the differentially expressed proteins in FDD_{KI} mice involved the kinesin family member 5A (Kif5a), a microtubule-dependent motor protein involved in the axonal transport of neurofilament proteins and organelles, and the kinesin family member 5C (Kif5c), involved in organelle transport. Interestingly, Kif5a and an additional protein identified in this study in multiple deregulated spots (spots 890, 891, 918, and 957), namely, dihydropyrimidinase-related protein 2 (Dpysl2), were found as differentially expressed during a proteomic profiling of an AD-transgenic model with preplaque (2 months) and plaque (24 months) phenotypes [32].

The DAVID database, which analyzes gene or protein lists deriving from high-throughput experiments and systematically extracts biological meaning from them [25, 26], was also used to highlight the functional annotation clustering inside the potential protein network identified by our proteomic analysis. The main descriptor found for molecular functions was the "nucleoside-triphosphatase activity" (GOTERM_MF_ALL; $P = 6.2E-5$), which included 6 out of the 13 identified proteins (Atp6v1a, Kif5a, Kif5c, Gnb1, Gnb2, and Hspa8; Figure 2, proteins inside the blue box). An additional cluster was associated to the "MAPK signaling pathway" and included heat shock cognate 71 kDa protein (Hspa8) and two phosphatases, namely, protein phosphatase 3, catalytic subunit, alpha isoform (Ppp3ca), and dual specificity phosphatase 3 (Dusp3) (KEGG_Pathway $P = 6.2E-2$) (Figure 2, green box). These phosphatases, although at a lower statistical value, were also annotated with the ATPase, H^+ transporting, lysosomal V1 subunit A (Atp6v1a) in the biological process "phosphate metabolic process" (GOTERM_BP_FAT $P = 2.7E-1$).

3.3. Validation of 2D-DIGE Results by Western Blot Analysis of Proteins Differentially Expressed in FDD_{KI} Mice. Differentially expressed proteins from 2D-DIGE analysis were mainly classified according to their functional annotation into "nucleoside-triphosphatase activity" or their involvement in "MAPK signaling pathway" (Figure 2). We then selected some representative members of the two groups, namely Kif5a and Dpysl2, together with Ppp3ca and Dusp3, respectively, to validate our expression results by an alternative method, such as western blotting. An additional downregulated protein, namely Dlg4/Psd95, which is a prominent scaffold protein in synaptosomal architecture/function, and is also associated with nucleoside-triphosphatase activity, was also assayed.

Western blotting analysis definitively demonstrated that Dlg4/Psd95 was slightly downregulated in synaptosomal extracts from FDD_{KI} mice, in strong agreement with 2D-DIGE data (expression ratio -1.27, $P = 0.025$; see Table 1) (Figure 3(a)). In contrast, no positive confirms were observed for the selected proteins associated with "nucleoside-triphosphatase activity," namely, Kif5a and Dpysl2

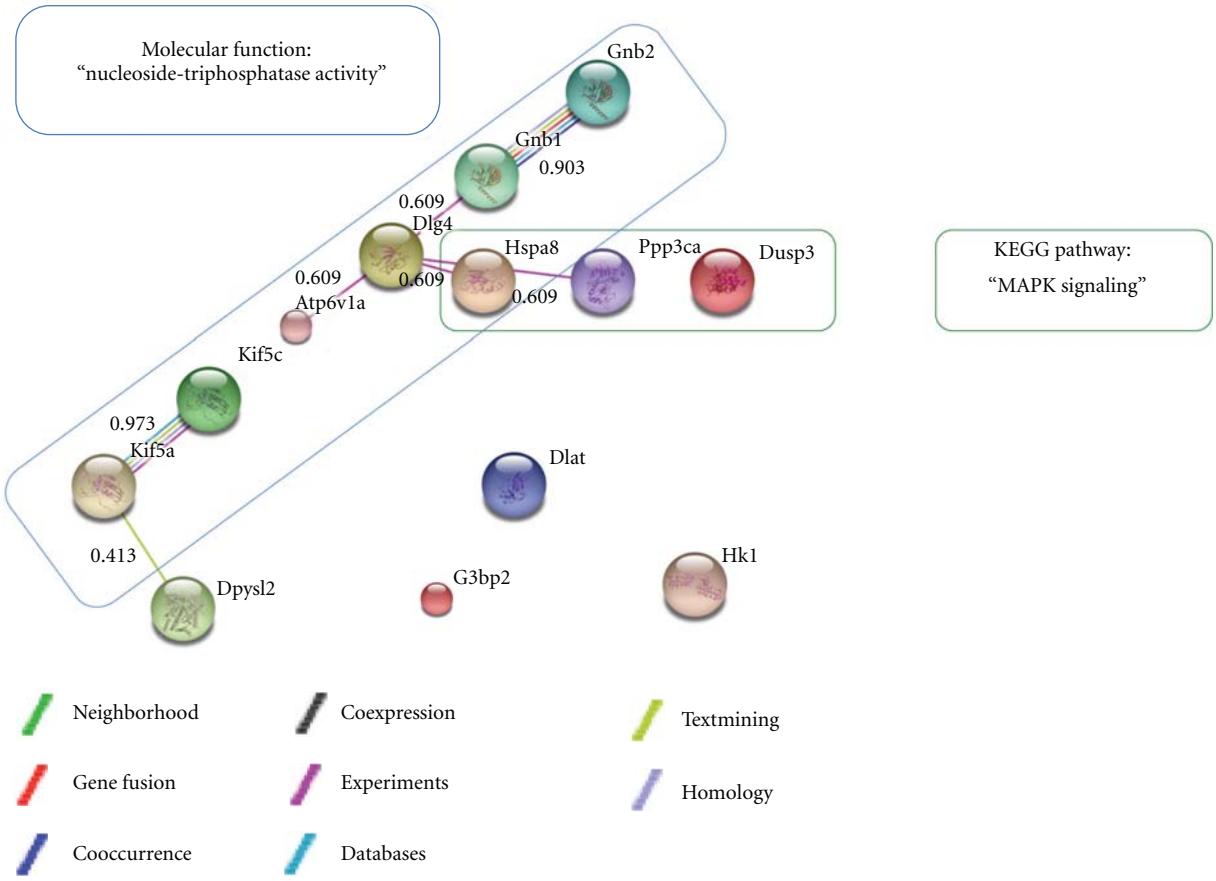

Figure 2: Bioinformatic analysis of the differentially expressed proteins.The list of the MS-identified protein spots from 2D-DIGE was subjected to String (v. 8.3) analysis to reveal functional interactions between the deregulated proteins. Interacting proteins are connected by lines of different colors, according to the color code shown at the bottom of the figure. The reported values close to the lines indicate the confidence scores, as revealed by the functional interaction analysis. The original graphic output was modified to fit the proteins in the blue and green boxes, according to their classification under the gene ontology descriptors "Molecular function: nucleoside triphosphatase activity" and "KEGG pathway: MAPK signaling pathway," as revealed by the DAVID (v. 6.7) annotation system.

(Figure 3(a)). Alternative results were obtained for phosphatase members of the "MAPK signaling cascade." In fact, a good correlation between 2D-DIGE and western blotting analysis was observed for Dusp3, while contradictory results were obtained for Ppp3ca (Figure 3(a)). Negative correlation data between the two analytical methods were easily explained on the basis of the differential expression of specific protein isoforms bearing posttranslational modifications. Thus, post-transcriptional events should regulate abundance of specific protein isoforms in FDD_{KI} synaptosomes. In this context, protein phosphorylation and dephosphorylation is a relevant process in synaptic activity. For example, after exocytosis for neurotransmitter release, the synaptic vesicles are retrieved by endocytosis to accomplish additional cycles of synaptic transmission. In the paradygm, several proteins involved in synaptic function are dephosphorylated, during synaptic vesicle endocytosis, and rephosphorylated after recycling to guarantee the maintenance of synaptic transmission [33]. Ppp3ca phosphatase is associated to these activities. Although global levels of this protein seemed unchanged in the FDD_{KI} synaptosomes by western blotting, 2D-DIGE analysis suggested downregulation of a specific Ppp3ca isoform. On the contrary, Dusp3 downregulation in the FDD_{KI} synaptosomes was definitively validated in the synaptosomal preparations, as a nongeneralized phenomenon in mouse brain. In fact, western blot analysis of Dusp3 in crude brain lysates showed slightly increased protein levels in the unfractionated FDD_{KI} samples (Figure 3(b)). Dual-specificity phosphatases constitute a heterogeneous group of enzymes with the ability to recognize either phospho-Tyr or phospho-Ser/Thr substrates and act in the regulation of JNK- and Erk-mediated pathways [34]. At the present, no evidences have been published that support a Dusp3 function in the nerve system and in synaptic functionality, although one can speculate the involvement of this phosphatase also in the central nerve system, given the relevant functions of the ERK kinases in the signal transduction mechanisms in the brain [35].

4. Conclusions

The results of this work outline a differential expression of selected proteins in the synaptosomes of FDD_{KI} mice. Eight

Table 1: Relative expression and nanoLC-ESI-LIT-MS/MS-based identification of differentially expressed proteins, as revealed by 2D-DIGE analysis of synaptosomal preparations.

Spot	Ratio	*P* value	Accession	Protein	Short name	pI/Mw theoretical (kDa)	Peptides	Sequence coverage	Mascot score
144	−1.85	0.029	P33175	Kinesin heavy chain isoform 5A	Kif5a	5.67/117	2	2	131
162	−1.53	0.049	P28738	Kinesin heavy chain isoform 5C	Kif5c	5.84/109	6	8	281
288	−1.41	0.047	P17710	Hexokinase-1	Hk1	6.44/108	10	12	407
425	−1.27	0.025	Q62108	Disks large homolog 4	Dlg4	5.56/80	3	4	116
890	1.51	0.043	P50516	V-type proton ATPase catalytic subunit A	Atp6v1a	5.42/68	5	11	323
			P63017	Heat shock cognate 71 kDa protein	Hspa8	5.37/71	7	12	264
			O08553	Dihydropyrimidinase-related protein 2	Dpysl2	5.95/62	3	6	163
891	−1.38	0.045	P50516	V-type proton ATPase catalytic subunit A	Atp6v1a	5.42/68	8	14	430
			P63017	Heat shock cognate 71 kDa protein	Hspa8	5.37/71	5	9	287
			O08553	Dihydropyrimidinase-related protein 2	Dpysl2	5.95/62	3	5	123
918	1.38	0.014	P50516	V-type proton ATPase catalytic subunit A	Atp6v1a	5.42/68	9	17	433
			O08553	Dihydropyrimidinase-related protein 2	Dpysl2	5.95/62	5	12	427
			P63017	Heat shock cognate 71 kDa protein	Hspa8	5.37/71	8	13	336
957	1.31	0.041	O08553	Dihydropyrimidinase-related protein 2	Dpysl2	5.95/62	13	31	925
			P97379	Ras GTPase-activating protein-binding protein 2	G3bp2	5.44/54	3	6	146
1043	1.35	0.026	Q8BMF4	Dihydrolipoyllysine-residue acetyltransferase component of pyruvate dehydrogenase complex, mitochondrial	Dlat	5.70/59	5	9	260
2632	−1.26	0.018	P62874	Guanine nucleotide-binding protein G(I)/G(S)/G(T) subunit beta-1	Gnb1	5.60/37	6	21	361
			P62880	Guanine nucleotide-binding protein G(I)/G(S)/G(T) subunit beta-2	Gnb2	5.60/37	6	21	327
2872	−1.29	0.041	P63328	Serine/threonine-protein phosphatase 2B catalytic subunit alpha isoform	Ppp3ca	5.58/59	4	10	180
3391	−1.50	0.043	Q9D7X3	Dual specificity protein phosphatase 3	Dusp3	6.07/20	3	24	217

protein spots were downregulated, while four protein spots were upregulated in the FDD_{KI} synaptosomal extracts. Western blot analysis on selected proteins, guided by the results of bioinformatic classification of the deregulated proteins, showed that two signalling proteins, namely, Dlg4/Psd95 and Dusp3, were actually downregulated in the available animal model of FDD. The first one (Dlg4/Psd95) is a well-known scaffold protein in synaptic function, and its downrepresentation in the synaptosomes of FDD_{KI} mice may impair synaptic transmission and activity. The second protein (Dusp3), a know regulator of Jnk- and Erk-mediated pathways, is not as well studied in the central nerve system. However, the evidence provided may stimulate further studies at the phosphoproteomic and functional levels, to assess its synaptosomal targets, and to define the role of its downregulation in brain physiology and in the mechanisms associated with FDD and additional neurodegenerative disorders, including FBD and AD.

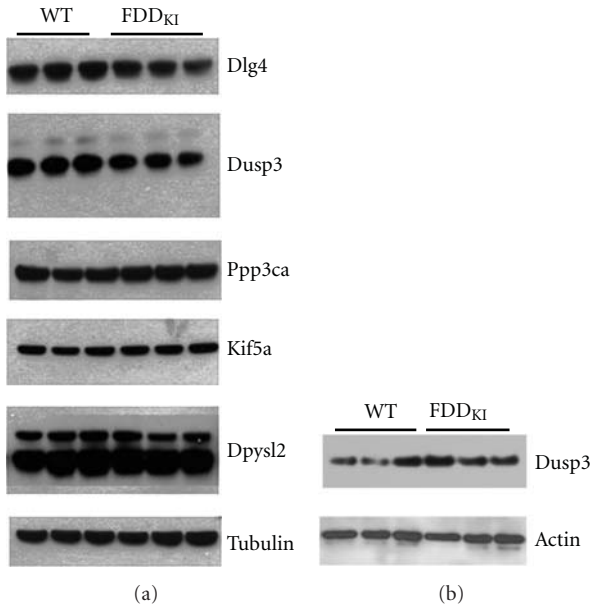

Figure 3: Validation of the 2D-DIGE results by western blot analysis. (a) Triplicate synaptosomal preparations from wild-type and FDD_{KI} mouse synaptosomes were separated on SDS-PAGE gels and transferred to membranes for western blot analysis with antibodies against the indicated proteins. Actual downregulation in the synaptosomal samples of FDD_{KI} mice can be observed for Dlg4/Psd95 and Dusp3 proteins. α-Tubulin antibody was used to show equal loading of the protein extracts. (b) Total brain homogenates from wild-type and FDD_{KI} mice were analyzed by western blot with antibodies against Dusp3. Actin antibody was used to show equal loading of the protein extracts.

Abbreviations

2-DE:	Two-dimensional electrophoresis
2D-DIGE:	Two-dimensional differential in-gel electrophoresis
AD:	Alzheimer's disease
FBD:	Familial British Dementia
FDD:	Familial Danish Dementia
MS:	Mass spectrometry
nanoLC-ESI-LIT-MS/MS:	Nanoliquid chromatography coupled to electrospray-linear ion trap tandem mass spectrometry
SDS-PAGE:	Sodium dodecyl sulphate-polyacrilamide gel electrophoresis.

Acknowledgments

N. Zambrano has been supported by funds from Ministero dell'Università e della Ricerca Scientifica (PS 126-Ind) and from Regione Campania (L.R. n. 5, Annualità 2007), and L. D'Adamio has been supported by Grants from Alzheimer's Association (IIRG-09-129984 and ZEN-11-201425), the Edward N. & Della L. Thome Memorial Foundation grant, and the National Institutes of Health (NIH; R01AG033007). Authors thank T. Russo and the Centro Regionale di Competenza Genomics for Applied Research, Regione Campania (GEAR) for granting access to the 2D-DIGE facility. M. Vitale and G. Renzone gave an equal contribution to this work.

References

[1] G. T. Plant, T. Revesz, R. O. Barnard, A. E. Harding, and P. C. Gautier-Smith, "Familial cerebral amyloid angiopathy with nonneuritic amyloid plaque formation," *Brain*, vol. 113, no. 3, pp. 721–747, 1990.

[2] R. Vidal, T. Révész, A. Rostagno et al., "A decamer duplication in the 3′ region of the BRI gene originates an amyloid peptide that is associated with dementia in a Danish kindred," *Proceedings of the National Academy of Sciences of the United States of America*, vol. 97, no. 9, pp. 4920–4925, 2000.

[3] J. L. Holton, T. Lashley, J. Ghiso et al., "Familial Danish dementia: a novel form of cerebral amyloidosis associated with deposition of both amyloid-Dan and amyloid-Beta," *Journal of Neuropathology and Experimental Neurology*, vol. 61, no. 3, pp. 254–267, 2002.

[4] R. Vidal, B. Franglone, A. Rostagno et al., "A stop-codon mutation in the BRI gene associated with familial British dementia," *Nature*, vol. 399, no. 6738, pp. 776–781, 1999.

[5] J. Ghiso, A. Rostagno, Y. Tomidokoro et al., "Genetic alterations of the BRI2 gene: familial British and Danish dementias," *Brain Pathology*, vol. 16, no. 1, pp. 71–79, 2006.

[6] J. L. Holton, J. Ghiso, T. Lashley et al., "Regional distribution of amyloid-Bri deposition and its association with neurofibrillary degeneration in familial British dementia," *American Journal of Pathology*, vol. 158, no. 2, pp. 515–526, 2001.

[7] A. Rostagno, T. Revesz, T. Lashley et al., "Complement activation in chromosome 13 dementias: similarities with Alzheimer's disease," *The Journal of Biological Chemistry*, vol. 277, no. 51, pp. 49782–49790, 2002.

[8] M. Tsachaki, J. Ghiso, and S. Efthimiopoulos, "BRI2 as a central protein involved in neurodegeneration," *Biotechnology Journal*, vol. 3, no. 12, pp. 1548–1554, 2008.

[9] S. Matsuda, L. Giliberto, Y. Matsuda et al., "The familial dementia BRI2 gene binds the alzheimer gene amyloid-β precursor protein and inhibits amyloid-β production," *The Journal of Biological Chemistry*, vol. 280, no. 32, pp. 28912–28916, 2005.

[10] S. Matsuda, L. Giliberto, Y. Matsuda, E. M. McGowan, and L. D'Adamio, "BRI2 inhibits amyloid β-peptide precursor protein processing by interfering with the docking of secretases to the substrate," *Journal of Neuroscience*, vol. 28, no. 35, pp. 8668–8676, 2008.

[11] S. Matsuda, Y. Matsuda, E. L. Snapp, and L. D'Adamio, "Maturation of BRI2 generates a specific inhibitor that reduces APP processing at the plasma membrane and in endocytic vesicles," *Neurobiology of Aging*, vol. 32, no. 8, pp. 1400–1408, 2011.

[12] A. Fotinopoulou, M. Tsachaki, M. Vlavaki et al., "BRI2 interacts with amyloid precursor protein (APP) and regulates amyloid β(Aβ) production," *The Journal of Biological Chemistry*, vol. 280, no. 35, pp. 30768–30772, 2005.

[13] S. Matsuda, R. Tamayev, and L. D'Adamio, "Increased AβPP processing in familial danish dementia patients," *Journal of Alzheimer's Disease*, vol. 27, no. 2, pp. 385–391, 2011.

[14] H. J. Garringer, J. Murrell, L. D'Adamio, B. Ghetti, and R. Vidal, "Modeling familial British and Danish dementia," *Brain Structure and Function*, vol. 214, no. 2-3, pp. 235–244, 2010.

[15] F. Pickford, J. Coomaraswamy, M. Jucker, and E. McGowan, "Modeling familial British dementia in transgenic mice," *Brain Pathology (Zurich, Switzerland)*, vol. 16, no. 1, pp. 80–85, 2006.

[16] R. Vidal, A. G. Barbeito, L. Miravalle, and B. Ghetti, "Cerebral amyloid angiopathy and parenchymal amyloid deposition in transgenic mice expressing the Danish mutant form of human BRI2," *Brain Pathology (Zurich, Switzerland)*, vol. 19, no. 1, pp. 58–68, 2009.

[17] J. Coomaraswamy, E. Kilger, H. Wölfing et al., "Modeling familial Danish dementia in mice supports the concept of the amyloid hypothesis of Alzheimer's disease," *Proceedings of the National Academy of Sciences of the United States of America*, vol. 107, no. 17, pp. 7969–7974, 2010.

[18] L. Giliberto, S. Matsuda, R. Vidal, and L. D'Adamio, "Generation and initial characterization of FDD knock in mice," *PLoS ONE*, vol. 4, no. 11, Article ID e7900, 2009.

[19] R. Tamayev, S. Matsuda, M. Fà, O. Arancio, and L. D'Adamio, "Danish dementia mice suggest that loss of function and not the amyloid cascade causes synaptic plasticity and memory deficits," *Proceedings of the National Academy of Sciences of the United States of America*, vol. 107, no. 48, pp. 20822–20827, 2010.

[20] R. Tamayev, L. Giliberto, W. Li et al., "Memory deficits due to familial British dementia BRI2 mutation are caused by loss of BRI2 function rather than amyloidosis," *Journal of Neuroscience*, vol. 30, no. 44, pp. 14915–14924, 2010.

[21] F. Talamo, C. D'Ambrosio, S. Arena et al., "Proteins from bovine tissues and biological fluids: defining a reference electrophoresis map for liver, kidney, muscle, plasma and red blood cells," *Proteomics*, vol. 3, no. 4, pp. 440–460, 2003.

[22] G. S. Scippa, M. Rocco, M. Ialicicco et al., "The proteome of lentil (Lens culinaris Medik.) seeds: discriminating between landraces," *Electrophoresis*, vol. 31, no. 3, pp. 497–506, 2010.

[23] W. J. Qian, T. Liu, M. E. Monroe et al., "Probability-based evaluation of peptide and protein identifications from tandem mass spectrometry and SEQUEST analysis: the human proteome," *Journal of Proteome Research*, vol. 4, no. 1, pp. 53–62, 2005.

[24] D. Szklarczyk, A. Franceschini, M. Kuhn et al., "The STRING database in 2011: functional interaction networks of proteins, globally integrated and scored," *Nucleic Acids Research*, vol. 39, supplement 1, pp. D561–D568, 2011.

[25] D. W. Huang, B. T. Sherman, and R. A. Lempicki, "Systematic and integrative analysis of large gene lists using DAVID bioinformatics resources," *Nature Protocols*, vol. 4, no. 1, pp. 44–57, 2009.

[26] D. W. Huang, B. T. Sherman, and R. A. Lempicki, "Bioinformatics enrichment tools: paths toward the comprehensive functional analysis of large gene lists," *Nucleic Acids Research*, vol. 37, no. 1, pp. 1–13, 2009.

[27] H. Husi, M. A. Ward, J. S. Choudhary, W. P. Blackstock, and S. G. N. Grant, "Proteomic analysis of NMDA receptor-adhesion protein signaling complexes," *Nature Neuroscience*, vol. 3, no. 7, pp. 661–669, 2000.

[28] M. O. Collins, H. Husi, L. Yu et al., "Molecular characterization and comparison of the components and multiprotein complexes in the postsynaptic proteome," *Journal of Neurochemistry*, vol. 97, supplement 1, pp. 16–23, 2006.

[29] E. Fernández, M. O. Collins, R. T. Uren et al., "Targeted tandem affinity purification of PSD-95 recovers core postsynaptic complexes and schizophrenia susceptibility proteins," *Molecular Systems Biology*, vol. 5, article 269, 2009.

[30] E. Kim and M. Sheng, "PDZ domain proteins of synapses," *Nature Reviews Neuroscience*, vol. 5, no. 10, pp. 771–781, 2004.

[31] A. Alexa, J. Varga, and A. Reményi, "Scaffolds are "active" regulators of signaling modules," *FEBS Journal*, vol. 277, no. 21, pp. 4376–4382, 2010.

[32] N. Guerreiro, M. Staufenbiel, and B. Gomez-Mancilla, "Proteomic 2-D DIGE profiling of APP23 transgenic mice brain from pre-plaque and plaque phenotypes," *Journal of Alzheimer's Disease*, vol. 13, no. 1, pp. 17–30, 2008.

[33] V. Anggono, K. J. Smillie, M. E. Graham, V. A. Valova, M. A. Cousin, and P. J. Robinson, "Syndapin I is the phosphorylation-regulated dynamin I partner in synaptic vesicle endocytosis," *Nature Neuroscience*, vol. 9, no. 6, pp. 752–760, 2006.

[34] K. I. Patterson, T. Brummer, P. M. O'Brien, and R. J. Daly, "Dual-specificity phosphatases: critical regulators with diverse cellular targets," *Biochemical Journal*, vol. 418, no. 3, pp. 475–489, 2009.

[35] J. D. Sweatt, "Mitogen-activated protein kinases in synaptic plasticity and memory," *Current Opinion in Neurobiology*, vol. 14, no. 3, pp. 311–317, 2004.

Hindawi Publishing Corporation
Journal of Biomedicine and Biotechnology
Volume 2012, Article ID 568567, 11 pages
doi:10.1155/2012/568567

Review Article

Patient-Derived Xenografts of Non Small Cell Lung Cancer: Resurgence of an Old Model for Investigation of Modern Concepts of Tailored Therapy and Cancer Stem Cells

Massimo Moro,[1] Giulia Bertolini,[1] Monica Tortoreto,[2] Ugo Pastorino,[3] Gabriella Sozzi,[1] and Luca Roz[1]

[1] *Tumor Genomics Unit, Department of Experimental Oncology and Molecular Medicine, IRCCS Foundation National Cancer Institute, Via Venezian 1, 20133 Milan, Italy*
[2] *Molecular Pharmacology Unit, Department of Experimental Oncology and Molecular Medicine, IRCCS Foundation National Cancer Institute, Via Venezian 1, 20133 Milan, Italy*
[3] *Thoracic Surgery Unit, Department of Surgery, IRCCS Foundation National Cancer Institute, Via Venezian 1, 20133 Milan, Italy*

Correspondence should be addressed to Luca Roz, luca.roz@istitutotumori.mi.it

Received 28 December 2011; Accepted 10 January 2012

Academic Editor: Andrea Vecchione

Current chemotherapy regimens have unsatisfactory results in most advanced solid tumors. It is therefore imperative to devise novel therapeutic strategies and to optimize selection of patients, identifying early those who could benefit from available treatments. Mouse models are the most valuable tool for preclinical evaluation of novel therapeutic strategies in cancer and, among them, patient-derived xenografts models (PDX) have made a recent comeback in popularity. These models, obtained by direct implants of tissue fragments in immunocompromised mice, have great potential in drug development studies because they faithfully reproduce the patient's original tumor for both immunohistochemical markers and genetic alterations as well as in terms of response to common therapeutics They also maintain the original tumor heterogeneity, allowing studies of specific cellular subpopulations, including their modulation after drug treatment. Moreover PDXs maintain at least some aspects of the human microenvironment for weeks with the complete substitution with murine stroma occurring only after 2-3 passages in mouse and represent therefore a promising model for studies of tumor-microenvironment interaction. This review summarizes our present knowledge on mouse preclinical cancer models, with a particular attention on patient-derived xenografts of non small cell lung cancer and their relevance for preclinical and biological studies.

1. Introduction

The continuously growing body of knowledge about molecular events driving oncogenesis has led to the identification of new potential targets for therapy and has consequently paved the way for the design of targeted compounds, offering potential new tools to improve the clinical outcome of cancer patients. The therapeutic efficacy of this large number of new compounds compared to standard treatments (or in association with them) has to be ultimately assessed through clinical trials [1] but drug development process includes many steps and requires investments both in time and resources as well as the recruitment of patients who agree to take part in human clinical trials. Typically, the developmental plan for a cancer chemotherapy agent involves sequential steps such as *in vitro* studies to identify the basic properties of the compound; rodent studies to assess its potential activity; pharmacology studies to define drug absorption, distribution, metabolism, and elimination; toxicology studies to define a starting dose for humans [2]. The most expensive steps are associated with preclinical toxicology and pharmacology studies and for this reason it is of primary importance to recognize early in the process compounds unworthy of further development. Many different *in vitro*

assays have been used to identify lead compounds as exemplified by the 60 human tumor cell line anticancer drug screen (NCI60) developed by the US National Cancer Institute in the late 1980s as an *in vitro* drug discovery tool which has proved valuable for high-throughput screens and initial assessment of novel compounds. The subsequent efficacy assessment in rodents, however, plays a crucial role in identifying those drugs which deserve further development. In fact, compounds that showed some activities as anticancer drugs on the NCI60 panel must undergo *in vivo* studies to be presented to the Drug Development Group as candidates for NCI development or licensing [3] highlighting the need for animal models that closely recapitulate human disease for efficient drug development.

2. Mouse Preclinical Cancer Models

In general the reliability of rodent-based preclinical cancer models can be questioned because of their imperfect correlation with human clinical outcomes [4]. However, although some drugs that show activity against human tumor xenografts (XGs) have failed to show activity in human clinical trials, many of the clinically approved drugs in use today have demonstrated and continue to demonstrate activity in a variety of preclinical models [4–7]. In addition, it is noteworthy to remember that mouse models are the most valuable tool for preclinical evaluation of novel therapeutic strategies in cancer primarily because humans and mice are genetically closely related and consequently the major signaling pathways are conserved between the two species. The mouse is also small and relatively inexpensive to breed and house. Moreover, the mouse germ line can be modified to generate many different mouse strains modeling different aspects of cancerogenesis. In the early 1980s, immunologically compromised mice, capable of supporting growth of human tumors, became more widely available [8], resulting in the development of human tumor xenografts models which represent, together with genetically engineered models (GEMs), the main categories of preclinical cancer models used for current preclinical efficacy studies. Distinct advantages and disadvantages of the different models are summarized in Table 1.

2.1. Genetically Engineered Mice (GEMs). A genetically modified mouse is a mouse whose genome has been altered by genetic engineering techniques. The genome of these mice is altered in genes known to be involved in malignant transformation, that can be mutated, deleted, or overexpressed; subsequently, the effect of altering these genes is studied over time to evaluate the effect on tumorigenesis (both spontaneous or induced) and eventually therapeutic responses may be followed *in vivo* [9–11].

There are two basic technical approaches to produce genetically modified mice. The first involves pronuclear injection into a single cell of the mouse embryo, where it will randomly integrate into the mouse genome [12] generating a transgenic mouse. The second approach involves modifying embryonic stem cells with a DNA construct containing DNA sequences homologous to the target gene [13]. This method is used to manipulate a single gene, in most cases "knocking out" the target gene, although more subtle genetic manipulation can occur (e.g., only changing single nucleotides).

The peculiar features of GEMs (germline alterations) make them particularly suitable to follow tumor development from early time points. Moreover, the development of a tumor resembling the human counterpart in a genetically modified mouse can be very useful for refined studies of relationship with the microenvironment, that can also be manipulated in mice trough specific genetic manipulations or using bone marrow transplantation. Furthermore, the possibility to cross GEMs with other inbred mice strains provides the opportunity to investigate the role of different genetic alterations in tumor development. It should however be stressed that GEMs tumors are murine tumors and although they might present characteristics closely resembling the human counterpart, they could never fully recapitulate a human tumor [14, 15]. Moreover, the number of modified genes is usually too limited to be representative of the heterogeneity of human solid tumors and the development of a genetically modified mouse strain is very costly and time consuming.

2.2. Mouse Xenograft Models. Xenotransplantation is defined as any procedure that involves the transplantation of living cells, tissues or organs from one species to another.

The growth of human tumors in a different species (e.g., mouse) requires immunodeficiency in the host animal to prevent rejection of the transplanted foreign tissues. There are many strains of genetically determined immunodeficient mice containing single mutations (e.g., nude, scid, beige, xid, rag-1 null, rag-2 null) or combined mutations, (e.g., bg/nu, bg/nu/xid, nude/scid, nod/scid) available for cancer research [16–18]. These strains have different immunological impairment and the availability of more permissive mouse strains can strongly increase the efficiency of xenotransplantation; however severely immunocompromised mice also have a higher cost and their manipulation can be extremely demanding requiring controlled husbandry environment and highly trained personnel. It is therefore mandatory to choose the immunocompromised strain with the best "efficiency of transplantation/costs" ratio for each application.

Successful xenografting of human tumors into nude mice was first reported in the late 1960s [19, 20]. Nude mouse models are now extensively used in the development of potential anticancer drugs and studies of tumor biology and mice with severe combined immunodeficiencies (e.g., SCID, beige, xid) have widened the spectrum of possible models and enabled engraftments of human tumors that were previously difficult to implant.

Tumor xenograft (XG) models can be broadly derived either from the injection in immunocompromised mice of human established tumor cell lines or from direct implant of patient's tumor fragments. This latter model has been referred to by different researchers as "tumorgraft," "primary-tumor xenograft," or "patient-derived xenograft" to

Table 1: Main advantages and disadvantages of GEM, XG, and PDX mouse models.

	Advantages	Disadvantages
Genetically engineered mice (GEM)	(i) Studies on defined mutations (ii) Possibility to follow tumor development from early time points (iii) Tumor microenvironment is representative of the studied tumor (iv) Potential analysis of effects of mutations in many genetic backgrounds by using a variety of mouse strains	(i) Limited number of genes (usually not representative of the heterogeneity of the tumor) (ii) Development costly and time consuming (iii) Tumor development in animals slow and variable (iv) Both, tumor and microenvironment are murine
Xenograft (XG)	(i) Allows a rapid analysis of response to a therapeutic regimen (ii) Source of material virtually unlimited for immortal cell lines (iii) Can predict drug response of human patient's tumor	(i) Human tumor microenvironment is not represented (ii) Orthotopic implant is often technically complicated (iii) Cells can undergo genetic modification as well as subpopulation rearrangements when cultured
Patient-derived xenograft (PDX)	(i) Provides a realistic representation of the heterogeneity of tumor cell subpopulations (ii) Can predict drug response of human patient's tumor (iii) Stromal component is representative of the parental tumor in the initial passages	(i) Orthotopic implant is often technically complicated (ii) Surgical fragments must be processed rapidly (iii) Limited source of original material

point out the difference from conventional "xenografts" generally intended as injection of suspensions of tumor cell lines. For clarity throughout this paper we will refer to the implantation of patient's tumor fragments as "patient-derived xenograft" (PDX), while the whole cohort of mice carrying the expansion of tumor fragments derived from the same patient will be defined as "xenopatients" (XP).

In general, established tumor cell lines have a much higher take rate when inoculated as a suspension into nude mice than human solid tumors of the same histological type that are transplanted directly from the patient [21]. On the other hand, culturing tumor cells could lead to changes in gene expression [22] as well as rearrangements in the composition of the cellular populations that constitute the original human tumor resulting in the xenotransplant of a cellular population that is not fully representative of the original tumor heterogeneity. Moreover, studies on XGs of human cell lines to test drug responses do not often correlate with clinical activity in patients [23], especially when cells are injected subcutaneously. By contrast, when cells are used as an orthotopic XG, there is a stronger predictive response value, especially when a clinically relevant drug dosage is used [23–25].

Implantation of either cells or tumor fragments is usually performed subcutaneously rather than orthotopically, because of the technical difficulties often encountered in these assays. This can raise doubts about the development of tumor vasculature and tumor-stroma interactions compared to those observed in the human tumor of origin. Interestingly, as will be discussed more in detail later in this paper, PDXs maintain the whole structure of the human parental tumor during the initial passages in mouse making them suitable also for microenvironment studies.

3. Patient-Derived Xenografts

Direct implantation of small tumor fragments in immunocompromised mice can result in growth of patient-derived xenografts that accurately reproduce the heterogeneity of human cancers, especially if a large set of a different tumor subtypes is available. These models can be serially propagated in mice by subsequent passaging as tissue explants and the use of standardized procedures for the assessment of therapeutic efficacy of different drugs using PDXs allows a rapid evaluation of combined therapies on a relatively large set of tumors. However, in order to be relevant as a useful tool for preclinical studies, a PDX panel should accurately reproduce human cancers representing their various subcategories and a particular PDX should accurately reproduce the original patient's tumor. Furthermore, there should be a high correlation between preclinical and clinical results in terms of therapeutic efficacy, with the gold standard being represented by PDXs that closely mimic (or even predict) the clinical response of the patient's tumor they derive from. All these features have been recently investigated in PDXs from different human tumors resulting in the observation that PDXs might represent a suitable model for preclinical studies intended as a "quick" evaluation of the response to different therapeutic treatments. Although the rapidity of this kind of approach is relative, being dependent on the rate of implant of the tumor, it can nonetheless give very relevant information in different clinical settings. On the one hand, while the models are being established and the patients are undergoing first-line treatment, it is possible to acquire proof-of-concept information on relative sensitivity or resistance to the different regimens to be correlated with the molecular features of the PDXs, while on the other it is

possible to imagine an immediate clinically relevant use of these models in selecting the best second line treatment for a specific patient.

Hidalgo et al. recently reported their results obtained with various advanced solid tumors resected from 14 patients, propagated in immunodeficient mice, and treated with 63 drugs in 232 treatment regimens. They showed an overall remarkable correlation between drug activity in the model and clinical outcome, both in terms of resistance and sensitivity. Their results emphasize the relevance of PDX panels in preclinical studies of anticancer treatments. The treatments they selected for each patient, based on the results obtained with the correspondent PDX, would not have been the first choice for a second- or third-line treatment, nonetheless the objective response rate they obtained was 88% for treatments deemed effective by the model and tested in the patient, with 11 of 14 patients achieving a partial response. This work highlights that personalized PDXs can be used to investigate drug response with the final aim to select best personalized treatments to increase the response rate of the patients [26].

Another preclinical setting in which PDXs can be extremely relevant is represented by the evaluation of the potential of new drugs in cancer treatment. Taking advantage from a panel of PDX which faithfully represents the heterogeneity of a cancer type, new drugs can be tested and can lead to the identification of the best treatment regimen for a specific subtype of tumor as well as to the identification of new biological pathways involved in the development of the tumor.

Encouraging results, which emphasize the potential of this kind of preclinical model, were recently obtained with metastatic colorectal cancer (mCRC) by Bertotti et al. that established a large PDX cohort from 85 patient-derived mCRC samples. Firstly, they validated the robustness of the cohort of xenopatients showing that they responded to the anti-EGFR antibody Cetuximab with analogous rates compared to those observed in the clinic. Then, they stratified their PDXs in responders and nonresponders and found an enrichment of tumors with HER2 amplification in Cetuximab-resistant KRAS/NRAS/BRAF/PIK3CA wild-type cases (36% versus 2.7% in unselected tumors). This approach allowed them to discover that inhibition of HER2 in combination with anti-EGFR antibodies induced overt, long-lasting tumor regression in Cetuximab-resistant colorectal cancers, an observation worthy of further clinical investigation [27].

Cetuximab response was also investigated in 79 different PDXs generated from colon, gastric, head and neck, lung and mammary cancer, leading to the identification of MET activation as a mechanism for drug resistance. In particular these models were used for an in-depth analysis of different molecular characteristics of the tumors, including EGFR expression and activation, mutational status of KRAS, BRAF, and NRAS, expression of EGFR ligands and activation of HER3 (ErbB3), and hepatocyte growth factor receptor (MET). High expression and activation of EGFR and its ligands epiregulin or amphiregulin were identified as positive predictive factors regulating Cetuximab response, whereas negative factors were markers for downstream pathway activation independent of EGFR. Interestingly, overexpression due to gene amplification and strong activation of MET was specifically identified in Cetuximab resistant NSCL adenocarcinomas [28].

4. PDX Models of Non Small Cell Lung Cancer

4.1. Establishment and Preclinical Relevance. Due to its high incidence and mortality lung cancer is the leading cause of cancer deaths worldwide. The two major forms of lung, cancer are non small cell lung cancer (NSCLC, about 85% of all lung cancer) and small cell lung cancer (SCLC, about 15%). NSCLC can be divided into three major histological subtypes: squamous cell carcinoma, adenocarcinoma, and large cell carcinoma. Smoking is the main etiological factor for all types of lung cancer although it is most strongly linked with SCLC and squamous cell carcinoma; on the other hand adenocarcinoma is the most common type of lung tumor in patients who have never smoked [29, 30]. Currently most NSCLC are diagnosed in advanced stages where five-year survival rates are less than 10%. Since available therapies only provide a modest survival benefit a better understanding of the molecular basis of the disease and novel therapies are needed to significantly improve patients' outcome. The establishment of PDXs from lung cancer specimens has therefore been investigated by us and others both as a source of therapeutically relevant information and as a supply of precious biological material.

After approval from the internal review board, samples of primary non small cell lung cancer are obtained from patients undergoing surgical resection. Each sample is immediately cut in small pieces (25–30 mm^3) in antibiotic-containing buffer (PBS 1x, 200 U/mL penicillin, 200 ug/mL streptomycin) and implanted subcutaneously in the flank region of 4 to 6 weeks old female nude or SCID (severe combined immunodeficient) anesthetized mice. In detail, animals are anesthetized with an intraperitoneal injection of ketamine/xylazine/saline mixture (20 : 2.5 : 77.5 v/v/v) at a dose of 10 mL/kg body weight. Fragments are then implanted using a trocar gauge and mice are maintained in rooms with constant temperature and humidity (Figure 1). Tumor size is evaluated once per week by caliper measurements and the relative tumor weight is estimated, assuming the PDX as an ellipsoid with a specific density of 1.0 g/cm^3, through the $(Lxl^2)/2$ (mg) formula, where L is the longest diameter and l the shortest [31].

Typically, after a variable lag time, the tumor begins to grow exponentially until it reaches a plateau level where the growth slows down; it is important to transfer the tumor to a new mouse in the period of exponential growth, mostly not only for ethical reasons (tumor charge must never exceed 1/10 of the mouse body weight), but also because the probability of necrotic areas within the PDX increases when it reaches a higher mass. Highly necrotic tumors are difficult to propagate and great care should be taken to avoid this occurrence. Successive rounds of expansion from donor to

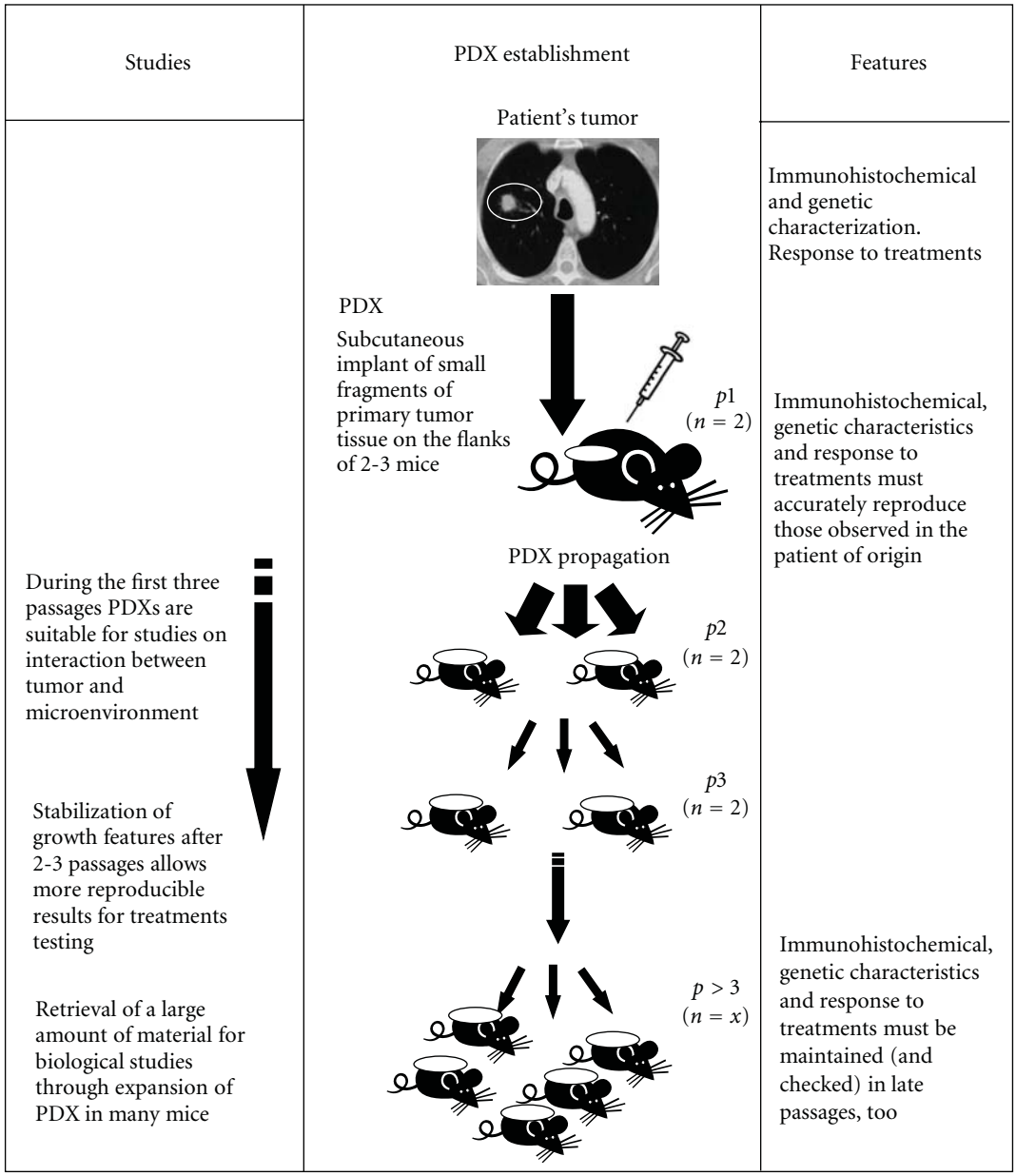

Figure 1: Flow-chart of establishment of patient-derived xenografts. Fragments of primary tumor samples are initially implanted subcutaneously in both flanks of 1-2 immunocompromised mice, depending on tissue availability ($p0$). When tumors reach the exponential growth phase they are removed from donor mice, reduced into fragments, and serially transplanted in new recipient mice ($p1$). For investigational purposes (i.e., drug treatments or subpopulation analysis) PDXs can be expanded in a higher number of mice in order to obtain statistical relevant results or sufficient biological material for analysis, respectively. (p: sequential passage in immunocompromised mouse; n: number of mice.)

recipient mice can produce a sizable cohort of xenopatients suitable for pharmacological experiments.

Each model has its specific characteristics when implanted subcutaneously in different immunodeficient mouse strains, so it is very important to monitor tumor progression using parameters that can be useful in subsequent experiments designed to evaluate the effects of different compounds on individual PDXs.

The first parameter that should be evaluated is the percentage of the tumor take in mice. Usually, for lung cancers about 30–40% of the patient-derived tumors are successfully implanted subcutaneously in nude mice. Interestingly, it has been reported a correlation between the ability to form PDXs and the risk of disease recurrence in early-stage NSCLC [32]. In this study 40% of NSCLC implanted resulted in a successful PDX with KRAS-mutated tumors engrafting more efficiently than EGFR-mutated ones and positive engraftment correlating with shorter disease-free survival in a multivariate analysis including age, sex, stage, and mutations.

Other useful parameters are related to the growth characteristics of the PDX. As previously described one feature defining PDX is its lag time before exponential growth that can be stable or variable during subsequent passages of the tumor. In our experience the lag time is generally higher for the first two-three passages and then reaches a steady state level, probably due to the progressive substitution of the original human tumor stroma with murine stroma.

Beyond the lag time, the parameters to follow during PDX establishment are specifically related to the growth characteristics of the model: growth rate, doubling time, time before implantation in another mouse are all useful tools to catalogue a panel of PDX in groups with similar characteristics. Mouse general health should also be monitored during the whole process of PDX implantation. Indeed we have observed that some tumors can induce a general health's worsening when implanted subcutaneously in mice in a way reminiscent to the cachexia-inducing potential of some human tumors. In these situations, if the growth of the model can be supported in a different strain, transferring the PDX in a less immunocompromised mouse strain (i.e., from SCID to nude mice) can clear up these kind of cachexia-related issues resulting in a fast-growing "healthy" PDX. This could be suggestive of a higher aggressiveness of tumors with such features, that are probably too aggressive to be sustained by an organism with a deeply compromised immune system, but further data are needed to confirm this observation.

According to our experience, PDXs can maintain the same characteristics of the human primary tumor for several passages (up to 20), highlighting their value as a resource for multiple studies [33]. Since it can be very expensive and unpractical to continuously passage PDXs in mice it is therefore useful to set up a stock of frozen PDX samples. A good practice is to store samples from earlier passage and then other samples every ten–fifteen passages. To obtain successful thawing of preserved samples, freshly processed tissue fragments should be immediately frozen in a solution of 90% fetal bovine serum and 10% DMSO and preserved at -80°C.

Also for lung cancer the relevance of PDXs for the evaluation of new therapeutic strategies has been reported. Patient-derived NSCLC PDXs have been established by Fichtner and collaborators in order to identify predictive biomarkers. Starting from 102 surgically resected early stage (T2/T3) NSCLC specimens, they set up 25 transplantable PDXs. They showed how, in early passages, PDXs maintain a high degree of similarity with the original clinical tumor sample with regard to histology, immunohistochemistry and mutational status. Also the chemotherapeutic responsiveness of the PDXs panel resembled the clinical situation. Interestingly, they observed a correlation between KRAS mutations and Erlotinib resistance but no correlation between anti-EGFR therapy and mutations in EGFR or p53. Moreover, after treatment with Cetuximab, a down regulation of EGFR was observed in 2 of 6 sensitive PDXs but in none of the resistant PDXs [34].

The same group used 22 well-characterized NSCLC PDX to support the clinical development of the anticancer drug Sagopilone (a fully synthetic low molecular weight analogue of epothilone) involved in an integrative preclinical phase II design. According to clinical trial criteria, 64% (14 of 22) of lung cancer PDXs were sensible to Sagopilone. Interestingly, tumors with wild-type TP53 as well as with a high expression of genes involved in cell adhesion/angiogenesis were more likely to be resistant to Sagopilone. Therefore a combination of Sagopilone with Bevacizumab and Sorafenib, drugs targeting vascular endothelial growth factor signaling, was tested in Sagopilone-resistant models, restoring antitumor activity [35].

These data confirm the potential relevance of well-annotated PDX panels to stratify the observed responses on the basis of specific molecular alterations. This holds great promise not only for evaluating conventional therapeutics, but also for testing novel drug candidates as well as to identify rationale combination therapies to be tested in clinical trials.

At the other end, for studies on personalized chemotherapy, intended as a "quick" evaluation of the putative treatment response of the individual patient, lung cancer and in particular NSCLC-derived PDXs appear currently not very suitable due to their relative low take rate (30–40%) if implanted subcutaneously and also for the slow growth rate (often several months). An interesting approach to bypass these issues has been proposed by Dong and colleagues who established PDX from 32 untreated, completely resected patients' NSCLCs. They obtained an engraftment rate of 90% implanting small pieces of tumors under the renal capsules of NOD/SCID mice. Treating these xenopatients with either cisplatin + vinorelbine, cisplatin + docetaxel, or cisplatin + gemcitabine they quickly assessed (in 6–8 weeks) the chemosensitivity of patients' cancers and selected the most effective regimen. Only 16 of the 32 tumors provided sufficient tissue for testing all three chemotherapeutic regimens, but it is noteworthy that 11 patients had adjuvant therapy that matched the regimen used for the corresponding PDX with good concordance between the results obtained in the animal model and clinical response, in particular in relation to resistance to conventional therapy (six of seven patients who developed recurrence/metastasis during followup were nonresponsive in mice) highlighting the need for novel strategies [36]. However, the technique of engraftment under the renal capsules is certainly more difficult compared to subcutaneous implantation of the tumor fragments and NOD/SCID mice are more costly and also more difficult to breed than SCID or nude mice, which are usually utilized to set up a PDX model.

Setting up a panel of PDX that can be used to test new agents is costly and time and resource consuming, moreover the selection of compounds for advancement to human clinical trials is based, in part, on *in vivo* efficacy studies. It is therefore of primary importance to validate the efficacy of the PDX panel in their representation of the human tumor. As previously mentioned, PDXs must show histological and genetic characteristics similar to patient's tumors they are derived from. These characteristics should be checked to remain unvaried after several passages in mouse, too. Furthermore, the panel of PDXs available for a study must be representative of the heterogeneity of the selected cancer type as well as possible. In the case of lung

cancers it is mandatory to obtain a PDX panel covering all the three major histological subtypes previously described (i.e., squamous cell carcinoma, adenocarcinoma, and large cell lung cancer; whereas a study on NSCLC in nonsmokers should be mainly derived from adenocarcinomas) and to evaluate the response to the common chemotherapeutic(s) utilized in clinic (e.g., cisplatin), that should mimic the patients' response tumor. These data, together with histological and genetic characteristics, could provide the basis for a classification of the PDXs in groups of tumors with similar features and similar behavior and will be very useful in testing the activity of new compounds for NSCLC.

4.2. Relevance for Biological Research. The availability of fresh tissue from primary human lung cancers expanded *in vivo* as PDXs also constitutes an important repository of biological material for different studies ranging from investigation of tumor-microenvironment interaction to evaluation of tumor heterogeneity and investigation of dynamics of different subpopulations during therapy.

Investigations have been carried out to define the preservation of tissue architecture in PDXs, including stroma components and resulted in the observation of a remarkable stability of the models even when murine cells have substituted the human counterpart [37, 38]. On the other hand the presence of human stroma in early passages of PDXs can be initially exploited to study interaction between tumor cells and microenvironment. In particular studies on tumor microenvironment on PDXs of NSCLC at early passages have been carried out by Simpson-Abelson and collaborators. They implanted nondisrupted pieces of primary human lung tumor in severely immunodeficient mouse (NOD/SCID IL2Rgamma null mice) obtaining PDXs in which tissue architecture, including tumor-associated leukocytes, stromal fibroblasts, and tumor cells were preserved for prolonged periods. They observed that plasma cells remained functional in PDX-bearing mice, as evidenced by production of human immunoglobulins, for up to 9 weeks after engraftment. Moreover, tumor-associated T cells were found to migrate from the microenvironment of the PDX to the lung, liver, and primarily to the spleen at 8 weeks post engraftment. These data confirmed the relevance of the PDX model in studying tumor and tumor-stromal cell interactions *in situ* [39]. Interestingly the same architecture was not maintained when tissue fragments were implanted in CB17-scid mice, indicating once more the need to select the appropriate model for different biological investigations.

PDXs can also be very useful as a source of material for studies on tumor subpopulations and their modulation after drug treatments, leading to a more comprehensive knowledge of tumor development as well as mechanisms of drug resistance. Foci of resistant cells have been identified after cisplatin + vinorelbine, cisplatin + docetaxel, or cisplatin + gemcitabine treatment in responsive NSCLC PDXs by Dong and collaborators [36]. The authors suggested that these drug-resistant cells could be responsible for tumor recurrence as it frequently occurs in patients after partial or even complete response. This observation fits very well with the hypothesis of the presence of small subpopulations of tumor initiating cells within the tumor. This theory, known as the cancer stem cell (CSC) theory has been proposed to explain tumor heterogeneity and the carcinogenesis process [40, 41]. Accordingly to this model, tumor can be represented as the result of abnormal organogenesis driven by CSCs, defined as self-renewing tumor cells able to initiate the tumor formation and to maintain tumor heterogeneity [42, 43]. Cells with features of CSCs have been identified in acute myeloid leukemia [44], glioblastoma [45–47], melanoma [48, 49], and different epithelial cancers [50–56].

Two main techniques are generally used to identify tumor initiating cells: (i) prospective flow cytometry-based cell sorting using tissue-specific surface markers or (ii) sphere forming assays in selective cells culture medium. Due to the relative paucity of the cancer stem cell fraction in the tumor population it is highly desirable to have a substantial amount of tumor samples available for thorough investigation but this is not easily obtained from surgical specimens. Since human cancer PDX models are similar to the patients' tumors not only in terms of genetic, immunohistochemical, and microenvironment features but also in terms of heterogeneity of the tumor cellular composition they are a useful model also in studies of subpopulations with cancer stem cell characteristics (Figure 2). As a matter of fact the possibility to expand the patient-derived tumor in immunocompromised mice yields a large amount of material for studies such as flow cytometry-based cell sorting. Using this approach our group has recently been successful in identifying a highly tumorigenic $CD133^+$ subpopulation in non small cell lung cancers which displays stem-like features and is spared by cisplatin treatment [33, 57].

PDXs as a tool for CSC studies have been also developed for pancreatic cancer. Jimeno et al. showed that the chemotherapeutic treatment of pancreatic PDXs resulted in an increase of CSC markers (ALDH and CD24), in the residual tumor population, supporting the idea of an enhanced chemoresistance of the cancer stem cells subpopulation. Moreover, the authors showed that CSCs targeting could increase the efficacy of conventional treatment. Combining gemcitabine with an inhibitor of the hedgehog pathway, that is fundamental for the maintenance of CSCs, they induced tumor regression and a decrease in CSC fraction [58]. Similar results were obtained with PDXs derived from other cancer types [59, 60], suggesting that combination therapy using conventional chemotherapy and drugs against CSC specific targets can lead to better therapeutic results, both in terms of tumor growth as well as in terms or tumor relapse.

Furthermore, subpopulations isolated from expanded PDXs can also be studied *in vivo* if reinjected in immunocompromised mice and their characteristics in terms of tumorigenicity as well as in term of response to chemotherapeutics can be directly compared with the characteristics of the parental tumor. This gives the possibility to identify treatment resistant subpopulations and to study the tumorigenic potential of prospectively identified putative CSCs. The relevance of these models in identifying and isolating CSC subpopulation has been proved also for other cancer

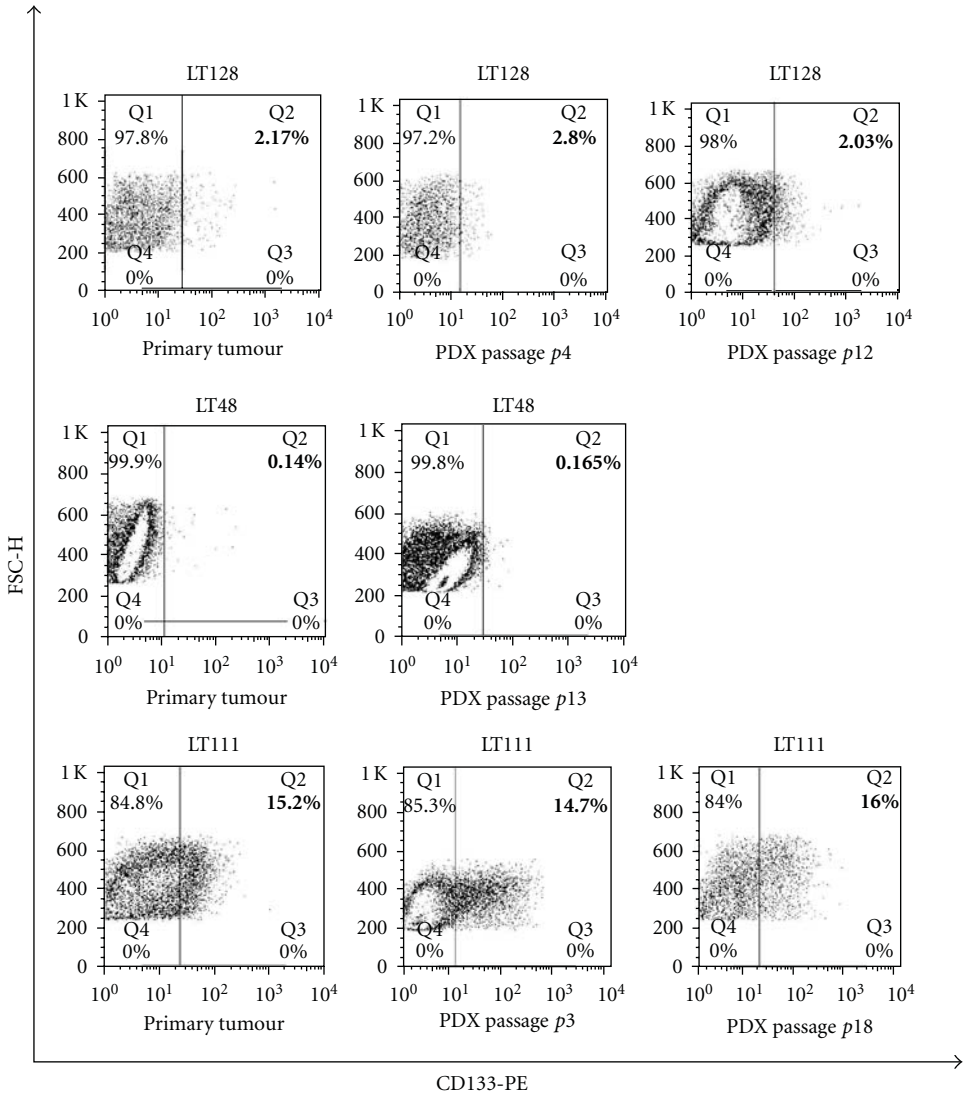

Figure 2: Frequency of CD133$^+$ cells in primary tumors is maintained in PDXs during passaging in mice independently of their initial content. Dot plots showing that the percentage of CD133$^+$ cells, previously demonstrated to display stem-like features and to be spared by cisplatin treatment [REF], is similar in the primary tumor and in PDXs. CD133$^+$ cells levels remain stable also after several passages in immunocompromised mice in PDX models established from low, intermediate and high CD133-expressing tumors (LT48, LT128, LT111 resp.). p = number of serial transplant in mouse. FACs analysis of CD133 expression was performed with CD133/1-phycoerythrin antibody (50 μg/mL; AC133 clone; Miltenyi Biotech).

types, such as breast cancer [60], colon carcinoma [61], and pancreatic adenocarcinoma [62, 63].

5. Conclusive Remarks

A growing number of research groups have established panels of patient-derived xenografts, demonstrating their relevance in drug development studies as well as in the discovery of novel predictive biomarkers to be used in the clinical setting.

It is therefore of primary importance to set up panels of PDXs highly representative of the cancer type under investigation and to validate the models through extensive immunohistochemical and genetic characterization to confirm similarities with the human tumor and also in terms of response to common chemotherapeutics to confirm the robustness of the model in testing the efficacy of new treatments. In our experience, growth features of PDX such as lag time and growth rate reach stability after two-three passages in mouse; it is therefore advisable to carry out drug efficacy tests with PDXs that have reached a certain stability in their growth characteristics.

This kind of preclinical model is also exploitable in research fields such as tumor-microenvironment interaction, cancer stem cells identification and modulation after drug treatment. Human cancer PDXs are particularly suitable for this kind of research because they provide a large amount

of material reproducing the original human tumor and its microenvironment and could therefore be more extensively utilized not only in preclinical studies but also in basic research. However, it is always noteworthy to remember that when using animal models for biological purposes, the guidelines for the welfare and use of animals in cancer research should be always kept in mind and strictly followed [64].

Acknowledgments

L. Roz and G. Sozzi are supported by grants from Associazione Italiana per la Ricerca sul Cancro (AIRC) and from the European Community Seventh Framework Programme Collaborative Project CURELUNG (to L. Roz).

References

[1] D. Decaudin, "Primary human tumor xenografted models ("tumorgrafts") for good management of patients with cancer," *Anti-Cancer Drugs*, vol. 22, no. 9, pp. 827–841, 2011.

[2] S. Venkatesh and R. A. Lipper, "Role of the development scientist in compound lead selection and optimization," *Journal of Pharmaceutical Sciences*, vol. 89, no. 2, pp. 145–154, 2000.

[3] R. H. Shoemaker, "The NCI60 human tumour cell line anticancer drug screen," *Nature Reviews Cancer*, vol. 6, no. 10, pp. 813–823, 2006.

[4] S. A. Burchill, "What do, can and should we learn from models to evaluate potential anticancer agents?" *Future Oncology*, vol. 2, no. 2, pp. 201–211, 2006.

[5] C. A. Carter, C. Chen, C. Brink et al., "Sorafenib is efficacious and tolerated in combination with cytotoxic or cytostatic agents in preclinical models of human non-small cell lung carcinoma," *Cancer Chemotherapy and Pharmacology*, vol. 59, no. 2, pp. 183–195, 2007.

[6] T. Voskoglou-Nomikos, J. L. Pater, and L. Seymour, "Clinical predictive value of the in vitro cell line, human xenograft, and mouse allograft preclinical cancer models," *Clinical Cancer Research*, vol. 9, no. 11, pp. 4227–4239, 2003.

[7] L. Q. M. Chow and S. G. Eckhardt, "Sunitinib: from rational design to clinical efficacy," *Journal of Clinical Oncology*, vol. 25, no. 7, pp. 884–896, 2007.

[8] J. Fogh and B. C. Giovanella, *The Nude Mouse in Experimental and Clinical Research*, Academic Press, 1978.

[9] H. Castrop, "Genetically modified mice-successes and failures of a widely used technology," *Pflugers Archiv European Journal of Physiology*, vol. 459, no. 4, pp. 557–567, 2010.

[10] D. J. Wells, "Genetically modified animals and pharmacological research," *Handbook of Experimental Pharmacology*, vol. 199, pp. 213–226, 2010.

[11] M. A. G. Sosa, R. De Gasperi, and G. A. Elder, "Animal transgenesis: an overview," *Brain Structure and Function*, vol. 214, no. 2-3, pp. 91–109, 2010.

[12] J. W. Gordon, G. A. Scangos, and D. J. Plotkin, "Genetic transformation of mouse embryos by microinjection of purified DNA," *Proceedings of the National Academy of Sciences of the United States of America*, vol. 77, no. 12, pp. 7380–7384, 1980.

[13] K. R. Thomas and M. R. Capecchi, "Site-directed mutagenesis by gene targeting in mouse embryo-derived stem cells," *Cell*, vol. 51, no. 3, pp. 503–512, 1987.

[14] J. H. Lin, "Applications and limitations of genetically modified mouse models in drug discovery and development," *Current Drug Metabolism*, vol. 9, no. 5, pp. 419–438, 2008.

[15] B. Bolon, "Genetically engineered animals in drug discovery and development: a maturing resource for toxicologic research," *Basic and Clinical Pharmacology and Toxicology*, vol. 95, no. 4, pp. 154–161, 2004.

[16] R. Clarke, "Animal models of breast cancer: experimental design and their use in nutrition and psychosocial research," *Breast Cancer Research and Treatment*, vol. 46, no. 2-3, pp. 117–133, 1997.

[17] J. K. Peterson and P. J. Houghton, "Integrating pharmacology and in vivo cancer models in preclinical and clinical drug development," *European Journal of Cancer*, vol. 40, no. 6, pp. 837–844, 2004.

[18] B. Firestone, "The challenge of selecting the "right" *in vivo* oncology pharmacology model," *Current Opinion in Pharmacology*, vol. 10, no. 4, pp. 391–396, 2010.

[19] J. Rygaard and C. O. Povlsen, "Heterotransplantation of a human malignant tumour to "Nude" mice," *Acta Pathologica et Microbiologica Scandinavica*, vol. 77, no. 4, pp. 758–760, 1969.

[20] B. C. Giovanella, S. O. Yim, J. S. Stehlin, and L. J. Williams, "Development of invasive tumors in the "nude" mouse after injection of cultured human melanoma cells," *Journal of the National Cancer Institute*, vol. 48, no. 5, pp. 1531–1533, 1972.

[21] B. C. Giovanella, D. M. Vardeman, L. J. Williams et al., "Heterotransplantation of human breast carcinomas in nude mice. Correlation between successful heterotransplants, poor prognosis and amplification of the HER-2/neu oncogene," *International Journal of Cancer*, vol. 47, no. 1, pp. 66–71, 1991.

[22] V. C. Daniel, L. Marchionni, J. S. Hierman et al., "A primary xenograft model of small-cell lung cancer reveals irreversible changes in gene expression imposed by culture *in vitro*," *Cancer Research*, vol. 69, no. 8, pp. 3364–3373, 2009.

[23] R. S. Kerbel, "Human tumor xenografts as predictive preclinical models for anticancer drug activity in humans: better than commonly perceived-but they can be improved," *Cancer biology & therapy*, vol. 2, no. 4, pp. S134–S139, 2003.

[24] J. I. Johnson, S. Decker, D. Zaharevitz et al., "Relationships between drug activity in NCI preclinical in vitro and in vivo models and early clinical trials," *British Journal of Cancer*, vol. 84, no. 10, pp. 1424–1431, 2001.

[25] C. C. Scholz, D. P. Berger, B. R. Winterhalter, H. Henss, and H. H. Fiebig, "Correlation of drug response in patients and in the clonogenic assay with solid human tumour xenografts," *European Journal of Cancer*, vol. 26, no. 8, pp. 901–905, 1990.

[26] M. Hidalgo, E. Bruckheimer, N. V. Rajeshkumar et al., "A pilot clinical study of treatment guided by personalized tumorgrafts in patients with advanced cancer," *Molecular Cancer Therapeutics*, vol. 10, no. 8, pp. 1311–1316, 2011.

[27] A. Bertotti, G. Migliardi, F. Galimi et al., "A molecularly annotated platform of patient-derived xenografts ("Xenopatient") identifies HER2 as an effective therapeutic target in cetuximab-resistant colorectal cancer," *Cancer Discovery*, vol. 1, no. 6, pp. 508–523, 2011.

[28] R. Krumbach, J. Schüler, M. Hofmann, T. Giesemann, H. -H. Fiebig, and T. Beckers, "Primary resistance to cetuximab in a panel of patient-derived tumour xenograft models: activation of MET as one mechanism for drug resistance," *European Journal of Cancer*, vol. 47, no. 8, pp. 1231–1243, 2011.

[29] S. Sun, J. H. Schiller, and A. F. Gazdar, "Lung cancer in never smokers—a different disease," *Nature Reviews Cancer*, vol. 7, no. 10, pp. 778–790, 2007.

[30] A. Spira, J. Beane, V. Shah et al., "Effects of cigarette smoke on the human airway epithelial cell transcriptome," *Proceedings of the National Academy of Sciences of the United States of America*, vol. 101, no. 27, pp. 10143–10148, 2004.

[31] J. Plowman, D. J. Dykes, M. Hollingshead, L. Simpson-Herren, and M. C. Alley, "Human tumor xenograft models in NCI drug development," in *Anticancer Drug Development Guide: Preclinical Screening, Clinical Trials and Approval*, B. Teicher, Ed., pp. 101–125, Humana Press, Totowa, NJ, 1997.

[32] T. John, D. Kohler, M. Pintilie et al., "The ability to form primary tumor xenografts is predictive of increased risk of disease recurrence in early-stage non-small cell lung cancer," *Clinical Cancer Research*, vol. 17, no. 1, pp. 134–141, 2011.

[33] G. Bertolini, L. Roz, P. Perego et al., "Highly tumorigenic lung cancer CD133$^+$ cells display stem-like features and are spared by cisplatin treatment," *Proceedings of the National Academy of Sciences of the United States of America*, vol. 106, no. 38, pp. 16281–16286, 2009.

[34] I. Fichtner, J. Rolff, R. Soong et al., "Establishment of patient-derived non-small cell lung cancer xenografts as models for the identification of predictive biomarkers," *Clinical Cancer Research*, vol. 14, no. 20, pp. 6456–6468, 2008.

[35] S. Hammer, A. Sommer, I. Fichtner et al., "Comparative profiling of the novel epothilone, sagopilone, in xenografts derived from primary non-small cell lung cancer," *Clinical Cancer Research*, vol. 16, no. 5, pp. 1452–1465, 2010.

[36] X. Dong, J. Guan, J. C. English et al., "Patient-derived first generation xenografts of non-small cell lung cancers: promising tools for predicting drug responses for personalized chemotherapy," *Clinical Cancer Research*, vol. 16, no. 5, pp. 1442–1451, 2010.

[37] E. Marangoni, A. Vincent-Salomon, N. Auger et al., "A new model of patient tumor-derived breast cancer xenografts for preclinical assays," *Clinical Cancer Research*, vol. 13, no. 13, pp. 3989–3998, 2007.

[38] L. De Plater, A. Laugé, C. Guyader et al., "Establishment and characterisation of a new breast cancer xenograft obtained from a woman carrying a germline BRCA2 mutation," *British Journal of Cancer*, vol. 103, no. 8, pp. 1192–1200, 2010.

[39] M. R. Simpson-Abelson, G. F. Sonnenberg, H. Takita et al., "Long-term engraftment and expansion of tumor-derived memory T cells following the implantation of non-disrupted pieces of human lung tumor into NOD-scid IL2R*γ*null Mice," *Journal of Immunology*, vol. 180, no. 10, pp. 7009–7018, 2008.

[40] T. Reya, S. J. Morrison, M. F. Clarke, and I. L. Weissman, "Stem cells, cancer, and cancer stem cells," *Nature*, vol. 414, no. 6859, pp. 105–111, 2001.

[41] R. Pardal, M. F. Clarke, and S. J. Morrison, "Applying the principles of stem-cell biology to cancer," *Nature Reviews Cancer*, vol. 3, no. 12, pp. 895–902, 2003.

[42] M. F. Clarke, "Self-renewal and solid-tumor stem cells," *Biology of Blood and Marrow Transplantation*, vol. 11, no. 2, pp. 14–16, 2005.

[43] M. F. Clarke, J. E. Dick, P. B. Dirks et al., "Cancer stem cells—perspectives on current status and future directions: AACR workshop on cancer stem cells," *Cancer Research*, vol. 66, no. 19, pp. 9339–9344, 2006.

[44] D. Bonnet and J. E. Dick, "Human acute myeloid leukemia is organized as a hierarchy that originates from a primitive hematopoietic cell," *Nature Medicine*, vol. 3, no. 7, pp. 730–737, 1997.

[45] S. K. Singh, I. D. Clarke, M. Terasaki et al., "Identification of a cancer stem cell in human brain tumors," *Cancer Research*, vol. 63, no. 18, pp. 5821–5828, 2003.

[46] H. D. Hemmati, I. Nakano, J. A. Lazareff et al., "Cancerous stem cells can arise from pediatric brain tumors," *Proceedings of the National Academy of Sciences of the United States of America*, vol. 100, no. 25, pp. 15178–15183, 2003.

[47] R. Galli, E. Binda, U. Orfanelli et al., "Isolation and characterization of tumorigenic, stem-like neural precursors from human glioblastoma," *Cancer Research*, vol. 64, no. 19, pp. 7011–7021, 2004.

[48] D. Fang, T. K. Nguyen, K. Leishear et al., "A tumorigenic subpopulation with stem cell properties in melanomas," *Cancer Research*, vol. 65, no. 20, pp. 9328–9337, 2005.

[49] T. Schatton, G. F. Murphy, N. Y. Frank et al., "Identification of cells initiating human melanomas," *Nature*, vol. 451, no. 7176, pp. 345–349, 2008.

[50] M. Al-Hajj, M. S. Wicha, A. Benito-Hernandez, S. J. Morrison, and M. F. Clarke, "Prospective identification of tumorigenic breast cancer cells," *Proceedings of the National Academy of Sciences of the United States of America*, vol. 100, no. 7, pp. 3983–3988, 2003.

[51] S. A. Bapat, A. M. Mali, C. B. Koppikar, and N. K. Kurrey, "Stem and progenitor-like cells contribute to the aggressive behavior of human epithelial ovarian cancer," *Cancer Research*, vol. 65, no. 8, pp. 3025–3029, 2005.

[52] A. T. Collins, P. A. Berry, C. Hyde, M. J. Stower, and N. J. Maitland, "Prospective identification of tumorigenic prostate cancer stem cells," *Cancer Research*, vol. 65, no. 23, pp. 10946–10951, 2005.

[53] L. Ricci-Vitiani, D. G. Lombardi, E. Pilozzi et al., "Identification and expansion of human colon-cancer-initiating cells," *Nature*, vol. 445, no. 7123, pp. 111–115, 2007.

[54] C. A. O'Brien, A. Pollett, S. Gallinger, and J. E. Dick, "A human colon cancer cell capable of initiating tumour growth in immunodeficient mice," *Nature*, vol. 445, no. 7123, pp. 106–110, 2007.

[55] P. Dalerba, S. J. Dylla, I. K. Park et al., "Phenotypic characterization of human colorectal cancer stem cells," *Proceedings of the National Academy of Sciences of the United States of America*, vol. 104, no. 24, pp. 10158–10163, 2007.

[56] A. Eramo, F. Lotti, G. Sette et al., "Identification and expansion of the tumorigenic lung cancer stem cell population," *Cell Death and Differentiation*, vol. 15, no. 3, pp. 504–514, 2008.

[57] G. Bertolini, L. Gatti, and L. Roz, "The "stem" of chemoresistance," *Cell Cycle*, vol. 9, no. 4, pp. 628–629, 2010.

[58] A. Jimeno, G. Feldmann, A. Suárez-Gauthier et al., "A direct pancreatic cancer xenograft model as a platform for cancer stem cell therapeutic development," *Molecular Cancer Therapeutics*, vol. 8, no. 2, pp. 310–314, 2009.

[59] T. Hoey, W. C. Yen, F. Axelrod et al., "DLL4 blockade inhibits tumor growth and reduces tumor-initiating cell frequency," *Cell Stem Cell*, vol. 5, no. 2, pp. 168–177, 2009.

[60] C. Ginestier, S. Liu, M. E. Diebel et al., "CXCR1 blockade selectively targets human breast cancer stem cells in vitro and in xenografts," *Journal of Clinical Investigation*, vol. 120, no. 2, pp. 485–497, 2010.

[61] S. J. Dylla, L. Beviglia, I. K. Park et al., "Colorectal cancer stem cells are enriched in xenogeneic tumors following chemotherapy," *PLoS One*, vol. 3, no. 6, Article ID e2428, 2008.

[62] Z. A. Rasheed, J. Yang, Q. Wang et al., "Prognostic significance of tumorigenic cells with mesenchymal features in pancreatic adenocarcinoma," *Journal of the National Cancer Institute*, vol. 102, no. 5, pp. 340–351, 2010.

[63] M. P. Kim, J. B. Fleming, H. Wang et al., "ALDH activity selectively defines an enhanced tumor-initiating cell population relative to CD133 expression in human pancreatic

adenocarcinoma," *PLoS One*, vol. 6, no. 6, Article ID e20636, 2011.

[64] P. Workman, E. O. Aboagye, F. Balkwill et al., "Guidelines for the welfare and use of animals in cancer research," *British Journal of Cancer*, vol. 102, no. 11, pp. 1555–1577, 2010.

Hindawi Publishing Corporation
Journal of Biomedicine and Biotechnology
Volume 2012, Article ID 131324, 6 pages
doi:10.1155/2012/131324

Review Article

Canine Liver Transplantation Model and the Intermediate Filaments of the Cytoskeleton of the Hepatocytes

Consolato Sergi,[1,2] Reem Abdualmjid,[1] and Yasser Abuetabh[1]

[1] *Department of Laboratory Medicine and Pathology, University of Alberta, Edmonton, AB, Canada T6G 2B7*
[2] *Department of Laboratory Medicine and Pathology, Walter Mackenzie Health Sciences Centre, 5B4.09, 8440-112 Street, Edmonton, AB, Canada T6G 2B7*

Correspondence should be addressed to Consolato Sergi, biotechlab@gmail.com

Received 10 December 2011; Accepted 27 January 2012

Academic Editor: Andrea Vecchione

Liver transplantation has been a successful therapy for liver failure. However, a significant number of recipients suffer from graft dysfunction. Considerably, ischemia and reperfusion (I/R) injury is the most important factor leading to organ dysfunction, although the pathogenesis has not been fully described. I/R injury have several established features that are accompanied by and/or linked to bile duct loss or ductopenia, cholestasis, and biliary ductular proliferations in the posttransplant liver biopsy. However, biliary marker levels increase usually only 5–7 days after transplantation. Intermediate filaments are one of the three cytoskeletal proteins that have a major role in liver protection and maintaining both cellular structure and integrity of eukaryotic cells. We reviewed the canine liver transplantation model as I/R injury model to delineate the intermediate filaments of the cytoskeleton that are probably the determinants in changing the phenotype of hepatocytes to cholangiocytes. Remarkably, this interesting feature seems to occur earlier than frank cholestasis. We speculate that I/R liver injury through a phenotypical switch of the hepatocytes may contribute to the poor outcome of the liver graft.

1. Introduction

Liver transplantation is an established therapy for both acute and chronic liver failure. However, graft dysfunction remains a problem affecting up to one-third of the recipients, despite reports of good to excellent long-term outcome. The organ dysfunction is considered multifactorial, but ischemia and reperfusion (I/R) injury is probably the most important contributing factor, although the detailed steps of pathogenesis are controversially debated. I/R injury is a major cause of liver graft dysfunction resulting in adenosine triphosphate (ATP) decrease, evidence of intracellular acidosis, and cell swelling of the hepatocytes. This aspect is also accompanied by or linked to bile duct loss or ductopenia, cholestasis, and biliary ductular proliferations in the posttransplant liver biopsy. However, biliary marker levels increase usually only 5–7 days after transplantation stimulating several fields of research in the last couple of decades. Cholestasis is associated with high morbidity and mortality in patients undergoing liver transplantation, and the steps reaching this state are not completely understood. We reviewed the canine liver transplantation model as I/R injury model to delineate in detail the intermediate filaments of the cytoskeleton that are probably the determinants in changing the phenotype of hepatocytes to cholangiocytes, which seems to be a post-transplant event occurring in the liver at an earlier stage than frank cholestasis. Here, we speculate that I/R liver injury through a phenotypical switch of the liver cells may contribute to the poor outcome of the liver graft.

2. Liver Transplantation

Liver transplantation is widely known as the most effective therapy for both acute and chronic liver failure [1]. In 1963, Thomas Starzl, an American surgeon, Northwestern University Medical School graduate with degrees in anatomy, neurophysiology, and medicine, was the first to perform the

liver transplantation on a child suffering from biliary atresia [2]. Despite the significant success of liver transplantation, infection, poor graft function, and rejection are major problems that may still contribute to death of the transplanted patient or to deterioration of the graft. Reperfusion following long ischemia of liver during liver transplantation causes severe injury, which is now universally indicated as I/R injury [1]. I/R injury of liver is a major cause of morbidity and mortality in patients undergoing liver transplantation [3]. Several mechanisms and distinct pathways may involve I/R leading to both initial poor function and primary nonfunction of the liver allograft [4]. Three cytoskeletal proteins form a network that provide the cellular structure and fundamental integrity of the eukaryotic cells: microfilaments, microtubules, and intermediate filaments. The intermediate filament proteins have an important role in liver protection against mechanical and nonmechanical injury, which have been demonstrated in animal models. Overexpression of proteins and mutations of the corresponding keratin genes have been reported to contribute to several human oncological and nononcological diseases [5].

3. Cytoskeleton and Keratins Are Involved in the Development of the Intrahepatic Biliary System (K19 and K7)

Eukaryotic cells have a unique cytoplasmic structure labeled as cytoskeleton, which consists of three distinct kinds of cytoskeletal filaments, including microfilaments, microtubules, and intermediate filaments. Besides giving the rigidity of the cell and maintaining cell shape and borders or cell "scaffolding," cytoskeleton plays important and probably crucial roles in intracellular transport, cell division, gene regulation, and signal transduction of the genetic information [6, 7]. Actin, which is widely accepted to be a highly conserved structure among different species, is the major protein that constitutes the microfilaments. There are three known classes of human actin gene that have been identified as β-, α-, and γ-actin. Cell-cell interaction, signal transduction, cell shape maintenance, and cell motility are the central functions of actin [7]. Microtubules, which have a diameter of around 23 nm, are protofilaments that are important for the intracellular transport, movement of cilia and flagella, mitotic spindle, and cell wall synthesis. Tubulins are the major component of microtubules. Both microfilaments and microtubules have several groups of binding proteins that modulate their stability and biological functions, such as signal transduction [7]. Intermediate filaments with around 10 nm of diameter are more stable than actin filaments and function in the maintenance of cell shape by carrying tension. Intermediate filaments, which include, for example, vimentin, glial fibrillary acidic protein, neurofilament proteins, keratins, and nuclear lamins, organize the internal 3D cell structure anchoring cyto-organelles and serving as structural scaffolds of the nucleus and cytoplasm. Cytokeratins (Ks) are the main protein family that constitutes the intermediate filaments with more than fifty members that have been identified [8]. Polypeptides of the Ks are variants and have been divided into type I and type II, or acidic and basic, respectively [9]. Studies have shown that each epithelial cell has a distinct content of cytokeratins (i.e., expression of keratins is described as tissue-specific manner) playing a major role in the tissue identification of metastasis of unknown primary carcinomas [10]. Ks usually present in cells as heteropolymers pairs composed of type I (K9–K20) and type II (K1–K8). Similar to microfilaments and microtubules, keratins have numbers of their preferential binding proteins. K8 (MW 52KD) and K18 (MW 45KD) are considered as the only Ks that are normally expressed in human hepatocytes [10]. Moreover, both K8 and K18 have been found to be expressed in early development stage of mouse embryos [11]. Immunohistochemical studies have revealed that cholangiocytes (bile duct cells) express K7 (54 KD) and K19 (40 KD) in addition to K8 and K18 [12], and those Ks have been used as valid markers for both studies on development of the intrahepatic biliary system and for assessment of bile duct damage [9]. It has also been well established that cholangiocytes are derived from hepatoblasts found around portal vein [13]. These cells show a particularly intense expression of K8 and K18. As indicated above, K7 and K19 have been linked to development of the intrahepatic bile duct system in both humans and animal models. The expression of K19 is useful to identify primitive biliary cells, while the expression of K7 appears after 20 weeks of gestation in humans [13]. Both K7 and K19 are consistently expressed in the development of the intrahepatic bile duct with elevated levels until one month of postnatal age. Thus, in order to phenotypically switch hepatoblasts into cholangiocytes, these cells should firstly express K19 followed by expression of K7 [13]. However, it has been shown that hepatocytes might express K7 in response to different conditions, such as ductopenia and cholestasis [14], and, interestingly, it has been found that hepatocellular carcinoma cells expressing K19 are significantly associated with reoccurrence of neoplasm after transplantation [15]. A recent study has demonstrated that hepatocytes are frequently expressing K7 in case of chronic liver allograft rejection [14]. Sergi et al. have demonstrated that hepatocytes intensively expressed K7 and K19 early following cold ischemia in a canine isolated perfused liver transplantation model [16]. Furthermore, they demonstrated that bile duct cytokeratins are very useful markers to diagnose an early sign of cholestasis. It has become clear that cholestasis is significantly associated with high morbidity and mortality in patients undergoing liver transplantation. Therefore, investigations that lead to discover the mechanisms of the cholestasis are dramatically required.

4. Ischemia/Reperfusion (I/R) Injury

I/R injury is a phenomenon that occurs when blood flow and oxygen delivery return to reperfused tissue [17]. It is considered one of the major causes of morbidity and mortality among patients undergoing liver transplantation [3]. I/R injury has been demonstrated in several diseases such as cerebrovascular diseases, peripheral vascular diseases, sepsis, myocardial infarction, and organ transplantation

[18]. It involves several mechanisms, which lead to organ failure, circulatory dysfunction, and, finally, death of the transplanted patient [1]. Cellular mechanisms of I/R injury include a few essential cell cascades that suggest the role of activation of endothelial cells, Kupffer cells, reactive oxygen species (ROS), and polymorphonuclear leukocytes (PMN) or neutrophils in the pathogenesis of I/R injury [19]. There may also be mechanisms involving T lymphocytes that seem to have a key role in short- and long-term damage during I/R injury. T lymphocytes act as mediator in the subacute inflammatory phase of neutrophilic recruitment following I/R injury [20]. Another important constituent of tissue injury following I/R injury that needs to be emphasized is the production of oxygen free radicals (OFRs). These OFRs can arise from different sources, such as Kupffer cells, PMN [1], and xanthine oxidase (XO) that is the most significant source [21]. Several etiological factors are involved in I/R injury, including ATP reduction [16], activation of proteases, and alteration in the intracellular concentration of cytokines and chemokines [22], and cell swelling [16]. Investigations of posttransplantation surgery have indicated that reperfusion plays an essential role in primary graft nonfunction, which is one of the most serious complications of liver transplantation [23]. The incidence of primary graft dysfunction is up to 20% [16]. I/R injury also causes early organ failure up to 10% as well as increases the acute and chronic rejection [1]. Several studies demonstrated that during I/R injury, morphological changes of liver tissues occur, and these changes can have a prognostic significance.

5. Intermediate Filaments of Cytoskeleton

The intermediate filament (IF) cytoskeletal protein is one of the three major cytoskeletal proteins whose result is important in maintaining both cellular structure and integrity of eukaryotic cells. The other two filament proteins are microfilaments (MF) and microtubules (MT) [5]. Beside their cellular functions like cell motility, division, and stress responses, they also have an essential role in human diseases due to mutations in filament proteins. For example, mutation in actin microfilaments will cause cardiac and noncardiac myopathies [5]. IF proteins consist of five types of keratins according to structure of genome and composition of amino acid, IF proteins types I–IV are cytoplasmic, and type V IF contain nuclear lamins [7]. The keratins are obligating noncovalently heteropolymers because they consist of one of each type I and type II keratins as pairs [9]. Type I or "acidic" and type II or "neutral to basic" keratins are the largest group of IF proteins [7] classified as type I (K9–K20) and type II (K1–K8) [24]. Another type of IF proteins is type III IF that includes vimentin, peripherin, glial fibrillary acidic protein, and desmin of mesenchymal cells, peripheral neurons, glia cells and astrocytes, and muscle cells, respectively [7]. Type IV IF proteins include neurofilament proteins (NF-L, NF-M, and NF-H), synemin, nestin, syncoilin, and α-internexin; lamins A–C for type V IF proteins [24]. They are the major IF proteins in the liver [5]. As indicated above, the adult hepatocytes express K8 and K18 only compared to other epithelial cells that express 2 or more type I or type II keratins [9] such as bile duct, which expresses additional keratins K7 and K19 [8]. Furthermore, alteration of the cytoskeletal proteins leads to several diseases and disorders. The first disease to be discovered related to keratin mutation was epidermolysis bullosa simplex (EBS) with mutations in K5 and K14. White sponge nevus syndrome is another disease caused by mutations in K4 and K13. It affects noncornifying stratified squamous epithelia in mouth, esophagus, and anogenital mucosa [25]. Additionally, mutations in K8 and/or K18 lead to acute or chronic liver diseases [26]. Normally in hepatocytes, the microfilaments are distributed in plasma membrane and region of the bile canaliculus. Further studies indicated that reperfusion alone causes alteration of theses microfilaments (F-actin) leading to contraction of canaliculi, relocalization of enzymes and transporters of canaliculi, and increasing permeability of cellular tight junction [16]. Cholestatic liver disease occurs when there is a decrease in bile flow, which is an abnormal physiologic state, and retention of toxic bile acids [27]. All three filament cytoskeletal proteins are remarkably altered in cholestatic liver disease. Clear cytoplasmic hepatocytes (cholate stasis) presented in cirrhotic nodules and showed a decrease in keratin IF network in the cytoplasm [28]. Studies on mice reported that keratin was overexpressed in epithelia of bile duct due to ligation of bile duct and in hepatocytes. In cholestatic liver disease, bile duct epithelial-type keratin (K7 and K19) was expressed in hepatocytes, too. Intermediate hepatocytes express K7, while reactive bile ductules express K7 and K19 [28]. In post-transplant period, morphological changes in liver tissue have also been demonstrated. Keratins of biliary type were detected in the hepatocytes in the early period of I/R injury. Moreover, bile canaliculus progressively dilate after ischemia, and a change of the microvillous integrity is demonstrable [16].

6. Canine Liver Transplantation Model

The liver is one of the organs with an incredible capacity for *in vivo* tissue engineering which allow restoration of the liver architecture and reestablishment of certain vital functions. The study of liver regeneration in humans arise ethical issues, and it is difficult to carry out because of a plethora of heterogeneous liver lesions. Accordingly, using experimental animal models is more useful and helpful for studying liver regeneration [29]. *In vitro* studies need to be followed by in vivo ones to simulate the interaction between liver cell populations. In our opinion, the use of large animals such as dog, pig, or sheep is more advantageous than small animals like rat or mouse; large animals are similar to human beings in their physiology and anatomy, and techniques of microsurgery are not necessary to carry out determinate experiments [29]. Only few studies have been carried out on I/R animal models in liver [21]. The canine liver model following I/R injury has been used as a liver transplantation model to study excretion of bile and intrahepatic intermediate filaments expression involved in morphological changes of the biliary system [16]. To the best of our knowledge, in a canine isolated and

perfused liver model, there was the first clear-cut evidence of cholestatic changes starting early following cold ischemia despite prompt recovery of the bile flow. According to some other authors, the use of the canine liver transplantation model seems to allow a better vascular perfusion under *ex vivo* conditions in contrast to the rat model [5]. Sergi et al.'s study revealed an ischemia-dependent impairment of an experimental biliary dye excretion during early stage of reperfusion and a progressive cytokeratin expression of biliary type in the hepatocytes despite a prompt recovery of the bile flow after I/R. The recovery of the bile output after I/R represents a key event in LT. The nonstimulated bile flow rate was unaffected by cold ischemia up to 10 h in our canine isolated perfused liver model, but the decrease of the biliary dye excretion during early stage of reperfusion correlated with the peak output rate of the dye across the canalicular membrane. The transhepatic transit time was prolonged with increasing ischemia time. Remarkably, the dye uptake at the sinusoidal membrane was not affected by cold ischemia, leading to a possible accumulation of toxic compounds in the hepatocytes. Hepatic elimination of the dye following I/R has been analyzed mainly by plasma clearance [4]. Very importantly was the study of the hepatic elimination of the dye after a bolus injection by compartmental spectrophotometric analysis both in the perfusate by transhepatic sampling and in the bile. In fact, this reflects the "effective" vectorial hepatocellular transport. Differential mechanisms can be suggested for the impaired biliary excretion of organic anions following I/R. Previously, a positive correlation between biliary dye excretion, viability of the graft, and hepatic ATP content has been found in cholestatic liver disease, and reduced biliary dye excretion has been attributed to the lack of ATP [17]. ATP content does not seem to be the main limiting factor for the hepatocellular transport following I/R. An impairment of the intracellular transport or a decreased transport rate across the canalicular membrane might play a major role as contributing factor. The step across the canalicular membrane generally represents the rate-limiting one in the hepatocellular transport [18]. In the canine liver transplantation model, the flow in the portal vein was continuous, because roller pump, oxygenator, and heat exchanger in the perfusion line were connected in series with the roller pump upstream. The oxygen content of the saline reperfusion solution was 2% in volume (10% of arterial hepatic blood and about 15% of the portal venous blood). The pO_2 values were almost five times higher than in blood. Thus, one can expect to have reactive-oxygen-species- (ROS-) linked damage at the beginning of the reperfusion after 8 or 10 h of ischemia. However, the excellent reperfusion results of the control group and data of the 2 h ischemia group indicate that this is not a general problem, but may be an ischemia-time-linked problem. High O_2 partial pressure in the liver stimulates ROS formation after extensive long ischemia times, and this may be one of the most important limiting factors of the ischemia tolerance [22]. Electron microscopy studies in hepatocytes revealed microfilaments, which are distributed along the plasma membrane and in the region of the bile canaliculus. As indicated above, cytoskeleton filaments are also essential for the maintenance of cell shape, bile canalicular architecture, and integrity of the cellular tight junctions. The microfilaments network surrounding the canalicular pole and extending into the canalicular microvilli is damaged during cholestasis. Reperfusion, but not ischemia, has been considered faulty, inducing an alteration of F-actin microfilaments, suggesting an impairment of the canalicular contraction, an increase of the tight junction permeability, and a probable relocalization of canalicular enzymes and transporters. Bile canalicular size change as detected in our study may be coincident with the reorganization of the pericanalicular filaments and the colocalization of actin and myosin. In fact, contraction in this study has been associated with shortening and/or twisting of bile canaliculi [5].

7. Summary

Liver transplantation is an established therapy for both acute and chronic liver failure. However, graft dysfunction remains a problem affecting up to one-third of the recipients, despite good to excellent long-term outcome. The organ dysfunction is considered multifactorial, but I/R injury is probably the most important contributing factor. The detailed steps of the pathogenesis of I/R injury continue to be a topic of vivid debate. I/R injury is a major cause of liver graft dysfunction resulting in ATP decrease, intracellular acidosis, and cell swelling of the hepatocytes. This feature is also linked to bile duct loss or ductopenia, cholestasis, and biliary ductular proliferations in the liver biopsy. However, the plasmatic levels of biliary markers increase usually only 5–7 days after transplantation prompting on-going research to address new markers of early liver damage. This could also be a stimulus to support more grant approvals for liver posttransplantation studies. Cholestasis is associated with high morbidity and mortality in patients undergoing liver transplantation, but the steps reaching this state are still deemed elusive. We reviewed the canine LT model as an I/R injury model and reviewed the intermediate filaments of the cytoskeleton that are probably the determinants in changing the phenotype of hepatocytes to cholangiocytes. In fact, this phenotypic switch of the liver cells, which is also sometimes called pseudo- or neoacinar transformation in diseases with cholestasis [30], seems to occur at a stage earlier than frank cholestasis. We emphasized that I/R injury through this peculiar phenotypic switch of the hepatocytes may be a milestone to investigate the pathways contributing to the poor outcome of the liver graft. Reperfusion injury following ischemia affects graft function in liver transplantation by induction of phenotypical changes in hepatocellular keratins. Keratin phenotype of hepatocytes leads to hepatocellular damage that is intimately connected to several intracellular processes, which are under intense investigation in our laboratory, and the appropriate choice of an animal model is crucial in forwarding research in very complex areas requiring not only human, but also comparative (veterinary) pathology knowledge.

Acknowledgments

The authors are very grateful to the Saudi Cultural Bureau, Ottawa, ON, Canada, for the financial support of two graduate students (R. Abdualmjid and Y. Abuuetabh.).They are also very grateful to Tyrolean Cancer Research Fund, Innsbruck, Austria and University of Alberta for some extra- and intramural funding, respectively. This work is dedicated to the memory of Professor Dr. h.c. Herwart F. Otto, formerly chairman and emeritus professor of pathology at the Institute of Pathology, Ruperto-Carola University of Heidelberg, Germany.

References

[1] J. W. Kupiec-Weglinski and R. W. Busuttil, "Ischemia and reperfusion injury in liver transplantation," *Transplantation Proceedings*, vol. 37, no. 4, pp. 1653–1656, 2005.

[2] T. E. Starzl, T. L. Marchioro, K. N. Vonkaulla, G. Hermann, R. S. Brittain, and W. R. Waddell, "Homotransplantation of the liver in humans," *Surgery, Gynecology & Obstetrics*, vol. 117, pp. 659–676, 1963.

[3] F. Dünschede, K. Erbes, A. Kircher et al., "Reduction of ischemia reperfusion injury after liver resection and hepatic inflow occlusion by α-lipoic acid in humans," *World Journal of Gastroenterology*, vol. 12, no. 42, pp. 6812–6817, 2006.

[4] P. A. Clavien, P. R. C. Harvey, and S. M. Strasberg, "Preservation and reperfusion injuries in liver allografts: an overview and synthesis of current studies," *Transplantation*, vol. 53, no. 5, pp. 957–978, 1992.

[5] M. B. Omary, N. O. Ku, and D. M. Toivola, "Keratins: guardians of the liver," *Hepatology*, vol. 35, no. 2, pp. 251–257, 2002.

[6] E. Frixione, "Recurring views on the structure and function of the cytoskeleton: a 300-year epic," *Cell Motility and the Cytoskeleton*, vol. 46, no. 2, pp. 73–94, 2000.

[7] N. O. Ku, X. Zhou, D. M. Toivola, and M. B. Omary, "The cytoskeleton of digestive epithelia in health and disease," *American Journal of Physiology*, vol. 277, no. 6, pp. G1108–G1137, 1999.

[8] P. Strnad, C. Stumptner, K. Zatloukal, and H. Denk, "Intermediate filament cytoskeleton of the liver in health and disease," *Histochemistry and Cell Biology*, vol. 129, no. 6, pp. 735–749, 2008.

[9] P. Van Eyken and V. J. Desmet, "Cytokeratins and the liver," *Liver*, vol. 13, no. 3, pp. 113–122, 1993.

[10] R. Moll, W. W. Franke, and D. L. Schiller, "The catalog of human cytokeratins: patterns of expression in normal epithelia, tumors and cultured cells," *Cell*, vol. 31, no. 1, pp. 11–24, 1982.

[11] B. W. Jackson, C. Grund, and E. Schmid, "Formation of cytoskeletal elements during mouse embryogenesis. Intermediate filaments of the cytokeratin type and desmosomes in preimplantation embryos," *Differentiation*, vol. 17, no. 3, pp. 161–179, 1980.

[12] P. Van Eyken, R. Sciot, B. Van Damme, C. De Wolf-Peeters, and V. J. Desmet, "Keratin immunohistochemistry in normal human liver. Cytokeratin pattern of hepatocytes, bile ducts and acinar gradient," *Virchows Archiv*, vol. 412, no. 1, pp. 63–72, 1987.

[13] P. Van Eyken, R. Sciot, F. Callea, K. Van der Steen, P. Moerman, and V. J. Desmet, "The development of the intrahepatic bile ducts in man: a keratin-immunohistochemical study," *Hepatology*, vol. 8, no. 6, pp. 1586–1595, 1988.

[14] A. M. Bellizzi, R. D. LeGallo, J. C. Boyd, and J. C. Iezzoni, "Hepatocyte cytokeratin 7 expression in chronic allograft rejection," *American Journal of Clinical Pathology*, vol. 135, no. 2, pp. 238–244, 2011.

[15] A. Durnez, C. Verslype, F. Nevens et al., "The clinicopathological and prognostic relevance of cytokeratin 7 and 19 expression in hepatocellular carcinoma. A possible progenitor cell origin," *Histopathology*, vol. 49, no. 2, pp. 138–151, 2006.

[16] C. Sergi, W. Gross, M. Mory, M. Schaefer, and M. M. Gebhard, "Biliary-type cytokeratin pattern in a canine isolated perfused liver transplantation model," *Journal of Surgical Research*, vol. 146, no. 2, pp. 164–171, 2008.

[17] E. E. Montalvo-Jave, T. Escalante-Tattersfield, J. A. Ortega-Salgado, E. Piña, and D. A. Geller, "Factors in the Pathophysiology of the Liver Ischemia-Reperfusion Injury," *Journal of Surgical Research*, vol. 147, no. 1, pp. 153–159, 2008.

[18] G. Bilbao, J. L. Contreras, D. E. Eckhoff et al., "Reduction of ischemia-reperfusion injury of the liver by in vivo adenovirus-mediated gene transfer of the antiapoptotic Bcl-2 gene," *Annals of Surgery*, vol. 230, no. 2, pp. 185–193, 1999.

[19] C. Fondevila, R. W. Busuttil, and J. W. Kupiec-Weglinski, "Hepatic ischemia/reperfusion injury—a fresh look," *Experimental and Molecular Pathology*, vol. 74, no. 2, pp. 86–93, 2003.

[20] R. M. Zwacka, Y. Zhang, J. Halldorson, H. Schlossberg, L. Dudus, and J. F. Engelhardt, "CD4+ T-lymphocytes mediate ischemia/reperfusion-induced inflammatory responses in mouse liver," *Journal of Clinical Investigation*, vol. 100, no. 2, pp. 279–289, 1997.

[21] H. Ajamieh, N. Merino, E. Candelario-Jalil et al., "Similar protective effect of ischaemic and ozone oxidative preconditionings in liver ischaemia/reperfusion injury," *Pharmacological Research*, vol. 45, no. 4, pp. 333–339, 2002.

[22] V. Kohli, W. Gao, C. A. Camargo, and P. A. Clavien, "Calpain is a mediator of preservation-reperfusion injury in rat liver transplantation," *Proceedings of the National Academy of Sciences of the United States of America*, vol. 94, no. 17, pp. 9354–9359, 1997.

[23] L. Benkoël, F. Dodero, J. Hardwigsen et al., "Effect of ischemia-reperfusion on bile canalicular F-actin microfilaments in hepatocytes of human liver allograft: image analysis by confocal laser scanning microscopy," *Digestive Diseases and Sciences*, vol. 46, no. 8, pp. 1663–1667, 2001.

[24] M. Hesse, T. M. Magin, and K. Weber, "Genes for intermediate filament proteins and the draft sequence of the human genome: novel keratin genes and a suprisingly high number of pseudogenes related to keratin genes 8 and 18," *Journal of Cell Science*, vol. 114, no. 14, pp. 2569–2575, 2001.

[25] A. D. Irvine and W. H. I. McLean, "Human keratin diseases: the increasing spectrum of disease and subtlety of the phenotype-genotype correlation," *British Journal of Dermatology*, vol. 140, no. 5, pp. 815–828, 1999.

[26] N. O. Ku, R. Gish, T. L. Wright, and M. B. Omary, "Keratin 8 mutations in patients with cryptogenic liver disease," *New England Journal of Medicine*, vol. 344, no. 21, pp. 1580–1587, 2001.

[27] G. F. Hutchins and J. L. Gollan, "Recent developments in the pathophysiology of cholestasis," *Clinics in Liver Disease*, vol. 8, no. 1, pp. 1–26, 2004.

[28] K. Zatloukal, C. Stumptner, A. Fuchsbichler et al., "The keratin cytoskeleton in liver diseases," *Journal of Pathology*, vol. 204, no. 4, pp. 367–376, 2004.

[29] D. Palmes and H. U. Spiegel, "Animal models of liver regeneration," *Biomaterials*, vol. 25, no. 9, pp. 1601–1611, 2004.

[30] L. Dorn, L. F. Menezes, G. Mikuz, H. F. Otto, L. F. Onuchic, and C. Sergi, "Immunohistochemical detection of polyductin and co-localization with liver progenitor cell markers during normal and abnormal development of the intrahepatic biliary system and in adult hepatobiliary carcinomas," *Journal of Cellular and Molecular Medicine*, vol. 13, no. 7, pp. 1279–1290, 2009.

Hindawi Publishing Corporation
Journal of Biomedicine and Biotechnology
Volume 2012, Article ID 845618, 10 pages
doi:10.1155/2012/845618

Review Article

Classic and New Animal Models of Parkinson's Disease

Javier Blesa,[1,2] Sudarshan Phani,[1,2] Vernice Jackson-Lewis,[1,2,3] and Serge Przedborski[1,2,3]

[1] *Department of Pathology and Cell Biology, Columbia University, New York, NY 10032, USA*
[2] *Center for Motor Neuron Biology and Disease, Columbia University, New York, NY 10032, USA*
[3] *Department of Neurology, Columbia University, New York, NY 10032, USA*

Correspondence should be addressed to Serge Przedborski, SP30@Columbia.edu

Received 9 January 2012; Accepted 23 January 2012

Academic Editor: Monica Fedele

Neurological disorders can be modeled in animals so as to recreate specific pathogenic events and behavioral outcomes. Parkinson's Disease (PD) is the second most common neurodegenerative disease of an aging population, and although there have been several significant findings about the PD disease process, much of this process still remains a mystery. Breakthroughs in the last two decades using animal models have offered insights into the understanding of the PD disease process, its etiology, pathology, and molecular mechanisms. Furthermore, while cellular models have helped to identify specific events, animal models, both toxic and genetic, have replicated almost all of the hallmarks of PD and are useful for testing new neuroprotective or neurorestorative strategies. Moreover, significant advances in the modeling of additional PD features have come to light in both classic and newer models. In this review, we try to provide an updated summary of the main characteristics of these models as well as the strengths and weaknesses of what we believe to be the most popular PD animal models. These models include those produced by 6-hydroxydopamine (6-OHDA), 1-methyl-1,2,3,6-tetrahydropiridine (MPTP), rotenone, and paraquat, as well as several genetic models like those related to alpha-synuclein, PINK1, Parkin and LRRK2 alterations.

1. Introduction

Parkinson's disease (PD) is the second most common neurodegenerative disease, affecting 1% of the population over 55 years of age [1]. This disease is characterized by the loss of ~50–70% of the dopaminergic neurons in the substantia nigra pars compacta (SNc), a profound loss of dopamine (DA) in the striatum, and the presence of intracytoplasmic inclusions called Lewy bodies (LB), which are composed mainly of α-synuclein and ubiquitin. Although mutations in the α-synuclein gene have thus far been associated only with rare familial cases of PD, α-synuclein is found in all LBs [2]. Therefore, this protein may play an important role in the pathogenesis of this disease. The main features of PD are tremor, rigidity, bradykinesia, and postural instability; however, these motor manifestations can be accompanied by nonmotor symptoms such as olfactory deficits, sleep impairments, and neuropsychiatric disorders [3–5]. Although the complete PD disease process is not yet understood, we have gained a better understanding of its etiology, pathology, and molecular mechanisms, thanks to various animal models [6]. For example, reserpine administration in animals was found to produce a profound depletion of monoamines, including DA, in the brains of injected animals resulting in reserpine syndrome. The symptoms of this syndrome consisted of slowness of movement and rigidity [7] now commonly associated with PD. Interestingly, it was found that L-DOPA was able to reverse many of the symptoms associated with reserpine administration [8], furthering the hypothesis that DA depletion was at the root of PD symptomatology.

For the past several decades, animal models of PD have come in a variety of forms. Typically, they can be divided into those using environmental or synthetic neurotoxins or those utilizing the in vivo expression of PD-related mutations (genetic).

Of the neurotoxic models, compounds that produce both reversible (reserpine) and irreversible (MPTP, 6-OHDA, paraquat, rotenone) effects have been used effectively; however recent studies have focused more on irreversible toxins to produce PD-related pathology and symptomatology. Therefore, the neurotoxins covered in this paper will focus on those that produce an irreversible effect. Neurotoxin-based

models produced by 6-hydroxydopamine (6-OHDA) and 1-methyl-1,2,3,6-tetrahydropyridine (MPTP) administration are the most widely used toxic models, while paraquat and rotenone are more recent additions to the stable of toxic agents used to model PD [6, 9]. A common feature of all toxin-induced models is their ability to produce an oxidative stress and to cause cell death in DA neuronal populations that reflect what is seen in PD. Oxidative stress results from increased production of extremely reactive free radicals, including reactive oxidative species (ROS) and peroxynitrite. ROS may be formed during a number of cellular processes, including mitochondrial oxidative respiration and metabolism. There are some drawbacks to the use of these models such as the time factor in these models versus the time factor in the human condition, but these do not negate the value of neurotoxin-based animal models in the study of PD.

Recently, the identification of different genetic mutations (α-synuclein, parkin, LRKK2, PINK1, DJ-1) has led to the development of genetic models of PD [10]. It is important to remember that, at best, only ~10% of PD cases are due to genetic mutations [6], while the vast majority of PD cases arise as sporadic, that is, from unknown origins. Although the above-mentioned genes are mutated in PD and are not overexpressed or knocked out, nonetheless, these animal models are important in that they may reveal specific molecular events that lead to the death of the DA neurons and potential therapeutic targets. In this paper, we try to describe the advantages and disadvantages of all of these animal models and their potential roles in revealing the mechanisms for PD pathogenesis and in testing experimental therapeutics (Table 1).

2. Neurotoxic Models

2.1. 6-Hydroxydopamine. 6-OHDA is the classic and oft utilized toxin-based animal model of PD [11–13]. A lot of information on the behavioral, biochemical, and physiological effects of dopamine in the CNS has been derived from this model. 6-OHDA was first isolated in the 1950s [14]. Ungersted [15] first used this neurotoxin to lesion the nigro-striatal dopaminergic pathway in the rat nearly 50 years ago, and the use of 6-OHDA remains widespread today for both *in vitro* and *in vivo* investigations. Mice, cats, dogs, and monkeys are all sensitive to 6-OHDA; however it is used much more frequently in rats [16–19]. Even though 6-OHDA exhibits a high affinity for several catecholaminergic transporters such as the dopamine transporter (DAT) and norepinephrine transporter (NET) [20], it is often used in conjunction with a selective noradrenaline reuptake inhibitor such as desipramine in order to spare the noradrenergic neurons from damage in animal models of PD [21].

Although the structure of 6-OHDA is similar to that of dopamine, the presence of an additional hydroxyl group makes it toxic to dopaminergic neurons. This compound does not cross the blood-brain barrier, which necessitates its direct injection into the SNpc, medial forebrain bundle (MFB), or the striatum [22, 23]. It is well known that 6-OHDA destroys catecholaminergic neurons by a combined

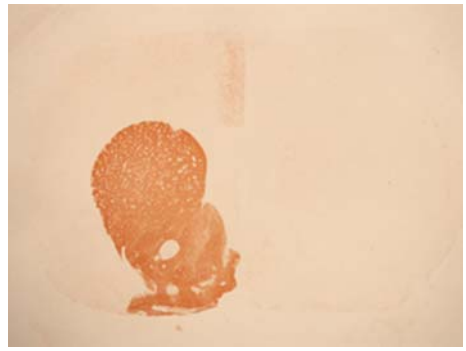

Figure 1: Photomicrograph of a 6-OHDA lesioned rat striatum immunostained for tyrosine hydroxylase (TH). Densities of TH-immunoreactivity striatal fibers are clearly reduced after the 6-OHDA injection (right side) as compared to the densities of striatal TH-immunoreactivity fibers in control rat (left side).

effect of ROS and quinones [24], and it can induce inflammation in the brain which tends to wane over time. The most common use of 6-OHDA is via unilateral injection into the rat medial forebrain bundle. Injection of 6-OHDA into the SNpc kills approximately 60% of the tyrosine hydroxylase- (TH-) containing neurons in this area of the rodent brain with subsequent loss of TH-positive terminals in the striatum [25] (Figure 1). Several studies have injected this compound directly into the striatum in order to test the hypothesis of retrograde degeneration, explicitly, that TH-positive terminals in the striatum die prior to TH-positive neurons in the SNpc, seemingly a replicate of PD in humans [23, 26, 27]. The magnitude of the lesion depends on the amount of 6-OHDA injected, the site of injection, and the animal species used. This model does not mimic all of the clinical features of PD. Dopamine depletion, nigral dopamine cell loss, and neurobehavioral deficits have been successfully achieved using this model, but it does not seem to affect other brain regions, such as olfactory structures, lower brain stem areas, or locus coeruleus. Although 6-OHDA does not produce or induce proteinaceous aggregates or Lewy-like inclusions like those seen in PD, it has been reported that 6-OHDA does interact with α-synuclein [25]. 6-OHDA is frequently used as a unilateral model because the bilateral injection of this compound into the striatum produces severe adipsia, aphagia, and also death [28, 29] due to the animal's inability to care for itself. One of the most attractive features of the unilateral 6-OHDA model is the fact that each animal can serve as its own control as there is a lesioned and an unlesioned hemisphere. This is particularly useful in behavioral analyses [15] as turning behavior to amphetamine or apomorphine following the unilateral application of 6-OHDA gauges the extent of the induced SNpc or striatal lesion and the efficacy of potential PD therapeutic agents and gene therapies [11, 30].

6-OHDA is an attractive candidate as a possible endogenous toxin for the initiation of the PD neurodegenerative process as it is a product of dopamine metabolism [31], and it is the result of hydroxyl radical attack with the presence of

Table 1

Model	Behavioral symptoms	Nigrostriatal damage	Synuclein aggregation/Lewy body formation	Uses of the model	Disadvantages
6-OHDA	Rotational behavior after unilateral injection	Loss of DA innervation at injection site (striatum)	No inclusions	Screen therapies that may improve PD symptoms. Study mechanisms of cell death	Requires intracerebral injection, very little synuclein involvement.
MPTP	Motor impairments in primates Less obvious motor impairments in acute rodent models	Loss of DA neurons dependent on dosing regimen, reaching 95% in acute high-dose conditions. Reduced DA levels in striatum concurrent with midbrain DA neuron loss	Inclusions not prevalent. Few cases of synuclein aggregation in nonhuman primates, as well as increased synuclein immunoreactivity in rodents.	Screen therapies that may improve PD symptoms. Study mechanisms of cell death	Nonprogressive model of cell death. Inclusiones are rare.
Rotenone	Reports of decreased motor activity in rodents	Loss of DA neurons accompanied by reduced DA innervation in striatum	Synuclein aggregation in DA neurons.	Test neuroprotective compounds	Substantial morbidity and mortality. Labor and time intensive.
Paraquat	No clear motor deficits	Decreased striatal TH immunoreactivity	No inclusions present, but increased synuclein immunoreactivity in DA neurons of the SN	Test neuroprotective strategies	Not extensively tested. Effects in other neurotransmitter systems.
α-synuclein	Severe motor deficits in the A53T model, less in the A30P model	Generally no DA neuron degeneration observed	Synuclein aggregation found in DA neurons, generally restricted to A53T model	Study the role of synuclein aggregation in PD, as well as the normal role of synuclein	Generally no DA neuron death observed with synuclein models
LRRK2	Few behavioral deficits seen in Drosophila mutation models	No effect on DA development or maintenance in knockouts, minimal levels of degeneration in mutation models	Generally not observed	Study the role of LRRK2 mutations related to PD	General lack of degeneration and general lack of synuclein aggregation.

excess dopamine; as a neurotoxin, it does produce lesions in the nigrostriatal DA pathway. However, although it has been measured in the brains of levodopa-treated rats subjected to MPTP treatment, 6-OHDA has yet to be recovered from the PD brain. Despite its limitations, this model has contributed enormously to our understanding of PD pathology. 6-OHDA will continue to afford PD researchers a useful animal model for PD research for long time.

2.2. MPTP. In 1982, MPTP was accidentally discovered in a synthesis process gone awry, and, although it may have caused some mayhem in certain circles, today it represents the most important and most frequently used parkinsonian toxin applied in animal models. Young drug addicts developed an idiopathic parkinsonian syndrome after intravenous injection of this compound. After investigating the etiology of their condition, it was found that MPTP was the neurotoxic contaminant responsible for the parkinsonian effect [32]. Oxidative stress, ROS, energy failure, and inflammation have consistently been pointed to as hallmarks of PD. It has been repeatedly demonstrated that MPTP is indeed the gold standard for toxin-based animal models of PD among PD researchers for replicating almost all of these hallmarks [32]. Unfortunately, lacking in this list is the definitive characteristic of PD, LB formation [33, 34]. Interestingly, some studies have demonstrated the production of Lewy body-like inclusions after MPTP administration [35, 36] although these studies have been difficult to replicate. These studies suggest that, under the right circumstances, we may be able to reproduce the majority of hallmarks found in PD.

MPTP is highly lipophilic and after systemic administration rapidly crosses the blood-brain barrier. Once in the brain, MPTP enters astrocytes and is metabolized into MPP+, its active metabolite, by monoamine oxidase-B (MAO-B). Recent findings show that once released from the astrocytes into the extracellular space via the OCT-3

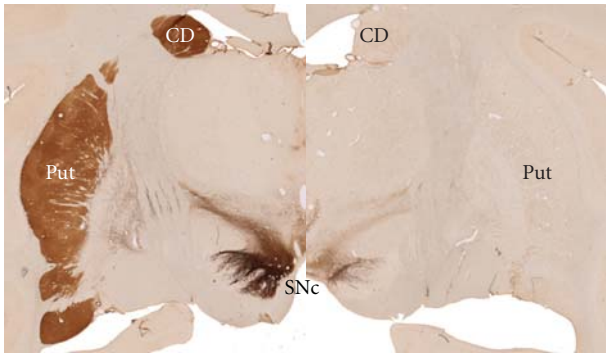

(a) (b)

Figure 2: Photomicrographs of nonhuman primate immunostained for tyrosine hydroxylase (TH). Dopaminergic neurons located in the substantia nigra compacta (SNc) project to the caudate (CD) and putamen (PUT). Note the markedly reduced TH immunoreactivity in the substantia nigra and striatum (CD and PUT) in the MPTP-treated monkey (b) compared to control (a).

transporter [37], MPP+ is taken up into the neuron by the dopamine transporter (DAT) and can be stored in vesicles via uptake by the vesicular monoamine transporter (VMAT2) [38]. Consequently, mice lacking the DAT are protected from MPTP toxicity [39]. Once inside the neuron, MPP+ is able to inhibit complex 1 of the mitochondrial electron transport chain, resulting in the release of ROS as well as reduced ATP production. Storing into vesicles can decrease MPP+ toxicity [40–42]. Additionally, MPP+ stored in vesicles is thought to expel DA out into the intercellular space where it can be metabolized into a number of compounds, including toxic metabolites, such as DOPAL and where it is can be subjected to superoxide radical (5-cysteinyl-DA) and hydroxyl radical (6-OHDA) attack [43, 44].

MPTP is used mainly in nonhuman primates and mice but has also been used in many other species such as dogs and cats [45]. For unknown reasons, rats are resistant to MPTP and mouse strains vary widely in their sensitivity to the toxin [46]. MPTP can be administered by a variety of regimens, but the most common and reproducible form is still systemic injection (subcutaneous, intravenous) [47]. When MPTP is administered to nonhuman primates, they exhibit behavioral and neuroanatomical similarities to the human condition showing a bilateral parkinsonian syndrome [48] (Figure 2). Another commonly used route is the unilateral intracarotid injection. This causes mostly a unilateral parkinsonism, whose benefits as an animal model were described earlier, but is technically more complicated to perform [49].

Usually monkeys are treated with high doses of MPTP for a short time (acute model). Recently, however, new schedules have introduced lower doses of the neurotoxin for longer periods of time (subacute to chronic) to replicate more closely the human pathology [50]. There are recent studies attempting to develop a more progressive model of PD. In addition, models are being developed to study compensatory mechanisms or recovery. These models use low to intermittent doses administered once or twice per week [51–54]. It is well known that monkeys exhibit variability in MPTP susceptibility and that older primates are often more susceptible to MPTP [55]. MPTP-treated monkeys respond well to antiparkinsonian treatments like L-DOPA or apomorphine and, like human pathology, after the treatment develop dyskinesias. Recently, some studies have been taken in order to study and evaluate the nonmotor symptoms of the disease using this model [56–61]. This model has also been used for electrophysiological studies, leading to important findings, including the emergence of deep brain stimulation, which is currently the best surgical method to ameliorate symptoms in PD patients [62, 63].

Currently, the MPTP model is used more in mice than in monkeys. Aside from the obvious financial benefits, the mouse model is employed to test theories about cell death in PD, to work out events in the neuronal death process, and to study other pathological effects of PD. It is also extremely useful as an initial screening tool to test potential treatments for PD. On the other hand, the MPTP monkey model is mainly used to discern behavioral and symptomatic components of PD, as mice do not develop a level of impairment equal to the human condition. Monkeys also represent the last level of PD treatment research prior to any treatment being administered to humans [64]. However, the data generated by mouse models has led to a better understanding of molecular mechanisms involved in PD, and its utility has proven invaluable. One of the most important aspects of the MPTP mouse model is the possibility to work with genetically modified mice [65, 66]. This model can be useful for testing neuroprotective therapies. Currently, MPTP is the standard bearer for toxin-based PD animal models.

3. Pesticide/Herbicide Models

3.1. Paraquat. Paraquat (N,N′-dimethyl-4-4-4′-bypiridinium) (PQ) is a herbicide widely used in agriculture that exhibits a structural resemblance to MPP+, and, because of this structural similarity, it was reasoned that PQ should behave like MPP+. Epidemiological reports suggest that pesticide use increases the risk of developing PD, but, in the case of PQ, there have been only 95 cases of PD linked to its toxicity in humans [67]. PQ exerts its deleterious effects through oxidative stress mediated by redox cycling, which generates ROS. In particular, the superoxide radical, hydrogen peroxide, and hydroxyl radicals lead to the damage of lipids, proteins, DNA and RNA [68, 69]. Recent evidence on the effects of PQ in the nigrostriatal DA system is somewhat ambiguous as some researchers report that, following the systemic application of this herbicide to mice, animals exhibit reduced motor activity and a dose-dependent loss of striatal TH-positive striatal fibers and midbrain SNpc neurons [70, 71]. Other researchers claim that no PQ-induced changes occur in the nigrostriatal DA system [72, 73]. However, in a newer recent study, Rappold et al. [74] demonstrate that PQ, in high doses, employs the organic cationic transporter-3 (OCT-3) and the dopamine transporter (DAT) and is toxic to the DA neurons in the SN. Furthermore, they suggest that the damage done by PQ is caused by radicalized PQ and

facilitated by the glial cells. This means that PQ behaves like MPP+ in exerting its toxic effects. Although this study increases our understanding of how PQ may work, it does not end the controversy about PQ and PD.

PQ's importance to PD researchers is its ability to induce increases in α-synuclein in individual DA neurons in the SNpc and its ability to induce LB-like structures in DA neurons of the SNpc [75]. The relation of dopaminergic neuron loss with α-synuclein upregulation and aggregation suggests that this model could be valuable for capturing a PD-like pathology. However, the molecular link between oxidative stress and cell death in this model is still unknown. Thus, the significance of PQ in PD research is often limited to the study of the process of LB formation in DA neurons as well as the role of α-synuclein in PD. PQ is only one of the many agricultural chemicals known to cause damage to the dopaminergic system. Maneb (manganese ethylenebisdithiocarbamate) has been shown to decrease locomotor activity and potentiate both the MPTP and the PQ effects [73, 76, 77]. Moreover, the combination of PQ and maneb produced greater effects on the dopaminergic system than either of these chemicals alone. These compounds give credence to the theory that environmental pesticides can cause PD [67, 78–80]. In fact, recent studies have demonstrated that those exposed to PQ or fungicides like maneb or ziram experience a greater risk of developing PD [81, 82]. Further investigations using these models are needed to determine the involvement of environmental exposures in the etiology of PD.

3.2. Rotenone. Unlike PQ, which is a pure herbicide rotenone, is both a herbicide and an insecticide [83]. It is the most potent member of the rotenoid family of neurotoxins found naturally in tropical plants. The half-life of rotenone is 3–5 days depending on its exposure to sunlight, and it is rapidly broken down in soil and in water [83]. For these reasons, rotenone is not considered to be a groundwater pollutant. Rotenone is highly lipophilic and readily crosses the blood-brain barrier. Chronic exposure to low doses of rotenone results in inhibition of the mitochondrial electron transport chain in the rat brain. In animals, rotenone has been administered by different routes. Oral administration appears to cause little neurotoxicity [84, 85]. Chronic systemic administration using osmotic pumps has been the most common delivery regimen, especially in the Lewis rat, which may be more sensitive to rotenone than other strains of rats [86]. Intraperitoneal injections have been reported to elicit behavioral and neurochemical deficits, although mortality is very high [87]. Intravenous administration is able to cause damage to nigrostriatal DA neurons that is accompanied by α-synuclein aggregation, Lewy-like body formation, oxidative stress, and gastrointestinal problems [88]. The apparent beauty of this model is that, like paraquat, it seems to replicate almost all of the hallmarks of PD including causing α-synuclein aggregation and Lewy-like body formation [89, 90]. Interestingly, a subsequent study has found that rotenone is not specific to the DA system and has deleterious effects on other neuronal populations. Likewise, in PD in which neurodegeneration extends beyond the dopaminergic system, rotenone is associated with 35% reduction in serotonin, 26% in noradrenergic, and 29% in cholinergic neurons [89]. However, when rotenone was administered chronically at lower doses to achieve complex I inhibition similar to that observed in patients, it seems to produce a highly selective nigrostriatal degeneration [86] although only about 50% of the treated rats exhibit nigrostriatal lesions. The controversy about the use of rotenone as a model of PD is that although it does augment DA oxidation, evidence is slim on depletion of DA in the nigrostriatal system [91]. Attempts to lesion other animal species such as mice or monkeys have not been successful at all [72, 92]. However, recent studies by two groups have demonstrated that oral administration of rotenone to mice causes nigral degeneration, a decrease of striatal dopamine levels, and motor dysfunction [85, 93, 94]. They also demonstrated α-synuclein aggregation in different areas of the brain [95]. Furthermore, there are no documented cases of rotenone-induced PD in humans. Thus, it is not clear that this model offers any advantage over other toxic models, such as that of 6-OHDA or MPTP.

4. Genetic Models

The underlying principle for studying genetic mutations of a disease is the belief that the clinical similarities between the inherited and sporadic forms of the disease share a common mechanism that can lead to the identification of molecular and biochemical pathways involved in the disease pathogenesis. Genetic mutations in PD are rare and represent only about 10% of all PD cases [6]. And animal models of these mutations (α-synuclein and LRRK2, autosomal dominant PD) and (PINK1/Parkin and DJ-1, autosomal recessive PD) are important as they represent potential therapeutic targets. However, we must first understand the workings of these animal models because it is becoming clearer that there are many facets to PD disease.

Mutations to the α-synuclein gene, which is normally thought to play a role in the synaptic vesicle recycling, were the earliest evidence for genetic link to PD. Two mutations in the α-synuclein gene (A53T, A30P) cause a dominantly inherited form of PD [96] and have been used to create transgenic mice in an effort to recapitulate the pathophysiology of PD. Studies done using α-synuclein transgenic mice have yielded considerable progress, showing that A53T mutations in mice can result in a severe motor phenotype which can eventually lead to paralysis and death [97]. Additionally, mutations to the α-synuclein gene in mice produce inclusions that resemble LBs [98]. However this phenotype is generally restricted to the A53T mutation and not found in A30P transgenic mice. Indeed, it has been shown that knocking out α-synuclein does not affect DA neuron development or maintenance [99, 100] suggesting that the loss of α-synuclein probably plays no role in the degeneration of DA neurons that is seen in PD. Interestingly, studies done in *Drosophila* expressing mutant α-synuclein show dopaminergic cell loss, reduced TH expression in the SN, filamentous intraneuronal inclusions, and motor deficits [101]. Some of the α-synuclein transgenic mice have olfactory impairments and colonic dysfunction, and it seems

that there are other nonmotor abnormalities [102]. Understanding these nonmotor symptoms could offer new model for testing therapies focused on the nonmotor symptoms. However, since the function of α-synuclein has yet to be figured out, the actual role of α-synuclein in PD still remains elusive.

Mutations to the LRRK2 gene have been shown to cause a dominant form of PD [103]. Unlike α-synuclein which is ubiquitous, LRRK2 (leucine rich repeat kinase 2) is localized to membranes. However, similar to α-synuclein transgenic mice, it has been determined that knocking out LRRK2 has no effect on DA neuron development and maintenance [102]. Moreover, *Drosophila* models are limited in their translation to the human condition, and the LRRK2 mouse model is not particularly a strong model as it shows only minimal levels of neurodegeneration [104].

Mutations to parkin (which accounts for about 50% of the familial cases of PD and 20% of the young onset PD cases), DJ1 (a redox sensitive molecular chaperone and regulator of antioxidant gene expression), and PINK1 (phosphatase and tensin homolog—PTEN-induced novel kinase 1, which is localized to the mitochondrial intermembrane space) cause autosomal recessive forms of PD. Knock-out rodent models of these genes do not demonstrate any nigrostriatal degeneration, present with intranucelar inclusions, or displays any form of DA neuron loss that resembles idiopathic or inherited PD and fail to develope any type of behavioral or pathological phenotype (only PINK1 knockout mice display reduced DA release in the striatum) [105]. However, recently it has been shown that knocking out parkin in mice at adult age causes neurodegeneration in the SNc [106].

Overall, this genetic mouse models are able to recapitulate specific aspects of PD, although none produce the neuronal degeneration associated with PD; therefore these themselves may be defective and may require additional modulations or modifications, like for example the human environment [107].

5. Conclusions

Animal model systems are the closest to humans that we are able to study. A number of animal models of PD have been developed to understand the pathogenesis and test potential therapeutics of this disease. In this paper we have summarized the most prominent aspects characterizing the most popular toxic and genetic models of PD. Each model has advantages and disadvantages as we have discussed in this paper. Toxic models offer some of the hallmarks of PD while genetic models offer others. Meanwhile the toxic models are useful to screen drugs for symptomatic treatment of the disease; transgenic or knockout models are useful for evaluating the role of genetics in PD. The drawback of the toxin models is that most of them resemble PD at late stages, whereas genetic animal models use either overexpression or knock-out technology to model disease from early on. The choice of the model to be used depends on the questions being asked. With toxin models, we are working toward developing a progressive model by tempering the toxic doses used. With genetic models, we are trying to come up with the right balance of contributing components through knock-in or conditional technology. However, there is much progress to be made, because it seems unlikely that a single model, be it toxic or genetic, can fully recapitulate the complexity of human PD. Future models should involve a combination of neurotoxin-induced and genetically induced models ideally taking into account factors of aging and environmental insults.

Acknowledgments

The authors are supported by grants from the National Institutes of Health (NS042269, NS064191, NS38370, NS070276, and NS072182), the US Department of Defense (W81XWH-08-1-0522, W81XWH-08-1-0465, and W81XWH-09-1-0245), the Parkinson Disease Foundation, the Thomas Hartman Foundation For Parkinson's Research, Project A.L.S, the Muscular Dystrophy Association/Wings over Wall Street. J. Blesa is supported by a fellowship from the Spanish Ministry of Education.

References

[1] A. J. Lees, J. Hardy, and T. Revesz, "Parkinson's disease," *The Lancet*, vol. 373, no. 9680, pp. 2055–2066, 2009.

[2] M. G. Spillantini, M. L. Schmidt, V. M. Y. Lee, J. Q. Trojanowski, R. Jakes, and M. Goedert, "α-synuclein in Lewy bodies [8]," *Nature*, vol. 388, no. 6645, pp. 839–840, 1997.

[3] L. S. Forno, "Neuropathology of Parkinson's disease," *Journal of Neuropathology and Experimental Neurology*, vol. 55, no. 3, pp. 259–272, 1996.

[4] H. Braak, E. Ghebremedhin, U. Rüb, H. Bratzke, and K. Del Tredici, "Stages in the development of Parkinson's disease-related pathology," *Cell and Tissue Research*, vol. 318, no. 1, pp. 121–134, 2004.

[5] K. R. Chaudhuri, D. G. Healy, and A. H. V. Schapira, "Non-motor symptoms of Parkinson's disease: diagnosis and management," *Lancet Neurology*, vol. 5, no. 3, pp. 235–245, 2006.

[6] W. Dauer and S. Przedborski, "Parkinson's disease: mechanisms and models," *Neuron*, vol. 39, no. 6, pp. 889–909, 2003.

[7] A. Carlsson, M. Lindqvist, and T. Magnusson, "3,4-Dihydroxyphenylalanine and 5-hydroxytryptophan as reserpine antagonists," *Nature*, vol. 180, no. 4596, p. 1200, 1957.

[8] A. Carlsson, "The occurrence, distribution and physiological role of catecholamines in the nervous system," *Pharmacological reviews*, vol. 11, no. 2, pp. 490–493, 1959.

[9] R. Betarbet, T. B. Sherer, and J. Timothy Greenamyre, "Animal models of Parkinson's disease," *BioEssays*, vol. 24, no. 4, pp. 308–318, 2002.

[10] T. M. Dawson, H. S. Ko, and V. L. Dawson, "Genetic Animal Models of Parkinson's Disease," *Neuron*, vol. 66, no. 5, pp. 646–661, 2010.

[11] R. K. W. Schwarting and J. P. Huston, "Unilateral 6-hydroxydopamine lesions of meso-striatal dopamine neurons and their physiological sequelae," *Progress in Neurobiology*, vol. 49, no. 3, pp. 215–266, 1996.

[12] R. K. W. Schwarting and J. P. Huston, "The unilateral 6-hydroxydopamine lesion model in behavioral brain research. Analysis of functional deficits, recovery and treatments," *Progress in Neurobiology*, vol. 50, no. 2-3, pp. 275–331, 1996.

[13] R. K. W. Schwarting and J. P. Huston, "Behavioral and neurochemical dynamics of neurotoxic meso-striatal dopamine lesions," *NeuroToxicology*, vol. 18, no. 3, pp. 689–708, 1997.

[14] S. Senoh and B. Witkop, "Non-enzymatic conversions of dopamine to norepinephrine and trihydroxyphenethylamines," *Journal of the American Chemical Society*, vol. 81, no. 23, pp. 6222–6231, 1959.

[15] U. Ungerstedt, "6-hydroxy-dopamine induced degeneration of central monoamine neurons," *European Journal of Pharmacology*, vol. 5, no. 1, pp. 107–110, 1968.

[16] T. A. P. Roeling, G. J. Docter, P. Voorn, B. P. C. Melchers, E. C. Wolters, and H. J. Groenewegen, "Effects of unilateral 6-hydroxydopamine lesions on neuropeptide immunoreactivity in the basal ganglia of the common marmoset, Callithrix jacchus, a quantitative immunohistochemical analysis," *Journal of Chemical Neuroanatomy*, vol. 9, no. 3, pp. 155–164, 1995.

[17] H. Valette, P. Deleuze, A. Syrota et al., "Canine myocardial beta-adrenergic, muscarinic receptor densities after denervation: a PET study," *Journal of Nuclear Medicine*, vol. 36, no. 1, pp. 140–146, 1995.

[18] L. E. Annett, E. M. Torres, D. J. Clarke et al., "Survival of nigral grafts within the striatum of marmosets with 6-OHDA lesions depends critically on donor embryo age," *Cell Transplantation*, vol. 6, no. 6, pp. 557–569, 1997.

[19] R. Ruffy and M. Leonard, "Chemical cardiac sympathetic denervation hampers defibrillation in the dog," *Journal of Cardiovascular Electrophysiology*, vol. 8, no. 1, pp. 62–67, 1997.

[20] C. Sachs and G. Jonsson, "Mechanisms of action of 6-hydroxydopamine," *Biochemical Pharmacology*, vol. 24, no. 1, pp. 1–8, 1975.

[21] G. E. Martin, R. D. Myers, and D. C. Newberg, "Catecholamine release by intracerebral perfusion of 6 hydroxydopamine and desipramine," *European Journal of Pharmacology*, vol. 36, no. 2, pp. 299–311, 1976.

[22] D. A. Perese, J. Ulman, J. Viola, S. E. Ewing, and K. S. Bankiewicz, "A 6-hydroxydopamine-induced selective parkinsonian rat model," *Brain Research*, vol. 494, no. 2, pp. 285–293, 1989.

[23] S. Przedborski, M. Levivier, H. Jiang et al., "Dose-dependent lesions of the dopaminergic nigrostriatal pathway induced by intrastriatal injection of 6-hydroxydopamine," *Neuroscience*, vol. 67, no. 3, pp. 631–647, 1995.

[24] G. Cohen, "Oxy-radical toxicity in catecholamine neurons," *NeuroToxicology*, vol. 5, no. 1, pp. 77–82, 1984.

[25] F. Blandini, M. T. Armentero, and E. Martignoni, "The 6-hydroxydopamine model: news from the past," *Parkinsonism and Related Disorders*, vol. 14, no. 2, pp. S124–S129, 2008.

[26] H. Sauer and W. H. Oertel, "Progressive degeneration of nigrostriatal dopamine neurons following intrastriatal terminal lesions with 6-hydroxydopamine: a combined retrograde tracing and immunocytochemical study in the rat," *Neuroscience*, vol. 59, no. 2, pp. 401–415, 1994.

[27] C. S. Lee, H. Sauer, and A. Björklund, "Dopaminergic neuronal degeneration and motor impairments following axon terminal lesion by intrastriatal 6-hydroxydopamine in the rat," *Neuroscience*, vol. 72, no. 3, pp. 641–653, 1996.

[28] U. Ungerstedt, "Adipsia and aphagia after 6-hydroxydopamine induced degeneration of the nigro-striatal dopamine system," *Acta Physiologica Scandinavica, Supplement*, vol. 367, pp. 95–122, 1971.

[29] W. M. Bourn, L. Chin, and A. L. Picchioni, "Enhancement of audiogenic seizure by 6-hydroxydopamine," *Journal of Pharmacy and Pharmacology*, vol. 24, no. 11, pp. 913–914, 1972.

[30] J. Knoll, "The pharmacology of (-)deprenyl," *Journal of Neural Transmission. Supplementum*, vol. 22, pp. 75–89, 1986.

[31] J. D. Graham, M. J. Lewis, and J. Williams, "Proceedings: The effect of delta-1-tetrahydrocannabinol on the noradrenaline and dopamine content of the brain and heart of the rat," *British Journal of Pharmacology*, vol. 52, no. 3, p. 446, 1974.

[32] J. W. Langston, P. Ballard, J. W. Tetrud, and I. Irwin, "Chronic parkinsonism in humans due to a product of meperidine-analog synthesis," *Science*, vol. 219, no. 4587, pp. 979–980, 1983.

[33] L. S. Forno, L. E. DeLanney, I. Irwin, and J. W. Langston, "Similarities and differences between MPTP-induced parkinsonsim and Parkinson's disease. Neuropathologic considerations," *Advances in neurology*, vol. 60, pp. 600–608, 1993.

[34] G. Halliday, M. T. Herrero, K. Murphy et al., "No Lewy pathology in monkeys with over 10 years of severe MPTP parkinsonism," *Movement Disorders*, vol. 24, no. 10, pp. 1519–1523, 2009.

[35] N. W. Kowall, P. Hantraye, E. Brouillet, M. F. Beal, A. C. McKee, and R. J. Ferrante, "MPTP induces alpha-synuclein aggregation in the substantia nigra of baboons," *NeuroReport*, vol. 11, no. 1, pp. 211–213, 2000.

[36] F. Fornai, O. M. Schlüter, P. Lenzi et al., "Parkinson-like syndrome induced by continuous MPTP infusion: convergent roles of the ubiquitin-proteasome system and α-synuclein," *Proceedings of the National Academy of Sciences of the United States of America*, vol. 102, no. 9, pp. 3413–3418, 2005.

[37] M. Cui, R. Aras, W. V. Christian et al., "The organic cation transporter-3 is a pivotal modulator of neurodegeneration in the nigrostriatal dopaminergic pathway," *Proceedings of the National Academy of Sciences of the United States of America*, vol. 106, no. 19, pp. 8043–8048, 2009.

[38] J. A. Javitch, R. J. D'Amato, S. M. Strittmatter, and S. H. Snyder, "Parkinsonism-inducing neurotoxin, N-methyl-4-phenyl-1,2,3,6-tetrahydropyridine: Uptake of the metabolite N-methyl-4-phenylpyridine by dopamine neurons explains selective toxicity," *Proceedings of the National Academy of Sciences of the United States of America*, vol. 82, no. 7, pp. 2173–2177, 1985.

[39] E. Bezard, C. E. Gross, M. C. Fournier, S. Dovero, B. Bloch, and M. Jaber, "Absence of MPTP-induced neuronal death in mice lacking the dopamine transporter," *Experimental Neurology*, vol. 155, no. 2, pp. 268–273, 1999.

[40] R. R. Gainetdinov, F. Fumagalli, Y. M. Wang et al., "Increased MPTP neurotoxicity in vesicular monoamine transporter 2 heterozygote knockout mice," *Journal of Neurochemistry*, vol. 70, no. 5, pp. 1973–1978, 1998.

[41] T. S. Guillot, K. R. Shepherd, J. R. Richardson et al., "Reduced vesicular storage of dopamine exacerbates methamphetamine-induced neurodegeneration and astrogliosis," *Journal of Neurochemistry*, vol. 106, no. 5, pp. 2205–2217, 2008.

[42] T. S. Guillot and G. W. Miller, "Protective actions of the vesicular monoamine transporter 2 (VMAT2) in monoaminergic neurons," *Molecular Neurobiology*, vol. 39, no. 2, pp. 149–170, 2009.

[43] W. J. Burke, V. B. Kumar, N. Pandey et al., "Aggregation of α-synuclein by DOPAL, the monoamine oxidase metabolite of dopamine," *Acta Neuropathologica*, vol. 115, no. 2, pp. 193–203, 2008.

[44] W. M. Panneton, V. B. Kumar, Q. Gan, W. J. Burke, and J. E. Galvin, "The neurotoxicity of DOPAL: behavioral and stereological evidence for its role in Parkinson disease pathogenesis," *PLoS One*, vol. 5, no. 12, Article ID e15251, 2010.

[45] M. J. Zigmond, T. W. Berger, A. A. Grace, and E. M. Stricker, "Compensatory responses to nigrostriatal bundle injury. Studies with 6-hydroxydopamine in an animal model of parkinsonism," *Molecular and Chemical Neuropathology*, vol. 10, no. 3, pp. 185–200, 1989.

[46] C. C. Chiueh, S. P. Markey, and R. S. Burns, "Neurochemical and behavioral effects of systemic and intranigral administration of N-methyl-4-phenyl-1,2,3,6-tetrahydropyridine in the rat," *European Journal of Pharmacology*, vol. 100, no. 2, pp. 189–194, 1984.

[47] S. Przedborski, V. Jackson-Lewis, A. B. Naini et al., "The parkinsonian toxin 1-methyl-4-phenyl-1,2,3,6-tetrahydropyridine (MPTP): a technical review of its utility and safety," *Journal of Neurochemistry*, vol. 76, no. 5, pp. 1265–1274, 2001.

[48] J. W. Langston, E. B. Langston, and I. Irwin, "MPTP-induced parkinsonism in human and non-human primates—clinical and experimental aspects," *Acta Neurologica Scandinavica*, vol. 70, supplement 100, pp. 49–54, 1984.

[49] K. S. Bankiewicz, E. H. Oldfield, and C. C. Chiueh, "Hemiparkinsonism in monkeys after unilateral internal carotid artery infusion of 1-methyl-4-phenyl-1,2,3,6-tetrahydropyridine (MPTP)," *Life Sciences*, vol. 39, no. 1, pp. 7–16, 1986.

[50] M. M. Iravani, E. Syed, M. J. Jackson, L. C. Johnston, L. A. Smith, and P. Jenner, "A modified MPTP treatment regime produces reproducible partial nigrostriatal lesions in common marmosets," *European Journal of Neuroscience*, vol. 21, no. 4, pp. 841–854, 2005.

[51] P. Hantraye, M. Varastet, M. Peschanski et al., "Stable parkinsonian syndrome and uneven loss of striatal dopamine fibres following chronic MPTP administration in baboons," *Neuroscience*, vol. 53, no. 1, pp. 169–178, 1993.

[52] E. Bezard, C. Imbert, X. Deloire, B. Bioulac, and C. E. Gross, "A chronic MPTP model reproducing the slow evolution of Parkinson's disease: evolution of motor symptoms in the monkey," *Brain Research*, vol. 766, no. 1-2, pp. 107–112, 1997.

[53] S. Mounayar, S. Boulet, D. Tandé et al., "A new model to study compensatory mechanisms in MPTP-treated monkeys exhibiting recovery," *Brain*, vol. 130, no. 11, pp. 2898–2914, 2007.

[54] J. Blesa, C. Juri, M. Collantes et al., "Progression of dopaminergic depletion in a model of MPTP-induced Parkinsonism in non-human primates. An 18F-DOPA and 11C-DTBZ PET study," *Neurobiology of Disease*, vol. 38, no. 3, pp. 456–463, 2010.

[55] A. Ovadia, Z. Zhang, and D. M. Gash, "Increased susceptibility to MPTP toxicity in middle-aged rhesus monkeys," *Neurobiology of Aging*, vol. 16, no. 6, pp. 931–937, 1995.

[56] M. Pessiglione, D. Guehl, E. C. Hirsch, J. Féger, and L. Tremblay, "Disruption of self-organized actions in monkeys with progressive MPTP-induced parkinsonism. I. Effects of task complexity," *European Journal of Neuroscience*, vol. 19, no. 2, pp. 426–436, 2004.

[57] JS Schneider, *Modeling Cognitive Deficits Associated with Parkinsonism in the Chronic-Low-Dose MPTP-Treated Monkey*, CRC Press, Boca Raton, Fla, USA, 2006.

[58] G. Anderson, A. R. Noorian, G. Taylor et al., "Loss of enteric dopaminergic neurons and associated changes in colon motility in an MPTP mouse model of Parkinson's disease," *Experimental Neurology*, vol. 207, no. 1, pp. 4–12, 2007.

[59] S. H. Fox, R. Chuang, and J. M. Brotchie, "Serotonin and Parkinson's disease: on movement, mood, and madness," *Movement Disorders*, vol. 24, no. 9, pp. 1255–1266, 2009.

[60] Q. Barraud, I. Obeid, I. Aubert et al., "Neuroanatomical study of the A11 diencephalospinal pathway in the non-human primate," *PLoS One*, vol. 5, no. 10, Article ID e13306, 2010.

[61] J. Vezoli, K. Fifel, V. Leviel et al., "Early presymptomatic and long-term changes of rest activity cycles and cognitive behavior in a MPTP-monkey model of Parkinson's disease," *PLoS One*, vol. 6, no. 8, Article ID e23952, 2011.

[62] H. Bergman, T. Wichmann, and M. R. DeLong, "Reversal of experimental Parkinsonism by lesions of the subthalamic nucleus," *Science*, vol. 249, no. 4975, pp. 1436–1438, 1990.

[63] J. Guridi, M. T. Herrero, M. R. Luquin et al., "Subthalamotomy in parkinsonian monkeys. Behavioural and biochemical analysis," *Brain*, vol. 119, no. 5, pp. 1717–1727, 1996.

[64] E. Bezard and S. Przedborski, "A tale on animal models of Parkinson's Disease," *Movement Disorders*, vol. 26, no. 6, pp. 993–1002, 2011.

[65] M. Vila, V. Jackson-Lewis, S. Vukosavic et al., "Bax ablation prevents dopaminergic neurodegeneration in the 1-methyl-4-phenyl-1,2,3,6-tetrahydropyridine mouse model of Parkinson's disease," *Proceedings of the National Academy of Sciences of the United States of America*, vol. 98, no. 5, pp. 2837–2842, 2001.

[66] W. Dauer, N. Kholodilov, M. Vila et al., "Resistance of α-synuclein null mice to the parkinsonian neurotoxin MPTP," *Proceedings of the National Academy of Sciences of the United States of America*, vol. 99, no. 22, pp. 14524–14529, 2002.

[67] C. Berry, C. La Vecchia, and P. Nicotera, "Paraquat and parkinson's disease," *Cell Death and Differentiation*, vol. 17, no. 7, pp. 1115–1125, 2010.

[68] B. J. Day, M. Patel, L. Calavetta, L. Y. Chang, and J. S. Stamler, "A mechanism of paraquat toxicity involving nitric oxide synthase," *Proceedings of the National Academy of Sciences of the United States of America*, vol. 96, no. 22, pp. 12760–12765, 1999.

[69] S. Przedborski and H. Ischiropoulos, "Reactive oxygen and nitrogen species: weapons of neuronal destruction in models of Parkinson's disease," *Antioxidants and Redox Signaling*, vol. 7, no. 5-6, pp. 685–693, 2005.

[70] A. I. Brooks, C. A. Chadwick, H. A. Gelbard, D. A. Cory-Slechta, and H. J. Federoff, "Paraquat elicited neurobehavioral syndrome caused by dopaminergic neuron loss," *Brain Research*, vol. 823, no. 1-2, pp. 1–10, 1999.

[71] A. L. McCormack, M. Thiruchelvam, A. B. Manning-Bog et al., "Environmental risk factors and Parkinson's disease: selective degeneration of nigral dopaminergic neurons caused by the herbicide paraquat," *Neurobiology of Disease*, vol. 10, no. 2, pp. 119–127, 2002.

[72] C. Thiffault, J. W. Langston, and D. A. Di Monte, "Increased striatal dopamine turnover following acute administration of rotenone to mice," *Brain Research*, vol. 885, no. 2, pp. 283–288, 2000.

[73] M. Thiruchelvam, B. J. Brockel, E. K. Richfield, R. B. Baggs, and D. A. Cory-Slechta, "Potentiated and preferential effects of combined paraquat and maneb on nigrostriatal dopamine systems: environmental risk factors for Parkinson's disease?" *Brain Research*, vol. 873, no. 2, pp. 225–234, 2000.

[74] P. M. Rappold, M. Cui, A. S. Chesser et al., "Paraquat neurotoxicity is mediated by the dopamine transporter and

organic cation transporter-3," *Proceedings of the National Academy of Sciences of the United States of America*, vol. 108, no. 51, pp. 20766–20771, 2011.

[75] A. B. Manning-Bog, A. L. McCormack, J. Li, V. N. Uversky, A. L. Fink, and D. A. Di Monte, "The herbicide paraquat causes up-regulation and aggregation of α-synuclein in mice: paraquat and α-synuclein," *Journal of Biological Chemistry*, vol. 277, no. 3, pp. 1641–1644, 2002.

[76] R. N. Takahashi, R. Rogerio, and M. Zanin, "Maneb enhances MPTP neurotoxicity in mice," *Research Communications in Chemical Pathology and Pharmacology*, vol. 66, no. 1, pp. 167–170, 1989.

[77] A. Kachroo, M. C. Irizarry, and M. A. Schwarzschild, "Caffeine protects against combined paraquat and maneb-induced dopaminergic neuron degeneration," *Experimental Neurology*, vol. 223, no. 2, pp. 657–661, 2010.

[78] P. G. Butterfield, B. G. Valanis, P. S. Spencer, C. A. Lindeman, and J. G. Nutt, "Environmental antecedents of young-onset Parkinson's disease," *Neurology*, vol. 43, no. 6, pp. 1150–1158, 1993.

[79] J. M. Gorell, C. C. Johnson, B. A. Rybicki, E. L. Peterson, and R. J. Richardson, "The risk of Parkinson's disease with exposure to pesticides, farming, well water, and rural living," *Neurology*, vol. 50, no. 5, pp. 1346–1350, 1998.

[80] B. K. Barlow, E. K. Richfield, D. A. Cory-Slechta, and M. Thiruchelvam, "A fetal risk factor for Parkinson's disease," *Developmental Neuroscience*, vol. 26, no. 1, pp. 11–23, 2004.

[81] C. C. Tang, K. L. Poston, V. Dhawan, and D. Eidelberg, "Abnormalities in metabolic network activity precede the onset of motor symptoms in Parkinson's disease," *Journal of Neuroscience*, vol. 30, no. 3, pp. 1049–1056, 2010.

[82] C. M. Tanner, F. Kame, G. W. Ross et al., "Rotenone, paraquat, and Parkinson's disease," *Environmental Health Perspectives*, vol. 119, no. 6, pp. 866–872, 2011.

[83] J. Hisata, *Lake and stream rehabilitation: rotenone use and health risks. Final supplemental environmental impact statement*, Washington Satet Deparment of Fish and Wildlife, 2002.

[84] M. Inden, Y. Kitamura, H. Takeuchi et al., "Neurodegeneration of mouse nigrostriatal dopaminergic system induced by repeated oral administration of rotenone is prevented by 4-phenylbutyrate, a chemical chaperone," *Journal of Neurochemistry*, vol. 101, no. 6, pp. 1491–1504, 2007.

[85] M. Inden, Y. Kitamura, M. Abe, A. Tamaki, K. Takata, and T. Taniguchi, "Parkinsonian rotenone mouse model: reevaluation of long-term administration of rotenone in C57BL/6 mice," *Biological and Pharmaceutical Bulletin*, vol. 34, no. 1, pp. 92–96, 2011.

[86] R. Betarbet, T. B. Sherer, G. MacKenzie, M. Garcia-Osuna, A. V. Panov, and J. T. Greenamyre, "Chronic systemic pesticide exposure reproduces features of Parkinson's disease," *Nature Neuroscience*, vol. 3, no. 12, pp. 1301–1306, 2000.

[87] M. Alam, A. Mayerhofer, and W. J. Schmidt, "The neurobehavioral changes induced by bilateral rotenone lesion in medial forebrain bundle of rats are reversed by L-DOPA," *Behavioural Brain Research*, vol. 151, no. 1-2, pp. 117–124, 2004.

[88] J. R. Cannon, V. Tapias, H. M. Na, A. S. Honick, R. E. Drolet, and J. T. Greenamyre, "A highly reproducible rotenone model of Parkinson's disease," *Neurobiology of Disease*, vol. 34, no. 2, pp. 279–290, 2009.

[89] G. U. Höglinger, J. Féger, A. Prigent et al., "Chronic systemic complex I inhibition induces a hypokinetic multisystem degeneration in rats," *Journal of Neurochemistry*, vol. 84, no. 3, pp. 491–502, 2003.

[90] T. B. Sherer, J. H. Kim, R. Betarbet, and J. T. Greenamyre, "Subcutaneous rotenone exposure causes highly selective dopaminergic degeneration and α-synuclein aggregation," *Experimental Neurology*, vol. 179, no. 1, pp. 9–16, 2003.

[91] Y.-N. Wu and S. W. Johnson, "Dopamine oxidation facilitates rotenone-dependent potentiation of N-methyl-d-aspartate currents in rat substantia nigra dopamine neurons," *Neuroscience*, vol. 195, pp. 138–144, 2011.

[92] R. J. Ferrante, J. B. Schulz, N. W. Kowall, and M. F. Beal, "Systemic administration of rotenone produces selective damage in the striatum and globus pallidus, but not in the substantia nigra," *Brain Research*, vol. 753, no. 1, pp. 157–162, 1997.

[93] H. Takeuchi, T. Yanagida, M. Inden et al., "Nicotinic receptor stimulation protects nigral dopaminergic neurons in rotenone-induced Parkinson's disease models," *Journal of Neuroscience Research*, vol. 87, no. 2, pp. 576–585, 2009.

[94] F. Pan-Montojo, O. Anichtchik, Y. Dening et al., "Progression of Parkinson's disease pathology is reproduced by intragastric administration of rotenone in mice," *PLoS One*, vol. 5, no. 1, Article ID e8762, 2010.

[95] F. J. Pan-Montojo and R. H. W. Funk, "Oral administration of rotenone using a gavage and image analysis of alpha-synuclein inclusions in the enteric nervous system," *Journal of Visualized Experiments*, no. 44, Article ID e2123, 2010.

[96] R. Krüger, W. Kuhn, T. Müller et al., "Ala30Pro mutation in the gene encoding α-synuclein in Parkinson's disease," *Nature Genetics*, vol. 18, no. 2, pp. 106–108, 1998.

[97] B. I. Giasson, J. E. Duda, S. M. Quinn, B. Zhang, J. Q. Trojanowski, and V. M. Y. Lee, "Neuronal α-synucleinopathy with severe movement disorder in mice expressing A53T human α-synuclein," *Neuron*, vol. 34, no. 4, pp. 521–533, 2002.

[98] E. Masliah, E. Rockenstein, I. Veinbergs et al., "Dopaminergic loss and inclusion body formation in α-synuclein mice: Implications for neurodegenerative disorders," *Science*, vol. 287, no. 5456, pp. 1265–1269, 2000.

[99] A. Abeliovich, Y. Schmitz, I. Fariñas et al., "Mice lacking α-synuclein display functional deficits in the nigrostriatal dopamine system," *Neuron*, vol. 25, no. 1, pp. 239–252, 2000.

[100] B. Thomas, A. S. Mandir, N. West et al., "Resistance to MPTP-Neurotoxicity in α-synuclein knockout mice is complemented by human α-synuclein and associated with increased β-synuclein and Akt activation," *PLoS One*, vol. 6, no. 1, Article ID e16706, 2011.

[101] M. B. Feany and W. W. Bender, "A Drosophila model of Parkinson's disease," *Nature*, vol. 404, no. 6776, pp. 394–398, 2000.

[102] D. Wang, B. Tang, G. Zhao et al., "Dispensable role of Drosophila ortholog of LRRK2 kinase activity in survival of dopaminergic neurons," *Molecular Neurodegeneration*, vol. 3, no. 1, article no. 3, 2008.

[103] A. Zimprich, S. Biskup, P. Leitner et al., "Mutations in LRRK2 cause autosomal-dominant parkinsonism with pleomorphic pathology," *Neuron*, vol. 44, no. 4, pp. 601–607, 2004.

[104] Y. Li, W. Liu, T. F. Oo et al., "Mutant LRRK2R1441G BAC transgenic mice recapitulate cardinal features of Parkinson's disease," *Nature Neuroscience*, vol. 12, no. 7, pp. 826–828, 2009.

[105] D. J. Moore and T. M. Dawson, "Value of genetic models in understanding the cause and mechanisms of Parkinson's disease," *Current Neurology and Neuroscience Reports*, vol. 8, no. 4, pp. 288–296, 2008.

[106] J.-H. Shin, H. S. Ko, H. Kang et al., "PARIS (ZNF746) repression of PGC-1α contributes to neurodegeneration in parkinson's disease," *Cell*, vol. 144, no. 5, pp. 689–702, 2011.

[107] J. Peng, M. L. Oo, and J. K. Andersen, "Synergistic effects of environmental risk factors and gene mutations in Parkinson's disease accelerate age-related neurodegeneration," *Journal of Neurochemistry*, vol. 115, no. 6, pp. 1363–1373, 2010.

Hindawi Publishing Corporation
Journal of Biomedicine and Biotechnology
Volume 2012, Article ID 541872, 12 pages
doi:10.1155/2012/541872

Review Article

PET/CT Imaging in Mouse Models of Myocardial Ischemia

Sara Gargiulo,[1,2] Adelaide Greco,[1,2] Matteo Gramanzini,[1,2] Maria Piera Petretta,[1,3] Adele Ferro,[1] Michele Larobina,[1] Mariarosaria Panico,[1] Arturo Brunetti,[1,2] and Alberto Cuocolo[1,2]

[1] *Department of Biomorphological and Functional Sciences and Institute of Biostructures and Bioimages of National Council of Research, University of Naples Federico II, Naples, Via S. Pansini 5, 80131 Naples, Italy*
[2] *CEINGE-Biotecnologie Avanzate scarl, Via G. Salvatore 486, 80145 Naples, Italy*
[3] *Department of Internal Medicine, Cardiovascular and Immunological Sciences, University of Naples Federico II, Via S. Pansini 5, 80131 Naples, Italy*

Correspondence should be addressed to Sara Gargiulo, sara.gargiulo@ibb.cnr.it and Alberto Cuocolo, cuocolo@unina.it

Received 4 November 2011; Revised 16 December 2011; Accepted 30 December 2011

Academic Editor: Andrea Vecchione

Different species have been used to reproduce myocardial infarction models but in the last years mice became the animals of choice for the analysis of several diseases, due to their short life cycle and the possibility of genetic manipulation. Many techniques are currently used for cardiovascular imaging in mice, including X-ray computed tomography (CT), high-resolution ultrasound, magnetic resonance imaging, and nuclear medicine procedures. Cardiac positron emission tomography (PET) allows to examine noninvasively, on a molecular level and with high sensitivity, regional changes in myocardial perfusion, metabolism, apoptosis, inflammation, and gene expression or to measure changes in anatomical and functional parameters in heart diseases. Currently hybrid PET/CT scanners for small laboratory animals are available, where CT adds high-resolution anatomical information. This paper reviews mouse models of myocardial infarction and discusses the applications of dedicated PET/CT systems technology, including animal preparation, anesthesia, radiotracers, and images postprocessing.

1. Introduction

Cardiovascular diseases, such as coronary heart disease (CHD), are common causes of morbidity and mortality in developed countries. Currently CHD is a relevant cause of permanent disability in workers and congestive heart failure, which is frequently secondary to myocardial infarction (MI). Despite progress in the diagnosis and treatment of CHD, appropriate animal models play a central role to investigate the mechanisms involved in the pathogenesis and for the advancement of diagnosis and therapies. Rodents, in particular mice, are often used in cardiovascular research, since they are not expensive, easy to handle and to house, are easily prone to genetic manipulations and show anatomic similarity in developmental and postnatal heart compared with humans. Therefore, conventional wild-type and genetically altered mice are becoming interesting models for better understanding the pathogenesis and improvement in diagnosis, prevention, and therapy of CHD in humans. Noninvasive *in vivo* imaging has acquired a critical role in mouse cardiovascular research; however, the small size and rapid rate of the mouse heart pose significant challenges for cardiac imaging, requiring expensive equipment and established expertise (Figure 1). Since the left ventricle wall is thinner than 1 mm, high spatial resolution is mandatory. At the same time, the rapid heart movement requires high temporal resolution. Table 1 indicates several imaging techniques that are currently used for morphological and functional phenotyping of mouse cardiovascular system, including high-resolution ultrasound, X-ray computed tomography (CT), magnetic resonance, and nuclear medicine procedures. Molecular imaging with positron emission tomography (PET) allows evaluating, in a non-invasive and longitudinal manner, biological processes

Table 1: Principal characteristics of small animal imaging techniques in cardiovascular research.

Imaging technique	Physical principle	Spatial resolution	Advantages	Disadvantages
UBM	High frequency sound waves	50 μm	Real-time cardiovascular morphofunctional assessment	Strongly operator dependent, difficult assessing of right ventricle
CT	X-rays	100 μm	Left ventricle morphology	Radiation dose
MRI	High intensity magnetic field	200 μm	High tissue contrast and functional parameters	Most expensive and availability
SPECT	Gamma emitters	Max 0.62 mm FWHM	Molecular imaging, myocardial metabolism and perfusion, 10^{-10}-10^{-11} M sensitivity	Low spatial resolution, radiation dose
PET	Positron emitters	Max 1 mm FWHM	Molecular imaging, myocardial metabolism and perfusion, 10^{-11}-10^{-12} M sensitivity	Low spatial resolution, radiation dose

UBM: ultrasound biomicroscopy; CT: computed tomography; MRI: magnetic resonance imaging; SPECT: single-photon emission computed tomography; PET: positron emission tomography; FWHM: full width at half maximum.

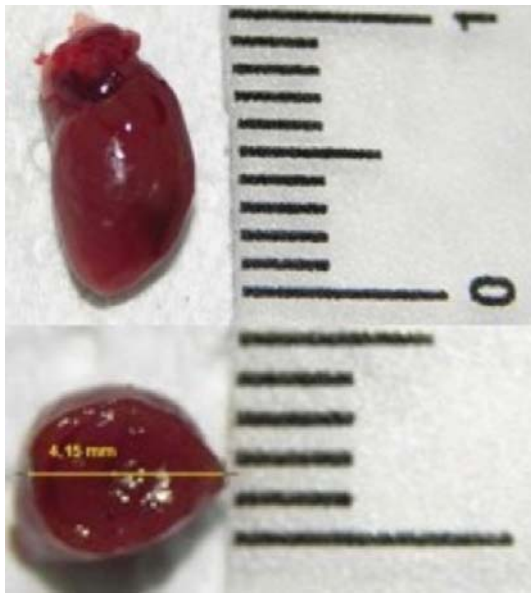

Figure 1: Longitudinal and transversal dimensions (mm) of mouse heart.

at a cellular and subcellular level in early steps of heart diseases, to perform quantitative analysis, to study apoptosis, angiogenesis, hypoxia, inflammation, receptor density, and gene expression. In spite of the great specificity and sensitivity of PET, molecular imaging approach can take advantage from simultaneous acquisition of morphological information for localization and quantification. Therefore, hybrid imaging with PET/CT systems is becoming the most used approach in cardiovascular imaging. In this paper we review mouse models of myocardial infarction and discuss the applications of dedicated PET/CT systems technology, including animal preparation, anesthesia, radiotracers, and images postprocessing.

2. Models of Myocardial Infarction

In an animal model the induced disorder should closely resemble the disorder in human. None of the currently available animal models can entirely reproduce the full spectrum of cardiovascular diseases in humans. Rodents, especially rats and mice, are commonly used in cardiovascular research because they are less expensive and are easier to handle and to house compared to large animals [1]. Since a broad variety of genetically modified mice are produced and knockin and knockout techniques are well developed on mice, mouse models are increasingly adopted to study cardiovascular human diseases and to identify new therapeutic targets. The most frequently used include MI or ischemia-reperfusion by ligation of the left coronary artery [2, 3]. Despite several anatomic differences, the value and clinical translatability of mouse models of cardiac diseases have been proven. The mouse heart is similar to the human concerning ventricular structure and valves. The major anatomical differences are seen in the atria and venous pole of the heart (Figure 2). In human, left atrium receives four pulmonary veins, while in the mouse the pulmonary veins join in a single vessel. During organogenesis, in human left cranial caval vein regresses and the proximal portion becomes the coronary sinus, while the distal portion gives rise to the ligament of Marshall and the oblique vein [4]. In the mouse, the left cranial caval vein does not regress and persist in postnatal life. These differences in venous tributaries into atrial chambers are the likely reasons for the relatively small size of atria in murine heart [5]. The mouse coronary anatomy has some differences compared to human. Mice have a single septal coronary artery, arising from separate ostia from the right sinus of Valsalva or as a proximal branch of the right coronary artery, while in man the interventricular septum is perfused by septal perforator arteries arising from the left anterior descending or posterior descending coronary arteries. Mouse left coronary artery does not divide proximally into left anterior descending and circumflex artery, but courses obliquely across the left ventricular (LV) free wall and branches in a variable

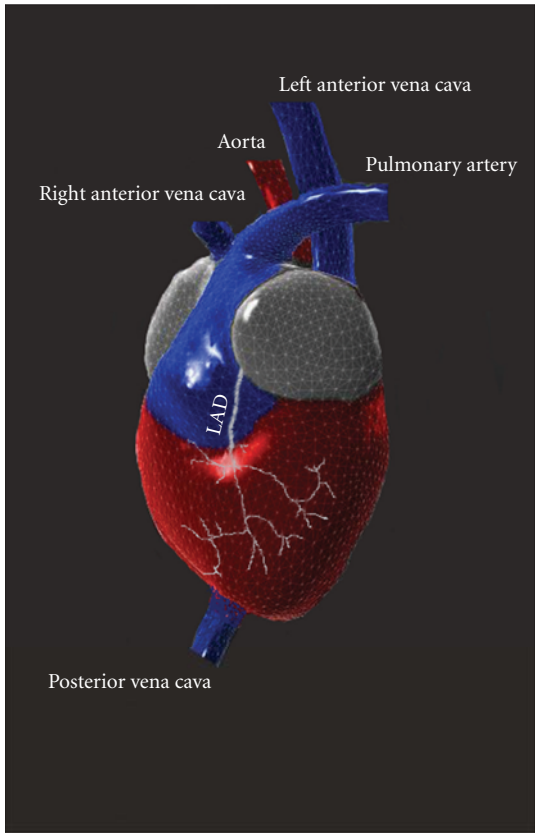

Figure 2: Tridimensional reconstruction of mouse heart, representing the peculiar features of venous pole and left coronary artery anatomy.

fashion, similar to the ramous intermedius artery in man. The right coronary artery branches proximal into a right ventricular and circumflex vessel supplying the LV posterior wall. Therefore, the distinct mouse coronary artery anatomy results in different regionality of infarction compared with human, because ligation of the left coronary artery in mice produces ischemia in the anterolateral, posterior, and apical regions of the heart, sparing the septum [2]. Also the anatomy of conduction system is different from human, because the sinoatrial node is located in the superior caval vein above its junction with the right atrium, not in the atrium itself [6]. Mouse model of myocardial ischemia has highlighted the mechanisms of infarct and LV remodeling and is often the first choice for testing new therapies such as stem cell myocardial repair. Animal models mimicking the characteristics and development of human MI and heart failure related to CHD have been developed with various strategies and methods. In humans CHD is related to chronic narrowing by atherosclerotic plaques or by acute occlusion by thrombosis of coronary arteries. In animals, atherosclerosis can be reproduced inducing hypercholesterolemia by fat-/cholesterol- rich diet or by genetic manipulation. However, time point and site of coronary occlusion occur accidentally in these models and, in the latter case, the etiology is different from that naturally occurring in humans. Various pathologic conditions mimicking human cardiovascular diseases can be induced by microsurgery. For example, surgical induction of narrowing or occlusion of coronary arteries allows facilitating a precise timing, location, reproducibility, and extent of coronary disease. According to the duration and extent of coronary blood flow impairment, surgical models can be classified as MI, cardiac ischemia-reperfusion injury, and chronic cardiac ischemia. In recent years, the mouse is the species increasingly used to characterize MI induced by coronary artery ligation. This is the major animal model of LV dysfunction progressing to failure. A main technical challenge to perform cardiovascular surgery in mice is the little size of mouse heart and coronary arteries. A microscope is required to clearly detect and bind the small left coronary artery. Moreover, dedicated microsurgical instruments, thin sutures and needles, and a customized mouse ventilator should be employed. To perform surgery, the mouse is anesthetized with intraperitoneal or inhalant agents. It is important to not disturb the animal prematurely, since this will induce stress and affect the quality of the subsequent procedure. After an adequate depth of anesthesia is attained, the mouse is fixed in a supine position on a heating table to prevent hypothermia and is intubated to provide assisted ventilation. Tracheal intubation of mice is challenging, due to their small mouth and then the difficulty to visualize vocal cord opening. If performed by nontrained operators, there is a high risk of pharyngeal or tracheal damage, such as perforation or stenosis. Intubation can be made with a customized tracheal cannula or a modified 18–20 gauge intravenous Teflon catheter, of about 25 mm of length, inserted through the oral cavity or after tracheotomy/tracheostomy. Visualization of vocal cord opening can be facilitated with appropriate positioning and using dedicated "self-made" device [7–12]. A drop of 1% lidocaine can be applied on the tip of the tracheal cannula to reduce laryngeal reflex. After intubation, the mouse is connected to a mouse ventilator, providing oxygen 2 liters/min and in case an inhalant anesthetic, with a tidal volume of 200 μL and a respiratory rate of about 133 breaths/min. Prior to the incision, the chest is trichotomized and disinfected with iodopovidone solution, and 0.1 mL of 0.1% lidocaine is injected subcutaneously. The thoracotomy is performed by a transverse 5 mm incision of the left fourth intercostal space, 2 mm away from the left sternal border. It is important to avoid bleeding caused by damage intercostal or internal thoracic veins. Chest retractor is gently inserted to facilitate heart exposition. The pericardial sac is gently opened, taking care to avoid the rupture of the wall of the left superior vena cava. The left coronary artery is visualized as a pulsating bright red vessel, running in the middle of the heart wall from the left atrium toward the apex. Ligation is performed with a 7-0 suture passed with a thin needle under the artery, 1-2 mm lower than the tip of the left auricle, which induces 40–50% ischemia of the left ventricle. It is important to not enter the cavity of the ventricle with the needle, but also to not be too superficial, as suture will cut through the wall ventricle. Blanching of the tissue distal to the ligation can recognize the occlusion of the artery. It is important to overinflate lungs by shutting off with a finger the outflow of the ventilator for 1-2 seconds. In fact, the

lungs could be partially compressed by the retractor and their collapse could result in respiratory distress and poor recovery after surgery. The chest cavity is closed by bringing together the 4th and the 5th ribs, muscles, and skin with 7-0 absorbable sutures. The duration of the whole procedure is reported of about 20 minutes for trained personnel. The permanent occlusion of left coronary artery is followed by an extensive myocardial remodeling, a hypertrophy of the viable myocardium and thinning of the necrotic area [13]. Genetic background, age, and sex of animals should be considered because they can influence both infarct size and the disease progression [14, 15]. Similar to the MI animal models, to perform ischemia-reperfusion models the left coronary artery is legated, but a small plastic tube is placed between the legated vessel and the node, allowing for easier and safe relief of the occlusion. Ischemia can be verified by sudden regional paleness of the myocardium, whereas reperfusion is verified by the appearance of hyperemia in the previously pale region. During the period of occlusion, the chest opening should be covered with a sterile gauze to prevent drying and loss of heat. This model is characterized by a high infiltration of inflammatory cells, attenuated fibrotic remodeling and angiogenesis in the necrotic area [13]. To minimize the influence of surgery on inflammatory process, a "closed chest" ligation model of myocardial ischemia-reperfusion injury in the mouse has also been developed: briefly, after thoracotomy, a thin suture is passed under the left coronary artery and the end of the suture are inserted into a piece of polyethylene-10 tubing and exteriorized through the chest wall [16]. Then thoracic incision is closed and ischemia-reperfusion experiment is performed a few days later, pulling or releasing the suture ends, when inflammatory process induced by surgery is ended. The surgical murine model of MI is different from human pathological condition for several aspects: left coronary artery ligation produces in mice a transmural MI, whereas in human the development of collateral circulation and the potential cardioprotective effects of repeated mild ischemic events associated with CHD produce smaller, nontransmural infarct. In 1994, Miller and colleagues showed that "preconditioning" in the myocardium can induce a reduction of the infarct size of about 50%. For preconditioning, the mouse undergoes three cycles of 5 minutes of artery occlusion, followed by 5 minutes of reperfusion, and then 30 minutes of artery occlusion followed by 2 hours of reperfusion. Mortality associated with MI induction in mice is about 10%, due to acute malignant arrhythmias such as ventricular fibrillation after reperfusion or within 1 hour after surgery, that can be prevented by intraperitoneal injection of lidocaine (6 mg/kg) [13].

3. Cardiac PET/CT Imaging

Traditional cardiac imaging is based on detection of changes in the anatomy and physiological features of heart, such as blood flow or contractile function. Instead, molecular imaging is characterized by visualization and measurement of biochemical and cellular mechanisms of diseases, including altered energy metabolism, inflammation, apoptosis, thrombosis, and angiogenesis, thus improving early diagnosis and therapeutic approaches. Cardiac imaging in mice is difficult, due to the small ventricle volume and high heart rate. The use of molecular imaging in preclinical cardiovascular research has become possible by advances in imaging technology. In the last years, small animal PET systems with high spatial resolution and great sensitivity have been developed. The advantages of PET include higher sensitivity enabling dynamic imaging, creation of radiolabeled probes with natural radioisotopes that do not alter chemical behavior, well-established methods for attenuation correction, and the potential of absolute and semiquantitative accurate image quantification. PET allows measurement of functional processes like myocardial blood flow, cardiac output, metabolism of glucose or free fatty acid, or oxygen consumption in absolute units or, more simply, in a semiquantitative manner. Dynamic scans are required to measure the arterial input function and the tissue time activity curve. In humans and in larger animal models, these parameters are evaluated through repeated blood samples, or noninvasively by assessing the activity of the arterial blood pool in the LV cavity on PET images. Catheter-based arterial blood sampling is the gold standard method for measuring the input function in mice. Nevertheless, in mice arterial sampling is technically difficult because of the relatively small diameters and fragility of the mouse blood arteries [17]. In addition, the total blood volume of a mouse is very limited (1.7 mL), making repeated blood sampling impossible without affecting the homeostasis of the mice. To minimize blood loss and difficulty in sampling blood from a mouse during a dynamic small animal PET scan, a microblood sampling technique has been developed [18], but the number of blood samples that can be withdrawn is limited. To avoid these problems, various methods have been proposed to estimate the input function noninvasively, such as the derivation of liver time-activity curve from small-animal PET dynamic images [17, 19] or measurement of blood pool activity from a LV volume of interest [20–24]. However, in small animal imaging, hearts and arteries are small compared with the scanner spatial resolution and in association with cardiac and respiratory motion causes blurring and partial volume effect artifacts. The correction of the partial volume related underestimation of the blood tracer concentration could be made determining recovery coefficient by different sizes rod phantoms [22] or using a four-dimensional virtual mouse phantom [25]. Moreover, the fast heart rate needs the correction for tracer recirculation. Since blood samples could not be obtained rapidly during the initial bolus transits through the central circulation, an early time point 20–35 seconds after injection has been proposed for blood-sampling-derived values. At this time, equivalent to several circulation times, the radiotracer concentration is relatively constant [20]. Implementation of clustering [26] or factor analysis algorithms [27] enables minimally invasive extraction of accurate input functions and myocardial time-activity curves from dynamic micro-PET images of rodents without the need to draw regions of interest, and overcoming the limitation related to partial-volume effect, spillover from the myocardium and motion

blurring. Therefore, although the quantification of the metabolic rate of energetic substrates utilization improves the accuracy of measuring the extent of the infarct, in mice are commonly adopted semiquantitative approaches for analysis of the distribution of radiotracers. Measurement of infarct size is an important clinical goal for prognostic assessment and evaluation of therapeutic interventions [28]. Although the quantification of infarct size has been well-established in humans, this approach is more challenging in small animals due to their smaller size. In cardiovascular research, histological measurements are widely accepted as the gold standard for quantifying infarct size, also to validate imaging-based approach. Nevertheless, histomorphometry cannot provide serial measurements in the same animal over time, which are useful to monitor the evolution of a disease or the response to a treatment. Therefore, there is a great interest to develop an accurate and noninvasive method to evaluate infarct size in living mice, improving the knowledge of metabolic and functional changes related to MI and the efficacy of interventional, pharmacological, or molecular therapies. Several imaging-based approaches to measure infarct size have been developed on animal models. It has been reported that infarct size quantification in mice can be obtained in an accurate and repeatable way with CT [29], magnetic resonance [30], single-photon emission computed tomography (SPECT) [31], or PET [32]. In particular, PET has several advantages, such as high spatial resolution and sensitivity. Since tridimensional images can be reconstructed from PET datasets, this technique is more suitable than others, such as 2D echocardiography, to study MI models, which are characterized by greatly modified ventricular shape and irregular wall thickness [14]. Furthermore, with the advent of dedicated image reconstruction and quantification software, it is now possible to perform quantitative clinical measures in rodent heart.

Disadvantages of PET include the use of ionizing radiation and the physic intrinsic limit to the maximum spatial resolution achievable. Currently most micro-PET imaging systems are fused with micro-CT, to create hybrid-imaging systems that overcome the inherent low resolution of the very sensitive nuclear imaging techniques and provide the site of molecular tracers uptake in greater anatomic detail. Hybrid imaging systems will facilitate the translation of molecular imaging-based approaches to man. CT is also useful to perform accurate correction for partial volume errors. Disadvantages of CT include the use of ionizing radiation and the limited spatial resolution achievable *in vivo*, related to the radiation dose administered to the animals.

4. PET Tracers for Models of Myocardial Infarction

Alterations in myocardial substrate metabolism are critical in the pathogenesis of many cardiovascular diseases. MI is associated with numerous biochemical and functional changes in the necrotic tissue, in the area at risk, and in the remote myocardium. PET imaging can provide *in vivo* a noninvasive, serial and quantitative assessment of myocardial perfusion, metabolism, apoptosis, and gene expression. Moreover, electrocardiographic and respiratory gating PET imaging can also be used to analyze anatomic and functional parameters, such as LV shape, end-diastolic and end-systolic volumes, stroke volume, cardiac output, ejection fraction, and regional contractility [32]. The principal characteristics of the most commonly used PET tracers are illustrated in Table 2. PET radiotracers used for evaluation of myocardial blood flow include N-13 ammonia, rubidium-82, and O-15 water [33]. However, their short half-life limits their widespread clinical use, because of the need for nearby cyclotron or generator. Among these, N-13 ammonia is the most widely used in preclinical studies, due to its relatively longer half-life of ten minutes, the high myocardium extraction, and reduced persistence in blood pool [34]. F-18 fluorodeoxyglucose (FDG) is the most widely used PET tracer and its uptake provides an established method in clinical practice to measure tissue viability in patients with advanced CHD and impaired LV function. Compared with the other tracers, FDG is more readily available in most PET centers and allows for better resolution images [35]. FDG traces myocyte glucose uptake and phosphorylation and can be used to quantify regional myocardial glucose metabolism in normal mice and in those with myocardial infarction (Figure 3). The uptake of FDG reflects the activity of various glucose transporters and hexokinase in manner similar to glucose, but unlike glucose-6-phosphate, FDG-6-phosphate is not further metabolized and is trapped into the cells, enhancing imaging quality. This radiotracer is also useful to study inflammation in course of acute myocardial ischemia-reperfusion injury and LV remodeling. As an alternative to glucose metabolism, PET studies with a variety of compounds with similar structure to the fatty acids radiolabeled with [18F] are useful for studying cardiac metabolism, since an ischemic event induces the use of glucose as preferential energy substrate instead of fatty acids, for a long time. C-11 acetate has been proposed as a marker of myocardial viability, because it evaluates residual oxidative metabolism, that is preserved in dysfunctional but viable myocardium, whereas it is severely depressed in irreversibly dysfunctional segments [27]. In the literature it has been described preclinical studies in rat with [18F]-RGD, a cyclic peptide that specifically recognizes receptors $\alpha v\beta 3$, and useful to evaluate angiogenesis after myocardial ischemia [36] and with 11C-epinephrine, demonstrating impaired uptake and storage of catecholamines in the myocardium after ischemia induction [37].

5. Technological Features of Dedicated PET/CT Systems

The development of PET systems dedicated to small laboratory animals started in the early 1990s. The first dedicated scanner commercialized was the "RatPET" in 1995 [38]. Since then, the main objective has been the improvement of the performances of these devices, considering that heart size is 10 times smaller and heart rate is 10 times faster

Table 2: Principal characteristics of PET tracers for cardiovascular imaging.

Tracer	Production	Half-life	Extraction	Myocardial uptake mechanism
^{13}N-ammonia	Cyclotron	10 min	80%	Diffusion/metabolic trapping (perfusion)
^{82}Rubidium	Generator	78 sec	50–60%	Na/K-ATPase (perfusion)
^{15}O-water	Cyclotron	2.1 min	100%	Free diffusion (perfusion)
F-18 FDG	Cyclotron	110 min	1–3%	Glucose transport/hexokinase (viability)

PET: positron emission tomography; Na/K-ATPase: sodium/potassium-ATPase; FDG: fluorodeoxyglucose.

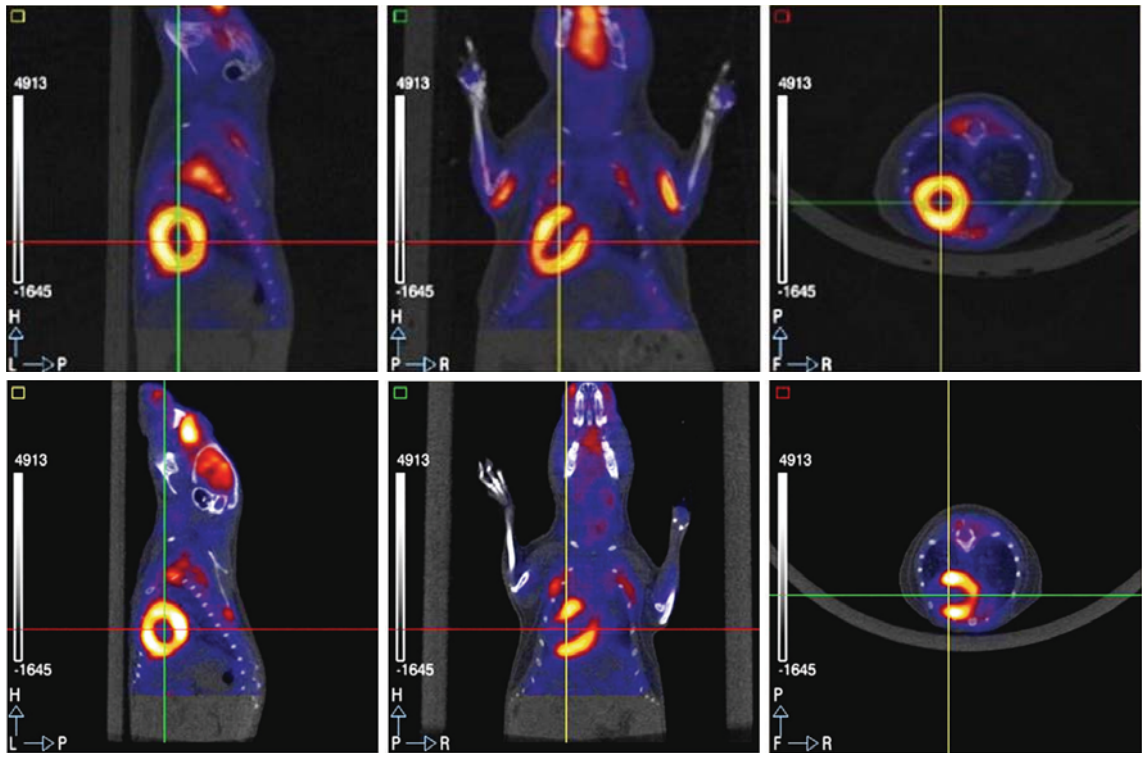

Figure 3: [^{18}F] FDG cardiac PET/CT in a normal mouse (top) and in a mouse with myocardial infarction (lower). FDG cardiac uptake is uniform in the normal mouse, while there is an area of absent uptake in the anteroapical region of the mouse with myocardial infarction.

in mice than humans. It is well known that PET is characterized by two intrinsic physical limits to the maximum spatial resolution achievable: the finite range of positron and the acollinearity of the two annihilation photons. It has been estimated that the distance which F-18 travels prior to annihilation produces a blurring effect of about 0.1–0.2 mm, whereas the deviation of annihilation photons from the 180° direction will produce an additional blur of 0.3 mm for a 15 cm detector diameter scanner. Therefore, the highest theoretically resolution achievable with F-18 is about 0.6 mm. Dedicated systems to date available have a spatial resolution between 1 and 2 mm full width at half maximum (FWHM) [39–41]. Problems related to nonuniformity of spatial resolution can be limited measuring depth of interaction of gamma rays in detectors composed of two joined scintillators with different decay time constant, for example LSO and GSO crystals. Nowadays the small animal scanner with higher spatial resolution is characterized by a detector system formed by layers of laminated lead with several holes that convert the incident gamma rays in electrons, and gas ionization chambers that detect these electrons. This peculiar detector system, associated with the use of a "*resolution recovery*" reconstruction algorithm, allows to achieve a spatial resolution of 1 mm FWHM [41]. System sensitivity, defined as the fraction of radioactive decays detected per volumetric resolution elements, is the other important parameter affecting image quality. The detector material, thickness, and geometry are the main factors affecting sensitivity. Currently both human and preclinical PET scanners detect about 2–5% of the coincident annihilation photons at the center of field of view. The main challenge of dedicated imaging systems is to obtain at the same time a high spatial resolution and sensitivity. The difficulty to reach this goal is in the design and realization of the detectors. To achieve a high spatial resolution in a dedicated PET scanner with inorganic crystals (BGO, LSO(Ce), GSO(Ce)) detectors, the size of the crystals cross-section must be reduced. As a consequence, the solid angle

covered by a single detector is limited, decreasing the system sensitivity. Moreover, a reduction of crystals size increases the number of gamma rays obliquely incident on their surface, causing parallax error that degrades spatial resolution from the center toward the edge of the field of view. On the other hand, the increase in the numbers of discrete small crystals poses some difficulties in terms of light collection and readout electronics. Theoretically, the coincidence photon detection efficiency should be improved by a factor of 1000 scaling from clinical to mouse imaging, but it is possible to achieve a 200-fold increase in 2D and a 30-fold increase in 3D data acquisition mode. The resolution-sensitivity offset also strongly affects dynamic scans, because reconstruction of short time frames of PET data may result in unacceptable low signal-to-noise ratio [40]. Iterative statistical algorithms can optimize tradeoff between signal-to-noise ratio and spatial resolution [42]. Image quality is also influenced by the total amount of radioactivity in the field of view, and the scan time. In order to collect an adequate amount of events for good quality image reconstruction, administered dose can be increased securely for probes of endogenous compounds such as the analogue of glucose FDG, overcoming some of the sensitivity limitations. For probes targeting biological markers in nanomolar concentration in tissues, an increase in specific activity allows more radioactivity to be injected into an animal. The number of detected events can be also incremented by long scan time, whereas this approach is limited by radionuclide half-life, radiotracers clearance, and animal anesthesia duration [40]. In molecular imaging, PET provides the possibility to visualize metabolic processes at cellular level noninvasively, quantitatively, and repeatedly, but does not allows a precise anatomic localization of lesions. The introduction of micro-PET/CT hybrid systems for imaging of small animals has greatly enhanced the performance and the accuracy of nuclear imaging, allowing a fine spatial localization of the radiotracer biodistribution and will facilitate the translation of molecular-based imaging to humans. Delayed enhancement micro-CT, using blood-pool and conventional iodinated contrast agent can help to optimize measurement of infarct size, since molecular targets and biological processes differ greatly between necrotic and remote myocardium [29]. Micro-CT can be also useful to perform attenuation correction that can result in underestimation of regional radiotracer activity. Whereas attenuation of the 511 KeV photons is about 22% for a mouse [41], CT-based attenuation correction has been shown to be accurate in small animal PET, allowing to reduce noise and significantly improve the accuracy of semiquantitative uptake measurements [43]. Several scanner designs are suited for different preclinical research fields. Generally, micro-CT provides higher spatial resolution (<500 μm) than current clinical scanner (from 450 to 600 μm). Scaling down CT imaging to the size of a mouse is challenging: to acquire CT data with detail of internal organs comparable to clinical CT scan, a resolution of about 100 μm is required. The heart rate of a mouse is about 400–600 min^{-1} and to use the diastole as the phase of the heart cycle that show the minimum amount of motion, a CT temporal resolution of almost 50 ms is necessary in comparison to 300 ms in humans. In order to achieve high spatial and contrast resolution, high X-ray doses are needed, ranging from 250 to 500 mGy, in comparison to <50 mGy for a clinical scanner. Currently, flat-panel-based mini-CT systems offer a valuable tradeoff among resolution (200 μm), scan time (0.5 s), and applied X-ray dose. Although these values remain below the lethal level for the mouse (6 Gy), repeated exposure to small X-ray dosages can have biological effects, which might interfere with longitudinal imaging protocols, for example, on tumor growth or hematopoiesis [44].

6. Animal Preparation for Cardiac PET/CT Imaging

Parallel to the development of dedicated PET scanners, the need to optimize the operative protocols for small rodents imaging has been profiled. For human F-18 FDG studies, standard protocols have been established, whereas procedures for animal imaging vary widely. In planning longitudinal PET studies in mice, many variables interfering with the accuracy of the experimental results must be taken into account. Several factors may influence the kinetics and biodistribution of radiopharmaceuticals, such as the mouse preparation, the type of radiotracer employed, methods and timing of radiopharmaceutical administration, and anesthesia. Mice attending personnel should be trained for resolutel and gentle manipulation. In fact, stress related to physical restraint can induce corticosteroid and epinephrine release, stimulate cardiovascular and respiratory functions, and increase glucose levels, body temperature, and anesthetic dosages [45]. Moreover, restraint distress during F-18 FDG injection can cause evident uptake of radiotracer in inter-scapular brown fat and paraspinal muscles, interfering with visualization of heart [45]. Several studies have investigated the effects of fasting, warming, and anesthesia on small animal PET studies with FDG [46]. Under normal resting conditions, myocardium derives the majority of energy from long chain fatty acids, but it can rapidly change their energy source to glucose in response to catecholamine or insulin stimulation, or acute ischemia. It is reported that in fasted mice myocardium should use fatty acids as its major energy source, with consequently reduced glucose or FDG uptake [47, 48]. In humans, glucose loading and insulin administration are commonly used to improve image quality and diagnostic accuracy. A glucose/insulin stimulation protocol was successfully applied in rats [49] and in mice [50], to standardize metabolic conditions for all animals and produce a 50-fold increase of FDG uptake into the myocardium. This protocol provides intraperitoneal administration of 8 mU/g of human insulin and 1 mg/g of glucose thirty minutes before FDG injection, and a biodistribution of thirty minutes prior to a static PET scan of heart. Keeping patients warm from before the FDG injection to the end of PET scanning is a standard practice, commonly adopted for reducing inter-scapular brown fat uptake [45]. Fueger et al. [46] reported that in mice warming significantly reduces the intense FDG uptake in brown adipose tissue, which could interfere with a clear visualization of heart. In fact, at a so-called "zone

of thermoneutrality" room temperature (30–34°C), body temperature is controlled by heat convection and activation of brown adipose tissue and muscle activity are not required to maintain it stable. Anesthesia can influence myocardial metabolism and several haemodynamic parameters, such as myocardial blood flow. Lee et al. [51] compared the effects of ketamine-xylazine and pentobarbital anesthesia on FDG biodistribution in fasted mice. They found that after 4 hours fast, both anesthetic protocols reduced FDG uptake in myocardium. This finding can be explained by the significant increase in plasma glucose level brought by xylazine and by the increased insulin level brought by pentobarbital. Hildebrandt et al. [45] reported that isoflurane, compared to ketamine-xylazine, induces mild hyperglycemia, reduces FDG uptake by brown adipose tissue and increases it in myocardium. Woo et al. [52] observed a dose-dependent increase in FDG uptake in heart under isoflurane anesthesia, likely related to a dose-dependent decrease in blood pressure, proportional to anesthetic depth.

Kober et al. [53] carried out regional myocardial blood flow under two commonly used anesthetic regimens in mice. They reported that under ketamine 100 mg/kg and xylazine 5 mg/kg or isoflurane 1.25% the mean blood flow value in the LV myocardium was comparable. However, under isoflurane concentration of about 2%, myocardial blood flow, and then the uptake of FDG or other radiotracers increased remarkably. In fact, isoflurane has been shown to have effects on blood flow and vascular resistance in many tissues including the heart. Its dose-dependent vasodilatory effect on coronary microvessels has been assessed *in vivo* in various animal models and in tissue preparations [53] and is based on a mechanism of mitochondrial adenosine triphosphate regulated potassium (mitoK_{ATP}) channels opening [54]. Ketamine/xylazine could enhance myocardial uptake of radiotracers that interact with catecholamine receptors. Such behavior seems to be due to a reduced blood norepinephrine concentration and radiolabeled analogues activity, brought about by the inhibition of norepinephrine release via α2-adrenoreceptors agonist [55]. The volume of radiotracer bolus should not exceed in mice 200 μL for the risk of iatrogenic hypervolemia and lung edema. Therefore, short half-life radionuclides have a maximum time of use in small rodents. Moreover their specific activity decreases over time, increasing the number of molecules injected and the potential appearance of side effects. This problem is critical in mice, because they receive a radiotracer dose greater of humans: for example, in mouse is commonly used a dosage of 0.2 mCi of F-18 FDG, that is, 50 times greater than the human one (10 mCi), taking into account the body weight. This factor is important to improve image quality but is related to a higher radiation dose (about 40 cGy for F-18 PET) [45]. The route of administration is another factor that could influence kinetics and biodistribution of radiopharmaceuticals. In humans, radiotracers are commonly administered intravenously and injection error occurs in about 1% of patients [56]. The two most common ways used in mice are intravenous and intraperitoneal injection. In preclinical PET studies, intravenous injection is preferred, because the circulation time is faster, the behavior of tracer kinetic is analogue to human and no residual tracer remains in peritoneum. The intraperitoneal route can be associated with modifications in tracer kinetics, wide variability of acquired data, wrong radiotracer injection in internal organs, and interference with abdominal studies. However, due to the very small diameter of murine tail veins, partial paravenous injection is common, leading to a net underestimation of the injected dose. Therefore, like in humans [56], it has been suggested the opportunity to measure residual radioactivity in the tail with a short PET scan to correct the injected dose for radioactivity deposition [57]. Moreover, Fueger et al. [46] found that at 60 minutes after injection, FDG biodistribution is comparable for intravenous and intraperitoneal route.

7. Postprocessing of PET/CT Images in Models of Myocardial Infarction

The use of N-13 ammonia, rubidium-82, and F-18 FDG PET for myocardial perfusion and viability imaging in patients with CHD has increased significantly over the last decade [58–60]. PET allows noninvasive measurements of physiological parameters in absolute units or semiquantitative data. The quantitative assessment of regional tracer distribution has represented the main improvement in clinical nuclear cardiology. A reliable, automated, and reproducible analysis of cardiac SPECT or PET data is an important goal and several software programs perform quantitative analysis of myocardial perfusion and viability, according to a scheme divided into some basic steps. First, the myocardial emission activity from the left ventricle is "segmented," that is isolated from any other adjacent emission activity. Since tomographic PET images are usually acquired transaxially to the long axis of the patient, the cardiac images must be reoriented by defining its long axis. Some software programs also allow defining the valve plane and the junction between left and right ventricle. At this point, the tomographic PET data of the heart can be reprocessed into short axis slices (from apex to the base, perpendicularly to the long axis of the heart), vertical long axis slices (from the posterior to anterior wall, parallel to long axis of the heart), horizontal long axis (from the lateral wall to septum, parallel to the long axis of the heart) to help the user in validating the reorientation. Assuming a simplified structural model of the left ventricle, described as a cylindrical structure in its basal two-thirds and spherical at the base, a regular sampling of maximal activity (in 30–60 equally spaced points) is conducted from each short axis section, and along rays normal to the myocardium. These data are used to compute a two-dimensional representation of midmyocardium called "circumferential profile." The epicardial and endocardial surfaces are located at fixed standard deviation values below the midmyocardial maxima. Circumferential profiles are arranged as a series of concentric circles, proportionally to the number of short axis slices, in a "polar map." A polar map is a two-dimensional representation of the three-dimensional distribution of the radiotracer in the heart, with the apex corresponding to the center, and the outermost

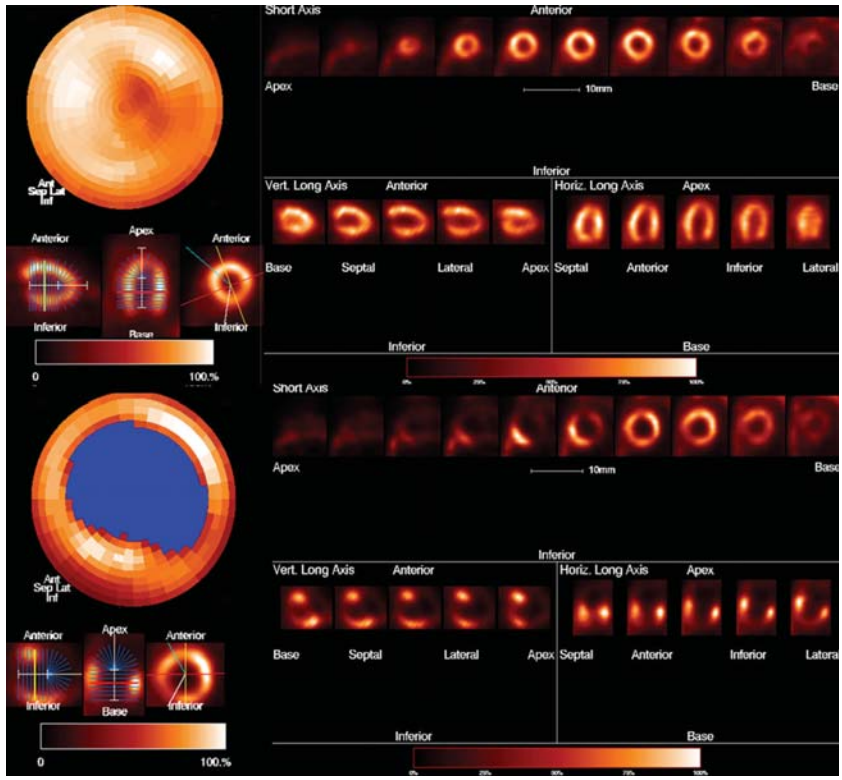

Figure 4: [^{18}F] FDG PET. Left ventricular polar map obtained in a normal mouse (top) and in a mouse with myocardial infarction (lower) by MunichHeart software.

circle corresponding to the base of the left ventricle [61–63]. Epicardial and endocardial surfaces can be used for displaying 3D rendering of myocardial perfusion that can be rotated and viewed as a color mapping of perfusion or as a wire-mesh frame. The regional distribution of radiotracer activity in LV myocardium (lateral, anterior, septal, inferior, and apical quadrant of the polar display) can be expressed in MBq/mL, standard uptake value, and standard deviation from maximal myocardial activity. However, a normal threshold for quantify infarct size has not yet been reported. Several algorithms for quantification of myocardial perfusion are based on the development and validation of a normal database or by measures obtained from anthropomorphic phantoms; others display all perfusion values below 50% as blackout pixels [61, 63, 64]. Generally polar maps are normalized for maximum activity value and scaled from 0 to maximum activity of 100%. Consequently, defects in perfusion are commonly expressed in percentage value by counting the number of pixels in the polar map whose the activity is below normal threshold and relate this value to the total number of pixels. Moreover, it is possible to determine the standard deviation from the normal threshold value for the pixels whose count is considered below normal [62] or measure infarct size in cm^2 using the calculated individual element size [61, 63]. Blackout pixels in the polar map are used as visual indication of perfusion defect size. Although the quantification of infarct size has been well established in humans with PET, this approach is more challenging in small animals due to their smaller size. In preclinical cardiovascular research, FDG PET is useful to accurately evaluate myocardial glucose metabolism and infarct size, monitoring *in vivo* and noninvasively the same animal. Its accurate and serial quantification may allow future applications in different knockout and to evaluate postischemic treatments, such as new drugs, gene therapy, or stem cells. The assessment of myocardial perfusion and viability by PET has been described in rodents, with the help of automated software owners [32, 65], clinical software's (Scion Image, ImageJ) [64, 66], or dedicated programs [31, 33, 49]. The validation of quantitative PET analysis methods developed for small laboratory rodents has been performed by histomorphometry [31, 49, 66] or by autoradiography as the gold standard [32, 64]. The threshold value of normal myocardial perfusion to accurately measure the extent of the necrotic area was determined by linear regression for comparison with histological measurements [46], or based on the method described by O'Connor et al. [67], providing that the pixel values less than 50% of maximum activity correspond to myocardial hypoperfused areas. Necrotic pattern was defined as relative tracer uptake of <50% of maximal myocardial uptake. PET can also be used to measure changes in anatomic and functional parameters, such as LV shape, end-diastolic and end systolic, volumes, stroke volumes, cardiac output, ejection fraction, and regional contractility [32], occurring in postinfarction cardiac remodeling (Figure 4).

8. Conclusions

In the last decades, murine models of MI have become useful tools to highlight the mechanisms underlying CHD and to test new therapeutic approaches, such as gene or stem cells therapy. At the same time, with technological advancements, small laboratory PET/CT imaging has emerged in cardiovascular research, providing *in vivo* a noninvasive, serial and quantitative assessment of myocardial perfusion and metabolism at a molecular level. PET/CT studies of myocardial perfusion and viability have been successful tools to perform a quantitative evaluation of myocardial metabolism and to measure infarct size in an accurate and repeatable way both in clinical and in preclinical research. Since the same animal can be imaged repeatedly and each animal can be its own control, the number of animals examined is significantly reduced and the variability caused by interindividual differences is removed, according to the principle of "*refinement, reduction, and replacement*."

Conflict of Interests

The authors declare no conflict of interests.

References

[1] F. A. Recchia and V. Lionetti, "Animal models of dilated cardiomyopathy for translational research," *Veterinary Research Communications*, vol. 31, no. 1, pp. 35–41, 2007.

[2] D. Kumar, T. A. Hacker, J. Buck et al., "Distinct mouse coronary anatomy and myocardial infarction consequent to ligation," *Coronary Artery Disease*, vol. 16, no. 1, pp. 41–44, 2005.

[3] K. M. Nilles and B. London, "Knockin animal models of inherited arrhythmogenic diseases: what have we learned from them?" *Journal of Cardiovascular Electrophysiology*, vol. 18, no. 10, pp. 1117–1125, 2007.

[4] B. Ciszek, D. Skubiszewska, and A. Ratajska, "The anatomy of the cardiac veins in mice," *Journal of Anatomy*, vol. 211, no. 1, pp. 53–63, 2007.

[5] A. Wessels and D. Sedmera, "Developmental anatomy of the heart: a tale of mice and man," *Physiological Genomics*, vol. 15, pp. 165–176, 2004.

[6] F. L. Meijler, "Atrioventricular conduction versus heart size from mouse to whale," *Journal of the American College of Cardiology*, vol. 5, no. 2 I, pp. 363–365, 1985.

[7] R. H. Hastings and D. Summers-Torres, "Direct laryngoscopy in mice," *Contemporary Topics in Laboratory Animal Science*, vol. 38, no. 6, pp. 33–35, 1999.

[8] R. H. Brown, D. M. Walters, R. S. Greenberg, and W. Mitzner, "A method of endotracheal intubation and pulmonary functional assessment for repeated studies in mice," *Journal of Applied Physiology*, vol. 87, no. 6, pp. 2362–2365, 1999.

[9] A. Vergari, A. Polito, M. Musumeci, S. Palazzesi, and G. Marano, "Video-assisted orotracheal intubation in mice," *Laboratory Animals*, vol. 37, no. 3, pp. 204–206, 2003.

[10] J. Winning, H. Huwer, J. Redjai et al., "Noninvasive mechanical ventilation of mice by using a balloon-tipped cannula," *Contemporary Topics in Laboratory Animal Science*, vol. 43, no. 6, pp. 39–41, 2004.

[11] E. N. Spoelstra, C. Ince, A. Koeman et al., "A novel and simple method for endotracheal intubation of mice," *Laboratory Animals*, vol. 41, no. 1, pp. 128–135, 2007.

[12] O. Moldestad, P. Karlsen, S. Molden, and J. F. Storm, "Tracheotomy improves experiment success rate in mice during urethane anesthesia and stereotaxic surgery," *Journal of Neuroscience Methods*, vol. 176, no. 2, pp. 57–62, 2009.

[13] O. Tarnavski, J. R. McMullen, M. Schinke, Q. Nie, S. Kong, and S. Izumo, "Mouse cardiac surgery: comprehensive techniques for the generation of mouse models of human diseases and their application for genomic studies," *Physiological Genomics*, vol. 16, pp. 349–360, 2004.

[14] D. A. Gorog, M. Tanno, A. M. N. Kabir et al., "Varying susceptibility to myocardial infarction among C57BL/6 mice of different genetic background," *Journal of Molecular and Cellular Cardiology*, vol. 35, no. 6, pp. 705–708, 2003.

[15] J. Takagawa, Y. Zhang, M. L. Wong et al., "Myocardial infarct size measurement in the mouse chronic infarction model: comparison of area- and length-based approaches," *Journal of Applied Physiology*, vol. 102, no. 6, pp. 2104–2111, 2007.

[16] T. O. Nossuli, V. Lakshminakayanan, G. Baumgarten et al., "A chronic mouse model of myocardial ischemia-reperfusion: essential in cytokine studies," *American Journal of Physiology*, vol. 278, no. 4, pp. H1049–H1055, 2000.

[17] L. A. Green, S. S. Gambhir, A. Srinivasan et al., "Noninvasive methods for quantitating blood time-activity curves from mouse PET images obtained with fluorine-18-fluorodeoxyglucose," *Journal of Nuclear Medicine*, vol. 39, no. 4, pp. 729–734, 1998.

[18] H. M. Wu, G. Sui, C. C. Lee et al., "In vivo quantitation of glucose metabolism in mice using small-animal PET and a microfluidic device," *Journal of Nuclear Medicine*, vol. 48, no. 5, pp. 837–845, 2007.

[19] A. S. Yu, H. D. Lin, S. C. Huang, M. E. Phelps, and H. M. Wu, "Quantification of cerebral glucose metabolic rate in mice using ^{18}F-FDG and small-animal PET," *Journal of Nuclear Medicine*, vol. 50, no. 6, pp. 966–973, 2009.

[20] M. C. Kreissl, H. M. Wu, D. B. Stout et al., "Noninvasive measurement of cardiovascular function in mice with high-temporal-resolution small-animal PET," *Journal of Nuclear Medicine*, vol. 47, no. 6, pp. 974–980, 2006.

[21] Y. H. D. Fang and R. F. Muzic Jr., "Spillover and partial-volume correction for image-derived input functions for small-animal 18F-FDG PET studies," *Journal of Nuclear Medicine*, vol. 49, no. 4, pp. 606–614, 2008.

[22] L. W. Locke, S. S. Berr, and B. K. Kundu, "Image-derived input function from cardiac gated maximum a posteriori reconstructed PET images in mice," *Molecular Imaging and Biology*, vol. 13, no. 2, pp. 342–347, 2011.

[23] J. K. Su, S. L. Jae, C. I. Ki et al., "Kinetic modeling of 3′-deoxy-3′-^{18}F-fluorothymidine for quantitative cell proliferation imaging in subcutaneous tumor models in mice," *Journal of Nuclear Medicine*, vol. 49, no. 12, pp. 2057–2066, 2008.

[24] L. Moerman, D. de Naeyer, P. Boon, and F. de Vos, "P-glycoprotein at the blood-brain barrier: kinetic modeling of 11C-desmethylloperamide in mice using a 18F-FDG μPET scan to determine the input function," *European Journal of Nuclear Medicine and Molecular Imaging*, vol. 1, pp. 12–21, 2011.

[25] W. P. Segars, B. M. W. Tsui, E. C. Frey, G. A. Johnson, and S. S. Berr, "Development of a 4-digital mouse phantom for molecular imaging research," *Molecular Imaging and Biology*, vol. 6, no. 3, pp. 149–159, 2004.

[26] S. Domenichelli, D. D'Ambrosio, S. Trespidi et al., "Quantitative cardiac dynamic imaging of small animal PET images using cluster analysis," in *Proceedings of the Computers in Cardiology (CAR '08)*, pp. 337–340, Bologna, Italy, September 2008.

[27] J. Kim, P. Herrero, T. Sharp et al., "Minimally invasive method of determining blood input function from PET images in rodents," *Journal of Nuclear Medicine*, vol. 47, no. 2, pp. 330–336, 2006.

[28] A. Saraste, S. G. Nekolla, and M. Schwaiger, "Cardiovascular molecular imaging: an overview," *Cardiovascular Research*, vol. 83, no. 4, pp. 643–652, 2009.

[29] M. Nahrendorf, C. Badea, L. W. Hedlund et al., "High-resolution imaging of murine myocardial infarction with delayed-enhancement cine micro-CT," *American Journal of Physiology*, vol. 292, no. 6, pp. H3172–H3178, 2007.

[30] J. Vogel-Claussen, C. E. Rochitte, K. C. Wu et al., "Delayed enhancement MR imaging: utility in myocardial assessment," *Radiographics*, vol. 26, no. 3, pp. 795–810, 2006.

[31] T. Wollenweber, C. Zach, C. Rischpler et al., "Myocardial Perfusion Imaging is Feasible for Infarct Size Quantification in Mice Using a Clinical Single-photon Emission Computed Tomography System Equipped with Pinhole Collimators," *Molecular Imaging and Biology*, vol. 12, no. 4, pp. 427–434, 2009.

[32] L. Stegger, A. N. Hoffmeier, K. P. Schäfers et al., "Accurate noninvasive measurement of infarct size in mice with high-resolution PET," *Journal of Nuclear Medicine*, vol. 47, no. 11, pp. 1837–1844, 2006.

[33] A. Cuocolo, W. Acampa, M. Imbriaco, N. De Luca, G. L. Iovino, and M. Salvatore, "The many ways to myocardial perfusion imaging," *Quarterly Journal of Nuclear Medicine and Molecular Imaging*, vol. 49, no. 1, pp. 4–18, 2005.

[34] M. Inubushi, M. C. Jordan, K. P. Roos et al., "Nitrogen-13 ammonia cardiac positron emission tomography in mice: effects of clonidine-induced changes in cardiac work on myocardial perfusion," *European Journal of Nuclear Medicine and Molecular Imaging*, vol. 31, no. 1, pp. 110–116, 2004.

[35] M. Ghesani, E. G. DePuey, and A. Rozanski, "Role of F-18 FDG positron emission tomography (PET) in the assessment of myocardial viability," *Echocardiography*, vol. 22, no. 2, pp. 165–177, 2005.

[36] T. Higuchi, F. M. Bengel, S. Seidl et al., "Assessment of $\alpha v\beta 3$ integrin expression after myocardial infarction by positron emission tomography," *Cardiovascular Research*, vol. 78, no. 2, pp. 395–403, 2008.

[37] G. Münch, N. T. B. Nguyen, S. Nekolla et al., "Evaluation of sympathetic nerve terminals with [^{11}C]epinephrine and [^{11}C]hydroxyephedrine and positron emission tomography," *Circulation*, vol. 101, no. 5, pp. 516–523, 2000.

[38] P. M. Bloomfield, S. Rajeswaran, T. J. Spinks et al., "The design and physical characteristics of a small animal positron emission tomograph," *Physics in Medicine and Biology*, vol. 40, no. 6, pp. 1105–1126, 1995.

[39] Y. Wang, J. Seidel, B. M. W. Tsui, J. J. Vaquero, and M. G. Pomper, "Performance evaluation of the GE healthcare eXplore VISTA dual-ring small-animal PET scanner," *Journal of Nuclear Medicine*, vol. 47, no. 11, pp. 1891–1900, 2006.

[40] M. Larobina, A. Brunetti, and M. Salvatore, "Small animal PET: a review of commercially available imaging systems," *Current Medical Imaging Reviews*, vol. 2, no. 2, pp. 187–192, 2006.

[41] K. P. Schäfers, A. J. Reader, M. Kriens, C. Knoess, O. Schober, and M. Schäfers, "Performance evaluation of the 32-module quadHIDAC small-animal PET scanner," *Journal of Nuclear Medicine*, vol. 46, no. 6, pp. 996–1004, 2005.

[42] A. Chatziioannou, J. Qi, A. Moore et al., "Comparison of 3-D maximum a posteriori and filtered backprojection algorithms for high-resolution animal imaging with microPET," *IEEE Transactions on Medical Imaging*, vol. 19, no. 5, pp. 507–512, 2000.

[43] P. L. Chow, F. R. Rannou, and A. F. Chatziioannou, "Attenuation correction for small animal PET tomographs," *Physics in Medicine and Biology*, vol. 50, no. 8, pp. 1837–1850, 2005.

[44] J. M. Boone, O. Velazquez, and S. R. Cherry, "Small-animal X-ray dose from micro-CT," *Molecular Imaging*, vol. 3, no. 3, pp. 149–158, 2004.

[45] I. J. Hildebrandt, H. Su, and W. A. Weber, "Anesthesia and other considerations for in vivo imaging of small animals," *ILAR Journal*, vol. 49, no. 1, pp. 17–26, 2008.

[46] B. J. Fueger, J. Czernin, I. Hildebrandt et al., "Impact of animal handling on the results of 18F-FDG PET studies in mice," *Journal of Nuclear Medicine*, vol. 47, no. 6, pp. 999–1006, 2006.

[47] M. C. Kreissl, D. B. Stout, K. P. Wong et al., "Influence of dietary state and insulin on myocardial, skeletal muscle and brain [18F]- fluorodeoxyglucose kinetics in mice," *European Journal of Nuclear Medicine and Molecular Imaging*, vol. 1, no. 6, pp. 1–22, 2011.

[48] T. Higuchi, S. G. Nekolla, A. Jankaukas et al., "Characterization of normal and infarcted rat myocardium using a combination of small-animal PET and clinical MRI," *Journal of Nuclear Medicine*, vol. 48, no. 2, pp. 288–294, 2007.

[49] G. Münch, N. T. B. Nguyen, S. Nekolla et al., "Evaluation of sympathetic nerve terminals with [^{11}C]epinephrine and [^{11}C]hydroxyephedrine and positron emission tomography," *Circulation*, vol. 101, no. 5, pp. 516–523, 2000.

[50] M. V. Simões, S. Egert, S. Ziegler et al., "Delayed response of insulin-stimulated fluorine-18 deoxyglucose uptake in glucose transporter-4-null mice hearts," *Journal of the American College of Cardiology*, vol. 43, no. 9, pp. 1690–1697, 2004.

[51] K. H. Lee, B. H. Ko, J. Y. Paik et al., "Effects of anesthetic agents and fasting duration on 18F-FDG biodistribution and insulin levels in tumor-bearing mice," *Journal of Nuclear Medicine*, vol. 46, no. 9, pp. 1531–1536, 2005.

[52] S. K. Woo, T. S. Lee, K. M. Kim et al., "Anesthesia condition for 18F-FDG imaging of lung metastasis tumors using small animal PET," *Nuclear Medicine and Biology*, vol. 35, no. 1, pp. 143–150, 2008.

[53] F. Kober, I. Iltis, P. J. Cozzone, and M. Bernard, "Myocardial blood flow mapping in mice using high-resolution spin labeling magnetic resonance imaging: influence of ketamine/xylazine and isoflurane anesthesia," *Magnetic Resonance in Medicine*, vol. 53, no. 3, pp. 601–606, 2005.

[54] H. Toyama, M. Ichise, J. S. Liow et al., "Evaluation of anesthesia effects on [18F]FDG uptake in mouse brain and heart using small animal PET," *Nuclear Medicine and Biology*, vol. 31, no. 2, pp. 251–256, 2004.

[55] B. H. Ko, J. Y. Paik, K. H. Jung et al., "Effects of anesthetic agents on cellular 123I-MIBG transport and in vivo 123I-MIBG biodistribution," *European Journal of Nuclear Medicine and Molecular Imaging*, vol. 35, no. 3, pp. 554–561, 2008.

[56] K. Miyashita, N. Takahashi, T. Oka et al., "SUV correction for injection errors in FDG-PET examination," *Annals of Nuclear Medicine*, vol. 21, no. 10, pp. 607–613, 2007.

[57] G. Porenta, W. Kuhle, J. Czernin et al., "Semiquantitative assessment of myocardial blood flow and viability using polar

map displays of cardiac PET images," *Journal of Nuclear Medicine*, vol. 33, no. 9, pp. 1628–1636, 1992.

[58] C. Nanni, C. Pettinato, V. Ambrosini et al., "Retro-orbital injection is an effective route for radiopharmaceutical administration in mice during small-animal PET studies," *Nuclear Medicine Communications*, vol. 28, no. 7, pp. 547–553, 2007.

[59] T. M. Bateman, G. V. Heller, A. I. McGhie et al., "Diagnostic accuracy of rest/stress ECG-gated Rb-82 myocardial perfusion PET: comparison with ECG-gated Tc-99m sestamibi SPECT," *Journal of Nuclear Cardiology*, vol. 13, no. 1, pp. 24–33, 2006.

[60] U. K. Sampson, S. Dorbala, A. Limaye, R. Kwong, and M. F. Di Carli, "Diagnostic accuracy of rubidium-82 myocardial perfusion imaging with hybrid positron emission tomography/computed tomography in the detection of coronary artery disease," *Journal of the American College of Cardiology*, vol. 49, no. 10, pp. 1052–1058, 2007.

[61] S. G. Nekolla, C. Miethaner, N. Nguyen, S. I. Ziegler, and M. Schwaiger, "Reproducibility of polar map generation and assessment of defect severity and extent assessment in myocardial perfusion imaging using positron emission tomography," *European Journal of Nuclear Medicine*, vol. 25, no. 9, pp. 1313–1321, 1998.

[62] H. Zaidi, *Quantitative Analysis in Nuclear Medicine Imaging*, Springer, 2006.

[63] G. S. Lin, H. H. Hines, G. Grant, K. Taylor, and C. Ryals, "Automated quantification of myocardial ischemia and wall motion defects by use of cardiac SPECT polar mapping and 4-dimensional surface rendering," *Journal of Nuclear Medicine Technology*, vol. 34, no. 1, pp. 3–17, 2006.

[64] M. C. Wu, D. W. Gao, R. E. Sievers, R. J. Lee, B. H. Hasegawa, and M. W. Dae, "Pinhole single-photon emission computed tomography for myocardial perfusion imaging of mice," *Journal of the American College of Cardiology*, vol. 42, no. 3, pp. 576–582, 2003.

[65] T. Kudo, K. Fukuchi, A. J. Annala et al., "Noninvasive measurement of myocardial activity concentrations and perfusion defect sizes in rats with a new small-animal positron emission tomograph," *Circulation*, vol. 106, no. 1, pp. 118–123, 2002.

[66] P. D. Acton, D. Thomas, and R. Zhou, "Quantitative imaging of myocardial infarct in rats with high resolution pinhole SPECT," *International Journal of Cardiovascular Imaging*, vol. 22, no. 3-4, pp. 429–434, 2006.

[67] M. K. O'Connor, T. Hammell, and R. J. Gibbons, "In vitro validation of a simple tomographic technique for estimation of percentage myocardium at risk using methoxyisobutyl isonitrile technetium 99m (sestamibi)," *European Journal of Nuclear Medicine*, vol. 17, no. 1-2, pp. 69–76, 1990.

Hindawi Publishing Corporation
Journal of Biomedicine and Biotechnology
Volume 2012, Article ID 184538, 11 pages
doi:10.1155/2012/184538

Research Article

Topical Application Effect of the Isolectin Hydrogel (Cramoll 1,4) on Second-Degree Burns: Experimental Model

Danielle dos Santos Tavares Pereira,[1] Maria Helena Madruga Lima-Ribeiro,[2,3] Ralph Santos-Oliveira,[4] Carmelita de Lima Bezerra Cavalcanti,[3] Nicodemos Teles de Pontes-Filho,[5] Luana Cassandra Breitenbach Barroso Coelho,[6] Ana Maria dos Anjos Carneiro-Leão,[4] and Maria Tereza dos Santos Correia[1,6]

[1] *Programa de Pós-Graduação em Ciências Biológicas, Universidade Federal de Pernambuco, 50670-901 Recife, PE, Brazil*
[2] *Programa de Pós-Graduação em Biociência Animal, Universidade Federal Rural de Pernambuco, 52171-900 Recife, PE, Brazil*
[3] *Laboratório de Imunopatologia Keizo Asami (LIKA), Universidade Federal de Pernambuco, 50670-901 Recife, PE, Brazil*
[4] *Divisão de Radiofarmácia, Instituto de Engenharia Nuclear, 21941-906 Rio de Janeiro, RJ, Brazil*
[5] *Departamento de Patologia, Universidade Federal de Pernambuco, 50670-901 Recife, PE, Brazil*
[6] *Departamento de Bioquímica, Centro de Ciências Biológicas, Universidade Federal de Pernambuco, 50670-901 Recife, PE, Brazil*

Correspondence should be addressed to Danielle dos Santos Tavares Pereira, dstpereira@yahoo.com.br

Received 24 August 2011; Revised 31 October 2011; Accepted 8 November 2011

Academic Editor: Monica Fedele

This study aimed at evaluating the use of hydrogel isolectin in the treatment of second-degree burns. Twenty male rats were randomly divided into two groups (G1 = treatment with hydrogel containing 100 μg/mL Cramoll 1,4 and G2 = Control, hydrogel). After 7, 14, 21, 28, and 35 days, animals were euthanized. On the 7th day, G1 showed intense exudates, necrosis and edema. On the 14th day, G1 showed tissue reepithelialization and moderate autolysis. On the 21st day, G1 showed intense fibroblastic proliferation, presence of dense collagen, and moderate fibrosis. On the 28th day, G1 showed complete tissue epithelialization. On the 35th day, G1 showed modeled dense collagen. The significant wound contraction was initiated from day, 14 in the G1. There were no significant differences in biochemical and hematological parameters analyzed. These results extend the potential of therapeutic applications for Cramoll 1,4 in the treatment of thermal burns.

1. Introduction

Since prehistory, plants and their by-products were used to treat wounds. Cramoll 1.4 is lectin extracted from seeds of *Cratylia mollis* Mart, a plant native to northeastern Brazil. Cramoll is specific for glucose/mannose. Four multiple forms have been purified from *C. mollis*—Cramoll 1, Cramoll 2, Cramoll 3, Cramoll 4—and preparations containing multiple combined forms as 1 and 4, named Cramoll 1.4 [2]. Studies have demonstrated that Cramoll 1,4 is capable of (i) isolating glycoproteins from human plasma [3], (ii) characterizing transformed mammary tissue [4], (iii) inducing mitogenic activity in human lymphocytes [5], (iv) producing IFN-y and nitric oxide [6], and (v) antitumor activities [7].

Burn wounds are one of the health problems in modern societies associated with irreparable harms and side many problems for patients and their families [8]. Burns are classified by their depth and severity such as 1st, 2nd, 3rd, and 4th degrees. The pathophysiologic reaction to a burn injury is complex and varies with the cause (thermal, chemical, electrical, or radiation). In thermal injuries, changes in the burn wound are mainly caused by heat direct effects, but superimposed on these are changes associated with the acute inflammatory process. It is these latter changes that account for the widespread and devastating effects of major burns on the entire body's homeostatic function [9]. In addition to the physiological morbidity of burns, these types of injuries are associated with a huge financial burden on the public health system.

In order to ease the pain of burning and minimize the number of dressing changes, several studies have been carried out in search of formulations that help in healing. The advent of dry bandages occurred in the nineteenth century due to the germ theory authored by Louis Pasteur. In the twentieth century, with advances in knowledge about the mechanisms involved in tissue lesion healing, the theory that the wounds in a wet environment have better healing capacity was developed [10]. In order to meet this need, the wet bandages containing natural and synthetic molecules have shown significant effect on the healing mechanism. In this sense, aiming to evaluate the effects of topical application of hydrogel containing 1, 4 Cramoll isolectin, this study investigated *in vivo* the clinical and histopathological features of second-degree thermal burns demonstrated experimentally in rats of Wistar strain.

2. Materials and Methods

2.1. Plant Material

2.1.1. Cratylia Mollis (Extraction and Purification). Cramoll 1,4 isolectin was purified from a 10% (w/v) seed extract of Cratylia mollis in 0.15 M NaCl according to the protocol reported in Correia and Coelho [11]. Briefly, all seeds (Camaratu bean) collected in Ibimirim City, State of Pernambuco, were washed with distilled water, dried at room temperature, and blended in 0.15 M NaCl. After 16 h of gently stirring at 4°C, the extract was filtered and centrifuged for 12 000 g. The extract was ammonium sulfate fractionated, dialysed against 0.15 M NaCl (fraction 40–60%) and affinity chromatographed on Sephadex G-75 (Sigma Chemical Company) in column (70.0 × 1.9 cm) containing 200 mL packed matrix, balanced with 0.15 M NaCl. After sample application, 0.15 M NaCl was passed through the column until $A280$ nm was less than 0.1; isolectin was eluted with 0.3 M glucose in 0.15 M NaCl. Fractions with highest $A280$ nm were pooled, exhaustively dialysed in buffer citrate phosphate and then lyophilized. The native isolectin has 8.5-8.6 pI measured by isoelectric focusing in polyacrylamide gel and 31 Kda main polypeptide.

2.2. Isolectin Hydrogel. Carbopol was used as vehicle suspended in boric acid buffer (pH 6.0) at 25°C. After extraction and purification, Cramoll 1,4 solutions were added in sufficient quantity to achieve the final concentration of 100 μg Cramoll 1,4 per mL of hydrogel. Irradiation was performed at room temperature using Co^{60} at 15 kGy h^{-2} [12].

2.2.1. Evaluation of Hemagglutinating Activity of the Isolectin Hydrogel. The hemagglutinating activity was performed in microtiter plates according to Correia and Coelho [11]. Samples of isolectin hydrogel (50 μL) were serially diluted in 0.15 M NaCl before adding 5 μL of a 2.5% (v/v) rabbit erythrocytes suspension previously treated with glutaraldehyde. The title was expressed as the highest dilution showing hemagglutinating activity. Assay performed in triplicate.

2.3. Animals and Experimental Wounds

2.3.1. Animals. All animals received humane care, and studies reported in this paper have been carried out in accordance with the guidelines for human treatment of animals set by the Brazilian College of Animal Experiment. The study was approved by the Committee on Animal Research at the Federal University of Pernambuco, Brazil (23076.015015/2009-31). A total of twenty male Wistar rats (*Rattus norvegicus*, albinus), 8–10-week-old and weighing approximately 250–300 g, were used in this study. Food pellets and water were provided ad *libitum* throughout the experiment.

2.3.2. Burn Injury. Animals were divided randomly into two groups of 10 (G1 and G2) and preanesthetized with atropine sulfate at 0.04 mg kg^{-1} intramuscularly. After ten minute, an anesthetic combination was used through an intramuscular injection of xylazine 10 mg kg^{-1} and ketamine 90 mg kg^{-1} with subsequent dorsum trichotomy by direct hair tension (area measuring approximately 3 cm^2) (Figure 1(a)) and antisepsis with 1% polyvinylpyrrolidone-iodine. Burns were symmetrically caused on depilated areas through contact with an aluminum bar (r = 10 mm), preheated for 100°C for 15 s (Figure 1(b)). After burn injury and animal awakening, once the procedure completed, analgesia was processed by means of intramuscular dipyrane application (0.01 mg kg^{-1}) to prevent pain. Injuries were observed during 35 consecutive days followed by the application of 100 μL hydrogel on the burn (Figure 1(c)). Group-1 was treated with empty hydrogel containing 100 μg Cramoll 1,4. Group-2 (control) was treated with hydrogel without isolectin.

2.4. Pathological Observations

2.4.1. Clinical Parameters. Burns surface was evaluated based on the following parameters for 35 consecutive days: edema, hyperemia, exudation and the firmness of wound surface, and presence or absence of granulation tissue and scar tissue. Wounds were considered closed if moist granulation tissue was no longer apparent and wounds seemed covered with new epithelium. Body weight was determined using electronic balance (accuracy to g) on the day of burn induction as well as days 7, 14, 21, 28, and 35 after wounding.

2.4.2. Wound Retraction Quantification. All the rats were examined weekly under anesthesia for observation of wound contracture. The wound retraction was evaluated in 7, 14, 21, 28, and 35 days after burn induction. Wound contraction was expressed as reduction in percentage of original wound size. % wound contraction on day-X = [(area on day 0 − open area on day X)/area on day 0] × 100 [13].

2.4.3. Biochemical and Hematological Evaluations. Blood from two animals per group were collected on days 7, 14, 21, 28, and 35 after burn induction for biochemical determination. Levels of creatinine, urea, glutamic pyruvic transaminase, glutamic oxalacetic transaminase, gamma

(a) (b) (c)

Figure 1: Induction of second-degree thermal burns in male Wistar rats. (a) Back trichotomy by direct hair tension, (b) depth second-degree thermal burn with $r = 10$ mm, (c) treatment of thermal burn using 100 μL hydrogel.

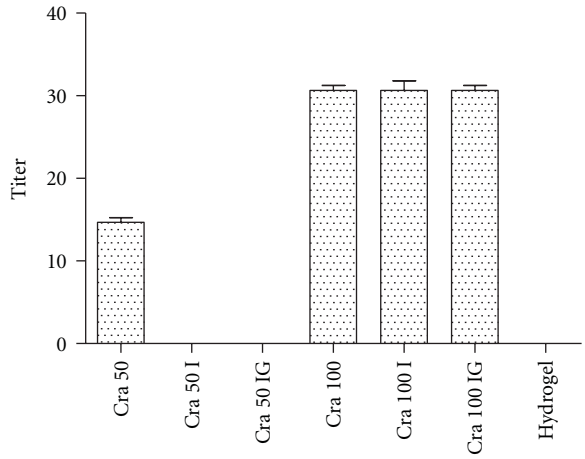

Figure 2: Evaluation of hemagglutinating activity of 1,4 Cramoll isolectin combined to the hydrogel excipient. Cra 50: Pure Cramoll 1,4 isolectin at 50 μg/mL. Cra 50 I: Pure Cramoll 1,4 isolectin at 50 μg/mL irradiated (15 k Gy h^{-2}). Cra IG: Pure Cramoll 1,4 isolectin at 50 μg/mL associated with hydrogel excipient and irradiated (15 k Gy h^{-2}). Cra 100: Pure Cramoll 1,4 isolectin at 100 μg/mL. Cra 100 I: Pure Cramoll 1,4 isolectin at 100 μg/mL irradiated (15 k Gy h^{-2}). Cra IG 100: Pure Cramoll 1,4 isolectin at 100 μg/mL associated with hydrogel excipient and irradiated (15 k Gy h^{-2}). Hydrogel irradiated without lectin. The title was expressed as the highest dilution showing hemagglutinating activity. Values are mean ± SEM.

glutamyl transferase, amylase, alkaline phosphatase, calcium, prothrombin, and fibrinogen were determined. Hematological parameters (erythrocytes, leukocytes, and platelets) were determined immediately after blood collection. Evaluations performed in triplicate. Animals in both G1 and G2 were sacrificed by injecting 30 mg kg^{-1} thiopental sodium.

2.4.4. Histopathology. After collection, tissue samples were fixed in 4% formaldehyde (v/v) prepared in PBS (0.01 M, pH 7.2) followed by histological processing through paraffin embedding, microtome with 4 μm cuts, and Masson's trichrome and hematoxylin-eosin staining. Histological analysis was performed by comparative descriptive analysis of experimental groups in binocular optical microscope (Zeiss-Axiostar model), where cellular and tissue characteristics of skin were evaluated after thermal injury and subsequent healing pattern.

2.5. Statistical Analysis. Data were analyzed using nonparametric tests. To detect differences between groups, the Mann-Whitney U test was used. All results were expressed as mean values of groups ± standard deviation and analyzed considering $P < 0.05$ as statistically significant.

3. Results and Discussion

Overall, all animals were clinically well (showing normal behavior of species and ingestion of food and water) during the experiments. There was no bleeding during surgery. Neither the rats under treatment nor the control group showed any statistically significant changes on the body weight throughout the experiments, showing that analgesia was adequate for the injury caused. As reported by Hellebrekers [1], the main signs of pain in laboratory animals subjected to experimental procedures are directly related to changes in behavior, with anorexia being one of the most significant signs.

3.1. Hemagglutinating Activity. Due to the immunostimulating and mitogenic activities attributed to lectins, the therapeutic use of these proteins in tissue repair processes has been subject of much research either related to the lectin concentration or the formulation used [14].

Lectins or hemagglutinins can be detected and characterized by their ability to agglutinate erythrocytes. In the evaluation of hydrogel containing 1,4 isolectin Cramoll was observed that Cramoll-1,4 at 50 μg/mL in both pure and

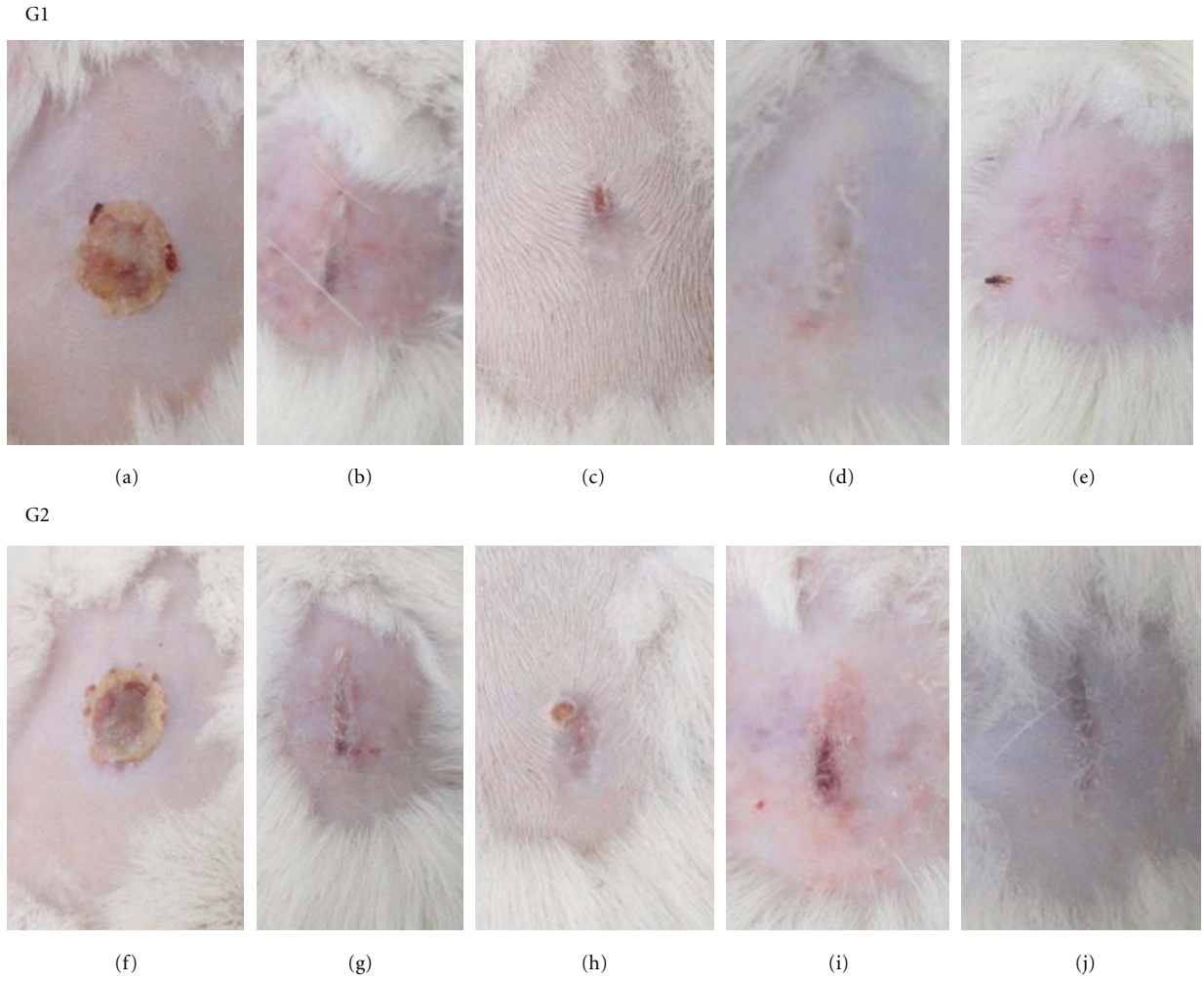

Figure 3: Clinical evaluation of second-degree burn healing in Wistar male rats. G1: experimental group treated with hydrogel containing isolectin Cramoll 1,4 at 100 μg/mL. (a) Thermal lesion aspect after 7 days: macroscopically shows thin and dry crust with detachment of edges. (b) Thermal lesion aspect after 14 days of treatment: absence of crust and the presence of scar tissue. (c) Thermal lesion aspect after 21 days of treatment: presence of scar tissue and a small detachment point of the crust. (d) Thermal lesion aspect after 28 days of treatment: presence of scar tissue only. (e) Thermal lesion aspect after 35 days of treatment: view of a discrete scar tissue. G2: control group treated by topical application of hydrogel excipient. (f) Thermal lesion aspect in control animals after 7 days: view of thin and dry crust with detachment of edges. (g) Thermal lesion aspect in control animals after 14 days: absence of crust and the presence of scar tissue. (h) Thermal lesion aspect in control animals after 21 days: presence of scar tissue, with the point of detachment of the crust. (i) Thermal lesion aspect in control animals after 28 days: presence of scar tissue and a second crust. (j) Thermal lesion aspect in control animals after 35 days: view of scar tissue.

gel formulation after irradiation lost their hemagglutinating activity. On the other hand, the concentration 100 μg/mL remained constant for the irradiated pure isolectin and that combined to the hydrogel excipient (Figure 2).

Several aspects make the hydrogel an ideal bandage for treatment of tissue lesions, such as hydrophilicity, biocompatibility, nontoxicity, biodegradability, easy replacement, transparency, adhesion, absorption, and prevention of body fluid losses [15, 16]. Burd [17] evaluated the use of hydrogel sheet dressings in comprehensive burn wound care, noting that use of hydrogel in burn wound care reduces patient's pain sensation. Osti [18] evaluated the use of a transparent adhesive film possessing selective permeability combined with a hydrogel (Burnshield) in burns treatment. For about 2 years, this type of therapy was used in the first aid treatment of 48 burn patients, 4 were lost during therapy and 4 were unavailable for followingup. In the reepithelialization phase complications were recorded in 8 of the 40 patients: 7 (18%) had residual inflammation and 1 (2%) had hypertrophic scar. During the followup, late complications were recorded in 2 (5%) of the 40 patients. A gel was used in 8 patients: in 6 of the 7 patients with residual inflammation, the complication was solved, while in 1, despite therapy, the residual inflammation evolved into hypertrophic scarring.

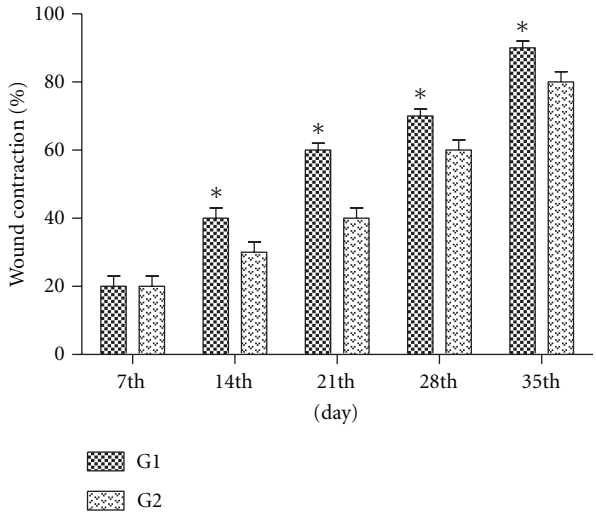

Figure 4: Effect of hydrogel topical application on the burn wound expressed as percentage of wound contraction. G1 = Treatment, G2 = Control. $n = 2$. Values are mean ± SEM. $^*P < 0.05$.

3.2. Clinical Parameters. Wound cooling caused by burn is an urgency measure, which proved to be beneficial in clinical and experimental practices. Hydrogels are cross-linking three-dimensional structures with high water percentage that can be transferred from the gel to the scar wound to facilitate hydration. The healing process of animals with aseptic experimental thermal burns treated topically with isolectin had better response than the control in the clinical examination in several ways such as (1) presence of edema in the first 24 h after induction of second-degree thermal burn, (2) thickening of the crust, which began to emerge spontaneously in 6 days of experiment, (3) discrete hyperemia observed in the range between 24 and 48 h after injury and (4) presence of scar tissue with 13 days of experiment (Figure 3). During the study period, lesions showed no signs of infection. Severely burned skin ceases to perform its natural protective and barrier role and allows a dramatic increase in water loss and can become a portal for bacterial invasion. The local treatment of second-degree burns is targeted at maintaining a wet microenvironment and stimulating the formation of a well-vascularised granulation tissue, and the reepithelization of the lesion while counteracting the development of microorganisms, which is able to delay or prevent the biological phenomena of cicatrization and reepithelization [19].

3.3. Wound Retraction Quantification. The wound contraction is a parameter used for assessing wound healing. The lesion area decreased gradually with the progress of healing time in both groups. The significant wound contraction was initiated from day 14 in the G1 that showed highest rate of lesion contraction compared with G2, indicating that isolectin has an inducing effect on the lesion contraction as illustrated in Figure 4. These results are consistent with studies *in vitro* and *in vivo* performed by Sezer et al. [20], which demonstrated the efficacy of hydrogels in the treatment of dermal burns in rabbit model revealing that the application of fucoidan-chitosan hydrogel promotes burn wound contraction and induces healing.

Wound contraction, wound shrinking process, depends on the tissue's reparative abilities, type, and damage extent and tissue health general state [21]. On the other hand, the wound contraction is rarely able to take to its permanent closure, which is mainly due to the presence of fibroblasts found in the granulation tissue that later differentiates into myofibroblasts [22].

3.4. Biochemical and Hematological Evaluation. Hematological values obtained in this study showed no significant changes as a function of burn induction during the period analyzed (erythrocytes: 7.6 ± 0.48, hemoglobin, 13.65 ± 0.5; platelets: 846400 ± 0.71, leukocytes: 7980 ± 0.71, basophils: 0.2 ± 0.05, eosinophils: 1.38 ± 0.18, lymphocytes: 82.37 ± 0.83, and Monocytes: 1.9 ± 0.2) (Table 1), revealing normal values in rats [23]. Rats, like other mammals, have to maintain strict control of the internal environment thus ensuring homeostasis. It is known that rats can produce changes in these parameters as a result of pathological processes or external factors such as sex, ancestry, age, diet, handling, and environment [24].

However, average values of biochemical parameters analyzed in this study were consistent with previously reported specific data to normal animals (calcium: 10.04 ± 0.42, pro-Thrombin: 9.94 ± 0.16, fibrinogen: 457.32 ± 0.25, alkaline phosphatase: 212.68 ± 0.52, glutamic oxalic transaminase: 180.02 ± 0.35, glutamic pyruvic transaminase: 53.28 ± 0.41, gamma-glutamyl transpeptidase: 5.76 ± 0.23, creatine: 0.54 ± 0.04, urea: 46.34 ± 0.04 and amylase: 842.06 ± 0.48) (Table 2). The biochemical evaluation revealed increased ALT levels in response to injury by burning and alkaline phosphatase-related to inflammatory period of the healing process. On the other hand, metabolic changes are considered high risk in third-degree burns with hyperglycemia [25] and high protein catabolism [26] as the main aggravating factors to the injury.

After burn trauma, inflammatory mediators, oxygen-free radicals, and arachidonic acid metabolites and complement [27], released in the wounds, promote a great edema. According to Beukelman et al. [28], liposomal hydrogel with 3% povidone-iodine (PVP-ILH, Repithel) has shown clinical benefit in settings where inflammation and/or reactive oxygen species are thought to impede wound healing (e.g., burns and chronic wounds in smokers). According to Møller-Kristensen et al. [29], the MBL, mannan-binding lectin, modulates not only inflammatory factors such as cytokines and chemokines, but also cell adhesion molecules, the binding growth factor protein, and, MPPs in particular, metalloproteinase matrix, which are most likely the direct effectors in scabs detachment.

Considering the influence of carbohydrates in numerous cell signaling phenomena whether physiological or pathological, the use of lectins in the treatment of cutaneous lesions among other diseases stimulates the activation and modulation events such as communication, cellular differentiation, and proliferation [30–32].

Table 1: Effect of topical administration of hydrogel containing 100 μg per mL isolectin Cramoll 1,4 on the hematological parameters of Wistar rats. Assays performed in triplicate for each parameter. G1 = Treatment, G2 = control. Mean ± SD ($n = 2$).

Parameters	7th day		14th day		21st day		28th day		35th day	
	G1	G2	G1	G2	G1	G2	G1	G2	G1	G2
Erythrogram										
Erythrocytes mil/mm^3	6.7 ± 0.01	7.2 ± 0.14	7.1 ± 0.16	7.57 ± 0.69	7.6 ± 0.69	7.5 ± 0.42	6.32 ± 0.56	8.1 ± 0.21	6.3 ± 0.71	7.7 ± 0.92
Hemoglobin g/dL	13.9 ± 0.01	13 ± 0.14	14.8 ± 0.52	15.59 ± 0.41	15.6 ± 0.41	12.4 ± 0.64	13.7 ± 0.38	12.8 ± 0.49	14.1 ± 0.32	14.5 ± 0.42
Hematocrit %	38.7 ± 0.22	41.1 ± 0.49	40.6 ± 0.56	43.22 ± 0.96	43.2 ± 0.96	41 ± 0.85	38.5 ± 0.55	39.8 ± 0.92	41.9 ± 0.84	40.8 ± 0.49
Platelet count										
Platelets mil/mm^3	844000 ± 0.71	805000 ± 0.71	656000 ± 0.71	926000 ± 071	788000 ± 0.71	820000 ± 0.71	844000 ± 0.71	789000 ± 0.71	749000 ± 0.71	892000 ± 0.71
WBC										
Leukocytes %	7200 ± 0.71	8000 ± 0.71	8100 ± 0.71	7900 ± 0.71	12000 ± 0.71	8100 ± 0.71	9300 ± 0.71	7900 ± 0.71	8000 ± 0.71	8000 ± 0.71
Neutrophils %	15.1 ± 0.07	26.8 ± 0.78	26.4 ± 0.28	31.3 ± 0.56	8.7 ± 0.63	28.8 ± 0.42	14.7 ± 0.71	27.5 ± 0.71	16.1 ± 0.2	33.1 ± 0.99
Eosinophils %	0 ± 0	0.1 ± 0.14	0.1 ± 0.07	1.6 ± 0.28	0.1 ± 0.07	2.4 ± 0.28	0.1 ± 0.14	1.3 ± 0.14	0.1 ± 0	1.5 ± 0.07
Basophils %	0.2 ± 0	0.2 ± 0.14	0.2 ± 0.07	0.2 ± 0	0.2 ± 0	0.2 ± 0.14	0.2 ± 0	0.2 ± 00	0.2 ± 0	0.1 ± 0
typical lymphocytes %	81.4 ± 0.64	81.5 ± 0.49	68.5 ± 0.70	86.85 ± 0.78	87.1 ± 0.84	82.7 ± 0.49	81.5 ± 0.56	79.9 ± 0.71	83.7 ± 0.46	80.9 ± 0.78
atypical lymphocytes %	0 ± 0	0 ± 00	0 ± 00	0 ± 00	0 ± 0	0 ± 0	0 ± 0	0 ± 00	0 ± 0	0 ± 0
Monocytes %	1.4 ± 0.07	2 ± 0.71	1.2 ± 0.07	2 ± 00	1.2 ± 0.07	1.5 ± 0.71	1.4 ± 0.07	1.5 ± 0.71	1.2 ± 0.07	2.5 ± 0.71

Table 2: Effect of topical administration of hydrogel containing 100 μg per mL isolectin Cramoll 1,4 on the biochemical parameters of Wistar rats. Doses performed in triplicate for each parameter. G1 = Treatment, G2 = Control. Mean ± SD (n = 2).

Parameters	7th day		14th day		21st day		28th day		35th day	
	G1	G2	G1	G2	G1	G2	G1	G2	G1	G2
Prothrombin time %	10.1 ± 0.07	9.7 ± 0.02	9.62 ± 0.11	10.1 ± 0.21	9.2 ± 0.21	10.1 ± 0.28	10.5 ± 0.71	10.1 ± 0.436	10.5 ± 0.70	9.7 ± 0.56
Fibrinogen mg/dL	460.5 ± 0.71	457.9 ± 0.07	407.1 ± 0.14	460.8 ± 0.21	412 ± 0.71	465.6 ± 0.47	380 ± 0.92	440.1 ± 0.142	407.7 ± 0.41	462.2 ± 0.34
Calcium mg/dL	10.3 ± 0.14	9.6 ± 0.46	8.4 ± 0.98	9.6 ± 0.42	11.6 ± 0.14	9.4 ± 0.16	11.5 ± 0.71	11.5 ± 0.658	9.7 ± 0.59	10.1 ± 0.42
Alkaline phosphatase U/L	193.6 ± 0.56	199.6 ± 0.49	212.7 ± 0.42	201.4 ± 0.57	208 ± 0.71	198.2 ± 0.31	275 ± 0.71	244.6 ± 0.601	209.7 ± 0.38	219.6 ± 0.62
Gamma glutamyl transferase U/L	5 ± 00	5.9 ± 0.14	5.7 ± 0.35	5.7 ± 0.29	5.8 ± 0.14	5.9 ± 0.02	5.3 ± 0.07	5.2 ± 0.012	5.6 ± 0.14	6.1 ± 0.72
Oxalic transaminase glutamic U/L	142 ± 0.07	176.6 ± 0.54	136.5 ± 0.71	208.2 ± 0.33	193 ± 0.71	179.9 ± 0.04	141.5 ± 0.64	156.6 ± 0.506	177.9 ± 0.15	178.8 ± 0.31
Transaminase glutamico piruvica U/L	60.7 ± 0.42	50.8 ± 0.19	55.7 ± 0.04	54.5 ± 0.58	47 ± 0.42	48.7 ± 0.33	48.5 ± 0.63	51.9 ± 0.129	58.5 ± 0.71	60.5 ± 0.78
Urea mg/dL	46.3 ± 0.49	46.9 ± 0.05	43.7 ± 0.35	50.6 ± 0.91	40 ± 0.71	45.9 ± 0.06	41.5 ± 0.71	46.8 ± 0.331	37.9 ± 0.11	41.5 ± 0.68
Creatinine mg/dL	0.2 ± 0.07	0.6 ± 0.04	0.5 ± 0.07	0.6 ± 0.12	0.4 ± 0.07	0.6 ± 0.01	0.6 ± 0.04	0.50 ± 0.011	0.5 ± 0.14	0.4 ± 0.04
Amylase U/L	838 ± 0.14	846.6 ± 0.56	789 ± 0.71	866.7 ± 0.42	808.3 ± 0.87	887.5 ± 0.71	856.6 ± 0.84	799.7 ± 0.469	814.5 ± 0.71	809.8 ± 0.27

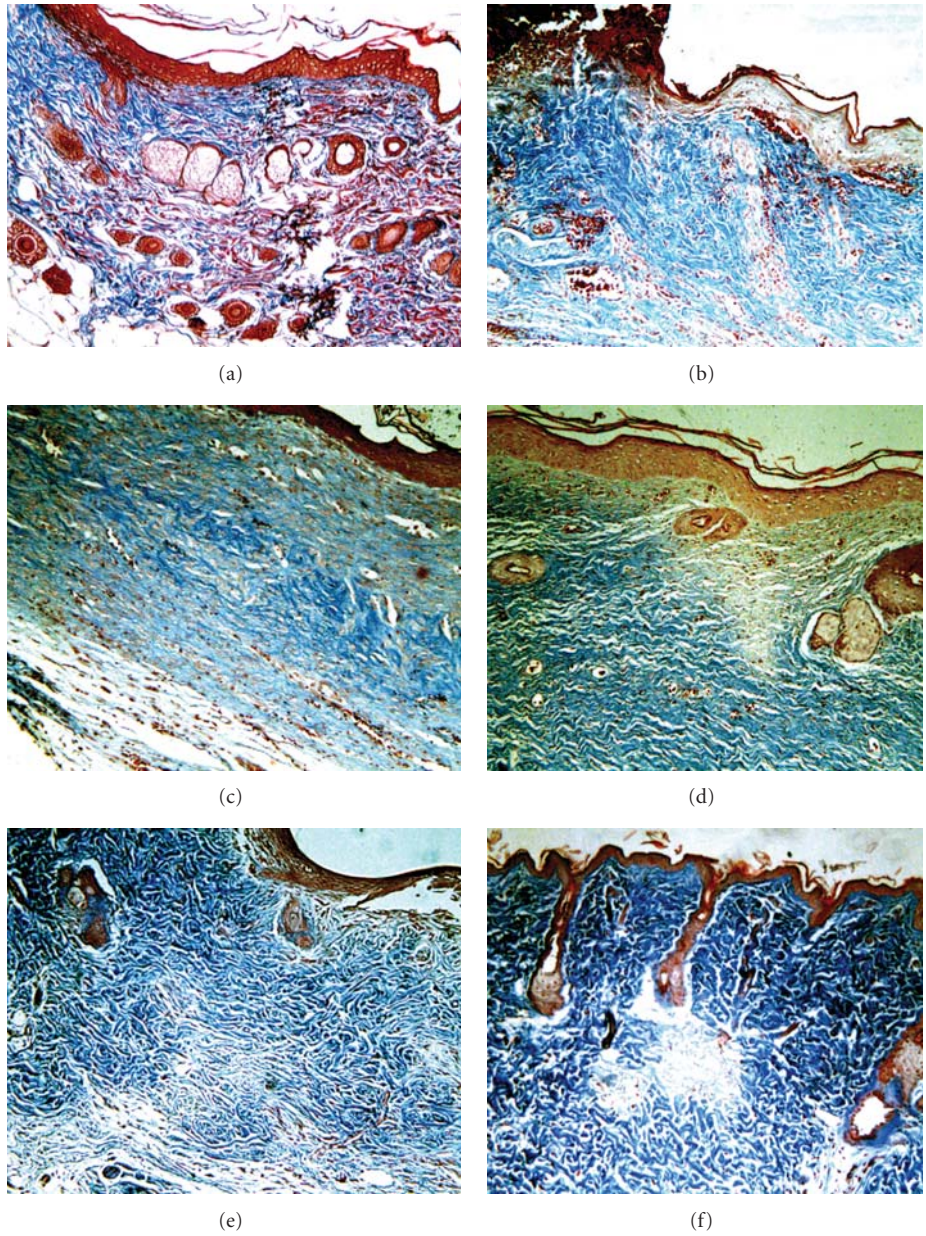

Figure 5: Epithelial tissue of rats in group 1 subjected to second-degree thermal burns. Masson's trichrome staining. 100x Magnification. (a) Normal epithelial tissue with all skin appendages. (b) Animal presenting epithelial tissue with complete destruction of the dermis and epidermis showing exudates albumin/leukocyte/macrophage intense, necrosis, edema, and crust at the 7th day after injury induction. (c) Animal at the 14th day with tissue reepithelialization, moderate autolysis, moderate exudate albumin/leukocyte/macrophage, intense neovascularization, and discrete fibroblast proliferation with the presence of loose collagen and mild fibrosis. (d) Animal at the 21st day with incomplete tissue reepithelialization, mild exudate albumin/leukocyte/macrophage, moderate neovascularization, intense fibroblastic proliferation, and presence of dense collagen, not modeled and moderate fibrosis. (e) Animal at the 28th day with complete tissue epithelialization, exudate albumin/leukocyte/macrophage discrete in the epidermis, moderate fibroblastic proliferation, presence of modeled dense collagen mesh and moderate fibrosis. (f) Animal at the 35th day with complete reepithelialization, mild fibroblastic proliferation, and presence of modeled dense collagen mesh and moderate fibrosis.

3.5. Histopathology. Deep partial thickness burns are injuries that cause partial or total destruction of nerve endings, hair follicles, and sweat glands. On the seventh day was observed intense fibroblastic proliferation, neovascularization, necrosis, and edema. In upper layer of dermis, most hair follicle walls, sebaceous follicles, and sudoriparous glands disappeared and only their residual bodies could be found. Capillary vessels were fractured. The epidermis showed necrosis with infiltration of large numbers of neutrophils and few monocytes, leukocytes, and plasma of the dermis

(Figure 5(b)). These data are similar to observations reported by Nunes et al. [33] that when evaluating the application of a collagen film containing acid usnic as bandage to treat second-degree thermal burns, an intense inflammatory response after 7 days with presence of neutrophils distributed throughout the length of the burn was found.

With 14 days of experiment, G1 and G2 showed granulation tissue with presence of discrete neovascularization and neoformation of skin appendages. Angiogenesis is essential to restore the supply of nutrients and oxygen during tissue healing [34]. In group 1, an increased number of fibroblasts was observed, and presence of collagen was organized in the lesion center (Figure 5(c)). Experiments performed by Sezer et al. [35] demonstrated that fibroblast and collagen amounts in fucosphere-treated groups increased at day 14 compared to that at day seven, but decreased at day 21. The reepithelialization time was lower for animals treated with isolectin hydrogel and started around the burn edge on the 14th day. Epithelialization is necessary in the repair of all type of wounds if water tight seal occurs. Protection from fluid and particulate-matter contamination and maintenance of internal milieu are dependent on keratin's physical characteristic [36]. The experimentally induced thermal injuries have been completely reepithelialized in both groups with 35 days.

Histopathology revealed the intense fibroblast proliferation at 21st day, presence of dense collagen, and not modeled and moderate fibrosis (Figure 5(d)). Collagen deposition in the fibroplasia phase is required for the efficient arrival of fibroblasts to the burn site. Mature fibroblasts produce a delicate matrix that gives mechanical support to the new capillaries [37]. The collagen deposited at the injury site will not have the same unique organization of an intact tissue, being required a period of two months to complete restructure [38]. The decrease in epithelium thickness on the day 21 was considered by Sezer et al. [39] as the result of higher healing rate, particularly on the superficial burn wound treated with chitosan film containing fucoidan.

After 28 days, both G1 and G2 showed gradual decrease in the number of fibroblasts with greater organization of the collagen matrix with reduced inflammatory infiltration (Figure 5(e)). Finally, 35 days after burn procedures, the injured tissue of group 1 is at the stage of maturation and remodeling, with the presence of few fibroblasts and inflammatory cells (Figure 5(f)). The histological analysis of liver sections in group G1 showed no cytotoxic effects resulting from topical application of isolectin hydrogel at the end of treatment after 35 days. These results are consistent with previous studies performed by our group that found the healing action of isoforms 1 and 4 of *Cratylia mollis* lectin in the repair of skin wounds in normal and immunosuppressed mice [40].

Several studies have confirmed the use of lectins in the immune system activation, enlisting neutrophils through indirect mechanisms [41], promoting proinflammatory effects in polymorphonuclear cells and inducing the cytokines release [42], as well as triggering fibroblasts proliferation [43]. Previous assays accomplished by our group have shown a potential proinflammatory and immunomodulatory activity induced by Cramoll 1,4 lectin. The importance of glycoproteins (including lectins) as components of *Aloe vera* extract gel has been asserted for promoting wound, burn, and frost-bite healing, and showing anti-inflammatory and antifungal properties [44]. Sell and Costa [45] also described improved effect of PHA lectin in the skin tissue repair process of Wistar rats compared to *Triticum vulgaris* (WGA) and *Artocarpus integrifolia* (jacalin) lectin.

4. Conclusion

The present study has demonstrated that the regular topical application of Cramoll 1,4 hydrogel containing in the treatment of second-degree burns accelerates the granulation, reepithelialization process, and wound retraction. These results extend the potential of therapeutic applications of isolectin Cramoll 1,4, which can be used in combination with other byproducts in the treatment of thermal burns.

Acknowledgments

The authors express their gratitude to Fundação de Amparo a Pesquisa do Estado de Pernambuco (FACEPE) for research grants, to Coordenação de Aperfeiçoamento de Pessoal de Nível Superior (CAPES) for financial support, and Adriana Cruz for technical assistance.

References

[1] L. J. Hellebrekers, "Fisiopatologia da dor em animais e sua conseqüência para a terapia analgésica," in *Dor Em Animais*, pp. 69–79, Manole, São Paulo, Brazil, 2002.

[2] G. A. Tavares, I. Caracelli, R. Burger, M. T. S. Correia, L. C. B. B. Coelho, and G. Oliva, "Crystallization and preliminary X-ray studies on the lectin from the seeds of *Cratylia mollis*," *Acta Crystallographica Section D*, vol. 52, no. 5, pp. 1046–1047, 1996.

[3] V. L. M. Lima, M. T. S. Correia, Y. M. N. Cechinel, C. A. M. Sampaio, J. S. Owen, and L. C. B. B. Coêlho, "Immobilized *Cratylia mollis* lectin as a potential matrix to isolate plasma glycoproteins, including lecithin-cholesterol acyltransferase," *Carbohydrate Polymers*, vol. 33, no. 1, pp. 27–32, 1997.

[4] E. I. C. Beltrão, M. T. S. Correia, J. Figueredo-Silva, and L. C. B. B. Coelho, "Binding evaluation of isoform 1 from *Cratylia mollis* lectin to human mammary tissues," *Applied Biochemistry and Biotechnology: Part A*, vol. 74, no. 3, pp. 125–134, 1998.

[5] E. V. M. Maciel, V. S. Araújo-Filho, M. Nakazawa, Y. M. Gomes, L. C. B. B. Coelho, and M. T. S. Correia, "Mitogenic activity of *Cratylia mollis* lectin on human lymphocytes," *Biologicals*, vol. 32, no. 1, pp. 57–60, 2004.

[6] C. M. L. de Melo, M. C. A. B. de Castro, A. P. de Oliveira et al., "Immunomodulatory response of Cramoll 1,4 lectin on experimental lymphocytes," *Phytotherapy Research*, vol. 24, no. 11, pp. 1631–1636, 2010.

[7] C. A. S. Andrade, M. T. S. Correia, L. C. B. B. Coelho, S. C. Nascimento, and N. S. Santos-Magalhães, "Antitumor activity of *Cratylia mollis* lectin encapsulated into liposomes," *International Journal of Pharmaceutics*, vol. 278, no. 2, pp. 435–445, 2004.

[8] L. S. Edelman, "Social and economic factors associated with the risk of burn injury," *Burns*, vol. 33, no. 8, pp. 958–965, 2007.

[9] G. L. Kramer, T. Lund, and D. Herndon, "Pathophysiology of burn shock and burn edema," in *Total Burn Care*, D. Herndon, Ed., pp. 78–87, Saunders, Philadelphia, Pa, USA, 2002.

[10] M. C. Guimarães, "História do curativo," in *Feridas e Curativos: Uma Forma Simples e Prática de Tratar*, Rubio, Ed., pp. 1–3, Rio de Janeiro, Brazil, 2011.

[11] M. T. S. Correia and L. C. B. B. Coelho, "Purification of a glucose/mannose specific lectin, isoform 1, from seeds of *Cratylia mollis* mart. (Camaratu Bean)," *Applied Biochemistry and Biotechnology*, vol. 55, no. 3, pp. 261–273, 1995.

[12] B. F. C. Patricio, M. H. M. Lima-Ribeiro, M. T. S. Correia et al., "Radiolabeling of Cramoll 1,4: evaluation of the biodistribution," *International Journal of Peptides*, vol. 2011, Article ID 945397, 3 pages, 2011.

[13] M. S. Kumar, R. Sripriya, H. V. Raghavan, and P. K. Sehgal, "Wound healing potential of *Cassia fistula* on infected albino rat model," *Journal of Surgical Research*, vol. 131, no. 2, pp. 283–289, 2006.

[14] N. Roy, N. Saha, P. Humpolicek, and P. Saha, "Permeability and biocompatibility of novel medicated hydrogel wound dressings," *Soft Materials*, vol. 8, no. 4, pp. 338–357, 2010.

[15] N. Roy, N. Saha, T. Kitano, and P. Saha, "Novel hydrogels of PVP-CMC and their swelling effect on viscoelastic properties," *Journal of Applied Polymer Science*, vol. 117, no. 3, pp. 1703–1710, 2010.

[16] A. Burd, "Evaluating the use of hydrogel sheet dressings in comprehensive burn wound care," *Ostomy Wound Management*, vol. 53, no. 3, pp. 52–62, 2007.

[17] E. Osti, "Cutaneous burns treated with hydrogel (Burnshield) and a semipermeable adhesive film," *Archives of Surgery*, vol. 141, no. 1, pp. 39–42, 2006.

[18] J. G. Hancok and J. L. Jorizzo, "Burns," in *Manual of Dermatologic Therapeutics*, K. A. Arndt and J. T. S. Hsu, Eds., Lippincott Williams & Wilkins, Philadelphia, Pa, USA, 7th edition, 2007.

[19] A. D. Sezer, E. Cevher, F. Hatipoğlu, Z. Oğurtan, A. L. Baş, and J. Akbuğa, "Preparation of fucoidan-chitosan hydrogel and its application as burn healing accelerator on rabbits," *Biological and Pharmaceutical Bulletin*, vol. 31, no. 12, pp. 2326–2333, 2008.

[20] N. S. Anuar, S. S. Zahari, I. A. Taib, and M. T. Rahman, "Effect of green and ripe *Carica papaya* epicarp extracts on wound healing and during pregnancy," *Food and Chemical Toxicology*, vol. 46, no. 7, pp. 2384–2389, 2008.

[21] R. O'Leary, E. J. Wood, and P. J. Guillou, "Pathological scarring: strategic interventions," *European Journal of Surgery*, vol. 168, no. 10, pp. 523–534, 2002.

[22] T. Yasuoka, M. Sasaki, T. Fukunaga et al., "The effects of lectins on indomethacin-induced small intestinal ulceration," *International Journal of Experimental Pathology*, vol. 84, no. 5, pp. 231–237, 2003.

[23] J. B. Messias, M. C. M. Caraciolo, I. M. Oliveira, U. R. Montarroyos, M. O. Guerra, and I. A. Souza, "Parâmetros hematológicos de *Rattus norvegicus* obtidos através de métodos automatizado e não automatizado," *Medicina Veterinaria*, vol. 3, no. 2, pp. 1–8, 2009.

[24] G. D. Carvalho, A. P. B. Masseno, M. S. Zanini et al., "Avaliação clínica de ratos de laboratório (*Rattus novergicus* linhagem Wistar): parâmetros sanitários, biológicos e fisiológicos," *Ceres*, vol. 56, no. 1, pp. 51–57, 2009.

[25] D. C. Gore, D. L. Chinkes, D. W. Hart, S. E. Wolf, D. N. Herndon, and A. P. Sanford, "Hyperglycemia exacerbates muscle protein catabolism in burn-injured patients," *Critical Care Medicine*, vol. 30, no. 11, pp. 2438–2442, 2002.

[26] A. A. Ferrando, M. Sheffield-Moore, S. E. Wolf, D. N. Herndon, and R. R. Wolfe, "Testosterone administration in severe burns ameliorates muscle catabolism," *Critical Care Medicine*, vol. 29, no. 10, pp. 1936–1942, 2001.

[27] Y. K. Youn, C. LaLonde, and R. Demling, "The role of mediators in the response to thermal injury," *World Journal of Surgery*, vol. 16, no. 1, pp. 30–36, 1992.

[28] C. J. Beukelman, A. J. J. van den Berg, M. J. Hoekstra, R. Uhl, K. Reimer, and S. Mueller, "Anti-inflammatory properties of a liposomal hydrogel with povidone-iodine (Repithel®) for wound healing *in vitro*," *Burns*, vol. 34, no. 6, pp. 845–855, 2008.

[29] M. Møller-Kristensen, M. R. Hamblin, S. Thiel, J. C. Jensenius, and K. Takahashi, "Burn injury reveals altered phenotype in mannan-binding lectin-deficient mice," *Journal of Investigative Dermatology*, vol. 127, no. 6, pp. 1524–1531, 2007.

[30] R. A. Moreira, I. L. Ainouz, J. T. de Oliveira, and B. S. Cavada, "Plant lectins, chemical and biological aspects," *Memorias do Instituto Oswaldo Cruz*, vol. 86, pp. 211–218, 1991.

[31] B. S. Cavada, C. F. Santos, T. B. Grangeiro et al., "Purification and characterization of a lectin from seeds of *Vatairea macrocarpa* duke," *Phytochemistry*, vol. 49, no. 3, pp. 675–680, 1998.

[32] H. J. Gabius and S. Gabius, *Glycosciences: Status and Perspectives*, Wiley-VCH, New York, NY, USA, 2nd edition, 2002.

[33] P. S. Nunes, R. L. C. Albuquerque-Jnior, D. R. R. Cavalcante et al., "Collagen-based films containing liposome-loaded usnic acid as dressing for dermal burn healing," *Journal of Biomedicine and Biotechnology*, vol. 2011, Article ID 761593, 9 pages, 2011.

[34] S. M. Bauer, R. J. Bauer, and O. C. Velazquez, "Angiogenesis, vasculogenesis, and induction of healing in chronic wounds," *Vascular and Endovascular Surgery*, vol. 39, no. 4, pp. 293–306, 2005.

[35] A. D. Sezer, E. Cevher, F. Hatipoğlu, Z. Oğurtan, A. L. Baş, and J. Akbuğa, "The use of fucosphere in the treatment of dermal burns in rabbits," *European Journal of Pharmaceutics and Biopharmaceutics*, vol. 69, no. 1, pp. 189–198, 2008.

[36] E. E. Peacock Jr., "Wound healing and wound care," in *Principles of Surgery*, S. I. Schwartz, Ed., p. 292, McGraw-Hill, Singapore, 4th edition, 1985.

[37] P. L. Williams, L. H. Bannister, M. N. Berry et al., *Gray's Anatomy*, Churchill Livingstone, Philadelphia, Pa, USA, 1995.

[38] J. Li, J. Chen, and R. Kirsner, "Pathophysiology of acute wound healing," *Clinics in Dermatology*, vol. 25, no. 1, pp. 9–18, 2007.

[39] A. D. Sezer, F. Hatipoğlu, E. Cevher, Z. Oğurtan, A. L. Baş, and J. Akbuğa, "Chitosan film containing fucoidan as a wound dressing for dermal burn healing: preparation and in vitro/in vivo evaluation," *AAPS PharmSciTech*, vol. 8, no. 2, article 39, pp. E94–E101, 2007.

[40] C. M. L. D. Melo, C. S. Porto, and M. R. Melo Jr., "Healing activity induced by Cramoll 1,4 lectin in healthy and

immunocompromised mice," *International Journal of Pharmaceutics*, vol. 408, no. 1-2, pp. 113–119, 2011.

[41] A. M. S. Assreuy, N. M. N. Alencar, B. S. Cavada et al., "Porcine spermadhesin PSP-I/PSP-II stimulates macrophages to release a neutrophil chemotactic substance: modulation by mast cells," *Biology of Reproduction*, vol. 68, no. 5, pp. 1836–1841, 2003.

[42] V. B. M. Alencar, N. M. N. Alencar, A. M. S. Assreuy et al., "Pro-inflammatory effect of *Arum maculatum* lectin and role of resident cells," *International Journal of Biochemistry and Cell Biology*, vol. 37, no. 9, pp. 1805–1814, 2005.

[43] A. M. Sell and C. P. da Costa, "Effects of plant lectins on in vitro fibroblast proliferation," *Brazilian Archives of Biology and Technology*, vol. 46, no. 3, pp. 349–354, 2003.

[44] S. Choi and M. H. Chung, "A review on the relationship between *Aloe vera* components and their biologic effects," *Seminars in Integrative Medicine*, vol. 1, no. 1, pp. 53–62, 2003.

[45] A. M. Sell and C. P. Costa, "Efeito inflamatório local induzido pelas lectinas PHA, WGA e Jacalina," *Arquivos de Ciências da Saúde*, vol. 6, no. 1, pp. 47–51, 2002.

Hindawi Publishing Corporation
Journal of Biomedicine and Biotechnology
Volume 2012, Article ID 519238, 14 pages
doi:10.1155/2012/519238

Review Article

Ultrasound Biomicroscopy in Small Animal Research: Applications in Molecular and Preclinical Imaging

A. Greco,[1,2,3] M. Mancini,[3,4] S. Gargiulo,[1,2] M. Gramanzini,[2,3] P. P. Claudio,[5,6] A. Brunetti,[1,2,3] and M. Salvatore[1,4]

[1] *Department of Biomorphological and Functional Sciences, University of Naples "Federico II", 80131 Naples, Italy*
[2] *CEINGE-Biotecnologie Avanzate, s.c.ar.l., 80145 Naples, Italy*
[3] *Institute of Biostructure and Bioimaging, Italian National Research Council (CNR), 80131 Naples, Italy*
[4] *SDN Foundation Instituto di Ricovero e Cura a Carattere Scientifico (M.M.), 80131 Naples, Italy*
[5] *Department of Biochemistry and Microbiology, Joan C. Edwards School of Medicine, Marshall University, Huntington, WV 25755, USA*
[6] *Department of Surgery, Joan C. Edwards School of Medicine, Marshall University, Huntington, WV 25755, USA*

Correspondence should be addressed to A. Greco, adegreco@unina.it

Received 1 August 2011; Accepted 12 August 2011

Academic Editor: Monica Fedele

Ultrasound biomicroscopy (UBM) is a noninvasive multimodality technique that allows high-resolution imaging in mice. It is affordable, widely available, and portable. When it is coupled to Doppler ultrasound with color and power Doppler, it can be used to quantify blood flow and to image microcirculation as well as the response of tumor blood supply to cancer therapy. Target contrast ultrasound combines ultrasound with novel molecular targeted contrast agent to assess biological processes at molecular level. UBM is useful to investigate the growth and differentiation of tumors as well as to detect early molecular expression of cancer-related biomarkers *in vivo* and to monitor the effects of cancer therapies. It can be also used to visualize the embryological development of mice in uterus or to examine their cardiovascular development. The availability of real-time imaging of mice anatomy allows performing aspiration procedures under ultrasound guidance as well as the microinjection of cells, viruses, or other agents into precise locations. This paper will describe some basic principles of high-resolution imaging equipment, and the most important applications in molecular and preclinical imaging in small animal research.

1. Introduction

Mice are widely used as models for studying many human diseases. The main advantage of research conducted in small animals is owed to their short life cycle and the possibility of genetic manipulation. However, most of the observations in small animals have been based in the past on surgery and histological postmortem analysis. Few years ago, research applications of noninvasive imaging methods such as optical imaging, computed tomography, magnetic resonance, micro-PET-SPECT, and ultrasound were limited to larger animals such as dogs and nonhuman primates. In the recent years, a new ultrasound technology, called ultrasound biomicroscopy (UBM) was optimized to evaluate animal models of human disease. UBM is a noninvasive real-time technique that allows accurate and reliable images of the heart and other organs in mice [1–3]. Additionally, this technique is useful to image the fetal mouse [4–6] and to obtain high-resolution images of mice tumors [7, 8]. The consistent ultrasound image obtained with the UBM can be used to visualize and guide injection into target organs [9, 10], including mouse embryo, to aid in targeted delivery of drugs and viral particles [7, 11]. UBM allows longitudinal data acquisition at low cost and noninvasively to investigate the growth and differentiation of tumors as well as to monitor the effects of cancer therapies; therefore, it reduces the number of animals needed to perform experiments [12].

The basic modalities include B-mode, M-mode, Doppler mode, 3D reconstruction, power mode, and an ECG-based Kilo-Herz visualization technology. Doppler ultrasound with color and power Doppler can be used to quantify blood flow

and to image microcirculation and the response of a tumor blood supply to cancer therapy [13]. Recently, the introduction of ultrasound contrast agents (lipid shell gas-filled 1–4 micron sized microbubbles) enhances UBM applications for detection and characterization of focal lesions. Recently, the introduction of ultrasound contrast microbubbles that is targeted to molecular markers expressed on the vasculature is able to image molecular events of disease and could be used for various applications including quantitative analysis of molecular biomarkers, perfusion studies, microvasculature targeting, and gene and drug delivery [7, 11].

Current applications of UBM are the following:

(i) studies on mouse development from early embryonic period to adulthood,

(ii) *in vivo* morphological and functional phenotyping of wild-type, transgenic and mutant mice and other mouse disease models,

(iii) tumor growth monitoring,

(iv) evaluation of effects of therapeutic interventions,

(v) imaging-guided intervention on mice,

(vi) microinjection for introducing genes or cells into the developing mouse embryos and follow-up of the effects,

(vii) ultrasound-guided catheterization (veins or bladder).

This paper describe basic principles of high-resolution imaging equipment and some applications in molecular and preclinical imaging in small animal research.

2. UBM Methodology

Human ultrasound scanners are limited to 2–20 MHz frequencies, since deep penetration and a axial spatial resolutions of 0.2–1 mm is required. UBM uses frequencies of 40–100 MHz. Higher frequencies are used to image cellular structures: the scanning acoustic microscopy (SAM) uses frequencies of 100 MHz-1 GHz for the evaluation of thickly sliced biological tissue or cells [14] and explore the acoustic properties of single cells with submicrometric resolution.

The choice of ultrasound frequency and the type of transducer represents a balance between image resolution and penetration depth.

The high-frequency ultrasound (20–100 MHz range) is used in mice imaging with mechanical sector scanhead with fixed focus or with electric probes with multiple focus. These transducers allow high-resolution imaging and require a mechanical support to perform the necessary micromovements for mice examinations (Figure 1).

At these frequencies, sound waves are transmitted through soft tissue relatively to the acoustic impedance of each tissues. The acoustic impedance of a particular tissue is the product of sound transmission velocity and tissue density. The transmission velocity in most soft tissue is nearly uniform at 1540 m/s; therefore, the acoustic impedance of most soft tissue is primarily a function of tissue density. In the frequency ranging from 20 to 100 MHz, only few studies of attenuation, backscatter, and speed of sound have been performed. The frequency dependence of attenuation is strongly dependence on the tissue type. The mechanism of the differences between various transducers is not well understood, but it is known that the concentration of collagen and other structural protein are of primary importance. In the case of a homogeneous soft tissue, an attenuation coefficient of 6.5 dB/mm can be expected at 60 MHz probe frequency [15]; therefore, a penetration of 6 mm would be expected for a system dynamic range of 80 dB.

Backscatter from blood at lower frequencies used in human diagnostic applications is predominantly dependent on shear rate due to the formation of red cells aggregates called "Roleaux." At frequencies greater than 40 MHz, the backscatter appears less dependent on shear rate, because the red blood cells begin to act as mirroring reflectors. At higher frequencies, the lumen of the vessel becomes isoechoic with the surrounding tissue, impeding accurate boundary discrimination. This natural enhancement of the blood signal is a benefit for Doppler analysis but at the expense of B-mode imaging quality.

Resolution is the ability to accurately distinguish two closely situated structures and becomes a crucial factor when imaging small targets like mouse organs (the diameter of an internal carotid artery is 0.2 mm, and the left ventricular posterior wall is approximately 1 mm thick [16]. Axial and lateral resolution improves with increasing frequencies. The axial resolution is dependent of the pulse spatial length and, therefore, for fixed cycles number is due to the wavelength.

The lateral resolution is the product of the transducer diameter, focal length, f-number, and wavelength. Therefore, the lateral resolution depends from transducers geometry and wavelength. The f-number equals the depth of returning echo (focal length) divided by the aperture of the beam (transducer diameter). It will be best (smallest) if there is a large aperture of the transducers and short wavelength (higher frequency).

Utilizing frequency of 40–60 MHz and a narrow beam width, a spatial resolution of 30–50 microns can be obtained. At these frequencies, the penetration is reduced to 1-2 cm. Hence, increasing axial and lateral resolution by increasing the frequency limits the depth penetration; however, this does not affect mice imaging, because most of the target organs are in the penetration depth range of the high frequency used.

Temporal resolution is the ability to distinguish two events in time and is an important factor when imaging mice hearts that have a heart rate of 400–600 beats/min. At heart rate of 400 beats/min, a frame rate of 30 Hz would result in only about 4 images for each cardiac cycle. Each image frame acquires 25% of the cardiac cycle, making the determination of the systolic and diastolic phase inaccurate. High-frequency ultrasound has low imaging frame rates (5–10 Hz) with relatively poor temporal resolution for moving structures. It is not important when imaging static or slow moving organs such as liver or xenografts, but it is indispensable for the evaluation of the heart. The Kilo-Herz visualization technology use B-mode frame synchronized with ECG trace that produce a postprocessing imaging equal to a real-time 1,000 Hz frame rate.

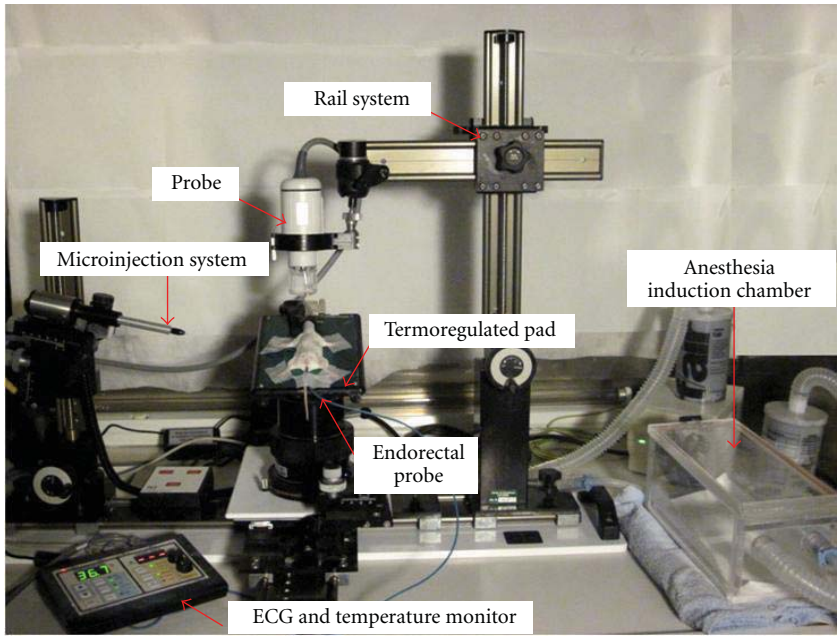

Figure 1: Ultrasound biomicroscopy integrated mechanical support with rail system. The microinjection system for visualization and guidance of injection and extraction procedures in real time. Ultrasound probe is mounted on a system securing the probe in a stationary position when the ultrasound scan is in the desired image plane. After anesthesia, the mouse is positioned on a termoregulated pad to monitor ECG and temperature (with endorectal probe) and ensure mouse comfort during imaging.

The UBM Doppler system using a typical duplex Doppler configuration operates at 20–55 MHz with a pulse repetition frequency of 1–20 KHz. The transducer is held stationary to obtain Doppler flow velocity spectra in real time for a sample volume located on the B-mode image. The default setting of Doppler system are pulse repetition frequency (PRF) from 1.0 to 120.0 kHz (transmit setting), the wall filter from 0 to 1000 Hz, and the Doppler gain from 1.0 to 10 dB (receive settings).

The Doppler sample volume size changes with the number of cycle per pulse and insonation frequency from 2.18 to 4.36 μL for 20 MHz to 0.46 to 0.93 μL for 40 MHz and 8–16 numbers of cycles per pulse. The high-frequency Doppler system is able to measure velocity from 37 cm/sec (max analyzed velocity at 0°) to a minimum velocity of 1 mm/sec. The system is able to detect low blood velocities in small vessels, and it can calculate blood flow with dedicated software.

3D UBM imaging allows viewing of the tissue of interest as a whole organ in different orientations. This application in experimental medicine can be useful in the detection of xenograft tumors in mice and in longitudinal growth. A set of consecutive 2D image planes of the tumor are acquired then reconstructed into 3D views for tumor estimation analysis [17, 18].

An automated method acquires the images, using dedicated 2D transducers. The probe is mounted on a rail system equipped with a 3D motor stage.

Based on operator-defined parameters, the 3D motor stage travels a set distance across the target object in a series of tiny steps. At each step, the probe takes a two-dimensional "slice." Each two-dimensional B-mode image slice is assembled with the other slices of acquired data and rendered by the software into a three-dimensional data set. The digitally stored volume data can be presented in a three-dimensional view of the acquired data (cube view), a three single, slidable image slice views (cross view), "transverse view," straight-on perspective of the *x*-*y* plane image slice, "sagittal view" and "coronal view" (Figure 2). 3D volumes can be created in 3D-mode or power 3D mode using parallel or rotational segmentation. For either method of segmentation, the system can perform a manual or semiautomated segmentation of the volume. When the manual segmentation procedure is followed, the operator draws each contour of the volume. After the semiautomated segmentation procedure is followed, the system draws two or more contours automatically.

Vascularization of tissues within the region of interest can also be assessed using 3D power-Doppler ultrasound and a percent vascularity value (PV) is provided after the volume has been created. The PV provides the percentage of the volume that contains flow detected from power Doppler mode.

3. Contrast Agent

The most used US contrast agents (both in preclinical and clinical research) consist of small, stabilized gas-encapsulated microparticles (<10 μm) defined microbubble contrast agents that we injected into the bloodstream behave similarly to red blood cells in the microcirculation providing a strongly reflective blood/gas interface. This allows the detection of purely intravascular molecular targets, whereas intracellular molecular events cannot be

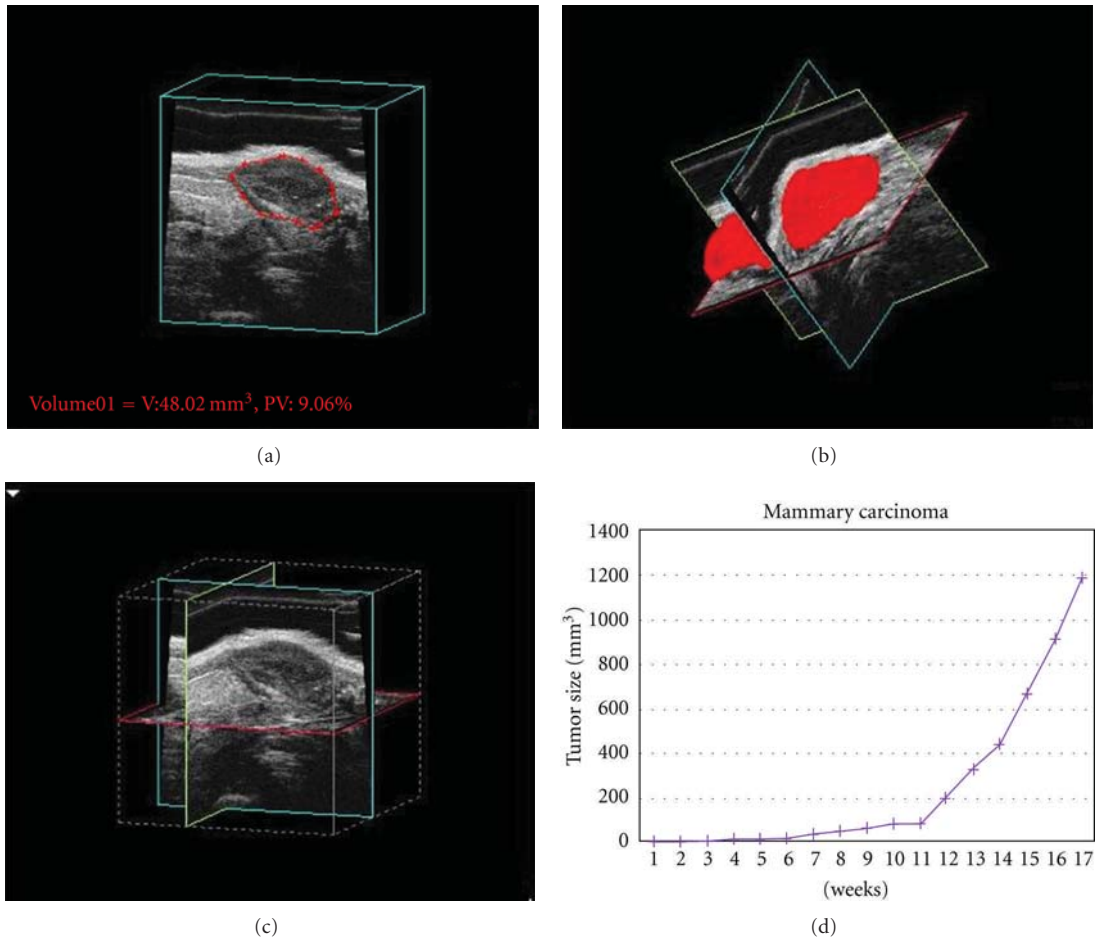

Figure 2: Various view of three-dimensional reconstructions of a subcutaneous tumor from two bidimensional successive parallel cross-section images. (a) Cube view. On the bottom, the segmentational volumetric analysis with a volume estimation of 48.02 mm^3. (b) Surface view. (c) Cross view. (d) Quantitative analysis of tumor growth in a mice model of mammary tumor. The tumor growth curve over time is showed in the diagram.

imaged. The microbubbles signal is dependent on a number of factors such as the filling gas property, for example, compressibility and solubility, the surrounding medium properties as viscosity and density, the frequency and power of ultrasound applied, the bubble size, and shell properties as elastic modules, thickness, and damping effects. The behavior of microbubbles depends on the amplitude of ultrasound to which they are exposed. A very low acoustic power (mechanical index <0.05–0.1) produces ultrasound scattering equal to the transmitted frequency. A slightly higher mechanical index of 0.1–0.3 produces a backscatter of a variety of frequencies (harmonics, subharmonics, and ultraharmonics). Higher acoustic pressures (MI > 0.3–0.6) destroy the microbubbles (Figure 3). This occurrence produces a high-intensity broadband signal, changes in the microenvironment, or even shell ballistic events that are important features for both perfusion imaging and therapeutic applications as local delivery of drug or genes.

It is possible to target microbubbles to specific region of disease. Actually, there are two mechanisms for targeting the contrast agent: a passive and an active mechanism of targeting.

The passive targeting mechanism is based on an unspecific electrostatic or chemical interaction between the microbubble shell and the receptors of the endothelial wall expressed by diseased tissues.

The active targeting mechanism is based on the specific binding between shell microbubbles' ligands and surface disease antigens. The "active targeting" uses the attachment of specific antibodies, such as anti-VEGF for example, to the surface of microbubbles with streptavidine-biotin interaction (Figure 4). This leads to the accumulation of targeted contrast agent to specific sites due to the use of adhesion ligands including antibodies, peptides, and polysaccharides. Since the microbubbles remain within the vasculature, because of their size in the micron range, specific marker molecules have to be located in the intravascular space and on the endothelium to be targeted during pathological events. Specific ultrasound imaging protocols are used to detect retention of targeted microbubbles (Figure 5). After the bolus injection of the targeted ultrasound contrast agent,

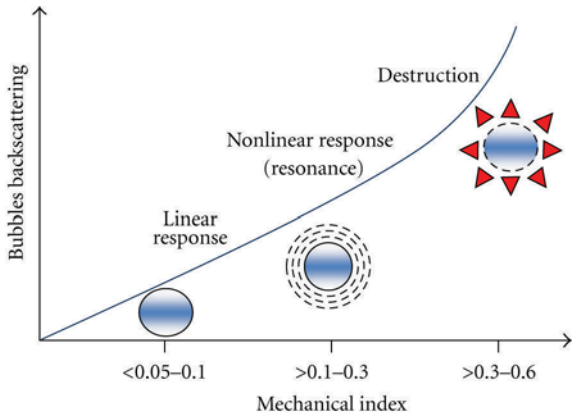

Figure 3: Behavior of microbubbles depends on the amplitude of ultrasound to which they are exposed. At very low acoustic power (mechanical index <0.05–0.1), microbubble oscillates in relatively symmetrical backscattering at the same frequency of incident ultrasound. At a slightly higher mechanical index of 0.1–0.3, the microbubble becomes somewhat oscillates in a nonlinear manner (nonlinear response), backscattering a variety of frequencies (harmonic). Higher acoustic pressures (MI > 0.3–0.6) destroy the microbubbles with high-intensity backscatter response.

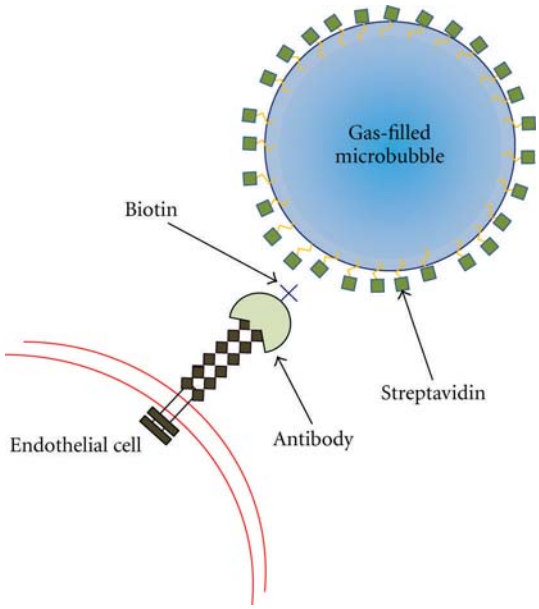

Figure 4: Schematic representation of active targeting of biotin-streptavidine bridges. Streptavidine is used for attachment of biotinylated ligands onto the shell of ultrasound contrast microbubbles. Molecularly targeted microbubbles selective bind to sites of molecular expression on the endothelium.

it is necessary to wait for 4 to 15 minutes before starting the contrast-enhanced imaging. This elapsed time allows retention and clearance of most circulating microbubbles from the blood pool. Sets of 300 frames (temporal resolution of 30 Hz in a period of 10 seconds) are then captured to obtain a signal from the tumor tissue background and contrast agent accumulated in the target site both retained and freely circulating microbubbles. Therefore, using destruction-subtraction algorithm the residual circulating contrast signal is measured. After destruction of microbubbles by 2 to 3 seconds of "break" frames performed with high mechanical index, a new set of 300 frames is captured to derive the signal only from tumor tissue and freely circulating microbubbles. The images acquired before breaking pulses and after breaking pulses are averaged and digitally subtracted to derive the signal representing only retained microbubbles. Late imaging modality of single intravenous injection of contrast media optimizes the signal coming from retained microbubbles with respect to the one coming from freely circulating microbubbles, since these latter are gradually removed from the blood pool. The signal from freely circulating microbubbles is very low, accounting for 15% of the contrast signal intensity on initial frames with the targeted agents. The entire imaging procedure typically lasts 30 minutes, then data analysis is performed offline, consisting mainly of digital subtraction and frame alignment, region-of-interest quantification and color map processing. Many researchers have used microbubbles in small animals for the detection of molecular markers of inflammation, angiogenesis, and atherosclerosis [19–22].

Ultrasound contrast agents are viable candidates for gene delivery/therapy. Ultrasound energy determines an increase of cell membrane permeability (a process known as sonoporation), which is being increasingly exploited for its role in drug-delivery applications to transfer therapeutic agents including genetic material, proteins, plasmid DNA, and chemotherapeutic agents, directly to the pathological tissue and organs. The use of US is based on the fact that the contrast agent can be identified at the target site and it can readily be insonated causing ultrasound-induced rupture of the drug-loaded microbubbles hence achieving targeted drug release. Most targeted ultrasound contrast agents are microbubbles, but other vehicles can be used including acoustically active liposomes and perfluorocarbon emulsions.

Echogenic liposomes can readily be conjugated to antibodies or other adhesion ligands, and thus are readily configured as targeted agents. Liposomes, are less than 1 mm in diameter and due to the small diameter, these agents are not entrapped in the microvasculature of the lung and have a long circulating time. Additionally, the liquid-like composition of liposomes makes them more resistant to pressure and mechanical stress than microbubbles. Another advantage of liposomes have been used to entrap gas and drugs for ultrasound controlled drug release and ultrasound-enhanced drug delivery [23]. Echogenic liposomes have been produced by different preparation methods, including lyophilization, pressurization, and biotin-avidin binding [24]. Additional benefits of liposomes are that lipids are small molecular structures and the lipid complexes can be made smaller by filtering or sonication techniques. Proteins and delivery agents made of proteins tend to break if they are manipulated to make them smaller. The difference lies in the rigidity of the protein, which has covalent bonds, *versus* the lipid, which is composed of small molecules held together by hydrophobic interactions [25].

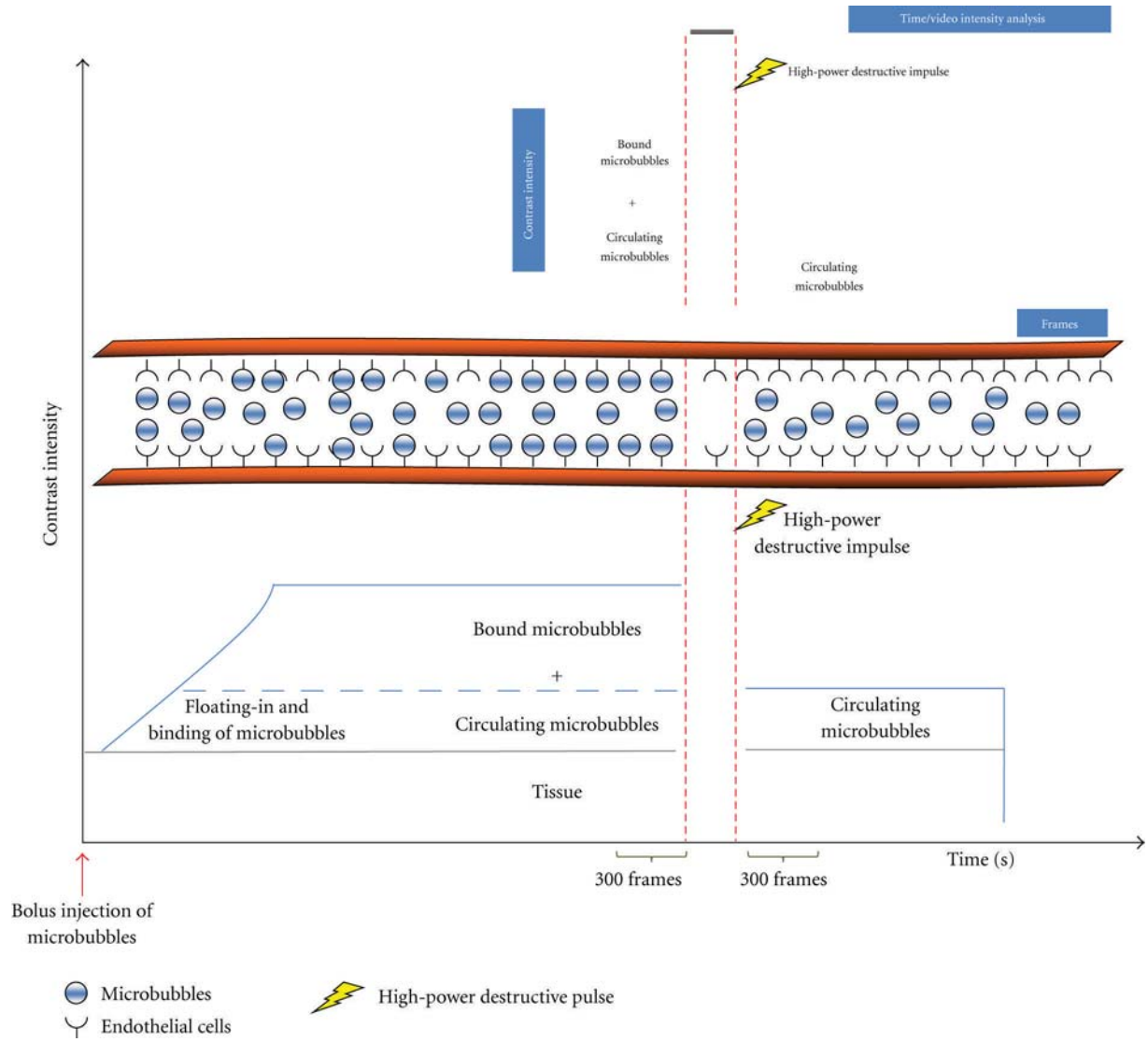

Figure 5: Targeted US of endothelial antigens in vessels of a tumor tissue. On the top of the figure time/video intensity analysis before and after high-power destructive pulse and bottom a diagram representation of destructive methodology. Endothelial cells of vessels (orange) of tumor tissues expresses specific antigens. After intravenous administration targeted microbubbles float in vessels and remaining exclusively in the vascular compartment. Many of them bind to antigens of endothelial cells , whereas others remains in the vessel lumen freely circulating. After high-power destructive pulse, all microbubbles are destroyed (bound + circulating), following circulating microbubbles that arrive from outside of scan plane, which remain freely circulating for several seconds. Contrast intensity is the sum of the intensity from tissue, intensity from microbubbles not bound to receptors (circulating microbubbles), and intensity from microbubbles bound to receptors on endothelial cells. After digital subtraction of the video intensity calculated on 300 predestruction frames from video intensity calculated on 300 postdestruction frames, resulting video intensity is due only to bound microbubbles.

Perfluorocarbon emulsion nanoparticles can be used as an ultrasound contrast agent. Due to their size (approximately 250 nm) in diameter and composition, these agents have the same qualities of gas encapsulated microbubble contrast agent and the liposomes [23, 26]. These nanoparticles avoid lung entrapment. They consist of a lipid encapsulated perfluorocarbon, which is a liquid at room temperature. The liquid composition makes it resistant to pressure and mechanical stress. However, due to their small size, their echogenicity is weak until they are deposited in a layer. This can be an advantage, as the low free-floating echogenicity results in a decreased background noise level. Submicron particles filled with liquid perfluorocarbon are currently being studied as a potential ultrasound targeted contrast agent.

Nanoparticles with directly conjugated tissue factor antibody demonstrated acoustic enhancement similar to that demonstrated with the avidin-biotin targeting approach with the advantage of one step targeting method [27].

Recently, acoustically activated submicron droplets of liquid perfluorocarbon have investigated as a "new class" of ultrasound contrast agent. In the liquid state, intravascular droplets can extrasavasated within tumors, resulting a candidate for an extravascular ultrasound contrast agent.

Table 1: Specific procedures related to UBM.

Procedures	Applications	References
Vein injection (jugular vein, femoral vein, and tail vein)	Contrast agent administration in single bolus	[34]
	Genes and drugs delivery	[31]
Blood vessels cannulation	Contrast agent administration in repeated bolus	[31, 32, 35, 36]
Ultrasound-guided microinjections	Viral vectors and gene delivery	[37]
	Drugs delivery	[38]
	Guided in utero microinjection	[33, 39, 40]
	Stem cells therapy	[9]
Biopsy	Tumor and organ histology	

Activation was accomplished by using burst of ultrasound to vaporize the droplets [28].

Finally, Bekeredjan et al. tested gold-bound microtubules to provide a backscattering that allowed microtubules to be potentially useful as an ultrasound contrast agent. Gold-bound microtubules provide a persistent contrast effect, suggesting their use as an ultrasonic contrast agent with the feasibility of antibody conjugation [29].

4. Animals Preparation to UBM Studies

Mice are anesthetized using 1.5%–2% isoflurane vaporized in oxygen with the aid of a precision vaporizer (we used the vaporizer manufactured by Vetequip Inc., Pleasanton, Calif, USA) to deliver the appropriate amount of anesthetic, with constant monitoring of their body temperature (with a rectal probe) and heart rate. Body temperature is maintained at 35°C–38°C using an infrared lamp and a heating pad. Hair is removed from the area of interest with a chemical hair remover to obtain a direct contact of the ultrasound gel to the skin of the animal and to minimize US attenuation. To provide a coupling medium for the transducer a prewarmed low-density ultrasound gel is used (we utilize the Aquasonic 100 ultrasound transmission gel, Parker, USA). Using all these cautions is possible to perform a safe UBM study on mice without particular regards to the anesthesia duration. The position of the two-dimensional image plane is obtained with the ultrasound probe fixed to a rail system that allows repeatable and precise examinations (Vevo Integrated rail System II).

5. Specific UBM Procedures

Some surgery procedures on mice can be necessary during studies: tail vein injection, cannulations, and microinjections (Table 1).

Tail vein injection is used to perform contrast UBM imaging for perfusion studies, for the administration of drugs or genetic materials contained in microbubbles. Before the injection, a vasodilatation is induced to better localize the lateral tail vein. It is important to avoid injection exceeding 200 μL to avoid hypervolaemia and lung edema.

Cannulation has several advantages compared to tail vein injection: it allows making injections in the jugular vein, and it is less traumatic for wall vessels and allows controlled and repeated injections during the same imaging study without changing the scanning plane.

Cannulation of the jugular vein [30] is an established method for studying drug pharmacokinetics and effects. After anesthesia, the skin between the ears and the right-hand side of the neck of the mouse needs to be shaven and the skin disinfected. A longitudinal incision of about 15 mm is made in the neck of the animal. After careful removal of the connective tissue surrounding the jugular vein, the cannula, filled with heparin solution (750 units/mL in water), is inserted into the vein in the caudal direction. The cannula is fixed to the jugular vein by ligation. Finally, the incision in the neck of the animal is closed using 5/0 Ethilon silk suture and a metal spring is firmly attached to the stitches (Figure 6(a)).

Cannulation of the lateral tail veins [31, 32] can also be performed in the mouse to inject contrast ultrasound agent. Animals are immobilized by taping the tail to an 18 cm × 7 cm plexiglass rectangle and by fastening a restraint tube (125 mL half-Nalgene bottle) using rubber bands. The tail is then washed and immersed in warm water (42°C) for approximately 45 seconds to dilate the tail veins. After this, the tail is cleaned and wiped with ethanol. A 27-gauge needle connected by PE 10 tubing to a 1 mL saline-filled syringe is inserted into the right lateral vein approximately 2 cm from the body and its intravascular position confirmed by drawing blood (Figure 6(b)). The needle is then removed, and a saline-heparin- (SH; 150 IU/mL) filled catheter is introduced through the access site. Proper position of the catheter in the vein is verified by the observation of blood backflow. The catheter is then secured to the tail using cyanoacrylate glue (we use Histoacryl, B Braun, Am Aesculap-Platz, Germany) at the point of insertion.

UBM-guided injections, such as targeted injections of retroviruses, cells, or genetic materials in mouse embryos, can be done manually [10] or by mechanical guide [33] and can be performed transcutaneously or with surgical exposure of the target organ. Injections can be performed with 50 μL Hamilton syringe and a 30 gauge needle [10] or with microinjector units and capillary glass needle that can inject very small volume (about 10 nL).

6. In Utero Microinjections

In utero ultrasound-guided microinjection of mouse embryos has proven a valuable tool for exploring the

(a) (b)

Figure 6: Cannulation of jugular and tail veins. The anesthetized mouse is immobilized by taping its harms on a termoregulated pad. A side of the neck or the tail of the mouse are disinfected. A 27-gauge needle connected by polyethylene tubing (PE10) to a 1 mL saline-filled cannula is inserted into the jugular vein or in the lateral tail vein approximately 2 cm from the body. The cannula, filled with heparin solution (750 units/mL in water), is inserted into the vein in caudal direction and fixed to the vein with cyanoacrylate glue (Histoacryl, B Braun, Am Aesculap-Platz, Germany). The proof of the correct position of the needle is given by blood visualization in the cannula. (a) Cannulation of jugular vein. (b) Cannulation of lateral tail vein.

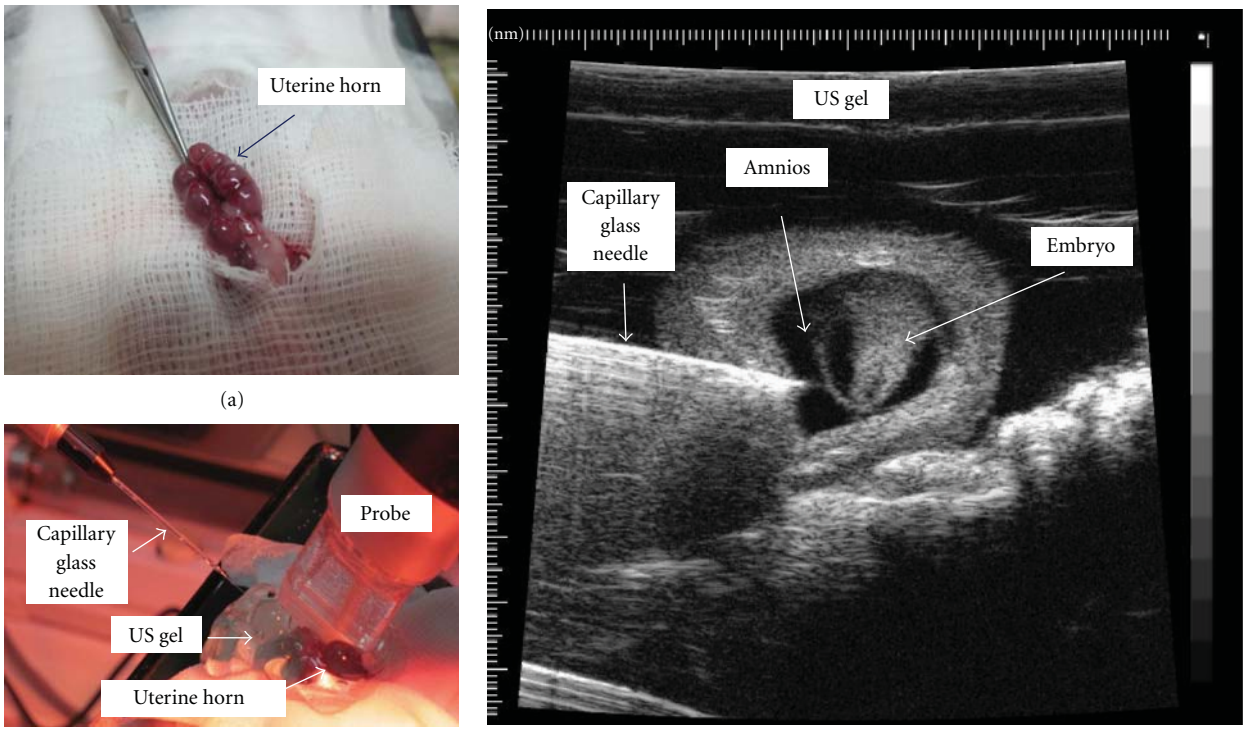

Figure 7: In utero microinjection: laparoscopy along the linea alba. The uterine horns are gently exteriorized to record implantation sites and simply positioned on sterile gauze and covered with sterile acoustic gel (a). A 40 Mhz probe is used to image in real time the embryos, and the microinjection is performed by an automatic microinjector equipped with a capillary glass needle. The needle is advanced with the use a micromanipulator under echo guidance until the needle tip is in the desired location (b). UBM images of a capillary glass needle advanced under echo guidance until the needle tip is in the amnions (c).

developmental consequences of altering gene expression using viral vectors and for injecting cells to study cell lineage or migration and to validate gene therapies. Pregnant females need to be monitored during anesthesia. Physiological parameters such as heart rate, respiratory frequency, and temperature are useful to assess anesthetic depth during the procedure and the maternal-fetal well-being. Microinjection procedure contemplate a laparoscopy along the linea alba after skin disinfection with 70% ethanol. The mouse is mounted on the stage of a rail system, which permits the operator to readily adjust the position of the mouse while maintaining the microinjection pipette within the transducer-imaging plane. The uterine horns are gently exteriorized to record implantation sites and simply positioned on sterile gauze and covered with sterile acoustic gel (Figure 7(a)).

A 40 Mhz probe is used to image in real time the embryos, and microinjection is performed with an automatic microinjector equipped with a capillary glass needle. The needle is advanced with the use a micromanipulator under echo guidance until the needle tip is in the desired location (Figure 7(b)). In this way, the procedure is less traumatic for the embryos, and a very small amounts of material can be injected, significantly reducing the risk of embryonic death. After microinjecting all sites, the gel is removed with a squeeze bottle containing sterile PBS, and embryos are placed back into the body cavity. The maternal abdomen is then closed using a 8–0 silk suture using a continuous stitch up, anesthesia is discontinued, and the mouse is placed in a heated recovery chamber. UBM is performed in the following two days to test the fetuses' health status.

Commonly, microinjection is performed at embryonic day 9.5 (E9.5) or greater, but recently, with advances in technology, it has been reported the possibility to accurately target specific regions of the embryos under high-resolution ultrasound guidance at E6.5 to E7.5 of gestation [33].

7. Applications

7.1. Oncology. High-Frequency ultrasound represents a significant advancement in the phenotypic assessment of mouse cancer models. Tumor size can be quantified by 2D and 3D ultrasound imaging in several xenograft models. Pezold et al. [41] demonstrated in a murine orthotopic oral cavity tumor model that tumor dimensions acquired with ultrasound measurements were not significantly different compared to histological measurement [42]. Moreover, high-frequency ultrasound allows noninvasive longitudinal assays [17]; UBM detects small tumor nodules in early stage with lower limit of detection at approximately 0.4 mm in volume (Figure 8). In a model of thyroid cancer UBM detected the presence of malignant thyroid nodules quite early, long before they were palpable, and UBM results were compared with histological findings [2].

In a model of human mammary cancer, 3D was used to monitor tumor growth every week and to detect tumor response after therapy, showing a better correlation with postmortem findings in comparison to other imaging technique like bioluminescence and positron emission tomography [43] (Figure 9).

Recently, Banihashemi et al. [44] demonstrated that UBM is able to detect apoptotic cell death in a preclinical tumor model of melanoma after treatment with photodynamic therapy in models of bladder and colorectal cancer.

Power Doppler ultrasound captures flow-dependent signals in blood vessels and can be used to assess neoangiogenesis. However, its sensitivity is limited to vessels larger than capillaries. Xuan et al. [13] reported the first application of high-frequency three-dimensional power Doppler ultrasound imaging in a genetically engineered mouse prostate cancer model. Tumor vascularity was quantified in power Doppler images by computing the color pixel density for the entire tumor and the peripheral part of the prostate tumor. The vascular architecture at different stages of tumor growth was detected comparing 3D power Doppler with contrast-enhanced micro-CT. Comparisons suggested that the smallest vessels reliably detected by power Doppler were from 100 to 150 μm diameter. Contrast agents revealed all perfused vessels by assessing stimulated acoustic emissions from microbubbles. Angiogenesis can be enhanced in neoplastic tissues by several mechanisms such as overexpression of angiogenetic factors or mobilization of angiogenetic proteins in the extracellular matrix [45], and the amount of new blood vessel growth is correlated with poor prognosis in several tumor types [46]. Therefore, there is a great interest in the development of antiangiogenetic drugs such as anti-VEGF treatments and of imaging techniques that could be helpful in quantifying tumor vasculature and the VEGF expression.

More recently, Willman et al. [35] demonstrated that angiogenesis is detected in angiosarcoma and malignant glioma in mice using microbubbles labeled with monoclonal antibodies against murine VEGF-R2. A dual-targeted contrast-enhanced US directed at both VEGF-R2 and alpha(v)beta(3) integrin improves *in vivo* visualization of tumor angiogenesis in a human ovarian cancer xenograft tumor model in mice.

A major challenge for tumor therapy is to obtain effects directly into an affected tissue of nucleic acids delivered in systemic circulation. Intravenous injections of a replication incompetent adenovirus with a cytokine displaying cancer selective-apoptosis profoundly inhibits prostate cancer growth in animals in which the tumor was insonated in comparison with the control groups injected with adenovirus but not insonated. These findings demonstrate the utility and the potential therapeutic applications of novel microbubbles guided gene therapy technology [7].

7.2. Cardiology. UBM provide an opportunity to characterize anatomy and physiology of heart and great vessels in a safe, reliable, and noninvasive modality in adult mice.

2D and 3D imaging have been used to evaluate cardiac structure and valves morphology and function in mice [1, 47, 48], to calculate cardiac function parameters such as stroke volume, cardiac output, ejection fraction, and fractional shortening, and to assess global left ventricular function and LV mass [8, 47–49] in normal and in models

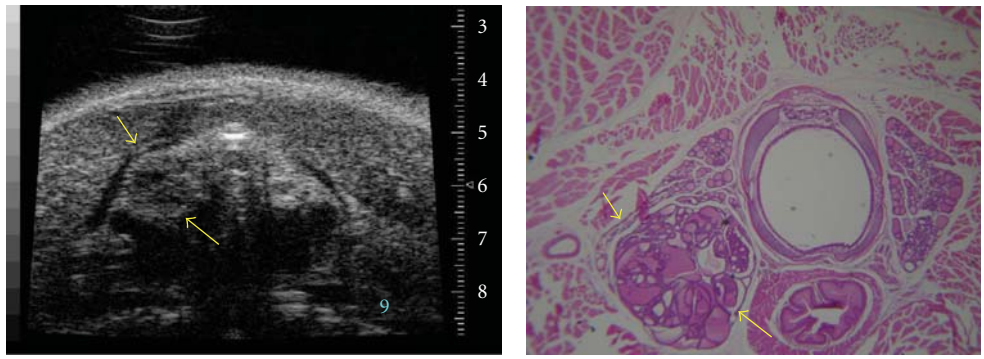

(a) (b)

Figure 8: (a) UBM microimaging of thyroid in living mice performed with a 35 MHz probe in a genetically engineered mice model of thyroid disease (TRK). The figure shows an enlarged left lobe with hypoechoic nodule (arrows). (b) Histopathology analysis shows a thyroid adenoma. From Mancini et al. *Endocrinology* [2].

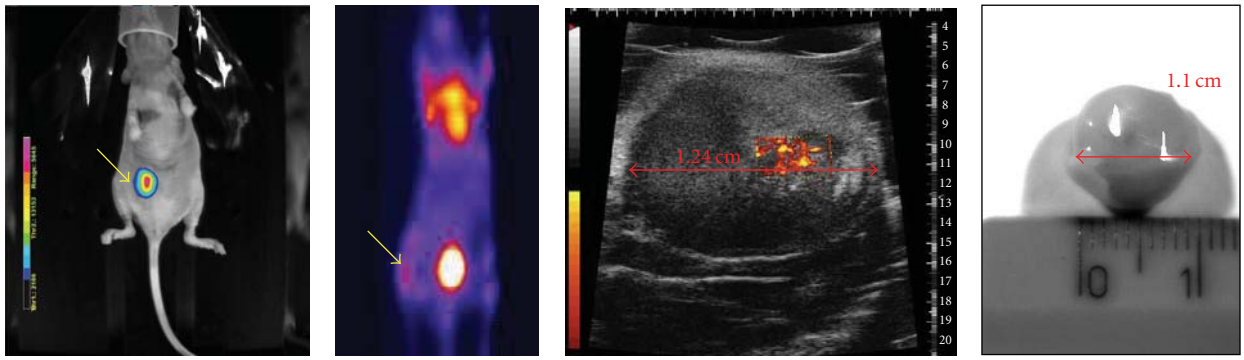

(a) Bioluminescence (b) PET (c) UBM (d) Necroscopy

Figure 9: Multimodality imaging of the lesion: human mammary tumor cells were implanted in the mammary fat pad of an athymic nude mice, 6 weeks old. There is a good correspondence between the morphology and the size of the tumor detected by UBM and necroscopic findings. (a) Bioluminescence of the tumor. (b) ^{18}F-flourothymidine total body PET, tumor uptake is evident (arrow). (c) UBM with measurements of neoplasia. (d) Post mortem dimension of the explanted tumor.

of cardiovascular diseases [50–54]. Pharmacological effects of various agents tested in mouse models have also been evaluated with echocardiography [55, 56].

Small heart size hampers accurate injection into the left ventricular (LV) wall and require surgical visualization of the heart, but that, however, do not prevent unintentional injection into the LV cavity. High-resolution echocardiography is able to guide cardiac injections accurately into the myocardial wall of mice with closet chest. This system was successful to target the injection of labeled cells into specific cardiac regions such as myocardium adjacent to ischemic area in a mouse myocardial infarction model or to treat ischemic myocardium implanting bone marrow cells and to guide left ventricular catheterization [9, 10].

Microbubbles have been applied mainly as blood pool agents to enhance the echogenicity of the cardiac chambers during echocardiography for better delineation of the myocardial borders and for perfusion assessment of the myocardium [57].

Using 2D B-mode imaging, fetal heart development can be detected in mice as early as embryonic day 8.5, when the linear heart tube begins to beat. On day 9.5, the U-shaped heart tube is clearly visible, and Doppler blood velocity waveforms can be recorded separately from the inflow and outflow regions of the heart tube (Figure 10(a)). On day 11.5, it is possible to detect the process of division of the outflow tract into the ascending aorta and main pulmonary artery (Figure 10(b)). At E12.5, the separation of the aorta and main pulmonary artery appears complete, but the interventricular septum is visibly incomplete, and flow streams from both ventricles can be seen entering the aorta (Figure 10(c)). At day 13.5, the embryonic ventricles are fully separated by a septum, the atrioventricular valves are visible, and the heart has a mature fetal form (Figure 10(d)). After day 15.5, the heart chambers begin to darken in the ultrasound image, and the ventricular wall, endocardium, and septum are easier to be discerned (Figure 10(e)). The improved contrast seen after day 15.5 means that ventricular chamber dimensions and wall thickness measurements become feasible [5, 58]. Fetal blood is echodense at UBM frequencies, due to nucleated erythroblasts, and this may facilitate assessment of major vascular development.

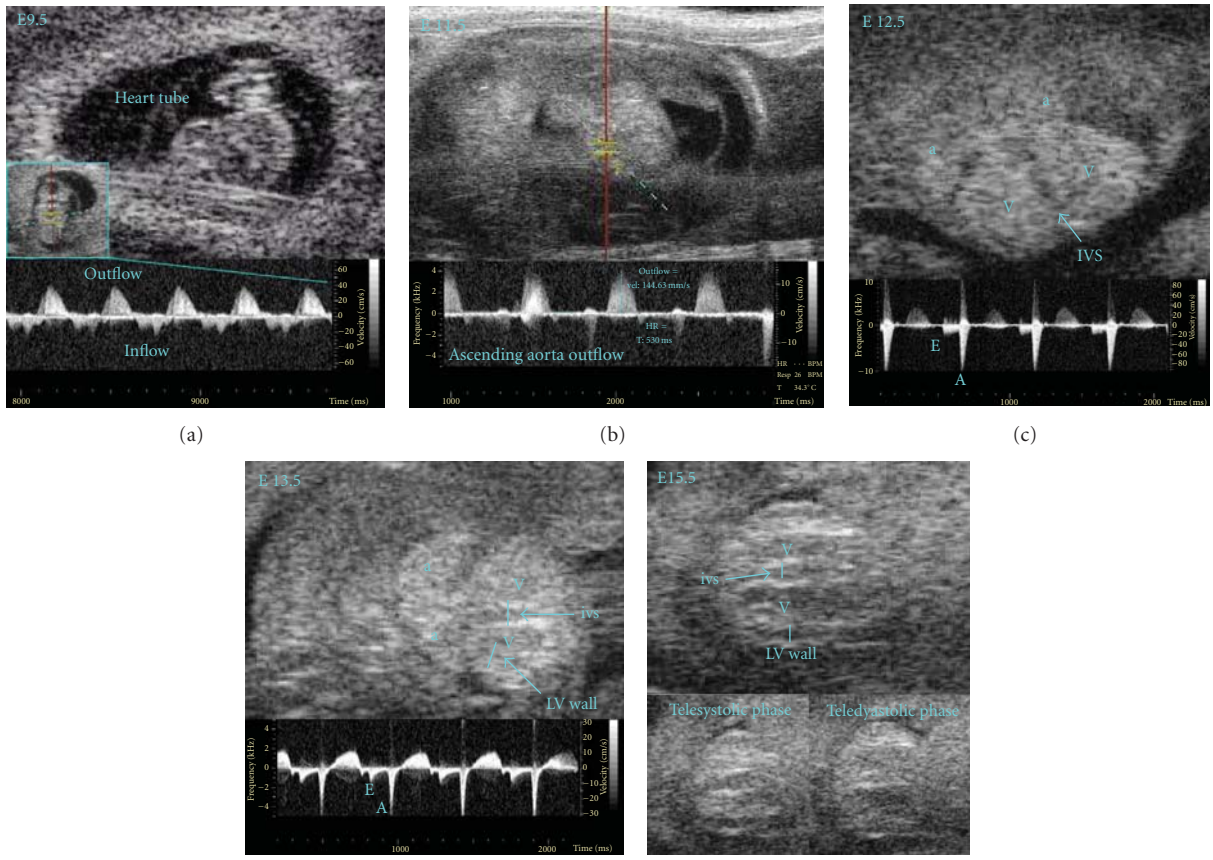

Figure 10: (a) E9.5: heart tube and doppler spectral trace of ventricular inflow and outflow at 9.5 gestational age. (b) E11.5: doppler spectral trace of ascending aorta outflow at 11.5 gestational age. (c) E12.5: bidimensional image of atrio-ventricular chambers (a–V) interventricular septum (IVS); and doppler spectral trace of ascending aorta outflow at 12.5 gestational age. (d) E13.5: bidimensional image of atrioventricular chambers, interventricular septum, and left ventricle wall (LV wall); doppler spectral trace of ventricular inflow and outflow at 13.5 gestational age. The atrial wave (A-wave) was dominant. The rapid ventricular filling (E-wave) is a measure of ventricular compliance. (e) E15.5: bidimensional image of ventricular chambers, interventricular septum, and left ventricle wall in telesystolic and telediastolic fase of heart cycle in a 15.5 days mouse embryo.

Noninvasive transthoracic echocardiography in newborn C57BL mice has been shown to define normal cardiac and great vessel anatomic measurements [59].

The mouse has become a powerful tool for studying genetic models of cardiac development and congenital heart disease and echocardiography is an ideal method for detecting and studying congenital malformations in living fetus, as it allows early recognition of abnormalities and the progression of disease can be followed in utero with longitudinal studies [5, 48, 59, 60].

7.3. Developmental Biology. In utero imaging of live mouse embryos allows studies of early embryonic developmental stages, embryonic neural tubes and heart development, and the effects of mutant phenotypes during embryogenesis.

UBM resolution is sufficient to visualize small anatomical structures, especially at embryonic and early postnatal stages [61] and to study the morphology of various organ systems throughout development.

The feasibility of UBM for *in vivo* morphometric quantification of embryonic growth and for estimating gestational age and embryonic body weight in utero as discussed elsewhere [62, 63].

At the earlier stage (E11.5), major features of the embryo can be identified, including amniotic membrane and cavity, yolk sac, placenta, umbilical vessels, and heart and brain ventricles. At later stages (>E13.5), brain, mouth, eyes, lungs, heart chambers, liver, kidneys, chest wall, spine, limbs, and tail are also clearly visualized.

In the semi-invasive approach, a small incision is made in the abdominal wall, and one or two embryos are exteriorized. It has the advantage to exclude the maternal abdominal wall, and intra-abdominal content to provide a better resolution of embryonic structures.

Doppler flow in the developing brain has also been obtained [59, 64]. Investigations about eyes limbs and spine and skin oculodentodigital dysplasias in mouse embryos have also been reported using this technology [39, 40, 65].

7.4. Ocular Applications. UBM is a good tool for imaging the anterior ocular segment anatomy and pathology, including the cornea, anterior chamber, iris, ciliary body, and lens

[31, 32, 34, 36, 66–69]. Throughout development until E18.5, anterior segment structures appear compressed, revealing little structural detail or differentiation from surrounding tissues. It is possible to perform several quantitative analysis: measurements of the corneal thickness, of the anterior chamber depth, of the trabecular-iris angle, and of the iridozonular distance. It is, thus, applicable for diagnostic imaging of corneal diseases, glaucoma, cysts, and tumors. Imaging of posterior structures of the eye, and in particular, the retina and the optical nerve can also be obtained. Normal embryonic development of the mouse eye can be studied by ultrasound biomicroscopy with a focus on the formation of the retina, lens, and cornea. The earliest stages of development that can be successfully imaged are at approximately E8.5, coinciding with the appearance of the optic placode and vesicle. At this point, the morphogenesis of the eye is very primitive, and features of the developing tissues are close to the resolution limit of the scanner. Subsequent development of the lens vesicle, retina, cornea, vitreous, and conjunctiva can be observed up to the birth of the mouse. No evidence of flow has yet been observed in the developing prenatal mouse eye.

8. Conclusions

Advantages of ultrasound imaging over other imaging techniques that use ionizing radiation (e.g., PET, SPECT, and CT) is that it less invasive, does not require specialized ancillary equipments, is safer for the animals and the operators, and, finally, is a low-cost technology.

However, ultrasound imaging has also some limitations as a research tool. In fact, it requires the knowledge and expertise of a well-trained sonographer to obtain accurate and repeatable images and is limited by bone- and gas-filled structures; therefore, ultrasound is not routinely used in brain, spinal cord, and lung imaging. The development of novel targeted contrast agents will foster future applications to study the molecular basis of animal models. UBM provide a noninvasive imaging of both embryos and adult mice anatomy and pathology. It is an excellent tool for cancer research and cardiovascular investigations to analyze ocular and abdominal structures and embryos development.

Acknowledgment

A. Brunetti and M. Salvatore contribute equally to this work.

References

[1] R. B. Hinton, C. M. Alfieri, S. A. Witt et al., "Mouse heart valve structure and function: echocardiographic and morphometric analyses from the fetus through the aged adult," *American Journal of Physiology—Heart and Circulatory Physiology*, vol. 294, no. 6, pp. H2480–H2488, 2008.

[2] M. Mancini, E. Vergara, G. Salvatore et al., "Morphological ultrasound microimaging of thyroid in living mice," *Endocrinology*, vol. 150, no. 10, pp. 4810–4815, 2009.

[3] Z. P. Shen, A. A. Brayman, L. Chen, and C. H. Miao, "Ultrasound with microbubbles enhances gene expression of plasmid DNA in the liver via intraportal delivery," *Gene Therapy*, vol. 15, no. 16, pp. 1147–1155, 2008.

[4] F. S. Foster, M. Zhang, A. S. Duckett, V. Cucevic, and C. J. Pavlin, "In vivo imaging of embryonic development in the mouse eye by ultrasound biomicroscopy," *Investigative Ophthalmology and Visual Science*, vol. 44, no. 6, pp. 2361–2366, 2003.

[5] C. F. Spurney, C. W. Lo, and L. Leatherbury, "Fetal mouse imaging using echocardiography: a review of current technology," *Echocardiography*, vol. 23, no. 10, pp. 891–899, 2006.

[6] D. H. Turnbull, T. S. Bloomfield, H. S. Baldwin, F. S. Foster, and A. L. Joyner, "Ultrasound backscatter microscope analysis of early mouse embryonic brain development," *Proceedings of the National Academy of Sciences of the United States of America*, vol. 92, no. 6, pp. 2239–2243, 1995.

[7] A. Greco, A. Di Benedetto, C. M. Howard et al., "Eradication of therapy-resistant human prostate tumors using an ultrasound-guided site-specific cancer terminator virus delivery approach," *Molecular Therapy*, vol. 18, no. 2, pp. 295–306, 2010.

[8] H. C. Manning, N. B. Merchant, A. C. Foutch et al., "Molecular imaging of therapeutic response to epidermal growth factor receptor blockade in colorectal cancer," *Clinical Cancer Research*, vol. 14, no. 22, pp. 7413–7422, 2008.

[9] M. L. Springer, R. E. Sievers, M. N. Viswanathan et al., "Closed-chest cell injections into mouse myocardium guided by high-resolution echocardiography," *American Journal of Physiology—Heart and Circulatory Physiology*, vol. 289, no. 3, pp. H1307–H1314, 2005.

[10] Y. Q. Zhou, L. Davidson, R. M. Henkelman et al., "Ultrasound-guided left-ventricular catheterization: a novel method of whole mouse perfusion for microimaging," *Laboratory Investigation*, vol. 84, no. 3, pp. 385–389, 2004.

[11] A. Greco, S. E. Kelly, P. P. Claudio, M. Salvatore, and A. Brunetti, "Ultrasound Contrast Agents for imaging and gene therapy," in *Proceedings of the AISAL Symposium "Imaging and Translational Medicine*, p. 25, 2010.

[12] F. S. Foster, M. Y. Zhang, Y. Q. Zhou et al., "A new ultrasound instrument for in vivo microimaging of mice," *Ultrasound in Medicine and Biology*, vol. 28, no. 9, pp. 1165–1172, 2002.

[13] J. W. Xuan, M. Bygrave, H. Jiang et al., "Functional neoangiogenesis imaging of genetically engineered mouse prostate cancer using three-dimensional power Doppler ultrasound," *Cancer Research*, vol. 67, no. 6, pp. 2830–2839, 2007.

[14] O. Balogun, G. D. Cole, R. Huber, D. Chinn, T. W. Murray, and J. B. Spicer, "High-spatial-resolution sub-surface imaging using a laser-based acoustic microscopy technique," *IEEE Transactions on Ultrasonics, Ferroelectrics, and Frequency Control*, vol. 58, no. 1, pp. 226–233, 2011.

[15] B. E. Treeby, E. Z. Zhang, A. S. Thomas, and B. T. Cox, "Measurement of the ultrasound attenuation and dispersion in whole human blood and its components from 0–70 MHz," *Ultrasound in Medicine and Biology*, vol. 37, no. 2, pp. 289–300, 2011.

[16] M. Tamaki, K. Kidoguchi, T. Mizobe et al., "Carotid artery occlusion and collateral circulation in C57Black/6J mice detected by synchrotron radiation microangiography," *Kobe Journal of Medical Sciences*, vol. 52, no. 5, pp. 111–118, 2006.

[17] K. C. Graham, L. A. Wirtzfeld, L. T. MacKenzie et al., "Three-dimensional high-frequency ultrasound imaging for longitudinal evaluation of liver metastases in preclinical models," *Cancer Research*, vol. 65, no. 12, pp. 5231–5237, 2005.

[18] L. A. Wirtzfeld, K. C. Graham, A. C. Groom et al., "Volume measurement variability in three-dimensional high-frequency

ultrasound images of murine liver metastases," *Physics in Medicine and Biology*, vol. 51, no. 10, pp. 2367–2381, 2006.

[19] J. R. Lindner, "Microbubbles in medical imaging: current applications and future directions," *Nature Reviews Drug Discovery*, vol. 3, no. 6, pp. 527–532, 2004.

[20] F. S. Villanueva, R. J. Jankowski, S. Klibanov et al., "Microbubbles targeted to intercellular adhesion molecule-1 bind to activated coronary artery endothelial cells," *Circulation*, vol. 98, no. 1, pp. 1–5, 1998.

[21] B. Walzog, D. Schuppan, C. Heimpel, A. Hafezi-Moghadam, P. Gaehtgens, and K. Ley, "The leukocyte integrin Mac-1 (CD11b/CD18) contributes to binding of human granulocytes to collagen," *Experimental Cell Research*, vol. 218, no. 1, pp. 28–38, 1995.

[22] M. Mancini, A. Greco, A. Speranza, and M. Salvatore, "Ultrasound molecular imaging by targeted microbubble contrast agents," *Minerva Biotecnologica*, vol. 21, no. 2, pp. 97–110, 2009.

[23] H. D. Liang and M. J. K. Blomley, "The role of ultrasound in molecular imaging," *British Journal of Radiology*, vol. 76, no. 2, pp. S140–S150, 2003.

[24] S. L. Huang, "Liposomes in ultrasonic drug and gene delivery," *Advanced Drug Delivery Reviews*, vol. 60, no. 10, pp. 1167–1176, 2008.

[25] C. K. Holland and D. D. McPherson, "Echogenic lipsomes for targeted drug delivery," in *Proceedings IEEE International Symposium of Biomedical Imaging (ISBI '09)*, pp. 755–758, July 2009.

[26] G. M. Lanza and S. A. Wickline, "Targeted ultrasonic contrast agents for molecular imaging and therapy," *Progress in Cardiovascular Diseases*, vol. 44, no. 1, pp. 13–31, 2001.

[27] O. Couture, P. D. Bevan, E. Cherin, K. Cheung, P. N. Burns, and F. S. Foster, "Investigating perfluorohexane particles with high-frequency ultrasound," *Ultrasound in Medicine and Biology*, vol. 32, no. 1, pp. 73–82, 2006.

[28] N. Reznik, R. Williams, and P. N. Burns, "Investigation of vaporized submicron perfluorocarbon droplets as an ultrasound contrast agent," *Ultrasound in Medicine and Biology*, vol. 37, no. 8, pp. 1271–1279, 2011.

[29] R. Bekeredjian, S. Behrens, J. Ruef et al., "Potential of gold-bound microtubules as a new ultrasound contrast agent," *Ultrasound in Medicine and Biology*, vol. 28, no. 5, pp. 691–695, 2002.

[30] H. A. Bardelmeijer, T. Buckle, M. Ouwehand, J. H. Beijnen, J. H. M. Schellens, and O. van Tellingen, "Cannulation of the jugular vein in mice: a method for serial withdrawal of blood samples," *Laboratory Animals*, vol. 37, no. 3, pp. 181–187, 2003.

[31] P. Haag, F. Frauscher, J. Gradl et al., "Microbubble-enhanced ultrasound to deliver an antisense oligodeoxynucleotide targeting the human androgen receptor into prostate tumours," *Journal of Steroid Biochemistry and Molecular Biology*, vol. 102, no. 1–5, pp. 103–113, 2006.

[32] Y. Miyake, K. Ohmori, J. Yoshida et al., "Granulocyte colony-stimulating factor facilitates the angiogenesis induced by ultrasonic microbubble destruction," *Ultrasound in Medicine and Biology*, vol. 33, no. 11, pp. 1796–1804, 2007.

[33] J. C. Slevin, L. Byers, M. Gertsenstein et al., "High resolution ultrasound-guided microinjection for interventional studies of early embryonic and placental development in vivo in mice," *BMC Developmental Biology*, vol. 27, no. 6, p. 10, 2006.

[34] D. Guo, X. Li, P. Sun et al., "Ultrasound/microbubble enhances foreign gene expression in ECV304 cells and murine myocardium," *Acta Biochimica et Biophysica Sinica*, vol. 36, no. 12, pp. 824–831, 2004.

[35] J. K. Willmann, A. M. Lutz, R. Paulmurugan et al., "Dual-targeted contrast agent for US assessment of tumor angiogenesis in vivo," *Radiology*, vol. 248, no. 3, pp. 936–944, 2008.

[36] A. Lyshchik, A. C. Fleischer, J. Huamani, D. E. Hallahan, M. Brissova, and J. C. Gore, "Molecular imaging of vascular endothelial growth factor receptor 2 expression using targeted contrast-enhanced high-frequency ultrasonography," *Journal of Ultrasound in Medicine*, vol. 26, no. 11, pp. 1575–1586, 2007.

[37] C. M. Howard, F. Forsberg, C. Minimo, J. B. Liu, D. A. Merton, and P. P. Claudio, "Ultrasound guided site specific gene delivery system using adenoviral vectors and commercial ultrasound contrast agents," *Journal of Cellular Physiology*, vol. 209, no. 2, pp. 413–421, 2006.

[38] M. R. Böhmer, A. L. Klibanov, K. Tiemann, C. S. Hall, H. Gruell, and O. C. Steinbach, "Ultrasound triggered image-guided drug delivery," *European Journal of Radiology*, vol. 70, no. 2, pp. 242–253, 2009.

[39] R. Pla, V. Borrell, N. Flames, and O. Marín, "Layer acquisition by cortical GABAergic interneurons is independent of Reelin signaling," *Journal of Neuroscience*, vol. 28, no. 26, pp. 6924–6934, 2006.

[40] C. Punzo and C. L. Cepko, "Ultrasound-guided in utero injections allow studies of the development and function of the eye," *Developmental Dynamics*, vol. 237, no. 4, pp. 1034–1042, 2008.

[41] J. C. Pezold, K. Zinn, M. A. Talbert, R. Desmond, and E. L. Rosenthal, "Validation of ultrasonography to evaluate murine orthotopic oral cavity tumors," *ORL*, vol. 68, no. 3, pp. 159–163, 2006.

[42] C. P. Chang, L. Chen, and G. R. Crabtree, "Sonographic staging of the developmental status of mouse embryos in utero," *Genesis*, vol. 36, no. 1, pp. 7–11, 2003.

[43] M. Zollo, N. Marino, A. Greco et al., "In vivo imaging methodologies applied to the murine xenografts of human breast cancer: a pre-clinical h-prune animal model," in *Proceedings of the European Symposium of Molecular Imaging*, p. 38, Naples, Italy, May 2007.

[44] B. Banihashemi, R. Vlad, B. Debeljevic, A. Giles, M. C. Kolios, and G. J. Czarnota, "Ultrasound imaging of apoptosis in tumor response: novel preclinical monitoring of photodynamic therapy effects," *Cancer Research*, vol. 68, no. 20, pp. 8590–8596, 2008.

[45] J. Folkman, "What is the evidence that tumors are angiogenesis dependent?" *Journal of the National Cancer Institute*, vol. 82, no. 1, pp. 4–6, 1990.

[46] C. Dazzi, A. Cariello, P. Maioli et al., "Prognostic and predictive value of intratumoral microvessels density in operable non-small-cell lung cancer," *Lung Cancer*, vol. 24, no. 2, pp. 81–88, 1999.

[47] M. Scherrer-Crosbie and H. B. Thibault, "Echocardiography in translational research: of mice and men," *Journal of the American Society of Echocardiography*, vol. 21, no. 10, pp. 1083–1092, 2008.

[48] J. Stypmann, M. A. Engelen, C. Troatz, M. Rothenburger, L. Eckardt, and K. Tiemann, "Echocardiographic assessment of global left ventricular function in mice," *Laboratory Animals*, vol. 43, no. 2, pp. 127–137, 2009.

[49] R. C. Fentzke, C. E. Korcarz, S. G. Shroff et al., "Evaluation of ventricular and arterial hemodynamics in anesthetized closed-chest mice," *Journal of the American Society of Echocardiography*, vol. 10, no. 9, pp. 915–925, 1997.

[50] P. Krishnamurthy, J. Rajasingh, E. Lambers, G. Qin, D. W. Losordo, and R. Kishore, "IL-10 inhibits inflammation and attenuates left ventricular remodeling after myocardial infarction via activation of STAT3 and suppression of HuR," *Circulation Research*, vol. 104, no. 2, pp. e9–e18, 2009.

[51] J. Takagawa, Y. Zhang, M. L. Wong et al., "Myocardial infarct size measurement in the mouse chronic infarction model: comparison of area- and length-based approaches," *Journal of Applied Physiology*, vol. 102, no. 6, pp. 2104–2111, 2007.

[52] T. P. Abraham, M. Jones, K. Kazmierczak et al., "Diastolic dysfunction in familial hypertrophic cardiomyopathy transgenic model mice," *Cardiovascular Research*, vol. 82, no. 1, pp. 84–92, 2009.

[53] L. Gavish, C. Rubinstein, A. Bulut et al., "Low-level laser irradiation inhibits abdominal aortic aneurysm progression in apolipoprotein E-deficient mice," *Cardiovascular Research*, vol. 83, no. 4, pp. 785–792, 2009.

[54] M. Ni, M. Zhang, S. F. Ding, W. Q. Chen, and Y. Zhang, "Micro-ultrasound imaging assessment of carotid plaque characteristics in apolipoprotein-E knockout mice," *Atherosclerosis*, vol. 197, no. 1, pp. 64–71, 2008.

[55] M. Walker, B. R. Campbell, K. Azer et al., "A novel 3-dimensional micro-ultrasound approach to automated measurement of carotid arterial plaque volume as a biomarker for experimental atherosclerosis," *Atherosclerosis*, vol. 204, no. 1, pp. 55–65, 2009.

[56] G. Bragagni, F. Lari, G. Magenta, R. Brogna, and G. Zoli, "Echocardiographic evaluation of anti-tumor necrosis factor-α therapy with infliximab in patients without cardiac pathologies," *Recenti Progressi in Medicina*, vol. 101, no. 7-8, pp. 289–292, 2010.

[57] J. Grönros, J. Wikström, U. Brandt-Eliasson et al., "Effects of rosuvastatin on cardiovascular morphology and function in an ApoE-knockout mouse model of atherosclerosis," *American Journal of Physiology—Heart and Circulatory Physiology*, vol. 295, no. 5, pp. H2046–H2053, 2008.

[58] B. A. Kaufmann, M. Lankford, C. Z. Behm et al., "High-resolution myocardial perfusion imaging in mice with high-frequency echocardiographic detection of a depot contrast agent," *Journal of the American Society of Echocardiography*, vol. 20, no. 2, pp. 136–143, 2007.

[59] S. Srinivasan, H. S. Baldwin, O. Aristizabal et al., "Noninvasive, in utero imaging of mouse embryonic heart development with 40-MHz echocardiography," *Circulation*, vol. 98, no. 9, pp. 912–918, 1998.

[60] C. K. L. Phoon, R. P. Ji, O. Aristizábal et al., "Embryonic heart failure in NFATc1-/- mice novel: mechanistic insights from in utero ultrasound biomicroscopy," *Circulation Research*, vol. 95, no. 1, pp. 92–99, 2004.

[61] N. Corrigan, D. P. Brazil, and F. M. Auliffe, "High-frequency ultrasound assessment of the murine heart from embryo through to juvenile," *Reproductive Sciences*, vol. 17, no. 2, pp. 147–157, 2010.

[62] D. H. Turnbull, J. A. Ramsay, G. S. Shivji et al., "Ultrasound backscatter microscope analysis of mouse melanoma progression," *Ultrasound in Medicine and Biology*, vol. 22, no. 7, pp. 845–853, 1996.

[63] M. Russo, L. Meomartino, A. Greco et al., "Pregnancy detection in mice using ultrasound," *Veterinary Record*, vol. 160, no. 13, pp. 446–447, 2007.

[64] J. Mu, J. C. Slevin, D. Qu, S. McCormick, and S. L. Adamson, "In vivo quantification of embryonic and placental growth during gestation in mice using micro-ultrasound," *Reproductive Biology and Endocrinology*, vol. 12, no. 6, p. 34, 2008.

[65] D. H. Turnbull, "In utero ultrasound backscatter microscopy of early stage mouse embryos," *Computerized Medical Imaging and Graphics*, vol. 23, no. 1, pp. 25–31, 1999.

[66] E. Bentley, P. E. Miller, and K. A. Diehl, "Use of high-resolution ultrasound as a diagnostic tool in veterinary ophthalmology," *Journal of the American Veterinary Medical Association*, vol. 223, no. 11, pp. 1617–1622, 2003.

[67] A. M. Flenniken, L. R. Osborne, N. Anderson et al., "A Gja1 missense mutation in a mouse model of oculodentodigital dysplasia," *Development*, vol. 132, no. 19, pp. 4375–4386, 2005.

[68] N. Nissirios, J. Ramos-Esteban, and J. Danias, "Ultrasound biomicroscopy of the rat eye: effects of cholinergic and anticholinergic agents," *Graefe's Archive for Clinical and Experimental Ophthalmology*, vol. 243, no. 5, pp. 469–473, 2005.

[69] S. W. M. John, R. S. Smith, O. V. Savinova et al., "Essential iris atrophy, pigment dispersion, and glaucoma in DBA/2J mice," *Investigative Ophthalmology and Visual Science*, vol. 39, no. 6, pp. 951–962, 1998.